بیست و سومین

کنفرانس شیمی فیزیک انجمن شیمی ایران

۲۲و۲۳دی۱۴۰۰کرمان، دانشگاه شهید باهنر

23RD Iranian Conference on Physical Chemistry
12-13-Jan 2022 – Shahid Bahonar University of Kerman

محورهای کنفرانس

ترمودینامیک شیمیایی | سینتیک شیمیایی | ترمودینامیک آماری

شیمی کوانتومی | طیف سنجی مولکولی | الکتروشیمی

شیمی سطح و حالت جامد | شیمی محاسباتی | شیمی فیزیک کاربردی | نانو شیمی فیزیک

شیمی فیزیک زیستی | مهندسی شیمی و آموزش شیمی

برگزارکنندگان

SCAN ME

دبیرخانه کنفرانس: کرمان - بزرگراه امام خمینی - میدان پژوهش - دانشگاه شهید با هنر کرمان - بخش شیمی

وبسایت کنفرانس : physchem23.uk.ac.ir

ایمیل کنفرانس : physchem23@conf.uk.ac.ir

تلفن تماس - واتس آپ :
۰۹۱۷۳۱۶۵۱۰۶

تلفن دبیرخانه: ۰۳۴-۳۱۳۲۲۱۲۶

بیست و سومین کنفرانس شیمی فیزیک انجمن شیمی ایران

مقالات پذیرفته شده

دانشکده علوم پایه بخش شیمی

دانشگاه شهید باهنر کرمان

۲۲ و ۲۳ دی ماه ۱۴۰۰

فهرست مطالب

پیشگفتار

ملکا ذکر تو گویم که تو پاکی و خدایی　　نروم جز به همان ره که توام راه نمایی
همه درگاه تو جویم همه از فضل تو پویم　　همه توحید تو گویم که به توحید سزایی

هم اکنون با گذشت ۵۰ سال از تاسیس دانشگاه شهید باهنر کرمان به همت و زحمات روانشاد مهندس علیرضا افضلی پور و همسر هنرمند ایشان زنده یاد بانو فاخره صبا، بخش شیمی دانشگاه شهید باهنر کرمان مفتخر است که با همراهی و مساعدت مجموعه ی دانشگاه شهید باهنر کرمان و با حمایت و مشارکت انجمن شیمی ایران و پایگاه استنادی علوم جهان اسلام، بیست و سومین کنفرانس شیمی‌فیزیک ایران را به صورت مجازی در روزهای چهارشنبه ۲۲ لغایت پنج شنبه ۲۳ دی سال ۱۴۰۰، با هدف آشنایی با آخرین دستاوردهای علمی پژوهشی ارزشمند انجام یافته توسط اساتید، دانشجویان و پژوهشگران در سطح کشور و به منظور فراهم نمودن بستری برای ارائه آخرین دستاوردهای علمی پژوهشی درحوزه های مختلف شیمی فیزیک و همچنین برقراری ارتباط بیشتر علمی بین پژوهشگران و متخصصان دانشگاهی و مراکز صنعتی برگزار نماید.

با اهدا ادب و سپاس فراوان

مریم دهستانی

رئیس بیست و سومین کنفرانس شیمی فیزیک ایران

حمایت کنندگان

بیست و سومین کنفرانس شیمی‌فیزیک انجمن شیمی ایران

دانشگاه شهید باهنر کرمان	انجمن شیمی ایران	وزارت علوم تحقیقات و فناوری
سیویلیکا	شرکت ملی صنایع مس ایران	پایگاه استنادی علوم جهان اسلام

کمیته علمی

بیست و سومین کنفرانس شیمی‌فیزیک انجمن شیمی ایران

دانشگاه شهید باهنر کرمان			
	دکتر مریم دهستانی	دکتر سید محمد علی حسینی	دکتر وحید صاحب
دانشگاه شهید باهنر کرمان			
	دکتر عفت جمالی زاده	دکتر طیبه شمسی پور	دکتر زهره رشیدی رنجبر
دانشگاه شهید باهنر کرمان			
	دکتر علی محبی	دکتر محمدرضا میر اولیائی	دکتر اسماعیل دره زرشکی

دانشگاه شهید باهنر کرمان			دانشگاه تحصیلات تکمیلی صنعتی و فناوری پیشرفته کرمان	
	دکتر حسن هاشمی پوررفسنجانی	دکتر فریبا فتحی		دکتر هادی بیت الهی
دانشگاه شیراز				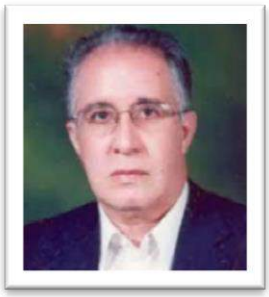
	دکتر افشان مهاجری	دکتر سید حسین موسوی پور		دکتر علی حیدر پاکیاری
دانشگاه شیراز			دانشگاه صنعتی شریف	
	دکتر مجتبی علی پور	دکتر زهرا جمشیدی		دکتر شهربانو رحمان ستایش
دانشگاه تهران				
	دکتر علی مقاری	دکتر حسن به نژاد		دکتر معصومه فروتن

دانشگاه خواجه نصیرالدین طوسی	 دکتر سیف اله جلیلی	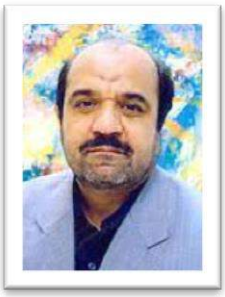 دکتر مجید جعفریان	دانشگاه علوم پزشکی تهران  دکتر مسعود امانلو
دانشگاه خوارزمی	 دکتر غلامرضا اسلامپور	 دکتر مهرداد قائمی	دانشگاه امیر کبیر  دکتر سعیده سرآبادانی
دانشگاه علم و صنعت ایران	 دکتر بهشته سهرابی	 دکتر سید مرتضی موسوی خوشدل	 دکتر سید مجید هاشمیان زاده
دانشگاه تربیت مدرس	 دکتر حسین غریبی	 دکتر ناصر هادی پور	دانشگاه فردوسی مشهد  دکتر الهه کفشدار گوهرشاد

دانشگاه یزد			
	دکتر منصور نمازیان	دکتر محمدرضا نوربالا	دکتر محمد کمالوند
دانشگاه مازندران			
	دکتر سعید یگانگی	دکتر عبداله عمرانی	دکتر عفت کیانپور

دانشگاه یاسوج			
	دکتر شاپور رمضانی	دکتر سید محمد اعظمی	دکتر مصطفی فضلی
دانشگاه سمنان			

دانشگاه علوم پزشکی زنجان		دانشگاه دامغان	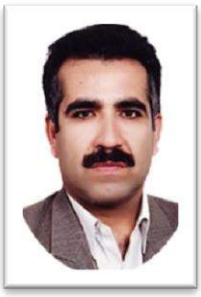	دانشگاه بوعلی سینا همدان	
	دکتر سعید قنبرزاده		دکتر داود عاجلو		دکتر سعید عزیزیان

دانشگاه زنجان			
	دکتر فرهاد خوئینی	دکتر محبوبه بهروزی	دکتر منیژه توضیحی
دانشگاه زنجان		دانشگاه تحصیلات تکمیلی زنجان 	
	دکتر جمال داودی	دکتر محسن لشگری	دکتر فخری السادات محمدی

دانشگاه گیلان			دانشگاه خلیج فارس 
	دکتر علی قنادزاده	دکتر محمدحسن لقمانی	دکتر حسین اسلامی

دانشگاه کردستان	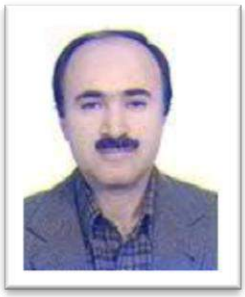	دانشگاه تبریز		پژوهشگاه علوم و فنون هسته ای 
	دکتر خالد عزیزی		دکتر حمایت شکاری	دکتر یاور تقی پور آذر

دانشگاه علوم پزشکی اصفهان

دکتر محمود میرزایی

دانشگاه رازی کرمانشاه

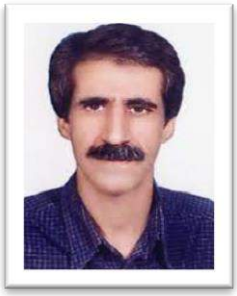

دکتر شهرام رنجبر

دانشگاه نیشابور

دکتر بهزاد حقیقی

دانشگاه حکیم سبزواری

دکتر حامد اکبرزاده

دانشگاه پیام نور

دکتر رضا بهجت منش

کمیته اجرایی

بیست و سومین کنفرانس شیمی‌فیزیک انجمن شیمی ایران

اعضای هیات علمی			
			
دکتر مریم دهستانی رییس کنفرانس	دکتر وحید صاحب دبیر علمی کنفرانس	دکتر سید محمد علی حسینی دبیر اجرایی	دکتر عفت جمالی زاده دبیر اجرایی
			
دکتر کامبیز افروز مدیریت فناوری اطلاعات و ارتباطات	دکتر محمد ابراهیمی عضو کمیته اجرایی		

کارمندان

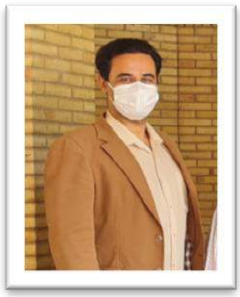			
ایمان ابراهیم ملکی پشتیبانی و سخت افزار	معین فروزنده	کریمه شیروانی سعادت آبادی	زهره پور مهدی زاده

دانشجویان

				
دانیال محمدی مدیر کمیته اجرایی	علیرضا قا ئم پناه عضو کمیته اجرایی	آسیه کیهانی زاده عضو کمیته اجرایی	صدیقه پوراسترآبادی عضو کمیته اجرایی	امیر فلاح عضو کمیته اجرایی
		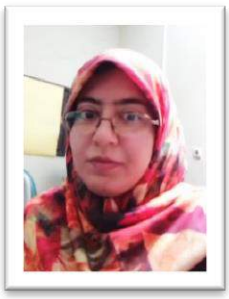		
آریا صبوری عضو کمیته اجرایی	دکتر راضیه علی پور مجری	افسانه نظری عضو کمیته اجرایی	سارا احمدیان عضو کمیته اجرایی	

برنامه زمان بندی

بیست و سومین کنفرانس شیمی‌فیزیک انجمن شیمی ایران

روز اول (چهارشنبه مورخ ۲۲ دی ماه ۱۴۰۰)

عنوان	زمان
افتتاحیه	۸:۱۵-۱۰:۳۰
استراحت	۱۰:۳۰-۱۱:۰۰
سخنران مدعو	۱۱:۰۰-۱۲:۰۰
استراحت و نهار	۱۲:۰۰-۱۴:۰۰
سخنران مدعو	۱۴:۰۰-۱۵:۰۰
سخنرانی ها	۱۵:۰۵-۱۶:۱۵
استراحت	۱۶:۱۵-۱۶:۳۰
سخنرانی ها	۱۶:۳۰-۱۹:۰۰
سخنران مدعو	۱۹:۱۰-۲۰:۱۰

روز دوم (پنجشنبه مورخ ۲۳ دی ماه ۱۴۰۰)

عنوان	زمان
سخنران مدعو	۸:۰۰-۹:۰۰
سخنرانی ها	۹:۰۰-۱۰:۱۵
استراحت	۱۰:۱۵-۱۰:۳۰
سخنرانی ها	۱۰:۳۰-۱۲:۳۰
استراحت و نهار	۱۲:۳۰-۱۳:۱۰
کارگاه آموزشی اول	۱۳:۱۰-۱۴:۴۰
کارگاه آموزشی دوم	۱۴:۴۵-۱۶:۱۵
استراحت	۱۶:۱۵-۱۶:۳۰
سخنران مدعو	۱۶:۳۰-۱۷:۳۰
سخنرانی ها	۱۷:۳۵-۱۸:۴۵
استراحت	۱۸:۴۵-۱۹:۰۰
اختتامیه	۱۹:۰۰-۲۰:۰۰

▷ Conference Program

Opening and Closing

Day1:12-Jan 2022

Time	Title	Link
8:15 –10:30 (AM)	Opening Ceremony	M

Day2: 13-Jan 2022

Time	Title	Link
7:00–8:00 (PM)	Closing Ceremony	M

Day 1: 12-Jan 2022	
Time	**Title**
8:15 AM-10:30 AM	Opening Ceremony
10:30 AM-11:00 AM	Break
11:00 AM-12:00 PM	Invited Talk
12:00 PM - 2:00 PM	Lunch Break
2:00 PM - 3:00 PM	Invited Talk
3:05 PM - 4:15 PM	Parallel Lectures
4:15 PM - 4:30 PM	Break
4:30 PM - 7:00 PM	Parallel Lectures
7:10 PM – 8:00 PM	Invited Talk

Day 2: 13-Jan 2022	
Time	**Title**
8:00 AM-9:00AM	Invited Talk
9:05 AM-10:15 AM	Parallel Lectures
10:15 AM-10:30 AM	Break
10:30 AM-12:30 PM	Parallel Lectures
12:30 PM-1:10 PM	Lunch Break
1:10 PM- 2:40 PM	Workshop 1
2:45 PM-4:15 PM	Workshop 2
4:15 PM-4:30 PM	Break
4:30 PM-5:30 PM	Invited Talk
5:35 PM-6:45 PM	Parallel Lectures
6:45 PM-7:00 PM	Break
7:00 PM-8:00 PM	Closing Ceremony

Invited Talks

Day 1:

Time	Speaker	Title	Link
11:00(AM)-12:00(PM)	Dr. Beheshteh Sohrabi	Surface Engineering of Graphene and Its Derivatives for Various Applications	T1
2:00-3:00 (PM)	Dr. Mohammad Hossein Keshavarz	The University and Industry Relationship	T2
7:10-8:10 (PM)	Dr. Gunnar Nyman	Chemical Kinetics and Tunnelling on Interstellar Dust Grains	T1

Day 2:

Time	Speaker	Title	Link
8:00–9: (AM)	Dr. Shahab Derakhshan	Heavy Element Transition Metal Oxides; Geometric Magnetic Frustration vs. Low Dimensional Magnetism	T1
4:30–5:30 (PM)	Dr. Aminreza Zolghadr	TiO2 Nanotubes: Simulation, Synthesis, and Application	T2

Parallel Lectures

Day 1: Theoretical

Time	Author(s)	Title
3:05 - 3:25 PM	Maryam A. Rafiei, Ali Maghari	Oxygen permeation through graphdiyne membrane
3:30 - 3:50 PM	Mojtaba Alipour, Niloofar Karimi	Photophysical properties of thermally activated delayed fluorescence emitters from the perspective of single-hybrid and double-hybrid density functional theory
3:55- 4:15 PM	Kobra Taji, Fatemeh Moosavi	Removal of Carbon Dioxide by Phosphonium-Based Amino Acid Ionic Liquids: Molecular Dynamics Simulation
4:30 PM - 4:50 PM	Masumeh Foroutan, Borhan Mostafavi Bavani	Anisotropic wetting characteristics of water droplet on phosphorene: A molecular dynamics simulation approach
4:55 PM - 5:15 PM	Faezeh Taravat, Seifollah Jalili	A new Carbon allotrope: 2D Twin Graphene

Practical

Time	Author(s)	Title
3:05 - 3:25 PM	Negin Mokhtari, Shahrbanoo Rahman Setayesh	Synthesis of solar light responsive nanocatalysts and investigation of their performance in water splitting reaction
3:30 PM - 3:50 PM	Zahra Dourandish, Farib Garkani Nejad, Iran Sheikhshoaie, Hadi Beitollahi	Screen-printed electrode modified with graphene quantum dots for detection of acetylcholine
3:55 PM - 4:15 PM	Beheshteh Sohrabi	The synthesis of smart nanoparticles to pH and their applications in industry and Medicine
4:30 PM - 4:50 PM	Zohreh Rashidi Ranjbar, Mozhde Salari Nasab	The Investigation of La(III)Ions-Doping effect on band gap of BiFeO3 perovskite
4:55 PM - 5:15 PM	Rahimi Nasim, Dalouji Vali	Effect of metal (Cu-Al)-dopants on the absorption edge of ZnO films

5:20 PM - 5:40 PM	Fatemeh Nazari, Nina Alizadeh	Inclusion complexes between β-cyclodextrin as a nanocarrier with thymol: Molecular modeling studies	5:20 PM - 5:40 PM	Rezvaneh Amrollahi	Room temperature selective (photo) catalytic oxidation of ethanol to acetaldehyde over Pt/WO3
5:45 PM - 6:05 PM	Elahe Khosravi-Mashizi, Maryam Dehestani, Elahe Mirzaie-Khaliabadi	Conical Intersection and Non-adiabatic Dynamics on Potential Energy Surfaces of H2S+ ion	5:45 PM - 6:05 PM	Ali Mehrizad	Kinetics study of catalytic ozonation process using NiO-Fe2O3 catalyst for treatment of food industrial effluent
6:10 PM - 6:35 PM	Leila Karami	Molecular features of interaction between VEGFR-2 and Linifanib and Semaxanib using a combination of computational methods	6:10 PM - 6:35 PM	Nazila Farsad Layegh, Vahid Mohammadzadeh, Iraj Ahadzadeh, Mir Ghasem Hosseini	An inexpensive glucose biosensor based on a mixed culture microbial fuel cell (MFC) for BOD monitoring applications
6:40 PM - 7:00 PM	Rahele Masoumifard, Mohsen Oftadeh	Investigation of Transport Properties in pure SiNW and SiNW Doped with Boron	6:40 PM - 7:00 PM	Masoumeh Sohrabi, Pouneh S. Pourhosseini, Samira Ansari	Poly (ester-ether-urethane) networks and their interaction with human growth hormone: Conductometry

Day 2: Theoretical

Time	Author(s)	Title
9:05 AM - 9:25 AM	Monireh Dehkhodaei, Adel Reisi-Vanani	Computational study of the synergistic effect of N, S atoms co-doping into monolayer graphdiyne nanosheet on hydrogen adsorption and storage
9:30 AM - 9:50 AM	Razieh Razavi	Molecular Docking of Tramadol-mu-opioid Receptor
9:55 AM - 10:15 AM	Mojtaba Alipour, Zahra Safari	New optimally tuned range-separated hybrids for singlet fission relevant energetics
10:30 AM - 10:50 AM	Zeinab Ashrafi, Hossein Nikoofard	Prediction of oxidation potential for a series of oligopyrroles in THF solvent using DFT calculations
10:55 AM - 11:15 AM	Ali Esmaeili	Quantum Chemical study of the Jahn – Teller Effect on the Distortions of XO2 (X = O, S, Se, Te) Systems

Practical

Time	Author(s)	Title
9:05 AM - 9:25 AM	Mahsa Mirzaei, Seyed Yousef Ebrahimipour, Maryam Mohamadinejad, Tayebeh Shamspour,Fatemeh Mehrabi	Synthesis of a modified mesoporous silica for the targeted delivery of Quercetin in Buffer solution (pH=5.3)
9:30 AM - 9:50 AM	Solmaz Kia	Development of molecularly imprinted polymer on ferric oxide nanoparticles modified electrode as electrochemical sensor for detection of the amount of human chorionic gonadotropin (hCG)
9:55 AM - 10:15 AM	Tahereh Mohammadi, Mir Ghasem Hosseini	Transition Bimetal MOF Embedded Carbon Felt as Anode Electrode for Ethanol Fuel Cell
10:30 AM - 10:50AM	Alireza Khodabakhshi, Alireza Pouyamehr	The effect of solvent evaporation time on the properties and performance of polymer membranes based on a mixture of polyvinyl chloride and polymethyl methacrylate
10:55 AM - 11:15AM	Thorn A. Dramstad, Zahra Sohrabpour, Aaron M. Massari	Molecular Structure at the Interfaces of Submonolayer Thin Films of Sexithiophene

11:20 AM - 11:40AM	Fahimeh Mokhtari, Mohammad Kmalvand	The effect of wall structure on sound
11:45 AM - 12:05PM	Sahand Nikzat, Ali Nassimi	Proposing a trajectory-based algorithm to solve the quantum-classical Liouville equation in the mapping basis
12:10 PM - 12:30PM	Khadijeh Shekoohi, Mohammad Hadi Ghatee	Structural and Dynamic Properties of Cesium Metal by Molecular Dynamics Simulation
5:35 PM – 5:55 PM	Maryam Hamzeh Jouneghani, Masumeh Foroutan	Effects of Water on the Formation and the Stability of Interfacial Nano-bubble: A Molecular Dynamic Simulation
6:00 PM - 6:20 PM	Elham S. Tabatabaie, Maryam Daghigh Asli	Theoretical study of the CO dissociation mechanism in [(η5-C5H5) Fe (CO)2(η1-C5H5)]
6:25 PM – 6:45 PM	Reza Safari, Hamid Hadi*	Computational study of external electric field effect on the electronic properties of a simple molecular wire

11:20 AM - 11:40AM	Tahereh Mohammadi, Karim Asadpour-Zeynali ,Mir Reza Majidi, Mir Ghasem Hosseini	Novel electrocatalysts for Hydrazine fuel cells: enhanced power generation by optimizing Bimetallic Ni-Co nanoparticles on Nickel Foam (NF)/ reduced graphene oxide as anode and mixed metal oxides as cathode
11:45 AM - 12:05PM	Arash Vojood	Prebiotic Synthesis of Ethylene Glycol through Formose Reaction in Methanolic Medium
12:10 PM - 12:30PM	Vali Alizadeh*, Ahmad Jamali Moghadam	Study of tunneling electron transfer on Graphene nanoplatelet /Self assembled monolayer modified gold electrode by electrochemical techniques
5:35 PM – 5:55 PM	Akbar Mobaraki	Semi-industrial synthesis of magnetic Fe3O4@SiO2@Me nanopowder to visualization of latent fingerprints
6:00 PM - 6:20 PM	Goudarzi Samir, Dalouji Vali	Effect of Cu content on structural properties of Ni-Cu @ a-C: H thin films
6:25 PM – 6:45 PM	Elahe Keshavarz **Chemistry Learning**	Implementation of analogy method to enhance students' chemistry self-regulated learning skills

Workshop

Day2: 13-Jan 2022

Time	Title
1:10 – 2:40 (PM)	Molecular Dynamic Simulation, Principles and Apllications by **Dr.Ali Mohebbi**
2:45 – 4:15 (PM)	Natural Bond Orbital (NBO) Analysis by **Dr.Seyed Mohammad Azami**

برنامه ی افتتاحیه بیست و سومین کنفرانس شیمی فیزیک انجمن شیمی ایران

چهارشنبه مورخ ۲۲ دی ۱۴۰۰

عنوان	زمان
تلاوت قرآن مجید	۸:۱۵-۸:۲۰
سرود ملی جمهوری اسلامی ایران و سرود دانشگاه	۸:۳۰-۸:۲۰
خیر مقدم رئیس محترم بیست و سومین کنفرانس شیمی فیزیک انجمن شیمی ایران	۸:۳۰-۸:۴۰
نماهنگ بخش شیمی دانشگاه شهید باهنر کرمان	۸:۴۰-۸:۵۵
خیر مقدم و سخنرانی معاونت محترم پژوهشی و فناوری دانشگاه شهید باهنر کرمان	۸:۵۵-۹:۱۰
نماهنگ بنیان گذار دانشگاه شهید باهنر کرمان	۹:۱۰-۹:۲۵
سخنرانی رئیس محترم انجمن شیمی ایران	۹:۲۵-۹:۴۵
سخنرانی رئیس محترم کمیته ی تخصصی شیمی فیزیک انجمن شیمی ایران	۹:۴۵-۱۰:۰۰
نماهنگ آشنایی با استان کرمان	۱۰:۰۰-۱۰:۰۵
تقدیر از شیمیدان برجسته کشور در گرایش شیمی فیزیک	۱۰:۱۵-۱۰:۰۵
تقدیر از شیمیدان پیشکسوت دانشگاه شهید باهنر کرمان در گرایش شیمی فیزیک	۱۰:۱۵-۱۰:۳۰

مراسم تقدیر

بیست و سومین کنفرانس شیمی‌فیزیک انجمن شیمی ایران

شیمیدان برجسته کشور در گرایش شیمی فیزیک:

دکتر غلامـرضا اسلام پور

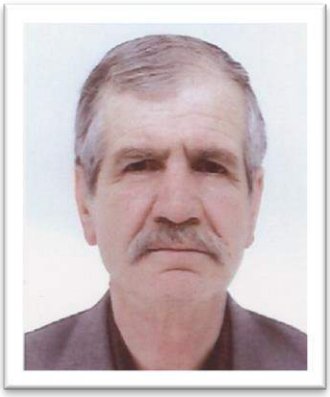

لینک دسترسی به رزومه

▶ Google Scholar

شیمیدان پیشکسوت دانشگاه شهید باهنر کرمان در گرایش شیمی فیزیک:

دکتر اسدالله ناصح زاده

لینک دسترسی به رزومه

▶ ACADEMIA

سخنرانان ویژه

بیست و سومین کنفرانس شیمی‌فیزیک انجمن شیمی ایران

- ✓ **دکتر بهشته سهرابی**

  از دانشگاه علم و صنعت ایران

- ✓ **دکتر محمد حسین کشاورز**

  از دانشگاه صنعتی مالک اشتر

- ✓ **دکتر گونار نیمان**

  از دانشگاه گوتنبرگ

- ✓ **دکتر شهاب درخشان**

  از دانشگاه ایالتی کالیفرنیا

- ✓ **دکتر امین رضا ذوالقدر**

  از دانشگاه شیراز

دانشگاه شهید باهنر کرمان

انجمن شیمی ایران
Iranian Chemical Society

23TH

Iranian Conference on Physical Chemistry

12-13 Jan 2022 – Shahid Bahonar University of Kerman

11:00(AM)-12:00(PM)

Dr. Beheshteh Sohrabi

■ Iran University of Science and Technology

Surface Engineering of Graphene and Its Derivatives for Various Applications

https://online2.uk.ac.ir/c_icspc_talk1/

2:00-3:00 (PM)

Dr. Mohammad Hossein Keshavarz

■ Malek-ashtar University of Technology

The University and Industry Relationship

https://online2.uk.ac.ir/c_icspc_talk2/

7:10-8:10 (PM)

Dr.Gunnar Nyman

■ University of Gothenburg

Chemical Kinetics and Tunneling on Interstellar Dust Grains

https://online2.uk.ac.ir/c_icspc_talk1/

1 First Day

12 Jan 2022

۲۲ دی ۱۴۰۰

دانشگاه شهید باهنر کرمان

23TH

Iranian Conference on Physical Chemistry

انجمن شیمی ایران

Iranian Chemical Society

12–13 Jan 2022 – Shahid Bahonar University of Kerman

8:00–9:00 (AM)

Dr. Shahab Derakhshan

■ California State University, Long Beach

Heavy Element Transition Metal Oxides;
Geometric Magnetic Frustration vs. Low Dimensional Magnetism

https://online2.uk.ac.ir/c_icspc_talk1/

4:30–5:30 (PM)

Dr. Aminreza Zolghadr

■ Shiraz University

TiO2 Nanotubes: Simulation, Synthesis, and Application

https://online2.uk.ac.ir/c_icspc_talk2/

2 Second Day

13 Jan 2022

۲۳ دی ۱۴۰۰

ارتباط دانشگاه و صنعت

سخنران: دکتر محمد حسین کشاورز

نام و نام خانوادگی: محمد حسین کشاورز

آدرس محل کار: اصفهان- شاهین شهر-دانشگاه صنعتی مالک اشتر- مجتمع دانشگاهی علوم کاربردی- دانشکده شیمی کاربردی

رشته تحصیلی: شیمی فیزیک

زمینه تحقیقاتی: ترمودینامیک و شیمی فیزیک

Email: mhkeshavarz@mut-es.ac.ir

Keshavarz7@gmail.com

افتخارات پژوهشی کسب شده

- ✓ جزء فهرست دانشمندان یک درصد در سطح بین المللی به لحاظ بیشترین تعداد مقاله و ارجاعات از سال ۱۳۸۸ تا کنون طبق اعلام مراجع رسمی
- ✓ کسب جایزه پژوهشگر برتر استان اصفهان در علوم پایه در سال ۱۳۸۹
- ✓ کسب رتبه دوم تحقیقات کاربردی بعنوان همکاری در اجرای طرح خط تولید مغناطیسهای سرامیکی سخت از چهاردهمین جشنواره بین‌المللی خوارزمی – بهمن ۱۳۷۹

مقالات علمی پژوهشی:

۳۱۳ مقاله ISI / ۱۲ مقاله علمی پژوهشی غیر ISI مورد تأیید وزارت علوم

پروژه های صنعتی:

۴۴ طرح پژوهشی خاتمه یافته با صنایع مختلف

کتابهای تصنیفی به زبان لاتین و فارسی

الف) کتابهای تصنیفی به زبان انگلیسی- چاپ ۴ کتاب و ۵ فصل کتاب به زبان انگلیسی

ب) چاپ کتاب تصنیفی به زبان فارسی-چاپ ۴ کتاب تصنیفی زیر به زبان فارسی

BOOKS

1. Keshavarz, M.H., Klapötke, T.M. and Klapotke, T.M., 2021. *The Properties of Energetic Materials: Sensitivity, Physical and Thermodynamic Properties*. Second Edition, Walter de Gruyter GmbH & Co KG.
2. Keshavarz, M.H. and Klapötke, T.M., 2020. *Energetic Compounds: Methods for Prediction of Their Performance*. Second Edition, Walter de Gruyter GmbH & Co KG.
3. Keshavarz, M.H., 2018. *Combustible Organic Materials: Determination and Prediction of Combustion Properties*. Walter de Gruyter GmbH & Co KG.
4. Keshavarz, M.H., 2018. *Liquid Fuels as Jet Fuels and Propellants: A Review of their Productions and Applications*. Nova Publisher.

BOOK CHAPTERS

1. M. H. Keshavarz, in An Introduction to Propellants, **Chapter 3**, *Recent simple methods for prediction of specific impulse of energetic compounds rather than using complex computer codes*, Ed.: S. K. Brar, Nova Science Publishers Inc., New York, pp. 47–106 (2020).
2. M. H. Keshavarz, in Hazardous Materials: Types, Risks and Control, **Chapter 4**, *Research Progress on Heats of Formation and Detonation of Energetic Compounds*, Eds.: C. Yu and Z. Wei, Nova Science Publishers Inc., New York, pp. 339–35 (2011).
3. M. H. Keshavarz, in Explosive Materials: Classification, Composition and Properties, **Chapter 4**, *Important Aspects of Sensitivity of Energetic Compounds: A Simple Novel Approach to Predict Electric Spark Sensitivity*, Ed. T. J. Janssen, Nova Science Publishers Inc., New York, pp. 103-123 (2011).
4. M. H. Keshavarz, in Explosive Materials: Classification, Composition and Properties, **Chapter 8**, *Predicting Detonation Performance In Non-Ideal Explosives By Empirical Methods*, Ed. T. J. Janssen, Nova Science Publishers Inc., New York, pp. 179-201 (2011).
5. M. H. Keshavarz, in New Research on Hazardous Materials, **Chapter 9**, *A Simple Theoretical Prediction of Detonation Velocities of Non-Ideal Explosives Only from Elemental Composition*, Ed. P. B. Warey, Nova Science Publishers Inc., New York, pp. 293-310 (2007).

۱- **م. ح. کشاورز**: **روشهای پیش بینی خواص ترموشیمیائی، انتقال فاز، قدرت انفجاری و دمای اشتعال مواد** پرانرژی، انتشارات دانشگاه صنعتی مالک اشتر (۱۳۹۵).

۲-**م. ح. کشاورز**: روشهای تعیین خواص شیمی فیزیکی و حساسیت انفجاری مواد منفجره قوی ، انتشارات دانشگاه صنعتی مالک اشتر (۱۳۹۲).

۳- ح.م. پوراعتدال و **م. ح. کشاورز**: فتوکاتالیست و فتوتخریب آلاینده های شیمیائی ، انتشارات دانشگاه صنعتی مالک اشتر (۱۳۹۰).

۴- **م. ح. کشاورز**، ح.م. پوراعتدال و ع. زالی: مواد پرانرژی: خواص ترموشیمیائی و کارائی ، انتشارات دانشگاه صنعتی مالک اشتر (۱۳۹۰).

Surface Engineering of Graphene and its Derivatives for Various Applications

سخنران: دکتر بهشته سهرابی

دانشگاه علم و صنعت ایران

زمینه های تحقیقاتی: ☐ مهندسی سطح ☐ شیمی نظری ☐ شیمی محاسباتی

Email: Sohrabi_b@iust.ac.ir

لینک دسترسی به رزومه

اختراعات:

استخراج ماده فعال سطحی مورد استفاده در صنعت از مواد طبیعی (گیاهی از خانواده سولارین ها)

افتخارات و جوایز:

- ✓ کسب رتبه اول در مقطع کارشناسی
- ✓ کسب رتبه اول در مقطع کارشناسی ارشد
- ✓ کسب رتبه اول در مقطع دکتری
- ✓ کسب رتبه برتر در میان مقالات چاپ شده در زمینه نانو در سال ۱۳۸۶
- ✓ ساخت دستگاه شبیه ساز خورشیدی

مقالات علمی پژوهشی:

۵۷ مقاله منتشر شده در مجله های خارجی / ۷ مقاله در مجلات داخلی / ۶۹ مقاله در کنفرانس های داخلی و خارجی

طرح های پژوهشی:

۱۰ طرح پژوهشی خاتمه یافته

ABSTRACT: Graphene has attracted a great deal of attention due to its excellent mechanical and electrical properties. This substance is one of the carbon allotropes and consists of carbon atoms with sp^2 hybridization arranged in a honeycomb hexagonal smooth lattice. It is usually considered as a suitable material for producing electronic devices such as transistors,[1] nanocomposites, [2] sensors,[3] and supercapacitors.[4] Due to the hydrophobicity of graphene, using it as a hydrophobic surface is one of the other applications of this useful material. One of the approaches for improving the properties of graphene is surface engineering e.g. doping. There are two means to doped graphene: interstitial and substitutional doping. In the first case, the dopant is considered as an adatom or admolecule on the graphene surface, and in the second case, lattice carbon atoms are replaced by doped atoms or bond them. Our group have studied doping of the fourth group elements of the periodic table, including Si, Ge, and Sn, computationally. This kind of doping can create roughness in the smooth lattice of graphene. This roughness can affect graphene properties and its application especially in the areas related to surface chemistry. In continue, we present a model to predict the water contact angle on a substrate coated by the monolayer of graphene and the fourth group element-doped graphene. Additionally, we try to correct this theoretical model by adding the polarization effect and separating the first layer and bulk terms in the theory. Since metal enhances the water dipole effect on graphene, dipole induced dipole interaction potential was considered which was neglected in our previous theory. The derived equation predicts the influence of interface potential on the wettability of graphene-coated metals and investigates how the interaction of Cu, Ag, and Au as a substrate besides water dipole moment, affect the hydrophobicity. In addition to computational and theory studies, graphene properties were investigated experimentally in our group as well. Since the Graphene is one of the most promising materials for spintronic fields, its application is limited due to its weak magnetic property. Despite many experimental and theoretical efforts for obtaining ferromagnetic graphene, still, a high degree of magnetization is an unsolved challenge. For the first time, we could develop a simple method for inducing magnetism obtained 0.4 emu/g in the graphene, as magnetization saturation at room temperature, which is higher than the reported values.

Keywords: Surface engineering; Graphene; Hydrophobicity; Ferromagnetic; Roughness

References

(1) Xia, F.; Former, D. B.; Lin, Y-M.; Avourois, P. Graphene Field- Effect Transistors with High on/off Current Ratio and Large Transport Band Gap at Room Temperature. Nano Lett. 2010, 10,
715−718.
(2) Hu, C.; Lu, T.; Chen, F.; Zang, R. A Brief Review of graphene− metal Oxide composites Synthesis and applications in photocatalysis. J. Chin. Adv. Mater. Soc. 2013, 1, 21−39.
(3) Wang, T.; Huang, D.; Yang, Z.; Xu, S.; He, G.; Li, X.; Hu, N.; Yin, G.; He, D.; Zhang, L. A Review on Graphene-Based Gas/Vapor Sensors with Unique Properties and Potential Applications. Nano-Micro Lett. 2016, 8, 95−119.
(4) Wang, Y.; Shi, Z.; Huang, Y.; Ma, Y.; Wang, C.; Chen, M.; Chen,Y. Supercapacitor Devices Based on Graphene Materials. J. Phys.Chem. C 2009, 113, 13103−13107.

Chemical Kinetics and Tunnelling on Interstellar Dust Grains

سخنران: دکتر گونار نیمان

University of Gothenburg

- Google Scholar
- University Link

Heavy Element Transition Metal Oxides; Geometric Magnetic Frustration vs. Low Dimensional Magnetism

سخنران: دکتر شهاب درخشان

CALIFORNIA STATE UNIVERSITY LONG BEACH

- Google Scholar
- Linkedin
- University Link

TiO2 nanotubes: simulation, synthesis, and application

سخنران: دکتر امین رضا ذوالقدر

دانشگاه شیراز

- Google Scholar
- University Link

کارگاه های آموزشی

بیست و سومین کنفرانس شیمی‌فیزیک انجمن شیمی ایران

شبیه سازی دینامیک مولکولی، اصول و کاربردها

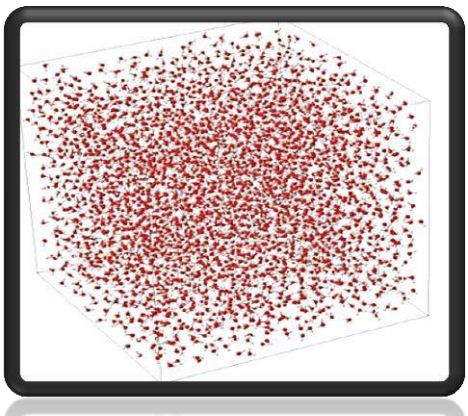

مدرس: دکتر علی محبی
دانشگاه شهید باهنر کرمان
مهندس حسین درانی
دانشگاه شهید باهنر کرمان

❖ Natural Bond Orbital Analysis

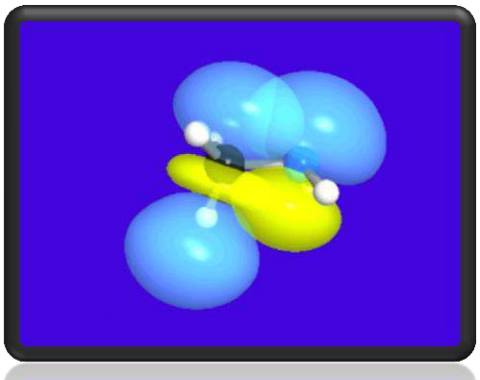

مدرس: دکتر سید محمد اعظمی
دانشگاه یاسوج

شبیه سازی دینامیک مولکولی، اصول و کاربردها

مدرس: دکتر علی محبی

دانشگاه شهید باهنر کرمان

Email: amohebbi@uk.ac.ir

زمینه های تحقیقاتی

نانو تکنولوژی محاسباتی (شبیه سازی دینامیک مولکولی)، آلودگی هوا، آب و مدلسازی آنها، کاربردهای نانو در محیط زیست، دینامیک سیالات محاسباتی، روشهای ازدیاد برداشت نفت، فرآیندهای گاز، نانو سیال، الگوریتم های بهینه سازی هوشمند

مشخصات مقالات و انتشارات

تعداد مقالات ژورنالی ، کنفرانسی و کتب

تعداد مقالات ژورنالی(علمی و پژوهشی و بین المللی)	تعداد مقالات کنفرانسی	راهنمایی پایان نامه کارشناسی ارشدو دکتری	مشاوره پایان نامه کارشناسی ارشد	کتب تالیفی و ترجمه
۱۲۰	بیش از ۱۵۰	۵۰	۲۵	۲(تالیف) ۲(ترجمه)

طرحهای پژوهشی خاتمه یافته: **۱۰ طرح**

افتخارات:

- جز دو درصد دانشمندان برتر جهان براساس شاخص **C-Score** اعلام شده توسط محققان دانشگاه استنفورد در سال ۲۰۲۱
- پژوهشگر برتر دانشگاه شهید باهنر کرمان در دانشکده فنی و مهندسی در سال ۱۳۹۸
- پژوهشگر برتر دانشگاه شهید باهنر کرمان در گروه فنی و مهندسی در سال ۱۳۹۷
- پژوهشگر برتر دانشگاه شهید باهنر کرمان در گروه فنی و مهندسی در سال ۱۳۸۶
- پژوهشگر برتر دانشگاه شهید باهنر کرمان در گروه فنی و مهندسی در سال ۱۳۸۷
- پژوهشگر برتر دانشگاه شهید باهنر کرمان در گروه فنی و مهندسی در سال ۱۳۸۸
- پژوهشگر برتر استان در گروه فنی و مهندسی در سال ۱۳۹۳
- پژوهشگر برتر دانشگاه شهید باهنر کرمان در گروه فنی و مهندسی در سال ۱۳۹۴
- سرپرست تیم دانشجویی مسابقات ملی مکانیک سیالات که در سال ۱۳۹۵ در بخش ساخت ویسکومتر مقامهای اول و دوم را کسب کرد.
- سرپرست تیم دانشجویی مسابقات ملی کمیکار که در سال ۱۳۹۵ در بخش پوستر مقام سوم را کسب کرد.
- سرپرست تیم دانشجویی مسابقات ملی کمیکار که در سال ۱۳۸۸ در ایران اول شد.
- سخنران کلیدی درکنفرانس **DOFIAC 2017** در چین
- سخنران کلیدی درکنفرانس **DOFIAC 2019** در چین

شبیه سازی دینامیک مولکولی، اصول و کاربردها

مدرس: مهندس حسین درانی

دانشگاه شهید باهنر کرمان

Email: dorranyir@yahoo.com

فعالیت های پژوهشی:

- ✓ تهیه نرم افزار تخمین منحنی تقطیر مخلوط برشهای نفتی با مواد خالص بر طبق استاندارد ASTM D86 به صورت متن باز
- ✓ شبیه سازی و موازنه انرژی واحد تصفیه لجن مس سرچشمه با نرم افزار Aspen Plus
- ✓ شبیه سازی و بهینه سازی انرژی ایستگاه تقلیل فشار گاز شهری کرمان با نرم افزار Aspen Hysys
- ✓ طراحی و شبیه سازی واحد بی کربنات سدیم(در مراحل پایانی) با نرم افزار Aspen Plus
- ✓ شبیه سازی واحدهای مختلف صنعتی از قبیل شیرین سازی و نم زدایی گاز، تولید اتانول، متانول، اتیل بنزن، استایرن، آکریلیک اسید و ...
- ✓ مدل سازی و مطالعه فرایندهای مختلف انتقال حرارت، انتقال جرم، طراحی راکتور و ترمودینامیک با استفاده از نرم افزار Matlab
- ✓ محاسبه خواص ترموفیزیکی مایعات یونی با استفاده از شبیه سازی دینامیک مولکولی (نرم افزار NAMD)
- ✓ محاسبه خواص ترموفیزیکی آب مایع با استفاده از پتانسیل های مختلف آب و شبیه سازی دینامیک مولکولی (نرم افزار های NAMD و LAMMPS)
- ✓ محاسبه خواص ترموفیزیکی فلزات با استفاده از میدان نیروی EAM در نرم افزار LAMMPS
- ✓ بررسی مکانیزم های انتقال جرم و انتقال حرارت در نانوسیالات با استفاده از شبیه سازی دینامیک مولکولی (نرم افزار LAMMPS)

Natural Bond Orbital Analysis

مدرس: دکتر سید محمد اعظمی

دانشگاه یاسوج

Email: azami@mail.yu.ac.ir

- Google Scholar
- Linkedin
- University Link

فهرست مقالات ارایه شده در کنفرانس

جهت دسترسی سریع به متن مقاله بر روی آیکن ◄ کلیک نمایید.

مقالات برگزیده در بخش سخنرانی

بیست و سومین کنفرانس شیمی‌فیزیک انجمن شیمی ایران

Practical

- **Tahereh Mohammadi, Karim Asadpour-Zeynali, Mir Reza Majidi, Mir Ghasem Hosseini**

  Novel electrocatalysts for Hydrazine fuel cells: enhanced power generation by optimizing Bimetallic Ni-Co nanoparticles on Nickel Foam (NF)/ reduced graphene oxide as anode and mixed metal oxides as cathode

- **Akbar Mobaraki**

  Semi-industrial synthesis of magnetic Fe_3O_4@SiO_2@Me nanopowder to visualization of latent fingerprints

- **Mahsa Mirzaei, Seyed Yousef Ebrahimipour, Maryam Mohamadinejad, Tayebeh Shamspour, Fatemeh Mehrabi**

  Synthesis of a modified mesoporous silica for the targeted delivery of Quercetin in Buffer solution (pH=5.3)

Theoretical

- **Mojtaba Alipour and Niloofar Karimi**

  Photophysical properties of thermally activated delayed fluorescence emitters from the perspective of single-hybrid and double-hybrid density functional theory

- **Masumeh Foroutan, Borhan Mostafavi Bavani**

  Anisotropic wetting characteristics of water droplet on phosphorene: A molecular dynamics simulation approach

- **Sahand Nikzat, Ali Nassimi**

  Proposing a trajectory-based algorithm to solve the quantum-classical Liouville equation in the mapping basis

متن مقالات

بیست و سومین کنفرانس شیمی‌فیزیک انجمن شیمی ایران

بیست و سومین کنفرانس شیمی فیزیک انجمن شیمی ایران
23rd ICS Physical Chemistry Conference
Chemistry Department,
Faculty of Science
Shahid Bahonar University of Kerman
Kerman, Iran
12-13 Jan 2022
ایران، کرمان
دانشگاه شهید باهنر کرمان
دانشکده علوم پایه، بخش شیمی
۲۳-۲۲ دی ماه ۱۴۰۰

Synthesis and characterization of Ni–Co Ferrite composite oxide nanocrystals as a reactive photocatalyst of phenol in aqueous solutions

Zeinab Taheri[a], Mahdiyeh Sheikhshoaei[b], Iran Sheikhshoaie[a]*

[a] *Department of Chemistry, Faculty of Science, Shahid Bahonar University of Kerman, 76175-133, Kerman, Iran*
E-mail: shoaie@uk.ac.ir
[b] *Department of Minning, Faculty of Engineeing, Shahid Bahonar University of Kerman, 76175-133, Kerman, Iran*

Abstract

The Ni–Co Ferrites composites have been successfully synthesized by hydrothermal process. The morphology, microstructure and electromagnetic properties were investigated by Fourier transform infrared spectrum (FT-IR), X-ray diffraction (XRD), scanning electron microscope (SEM), transmission electron microscope (TEM), network analyzer and vibrating sample was successfully synthesized by copreciptation method from a three salts: $MnCl_2$, $CoCl_2$ and $FeCl_3$. The synthesised composite could be the potential candidates for degradation of phenol from waste waters. In this study, a high sensitive electrochemical sensor for Phenol was established based on graphene oxide carbon paste electrode. The proposed sensor exhibited strong enrichment effect on phenol and gave superior catalytic activity towards the electro-oxidation of phenol.

Keywords: Nanocomposite; Ni oxide; Electrochemistry; Co oxide; FESEM; XRD; MAP; FT-Ir.

I. Introduction

Phenols based compounds are discharged in the environment due to their huge production. They are present in tap-water as a result of humic acids and phenol chlorination during disinfection, as biocides, as by-products of the reaction of chlorine or hypochlorite with phenolic acids, and also as degradation products of phenoxy herbicides. Also, phenols are present in wood preservatives and in paper industries and can be detecting as contaminants in water and waste water samples. Also, phenol is used as an intermediate for the synthesis of pesticides, phenolic resins, medicines, dyes and other organic based compounds. Phenol is used as a solvent for extracting sulfur and nitrogen compounds from coal. Therefore, fabrication of fast and sensitive sensor for determination of its in water and biological compounds is very important in environmental science. The need for high sensitive, fast and simple methods of nitrite determination comes from its potential toxicity to human health.

II. Methods

Preparation of the electrode

Ni–Co Ferrites /NPs//CPE was prepared by mixing of 0.80 g of the liquid paraffin, 0.2 g of Ni–Co Ferrites /NPs, and 0.8 g of graphite powder. Then the mixture was mixed well for 60 min until a uniformly wetted paste was obtained. A portion of

the paste was filled firmly into one glass tube as described above to prepare Ni–Co Ferrites/CPE. Unmodified carbon paste electrode was prepared by hand-mixing of 1.0 g of graphite powder plus paraffin at a ratio of 70:30 (w/w) and mixed well for 60 min until a uniformly wetted paste was obtained [1-3].

III. Results and discussion

Electrochemical investigation

The effect of pH value on the electrochemical behavior of phenol is performed in the range from 3.0 to 9.0 in 0.1 M PBS solutions. 0.1 M PBS with pH 7.0 is used as the supporting electrolyte in all subsequent experiments.

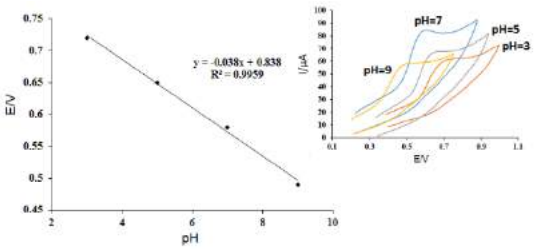

Fig. 1. Plot of potential, E, vs. pH for the electro-oxidation of 400 μM phenol at a surface of Ni–Co Ferrites/NPs/CPE.

The different electrochemical behaviors of modified electrode is investigated by cyclic voltammetry with 500.0 μM phenol as the target compound. After modification of electrode, it is found that the oxidation current increased, indicating the Ni–Co Ferrites can increase the conductibility of electrode and then increase the oxidation current for phenol.

IV. Conclusions

In this work, the modified Ni–Co Ferrites carbon paste electrode was used to investigate the electrochemical behaviors of phenol. The Ni–Co Ferrites/NPs/CPE showed great improvement to the electrode process of phenol compare to BCPE.

References

[1]. H.S. Hashim, Y.W. Fen, N.A.S. Omar, N.I.M. Fauzi, W.M.E.M. Daniyal *Measurement*, 2021, *184*, 109855.

[2]. J. Mathiyarasu, J. Joseph, K.L.N. Phani, V. Yegnaraman, 2004, Indian Journal of Chemical Technolog, 2004, 11, 797-803.

[3]. J. Abdullah, M. Ahmad, N. Karuppiah, L.Y. Heng, H. Sidek, 2006, *Sensors and Actuators B: Chemical*, *114*(2), 604-609.

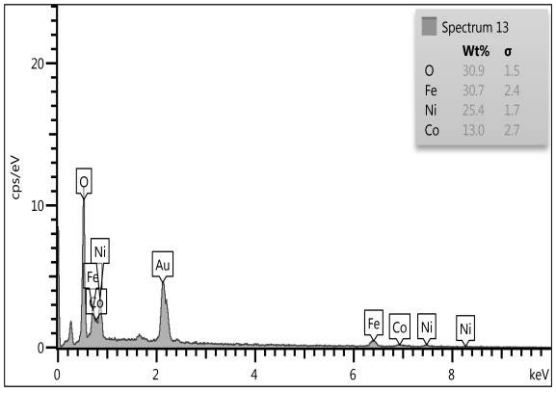

Fig. 2. EDX pattern of Ni-Co Ferrite nanocomposite

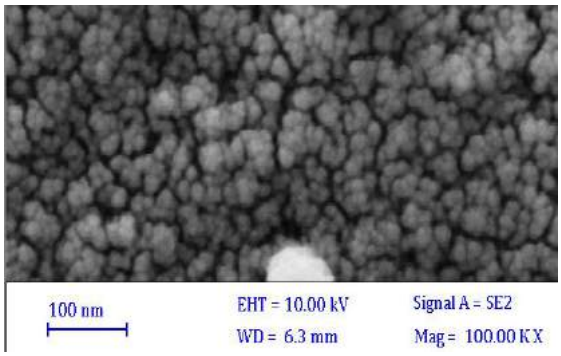

Fig. 3. SEM image of Ni-Co Ferrite nanocomposite

بیست و سومین کنفرانس شیمی فیزیک انجمن شیمی ایران
23rd ICS Physical Chemistry Conference
Chemistry Department,
Faculty of Science
Shahid Bahonar University of Kerman
Kerman, Iran
12-13 Jan 2022
ایران، کرمان
دانشگاه شهید باهنر کرمان
دانشکده علوم پایه، بخش شیمی
۲۳-۲۲ دی ماه ۱۴۰۰

Study of some magnetic properties of cobalt zinc ferrite nanoparticles

Hamid Hadi*, Reza Safari*

Department of chemistry, Faculty of science, University of Qom, Qom, Iran:
hadi.ha@fs.lu.ac.ac.ir and R.safari@qom.ac.ir

Abstract

In this work, zinc-cobalt mixed ferrite $Zn_xCo_{1-x}Fe_2O_4$ (where x = 0, 0.2 and 0.4) were synthesized, using thermal treatment method Also, some the structural and electronic/magnetic properties of these magnetic cobalt zinc ferrite nanoparticles were studied, using vibrating sample magnetometer (VSM) and X-ray diffraction (XRD) technique. Analysis of these results showed that cobalt concentration has a significant effect on the magnetic properties (such as saturated magnetism, Ms, magnetic residue, Mr, and gyromagnetic ratio, γ) of these nanoparticles.

Keywords: Super-paramagnetic nanoparticles; Magnetic properties; Spin-Spin relaxation time; gyromagnetic ratio.

I. Introduction

Today, nanomaterial's are widely used in different sciences such as medicine, electronics, etc [1]. Nanoparticle Contrast Agents ($Zn_xCo_{x-1}Fe_2O_4$), are a group of nanomaterial's that can be used to enhance the quality of molecular imaging [2]. Magnetic properties such as spin-spin relaxation time and gyromagnetic ratio are effective factors in selecting these nanoparticle as Contrast Agents [3-4]. Due to the many applications of magnetic/Super-paramagnetic nanoparticles in various sciences and technologies, in this research, some the structural and electronic /magnetic properties of cobalt zinc ferrite nanoparticles ($Zn_xCo_{1-x}Fe_2O_4$) were studied. In this regard, the X-ray, and VSM techniques are using.

II. Methods

In this work, zinc-cobalt mixed ferrite $Zn_xCo_{1-x}Fe_2O_4$ (where x = 0, 0.2 and 0.4) were synthesized, using thermal treatment method (Table 1). Also, to improve the solubility and limit the size of nanoparticles, polyvidone polymer (PVP) was used.

Table 1 A summary of the compounds is used in the preparation of the samples

Chemical formula	Zinc Nitrate, (m.mol)	Iron (III) nitrate, (m.mol)	Cobalt acetate, (m.mol)
$CoFe_2O_4$	1	2	0
$Zn_{0.2}Co_{0.8}Fe2O4$	0.2		0.8
$Zn_{0.4}Co_{0.6}Fe2O4$	0.4		0.6

III. Results and discussion

In this work, the structural properties (such as particles size, D) of these synthesized nanoparticles (at different concentrations of zinc) were evaluated, using the X-ray diffraction (XRD) method (Fig. 1).

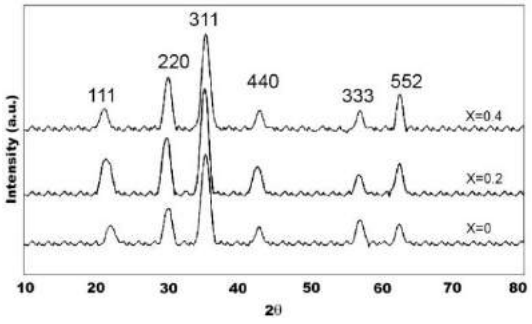

Fig. 1. The XRD pattern of $Zn_xCo_{1-x}Fe_2O_4$ (X = 0, 0.2, 0.4)

In addition, in order to investigate the magnetic properties of these nanoparticles, a vibrating sample magnetometer (VSM) was used. In this regard, the magnetic behavior/properties of these samples (at room temperature and in the presence of a magnetic field with 10 KOe intensity) was evaluated. Also, the value of the saturated magnetism (Ms), magnetic residue (Mr) and the forcing field (Hc) of these nanopatrticels were calculated (Table 2 and Fig.2).

Table 2 Magnetic parameters (saturation magnetization Ms, remanent magnetization Mr, coercitivity Hc) at room temperature of $Zn_xCo_{1-x}Fe_2O_4$ nanoparticles.

X	Size (nm)	Ms (emu/g)	Mr (emu/g)	Hc (Oe)	Mr/Ms	γ (MHz/T)
0	55	96	49	1427	0.5	33.92
0.2	59	117	34	451	0.3	27.63
0.4	66	109	15	137	0.1	29.05

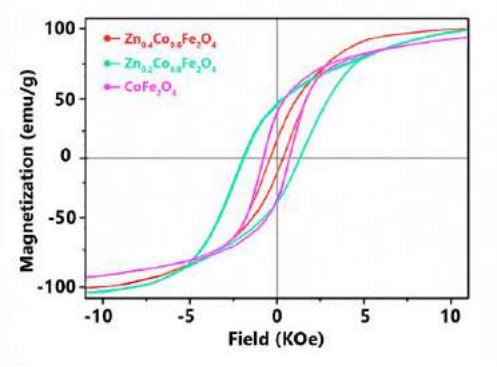

Fig. 2. Hysteresis ring (magnetic hysteresis) for $Zn_xCo_{1-x}Fe_2O_4$ nanoparticles (X = 0, 0.2, 0.4)

Moreover, the gyromagnetic ratio (γ) of these zinc-cobalt ferrite nanoparticles (x = 0, 0.2, 0.4) were calculated, using VSM data and following equations [5];

$$\mathbf{g} = \frac{\mathbf{h\nu}}{\boldsymbol{\beta\mu_s}} \qquad (1)$$

where h is the Planck constant, υ is the microwave frequency, β is the Bohr magneton, and H_r is the magnetic field. Also, γ given by:

$$\boldsymbol{\gamma} = \frac{\boldsymbol{g\mu_N}}{\hbar}, \text{ and } \frac{\boldsymbol{\mu_N}}{\hbar} = \mathbf{7.6225}\ (\boldsymbol{MHz/T}) \qquad (2)$$

$$\boldsymbol{\gamma} = \boldsymbol{g}(\mathbf{7.6225}) \qquad (3)$$

Here, μ_N is the nuclear magneton and g is the g-factor of the nucleus in question [5]. Using the Eqs. (1-6), the effect of concentration (x) on the coefficient $\boldsymbol{\gamma}$ was calculated. Some of these results are reported in Table 2.

IV. Conclusions

In this study, some of the structural and magnetic properties of zinc-cobalt ferrite nanoparticles were investigated. in this regard, the value of the saturated magnetism (Ms), magnetic residue (Mr), forcing field (Hc) and gyromagnetic ratio (γ) of these nanoparticles were calculated. Analysis of these results showed that cobalt concentration has a significant effect on the magnetic properties of synthesized nanoparticles. Therefore, by using the optimal concentrations of cobalt/iron in these synthetic nanoparticles, their magnetic properties can be managed and optimized.

Finally, it should be noted that the study of the mechanism of changes in the ratio of gyro-magnetic ratio of these synthetic nanoparticles with concentration, can be considered as an important parameter (or index) for optimal and controlled use of these nanoparticles in medicine and molecular imaging.

References

[1] R. Singh, W. Lillard W, Exp Mol Pathol, 2009, 86 (3), 215–223.

[2] G. Thirupathi, R. Singh, IEEE Transactions on Magnetics, 2012, 48(11), 3630-3633.

[3] M.Yue Tang, T. Wu Chen, X. Ming Zhang, X. Hua Huang, BioMed Research Int, 2014, 4, 312142.

[4] R. Kaur, A. Priya, K. Gagandeep, K. Manpreet, Ultrason Sonochem, 2015, 26, 229-240.

[5] K. Hentschel, D. Greenberger, and F. Weinert, in Compendium of Quantum Physics (Springer, Berlin, 2009).

بیست و سومین کنفرانس شیمی فیزیک انجمن شیمی ایران
23rd ICS Physical Chemistry Conference
Chemistry Department,
Faculty of Science
Shahid Bahonar University of Kerman
Kerman, Iran
12-13 Jan 2022
ایران، کرمان
دانشگاه شهید باهنر کرمان
دانشکده علوم پایه، بخش شیمی
۲۳-۲۲ دی ماه ۱۴۰۰

Transition Bimetal MOF Embedded Carbon Felt as Anode Electrode for Ethanol Fuel Cell

Tahereh Mohammadi[a], Mir Ghasem Hosseini[b,*]

[a, b] *Department of physical chemistry, Electrochemistry Research Laboratory, University of tabriz, Tabriz, Postal code 5166616471, Iran.*
E-mail: *mg-hosseini@tabrizu.ac.ir*

Abstract

The detection of resources to replace costly noble metals and their alloy for constructing effective non noble metal electrocatalysts has been received interest. Recently, metal-organic frameworks (MOFs) provide an opening for the construction of mixed metals distribution in the substrate carbon without any carbon precursor augmentative. In this study, porous NiCu-MOF nanosheets were supported on 3D carbon felt substrate as an anode electrode. The EOR activity of catalysts is investigated via CV, EIS, CA and CP techniques. Remarkably, the obtained NiCu-MOF/CF electrode delivered a power density of 6.074 mW cm^{-2} with a cell voltage of 0.87 V in 60℃.

Keywords: Metal organic framework; Carbon felt; Ethanol; Power density; Fuel cell.

I. Introduction

The reduction of environmental pollution and the improvement of new energy sources have become the main preference. Direct ethanol fuel cells (DEFCs) with advantages of low toxicity, high energy density, and easy fuel storage have been attended as the replacement for traditional energy resources. Since the precious metals that are commonly used as electro catalysts hinder the commercialization of FCs, so the identification of new effective and low-cost non-noble metal electrocatalysts with stability is essential. MOFs which along with many single and bi/multimetallic nanomaterials employed as electrodes display notable effects on the electrocatalytic properties. To improve EOR yield with nonprecious group metals, the direct growing of catalysts onto supports such as carbon felts (known as ‘gas diffusion layer, GDL’) lets a better catalyst usage. Herein, for the reason of relatively low price, porosity, flexibility, and stability against acidity carbon felt were applied to a PEMFC.

II. Methods

The composition of as-prepared samples was revealed by FTIR and the morphologies of samples were investigated by an SEM and EDX spectroscope. XRD data was recorded for measuring the crystallographic structures and phase purity (Fig. 1). Electrochemical experiments were carried out in a three-electrode system containing a certain amount of ink dropped onto the commercially available glassy carbon electrode as a working electrode.

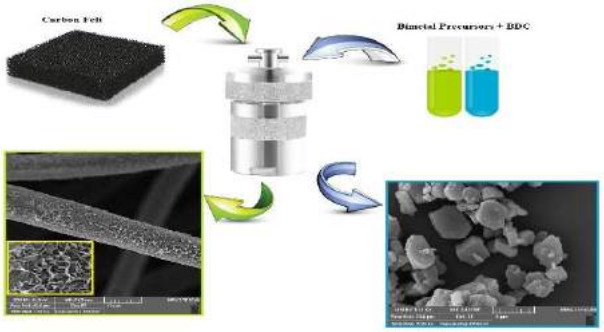

Scheme 1: Schematic Diagram of the Synthesis Process.

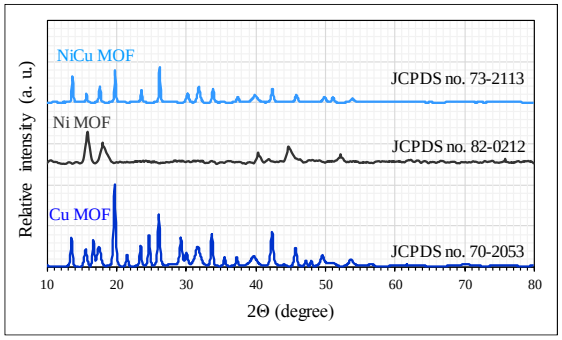

Fig. 1. Powder XRD patterns of as-prepared MOFs.

III. Results and discussion

By comparison of CVs of electrocatalysts (fig.2) it can be seen that the current density of EOR on different catalysts is increasing in the order of: NiCu-MOF/GCE > Ni-MOF/GCE > Cu-MOF/GCE. These results exhibit that CoCu-MOF/GCE has the highest mass-specific and area-specific activities of ~40 A g metal toward the anodic oxidation of ethanol. EIS and CA test express that the NiCu-MOF has a lower impedance and better stability comparative to Cu and Ni MOF. The 3D structure of MOF with free pores and synergistic effect between Ni and Cu enhanced the catalytic activity.

The single fuel cell practical application in direct ethanol fuel cells was studied using NiCu-MOF/CF as an anodic catalyst, and MEA with the loading of Pt/C as cathodic catalyst material. As shown in Fig. 2 it can be seen that few slope in polarization the single fuel cell practical application in DEFC was studied using NiCu-MOF/CF as an anodic catalyst, and MEA with the loading of Pt/C as cathodic catalyst material. As shown in Fig. 2 it can be seen that few slopes in the polarization curve and the maximum power density of cell at 60℃ for NiCu-MOF/CF-based DEFC were obtained 6.074 mW cm^{-2} which indicates relatively faster electrochemical kinetics.

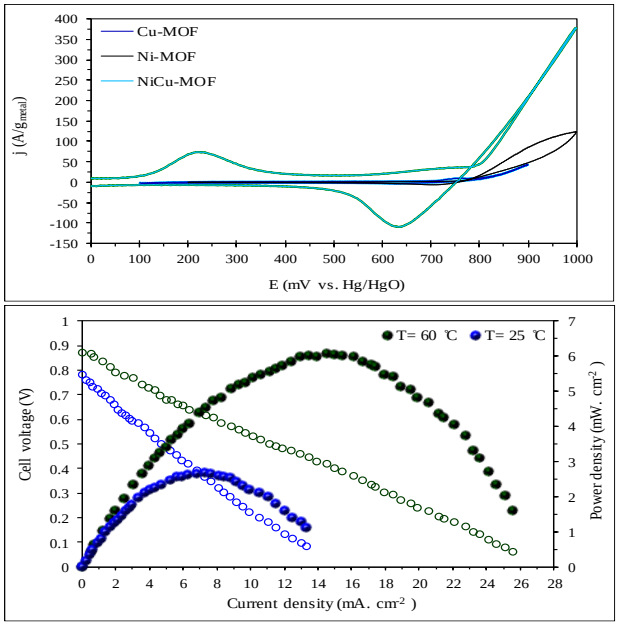

Fig. 2. EOR CV curves in 1 M NaOH + 0.5 M EtOH at scan rate of 20 mV s^{-1} (a), polarization and power density curves in 2 M NaOH + 2 M EtOH for NiCu-MOF/CF as anodic and Pt/C as cathodic catalyst (b).

IV. Conclusions

We focused on an easy procedure for the development NiCu-MOF/CF of the electrocatalyst. The resulting NiCu-MOF/CF not only demonstrates acceptable current density and stability for the EOR but also has outperformed activity over most reported non-noble-metal-based catalysts. Our work highlights an easy strategy for the advancement of earth-abundant electrocatalyst and may present a promising method to provide a low-cost and high-efficiency electrocatalyst for fuel cell performance.

References

[1] **G. Zhang, Z. Bao, B. Xie, *International Journal of Hydrogen Energy*, 46.3, 2021, 2978-2989.**
[2] **Sh. Zhu, A. Xie, and X. Tao,*Journal of Electroanalytical Chemistry*, 857, 2020.**
[3] **N. Delaporte, E. Rivard, *Nanomaterials*, 10, 2020, 1947.**
[4] **J. Wang, J. Li, *Frontiers in Materials*, 7, 2020, 194.**
[5] **S. Rizvi, N. Lqbal, *Catalysis Letters*, 10, 2019 1-11.**

بیست و سومین کنفرانس شیمی فیزیک انجمن شیمی ایران
23rd ICS Physical Chemistry Conference
Chemistry Department,
Faculty of Science
Shahid Bahonar University of Kerman
Kerman, Iran
12-13 Jan 2022
ایران، کرمان
دانشگاه شهید باهنر کرمان
دانشکده علوم پایه، بخش شیمی
۲۳-۲۲ دی ماه ۱۴۰۰

Study of photocatalytic degradation of Acid Red 1 by Sm-doped CdS under visible light irradiation from kinetics perspective

Ali Mehrizad*, Afsaneh Golzari khosroshahi

Department of Chemistry, Tabriz Branch, Islamic Azad University, Tabriz, Iran. Tel: 041 31966033; E-mail: mehrizad@iaut.ac.ir

Abstract

Photocatalytic degradation of Acid Red 1 by Sm-doped CdS catalyst was studied from kinetics perspective. To infer the kinetics of the process, experiments were conducted in the period of 0-100 min under visible light irradiation. The experimental data fitted well by the Langmuir-Hinshelwood's pseudo-first-order model.

Keywords: Photocatalysis; Acid Red 1; Sm-CdS; Kinetics.

I. Introduction

Textile and dyeing industries are considered the most significant water consumers; so, a considerable amount of wastewater is produced by these industries in different production stages [1]. Among different methods, the importance of the photocatalytic processes in the degradation of contaminants and their conversion into non-detrimental compounds is clear [2]. According to the extensive literature, the kinetics equation proposed by the Langmuir–Hinshelwood (equation 1) is the well-known and widely applied kinetics model in the studies of the photocatalytic degradation of dyes.

$$-\frac{dC}{dt} = \frac{kKC}{1 + KC + \sum K_i C_i} \qquad (1)$$

In this equation, k refers to the reaction rate constant (mg L^{-1} min^{-1}), K and K_i denote the adsorption equilibrium constant (L mg^{-1}). C and C_i are the dye and intermediates concentration (mg L^{-1}), respectively. According to the assumption suggested by Beltran-Heredia et al. [3], $KC + \sum K_i C_i$ is tantamount to KC_0 (C_0 stands for the initial dye concentration) and under these circumstances:

$$-\frac{dC}{dt} = \frac{kKC}{1 + KC_0} \qquad (2)$$

The equation (2) can be written as a pseudo-first order kinetics relation by defining the apparent rate constant (k_{ap}) as follows:

$$-\frac{dC}{dt} = \left(\frac{k_r K_{ads}}{1 + K_{ads} C_0}\right) C \xrightarrow{k_{ap} = \left(\frac{k_r K_{ads}}{1 + K_{ads} C_0}\right)} -\frac{dC}{dt} = k_{ap} C \rightarrow \ln\left(\frac{C_0}{C_t}\right) = k_{ap} t \qquad (3)$$

The present work aimed to kinetics study of photocatalytic degradation of Acid Red 1 by Sm-doped CdS under visible light irradiation.

II. Methods

Experiments were carried out in a crystallizing dish on a magnetic stirrer under a halogen lamp (300 W, Osram,

Germany). An appropriate amount of the photocatalyst (0.25-1.25 g L^{-1}) was dispersed in 100 mL of the AR1 solution (10-50 mg L^{-1}). The obtained suspension was stirred under irradiation of the halogen lamp using a filter with 420 nm cutoff. The suspension was sampled at the time intervals (0-100 min) and the absorbance of the centrifuged samples was monitored using a UV-Vis spectrophotometer (UV mini-1240 Shimadzu).

III. Results and discussion

To infer the kinetics of the process, experiments were conducted in the period of 0-100 min in the variation of initial dye concentration (10-50 mg L^{-1}) and catalyst dosages (0.25-1.25 g L^{-1}). The experimental data fitted well in a pseudo-first order kinetics model (equation 3), and Fig. 1 illustrates the plots of $\ln C_0/C_t$ against the irradiation time in various experiments. From Fig. 1 (a and b), it can be concluded that the photocatalytic degradation of Acid Red 1 by Sm-doped CdS is compatible and well-matched with the pseudo-first order kinetics model. Fig. 1 (a) shows that removal rate has a reverse relationship with the initial concentration of the dye. Contrariwise, according to Fig. 1 (b), degradation rate is increased by increasing the amount of catalyst.

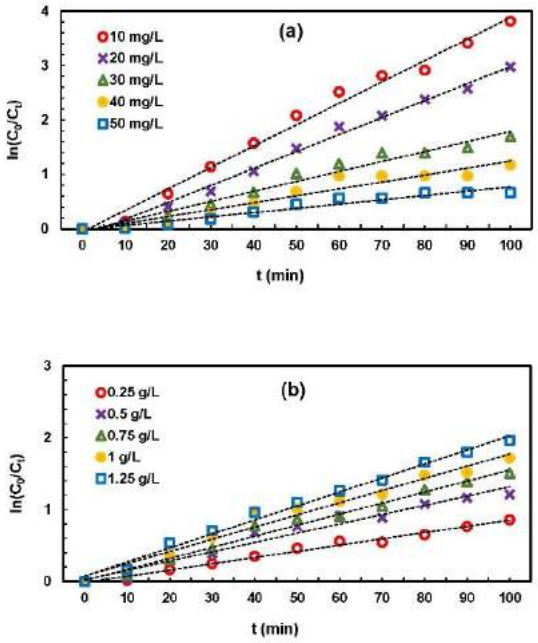

Fig. 1. The plot of the $\ln C_0/C_t$ versus time at different (a) initial concentration of dye (b) catalyst dosage.

IV. Conclusions

The photocatalytic degradation process of Acid Red 1 by Sm-doped CdS catalyst was studied from kinetics perspective. The experimental data fitted well in a pseudo-first order kinetics model. Based on the results, degradation rate increased by increasing the amount of catalyst and decreased by increasing the initial concentration of Acid Red 1.

References

[1] H. Wu, Z. Liu, A. Li, H. Yang, *Chemosphere*, 2017, 174, 200

[2] N.M. Gupta, *Renewable and Sustainable Energy Reviews*, 2017, 71, 585

[3] J. Beltran-Heredia, J. Torregrosa, J.R. Dominguez, J.A. Peres, *Journal of Hazardous Materials*, 2001, 83 255

بیست و سومین کنفرانس شیمی فیزیک انجمن شیمی ایران
23rd ICS Physical Chemistry Conference
Chemistry Department,
Faculty of Science
Shahid Bahonar University of Kerman
Kerman, Iran
12-13 Jan 2022
ایران، کرمان
دانشگاه شهید باهنر کرمان
دانشکده علوم پایه، بخش شیمی
۲۳-۲۲ دی ماه ۱۴۰۰

Kinetics study of catalytic ozonation process using NiO-Fe_2O_3 catalyst for treatment of food industrial effluent

Ali Mehrizad

Department of Chemistry, Tabriz Branch, Islamic Azad University, Tabriz, Iran. Tel: 041 31966033; E-mail: mehrizad@iaut.ac.ir

Abstract

In this research, catalytic ozonation process of food industrial effluent by NiO-Fe_2O_3 catalyst was studied from kinetics perspective. To infer the kinetics of the process, experiments were conducted in the period of 0-20 min in the absence and presence of catalyst (OP and COP). The experimental data fitted well in a pseudo-first order kinetics model. Based on the results, the presence of NiO-Fe_2O_3 as a catalyst in COP causes to double the reaction rate than OP.

Keywords: Catalytic ozonation; Food industrial effluent; NiO-Fe_2O_3; Kinetics.

I. I. Introduction

Food industries are one of the major sectors consuming huge amounts of water converting into effluents during various processes. Therefore, treatment and reuse of effluents produced by such industries are one of the environmental priorities [1]. Advanced oxidation processes like ozonation are an emergent approach to ameliorate the wastewater treatments. Ozone (O_3) is a powerful oxidizer, and the strong electrophilic nature of O_3 enables it to react with various organic compounds. In the ozonation process, the reaction between O_3 and pollutants can be explained by direct or indirect reactions, i.e. through the O_3 molecules or °OH radicals [2]. Nevertheless, low solubility and stability of O_3 in water and its slow reaction with some organics are the most common obstacles in OP, where the integration of O_3 with catalysts could overwhelm the drawbacks [3]. The present work aimed to kinetics study of catalytic ozonation process using NiO-Fe_2O_3 catalyst for treatment of food industrial effluent.

II. Methods

Experiments were conducted by using the experimental set-up described in Fig.1. Typically, 200 mL of effluent was poured into the reactor and mixed with appropriate amount of catalyst (5 gL^{-1}). Then, desired ozone dosage (10 $mgmin^{-1}$) were introduced into the reactor from an ozone generator model X-200 (Baku, Azerbaijan).

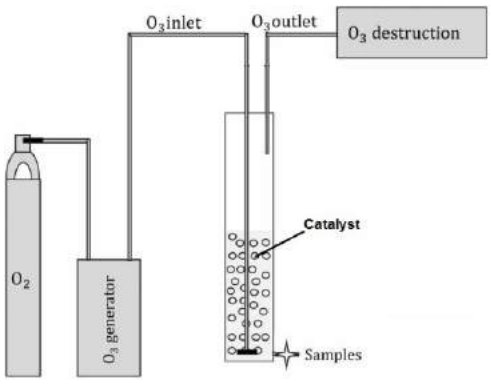

Fig. 1. Schematic diagram of the bench-scale system.

III. Results and discussion

Catalytic ozonation kinetics study can be used to evaluate the catalyst performance and achieve an accurate design of the

treatment system. As mentioned previously, the reaction between O_3 and micropollutions (M) can be explained by direct or indirect reaction, i.e. through reaction with O_3 or °OH:

$$O_3 + M \xrightarrow{ko_3} \text{Products} \quad (1)$$

$$^{\circ}OH + M \xrightarrow{k_{^{\circ}OH}} \text{Products} \quad (2)$$

Typically, a combination of two reactions is used to describe the kinetics of the process [4]:

$$-\frac{d[M]}{dt} = \left(k_{O_3}[O_3] + k_{^{\circ}OH}[^{\circ}OH]\right)[M] \quad (3)$$

Elovitz and Von Gunten [5] suggested that, the phrase of $\left(k_{O_3}[O_3] + k_{^{\circ}OH}[^{\circ}OH]\right)$ is equal to a new rate constant (observed rate constant, k_{obs}) and can be written:

$$-\frac{d[M]}{dt} = k_{obs}[M] \quad (4)$$

This viewpoint is widely accepted in the kinetics studies of COP, and Eq. (4) can be summarized as a pseudo-first order kinetics model after integration:

$$\ln[M]_t = -k_{obs}t + \ln[M]_0 \quad (5)$$

To infer the kinetics of the process, experiments were conducted in the period of 0-20 min in the absence and presence of catalyst (OP and COP). The experimental data fitted well in a pseudo-first order kinetics model (Eq. 5), and Fig. 2 illustrates the plot of the $\ln[M]_t$ versus time.

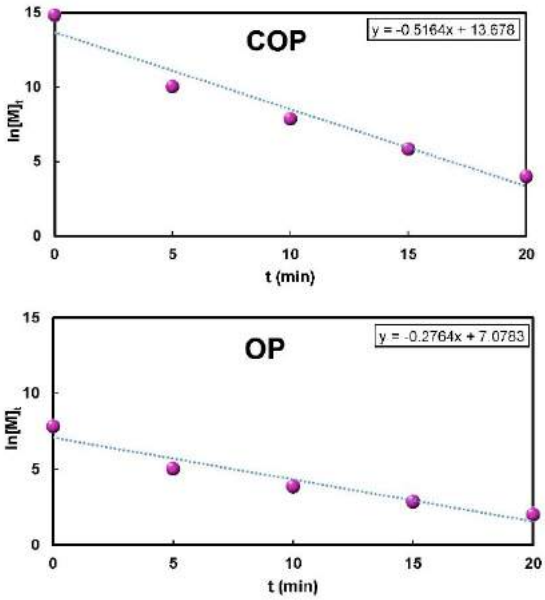

Fig. 2. The plot of the $\ln[M]_t$ versus time for ozonation process (OP) and catalytic ozonation process (COP).

IV. Conclusions

The catalytic ozonation process of food industrial effluent by NiO-Fe_2O_3 catalyst was studied from kinetics perspective. The experimental data fitted well in a pseudo-first order kinetics model. Based on the results, the presence of NiO-Fe_2O_3 as a catalyst in COP causes to double the reaction rate than OP.

References

[1] K. Hernández, C. Muro, R.E. Ortega, S. Velazquez, F. Riera, *Environmental technology*, 2021, 42, 775

[2] Y. He, X. Wang, J. Xu, J. Yan, Q. Ge, X. Gu, L. Jian, *Bioresource Technology*, 2013, 133, 150

[3] Y. Kaya, Z.B. Gönder, I. Vergili, A. Ongen, *Environmental Progress & Sustainable Energy*. 2019, 38, 13025

[4] J.L. Acero, K. Stemmler, U. Von Gunten, *Environmental Science and Technology*. 2000, 34, 591

[5] M.S. Elovitz, U. von Gunten, *Ozone: Science and Engineering*, 1999, 21, 239

بیست و سومین کنفرانس شیمی فیزیک انجمن شیمی ایران
23rd ICS Physical Chemistry Conference
Chemistry Department,
Faculty of Science
Shahid Bahonar University of Kerman
Kerman, Iran
12-13 Jan 2022
ایران، کرمان
دانشگاه شهید باهنر کرمان
دانشکده علوم پایه، بخش شیمی
۲۳-۲۲ دی ماه ۱۴۰۰

An inexpensive glucose biosensor based on a mixed culture microbial fuel cell (MFC) for BOD monitoring applications

Nazila Farsad Layegh[a*], Vahid Mohammadzadeh[a] , Iraj Ahadzadeh[a], Mir Ghasem Hosseini[b]

[a] *Research Laboratory for Electrochemical Instrumentation and Energy Systems, Department of Physical Chemistry, Faculty of Chemistry, University of Tabriz, Tabriz, Iran*
n.farsadlayegh99@ms.tabrizu.ac.ir
v.mohammadzadeh2014@gmail.com, irajahadzadeh@gmail.com
[b] *Electrochemistry Research Laboratory, Department of Physical Chemistry, Faculty of Chemistry, University of Tabriz, Tabriz, Iran*
mirghasem.h@gmail.com

Abstract

Microbial fuel cells (MFCs) are used for including electricity generation, wastewater treatment, and also biosensors. The purpose of the current research is to study an MFC as a biosensor to measure glucose as a biological oxygen demand (BOD) indicator. Results showed that there is a very good linear relationship by plotting open circuit potential (OCP), maximum power, and short circuit current of the MFC vs. glucose concentration in the 0.1-5 g/L range. So the developed biosensor can be scaled and used as a promising cost-effective glucose biosensor and/or BOD monitoring sensor in food industry-related applications.

Keywords: MFC; Glucose; BOD monitoring.

I. Introduction

Wastewater discharge into habitats has caused serious damage to the environment. It is necessary to prevent adverse effects of wastewater on the environment, using disposal standards, depending on the final disposal site [1-3]. Biological-based treatment systems, such as anaerobic digesters and activated sludge, require a considerable amount of energy [4]. MFCs are used as biosensors to measure parameters such as biological oxygen demand (BOD), chemical oxygen (COD), dissolved oxygen (DO), and toxins in wastewater. The main advantage of MFC-based biosensors is that they can operate without an additional signal converter or external power supply [5]. The purpose of the current research is to study a two-chamber MFC as a biosensor to measure glucose concentration to further develop a BOD monitoring sensor.

II. Methods

An anaerobic culture vessel for bacteria growth containing 0.1 g/L glucose was incubated for 128 h. After forming the biofilm on the graphite anode electrode, the anode was placed in a two-chamber MFC. Both anode and cathode electrodes (22 cm^2) are made of graphite. The anolyte solution includes 180 ml PBS with pH=7.2, 0.1 cm^3 of trace element, 5 g/L glucose. The catholyte solution contained 180 ml PBS and was continuously aerated with an air pump. A Sama 500 potentiostat connected to a PC were used for electrochemical measurements such as V-I and P-I data plotting. A 1 kΩ external resistor was connected to the MFC between two consecutive sets of polarization measurements. This operation

was repeated for glucose concentrations of 0.1, 1and 5g/L.

Results and discussion

Fig. 1 indicates V-I and P-I curves from which open circuit potential (OCP), short circuit current (I_{sc}), and maximum power (P_{max}) values were calculated and given in Table 1.

Table 1. Operational parameters of MFC.

Glucose concentration (g/L)	*OCP(mV)*	*I_{sc} (μA)*	*P_{max}(nW)*
0.1	63	130	2500
1	110	185	6000
5	385	362	49000

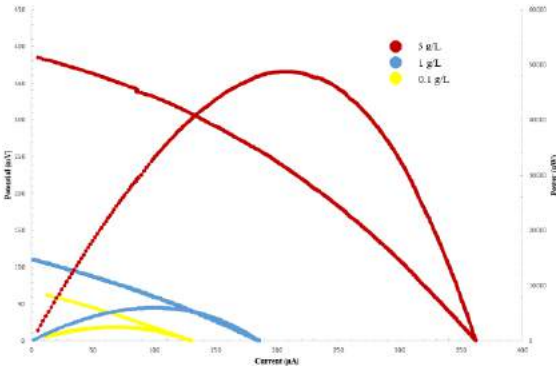

Fig. 1. V-I and P-I curves for MFC at various glucose concentrations.

The graphs of OCP, I_{sc}, and P_{max} vs. connection of glucose were given in Fig 2.

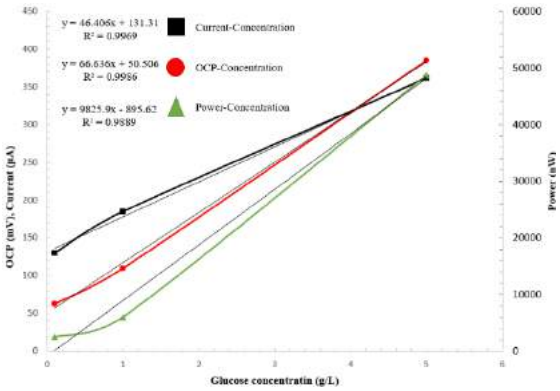

Fig. 1. Trends of OCP, I_{sc}, and P_{max} vs. concentration of glucose at 0.1, 1, and 5 g/L range.

It can be seen that there is a very good linear relationship by plotting OCP, I_{sc}, and P_{max} of the MFC vs. glucose concentration in the 0.1-5 g/L range, i.e. a 50-fold dynamic concentration range of the sensor can be realized.

III. Conclusions

Results showed in the 0.1-5 g/L range of glucose the developed MFC system can be scaled and used as a promising cost-effective glucose biosensor and/or BOD determination in food industry related wastewater applications.

References

[1] Tardy, G. M., Lóránt, B., Gyalai-Korpos, M., Bakos, V., Simpson, D., & Goryanin, I., *Biotechnology letters*, Microbial fuel cell biosensor for the determination of biochemical oxygen demand of wastewater samples containing readily and slowly biodegradable organics, 2021, 43(2), 445-454.

[2] Wang, S., Tian, S., Zhang, P., Ye, J., Tao, X., Li, F., Nabi, M., *Journal of environmental management*, Enhancement of biological oxygen demand detection with a microbial fuel cell using potassium permanganate as cathodic electron acceptor, 2019, 252, 109682.

[3] Do, M. H., Ngo, H. H., Guo, W., Chang, S. W., Nguyen, D. D., Deng, L., Nguyen, T. V., *Journal of Environmental Management*, Performance of mediator-less double chamber microbial fuel cell-based biosensor for measuring biological chemical oxygen, 2020, 276, 111279.

[4] Gao, Y., Wang, S., Yin, F., Hu, P., Wang, X., Liu, Y., & Liu, H., *Journal of Environmental Sciences*, Enhancing sensitivity of microbial fuel cell sensors for low concentration biodegradable organic matter detection: Regulation of substrate concentration, anode area and external resistance, 2021, 101, 227-235.

[5] Guo, F., Liu, Y., & Liu, H., *Science of the Total Environment*, Hibernations of electroactive bacteria provide insights into the flexible and robust BOD detection using microbial fuel cell-based biosensors, 2021, 753, 142244.

بیست و سومین کنفرانس شیمی فیزیک انجمن شیمی ایران
23rd ICS Physical Chemistry Conference
Chemistry Department,
Faculty of Science
Shahid Bahonar University of Kerman
Kerman, Iran
12-13 Jan 2022
ایران، کرمان
دانشگاه شهید باهنر کرمان
دانشکده علوم پایه، بخش شیمی
۲۳-۲۲ دی ماه ۱۴۰۰

Photophysical properties of thermally activated delayed fluorescence emitters from the perspective of single-hybrid and double-hybrid density functional theory

Mojtaba Alipour* and Niloofar Karimi
Department of Chemistry, School of Science, Shiraz University, Shiraz 71946-84795, Iran; E-mail: malipour@shirazu.ac.ir

Abstract

In this research, we dissect the accountability of parameterized and parameter-free single-hybrid (SH) and double-hybrid (DH) functionals through the time-dependent density functional theory (TD-DFT) and Tamm-Dancoff approximation (TDA) formalisms for the estimation of photophysical properties like absorption and emission energies as well as singlet-triplet energy gaps of thermally activated delayed fluorescence (TADF) emitters. We find that PBE0-1/3 with one-third of exact-like exchange as a parameter-free SH functional with one-third of exact-like exchange, the B2π-PLYP and B2GP-PLYP parameterized functionals, and the PBE-CIDH and PBE-QIDH parameter-free models provide more reliable descriptions of photophysical properties.

Keywords: Thermally activated delayed fluorescence; Density functional theory; Single-hybrid; Double-hybrid.

I. Introduction

As an approach for effective harvesting of both singlet and triplet excitons, the thermally activated delayed fluorescence (TADF) mechanism is of interest. Organic light emitting diodes (OLEDs) based on TADF emitters are also an attractive category of materials [1]. In the emitters exhibiting TADF with a small energy gap between the first singlet (S_1) and triplet (T_1) excited states, thermal energy can induce reverse intersystem crossing from the T_1 to the S_1 state. Since the radiative rate for the $S_1 \rightarrow S_0$ transition is much greater than the $T_1 \rightarrow S_0$ transition, it reduces the reliance on heavy rare earth metals and promotes the opportunity of exploiting exclusively organic materials. In this work, we have performed a detailed investigation based on the SH and DH functionals [2] for reliable prediction of photophysical properties of TADF emitters.

II. Methods

As systems under study, we have chosen two families of TADF emitters from the literature [3] as follows: One category with low (0.06-0.3 eV) and another class with high (0.3-0.8 eV) experimental singlet-triplet energy gaps (Fig. 1).

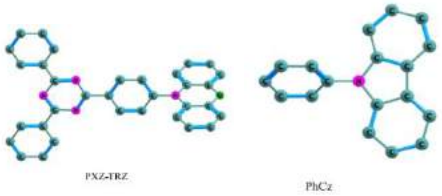

Fig. 1 Geometrical structures of two benchmarked molecules with low (PXZ-TRZ) and high (PhCz) singlet-triplet energy gaps. Other emitters are available in Ref. [4].

We employed the 6-31G* basis set for the SH calculations, while for the DH computations the def2-TZVP basis with the corresponding auxiliary functions was used. Besides the gas phase calculations, the solution phase has also been taken into account using the conductor-like screening

model. All the runs were implemented in ORCA and GAUSSIAN programs.

III. Results and discussion

According to our detailed analyses on the performance of SHs, the TDA-based parameter-free SH functional of PBE0-1/3 with one-third of exact-like exchange turned out to be the best performer in comparison to other functionals (Table 1).

Table 1. Comparison between TDA and full TD-DFT using the PBE0-1/3 and TPSS0-1/3 approximations for the singlet-triplet energy gaps. As metrics for gauging the performance of functionals, mean signed deviation (MSD), mean absolute deviation (MAD), maximum absolute deviation (MaxAD), and root mean square deviation (RMSD) were used.

	TDA		TD-DFT	
	PBE0-1/3	TPSS0-1/3	PBE0-1/3	TPSS0-1/3
MSD	0.00	0.14	0.31	0.48
MAD	0.15	0.25	0.34	0.48
MaxAD	0.32	0.65	0.82	1.01
RMSD	0.18	0.31	0.42	0.57

This is also indeed the case as compared to other approximations from various rungs [4]. We found also the same conclusion regarding the absorption and emission spectra (Fig. 2).

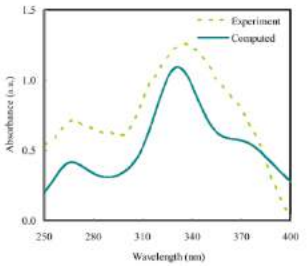

Fig. 2. Experimental (dashed line) and computed (solid line) absorption spectra using PBE0-1/3 functional for α-NPD [4].

From another perspective, considering this point that both nonlocal exchange and correlation are essential for reliable description of large charge-transfer excited states, capability of the parameterized and parameter-free DHs was also evaluated (Fig. 3). Perusing the role of exact-like exchange, perturbative-like correlation, and solvent effects, we find that the B2π-PLYP and B2GP-PLYP parameterized DHs and the PBE-CIDH and PBE-QIDH parameter-free models have better performances with respect to others.

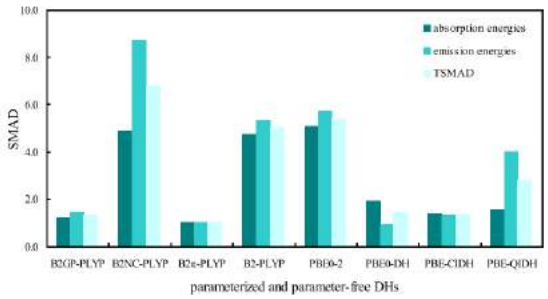

Fig. 3 Comparison of the general performance of parameterized and parameter-free DHs based on scaled MAD of a functional ($SMAD_f = MAD_f / MAD_{B2\pi\text{-}PLYP}$) and total SMAD (average of the SMAD values). All the functionals are compared with B2π-PLYP.

IV. Conclusions

We evaluated the performances of the SH and DHs for photophysical properties of TADF emitters with various singlet-triplet energy gaps [3]. Of the tested parameter-free SHs, the TDA-based functional PBE0-1/3 was found to be the best performers. The applicability of DHs for the absorption and emission energies was also assessed, where from parameterized parameter-free models, respectively, PBE-CIDH and B2π-PLYP were found to be the best performers. Hopefully, these methods can be used to design the TADF emitters with low singlet-triplet gap for OLED applications [4].

References

[1] H. Uoyama, K. Goushi, K. Shizu, H. Nomura, and C. Adachi, Nature 2012, 492, 234-238.
[2] S. Grimme, J. Chem. Phys. 2006, 124, 034108.
[3] D. Hait, T. Zhu, D. P. McMahon, and T. V. Voorhis, J. Chem. Theory Comput. 2016, 12, 3353.
[4] M. Alipour and N. Karimi, J. Chem. Phys. 2017, 146, 234304.

بیست و سومین کنفرانس شیمی فیزیک انجمن شیمی ایران
23rd ICS Physical Chemistry Conference
Chemistry Department,
Faculty of Science
Shahid Bahonar University of Kerman
Kerman, Iran
12-13 Jan 2022
ایران، کرمان
دانشگاه شهید باهنر کرمان
دانشکده علوم پایه، بخش شیمی
۲۳-۲۲ دی ماه ۱۴۰۰

Computational design of aptamer-based biosensors for the detection of small molecule Toxins

Fatemeh Salari[a*], Seifollah Jalili[b], Atena Pakzadiyan[c]

[a]Department of Chemistry, K. N. Toosi University of Technology, Tehran, Iran, sjalili@kntu.ac.ir
[b]Department of Chemistry, K. N. Toosi University of Technology, Tehran, Iran, sliftmh@gmail.com
[c]Department of Chemistry, K. N. Toosi University of Technology, Tehran, Iran, a.pakzadiyan@email.kntu.ac.ir

Abstract

In this study, the interaction of OBA3 aptamer with two molecules, ochratoxin A (OTA) and ochratoxin B (OTB) was theoretically explored. To this end, molecular dynamics (MD) simulations on aptamer-OTA and aptamer-OTB complexes were applied to assess their ability in the development of aptamer-based biosensors.

Keywords

OBA3 aptamer; ochratoxin A (OTA); ochratoxin B (OTB); molecular dynamics (MD) simulations; biosensor

Introduction

Aptamers are oligonucleotide sequences with a length of about 25–80 bases that mimic monoclonal antibodies. They generally fold into diverse three-dimensional structures that bind to specific targets. SELEX is still a gold-standard strategy for the generation of nucleic acid aptamers. The election cycle, whether for DNA or RNA sequences, on proteins, on cellular levels, or in living animals, requires three pivotal steps: (i) incubating a target with a library containing randomized sequences, (ii) partitioning bound sequences from non-bound sequences, and (iii) recovering and PCR amplifying the bound sequences [1]. Aptasensors are a class of biosensors where the biological recognition element is a DNA or RNA aptamer. Aptasensors represent a new type of biosensors that takes advantage of the unique properties of in vitro selected aptamers, in which the recognition reaction is independent of the transducer employed [2].

Methods

The initial structures of the OBA3OTA complex were obtained from the protein data bank (accession number:6J2W). All simulations were carried out using software GROMACS [3] version 4.6.1 with CHARMM27 [4] force fields. The energy minimization was carried on the system through 5000 descent steps. Molecular dynamics simulation at constant temperature and pressure (NPT) was performed for 20 nanoseconds at 310 K. The root-mean-square deviation (RMSD), Distribution of RMSD, and hydrogen bond by DSSR 3DNA software was analyzed.

Results and discussion

The root mean square deviation (RMSD) of the aptamer was calculated to estimate the system stability during the production simulation (Fig 1). In general, RMSD values of aptamer-OTA complex were a little lower than those of aptamer-OTB and aptamer-free.

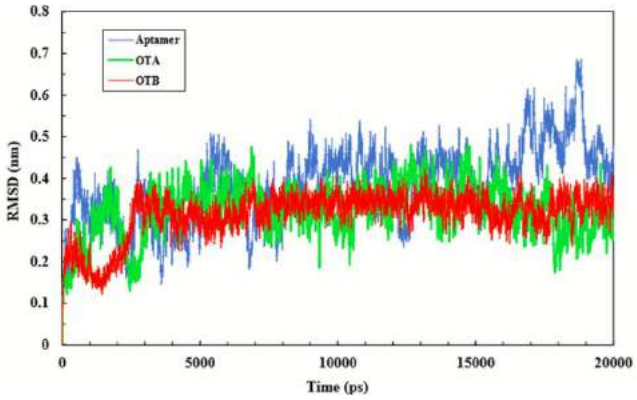

figure 1. RMSD time changes of all three systems: aptamer free (blue), aptamer-OTA complex (green) and aptamer-OTB complex (red), respectively.

Fig 2 shows that the probability distribution of RMSD plots of all systems has a peak. It means their RMSD is constant.

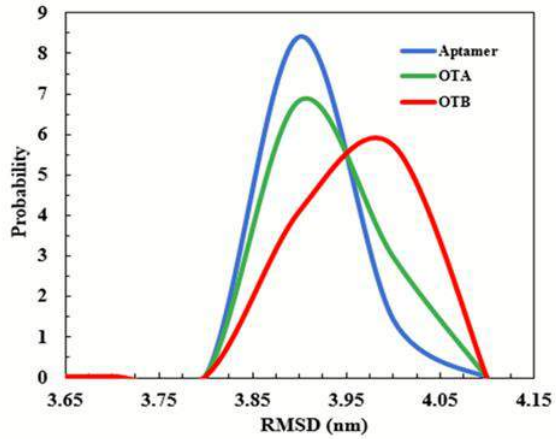

Figure 2. Probability distributions of RMSD values of all simulation systems.

Figure 3 shows the hydrogen bonding of base pairs of aptamers in all simulation systems. As shown in fig 3, The aptamer system has the lowest number of hydrogen bonds. the aptamer-OTA system compared to the aptamer-OTB system has the lowest number of hydrogen bonds Because the tamer-OTA system in index 5 (G5 base) has formed a halogen bond and has a stronger connection.

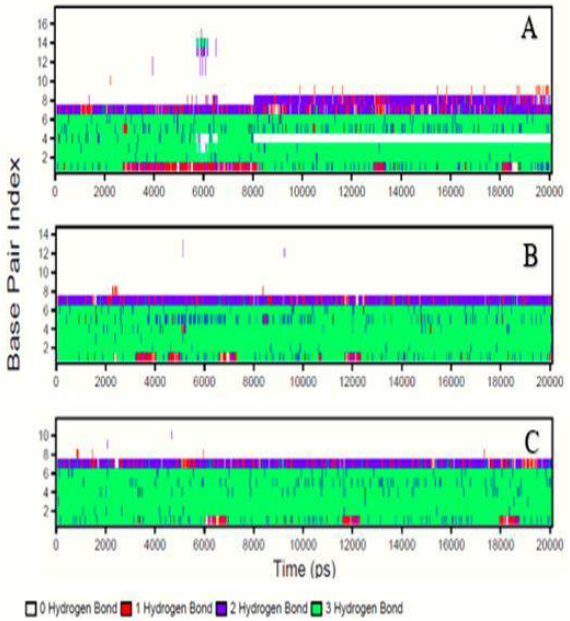

Figure 3. hydrogen bonding of base pairs of aptamer in all simulation systems.

Conclusion

The result of molecular dynamic simulation reveals that halogen bonds between the chlorine of OTA and G5 are responsible for discriminating between OTA and OTB.

References

[1] S. Ni, Z. Zhuo, Y. Pan, Y. Yu, F. Li, J. Liu, L. Wang, X. Wu, D. Li, Y. Wan, Recent progress in aptamer discoveries and modifications for therapeutic applications, ACS Appl. Mater. Interfaces. 13 (2020) 9500–9519.

[2] S. Song, L. Wang, J. Li, C. Fan, J. Zhao, Aptamer-based biosensors, TrAC Trends Anal. Chem. 27 (2008) 108–117.

[3] D. Van Der Spoel, E. Lindahl, B. Hess, G. Groenhof, A.E. Mark, H.J.C. Berendsen, GROMACS: fast, flexible, and free, J. Comput. Chem. 26 (2005) 1701–1718.

[4] U. Pentikainen, K.E. Shaw, K. Senthilkumar, C.J. Woods, A.J. Mulholland, Lennard− Jones Parameters for B3LYP/CHARMM27 QM/MM Modeling of Nucleic Acid Bases, J. Chem. Theory Comput. 5 (2009) 396–410.

بیست و سومین کنفرانس شیمی فیزیک انجمن شیمی ایران
23rd ICS Physical Chemistry Conference
Chemistry Department,
Faculty of Science
Shahid Bahonar University of Kerman
Kerman, Iran
12-13 Jan 2022
ایران، کرمان
دانشگاه شهید باهنر کرمان
دانشکده علوم پایه، بخش شیمی
۲۳-۲۲ دی ماه ۱۴۰۰

Calculation Of The Theory Of Thermodynamic Properties Of Ionic Liquids In Pure And Mixed State

Shaida Safaei, Ensieh Ghasemian Lemraski *

shaidasafaei56@gmail.com
e.ghasemian@gmail.com

Abstract:

Ionic liquids are defined as molten salts consisting of cations and anions. The structures and properties of ionic liquids are controlled by the interactions between the ions, so understanding the relationship between these interactions and the properties is essential to the design (group contribution method) of ionic liquids. In this article at first, 10 ionic liquids containing metal have been selected. In the second stage, the critical parameters have been calculated by the group contribution method. Equations for calculating the viscosity of ionic liquids containing different anions at different temperatures and molar fractions have been used.

Keywords: ionic liquids; critical points; viscosity.

I. Introduction: Thermodynamics studies the relationships between the macroscopic properties of a system. Chemical-physical and thermodynamic research play a very important role in understanding the interactions between particles and developing molecular aggregation patterns in pure and binary liquids. Thermodynamic parameters such as

Today, the use of chemical and technologies based on green chemistry is one of the important priorities in research and industry. Ionic liquids with very low volatility and unique properties are a good alternative to conventional solvent ionic liquids have low vapor pressure, are non-volatile and highly polarized and are resistant to heat, have high electrical conductivity, various enzymes in these compounds are easily soluble, can be changed by cation and anion, it forms various ionic liquids, the most common of which are imidazolium and pyridinium[3].

II. Methods

In this paper, first 10 ionic liquids containing metal are selected. In the second step, the critical parameters are calculated by group participation method. Equations have been used to calculate the viscosity of ionic liquids containing different anions at different temperatures and molar fractions. ; Group contribution method for ionic liquids containing metal proposed in this paper.

x_1	η_0(mpa.s)	B(k)	T_0(k)
0.0000	0.289	621.4	147.5
0.1016	0.268	643.1	144.0
0.2046	0.252	657.6	141.7
0.3035	0.245	662.1	140.7
0.4003	0.238	664.9	140.2
0.5041	0.227	674.7	138.8
0.5962	0.215	687.6	137.0
0.6955	0.200	706.5	134.6
0.7963	0.182	731.6	131.5
0.8901	0.162	768.2	126.9
1.0000	0.155	776.1	126.1

x_1	293/15	303/15	313/15	323/15	333/15	343/15	353/15
0.0000	20.59	15.65	12.30	9.93	8.21	6.92	5.93
0.1016	1./98	15.24	12.00	9.70	8.02	6.76	5.80
0.2046	19.36	14.80	11.67	9.44	7.81	6.59	5.64
0.3035	18.85	14.42	11.39	9.22	7.64	6.44	5.52
0.4003	18.38	14.08	11.12	9.01	7.46	6.30	5.40
0.5041	17.96	13.76	10.88	8.82	7.30	6.16	5.28
0.5962	17.57	13.48	10.65	8.64	7.15	6.03	5.17
0.6955	17.22	13.22	10.45	8.47	7.02	5.91	5.06
0.7963	16.81	12.91	10.21	8.27	6.85	5.77	4.93
0.8901	16.45	12.65	10.01	8.11	6.71	5.65	4.83
1.0000	16.14	12.44	9.82	7.95	6.58	5.53	4.72

Table1; Fitted Value of the Empirical parameters η_0, B, T0, for the Viscosities of [Emim][Al_2Cl_7](1) + [Emim][AlCl4] (2) Binary Mixtures of Mole Fraction x_1 .

III. Conclusions

Theoretical methods are of great importance in the development of science because of the saving of time, materials, and the provision of information that is not easily accessible through experimentation.

In this study, the pure state viscosity of 10 types of metal ions liquids containing metal based on imidazolium, pyridinium, etc. and studied by CSGC group contribution method. The obtained results were compared with the experimental data in the articales and discussed. The data obtained in the theory model and diagrams testify to the accuracy of this method and express the similar trend between the mentioned theory model and the experimental data and the low error percentage.

References

[1] Valderrama, J. O., & Robles, P. A. (2007). Critical properties, normal boiling temperatures, and acentric factors of fifty ionic liquids. Industrial & Engineering Chemistry Research, 46(4), 1338-1344.

[2]Lemraski, E. G., & Kargar, E. (2014). Standard Gibbs energy of adsorption and surface properties for ionic liquids binary mixtures. Journal of Molecular Liquids, 195, 17-21.

[3]Tomida, D., Kumagai, A., Kenmochi, S., Qiao, K., & Yokoyama, C. (2007). Viscosity of 1-hexyl-3-methylimidazolium hexafluorophosphate and 1-octyl-3-methylimidazolium hexafluorophosphate at high pressure. Journal of Chemical & Engineering Data, 52(2), 577-579.

بیست و سومین کنفرانس شیمی فیزیک انجمن شیمی ایران
23rd ICS Physical Chemistry Conference
Chemistry Department,
Faculty of Science
Shahid Bahonar University of Kerman
Kerman, Iran
12-13 Jan 2022
ایران، کرمان
دانشگاه شهید باهنر کرمان
دانشکده علوم پایه، بخش شیمی
۲۳-۲۲ دی ماه ۱۴۰۰

Density functional theory study of formamide adsorption on the pristine (8,0)Carbontube

Marjan Ghaffari [a,*], Hossein Mohammadi-Manesh[a], Forough Kalantari Fotooh[b]

[a] *Department of Chemistry, Yazd University, Yazd, Iran, ghafarimarjan@stu.yazd.ac.ir*

[b] *Department of chemistry, Yazd branch, Islamic Azad University, Yazd, Iran, f_kalantari_f@iauyazd.ac.ir*

Abstract

Adsorption of formamide (HCONH2,FM) molecule on (8,0) single-walled carbon nanotube (SWCNT) was studied by density functional theory (DFT) method. The FM molecule was adsorbed from the oxygen side on C_1 atom of nanotube and its geometric structure and electronic properties before and after FM adsorption were investigated

Keywords: Density functional theory; SWCNT ; HCONH2 adsorption; Electronic structure

I. Introduction

FM is the simplest member of the amide active group, which contains the prototypical NH-C=O linkage in peptides. This linkage is reactive at both amino and carbonyl sites and is expected to constitute a key building block for formation of nucleic acids[1]. Furthermore, FM is used for the manufacture of sulfa drugs, other pharmaceuticals, herbicides, pesticides and the manufacture of hydrocyanic acid. Nowadays, carbon nanotubes (CNTs) are a promising material which people pay more attention to. It is unique because of its wonderful properties, including the nanoscale size, high strength, high sensitivity and excellent electrical properties.. Therefore, carbon nanotube is used in an increasing number of practical applications, such as nano-diode, drug delivery, electrochemical biosensors, gas sensors and field-emission materials [2,3].

In this work ،The formamide molecule was adsorbed from the oxygen side on C_1 atom of nanotube.

II. Methods

The electronic structure and density of state calculations were carried out thorough the dispersion corrected DFT ,in the spin polarized mode.Employing the plane-wave pseudo potential technique and PBE formulation of generalized gradient approximation implemented Quantum Espresso package. The considered supercell contain 32 carbon atoms and has lattice constants of a = 31.75 Å and c = 4.260 Å .The Brillouin zones integrations were performed by using 1×1×11 Monkhorst-Pack meshe

III. Results and discussion

The relaxed adsorption energies were determined according to the expression:

$E_{ads}=E_{total}$(FM-SWCNT) $-E_{total}$(SWCNT) $-E_{total}$(FM)

Where E_{total}(FM-CNT) is the total energy of FM adsorbed CNT, E_{total}(CNT) is the total energy of the relaxed CNT in the absence of the FM, and E_{total}(FM) is the total energy of an isolated FM molecule. By defining the negative number of absorption energy(E_{ad}) -0.2445 ev is related to exothermic adsorption, which indicates the relative tendency of nanotube(8.0) to adsorb FM.

FM molecule is located on the nanotube so that its oxygen atom is close to the C_1 atom of SWCNT.The C_1–O bonding distance is 3.1635Å, The small adsorption energy and the long distance of FM after adsorption indicate the physical adsorption and very weak interaction of FM with nanotube (8.0). according to the table1 ,in band and DOS calculations before and after adsorption, fermi energy level has increased slightly and energy gap are not many changes, indicating that the nanotube are semiconductors before and after adsorption.

PDOS diagram of FM adsorption on C_1 atom nanotube in fig 1, doesn't show change significantly compared to the PDOS of C_1 atom isolate nanotube. Only the intensity of the lines has increased slightly, which has little effect on the fermi surface and the conductivity of the nanotube,This factor confirms the inefficiency of nanotube (8.0) on the FM molecule.

as shown in Fig 1. the two spin up and down states are symmetrical to each other, it means no spin polarization or zero magnetic moment in charge carriers and the density of states at the fermi level is zero.

Table1. Properties of CNT and CNT/FM data

system	E_g	E_{SCF}	E_f	μ
CNT band	0.5920	8025.5288	-3.5690	0
CNT /FM	0.5910	-9275.875	-3.0846	0
CNT dos	0.4000	8025.5288	-3.9461	0
CNT /FM	0.6000	9275.8750	-3.4581	0

Fig1.PDOS of s,p orbitals C_1 atom CNTand orbitals FM molecule

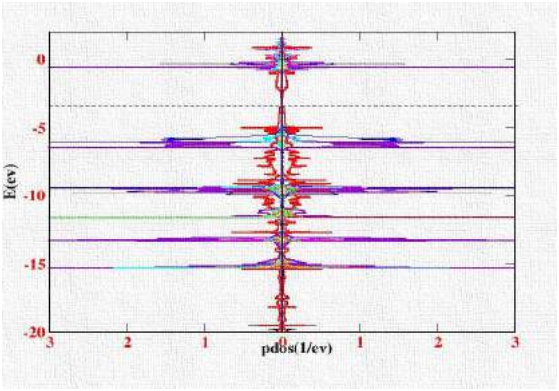

IV. Conclusions

The results show that the adsorption of FM molecule, dose not much change the properties of (8,0) SWCNT. It is suggested that by selecting larger nanotubes, the effect of nanotube size and possibly more accurate results be investigated.

[1]. H. L Barks, R .Buckley, G. A .Grieves, E .Di. Mauro, N. V. Hud, T. M. Orlando, ChemBioChem, 2010, 11, 1240.

[2].. M. Zhang, J. Li, Carbon nanotube in different shapes, Mater. Today, 2009, 12 ,12–18.

[3]. W. Li et al, Appl. Surf. Sci, 2016, 364 , 560.

بیست و سومین کنفرانس شیمی فیزیک انجمن شیمی ایران
23rd ICS Physical Chemistry Conference
Chemistry Department,
Faculty of Science
Shahid Bahonar University of Kerman
Kerman, Iran
12-13 Jan 2022
ایران، کرمان
دانشگاه شهید باهنر کرمان
دانشکده علوم پایه، بخش شیمی
۲۳-۲۲ دی ماه ۱۴۰۰

Molecular Dynamics Simulation of Mixture of Ionic Liquid 1-Ethyl-3-Methyl Imidazolium Methyl Sulfate and Water

Atefeh .mehraban , Farkhondeh.Mozaffari*

Department of Chemistry,Persian Gulf University, Bushehr, Iran
E-mail: atefi.mehraban@gmil.com
E-mail: farkhondeh mozaffarif@gmail.com

Abstract

Molecular dynamics simulations are applied to study 1-ethyl-3-methylimidazolium methyl sulfate ionic liquid/water mixture. The density, excess molar volume, water cluster size, radial distribution function, and hydrogen bonding are studied that are in good agreement with the literature. The number of hydrogen bonds of water-water increased with increasing water mole fraction in mixtures that is in agreement with large water clusters in high water mole fraction.

Keywords: Hydrogen bonding; Ionic liquid; Modeling and Simulation

I. Introduction

The addition of water to ionic liquids (ILs) can drastically change the structures and dynamical properties of ionic liquids such as viscosity [1], ionic diffusion coefficient [2] biological activity [3], density, melting point. Due to the importance of this topic, we are performed molecular dynamics (MD) simulation to investigate the water influence on different properties of [Emim][$MeSO_4$] at various water amount.

II. Methods

MD simulation in the isobaric-isothermal (NPT) ensemble is performed on [Emim][$MeSO_4$] IL and water mixtures at constant pressure, 101.3 kPa, and at constant temperature 300K. In this work, a standard all-atom force field is applied to characterize the potential energy function. The three-site Lennard-Jones (LJ) plus Coulombic potentials with the reaction field model were exerted to appraise the nonbonded interactions of the force field The applied cutoff distance is 1.1 nm and if the neighbor distance is less than 1.2 nm the neighbor is accounted. The effective dielectric constant of 30 and 71 for pure IL and pure water were considered for reaction field correction of the Coulombic interactions [4].

III. Results and discussion

The calculated mass density of the [Emim][$MeSO_4$]/water mixtures at different mole fractions of water indicated increasing in mixture density in low water mole fraction and decreasing of mixture density in high water mole fraction.The nonlinear changes of the mixture density indicated the non-ideality of these mixtures that can be determined with excess molar volume. The excess molar volume of this mixture as a function of water mole fraction

is investigated.The negative deviations from ideal behavior in low mole fraction $x_w s \leq 0.6$ showed that the mixing process of IL and water could eventuate to more close-packing and the attractive interactions between water and [Emim][$MeSO_4$]. This observation is in agreement with the negative excess enthalpy of Brennecke[5] for [Emim][$MeSO_4$]/water mixture that shows stronger interaction between the component of mixture. The water cluster size distribution results in the different water mole fractions indicate that larger clusters are formed in higher water mole fractions and hydrogen bond (HB) networks are formed between nearly all water molecules in these solutions. The center of mass radial distribution functions (RDFs) were applied to distinguish water–anion and water–cation correlation in mentioned mixtures. The RDFs of water–anion and water–cation are indicated in Figure 1. The comparison of water–cation RDF with water–anion RDF indicated the height of the first peak of water–anion is almost double that for water–cation. This observation demonstrates that the water molecules tend to be in the vicinity of anion compared to cation. Our results for the number of hydrogen bonding (nHB) indicated the average of nHB reduced for cation–anion, water–anion, and water–cation while nHB of water–water increased with increasing water mole fraction in mixtures.

Figure 1. RDF for water-anion and cation-water in [Emim][$MeSO_4$]/water mixtures. (The numbers in the legend indicate the water mole fraction) .

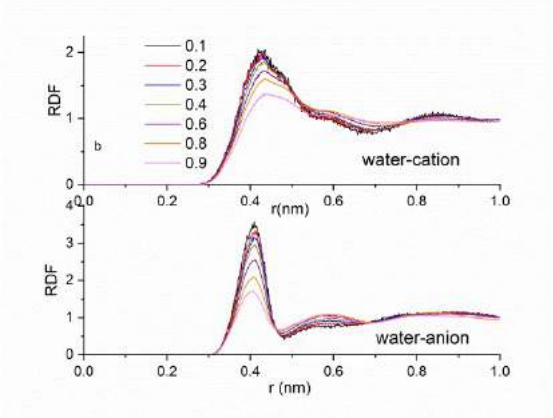

IV. Conclusions

The RDF curves indicate the water molecules tend to be in the vicinity of anion compared to cation. The water molecules begin to accumulate more homogeneously and start to indicate structural characteristics like those of pure water in solution with high water mole fraction.

References

[1] P.Sánchez, B. García, J. Salgado, J. González-Romero, E. ACS Sustainable Chem. Eng. 2016, 4, 5068−5077.

[2] M H. Kowsari, S. M. Torabi. NASHRIEH SHIMI VA MOHANDESI SHIMI IRAN (PERSIAN) 2018 , 37, 103-112.

[3]H. Ohno, Fujita, K. Kohno, Y. Is Seven the Phys. Chem. Chem. Phys. 2015, 17, 14454−14460.

[4] Allen,M. P. TILDESLEY, Dominic J. How to analyse the results. In: Computer Simulation of Liquids. Oxford University Press, 1987.

[5] L. E. Ficke, J., F. Brennecke, J. Phys. Chem. B, 2010, 114, 10496.

بیست و سومین کنفرانس شیمی فیزیک انجمن شیمی ایران
23rd ICS Physical Chemistry Conference
Chemistry Department,
Faculty of Science
Shahid Bahonar University of Kerman
Kerman, Iran
12-13 Jan 2022
ایران، کرمان
دانشگاه شهید باهنر کرمان
دانشکده علوم پایه، بخش شیمی
۲۳-۲۲ دی ماه ۱۴۰۰

Poly (ester-ether-urethane) networks and their interaction with human growth hormone: Conductometry

Masoumeh Sohrabi[a], Pouneh S. Pourhosseini[a,*], Samira Ansari[b]

[a] *Department of Biotechnology, Faculty of Biological Sciences, Alzahra University, Tehran, Iran. E-mail: m.sohrabi@student.alzahra.ac.ir, [*]E-mail: p.pourhosseini@alzahra.ac.ir*

[b] *1- CinnaGen Medical Biotechnology Research Center, Alborz University of Medical science, Karaj, Iran. 2-CinnaGen research and production co., Alborz, Iran. E-mail: Ansaris@gmail.com*

Abstract

In this study, the interaction between human growth hormone (hGH) with a di-cationic and a single-chain polymer of poly(ester-ether-urethane) was investigated by conductometry. Thermodynamic parameters of micellization were determined, such as critical micelle concentration (CMC), critical association concentration (CAC), protein saturation point (PSP), and the average degree of ionization (α) of micelles or complexes. The values of CMC for both polymers are low, indicating a good stability of supramolecular structures in aqueous solutions. A comparison of these parameters between both polymers provides a better understanding about their physicochemical behavior in interaction with the protein.

Keywords: Conductivity; Human growth hormone; Interaction; Polyurethane.

I. Introduction

Polyurethanes (PUs) are a family of versatile synthetic polymers that have a soft to hard structure and can be easily dispersed in solvents. Due to their biocompatibility and elastic behavior, which is very similar to soft tissues, they are used for in vivo applications [1, 2]. Also, urethane groups can be added to other compounds as a factor to control the rate of degradation [3]. The polymers used in this study, are synthetic having urethane, ether and ester bonds in their chains. The di-cationic polymer is actually a gemini surfactant, while the uncharged one is a single-chain polymer.

II. Methods

To prepare polymer nanoparticles, a 30 mg/ml dispersion of polymer was prepared in buffer (L-His, pH 6.2), which was ultrasonicated (Elma, S30H) to achieve a uniform distribution of micelles (20 min, 25 °C). Specific conductivity of buffer was measured using an LCR meter (GPS, 3138B, England). Titration of buffer with small volumes of polymer nanoparticles was performed several times and the conductance was measured at 298 K, a frequency of 1 kHz and a voltage of 0.1 V. Titration of hGH solution with polymer colloid was conducted similar to that performed for buffer.

III. Results and discussion

The plots of specific conductivity versus polymer concentration are represented in Fig.1. The breakpoint in diagrams "a" shows the CMC, while those in diagrams "b" represent the CAC and PSP. The (α) value was obtained by the ratio of the slopes above and below the CMC. The calculated

Table 1. Parameters obtained by conductometry. (*: in the presence of protein)

polymer	CMC (μM)	CAC (μM)	PSP (μM)	α (%)	α_1 (%)	α_2 (%)	CAC/ CMC	PSP/ CMC	$\Delta G°\ mic^*$ (kJ/mol)	$\Delta G°\ mic$ (kJ/mol)	$\Delta G°\ a$ (kJ/mol)	$\Delta G°\ Ps^*$ (kJ/mol)	$\Delta G°\ Ps$ (kJ/mol)
Non-ionic surfactant	4.7	4.8	17	0.52	0.67	0.42	1.02	3.62	-43	-45	-40.4	2.6	4.6
Di-cationic surfactant	5.4	5.6	19.1	0.52	0.54	0.43	1.04	3.54	-29.7	-30.3	-29.6	0.1	0.7

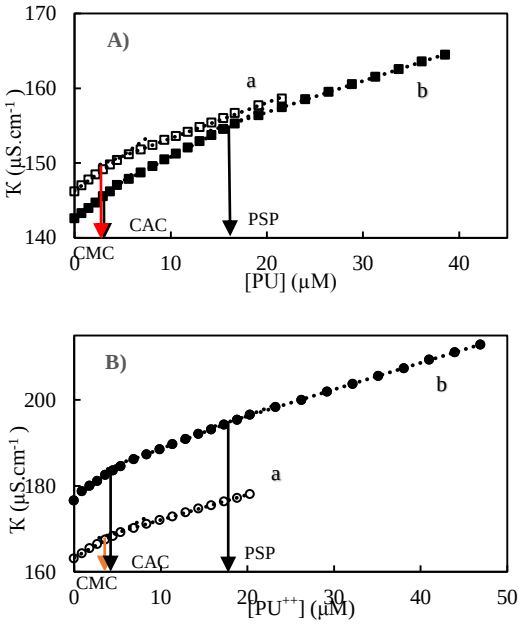

Figure 1. Specific conductivity versus surfactant concentration for the single-chain (A) and the gemini (B) surfactant, in the absence (a) and presence (b) of the protein.

parameters are summarized in Table 1. Furthermore, the standard Gibbs free energy of micellization ΔG^o_{mic}, the standard Gibbs energy for the transference of 1 mol of surfactant molecules from unperturbed micelles (i.e., in the absence of protein) to protein-bound micelles, ΔG^o_{PS}, was calculated. The negative values of ΔG^o_{mic} imply spontaneous micellization for both polymers. The ratio of CAC/CMC is almost unity, indicating that complex formation occurs between micelles and the protein. The ratio of PSP/CMC is greater than one, implying that after PSP the protein surface is saturated by polymers and free micelles are formed. Positive values for ΔG^o_{PS} in the absence of protein, indicate that ΔG^o_{mic} is more negative than $\Delta G°_{\ell}$. Therefore, free micelle formation is thermodynamically more desirable than complex formation [4]. In this case, if a molecule of complex is entered into a dish containing free micelles, the polymers migrate from the protein surface to form free micelles in the buffer.

IV. Conclusions

The conductivity of gemini surfactant dispersion in the presence of protein was higher than that of pure surfactant system. This is because of binding of larger surfactant cations to protein that may release some small cations from the stern layer near the negative charged amino acid residues of the protein. [5].

References

[1] Magnin, A., et al., Evaluation of biological degradation of polyurethanes. Biotechnology advances, 2020. 39: p. 107457.

[2] Nelson, D.M., et al., Controlled release of IGF-1 and HGF from a biodegradable polyurethane scaffold. Pharmaceutical research, 2011. 28(6): p. 1282-1293.

[3] Nazarpak, M.H., et al., Synthesis and characterization of conductive neural tissue engineering scaffolds based on urethane-polycaprolactone. International Journal of Polymeric Materials and Polymeric Biomaterials, 2018.

[4] Faustino, C., A. Calado, and L. Garcia-Rio, Gemini surfactant-protein interactions. 2008.

[5] Yin, T., M. Qin, and W. Shen, Physicochemical investigations on the interactions between gemini/single-chain cationic surfactants and bovine serum albumin. Colloids and Surfaces A: Physicochemical and Engineering Aspects, 2014. 461: p. 22-29.

بیست و سومین کنفرانس شیمی فیزیک انجمن شیمی ایران
23rd ICS Physical Chemistry Conference
Chemistry Department,
Faculty of Science
Shahid Bahonar University of Kerman
Kerman, Iran
12-13 Jan 2022
ایران، کرمان
دانشگاه شهید باهنر کرمان
دانشکده علوم پایه، بخش شیمی
۲۳-۲۲ دی ماه ۱۴۰۰

The Investigation of La(III)Ions-Doping effect on band gap of $BiFeO_3$ perovskite

Zohreh Rashidi Ranjbar, Mozhde Salari Nasab

Address: Department of Chemistry, Faculty of Sciences, Shahid Bahonar University of Kerman, Kerman, Iran;
**Email:zoh.rashidi@gmail.com*

Abstract

In the last few years, perovskite have received researchers' attention due to their applications in photovoltaic and photo-catalysis. These materials are semiconductor and it is one of the most important properties of them.

In this research, we synthesized bismuth ferrite ($BiFeO_3$) perovskite by co-precipitation method and doped La (III) to investigate any changes in band gap energy. Prepared structures were characterized by IR spectroscopy, X-ray powder Diffraction (XRD), Energy Dispersive X-ray Spectroscopy (EDAX). The band gap energies, HOMO and LUMO levels of synthesized compounds were calculated by using UV-Vis spectroscopy and Cyclic Voltammetry (CV).

Keywords: Semiconductor; Perovskite; Doping; Band gap

I. I. Introduction

Perovskites as semiconductor oxides have to be stable in aqueous solutions over an extended pH range with a bandgap 3.2 eV. Because of stability in water, perfect conduction band potentials and ease of synthesis; perovskites have been preferred as optoelectronics and photo-catalysis material [1]. However, TiO_2 is the first model of semiconductor oxide and remains the most common today [2]. In addition, another semiconductor such as SnO_2 and the SnO_2/TiO_2 core–shell material [3] have also been introduced for photovoltaic and photo-catalysis reasons. Every changes in band gap could effect on semiconductors properties and their applications. For example, in $BiFeO_3$ structure, Ca^{2+} (114 pm) doping at Bi^{3+} (117 pm) site and Oxygen vacancies can be easily incorporated into a lattice by substituting cation sites with dopants. Also, the bandgap can be brought down to 1.5 eV [4]. In this work, we synthesized bismuth ferrite ($BiFeO_3$) and doped La (III) at Bi^{3+} site to investigate the band gap energy.

II. Methods

To prepare $BiFeO_3$ with La (III) doping, stoichiometric amounts of bismuth nitrate and iron nitrate salts (1:1 ratio) were dissolved in 10 mL methanol. The 0.5 mmol of lanthanium(III) nitrate was dissolved in 5 mL methanol and added to the pervious solution. By adding NaOH up to the solution doped sample were precipitated.

III. Results and discussion

Two perovskites were characterized by IR spectroscopy, X-ray powder Diffraction (XRD), Energy Dispersive

X-ray Spectroscopy (EDAX). The band gaps of perovskites ($BiFeO_3$ and $BiFeO_3$/La(III) dopped) were estimated by absorption and emission spectra. The absorption and emission data are obtained from UV-Vis and PL spectroscopies. We prepared DMSO solution (0.001mM, 20ml) of perovskites for absorption and emission analysis. Absorption and emission spectra were acquired at room temperature. Band gap energies were obtained from UV-Vis spectra. Absorption bands are extending from 200 nm to 800 nm wavelengths and corresponding wavelengths to the band gaps were calculated by optical absorption data and Tauc plots (figure 1). To determine the possibilities of electron injection from the valance band (VB) to conduction band (CB) of dyes and electron drift in cell, HOMO and LUMO energy levels were measured by cyclic voltammetry data. Schematic diagram of energy levels in perovskites shows in figure 2.

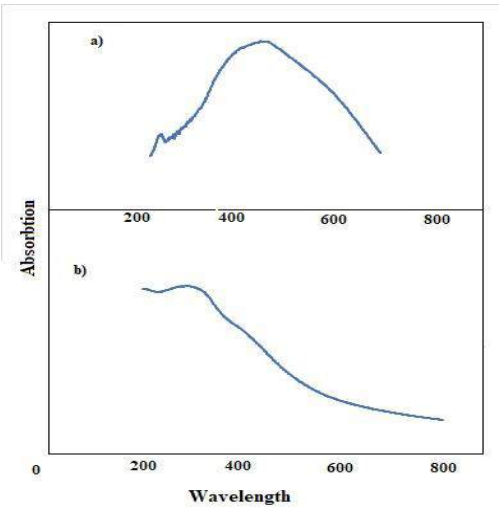

Fig. 3. UV-Vis spectra of a) $BiFeO_3$ b) $BiFeO_3$/La(III) dopped band gaps and energy levels

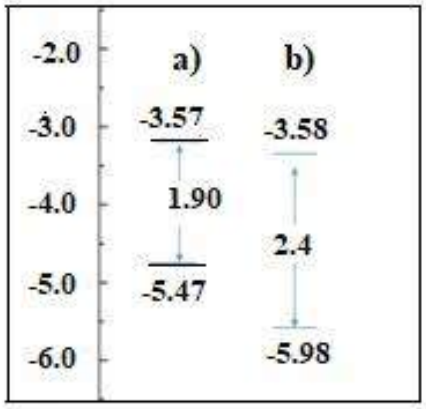

Fig. 2. a) $BiFeO_3$ b) $BiFeO_3$/La(III) dopped band gaps and energy levels

Conclusions

In this work, we synthesized two perovskites ($BiFeO_3$ and $BiFeO_3$/La(III) doped). The studies show after doping La(III) up to $BiFeO_3$ perovskite structure, band gap was increased. This phenomenon cause light absorption of two perovskites ($BiFeO_3$ and $BiFeO_3$/La(III) doped) as semiconductor perform.

Reference

[1] N. M. Laya, R. R. Zohreh, *Journal of Alloys and Compounds*, 2019, 785, 117-124.

[2] A. Hagfeldt, G. Boschloo, L. Sun, L. Kloo, H. Pettersson, *Chem. Rev.*, 2010, 110, 6595–6663.

[3] L. Alibabaei, B.D. Sherman, M.R. Norris, M.K. Brennaman, T.J. Meyer, *Proc. Natl. Acad. Sci*, 2015, 112, 5899–5902.

[4] N. Subhajit, K. Kulwinder, S. V. M. Pavana, B. R. K. Nanda, and C. Sudakar, *Journal of Applied Physics*, 2018, 124, 195108-195121

بیست و سومین کنفرانس شیمی فیزیک انجمن شیمی ایران
23rd ICS Physical Chemistry Conference
Chemistry Department,
Faculty of Science
Shahid Bahonar University of Kerman
Kerman, Iran
12-13 Jan 2022
ایران، کرمان
دانشگاه شهید باهنر کرمان
دانشکده علوم پایه، بخش شیمی
۲۳-۲۲ دی ماه ۱۴۰۰

Enhancement Efficiency of Quantum Dot perovskite Solar Cell by Plasmonic Nanoparticles

Saeedeh Zavari[a,*], Vahid Saheb [b], Hossein Rooholamini Nejad [c]

[a] *Address: Shahid Bahonar University of Kerman, Faculty of Physics; Tel: 0936 980 5493; E-mail: saeedeh.zavari@gmail.com*
[b] *Address: Shahid Bahonar University of Kerman, Faculty of chemistry; Tel: 0917 316 5106; E-mail: vskermanu@gmail.com*
[c] *Address: Shahid Bahonar University of Kerman, Faculty of Physics; Tel: 0913 243 0180; E-mail: rooholamini@uk.ac.ir*

Abstract

Perovskites are widely used in solar cells and solid-state lasers and light emitting diodes due to their high light absorption and ability to generate stable excitons. One of the major disadvantages and challenges of perovskite solar cells is their stability. Perovskite solar cells CsPbBr3 are less efficient than perovskite CsPbI3, but are better than perovskite CsPbI3 in terms of long-term stability. In this project, perovskite quantum dots CsPbBr3 were used due to more stability and also silver nanoparticles were used to increase the efficiency of solar cells and the efficiency of solar cells was increased from 2.65% to 3.5%.

Keywords: Perovskite; quantum dots; silver nanoparticles; solar cell.

I. Introduction

Solar energy is one of the cleanest and most accessible sources of energy supply that can be converted into other forms of energy. Among the types of solar cells, quantum dot perovskite solar cells have been considered due to the synthesis method, low manufacturing cost and other features. The structure of perovskite is structurally similar to that of calcium titanate, which is characterized by a structural formula that represents cations of different sizes (larger than) and is representative of the anion.

In halide perovskites, an anion is a group of halogens such as fluorine (F), chlorine (Cl), bromine (Br) and iodine (I) or a combination thereof, a divalent metal of the fourteen group such as tin (Sn) or Lead (Pb) or rare earth element (Eu) [1].

Quantum dot structures are used for a variety of applications, the most important of which has recently attracted the attention of researchers is the use of nanostructured solar cells, which reduces the cost of fabricating these cells and increases their conversion efficiency. One of the great properties of quantum dots is their adjustable energy gap. In this way, as the size of the quantum dots decreases, its energy gap increases [2].

Perovskite solar cells are one of the most important types of solar cells that can be used to produce cheaper solar energy.

II. Methods

Silver nanoparticles were first synthesized. Then perovskite quantum dots CsPbBr3 were synthesized. The construction of perovskite quantum dots is done in three steps. These steps include precursor synthesis, quantum dot formation, and centrifugation. To prepare the precursor, cesium carbonate, along with oleic acid and paraffin solvents, is first poured into three necked round bottom flask and prepared

under nitrogen atmosphere at 150 ° C. Then, when it is dissolved with olelamine, oleic acid and paraffin (at 170 ° C), we immediately inject the synthesized precursor. (Figure 1) Finally, to stop the reaction, we place the three-mouth container in an ice bath for 5 seconds [3].

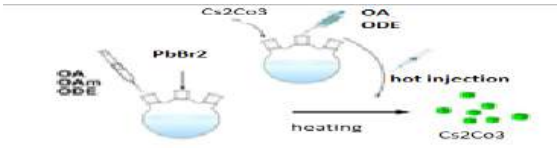

Figure 1: Construction of perovskite quantum dots

In this project, instead of using expensive Octadense solvent, paraffin was used, which has similar properties to this expensive solvent. The advantage of paraffin is its availability and cheapness.

III. Results and discussion

According to Figure 2, the absorption spectrum of CsPbBr3 quantum dots is in the visible region.

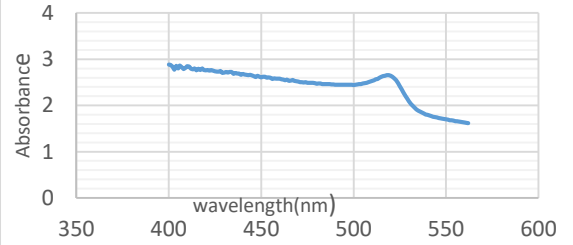

Figure 2: Ultraviolet-visible absorption spectra for perovskite quantum dots

In the imaging of the synthesized perovskite sample, Figure 3 was obtained. This image shows the cubic structure of perovskite nanoparticles, which is most efficient for use in solar cells.

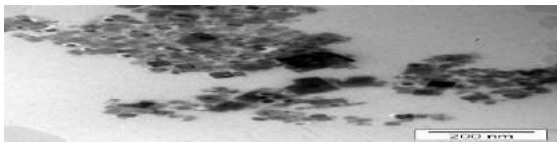

Figure 3: Electron microscopy of perovskite quantum dots

One of the most important analyzes in solar cells is the study of current-voltage curves. Current-voltage curve obtained from current and voltage measurements for different resistors is shown in Figure 4.

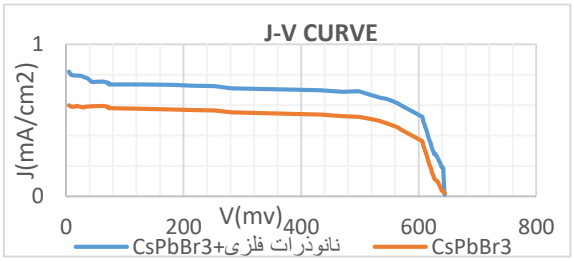

Figure 4: Current-voltage density curve for a perovskite quantum dot solar cell and a perovskite quantum dot cell mixed with metal nanoparticles under sunlight

IV. Conclusions

One of the challenges facing perovskites is their stability. Therefore, in this article, we have tried to use perovskite quantum dots CsPbBr3 instead of CsPbI3 quantum dots to reduce this problem, and to increase the efficiency, silver nanoparticles have been used. It was observed that the fusion of a perovskite solar cell with silver nanoparticles significantly increased the current compared to a solar cell without silver nanoparticles. The efficiency of a solar cell without silver nanoparticles is about 2.65%, while the combination of perovskite quantum dots with silver nanoparticles increases the efficiency of the solar cell by 3.5%.

References

[1] Elumalai, Naveen Kumar, et al. "Perovskite solar cells: progress and advancements." ***Energies*** **9.11 (2016): 861.**

[2] Song, Jung Hoon, and Sohee Jeong. "Colloidal quantum dot based solar cells: from materials to devices." ***Nano Convergence*** **4.1 (2017): 1-8.**

[3] Wang, Wei, et al. "A CsPbBr3 quantum dots/ultra-thin BN fluorescence sensor for stability and highly sensitive detection of tetracycline." ***Microchemical Journal*** **162 (2021): 105876.**

بیست و سومین کنفرانس شیمی فیزیک انجمن شیمی ایران
23rd ICS Physical Chemistry Conference
Chemistry Department,
Faculty of Science
Shahid Bahonar University of Kerman
Kerman, Iran
12-13 Jan 2022
ایران، کرمان
دانشگاه شهید باهنر کرمان
دانشکده علوم پایه، بخش شیمی
۲۳-۲۲ دی ماه ۱۴۰۰

Adsorption of CO molecules on the pure and V_n-doped BN nanotubes

Batoul Makiabadi[a]*, Mohammad Zakarianezhad

[a] *Department of Chemical Engineering, Sirjan University of Technology, Sirjan, Iran, bmakiabadi@yahoo.com*
[b] *Department of Chemistry, Payame Noor University, Tehran, Iran*

Abstract

Interaction of pure and Vn-doped (8, 0), (12, 0) and (16, 0) boron nitride nanotubes with CO molecules was studied using B3LYP/6-311++G(d) theoretical level. Substituting V instead of B atoms, increased the reactivity of nanotube. The complex stability depends on the direction and the number of the CO molecules interacted with the nanotube. The influence of the diameter of the nanotube on the electronic properties of the complexes was investigated. The charge transfer in complexes was calculated with NBO analysis.

Keywords: Boron Nitride Nanotube; Electronic Properties; HOMO-LUMO Gap; V-doped Nanotube.

I. Introduction

Unlike carbon nanotubes, BNNTs are noncytotoxic and are predicted that these nanotubes to be suitable in various medical fields relative to the CNTs [1]. The investigations show that defect or doping, enhances the application of BNNTs in different fields such as nanoelectronics, nanoscale biotechnology, and biosensors [2,3]. The doping effect of the elements on the adsorption of the various molecules on the BNNTs was investigated by the theoretical methods [4,5]. Carbon monoxide (CO) is a colorless, odorless, and a tasteless flammable gas. Many investigations have been performed on the CO adsorption on the pure and doped carbon nanotubes. In this work, we selected the V-doped BNNTs and investigated the interaction of Co molecules with the V-doped BN nanotubes. Analysis of the electronic properties of the structures was also investigated in the solution phase. The results of this study are useful for designing and developing of CO detectors.

II. Methods

All structures were optimized at the level with B3LYP exchange functional and 6-311++G(d) basis set using the Gaussian 09 software package [6]. The molecular descriptors such as the energy gap (Eg), the electronic chemical potential (μ), chemical hardness (η), chemical softness (S), electrophilicity index (ω) and the maximum amount of electronic charge of the system (ΔN_{max}) were evaluated. The charge analysis was performed at the B3LYP/6- 311++G(d) level of theory using the NBO analysis [7].

III. Results and discussion

We have examined all the possible positions for CO molecules adsorption on the boron nitride nanotubes. The interaction of the CO molecule with BNNTs includes two kinds of configurations (See Fig 1). In configurations **a** and **b**, C or O atom of CO

interacted with B atom of the nanotube, respectively. Based on the results, (CO)n/Vn−BNNT complexes are more stable than (CO)n/BNNT ones. Also, the configuration **a** is more stable than the **b**. This stability decreased with increasing the tube diameter. By doping of V atoms, the electronic properties of nanotube were changed and the energy gap of complexes decreased. Thus, the conductivity of nanotubes was increased upon complexation. The results show that the energy gap and chemical hardness of (CO)n/BNNTs are higher than those of (CO)n/Vn−BNNT complexes. Also, chemical potential, chemical softness, ΔN_{max}, and electrophilicity index for (CO)n/BNNTs are smaller than those of (CO)n/Vn−BNNT complexes. Therefore, it is predicted that after the doping of BNNTs, the stability and conductivity of the complexes were increased. According to the NBO results, in CO/BNNT complexes, charge transfer was carried out from CO molecules to nanotubes, while the opposite was observed in (CO)n/Vn−BNNT complexes. The values of charge transfer in (CO)n/ Vn−BNNT complexes is more than (CO)n/BNNT. By increasing the number of the CO molecules, the value of charge transfer between CO molecules and nanotubes was increased upon complexation.

IV. Conclusions

In this research, the effect of the interaction of CO molecules on the molecular descriptors of pure and Vn−doped (8, 0), (12, 0) and (16, 0) BNNTs were investigated. Based on the results, (CO)n/Vn−BNNT complexes are more stable than (CO)n/BNNT ones. It is predicted that after the doping of BNNTs, the stability and conductivity of the complexes were increased. Compared with previous works, the interaction of the CO molecules with the V-BNNTs is stronger than Al, Ga, Si-doped BNNTs and weaker than Ni, Pd and Pt-doped boron nitride nanotubes. It seems that the Vn−BNNTs could be appropriate for the adsorption of the CO molecules. It is predicted that the Vn-nanotubes with a larger diameter can be a better candidate for the adsorption of the CO molecules.

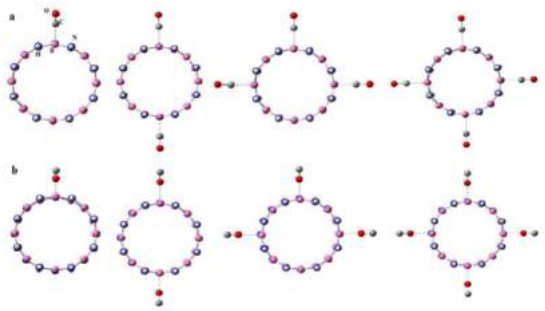

Fig. 1. Optimized structures for a and b configurations of (CO)n/(8,0) BNNT complexes, (n=1-4).

References

[1] Q. Weng, X. Wang, X. Wang, Y. Bando and D. Golberg. Chem. Soc. Rev., 2016, 45, 3989-4012.
[2] G. H. Fan, S. Zhu, X. K. Li, K. Ni and H. Xu. Comput. Theor. Chem., 2017, 1115, 208–216.
[3] M. B. Javan, A. Soltani, A. S. Ghasemi, E. T. Lemeski, N. Gholami and H. Balakheyli. Appl. Surf.Sci., 2017, 411, 1-10.
[4] E. Vessally, B. Dehbandi and L. Edjlali. Russ. J. Phys. Chem. A., 2016, 90, 1217-1223.
[5] M. Abdoli, H. Saeidian and A. Kakanejadifard, Comput. Theor. Chem., 2017, 1115, 323–329.
[6] M. Frisch, G. Trucks, H. B. Schlegel, G. Scuseria, M. Robb, J. Cheeseman, G. Scalmani, V. Barone, B. Mennucci and G. Petersson, Gaussian 09, Revision A. 02. Gaussian. Inc, Wallingford, 2009.
[7] A. E. Reed, L. A. Curtiss and F. Weinhold. Chem Rev., 1988, 88,899–926.

بیست و سومین کنفرانس شیمی فیزیک انجمن شیمی ایران
23rd ICS Physical Chemistry Conference
Chemistry Department,
Faculty of Science
Shahid Bahonar University of Kerman
Kerman, Iran
12-13 Jan 2022
ایران، کرمان
دانشگاه شهید باهنر کرمان
دانشکده علوم پایه، بخش شیمی
۲۳-۲۲ دی ماه ۱۴۰۰

Interaction of Tegafur drug with BN, AlN, and CN Nanotubes as drug delivery systems

Batoul Makiabadi[a]*, Mohammad Zakarianezhad

[a] *Department of Chemical Engineering, Sirjan University of Technology, Sirjan, Iran, bmakiabadi@yahoo.com*
[b] *Department of Chemistry, Payame Noor University, Tehran, Iran*

Abstract

In this work, the potential of BN, AlN, and CN nanotubes as the drug delivery systems of Tegafur (TG) was investigated by the density functional theory (DFT). The structural parameters, the interaction energies, and the electronic properties of formed complexes were evaluated. The strength of interactions in complexes was investigated using interaction energies, geometric parameters and topological properties.

Keywords: Drug delivery system; Interaction; Tegafur; Doped nanotubes; Electronic properties

I. Introduction

Cancers are a broad category of diseases that can affect any part of the body and involve abnormal cell growth to invade or spread to other parts of the body [1]. There are many types of cancer treatment. Nowadays, nanomaterials, as drug delivery systems, have attracted much attention due to their unique characteristics [2,3]. Researches show that nanotubes could deliver drugs to cancer cells without damaging target cells [4,5]. Tegafur (TG) is a chemotherapeutic prodrug of 5-fluorouracil (5-FU) used in the treatment of malignant tumors such as head and neck, breast, gallbladder, stomach, and colon cancers [6]. In this study, the structural. and electronic properties of pristine nanotubes complexed with Tegafur drug have been investigated as drug delivery systems

II. Methods

In this study, the pristine (5,5) BN, AlN, and CN nanotubes have been selected as a model. All structures were optimized at the level with M06-2X exchange functional and 6-31G(d) basis set using the Gaussian 09 software package [7]. The molecular descriptors such as the energy gap (Eg), the electronic chemical potential (μ), chemical hardness (η), chemical softness (S), electrophilicity index (ω) and the maximum amount of electronic charge of the system (ΔN_{max}) were evaluated. The NBO and AIM analysis was carried out at the M06-2X/6-31G(d) level of theory [8, 9].

III. Results and discussion

All the possible positions for the interaction of the TG molecule on BN, AlN, and CN nanotubes have been investigated (See Fig 1). The results reveals that the TG/AlNNT complexes are the most stable. The stability of the complexes is in the order of TG/AlNNT> TG/BNNT> TG/CNT. Thus, the interactions in TG/AlNNT nanotube are stronger than the TG/ BNNT and TG/CNT complexes. Also, the relative stability of

configurations decreases in the order A_{CN}> D_{CN}> C_{CN}> B_{CN}> for TG/CNT complexes and A_{BN}> D_{BN}> B_{BN}>C_{BN}> E_{BN} for TG/BNNT complexes and also A_{AlN}> B_{AlN}> C_{AlN}> D_{AlN}> E_{AlN} for TG/AlNNT complexes. To investigation of the electronic properties of TG/CNT, TG/BNNT and TG/AlNNT complexes, the HOMO–LUMO gap, electronic chemical potential (μe), hardness (η), softness (S), electrophilicity index (ω), work function, the Fermi level were calculated. The results show that the interaction of TG drug with nanotubes leads to a reduction in the energy gaps and an increase in the electrical conductivity of complexes compared to pristine nanotubes. The NBO analysis was performed to evaluate the charge transfer in complexes. Based on the NBO results, in TG/CNT, TG/BNNT, TG/AlNNT, the charge transfer takes place from TG to the nanotube. Based on the AIM analysis, the nature of interactions are electrostatic.

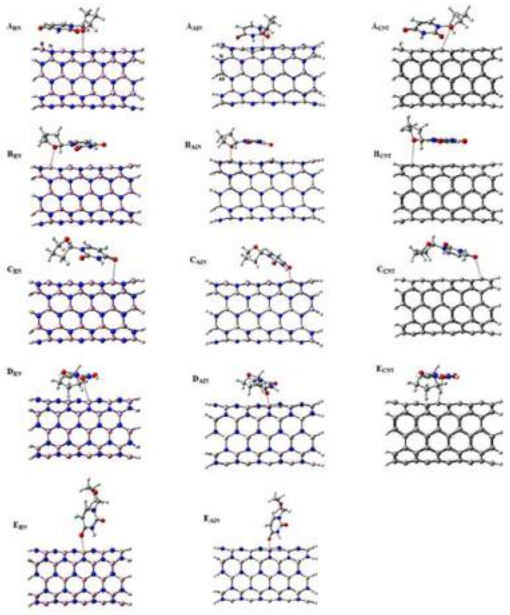

Fig. 1. Optimized structures for AlNNT, BNNT and CNT complexes.

IV. Conclusions

The results show that the tendency of TG drug for interaction with AlN nanotubes is the most. In all complexes, the most interaction energy is related to the A configuration. The results show that the intermolecular interactions in complexes are weak and of the Van der Waals type. Therefore, TG drug can physically be adsorbed on the surface of the nanotubes. The AlN and BN nanotubes are more suitable than CN nanotubes for carrying of Tegafur drugs. It seems that the selected nanotubes can be used as drug delivery systems for the transfer of TG drugs in living organisms.

References

[1] D. D. Ma and W. X. Yang. Oncotarget., 2016, 7, 40882–40903.
[2] C. Ding, and Z. Li Mater Sci Eng., 2017, 76,1440–1453
[3] H. Zhang, Y. Zhai, J. Wang and G. Zhai. Mater Sci Eng., 2016, 60, 560–568
[4] K. H. Son, J. H. Hong and J. W. Lee. Int J Nanomedicine., 2016, 11,5163–5185.
[5] C. D. Fahrenholtz, S. Ding, B. W. Bernish, M. L. Wright, Y. Zheng, M. Yang, X. Yao, G. L. Donati, M. D. Gross, U. Bierbach and R. Singh. J Inorg Biochem., 2016, 165,170–180.
[6] S. Chen, X. Z. Zhang, S. X. Cheng, R. X. Zhuo and Z. W. Gu Biomacromolecules., 2008, 9, 2578–2585.
[7] M. Frisch, G. Trucks, H. B. Schlegel, G. Scuseria, M. Robb, J. Cheeseman, G. Scalmani, V. Barone, B. Mennucci and G. Petersson, Gaussian 09, Revision A. 02. Gaussian. Inc, Wallingford, 2009.
[8] A. E. Reed, L. A. Curtiss and F. Weinhold. Chem Rev., 1988, 88,899–926.
[9] F. Biegler-König, J. Schönbohm and D. Bayles. J Comput Chem., 2001, 22, 545–559.

بیست و سومین کنفرانس شیمی فیزیک انجمن شیمی ایران
23rd ICS Physical Chemistry Conference
Chemistry Department,
Faculty of Science
Shahid Bahonar University of Kerman
Kerman, Iran
12-13 Jan 2022
ایران، کرمان
دانشگاه شهید باهنر کرمان
دانشکده علوم پایه، بخش شیمی
۲۳-۲۲ دی ماه ۱۴۰۰

Implementation of analogy method to enhance students' chemistry self-regulated learning skills

Elahe Keshavarz[a,*]

[a] *Department of Sciences, University of Farhangian, Tehran, Iran, keshavarz@cfu.ac.ir*

Abstract

The aim of this research was to investigate the effect of analogy method compared to traditionally designed chemistry instruction method on students' self-regulated learning skills. Participants were 80 Students fron Farhangian University. Two experimental groups were randomly selected. Motivated Strategies for Learning Questionnaire (MSLQ) were administered to both groups as pretest and posttest to determine students' self-regulated learning skills. The results showed that the analogy method was superior to the traditionally method on students' chemistry self-regulated learning skills.

Keywords: Analogy method; Chemistry concept; Self-regulated, MSLQ.

I. Introduction

Chemistry is one of the fields that learners have difficulties in learning. Expert teachers have introduced some appropriate strategies, such as analogy, to simplify comprehension of abstract concepts [1].

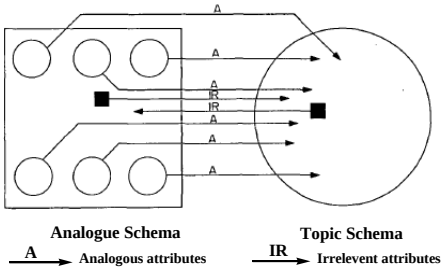

Fig. 1. The transfer of the analogous and the irrelevant attributes between the analogue schema and the topic schema [2].

An analogy is a system of relations between parts of the structure of two domains: the analogue and the target.

The analogue domain, also called the source or base domain, is a domain that exists in memory, from which the analogy is drawn. The target domain contains the scientific concept. An analogy involves the transfer of relational information from the analogue to the target (Fig. 1), which consists of finding the correspondences between the two systems [3].

Previous research studies suggested some instructional models for teaching with analogies. The FAR guide (Focus, Action, and Reflection) (table 1) is one of the most common models used in analogy learning in science [4]. In the Focus phase, the scientific concept and student familiarity with the analogue are considered. In the Action phase, students experience the analogical model and identify the similarities and differences of the analogue and the target concepts. In the Reflection phase the instructor reflects upon the clarity, and the conclusions drawn from the analogue.

Table 1 The three phases in the FAR guide model (Venville, 2008; Davis, 2013)

Focus phase	**Pre-lesson planning**
Concept	Is the concept difficult or abstract?
	What is difficult about the concept?
Students	What ideas do students currently have about the concept?
Experience	What familiar experiences do students have that I can use?

Action phase	In-lesson action
Similarities	Cue the student memory of the analogy
	Discuss ways in which the analogue is like the target
	Are there surface features or deep relations?
Differences	Discuss ways in which the analogue is unlike the target
Summary	Conclude by summarising the outcomes of using the analogy
Reflection phase	**Post-lesson reflection**
Conclusions	Was the analogy clear and useful, or confusing?
Improvements	What changes are needed for the following lesson?
	What changes are needed the next time I use this analogy?

The aim of this research was to investigate and compare the effect of analogy method and traditionally designed chemistry instruction method to enhancing university students' self-regulated learning skills.

II. Methods

The research method was quasi-experimental with pretest and posttest design. The statistical population included all students in the lesson of science education of Farhangian University of Guilan and the sample size was 80 students who were randomly assigned to girls and boys groups and some concepts of chemistry were trained by traditional and analogy methods. A screening test was used to select the sample and a MSLQ questionnaire was used to collect information. The validity and the reliability of the questionnaires was obtained through content and face validity, and using Cronbach's alpha, respectively.

III. Results and discussion

Self-regulatory is a complex process desiring a combination of metacognition, motivation and learning behaviors. Self-regulated students are aware of the need for using different learning strategies for different learning times [5].

It was found in this research that the students in the analogy method was better in self-regulated *learning strategies* which make learning more important than the grades received by students in traditional method group. On the other hand, there is no significant relationship between the effect of analogy education and *motivational beliefs* of self-regulated strategies.

IV. Conclusions

Due to the difficulty of chemistry concepts, current and conventional training has not been effective. Analogy method with exploratory and active basis allow the teachers to perform their facilitative role. The effectiveness of analogy can be tested with different chemistry topics. Also, Similar studies can be conducted in different types of universities and with a larger sample size.

References

[1] M. E. Gray and K. J. Holyoak, Mind, Brain, and Educ., 2021,15, 250-263.

[2] H. H. Zeitoun, Resrarch in Science & Technological Education, 1984, 2, 107-125.

[3] P. Sarantopoulos and G. Tsaparlis, Chem. Educ. Res. Pract., 2004, 5, 33–50.

[4] A. G. Harrison and R. K. Coll, Using analogies in middle and secondary science classrooms: The far guide–an interesting way to teach with analogies, 2007, CA: SAGE Publications.

[5] K.-A. Cansel and U.-K. Esen, Chem. Educ. Res. Pract., 2021, 22, 12-29.

بیست و سومین کنفرانس شیمی فیزیک انجمن شیمی ایران
23rd ICS Physical Chemistry Conference
Chemistry Department,
Faculty of Science
Shahid Bahonar University of Kerman
Kerman, Iran
12-13 Jan 2022
ایران، کرمان
دانشگاه شهید باهنر کرمان
دانشکده علوم پایه، بخش شیمی
۲۳-۲۲ دی ماه ۱۴۰۰

Thermodynamic Study of ZnO/SBA-16 as Drug Delivery System

Mohammad Hossein Fekri[a], Samaneh Soleymani[b,*], Maryam Razavi Mehr[c]

[a] *Department of Chemistry, Faculty of Basic Sciences, Ayatollah Borujerdi University, Borujerd, Iran; E-mail :Fekri188@gmail.com*

[b] *Department of Chemistry, Faculty of Basic Sciences, Ayatollah Borujerdi University, Borujerd, Iran; Tel: 09168622312; E-mail: samanesoleymani1988@gmail.com*

[c] *Department of Chemistry, Faculty of Basic Sciences, Ayatollah Borujerdi University, Borujerd, Iran; E-mail :ma.razavimehr@gmail.com*

Abstract

In this work, the thermodynamic parameters related to the loading of temozolomide drug on ZnO/SBA-16 nanocomposite were studied. Thermodynamic factors were computed for comprehend the loading process. The thermodynamic parameters ΔH°, ΔS°, and ΔG° were studied and evaluated at three temperatures of 30, 50 and 70 ℃. The results showed that drug loading is an exothermic and spontaneous process.

Keywords: ZnO/SBA-16; Temozolomide; Drug loading; Drug delivery system; Thermodynamic parameters

I. I. Introduction

The science of nanotechnology in the pharmaceutical industry very promising, because with the use of modern drug delivery systems, drugs can be much stronger and more effective. The design and construction of controlled drug release systems can be very useful in the management of drug treatment methods. So far, many substances have been introduced as drug delivery systems, of which mesoporous material is one. Mesoporous materials have been widely used in various fields, including medicine, due to their unique properties such as high surface-to-volume ratio, controllable pores size, as well as biocompatibility and biodegradability [1]. Among the mesoporous materials, SBA-16 was quickly noticed due to its desirable surface properties. SBA-16 is a group of three-dimensional silicate porous materials including Sio_2 groups and surface hydroxyl groups prepared using non-ionic copolymers. This composition has a cubic structure and belongs to the Im3m space group.

II. Methods

In this study, ZnO/SBA-16 nanocomposite was synthesized using post-synthesis method. The nanocomposite was then identified by XRD technique. After confirming the correctness of the synthesized structure, temozolomide was loaded on ZnO/SBA-16 nanocomposite and thermodynamic parameters were studied.

III. Results and discussion

Figure 1 shows the X-ray diffraction pattern of ZnO/SBA-16 nanocomposites. A peak is observed in the range of 2θ=23 with relatively low intensity.

The values of ΔH^0 and ΔS^0 were reached from the data of $\ln K_c$ versus 1/T (Fig. 2).

The outcomes are summarized in table 1. ΔH°, ΔS°, and ΔG° values have been determined as negative for studied three temperatures 30, 50, and 70 ^{o}C. The negative values of ΔG° display that the adsorption process onto the nanocarrier is spontaneous. It can be seen ΔG° values turn out to be extra positive with the increasing of temperature so, the increasing temperature isn't always desired in the adsorption process. The negative values of ΔH° indicated that the adsorption of TMZ onto the nanocarrier is an exothermic process [2,3]. The ΔS° values play a vital function in reflecting whether the order of adsorbate throughout the adsorption process will become less random ΔS°<0 or more random ΔS° > 0. Furthermore, negative the ΔS° value includes reducing in the degree of freedom of TMZ drug inside the solution. Additionally, the sign of ΔS° suggests whether or not the adsorption reaction is an associative or dissociative process. So, due to the fact ΔS°, has a negative cost, it is able to be an associative mechanism [4]. According to the value ΔH°, the adsorption between the drug and nanocarrier could be categorized as physical adsorption. Physical adsorption is based on weak reactions between the adsorbate and the surface sites of the adsorbent.

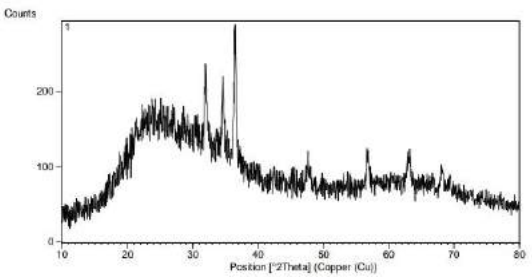

Fig. 1. X-ray diffraction pattern

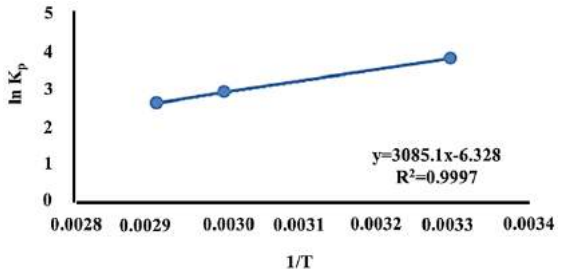

Fig. 2. Relationship between thermodynamic constants and temperature of TMZ onto nanocarrier.

Table 1. Thermodynamic parameters for the adsorption of TMZ drug onto "ZnO/SBA-16" at different temperatures (C_0= 10 mg L^{-1}).

Temperature (K)	Ln K_c	ΔH° (kJ. mol^{-1})	ΔS° (kJ. mol^{-1})	ΔG° (kJ. mol^{-1})	R^2
303	3.85	-25.64	-0.05261	-9.70	0.999
323	2.94			-8.65	
343	2.64			-7.6	

IV. Conclusions

The study was performed to determine the thermodynamic parameters of ZnO/SBA-16 nanocomposite as the drug delivery system of temozolomide. The ZnO/SBA-16 nanocomposite was successfully synthesized by the post- synthesis method. Thermodynamic studies showed that the drug loading process is exothermic and spontanrous.

References

[1] Poonia E., Dahiya M.S., Kumar S., Duhan S. Humidity sensing behavior of tin-loaded 3-D cubic mesoporous silica, *Physica E: Low-Dimensional Systems and Nanostructures.*, 2018, *101*: 284–293.

[2] M.H. Fekri, M. Banimahd Keivani, M. Razavi Mehr and B. Akbari-adergani, *J. Mazandaran Univ. Med. Sci.*, 2019, 29, 166.

[3] M.H. Fekri, M. Banimahd keivani, M. Darvishpour and H. Banimahd keivani, *Journal of Physical and Theoretical Chemistry*, 2012, 9,95.

[4] B.H. Aregawi and A.A. Mengistie, *Bulletin of the Chemical Society of Ethiopia*, 2013, 27, 35.

بیست و سومین کنفرانس شیمی فیزیک انجمن شیمی ایران
23rd ICS Physical Chemistry Conference
Chemistry Department,
Faculty of Science
Shahid Bahonar University of Kerman
Kerman, Iran
12-13 Jan 2022
ایران، کرمان
دانشگاه شهید باهنر کرمان
دانشکده علوم پایه، بخش شیمی
۲۳-۲۲ دی ماه ۱۴۰۰

Preparation of magnetic hydrogel based membrane using PVDF/Activated carbon/Fe3O4

Ensieh Ghasemian[a]*, Abolfazl Azimi

[a] *Department of Chemistry, Faculty of Science, Ilam university, Ilam,, Iran, e.ghasemian@ilam.ac.ir*

Abstract

In the present work, we try to prepare hydrogel-based film with PVDF, activated carbon, and Fe_3O_4 magnetic nanoparticles. incorporating of magnetic nano particles improved recovery capability of membrane. The prepared film is characterized by the thermal gravimetric analysis (TGA), Fourier transforms infrared spectroscopy (FT-IR), and N_2 adsorption desorption isotherm.

Keywords: magnetic; hydrogel; activated carbon; film.

I. Introduction

Among the chemical compounds, hydrogel are a group of materials carriers with outstanding applications [1,2]. Hydrogels are an important class of materials whose interaction with the guest molecule is based on non- covalent interactions [2,3]. Due to their special interactions with guest molecules, this class of materials can alter their morphology, structure, or performance in response to some stimuli such as temperature, pH, light, enzyme, and inhibitory factors [4].

II. Methods

In the first step, a solution contain 1.5 g polymer in 50 ml DMF was prepared. Due to the low solubility of the polymer in water, the solution was stirred for 10 hours and then sonicated for 30 min. Then 4 g of activated carbon was slowly added to it. The mixture was stirred for one hour to obtain a uniform solution. In the next step, the solution containing the polymer and activated carbon is gently mixed together and then casted into the petri dish to form a membrane and evaporate the solvent. Activated carbon with magnetic properties have been prepared by chemical synthesis of Fe3O4 in reflux condition.

III. Results and discussion

Thermal gravimetry analysis for PVDF/Activated carbon/Fe3O4 film are shown in Figure 1. As can be seen from Figure 1, chitosan showed two decomposition main stages. The first stage of decomposition (wt% 3.91) observed at 100 °C cause to the water loss. The other main stage at 220°C with a maximum of 485°C and 70% weight loss due to polymer decomposition and dissociation of the polymer chain. after protonation.

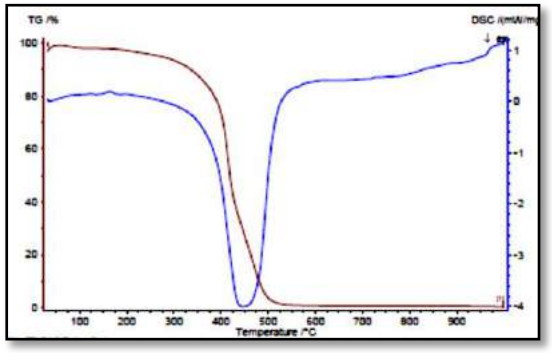

Fig. 1. Tga/dsc of PVDF/Activated carbon/Fe3O4.

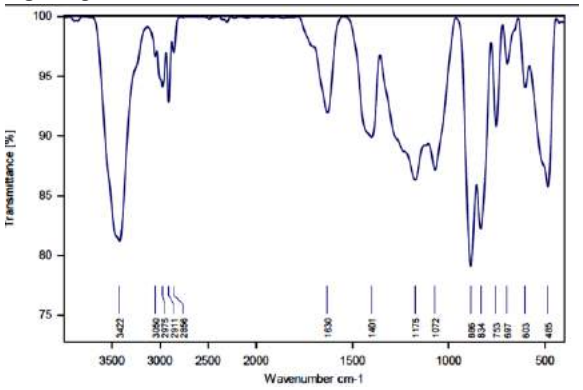

Fig. 2 FT-IR spectrum of the prepared PVDF/AC/Fe_3O_4 film

IV. Conclusions

This study assessed the prepared of PVDF based film using chemical method. The results indicated the formation of the magnetic film with proper porosity.

Investigation of the performance of the film have been confirmed by FTIR and TGA/DSC under air atmosphere conditions.

The spectrum of the PVDF/AC/Fe_3O_4 film is also shown in Figure 2. The intensity of peaks in regions 3100-3500 cm^{-1} reduced due to the interaction between surface activated carbon group and PVDF functional groups. Furthermore the characteristic peak at 1413 cm-1 attributed to the pyrrolidinyl group present in PVDF. In general, the position and intensity of the peaks do not change significantly in PVDF/AC/Fe_3O_4film. This small change can also be attributed to the interaction of the two polymers.

REFERENCES:

1. Turner RJ. Metal-Based Antimicrobial Strategies. *Microb. Biotechnol.* **2017**; *10*(5): 1062-5. DOI:10.1111/1751-7915.12785.
2. Lemir J, Harrison J, Turner R. Antimicrobial Activity of Metals: Mechanisms, Molecular Targets and Applications. *Nat. Rev. Microbiol.* **2013**; 11:371–84. DOI:10.1038/nrmicro3028.
3. 3. Azizi-Lalabadi M, Ehsani A, Divband B, Alizadeh Sani M. Antimicrobial Activity Of Titanium Dioxide and Zinc Oxide Nanoparticles Supported in 4A Zeolite and Evaluation The Morphological Characteristic. *Sci. Rep.* **2019**; *9*: 17439-49. DOI:10.1038/s41598-019-54025-0.
4. Tang S, Zheng J. Antibacterial Activity of Silver Nanoparticles: Structural Effects. *Adv. Healthcare. Mater.* **2018**; *7*(13): 1701503. DOI:10.1002/adhm.201701.

بیست و سومین کنفرانس شیمی فیزیک انجمن شیمی ایران
23rd ICS Physical Chemistry Conference
Chemistry Department,
Faculty of Science
Shahid Bahonar University of Kerman
Kerman, Iran
12-13 Jan 2022
ایران، کرمان
دانشگاه شهید باهنر کرمان
دانشکده علوم پایه، بخش شیمی
۲۳-۲۲ دی ماه ۱۴۰۰

Molecular Dynamics Study of the Graphene/Ionic Liquid Interface

Maryam Hamzeh Jouneghani*., Masumeh Foroutan

Department of Physical Chemistry, University of Tehran, Tehran, Iran, mrymhamzeh@ut.ac.ir

Abstract:

The results of classical molecular dynamics simulations on the behavior and properties of the ionic liquid 1-n-butyl-3-methylimidazolium hexafluorophosphate, a widely studied ionic liquid, and carbon nanostructures are reported in this work. The simulation results showed that the orientation of the ions near the substrate is such that it shows a non-wettability state of ionic liquid droplet on the graphene substrate.

Keywords: Ionic liquid**,** Contact angle, Molecular dynamics simulation

I. Introduction

Ionic liquids (ILs) are low melting point salts that are typically fluid below 100 °C. They often consist of an organic cation and a smaller anion .ILs can have many unique properties such as low vapor pressure, large liquid phase range, and non-flammability. These properties have stimulated extensive studies of ILs due to their promise for a number of technical applications (1).The use and applications of ionic liquids have traversed many areas of chemistry and biochemistry (2). Due to their no volatility, thermal stability, and recyclability, ionic liquids are classified as green solvents (3). Compared with traditional organic solvents, ILs are environmentally benign and designable. There are many combinations of different cations and anions, so one can design a specific ionic liquid for a specific application, which delivers an attractive feature to both academic institutes and industrial societies (4).

Although surface behavior of ionic liquids on graphene have been studied both using experimental and computational approaches (5), the characterization of liquid−surface interaction through contact angle measurements have so far been the subject of a reduced number of studies.

Molecular dynamics (MD) simulations are useful in the analysis of interactions at atomic detail. Classical MD simulations have been widely used to study the wetting properties of different solid surfaces since the pioneer work of Rahman and Stillinger (6). Although quantum mechanical calculations are more precise compared to MD simulation, they are limited to the system size.

II. Methods

The software package LAMMPS was used for MD simulation in this work. [BMIM][PF6] ionic liquid and carbon nanostructures were modeled according to the force field parametrization reported in Ref 7.The system represented with 2D periodic boundary conditions and the cutoff radius of non-bonded interactions was set to 12 Å. The system equilibrated at 300 K controlled with the Nose‒́ Hoover thermostat in the NVT ensemble.

III. Results and discussion

To investigate the wettability behavior of an ionic liquid droplet on a graphene substrate, the contact angle of ionic liquid droplet has been calculated. According to the results, little adhesion was observed at the graphene-ionic liquid interface.

IV. Conclusions

Using classical molecular dynamic simulations, we studied the structure of the IL/Graphene interfaces, The distribution of orientations of cations and anions at the graphene surface Refers to a non-wettability state of ionic liquid droplet.

References:

[1] M. Earle, K. Seddon, Pure Appl. Chem. 2000, 72, 1391.
[2] J. Anderson, D. Armstrong, Anal. Chem. 2003, 75, 4851.
[3] J. Wilkes, J. Mol. Catal. A: Chem, 2004, 214, 11.
[4] H. Shirota, E. Castner , J. Phys. Chem. B 2005, 109, 21576.
[5] M. Vijayakumar, B. Schwenzer, V. Shutthanandan, J. Hu, J. Liu, I. Aksay, Nano Energy 2014, 3, 152.
[6] A. Rahman, F. Stillinger, J. Chem. Phys. 1971, 55, 3336.
[7] B. Doherty; X. Zhong, S. Gathiaka, B. Li, O. Acevedo, J. Chem. Theory Comput. 2017, 13, 6131.

بیست و سومین کنفرانس شیمی فیزیک انجمن شیمی ایران
23rd ICS Physical Chemistry Conference
Chemistry Department,
Faculty of Science
Shahid Bahonar University of Kerman
Kerman, Iran
12-13 Jan 2022
ایران، کرمان
دانشگاه شهید باهنر کرمان
دانشکده علوم پایه، بخش شیمی
۲۳-۲۲ دی ماه ۱۴۰۰

Thermodynamic evaluation of the effect of Cu^{2+} ion on the interaction of Ribavirin drug with BSA

Saba Hadidi*

Department of Inorganic Chemistry, Faculty of Chemistry, Razi University, Kermanshah, Iran, s.hadidi@razi.ac.ir

Abstract

In this study, the effect of Cu^{2+} ion on the interaction between bovine serum albumin (BSA) and Ribavirin drug (Rib) was investigated by fluorescence spectroscopy. The negative sign of free energy (ΔG) confirmed that Rib-BSA reaction is spontaneous both in the absence and presence of Cu^{2+} ions. The positive values for ΔH and ΔS indicated that hydrophobic interactions play major roles in Rib-BSA association in the absence of Cu^{2+} ion, while in the presence of Cu^{2+} ion, it is the electrostatic interaction that play essential role in the binding process.

Keywords: Thermodynamic parameters; Ribavirin drug; BSA interaction; Copper ion; Hydrophobic interaction; Electrostatic force.

I. Introduction

Ribavirin, is an antiviral medication used to treat RSV infection, hepatitis C and some viral hemorrhagic fevers. It is known that the distribution, free concentration and the metabolism of various drugs are strongly affected by drug-protein interactions in the blood stream [1]. The molecular interactions are often monitored by spectroscopic techniques because these methods are sensitive and relatively easy to use. Among them, fluorescence spectroscopy is an appropriate method to determine both the binding and thermodynamic parameters, which characterize the main forces in the association reaction between drug and protein.

II. Methods

The stock solutions of BSA (1×10^{-4} M) and Ribavirin (1×10^{-3} M) were prepared in 0.1 M phosphate buffer at pH 7.4. Fluorescence measurements were performed on JASCO spectrofluorimeter Model FP-6200 by keeping the concentration of BSA constant (5×10^{-6} M) while varying the Ribavirin concentration from 0.0 to 1.3×10^{-4} M. To investigate Cu^{2+} ion effect, a 2 mL solution containing 5×10^{-6} M of BSA and 1.4×10^{-4} M of Cu^{2+} ion was titrated by different aliquots of Ribavirin solution (0.0 to 1.3×10^{-4} M) at different temperatures (288, 298, 310) in the wavelength range of 300-500 nm with exciting wavelength at 295 nm.

III. Results and discussion

The fluorescence spectra of BSA in the absence and presence of Cu^{2+} ion with varying concentrations of Ribavirin is shown in Fig. 1. As can be seen, BSA fluorescence intensity decreased gradually with the addition of Ribavirin with or without Cu^{2+} ion, but the decrease in the emission intensity in the absence of Cu^{2+} ion is higher.

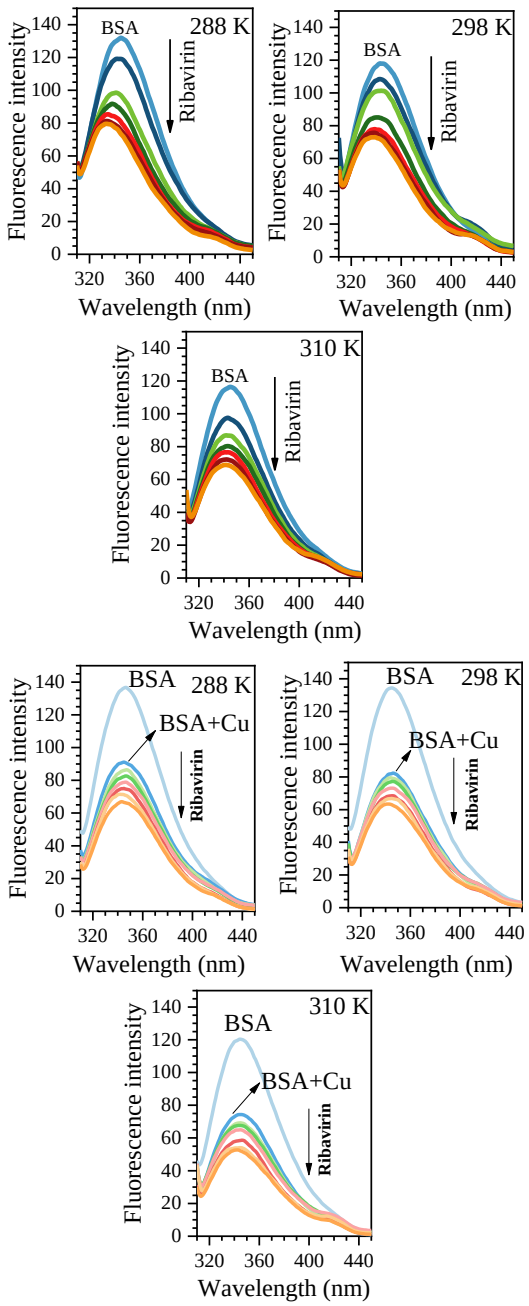

Fig. 1. Fluorescence emission spectra of BSA with Ribavirin concentration increasing in the absence and presence of Cu^{2+} ion

In order to estimate the intrinsic binding constant (K_b) the fluorescence data were analyzed using following equation and results summarized in Table 1.

$$Log\left(\frac{F_0 - F}{F}\right) = LogK_b + nLog[Q]$$

It is found that K_b decreases in the presence of Cu^{2+} ion. The thermodynamic parameters were estimated from the following relationship:

$$\Delta G = -RTLnK_b = \Delta H - T\Delta S$$

The negative sign of ΔG values supported the assertion that all binding processes are spontaneous. According to the positive sign of enthalpy and entropy change the hydrophobic interaction played an absolutely key role in the binding of Ribavirin to BSA in the absence of Cu^{2+} ion, while in the presence of Cu^{2+} ion, it is the electrostatic interaction that play essential role in the binding process [2].

Table 1 The binding and thermodynamic parameters for Ribavirin interaction with BSA

In the absence of Cu^{2+}			
T (K)	**288**	**298**	**310**
K_b (L mol^{-1})	1.5×10^4	2.3×10^4	3.3×10^4
ΔG (kJ mol^{-1})	-23.1	-24.9	-26.8
ΔH (kJ mol^{-1})	25.4		
ΔS (J mol^{-1} K^{-1})	168		
In the presence of Cu^2			
K_b (L mol^{-1})	7.1×10^3	6.2×10^3	4.6×10^3
ΔG (kJ mol^{-1})	-21.2	-21.6	-21.7
ΔH (kJ mol^{-1})	-14.9		
ΔS (J mol^{-1} K^{-1})	22		

IV. Conclusions

It was found that the presence of Cu^{2+} ion decreased the binding constants of Rib-BSA complex. Also, the main interaction force in the binding of Ribavirin to BSA was different in the absence (hydrophobic) and presence (electrostatic) of Cu^{2+} ion.

References

[1] J. Chen, X.Y. Jiang, X. Q. Chen, and Y. Chen, J. Mol. Struct., 2008, 876, 121-126.
[2] N. Shahabadi, F. Shiri, S. Hadidi, K. Farshadfar, M. Darbemamieh, and S. M. Roe, J. Mol. Liq., 2021, 335, 116290.

بیست و سومین کنفرانس شیمی فیزیک انجمن شیمی ایران
23rd ICS Physical Chemistry Conference
Chemistry Department,
Faculty of Science
Shahid Bahonar University of Kerman
Kerman, Iran
12-13 Jan 2022
ایران، کرمان
دانشگاه شهید باهنر کرمان
دانشکده علوم پایه، بخش شیمی
۲۳-۲۲ دی ماه ۱۴۰۰

Synthesis of a modified mesoporous silica for the targeted delivery of Quercetin in Buffer solution (pH=5.3)

Mahsa Mirzaei[a], Seyed Yousef Ebrahimipour[a,*], Maryam Mohamadinejad[b] Tayebeh Shamspour[a], Fatemeh Mehrabi[a]

[a] *Department of Chemistry, Shahid Bahonar University of Kerman, mahsa.mirzaee740@gmail.com*
[a] *Department of Chemistry, Shahid Bahonar University of Kerman, Ebrahimipoor@uk.ac.ir*
[b] *Pistachio Safety Research Center, Rafsanjan University of Medical Sciences, Rafsanjan, Iran, m.mohamadi@rums.ac.ir*
[a] *Department of Chemistry, Shahid Bahonar University of Kerman, tsh@uk.ac.ir*
[a] *Department of Chemistry, Shahid Bahonar University of Kerman, f_mehrabi2010@yahoo.com*

Abstract

In this work mesoporous silica was functionalized with (3-aminopropyl) triethoxysilane (APTES) as the carrier for anti-cancer drug Quercetin. The sample of nano carrier-drug complex was described by BET and an in-vitro drug release test. The release index of the aminopropyl-modified nano carrier exhibited release of Quercetin in applied media. Tests performed in Buffer solution (pH = 5.4) showed the best pharmaceutical availability.

Keywords: Mesoporous silica; Drug delivery; APTES; Quercetin; BET

I. Introduction

Today, intensive studies are underway to increase the use of ordered mesoporous materials in controlled drug delivery systems [1,2]. Release rate is a problem that may be solved by using mesoporous silica in drug delivery. Mesoporous materials are biocompatible, non-toxic and have adjustable pore size and structure, which makes them very attractive as drug carriers [1,2,3]. The aim of this study was to synthesize amino functionalized mesoporous silica and to investigate their potential application in Quercetin uptake and release [4].

II. Methods

First of all SBA-15 was synthesised by using a standard technique discovered by Zhao et al [5]. In the following step Surface functionalization Of SBA15 by APTES was applied by refelux [4,6]. Then loading of Quercetin in to the synthesised mesoporous was done by DMSO. In vitro degradation tests were performed to predict the in-vivo degradation patterns of MSNs. In this experiment, (0.001g) of mesoporous/TEOS/APTES/Quercetin was implanted in a dialysis tube. Then the tube put into 20 ml of phosphate buffer (pH=5.4), whereas the temperature was maintained at 37±3°C. In different time intervals (from 5-360 min), 2 ml of the buffer solution was withdrawn and replaced by 2 ml fresh buffer (in order to maintain a constant volume).

III. Results and discussion

The average size of the pore was obtained 7(nm) with BET analysis. The total pore volume (V total) was estimated from the amount of nitrogen adsorbed at a relative pressure of 0.99 (Fig. 1). Then The release

profile of Quercetin from the proposed mesoporous material was examined in different time intervals. According to Eq. (1) the loading percentage was calculated (Fig. 2):

$$\%\text{Release}=\frac{Weight\ of\ drug\ in\ solution}{Weight\ of\ drug\ in\ of\ Nano\ carrier}\times 100 \quad \text{Eq.(1)}$$

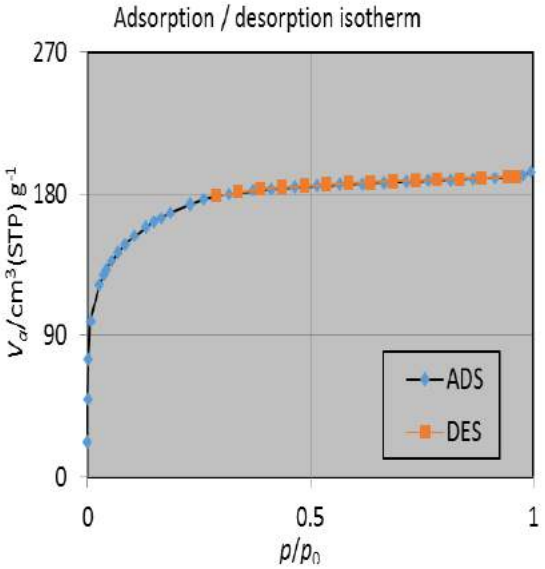

Fig. 1. Nitrogen adsorption–desorption isotherm of mesoporous silica/TEOS/APTE

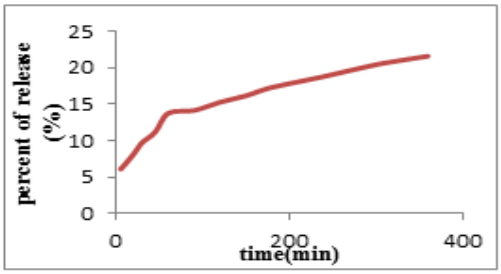

Fig. 2. The Quercetin release profile of Nano carrier**.**

IV. Conclusions

In the present study, the mesoporous silica nanocomposite was selected as host matrix for controlled drug delivery and its surface modified with polar groups (–NH2). Not only, the in-vitro results are very promising, but also more investigations are required to delineate the mechanism of action, toxicity, stability, and administration rout of the prepared formulation. In this case, the drug molecules are attached and adsorbed to the active parts of the mesoporous materials. In addition to drug release is well-done. Such a development would increase the clinical use of Quercetin.

References

[1] B. Murugan, L. Narashimhan Ramana, S. Gandhi, S. Sethuraman and U. M. Krishnan, J. Mater. Chem. B, 2013, 1, 3494–3505.
[2] L. Pasqua, F. Testa, R. Aiello, S. Cundari and J. B. Nagy, Microporous Mesoporous Mater, 2007, 103, 166–173.
[3] J. Gu, W. Fan, A. Shimojima and T. Okubo, Small, 2007, 3, 1740–1744.
[4] S. Hao, H. Chang, Q. Xiao, Y. Zhong, W. Zhu, J. Phys. Chem. C, 2011, 115, 12873-12882.
[5] Z. Zhou, S. Zhu and D. Zhang, J. Mater, Chem., 2007, 17, 2428–2433.
[6] Hall, S. R.; Fowler, C. E.; Lebeau, B.; Mann, S. Chem. Commun, 1999, 201–202.

بیست و سومین کنفرانس شیمی فیزیک انجمن شیمی ایران
23rd ICS Physical Chemistry Conference
Chemistry Department,
Faculty of Science
Shahid Bahonar University of Kerman
Kerman, Iran
12-13 Jan 2022
ایران، کرمان
دانشگاه شهید باهنر کرمان
دانشکده علوم پایه، بخش شیمی
۲۳-۲۲ دی ماه ۱۴۰۰

Effect of temperature and copper ion on Guaifenesin-DNA interaction: Calculation of thermodynamic parameters

Saba Hadidi*

Department of Inorganic Chemistry, Faculty of Chemistry, Razi University, Kermanshah, Iran, s.hadidi@razi.ac.ir

Abstract

In this study, the effect of temperature and Cu^{2+} ion on the interaction of Guaifenesin (Gua) with DNA was investigated. The binding constant increases with the increasing of temperature, shows that the temperature has a positive effect on binding reaction. Except for the temperature of 288 K, there was no significant difference between binding constants in the absence and in the presence of Cu^{2+} ion. The negative values of ΔG confirmed that all binding processes are spontaneous. Both ΔH and ΔS of the association reaction between DNA and Guaifenesin are positive, which confirmed hydrophobic interaction during binding process.

Keywords: DNA interaction; Guaifenesin drug; Effect of temperature; Copper ion; Thermodynamic parameters; Hydrophobic interaction.

I. Introduction

Guaifenesin is a medication used as an expectorant, intended to help cough out phlegm from the airways. DNA plays an important role in the life process because it carries heritage information. Studies on the binding mechanism of some small molecules with DNA have been identified as one of the key topics during the past few decades and it is of great help to understand the action mechanism of some drugs, and therefore, to design new and more efficient DNA targeted drugs to deal with genetic diseases [1].

II. Methods

Fluorescence measurements were performed on JASCO spectrofluorimeter by keeping the concentration of Guaifenesin constant (2.5×10^{-6} M) while varying DNA concentration from 0.0 to 1.3×10^{-4} M. To investigate Cu^{2+} ion effect, a 2 mL solution containing 2.5×10^{-6} M of Guaifenesin and 1.6×10^{-4} M of Cu^{2+} ion was titrated by different aliquots of DNA solution (0.0 to 1.3×10^{-4} M) at different temperatures (278, 283, 288) in the wavelength range of 270-425 nm with exciting wavelength at 270 nm.

III. Results and discussion

Fluorescence spectra of Guaifenesin were recorded in the presence of various amounts of DNA. As shown in Fig. 1, on increasing the concentration of DNA there is a gradual quenching of the fluorescence intensity both in the presence and in the absence of Cu^{2+} ion, which is direct evidence of the interaction between Guaifenesin and DNA. To investigate the effect of Cu^{2+} ion on the interaction process, the binding constants (K_b) were calculated from the following equation:

$$Log\left(\frac{F_0 - F}{F}\right) = LogK_b + nLog[Q]$$

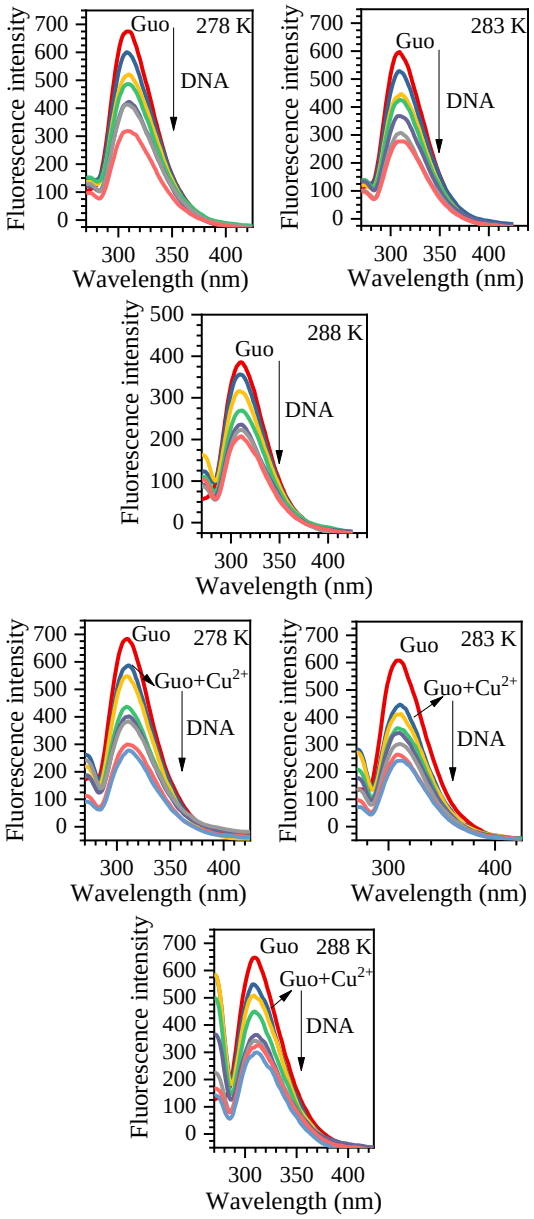

Fig. 1. Fluorescence emission spectra of Guaifenesin with DNA concentration increasing in the absence and presence of Cu^{2+} ion

It is found that the binding constant increases with the increasing of temperature, which shows that the temperature has a positive effect on Gua-DNA binding reaction. On the other hand, except for the temperature of 288 K, there was no significant difference between binding constants in the absence and in the presence of Cu^{2+} ion. The thermodynamic parameters were calculated from the following relationship:

$$\Delta G = -RTLnK_b = \Delta H - T\Delta S$$

The negative values of ΔG confirmed that all binding processes are spontaneous. Both ΔH and ΔS of the association reaction between DNA and Guaifenesin are positive, which confirmed hydrophobic interaction during binding process [2].

Table 1 The binding and thermodynamic parameters for Guaifenesin interaction with DNA

In the absence of Cu^{2+}			
T (K)	**278**	**283**	**288**
K_b (L mol^{-1})	2.7×10^4	4.1×10^4	1.6×10^5
ΔG (kJ mol^{-1})	-23.6	-24.9	-28.6
ΔH (kJ mol^{-1})	116.4		
ΔS (J mol^{-1} K^{-1})	502		
In the presence of Cu^2			
K_b (L mol^{-1})	2.6×10^4	4.4×10^4	7.9×10^4
ΔG (kJ mol^{-1})	-23.5	-25.2	-27.1
ΔH (kJ mol^{-1})	74.5		
ΔS (J mol^{-1} K^{-1})	352		

IV. Conclusions

In general, it was concluded that unlike Cu^{2+} ions, which did not have a significant effect on the interaction process, the increase in temperature had a positive effect. Also, hydrophobic interactions were identified as the main forces in the formation of Gua-DNA complex.

References

[1] A. Aggarwal, S. Naskar, A.K. Sahoo, S. Mogurampelly, A. Garai, P.K. Maiti, Curr. Opin. Struct. Biol., 2020, 64, 42-50.

[2] N. Shahabadi, F. Shiri, S. Hadidi, K. Farshadfar, S. Sajadimajd, and S. M. Roe, Spectrochim. Acta A, 2020, 235, 118280.

بیست و سومین کنفرانس شیمی فیزیک انجمن شیمی ایران
23rd ICS Physical Chemistry Conference
Chemistry Department,
Faculty of Science
Shahid Bahonar University of Kerman
Kerman, Iran
12-13 Jan 2022
ایران، کرمان
دانشگاه شهید باهنر کرمان
دانشکده علوم پایه، بخش شیمی
۲۳-۲۲ دی ماه ۱۴۰۰

Adsorption of commonly drug from aqueous solution by natural and modified zeolite

Yasaman Khaksarfard*, Ahmad Bagheri

Department of Chemistry, Semnan University, P.O. Box 35131-1911, Semnan, Iran

Abstract

This paper describes studies of evaluating natural and surface modification of a clinoptilolite zeolite with cetyltrimethyl ammonium chloride (CTAC), to investigate the adsorption efficiency for the removal of commonly drug from aqueous solution at bench scale. Modification of the zeolite with cationic surfactant (named ZMS) was based on the external cation exchange capacity.

Keywords: Zeolite; Clinoptilolite; Surfactant; Drug removal.

I. Introduction

In the last decade, presence of pharmaceuticals, typically at concentration levels of ng/L to µg/L, have been reported in the water cycle, including surface waters, groundwater, wastewater, and to a lesser volume, drinking water [1]. Diclofenac belongs to the family of non-steroidal anti-inflammatory drugs (NSAID) or cyclo-oxygenase (COX) inhibitors [2]. Zeolite as a rock was first discovered by Swedish geologist Alex Fredrik Cronstedt in 1756. Due to the hydrophilic surfaces and hydrated inorganic cations, natural zeolites have no affinity for adsorption of hydrophobic molecules, thus modification with cationic surfactants changes their surface, producing nanostructured composites well-known as Surface Modified Natural Zeolites (SMNZs) and enhancing adsorption of these molecules [3]. The adsorption of NSAIDs on SMNZs has been extensively examined as carriers for pharmaceutical active forms. It was found that the amounts of adsorbed DCF were about a few dozen mg/g and adsorption of the drugs increased with increasing of the initial drugs concentrations [4].

II. Methods

In this study, the elimination of a number of high-dose analgesics will be investigated using natural zeolite clinoptilolite. Also clinoptilolite zeolite as an inexpensive adsorbent in quantity. It is found a lot in the mines of Semnan province, to increase the adsorption efficiency, the surface of natural zeolite is modified using cationic surfactants. SEM, XRD, FT-IR and BET analyzes are used to characterize the zeolite surface in both two cases (natural, modified with cationic surfactant). Due to the active absorption of the studied drugs in the UV region, UV-Vis spectroscopic technique was used to determine the concentration of these drugs at each stage.

III. Results and discussion

For this purpose, for each drug, first the calibration curve was determined by determining the response range.

The obtained experimental data will be evaluated in different linear and non-linear forms using different adsorption isotherms (such as Langmuir, Freundlich, Temkin and Langmuir-Freundlich) and finally Propose the best model based on experimental data and the results will be interpreted from a molecular point of view. Also in different concentrations of pollutants, the adsorption process will be evaluated in two linear and non-linear forms using different kinetic models (such as pseudo-first order, pseudo-second order, fractal, IKL, etc.). Freundlich isotherm model is a good model to describe the removal diclofenac by zeolite. The constants k_f (related to adsorption capacity) and 1/n (related to removal intensity) were determined to be 11.46 mg/g and 0.113, respectively.

Table 1. Obtained constants of various isotherms for the adsorption of drug onto SMNZ

Isotherm Model	Q_m (mg/g)	K_f	K_L	1/n	R^2
Freundlich		11.46		0.113	0.955
Langmuir-Freundlich	17.06		0.037	2.804	0.992

The Lagmuir-Freundlich isotherm model was found to be the best model to describe the removal of diclofenac sodium indicating ideal adsorption processes for this pharmaceutical on the surface of zeolite.

IV. Conclusions

Natural and modified zeolite (clinoptilolite) is effective for removal of diclofenac sodium from aqueous solution. Zeolite is characterized by large surface area, microporous nature, high adsorption capacity, and easy availability. The effect of contact time, adsorbent dosage, and initial concentration of pharmaceuticals on the removal process was studied and kinetic and isotherm models were evaluated, the results shows that this adsorbent is useful for drug removal.

References

[1] A. Uheida, A. Mohamed, M. Belaqziz, W. S. Nasser, Technol, 2019, 110-118.
[2] E. Felis, K. Miksch, Water Science & Technology, 2009, 2253-2259.
[3] P. J. Reeve, H. J. Fallowfield, Journal of Environmental Management, 2018, 253-261.
[4] D. Smiljani, B. de Gennaro, F. Izzo, Microporous and Mesoporous Materials, 2020, 110057.

بیست و سومین کنفرانس شیمی فیزیک انجمن شیمی ایران
23rd ICS Physical Chemistry Conference
Chemistry Department,
Faculty of Science
Shahid Bahonar University of Kerman
Kerman, Iran
12-13 Jan 2022
ایران، کرمان
دانشگاه شهید باهنر کرمان
دانشکده علوم پایه، بخش شیمی
۲۳-۲۲ دی ماه ۱۴۰۰

New optimally tuned range-separated hybrids for singlet fission relevant energetics

Mojtaba Alipour* and Zahra Safari
Department of Chemistry, School of Science, Shiraz University, Shiraz 71946-84795, Iran; E-mail: malipour@shirazu.ac.ir

Abstract
Singlet fission (SF), namely generating two triplet excitons out of a single photon absorption, has recently come into the spotlight. Herein, we propose novel optimally tuned range-separated hybrids (OT-RSHs) for reliable prediction of the negative singlet-triplet and triplet-triplet (TT) energy gaps in the SF mechanism. The newly designed OT-RSHs outperform the related RSHs and screened-exchange approximations as well as other density functionals from different rungs for describing the SF energetics. Our proposed models can also be used for computational design of chromophores as promising candidates for the SF-based materials.

Keywords: Singlet fission; Density functional theory; Range-separated model, optimally tuning.

I. Introduction
With certain relations among the energies of the excited states of the chromophores, the singlet exciton may fission into two triplet excitons through a photophysical process called singlet fission (SF), resulting in twice the number of excitons with a longer life [1]. Two important energy criteria for efficient SF are as follows: $E(S_1) \geq 2E(T_1)$ and $E(T_2) \geq 2E(T_1)$, where $E(S)$ and $E(T)$ denote the singlet and triplet excited states energies, respectively, and the subscripts 1 and 2 indicate the first and second excited states. In this work, we propose novel OT-RSHs without invoking fitting procedures and only based on the satisfaction of the inherent constraints of density functionals for describing the excited states energetics in the SF process. The best proposed models will also be employed for the computational design of several SF-based chromophores.

II. Methods
Several experimentally known and theoretically designed SF chromophores have been investigated. (Fig. 1).

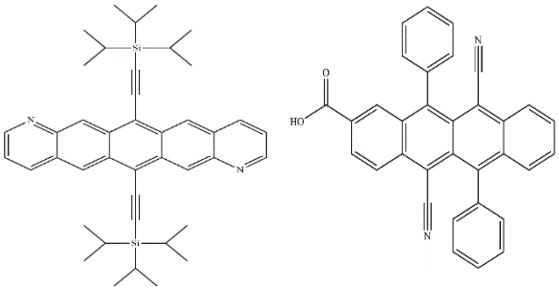

(a) (b)

Fig. 1 Chemical structures of two examples of experimental (a) and theoretically designed (b) SF chromophores. Other chromophores are available in Ref. [2].

The values of the range-separation parameter μ for all the systems are derived by minimizing a target function as follows:

$$J^2 = \sum_{i=0}^{1}\left[\varepsilon_{\mathrm{HOMO}}^{\mu}(N+i) + \mathrm{IP}^{\mu}(N+i)\right]^2 \qquad (1)$$

where $\varepsilon_{\mathrm{HOMO}}$ is the highest occupied molecular orbital (HOMO) energy, IP refers to ionization potential, and N is the number of electrons in the system. In the RSHs, the Hartree-Fock (HF) exchange contributions at short-range and long-range

domains are flexible as α and $\alpha+\beta$, respectively. We included a broad range for α, where the constraint of full HF exchange at the asymptotic distance, $\alpha+\beta=1$, was also imposed. The BLYP, PBE, and TPSS density functional approximations were employed during our study. Following the recent recommendations, we used 6-31+G(d) basis set. Solvent effects were modeled through polarizable continuum model and screened OT-RSHs with the same solvent as in the experiment. All the runs of proposed and benchmarked models were implemented in ORCA and GAUSSIAN programs.

III. Results and discussion

We carried out the optimally tuning of μ for all the considered systems (see, for instance, Fig. 2 for compound (a), while other plots are available in Ref. [2]). The polynomial fittings were applied to the curves and the optimal values of μ were determined for all the systems. The optimally tuned values of μ were found to be in the range of 0.12 to 0.22 Bohr^{-1}. These values were then used for the calculations of the energetic criteria of the SF chromophores (Fig. 3)

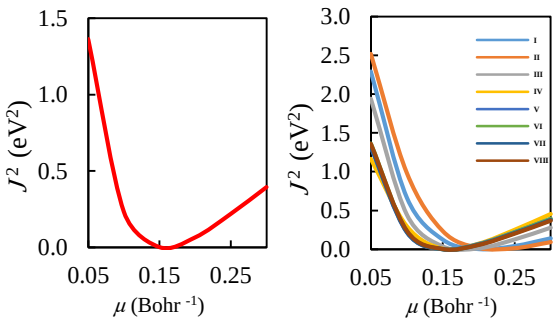

Fig. 2. (Left) Plot for the rang-separation parameter tuning for one of the experimentally known SF chromophore (compound (a) as a representative example) for the case of $\alpha=0.0$, $\beta=1.0$ using the BLYP density functional approximation. (Right) Same as left figure, but for all the experimental compounds I-VIII [2].

Overall, performing both optimally tuning and SF energetics computations with the TPSS- and PBE-based OT-RSHs $\alpha=0.10, \beta=0.90$ and $\alpha=0.15, \beta=0.85$, respectively, in the gas phase can be recommended as the models to reliably accounting for the SF process. These models perform also better than other functionals from various rungs [2].

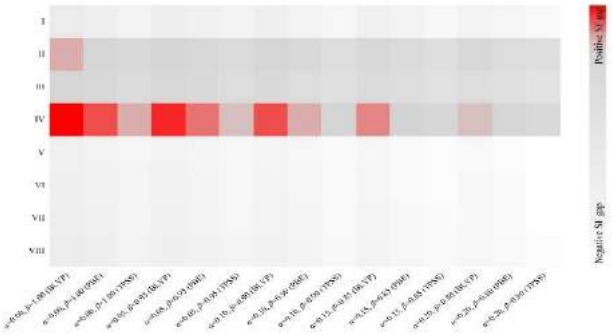

Fig. 3. Visualization of the SF energy gap for the experimentally known SF chromophores (compounds I-VIII are from Ref. [2]) using the proposed OT-RSHs based on different DFAs for all the combinations of the α and β parameters. The positive and negative gaps are represented based on the color bar.

Accountability of our proposed models was further validated for theoretically design of chromophores prone to be utilized in the SF materials, such as compound (b) in Fig. 1 (other designed chromophores are also available in Ref. [2]).

Conclusions

We proposed several variants of the OT-RSH approximations for predicting the singlet fission relevant energetic criteria not only for experimentally known SF chromophores but also for the theoretically designed chromophores.

References

[1] K. Miyata, F. S. Conrad-Burton, F. L. Geyer and X.-Y. Zhu, Chem. Rev., 2019, 119, 4261.
[2] M. Alipour and Z. Safari. Phys. Chem. Chem. Phys., 2020, 22, 27060.

بیست و سومین کنفرانس شیمی فیزیک انجمن شیمی ایران
23rd ICS Physical Chemistry Conference
Chemistry Department,
Faculty of Science
Shahid Bahonar University of Kerman
Kerman, Iran
12-13 Jan 2022
ایران، کرمان
دانشگاه شهید باهنر کرمان
دانشکده علوم پایه، بخش شیمی
۲۳-۲۲ دی ماه ۱۴۰۰

Tramadol-mu-opioid Receptor Molecular Docking

Razieh Razavi

Department of Chemistry, Faculty of Science, University of Jiroft, Jiroft Iran, r.razavi@ujiroft.ac.ir

Abstract

In this study, the molecular docking of tramadol with mu opioid receptor was theoretically examined. Energy binding and data of docking have been obtained that the best pharmacophores position of mu opioid receptor is alanine in B chain.

Keywords: mu opioid receptor; Molecular docking; Tramadol; Quantum chemical calculations.

I. Introduction

The existence of receptors for opiate drugs was first proposed in 1954 by Beckett and Casy based on their studies of structure-activity relationships for antinociceptive activity in a series of synthetic opiates. These receptors are called 'opioid' since we now know their endogenous ligands are peptides with effects resembling those of opiate drugs. Through structure-activity relationship analysis studies, Portoghese and colleagues suggested as early as 1965 that it may be necessary to propose the existence of more than one opioid receptor type or that multiple modes of interaction of ligands with opioid receptors were possible. High-affinity, stereospecific binding sites for opiate drugs were found in brain in 1973. The confirmed presence of specific receptors for opiate alkaloid and related synthetic drugs led to a search for endogenous ligands for these receptors and the discovery of the enkephalins β-endorphin, and dynorphins[1]. Tramadol[2] is one of the antidepressant drugs that act with opioid receptors therefore in this study molecular docking applied to obtain structural and binding position of tramadol in mu opioid receptor.

II. Methods

The initial structures of tramadol was optimized by DFT method and B3LYP/6-31G basis set method and mu opioid receptor was obtained from the protein data bank. Molecular docking was done by autodock4.0.

III. Results and discussion

The best pose of binding site of mu opioid receptor among of 77 poses illustrated in Fig. 1. And the best conformer of tramadol with at least RMSD=0.19 illustrated in Fig 2. The minimum binding energy obtained -8.56 kcal/mol.

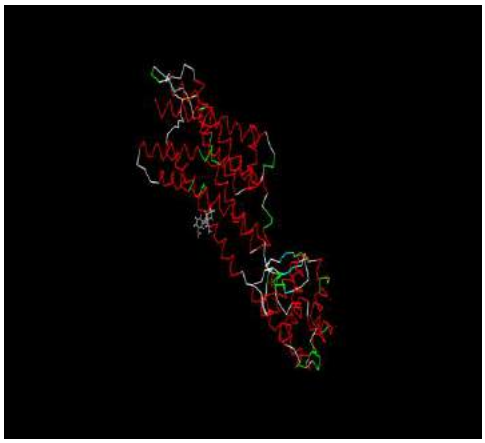

Fig. 1 The best pose of molecular docking of tramadol with mu opioid receptor.

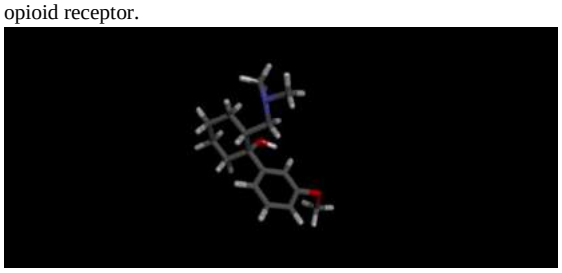

Fig. 2 Optimized structure of tramadol

IV. Conclusions

This study assessed the binding pose and binding energy of Tramadol with mu binding energy of docking is -8.56 kcal/mol and the best pose is alanine.

References

[1] Becheet Ah, Casy Af. J Pharm Pharmacol, 1954 , 6 (12), 986-1001.

[2] Matheus C. Fonseca, Clebio S. Nascimento Jr., Keyller B. Borges, Chemical Physics Letters, 2016, 645, 174-179.

بیست و سومین کنفرانس شیمی فیزیک انجمن شیمی ایران
23rd ICS Physical Chemistry Conference
Chemistry Department,
Faculty of Science
Shahid Bahonar University of Kerman
Kerman, Iran
12-13 Jan 2022
ایران، کرمان
دانشگاه شهید باهنر کرمان
دانشکده علوم پایه، بخش شیمی
۲۳-۲۲ دی ماه ۱۴۰۰

Effect of Cu content on structural properties of Ni-Cu @ a-C: H thin films

Goudarzi Samira, Dalouji Vali*

Address: Department of Physics, Malayer University, Malayer, Iran, Telephone and fax number: +988132355466; dalouji@yahoo.com

Abstract

In this study, Ni-Cu NPs @ a-C:H films with different Cu percentages, by co- deposition of RF-sputtering and RF- plasma enhanced chemical vapor deposition (RF-PECVD) were prepared using acetylene gas and Ni and Cu targets. The EDAX results show that the Ni and Cu are presented in the films successfully. With the increase of Cu percentages, the average diameter of CNTs was increased.

Keywords: Ni-Cu thin films, RF-PECVD system, Scanning Electron Microscope (SEM)

1. Introduction

Metallic nanoparticles in dielectric host have been the subject of extensive research due to their unique applications in many areas such as nonlinear optical switching, immunoassay labeling and Raman spectroscopy enhancement [1]. We have studied the growth of carbon nanotubes on copper substrates using a nickel thin film as a catalyst. Synthesis of carbon nanotubes (CNTs) using nickel catalyst on copper substrate has been attractive subject in the past few years [2, 3].

2. Experimental Details

In this study, Ni-Cu NPs @ a-C: H with the same values of Ni and different values from Cu were deposited by a capacitance coupled RF-PECVD system with 13.56 MHz power supply. The reactor contains of two different size electrodes Ni and Cu targets as powered electrodes were the smaller electrode at the first and second stages of films deposition, respectively. The distance of Ni and Cu targets to the substrate was 6 cm. The body of the stainless steel chamber was grounded via the larger electrode. All deposition process was carried out at room temperature over the larger electrode on a glass substrate. The chamber was vacuumed to a base pressure in the order of 10^{-5} mbar prior to the deposition then the pressure was increased to ambient pressure by acetylene gas. The RF power and the initial acetylene gas pressure were set at 200 W and 0.045 mbar respectively for growth of films in the first stage of deposition. Deposition times for films in room temperature were 20 min. After finishing of Cu deposition using Cu electrode, the electrode was changed to Ni electrode. In this processing, the different CNTs were obtained using constant Ni NPs and different values of Cu as 5%, 40% and
75%. EDAX mode of SEM was used for estimating of contents of the targets and films.

3. Results and discussion

Fig. 1shows a typical EDAX spectrum for the Ni-Cu target. In these spectra, there are Ni, O, Ca, Mg, Na and Si peaks. EDAX was used for structural analysis and determination of the chemical composition of a specimen and by installing it on electron microscopes can perform a qualitative and quantitative

analysis on a wide range of samples. The EDAX measurements were performed to confirm the presence of nickel and copper atoms in the target. It can be observed from the results obtained from EDAX data that the Ni and Cu are presented into the films successfully.

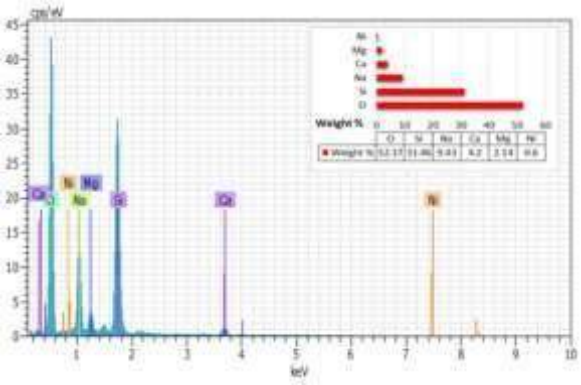

Fig. 1. Typical EDAX spectrum of composite Ni-Cu target.

Morphological properties of the thin films were investigated using SEM microscope and obtained gray-scale images. The SEM micrograph of CNTs grown on Ni NPs without Cu NPs thin layer and with Cu NPs thin films contenting 5%, 40%, 75% Cu are shown in Figs 2(a-d), respectively. We notice that adding of Cu NPs @ a-C: H with different percentages did change the surface morphology of samples. It can be seen that, the CNTs have different diameters and are generally the average diameter of the grown CNTs increases by increasing of Cu percentage of thin films. The average diameter of the grown CNTs on the Ni-Cu thin films with contenting 5%, 40% and 75% Cu were obtained to be about of 10.3, 12.5 and 16.2 nm, respectively. Also, these SEM images revealed that CNTs grown on the catalyst film with various Cu NPs contents have similar morphology and are not vertically aligned, but randomly tangled. A more noteworthy characteristic is the catalyst particle content that effects on the diameter of the CNTs and raises the CNTs diameter. As a result, Cu NPs @ a-C: H thin film has an important role in the growth of CNTs based on Ni NPs catalyst.

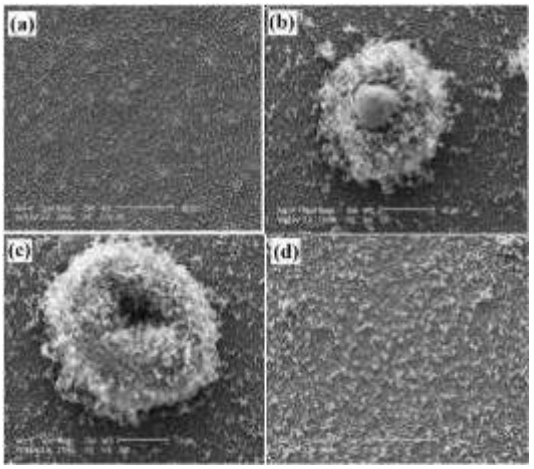

Fig. 2. SEM images of the prepared CNTs using (a) Ni NPs without Cu NPs @ a-C: H thin layer, (b) 5% Cu, (c) 40% Cu, (d) 75% Cu.

4. Result

It was found that the Cu NPs play an important role in the growth of CNTs based on Ni NPs catalyst. Multi-Walled Carbon Nanotubes, CNTs, synthesized have maximum value of the average diameters in films deposited with 75% Cu. It can be studied from the results obtained from EDAX data that the Ni and Cu are presented into the films successfully.

References

[1] DA Genov, K Seal, AK Sarychev, H Noh, VM Shalaev, ZC Ying, X Zhang X, H Cao, Applied Physics B, 2006 , 84(1), 205-210.

[2] J Garcia-Cespedes, S Thomasson, KB Teo, IA Kinloch, WI Milne, E Pascual, E Bertran, Carbon, 2009, 47(3), 613-621.

[3] G Atthipalli, R Epur, PN Kumta, BL Allen, Y Tang, A Star, JL Gray, Thin solid films, 2011, 519(16),5371-5375.

بیست و سومین کنفرانس شیمی فیزیک انجمن شیمی ایران
23rd ICS Physical Chemistry Conference
Chemistry Department,
Faculty of Science
Shahid Bahonar University of Kerman
Kerman, Iran
12-13 Jan 2022
ایران، کرمان
دانشگاه شهید باهنر کرمان
دانشکده علوم پایه، بخش شیمی
۲۳-۲۲ دی ماه ۱۴۰۰

Structural and Optical Study of Ni-Cu thin films with the different copper percentage

Goudarzi Samira, Dalouji Vali*

Address: Department of Physics, Malayer University, Malayer, Iran, Telephone and fax number: +988132355466; dalouji@yahoo.com

Abstract

In this paper, we report co-deposition of RF-sputtering and RF-PECVD for growth of Ni NPs @ a-C: H with different percentages of Cu. We studied optical constants of Ni-Cu thin films, with constant Ni content and different percentages of 5%, 40%, and 75 % from Cu atoms. With the increase of Cu percentage, the RMS roughness of films was decreased. All films exhibit a reflectance and transmittance of about 20% and 50%, respectively.

Keywords: thin films, Atomic Force Microscopy (AFM), Optical properties

1. Introduction

In recent years, nanoparticle based optical surface Plasmon sensors have drowned lot of attention among the research community because of their faster response and better resolution [1]. Carbon nanotubes (CNTs) with their attractive properties, one-dimensional geometry, and their large aspect ratio are ideal candidates for a variety of applications including energy storage, sensing, nano electronics, among others. The nickel–copper NPs have been used as catalysts to synthesis carbon nanotubes and dimethyl carbonate [2, 3].

2. Experimental Details

Ni-Cu NPs @ a-C: H with the same values of Ni and different values from Cu were deposited by a capacitance coupled RF-PECVD system with 13.56 MHz power supply. The reactor contains of two different size electrodes Ni and Cu targets as powered electrodes were the smaller electrode at the first and second stages of films deposition, respectively. The body of the stainless steel chamber was grounded via the larger electrode. All deposition process was carried out at room temperature over the larger electrode on a glass substrate. The chamber was vacuumed to a base pressure in the order of 10^{-5} mbar prior to the deposition then the pressure was increased to ambient pressure by acetylene gas. The RF power and the initial acetylene gas pressure were set at 200 W and 0.045 mbar respectively for growth of films in the first stage of deposition. Deposition times for films in room temperature were 20 min. After finishing of Cu deposition using Cu electrode, the electrode was changed to Ni electrode. In this processing, the different CNTs were obtained using constant Ni NPs and different values of Cu as 5%, 40% and 75%. A measured spectrum can be imported for comparison with the simulated one and for data fitting. AFM on non-contact mode was used to obtain average nanoparticle size and sample surface morphology.

3. Results and discussion

The AFM images of nanoparticles on the surface (3μm × 3μm) of the thin films are shown in Figs 1(a-d), respectively. Atomic
Force Microscopes (AFM) is a group of scanning probe microscopes that study of surface properties for samples. The RMS roughness of films with 5%, 40% and 75% Cu are obtained to be 3.6, 2.2 and 2 nm, respectively [4]. It turned out that by increasing of Cu percentage the surface of films becomes smooth, and it also seems that more bright points are revealed in AFM images. The general observation for the AFM images is that Cu with the different percentages over layer has an important effect on the surface morphology of the thin film.

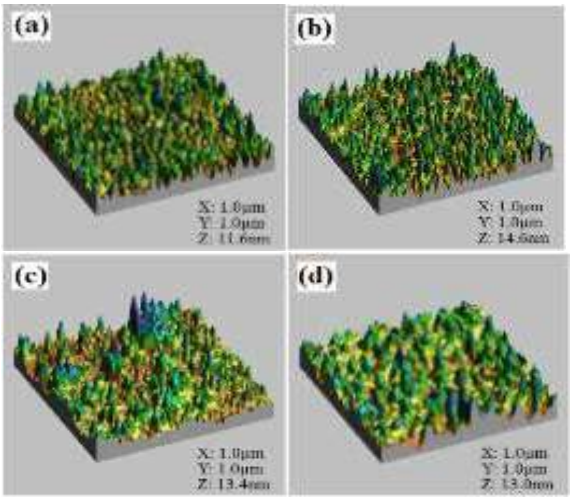

Fig. 1. AFM images of the prepared CNTs using **(a)** Ni NPs without Cu NPs @ a-C: H thin layer, **(b)** 5% Cu, **(c)** 40% Cu, **(d)** 75% Cu.

The spectral transmittance T and reflectance R of films were measured at normal incidence in the wavelength range 300-800 nm. Figs 2(a) and (b) show the optical transmittance spectra and reflectance spectra of films with pure Ni NPs without Cu NPs and with Cu NPs containing 5%, 40% and 75% Cu.

The transmittance and reflectance of the films remain nearly constant. This difference may be attributed to the effect of Cu doping and the Ni. It is clear from Fig 2(a) that by increasing of Cu percentage, transmittance spectra increase, and the invisible area is more than in UV area so the absorption edge stays on at fewer wavelengths. Fig 2(b) shows the reflectance spectra are increased by a decrease of Cu percentage in the visible area but reflectance spectra are more in the UV area. All films exhibit a reflectance and transmittance of about 20% and 50%, respectively.

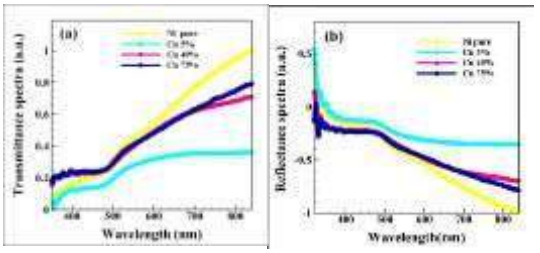

Fig. 2.(a) Transmittance spectra and **(b)** reflectance spectra of films with pure Ni NPs without Cu NPs and with Cu NPs containing 5%, 40% and 75% Cu.

4. Result

It was found that by increasing of Cu percentage of films the surface of films becomes smooth and it also seems that more bright points are revealed in AFM images. By increasing of Cu percentage, transmittance spectra increase, and the invisible area is more than in UV area so the absorption edge stays on at fewer wavelengths. The reflectance spectra are increased by a decrease of Cu percentage in the visible area but reflectance spectra are more in the UV area.

References

[1] AK Sharma, BD Gupta, Journal of Optics A: Pure and Applied Optics, 2007, 9(2), 180.
[2] T Ghodselahi, MA Vesaghi, A Gelali, H Zahrabi, S Solaymani , Applied surface science, 2011, 258(2), 727-731.
[3] J Bian, M Xiao, SJ Wang, YX Lu, YZ Meng, Catalysis Communications. 2009, 10(11), 1529-1533.
[4] S Goudarzi, V Dalouji, Optik, 2020 , 223,165585.

بیست و سومین کنفرانس شیمی فیزیک انجمن شیمی ایران
23rd ICS Physical Chemistry Conference
Chemistry Department,
Faculty of Science
Shahid Bahonar University of Kerman
Kerman, Iran
12-13 Jan 2022
ایران، کرمان
دانشگاه شهید باهنر کرمان
دانشکده علوم پایه، بخش شیمی
۲۳-۲۲ دی ماه ۱۴۰۰

Effect of metal (Cu-Al)-dopants on the absorption edge of ZnO films

Rahimi Nasim, Dalouji Vali*

Address: Department of Physics, Malayer University, Malayer, Iran, Telephone and fax number: +988132355466; dalouji@yahoo.com

Abstract

The CAZO films were deposited for 75min on glass substrates using RF magnetron co-sputtering at room temperature. Increasing annealing temperature causes to increase the kinetic energy of nanoparticles and increasing nanoparticle. The absorption of CAZO thin films in the UV range are due to their intrinsic optical band gap energy.

Keywords: Absorption coefficient; Atomic Force Microscopy; Zinc oxide; RMS roughness.

I. Introduction

There are extensive efforts to develop next-generation optoelectronic devices based on transparent conducting materials which are attracted more and more research interest owing to their superior electrical and optical properties making them suitable materials for various applications such as light-emitting diodes, solar cells, and gas sensors. [1] Zinc oxide, a wide bandgap (3.4eV) II-VI compound semiconductor. The high quality of ZnO nanostructure is strongly dependent on the lattice parameter and crystal structure of the substrates. [2] In this paper, Cu and Al will be mixed as a dopant in ZnO nanostructures. Cu-Al doped ZnO thin films which are a diluted magnetic semiconductor believed a promising candidate as a source of polarized spins and candidate in establishing room temperature ferromagnetism.

II. Methods

The CAZO films were deposited for 75min on glass substrates using RF magnetron co-sputtering (Vas PFG1000- RF) at room temperature. The basic pressure and initial vacuum of the sputtering process were 2×10^{5} and 2×10^{3} mbar, respectively, and the power of sputtering was set at 125W. The zinc metal was melted at 300°C, and then, appropriate amounts of aluminum and copper were added to the zinc melt The values obtained for the ratio of these three metals were 90 to 5 and 5% by weight of zinc, aluminum, and copper, respectively. Films were annealed in a furnace by argon flux at three different temperatures of 400, 500, and 600°C for 1 hour with the rate of 10°C/min. Transmittance and reflectance measurements of films were performed by Varian a Cary-500 spectrophotometer in the range of 200–2500nm (Varian Inc, CA, USA). Images were acquired in non-contact mode over square areas of $5\mu m \times 5\mu m$ with standard tipped CSC12 cantilever of 0.03N/m nominal stiffness (Veeco).

III. Results and discussion

Figure. 1 shows the topology of CAZO films which were performed by AFM analysis. With doping Cu-Al in ZnO films, and then, by increasing annealing temperature of films to 600°C the nanoparticles close to each other. RMS roughness of CAZO films in as deposited films and films annealed at 400, 500, and 600 °C were 2.43, 8.27, 8.78, and 9.58nm, respectively. We found that doping and temperature played a great role in this matter. As a result, with increase of annealing temperature films are to be rough and the size of the nanoparticles increased. Increasing annealing temperature cause to

increasing kinetic energy of nanoparticles and hence coalescence of nanoparticles and hence increasing nanoparticle.

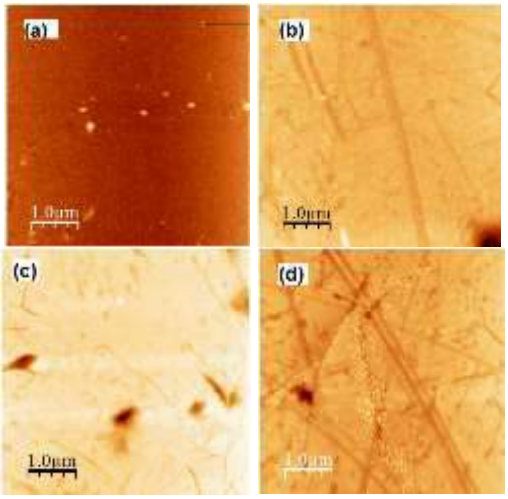

Figure 1. AFM images of (a) as deposited films and films annealed at (b) 400, (c) 500, and (d) 600°C.

Figure. 2 shows the optical transmittance and reflection spectra and the absorption of CAZO films. It is clear from Figure. 2 that it is seen reflectance and transmittance peak are shifted in doped films, the all films exhibit a reflectance and transmittance about 20% and 70% respectively. This Light difference may be attributed to the effect of Cu-Al doping and the temperature. It can be due to that thin films are not black. The optical band gap energy of CAZO films was estimated using the formula A=1−T−R. This can give a good estimate of the absorbance only for wavelengths larger than the guided-mode resonance, where propagation reflection orders are not allowed, exception of zeroth order. The results indicate that all films exhibit low absorption in the visible range but exhibit high absorption in the UV range.

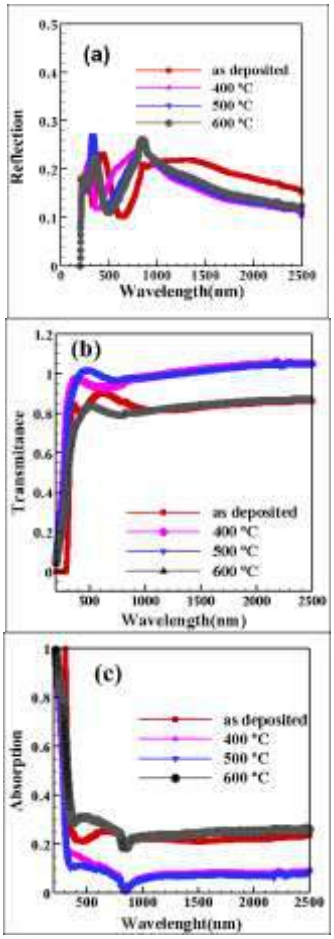

Figure .2 (a) Reflection spectra (b) and Transmission spectra (c) Absorption of CAZO films.

IV. Conclusions

with increase of annealing temperature films are to be rough and the size of the nanoparticles increased. the all films exhibit a reflectance and transmittance about 20% and 70% respectively.

References

[1] T. Minami, Y. Nishi and T. Miyata, *Thin Solid*, 2013, 549, 65–69.

[2] H. K. Park, S. P. Hong, Y. Rag, J. Electrochem. Soc, 2012, 159, 355–361.

بیست و سومین کنفرانس شیمی فیزیک انجمن شیمی ایران
23rd ICS Physical Chemistry Conference
Chemistry Department,
Faculty of Science
Shahid Bahonar University of Kerman
Kerman, Iran
12-13 Jan 2022
ایران، کرمان
دانشگاه شهید باهنر کرمان
دانشکده علوم پایه، بخش شیمی
۲۳-۲۲ دی ماه ۱۴۰۰

Influence of annealing processing on of nanoparticle size on surface of CZO films

Rahimi Nasim, Dalouji Vali*

Address: Department of Physics, Malayer University, Malayer, Iran, Telephone and fax number: +988132355466; dalouji@yahoo.com

Abstract

The CZO films were deposited for 75min on glass substrates using RF magnetron co-sputtering at room temperature. The wide variation in the surface morphology and grain sizes reveal the importance of the temperature in the synthesis of these film samples. RMS roughness of CZO films in as deposited films were 4.18nm and in 400ºC was 2.87nm and 500ºC, 600ºC were 4.48, 6.02nm, respectively.

Keywords: nanoparticle size; Atomic Force Microscopy; Zinc oxide; RMS roughness.

I. Introduction

There are extensive efforts to develop next-generation optoelectronic devices based on transparent conducting materials. [1] As an II–VI compound n-type semiconductor with a wide direct band gap (3.36eV), zinc oxide has a large exaction binding energy of 60mV with a hexagonal quartzite structure. [2] Recently, doping processing with Cu atoms has attracted increasing attention due to the lack of clustering and the fact that the secondary phases of Cu and copper oxides (Cu_2O and CuO) were not ferromagnetic (FM), also Cu-doped ZnO has shown significant improvement in relevant properties such as electrical, magnetic, photocatalytic performance and gas sensing.

II. Methods

The copper-doped ZnO films were deposited for 75min on glass substrates using RF magnetron co-sputtering (Vas PFG1000- RF) at room temperature. The basic pressure and initial vacuum of the sputtering process were 2×10^5 and 2×10^3 mbar, respectively, and the power of sputtering was set at 125W. The zinc metal was melted at 300°C, and then, appropriate amounts of aluminum and copper (99.99%-Merck company) were added to the zinc melt (99.99%). The values obtained for the ratio of these three metals were 90 to 5 and 5% by weight of zinc, aluminum, and copper, respectively. Films were annealed in a furnace by argon flux at three different temperatures of 400, 500, and 600°C for 1 hour with the rate of 10°C/min. Transmittance and reflectance measurements of films were performed by Varian a Cary-500 spectrophotometer in the range of 200–2500nm (Varian Inc, CA, USA). Topology and RMS roughness of films were determined by Veeco-Autoprobe in contact mode. Images were acquired in non-contact mode over square areas of $1\mu m \times 1\mu m$ with standard tipped CSC12 cantilever of 0.03N/m nominal stiffness (Veeco).

III. Results and discussion

EDX measurement was performed to confirm the pre-sence of Cu and the purity of the films. The EDX spectrum annealy from as deposited film shown that this Cu and Zn in films. The EDAX annealed of Cu – Zn target, with confirms the presence of Cu in the CZO target (table

(1)). It can be verified from the result of EDX that the Cu is successfully presented in the films. Figure. 1 shows surface morphology of CZO thin films. These images were used to estimate the mean size of nanoparticles. From this, it is concluded that the films have uniformly distributed spherical or distorted spherical grains giving the smooth surface morphology. The deformed shaped grains have been observed for (a) and (b) while nearly spherical grains were observed for the other two film larger crystallite size. The wide variation in the surface morphology and grain sizes reveal the importance of the temperature in the synthesis of these film samples. RMS roughness of CZO films in as deposited films were 4.18nm and in 400ºC was 2.87nm and 500ºC, 600ºC were 4.48, 6.02nm, respectively. As shown in Figure. 1(c), variation of the average of nanoparticle size of films have an increasing function with annealing temperature. With increasing annealing temperature up to 500°C, the size of nanoparticle smoothly increases however from 500 to 600°C the size of nanoparticle as significant changes. This figure may be used to interpret the distribution function of the particle size.

table. 1 Typical EDAX spectrum of Cu – Zn target

Element	Series	unn.C [wt. -%]	norm.C [wt. -%]	Atom. C [at. -%]
Copper	K series	3.94	4.12	4.13
Zinc	K series	90.26	94.24	91.97

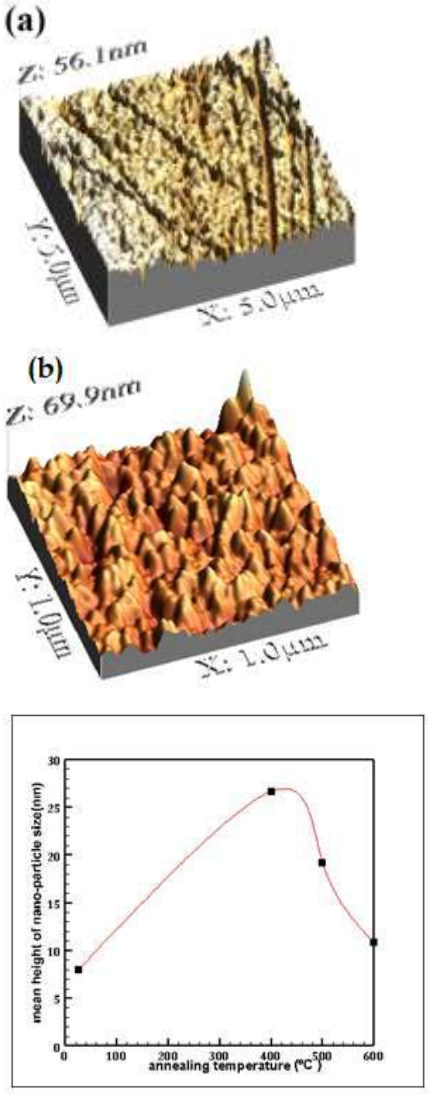

Fig. 1 AFM images of CZO thin films annealed at **(a)** 400ºC, **(b)** 600ºC, **(c)** Variation of nanoparticle size on surface of films with annealing temperature

IV. Conclusions

With increasing annealing temperature up to 500°C, the size of nanoparticle smoothly increases however from 500 to 600°C the size of nanoparticle as significant changes. This figure may be used to interpret the distribution function of the particle size.

References

[1] T. Minami, Y. Nishi and T. Miyata, *Thin Solid*, 2013, 549, 65–69.
[2] H. K. Park, S. P. Hong, Y. Rag, J. Electrochem. Soc, 2012, 159, 355–361.

بیست و سومین کنفرانس شیمی فیزیک انجمن شیمی ایران
23rd ICS Physical Chemistry Conference
Chemistry Department,
Faculty of Science
Shahid Bahonar University of Kerman
Kerman, Iran
12-13 Jan 2022
ایران، کرمان
دانشگاه شهید باهنر کرمان
دانشکده علوم پایه، بخش شیمی
۲۳-۲۲ دی ماه ۱۴۰۰

Preparation of NiMo/γ -Al_2O_3 Catalyst for the Oxidative Desulfurization of fuel

Sara Beshkoofeh[1,*], Zahra Shahidian[1], Zahra Sedghi[1]

[1]Iranian Institutes of Research and Design in Chemical Industries (IRDCI-Acecr), Tehran, Iran

Abstract

The subject is to prepare one of the ODS catalyst. The mesoporous NiMo/γ -Al_2O_3 catalyst was prepared by incipient wetness impregnation method. Molybdenum was as an active metal and nickel was as a promoter. The catalysts were characterized XRD, BET, and ICP-MS.

Keywords: Oxidative; desulfurization catalyst; NiMo/γ-Al_2O_3; catalyst; fuel desulfurization

I. Introduction

The major source of air pollution and acid rain was sulfur impurities which exists in the fuels. So, fuels should be free of polluting [1, 2].

The HDS process is the current method of removing sulfur of fuel. This process is conducted under high pressure, high temperature and in the present of catalysts. [3].

The ODS process is a better method for reducing sulfur components of fuel in comparison with HDS method. The sulfur components are oxidized to sulfones. These products can be removed by extraction, adsorption, distillation, or decomposition [4].

II. Method

The boehmite powder was used as the precursor. The other raw materials are hydroxyethyl cellulose, ammonium hepta molybdate tetra hydrate, nickel (II) nitrate hexahydrate. Boehmite powder was mixed with 5% HEC and water until to obtain homogeneous. The paste was extruded and dried at 25 ºC. It was dried at 120 ºC for 24 hr. Then it was calcined up to 600 ºC in furnace. Ni and Mo was impregnated on the γ-Al_2O_3 catalyst. Then, solution of the salts with γ-Al_2O_3 catalysts support was placed in the rotary evaporator at 50 ˚C for 2 hr. The samples were dried at 120 ˚C for 24 hr in an oven. Then catalyst was calcined up to 600 ºC in a furnace.

III. Results and discussion

The properties of γ-Al_2O_3 and NiMo/γ-Al_2O_3 catalyst are shown in Table 1. The BET reults shoes in Fig 1 and 2. According to the IUPAC classification and Figure 2, all of the prepared mesopore NiMo/γ-Al_2O_3 catalysts exhibited type IV isotherms with H_2 hysteresis loop. Typical mesoporous materials due to complex pore networks are made up of pores with wide pore size distribution [5].

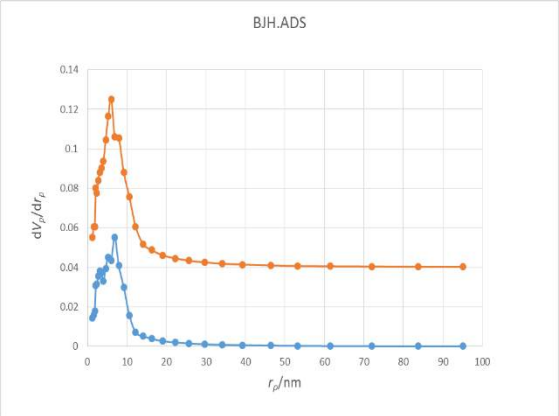

Figure 1. BJH plot

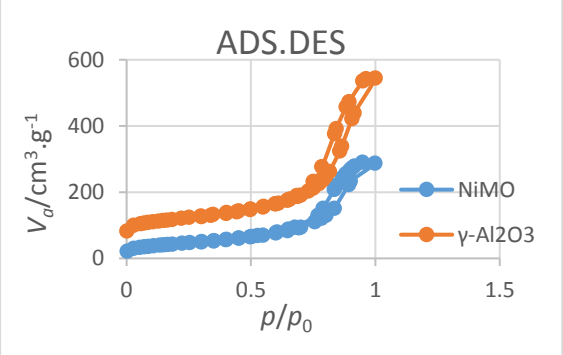

Figure. 2 Adsorption/Desorption isotherms

Table 1 shows the results of ICP-MS ICP-MS analysis of the prepared catalysts.

Table 1. ICP-MS results

Catalyst	Al wt.%	Mo wt.%	Co wt.%
γ-Al_2O_3	54.97	-	-
10%Ni15%Mo/γ-Al_2O_3	54.97	12.58	8.04

Figure 3 shows the XRD results of the prepared catalyst. The results of the tests indicate that the amorphous phase of MoO_3 is observed on the support. For nickel oxide (NiO) at 2θ= 32, 36, 37°, 40, 45° and 67° [12, 13], Two peaks exist at 2θ= 45° and 67° for NiO, are close to specific peaks of γ-Al_2O_3 and it can be assigned to the overlap of defect NiO and γ-Al_2O_3 [6,7].

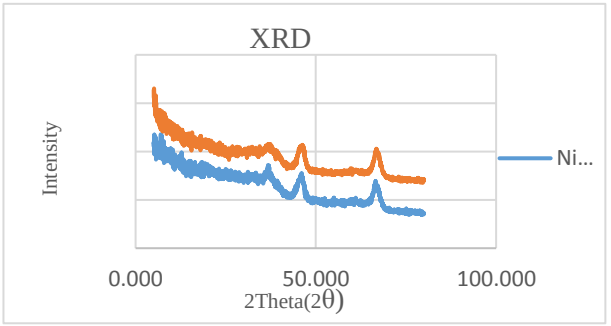

Figure 3. XRD plots

IV. Conclusions

In this article we added 10% nickel onto the 15wt% Mo /γ-Al_2O_3 catalysts. The BET results of NiMo/γ-Al_2O_3 catalyst showed that the NiO, MoO_3 and γ-Al_2O_3 are appeared on prepared catalyst and the prepared catalyst is the same with commercial catalyst.

References

[1] Saleh T. A., Trends in Environmental Analytical Chemistry, 2020, 25: e00080.
[2] Ghorbani N., Moradi G., *Chinese Journal of Chemical Engineering*, 2019, 27: 2759-2770.
[3] Subhan S., Rhman A. U., Yseen A., Rshid H., Ishaq M., Sahibzada M., Tong Z., *Fuel*, 2019, 273: 793-805.
[4] Ancheyta J., Introduction of deactivation of heavy oil hydroprocessing catalyst, John Wiley & Sons, Inc., Hoboken, New Jersey, 2016 .
[5] Wan Abu Bakar W., Rusmidah A., Abdul Aziz A., Wan Mokhtar W., *Modern Chemistry & Application*, 2015, 3: 1-3.
[6] Rang H., Kann J., Oja V., *Oil Shale*, 2008, 23: 164-176.
[7] Akbari A., Omidkhah M., Toufighi Darian J., Engineering and Technology International Journal of Chemical and Molecular Engineering, 2012, 6: 567-570.

بیست و سومین کنفرانس شیمی فیزیک انجمن شیمی ایران
23rd ICS Physical Chemistry Conference
Chemistry Department,
Faculty of Science
Shahid Bahonar University of Kerman
Kerman, Iran
12-13 Jan 2022
ایران، کرمان
دانشگاه شهید باهنر کرمان
دانشکده علوم پایه، بخش شیمی
۲۳-۲۲ دی ماه ۱۴۰۰

ZIF-67 derived cobalt sulfide/g-C_3N_4 nanohybrid as catalyst for electroreduction of chloramphenicol

Seyede Zohre Hosseini, Shahram Ghasemi*, Sayed Reza Hosseini
Faculty of Chemistry, University of Mazandaran, Babolsar, Iran, sghasemi@umz.ac.ir

Abstract

ZIF-67-derived cobalt sulfide wrapped by graphitic carbon nitride (g-C_3N_4) nanohybrid was synthesized and used for modification of glassy carbon electrode (GCE) to prepare chloramphenicol (CAP) sensor. The catalytic activity of the cobalt sulfide/g-C_3N_4/GCE toward CAP electroreduction has been investigated using cyclic voltammetry. At the surface of the electrocatalyst, the cathodic peak current for reduction of CAP is higher than that g-C_3N_4 and ZIF-67-derived cobalt sulfide at lower overpotential.

Keywords: Chloramphenicol; Electrochemical sensor; g-C_3N_4; Cobalt sulfide

I. Introduction

The increase in production of food for humans and animals has led to extensive use of antibiotics as essential medicines. Their accumulation in human body through food chain may induce serious health hazards [1]. CAP is a low cost and strong effective antibiotic drug. The excessive intake of CAP causes to serious side-effects such as leukemia, bone marrow and depression. Therefore, it is necessary to develop a selective and sensitive method for determination of CAP in food products [2]. Electrochemical sensors are emerging analytical tools for simple, low cost, specific and sensitive determination of antibiotics. g-C_3N_4 has been widely used in electrochemical sensors because of its good photo-electrocatalytic properties and high chemical and thermodynamic stability. Zeolitic imidazolate frameworks (ZIFs) as a subfamily of metal-organic frameworks have unique properties such as high specific surface area, porosity and flexibility [3]. In the current study, nanohybrid of g-C_3N_4 nanosheets with ZIF-67-derived cobalt sulfide was prepared to fabricate electrochemical sensor for determination of the CAP.

II. Methods

For the preparation of g-C_3N_4, 10 g of thiourea was heated to 550 °C in furnace with heating rate of 5 °C min^{-1} under air atmosphere and kept for 3 h. For preparation of g-C_3N_4/ZIF-67, 10 mg of g-C_3N_4 was dispersed into 20 mL methanol and treated with ultrasound for 1 h. Then, 0.87 g $Co(NO_3)_2.6H_2O$ was dissolved in methanol consisting of g-C_3N_4 and added into 20 mL of methanol containing 1.97 g of 2-methylimidazole under stirring for 30 min. The resulting mixture was kept at room temperature for 24 h. A purple solid was collected by centrifugation and then it was washed with methanol and dried at 60 °C for 6 h.

To prepare cobalt sulfide/g-C_3N_4, 80 mg of g-C_3N_4/ZIF-67 was dispersed into 40

mL ethanol and 0.12 g thioacetamide was added. The mixture was transferred into a Teflon-lined stainless steel autoclave and heated at 120 °C for 4 h. The product was collected by centrifugation and washed three times with ethanol and dried at 60 ° C for 12 h. The hybrid was characterized by different techniques.

For investigating the electrochemical behavior of active materials, the surface of GCE was modified and used as working electrode in three-electrode system.

III. Results and discussion

Figure 1 A shows XRD patterns of g-C_3N_4 and cobalt sulfide/g-C_3N_4. For g-C_3N_4, two peaks at 2Θ of 12 and 27º, corresponding to (100) and (002) crystal planes are observed. For cobalt sulfide/g-C_3N_4, the peaks appear at 16.5, 31, 47.3 and 55º are assigned to (111), (311), (422) and (440) planes of cubic Co_3S_4 (JCPDS No. 42-1448).

Figure 1B shows cyclic voltammograms of (a) GCE, (b) g-C_3N_4/GCE and (c) Co_3S_4/g-C_3N_4/GCE in the presence of 500 µM CAP in N_2 saturated phosphate buffer (pH=7). At surface of bare GCE, a small reduction peak is observed at high overpotential.

At g-C_3N_4/GCE, the current for CAP reduction increases and cathodic peak potential shifts to -0.61 V which show the facilitation of reduction process. At surface of Co_3S_4/g-C_3N_4/GCE, the reduction peak appears at -0.53 V and the current increases substantially which confirms the improvement in electron transfer and decrease in the overpotential of the reduction process.

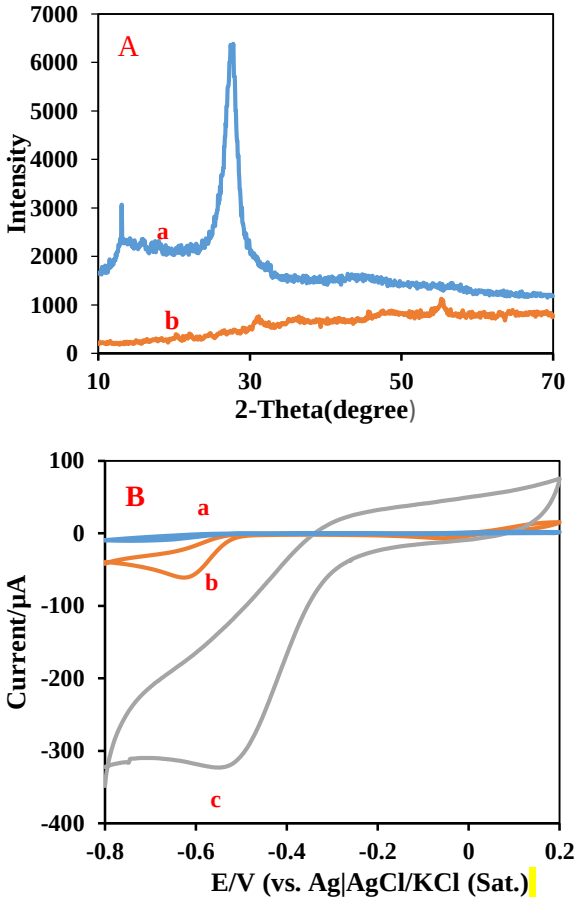

Figure 1: (A) XRD pattern of (a) g-C_3N_4 and (b) Co_3S_4/g-C_3N_4; (B) Cyclic voltammograms of (a) GCE, (b) g-C_3N_4/GCE and (c) Co_3S_4/g-C_3N_4/GCE in phosphate buffer solution containing 500 µM CAP at 50 mV s^{-1}.

IV. Conclusion

The studies on XRD patterns of g-C_3N_4 and cobalt sulfide/g-C_3N_4 showed the successful synthesis of the nanohybrid. The electrochemical investigation of the g-C_3N_4/Co_3S_4 nanohybrid in phosphate buffer solution in the presence of CAP showed an electroreduction peak with higher current and lower overpotential than that for g-C_3N_4 and Co_3S_4/g-C_3N_4.

References

[1] A. Joshi, K.H. Kim, Biosens. Bioelectron, 2020, 153, 112046.

[2] Xia, Y. M., Zhang, W., Li, M. Y., Xia, M., Zou, L. J., & Gao, W. W, Electrochem. Soc, 2019, 166(8), B654.

[3] Samadi-Maybodi, A, Ghasemi, S, & Ghaffari-Rad, H,Sens Actuators, B, 2015, 220, 627.

بیست و سومین کنفرانس شیمی فیزیک انجمن شیمی ایران
23rd ICS Physical Chemistry Conference
Chemistry Department,
Faculty of Science
Shahid Bahonar University of Kerman
Kerman, Iran
12-13 Jan 2022
ایران، کرمان
دانشگاه شهید باهنر کرمان
دانشکده علوم پایه، بخش شیمی
۲۳-۲۲ دی ماه ۱۴۰۰

Molecular features of interaction between VEGFR-2 and Linifanib and Semaxanib using a combination of computational methods

Leila Karami [a,*]

[a] *Department of Cell and Molecular Biology, Faculty of Biological Sciences, Kharazmi University, Tehran, Iran,l_karami@khu.ac.ir*

Abstract

Due to the importance of Vascular Endothelial Growth Factor Receptor type 2 (VEGFR-2) in angiogenesis of cancerous tumors, in this work, the molecular mechanism of interaction between the VEGFR-2 and linifanib and semaxanib as inhibitor was investigated using the molecular docking, molecular dynamics (MD) simulation. For this purpose, post MD analysis (structural and thermodynamics) were performed.

Keywords: VEGFR-2; molecular docking; Molecular dynamics simulations; Linifanib; Semaxanib.

I. Introduction

Vascular endothelial growth factor(VEGF) is an important signaling protein involved in vasculogenesis (the formation of the circulatory system) and angiogenesis (the growth of blood vessels from pre-existing vasculature). All types of VEGFs (VEGF-A, VEGF-B, VEGF-C, VEGF-D and VEGF-E) stimulate cellular responses by binding to tyrosine kinase receptors (the VEGFRs) on the cell surface, causing them to dimerize and become activated through transphosphorylation [1]. The VEGF receptors have an extracellular portion consisting of 7 immunoglobulin-like domains, a single transmembrane spanning region and an intracellular portion containing a split tyrosine-kinase domain. Among the VEGFRs (VEGFR-1, VEGFR-2 and VEGFR-3), VEGFR-2 is only as the protein kinase domain transmitting the angiogenic signals [2]. It is therefore crucial to inhibit the tyrosine kinase VEGFR-2 signaling pathway, which in turn stops the angiogenesis process in solid tumors.

II. Methods

The initial structures VEGFR-2 and inhibitors were obtained from protein data bank (PDB ID 3WZD) and DRUGBANK (DB11800 and DB08896) respectively. After the geometry optimizing of inhibitors using Gaussian 03 program at the B3LYP/6-31 ++G level of theory, AutoDock Vina [3] was applied to create receptor-inhibitor complex structures. The best pose of docking was selected based on the binding energy to be input for MD simulation. MD simulations was carried out using Gromacs 2019 [4] and Amber03 and GAFF force fields for protein and ligands, respectively. MD simulation protocol is as follows: 1) energy minimization with position restraint on complex heavy atoms, 2) two equilibrium phase in NVT and NPT ensembles and 3) production phase in NPT ensemble in 300K temperature and 1 bar pressure using Berendsen thermostat and barostat.

III. Results and discussion

The root mean square deviation (RMSD) and radius of gyration (Rg) as measures of the simulation stability and compactness of protein structure were calculated and plotted in Fig. 1 and Fig. 2, respectively. The RMSD of the protein-ligand complexes attained a value of 0.25 nm at 25 ns and remained almost constant till the end of simulation. RMSD plots display the more stability of VEGFR2-linifanib complex relative to VEGFR2-semaxanib complex.

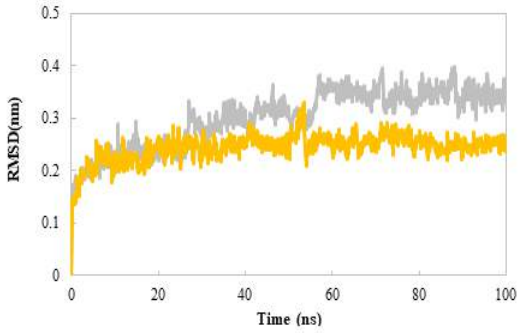

Fig. 1. The root mean square deviation (RMSD) of the alpha carbon atoms of VEGFR-2 in complex with a) semaxanib (gray) and b) linifanib (yellow).

The average Rg value for linifanib, and semaxanib were found to be 2.06 nm, and 2.11 nm, respectively. The VEGFR2-linifanib complex showed less Rg value as compared to the VEGFR2-semaxanib complexes, suggesting that it forms a more compact and stable complex.

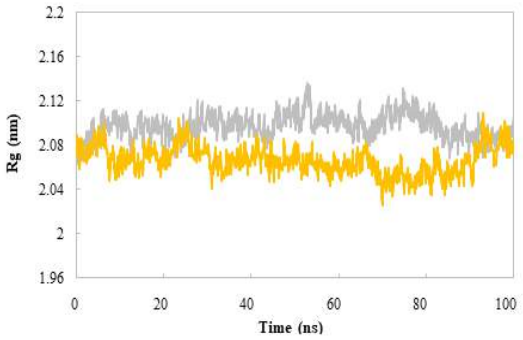

Fig. 2. Time dependence of the VEGFR-2 radius of gyration (Rg) in complex with a) semaxanib (gray) and b) linifanib (yellow).

To estimate the binding affinity of inhibitors to VEGFR2, $\Delta G_{binding}$ values were calculated using the MM-PBSA method to complement the structural analysis. The calculated $\Delta G_{binding}$ and detailed energy contribution were summarized in Table 1. For both complexes, the major favorable contributors are the van der Waals and electrostatic terms, whereas the polar solvation term opposes binding. As can be seen in Table 2, the binding affinity of linafinib to VEGFR2 is greater than that of semaxanib. This can be attributed to the interactions between linifanib and VEGFR2.

Table 1. Binding free energy (kJ/mol) of VEGFR2-inhibitor complexes calculated by MM-PBSA method

System	VEGFR2-linifanib	VEGFR2-semaxanib
ΔE_{vdW}	-265.3	-242.3
ΔE_{ele}	-64.5	-36.6
ΔG_{polar}	193.3	174.1
$\Delta G_{non\text{-}polar}$	-34.4	-31.5
$\Delta G_{binding}$	-146.8	-115.3

IV. Conclusions

MD simulation results (structural and thermodynamics analysis) of VEGFR2-inhibitor complexes showed that among the studied small molecules, linifanib is a better inhibitor for the receptor.

References

[1] M. Shibuya, Genes. Cancer., 2011, 2, 1097–1105.
[2] K. Holmes, O. L. Roberts, A. M. Thomas, and M. J. Cross, Cellular Signalling., 2007, 19, 2003–2012.
[3] O. Trott, and A. J. Olson, J. Comput. Chem., 2010, 31, 455-461.
[4] M. J. Abraham, D. van der Spoel, E. Lindahl, B. Hess and the GROMACS development team, http://www.gromacs.org.

بیست و سومین کنفرانس شیمی فیزیک انجمن شیمی ایران
23rd ICS Physical Chemistry Conference
Chemistry Department,
Faculty of Science
Shahid Bahonar University of Kerman
Kerman, Iran
12-13 Jan 2022
ایران، کرمان
دانشگاه شهید باهنر کرمان
دانشکده علوم پایه، بخش شیمی
۲۳-۲۲ دی ماه ۱۴۰۰

Synthesis of solar light responsive nanocatalysts and investigation of their performance in water splitting reaction

Negin Mokhtari[a], Shahrbanoo Rahman Setayesh[a,*]

Department of chemistry ,Sharif University of Technology, Tehran, Iran
Email:setayesh@sharif.edu

Abstract

A customary and feasible hydrothermal process was designed to synthesize $ZnMn_2O_4$/g-C_3N_4 nanocomposite catalyst. The surface morphology was characterized by FE-SEM method. by measuring the amount of oxygen evolution from water splitting, the optimum percentage of $ZnMn_2O_4$/g-C_3N_4 nanophotocatalyst was found to be 80/20.

Keywords: Water splitting; $ZnMn_2O_4$; g-C_3N_4; Nanophotocatalyst; Oxygen evolution .

I. Introduction

One of the most promising ways to provide clean and sustainable energy is using hydrogen, and reduce the use of non-renewable resources [1]. The use of hydrogen in combustion and fuel cells can lead to higher energy conversion efficiencies than internal combustion engines with fossil fuels. Today, the utilization of photocatalysts to produce cheap and pure hydrogen by water and sunlight is a good way to prevent environmental pollution [2]. The oxygen evolution reaction requires a high voltage relative to hydrogen due to its high kinetics energy barrier. Oxygen produced from water fission is used in metal-air batteries and fuel cells [3]. In this project, the n-p structure was used to separate the electron-hole pair created by light and prevent their recombination. We want to advance the fission reaction of water with proper efficiency of hydrogen and oxygen production by synthesizing $ZnMn_2O_4$/g-C_3N_4 nanophotocatalyst.

II. Methods

A: the synthesis of $ZnMn_2O_4$/g-C_3N_4

The $ZnMn_2O_4$/g-C_3N_4 nanocomposite was fabricated using the one step hydrothermal method. Sufficient amount of g-C_3N_4 was dispersed evenly in 50 mL of deionized water by ultrasound to form a homogeneous dispersion. Then appropriate amount of $Zn(NO_3)_2$ and $Mn(NO_3)_2$ were well dissolved in 50 mL of ethylene glycol. This solution were added to the homogeneous dispersion g-C_3N_4 and stirred for 30 minutes. ammonia aqueous solution (25 wt%) was used to adjust the pH of the solution to ~10. Subsequently, the mixed suspension was transferred to a 120 mL Teflon-lined stainless-steel autoclave and heated at 454 K for 20 h. Finally, the solid product was centrifuged, washed with deionized water, and then dried in air overnight to obtain ZMO/g-C_3N_4. pure ZMO was also synthesized

through a procedure similar to that was mentioned above without addition of g-C_3N_4[3].

B: The experiment of water splitting

Photocatalytic testing of water splitting was performed in a Pyrex cell with a capacity of 250 mL. Taking 0.1g of synthesized $ZnMn_2O_4$/g-C_3N_4 (80:20) as a non-homogeneous catalyst in 200 mL distilled water and a magnetic stirrer is used to ensure the catalyst was suspended. 40 W LED was used as a light source. The amount of water oxygen by flowing argon gas through the water becames zero. Oxygen meter sensor was placed in solution and the amount of oxygen was measured at the specified time.

III. Results and discussion

The surface morphology of the nanostructures was shown by FE-SEM. Fig. 1b indicated the structure of the ZMO particles were about 30-60 nanometers. Also, the morphology of the g-C_3N_4 nanosheets shown in Fig.1a . From the FE-SEM in Fig. 1c, it can be found that the nanoparticles were placed on the nanosheets and the particles size were 20-40 nm.

Fig.2 represent that coupling of g_C_3N_4 to $ZnMn_2O_4$ increased the amount of oxygen evolution, which is due to the decrease of the band gap energy and the electron-hole recombination in the nanocomposite.

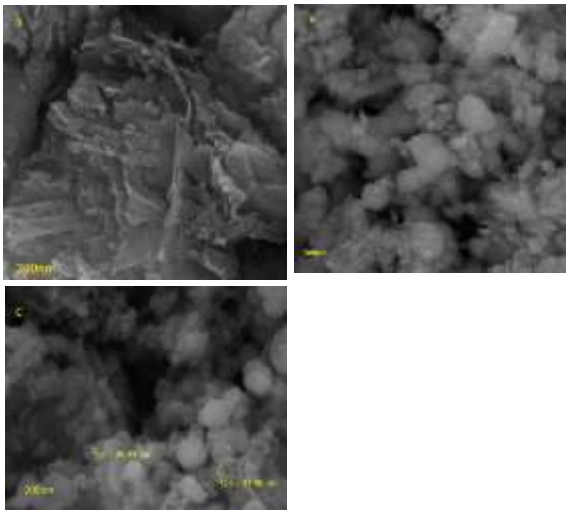

Fig. 1. FE-SEM images of g-C_3N_4(a), $ZnMn_2O_4$(b), ZMO@g-C_3N_4 (80:20) (c).

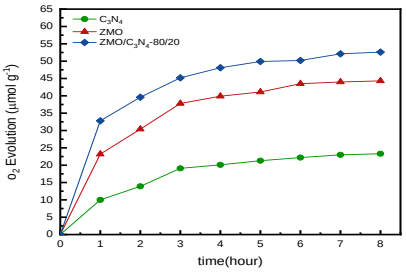

Fig. 2. Oxygen evolution of ZMO,g-C3N4,ZMO/g-C3N4(80/20)

IV. Conclusions

In this work, ZMO/g-C_3N_4 (80/20) nanocomposite was successfully synthesized by hydrothermal method. The nanocomposite image showed that the ZMO / g-C3N4 particles size were 20-40 nm. The optimum percentage of $ZnMn_2O_4$/g-C_3N_4 nanophotocatalyst was found to be 80/20. At the eighth hour and at a temperature of 25 °C, 55 μmol of oxygen was produced.

References

[1] G. Jingqi, F. Zhang , S. Kelly, R. Si, M. Dupuis, Nature Catalysis 1,2018,11,870.

[2] S.Jiang, J.Cao, M.Guo, D.Cao, S.Chen,Applied Surface Science,2021,149882.

[3] K. Aruchamy, R.Nagaraj, Materials Science and Engineering: B 2020, 252, 114481.

بیست و سومین کنفرانس شیمی فیزیک انجمن شیمی ایران
23rd ICS Physical Chemistry Conference
Chemistry Department,
Faculty of Science
Shahid Bahonar University of Kerman
Kerman, Iran
12-13 Jan 2022
ایران، کرمان
دانشگاه شهید باهنر کرمان
دانشکده علوم پایه، بخش شیمی
۲۳-۲۲ دی ماه ۱۴۰۰

Investigation of Transport Properties in pure SiNW and SiNW Doped with Boron

Rahele Masoumifard[a,*], Mohsen Oftadeh[b] , Kiomars Eskandari

[a] *Chemistry Department, Payame Noor University, 19395-4697 Tehran, I. R. Iran. E-mail: maasoumi.r@gmail.com*
[b] *Chemistry Department, Payame Noor University, 19395-4697 Tehran, I. R. Iran. E-mail: m_oftadeh@pnu.ac.ir*

Abstract

In this paper, to understand the electronic properties and conductivity of SiNWs, we have performed the band structure calculations of SiNWs in different modes of normal and boron-doped.

Keywords: Silicon Nanowires; Conductivity; Quantum Espresso; Density Functional Theory.

I. Introduction

Doping methods can control the electrical conductivity of semiconductor materials such as silicon (Si) [1, 2]. Boron (B) is the most popular p-type doped in silicones, so it is necessary that doping boron in Silicon nanowires (SiNWs) is of particular importance [3]. Studying the transport properties of SiNWs such as thermal and electrical conductivity is challenging.

II. Methods

The calculation of this work is based on the density functional theory by using the method of augmented plane waves and norm-conserving potential in quantum espresso computational package [4] with the generalized gradient approximation (GGA) for exchange-correlation. To investigate the transport properties of silicon nanowires, the structure was optimized and relaxed, and to obtain the transport properties, the computational package of Wannier 90 [5] was used.

III. Results and discussion

After optimizing the structure of pure and doped nanowires with B atoms, we obtained the electronic properties of these systems such as state density, band structure and quantum conductivity using the Quantum Espresso and the Wannier 90 computational package. Figure 1 shows the band structure of pure and neutral silicon nanowires with hydrogen atoms. In this figure it is clear that the energy bands in the Γ-X direction have very little dispersion and in the Γ-X direction the probability of transport is very low. Also it is clear from Figure 1-b that there is an energy gap between the capacity and conduction region. Therefore, the energy gap type for a pure silicon nanowire system neutralized with a hydrogen atom is indirect.

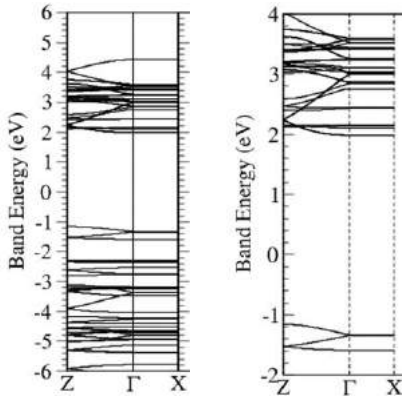

a b

Figure 1 Band structure of (a) pure and (b) hydrogen-passivated of silicon nanowires

Simultaneous examination of quantum conduction diagrams state densities, and band structure in the Figure 2 shows that wide quantum conduction bands occur where the energy bands have a high scattering and among these scatterings there are no flat bands but the boundaries of the scatter bands marked by bands and where the scattering of bands is low and the density of states is high, the amount of quantum conductivity has increased significantly.

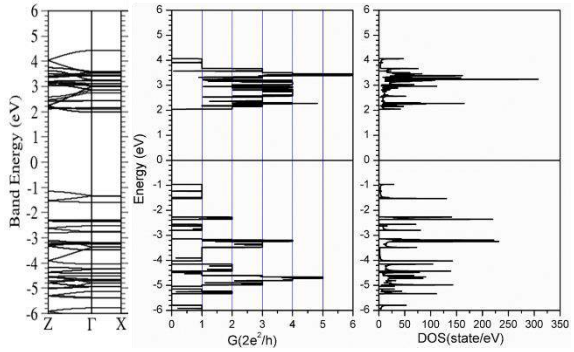

Figure 2 Comparison of quantum conduction diagrams, density of states and band structure in pure silicon nanowires

Figure 3 shows the band structure of a B-atom silicon nanowire. Here the band structure changes considerably relative to the pure state. Its electron states appear to be located in the band gap of the doped atoms, so Fermi energy shifts to the pure silicon nanowire capacity band, and plane states of energy bands are seen around Fermi energy. Therefore, it can be said that doped nanowire has created a p-type semiconductor in the system.

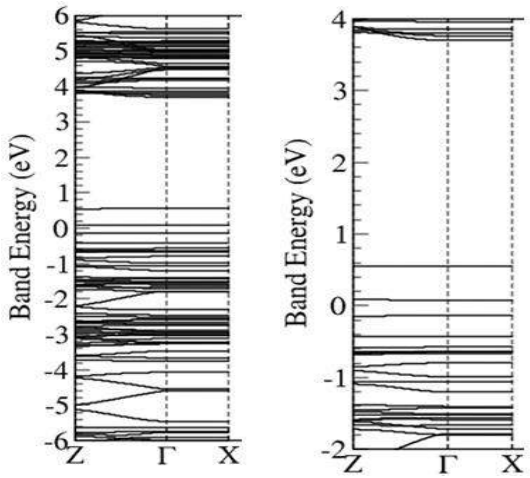

a b

Figure 3 Band structure of doped silicon nanowires with B atom

IV. Conclusions

Our results show that for pure silicon nanowires the energy gap is indirectly. In the conduction region, energy bands can be seen and have high scattering. There is no quantum conduction in the band gap energy range. Quantum conduction bands occur where energy bands have high scattering. Doping of the nanowire with B indicates that the doped produced a p-type semiconductor. The band gap of the B-doped silicon nanowire is straight.

References

[1] J. Jie, W. Zhang, K. Peng, G. Yuan, C. S. Lee and S. T. Lee, Advanced Functional Materials, 2008, 18(20), 3251-3257.

[2] R. Taniguchi and S. Inasawa, Crystal Growth, 2020, 547, 125796.

[3] D. D. D. Ma, C. S. Lee and S. T. Lee, Applied Physics Letters, 2001, 79(15), 2468-2470.

[5] G. Pizzi and V. Vitale, R. Arita, S. Blügel, F. Freimuth, G. Géranton and J. R. Yates, Physics: Condensed Matter, 2020, 32(16), 165902.

[6] P. Giannozzi, S. Bonini, N. Bonini, M. Calandra, R. Car and C. Cavazzoni, Phys Condens Matter, 2009, 21(39), 395502.

بیست و سومین کنفرانس شیمی فیزیک انجمن شیمی ایران
23rd ICS Physical Chemistry Conference
Chemistry Department,
Faculty of Science
Shahid Bahonar University of Kerman
Kerman, Iran
12-13 Jan 2022
ایران، کرمان
دانشگاه شهید باهنر کرمان
دانشکده علوم پایه، بخش شیمی
۲۳-۲۲ دی ماه ۱۴۰۰

Synthesis of piezoelectric nanomaterials and kinetics investigation of their performance for degradation of organic pollutants under ultrasonic vibrations

Samaneh Mashhadizadeh[a], Shahrbanoo Rahman Setayesh[a]*

Address: Department of Chemistry, Sharif University of Technology, Tehran, Iran
** E-mail: setayesh@sharif.edu*

Abstract

The piezocatalysis, a phenomenon of vibration exciting chemical reaction, is a promising water purification technology. In this project, the effect of $BiFeO_3/Bi_2WO_6$ nanocomposite was estimated through the decomposition of the methyl orange dye (MO). The results reveal that the $BiFeO_3/Bi_2WO_6$ (80:20) nanocomposite facilitates the degradation efficiency of MO solution compared to pristine $BiFeO_3$ and Bi_2WO_6. The enhancement is attributed to the electric field in the heterojunction which can separate the charge carriers effectively.

Keywords: piezocatalysis; piezocatalytic degradation; Bi_2WO_6; $BiFeO_3$

I. Introduction

Due to rapid industrialization on a wide scale, contamination of water becomes a major concern in the world. The best approach to contribute to the wellness of human health and the environment is providing clean and affordable water, one of the modern-time hurdles.

Mechanical energy is a very pervasive and available form of energy in the environment. Piezoelectric materials can obtain mechanical energy and convert it to electrical energy. When a piezoelectric material is subjected to mechanical energy like ultrasonic vibrations, the negative and positive charges are transferred to the opposite polar surfaces due to easy deformation of the material [1]. The charges displacement creates an internal electric field which enhances the separation of the electron-hole pairs and leads to swift degradation of dye molecules [2]. Herein, we report the enhanced piezocatalytic performance of $BiFeO_3$ nanoparticles by coupling with Bi_2WO_6 nanosheets, and the results demonstrated ultrasound assisted piezocatalytic degradation of MO solution.

II. Methods

$BiFeO_3/Bi_2WO_6$ nanocomposite was synthesized by hydrothermal method. Proper amounts of bismuth nitrate and iron chloride were mixed in acetone. An aqueous dispersion of Bi_2WO_6 was then added to the mixture. Then concentrated ammonia was added under vigorous stirring until the pH value reached 10-11. After filtering and rinsing with distilled water, the red co-precipitate was redispersed in NaOH solution. Next, the solution was placed inside an autoclave and heated at 140 °C for 48 hours. The final product was dried at 80 °C for 8 hours [3].

III. Results and discussion

Fig. 1(a-c) displays the FE-SEM morphologies of pristine $BiFeO_3$, Bi_2WO_6 and $BiFeO_3/Bi_2WO_6$ nanocomposite , respectively. In Fig. 1(a), $BiFeO_3$ nanoparticles with grain sizes of 90-180 nm can be seen. In the FE-SEM image of Bi_2WO_6 , smooth and sheet like morphology can be observed clearly. For the $BiFeO_3/Bi_2WO_6$ (80:20) nanocomposite (Fig. 1(c)), the $BiFeO_3$ nanoparticles are seen to be assembled on the Bi_2WO_6 nanosheets.

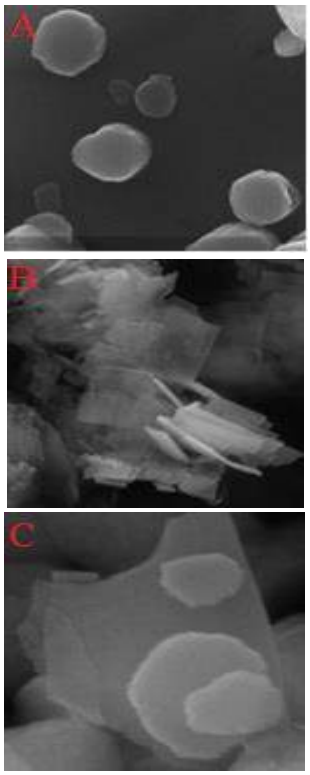

Fig. 1 (A-C) FE-SEM images of $BiFeO_3$, Bi_2WO_6 and $BiFeO_3/Bi_2WO_6$.

The piezocatalytic dye degradation process was investigated by exerting ultrasonic vibration to the suspension. Fig. 2 depicts the variation of MO concentration (C/C_0) with time. It is clearly observed that $BiFeO_3/Bi_2WO_6$ (80:20) has the best piezocatalytic activity towards MO degradation.

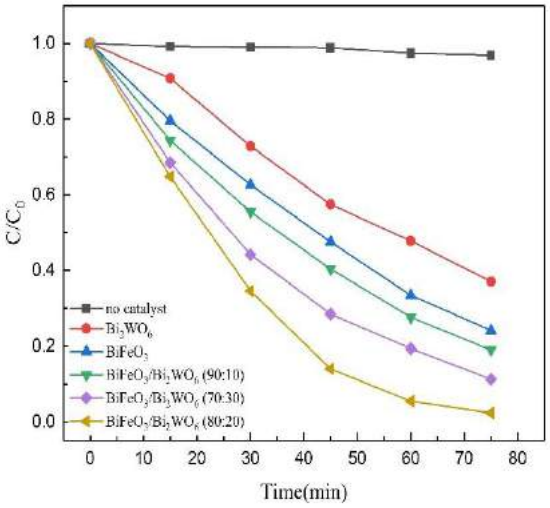

Fig. 2 The piezocatalytic MO degradation for different samples.

IV. Conclusions

In summary, the $BiFeO_3/Bi_2WO_6$ nanocomposite was successfully synthesized by hydrothermal method. The FE-SEM images represented that the $BiFeO_3$ nanoparticles were assembled on the Bi_2WO_6 nanosheets. The vibrational catalytic activity was significantly improved due to heterojunction of $BiFeO_3$ nanoparticles and Bi_2WO_6 nanosheets which can efficiently separate electron and hole pairs and inhibit their recombination.

References

[1] J. Wu, Y. Sun, W. Chang, J. Lee, Nano Energy, 2018, 46, 372-382.
[2] S. Feng, J. Xiong, Y. Tian, S. Liu, S. Kong, L, Environmental Science & Technology, 2017, 51, 6560-6569.
[3] A. Arazas, C. Wu, K. Chang, Ceramics International, 2018, 44, 14158-14162

بیست و سومین کنفرانس شیمی فیزیک انجمن شیمی ایران
23rd ICS Physical Chemistry Conference
Chemistry Department,
Faculty of Science
Shahid Bahonar University of Kerman
Kerman, Iran
12-13 Jan 2022
ایران، کرمان
دانشگاه شهید باهنر کرمان
دانشکده علوم پایه، بخش شیمی
۲۳-۲۲ دی ماه ۱۴۰۰

Use of compartmental model for evaluation of ^{137}Cs transfer and absorption coefficients

Baharak Eslami*[a], Somaye Malmir[b]

[a, b] *Department of Physics, Payame Noor University, Iran; bkeslami@yahoo.com; s_malmir84@yahoo.com*

Abstract

Cesium-137 is one of the most important radioactive nuclides, which released into the environment during nuclear accidents. In this article, by compartmental model transfer coefficients of ^{137}Cs in the root vegetables investigated. For the calculation of parameters in the plants, data of Fukushima accident used. Data of ^{137}Cs concentration in soil and in root of vegetables are as inputs.

Keywords:

Cesium 137; Nuclear Accident; Transfer Coefficients; Compartmental model.

I. Introduction

Some radioactive materials are widely released into the environment due to human activity [1]. These activities include nuclear tests, and in particular major accidents at nuclear power plants such as Chernobyl and Fukushima. External and internal radiation because of entry these radionuclides through food, drink, and inhalation of polluted air, into the body can pose potential and actual dangers to humans. One of the most important cases of nuclear pollution is cesium-137, which in the Chernobyl and Fukushima nuclear accidents, large amounts of it have entered the environment, which due to its half-life of about 30 years, remain in the environment for a long time [2, 3]. This metal remains in high layers of the soil and by the time, diffuse to the lower depths of the soil and absorbed by plant roots and finally it will enter the human chain and effects directly on the human health [4-6]. Therefore, the use of appropriate models for prediction of the ^{137}Cs absorption in root vegetables can help on the human health.

II. Methods

The amount of cesium on the soil surface depends on the weather conditions, the amount of rainfall and its distribution. To measure either the amount of cesium in the subsoil, the direct measurement method must use or the equation governing the influence of cesium in the soil can solved.

$$\frac{\partial C}{\partial t} = D\frac{\partial^2 C}{\partial h^2} - v\frac{\partial C}{\partial h} - \lambda C \qquad (1)$$

Equation (1) can solved by considering the density of sodium at different times on the soil. The best multi-part model for plants is to divide the plant into main parts, i.e. roots, stems and leaves. Equation (2) shows the equations governing the three-part model in the plant.

$$\begin{cases} \frac{dc_r}{dt} = k_x I(t) - \mathrm{k_l c_r} + \mathrm{k_2 c_s} - \lambda_R \mathrm{c_r} \\ \frac{dc_s}{dt} = k_l c_r - (k_2 + k_3)c_s + k_4 c_l - \lambda_R c_s \\ \frac{dc_l}{dt} = k_3 c_s - k_4 c_l - \lambda_R c_l \end{cases} \qquad (2)$$

$C_r(t), C_s(t), C_l(t)$ are the radiation in the roots, stems and leaves, respectively and K coefficients are the transfer coefficients between sections.

One of the useful numerical methods to solve the system of differential equations is the Runge Kutta method. In this article, this algorithm is implemented using MATLAB software and the system of equations governing the three-part model for root plants solved.

III. Results and discussion

Changes in sodium concentration indicate that the concentration of sodium decreases with increasing depth. To calculate the transfer coefficients, Equation (2) solved for a multi-part model for different k. To solve the equations Runge Kutta method used. The difference between this method and other methods is less error. Table 1 shows the calculated values for different K. The results show that the coefficients of cesium transfer from soil to root (k) correspond to the ratio of soil-to-plant radioactive cesium concentration (Cr), for loamy soil and root vegetables.

Table 1 calculated transfer coefficients

	K_1	K_2	K_3	K_4	k_x
potato	0.001	0.089	0.114	0.002	0.035
turnip cabbage	0.002	0.0078	0.09	0.002	0.038

IV. Conclusions

The result shows the calculated transfer coefficients for soil to root of vegetable is in the same order of reference for the loam soil of agricultural and root vegetables.

The calculated transfer coefficients are in a very good consistency to the recommended NCRP. This result can used for predicting the nuclear contamination in the nuclear accident.

References

[1] Korobova E, Romanov S. Experience of mapping spatial structure of Cs-137 in natural landscape and patterns of its distribution in soil toposequence, Journal of Geochemical Exploration, 2011 ; 109: 139–145.

[2] Timms D.N, Smith J.T., Cross M.A, Kudelsky A.V., Horton G., Mortlock R. A new method to account for the depth distribution of Cs-137 in soils in the calculation of external radiation dose rate, Journal of Environmental Radioactivity 2004; 72: 323–334

[3] Radiol J. Cesium-137 in the Environment: Radioecology and approaches to assessment and management. Journal of radiology protection, 2007; 27: 375–377

[4] Almgren S. Studies on the Gamma Radiation Environment in Sweden with Special Reference to ^{137}Cs. Department of Radiation Physics University of Gothenburg, Sweden Göteborg 2008

[5] Choi Y, Muk Lim K, Jun I, Kwon Keum D, Hee Han M, Gyu Kim I. Transport behavior and rice uptake of radio strontium and radio caesium in flooded paddy soils contaminated in two contrasting ways, Science of the total Environment, 2011; 248–256

[6] MEXT, Ministry of Education, Culture, Sports, Science and Technology, Japan. Monitoring Information of environmental radioactivity level. 2011.

بیست و سومین کنفرانس شیمی فیزیک انجمن شیمی ایران
23rd ICS Physical Chemistry Conference
Chemistry Department,
Faculty of Science
Shahid Bahonar University of Kerman
Kerman, Iran
12-13 Jan 2022
ایران، کرمان
دانشگاه شهید باهنر کرمان
دانشکده علوم پایه، بخش شیمی
۲۳-۲۲ دی ماه ۱۴۰۰

Evaluation of the mechanism of interaction of hydrogen peroxide with DNA bases

Somaye Malmir[a], Baharak Eslami[b*], Mariyam Malmir[c]

a, b Department of Physics, Payame Noor University, Iran; bkeslami@yahoo.com; s_malmir84@yahoo.com

c Department of chemistry, University of Kurdistan, Iran; maryam.86.67@gmail.com

Abstract

The interaction between hydrogen peroxide and double-stranded DNA constructing base pair, Adenine-Thymine and Guanine-Cytosine using the M062-X calculation and base set 6-31G (d) optimized. The structure parameters including hydrogen bonds and dihedral angle between the species of each base pair and electronic properties including change transfer between base pair and radical, the energy of HOMO and LUMO calculated for each complex. AIM2000 program to obtain critical points of the profile, the electron density and the Laplacian of the electron density is in the complexes.

Keywords: NA, Adenine-Thymine base pair; Guanine-Cytosine base pair, Hydrogen peroxide; cancer, AIM; NBO

I. Introduction

There are many different chemicals in the environment where they are very active and can be harmful to human health. (H2O2) is a widely used oxidizing and bleaching agent. Contact with this substance poses health risks [1] Furthermore, in recent years, DNA has received considerable attention because it is application in biotechnology, microelectronic devices, DNA-based computation, medicine and the pharmaceutical industry [2]. Therefore, it would be of interest to analyze the stability and quantum chemical aspects of complexes of hydrogen peroxide with DNA base pairs [3].

II. Methods

. In this paper, the interaction of chemical species such as hydrogen peroxide with pairs of DNA bases investigated. The main purpose of this study is the effect of this chemical species on hydrogen bonds between pairs. In addition, to what extent these species affect the properties of DNA bases. The structures of the (H_2O_2)/G-C, A-T pairs and its constituent monomers were optimized by the B3LYP level using the 6-31G*basis set within the Gaussian 09 program. . The error in this work has done in the AIM method at the M06 - 2 X / 6 - 31 G computing level. In the NBO method, natural orbitals used instead of molecular orbitals

III. Results and discussion

In figure (1) and (2) the optimized geometric structure of hydrogen peroxide with AT and GC is indicated. For the AT - H2O2 complex, the structure is A1.B 1 is the most stable condition for GC- H2O2.

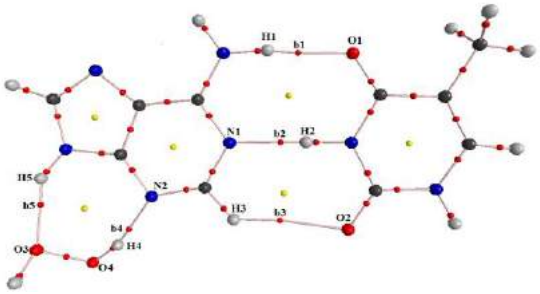

Fig. 1.. AT- H2O2 optimized complex structure at computational level m06 2x / 6 31g *

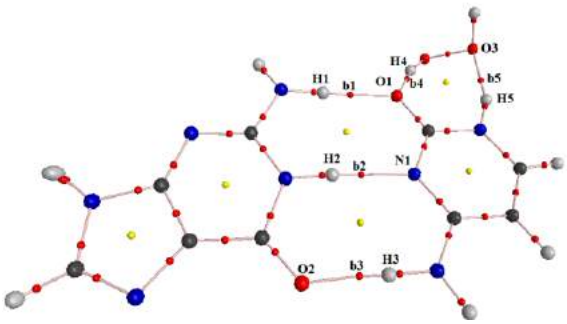

Fig. 2. GC- H_2O_2 optimized complex structure at computational level m06 2x / 6 31g *

In table (1) the hydrogen peroxide data is given with AT the structures in the A1 structure are more stable compounds. Because its energy is more negative than any other structure. It can be concluded that, with an interaction between AT and the joints between the base pair are shorter, and they are closer together and cause an AT structure out of the normal state. In fact, the change of the angle for the different structures of adenine and from the downstream direction is greater.in these structures, the variation of the angle aligned with the energy stability

Table 1. Investigation of electronic properties of AT complexes in the presence of H2O2 at computational level M06 2X / 6 31G

کمپلکس	برهمکنش	فاصله	Δr(A°)	ΔDH	ΔE(kJ/mol)	ΔH(kJ/mol)
	H1…..O1	1.9314				
AT	H2…..N1	1.8337	-	-	-	-
	H3…..O2	2.8532				
	H1…..O1	1.9463				
	H2…..N1	1.7855	B1:0.014			
A1	H3…..O2	2.7097	B2:-0.048	2.2452	-69.5454	-63.4324
	H5…..O3	1.8437	B3:-0.143			
	O4……H4	1.9487				
	H1…..O1	1.9508	B1:0.0190			
	H2…..N1	1.7816	B2:-			
A2	H3…..O2	2.7027	0.0521	2.4051	-67.6986	-60.4814
	H4…..N2	1.8516	B3:-			
	H5…..O3	2.2989	0.1505			
	H1…..O1	1.9316	B1:0.0020			
	H2…..N1	1.7808	B2:-			
A3	H3…..O2	2.7242	0.0529	0.8270	-65.2782	-58.6750
	H4…..O2	1.7897	B3:-			
	H5…..O3	2.3389	0.1290			
	H1…..O1	1.9737	B1:-			
	H2…..N1	1.7857	0.1747			
A4	H3…..O2	2.6785	B2:-	0.0382	-60.5929	-53.6051
	H4…..N2	1.8073	0.0480			
	H5…..O3	2.4019	B3:0.0423			

The structural properties of GC complexes with H2O2 listed in Table (2). According to the data of this table, the parameter B1 considered as the most negative in the most stable amount of energy. For the most stable structure, H_2O_2 interacts with cytosine base from above. The bond length $H_1…O_1$, which is the closest bond to H_2O_2, more affected than other bonds, causing the base pair to move closer together.

Table 2. Investigation of electronic properties of GC complexes in the presence of H_2O_2 at computational level M06 2X / 6 31G

کمپلکس	برهمکنش	فاصله	Δr(A°)	ΔDH	ΔE(kJ/mol)	ΔH(kJ/mol)
	H1…..O1	1.9115				
GC	H2…..N1	1.9186	-	-	-	-
	H3…..O2	1.7808				
	H1…..O1	1.9189				
	H2…..N1	1.9221	B1:0.0073			
B1	H3…..O2	1.7512	B2:0.0035	5.9533	-69.7164	-59.3235
	H4…..O1	1.7567	B3:-			
	H5…..O3	1.8621	0.0073			
	H1…..O1	1.8639	B1:-			
	H2…..N1	1.8994	0.0276			
B2	H3…..O2	1.8114	B2:-	3.1881	-66.6726	-55.2592
	H4…..N2	1.9666	0.0192			
	H5…..O3	1.8882	B3:0.0305			
	H1…..O1	1.8865	B1:-			
	H2…..N1	1.8983	0.0250			
B3	H3…..O2	1.7900	B2:-	2.4578	-55.0560	-45.3951
	H4…..N2	1.8611	0.0203			
	H5…..O3	2.4765	B3:0.0292			
	H1…..O1	1.9431				
	H2…..N1	1.8909	B1:0.0315			
	H3…..O2	1.8500	B2:-			
B4	H4…..N1	2.2082	0.0276	20.3133	-54.8147	-44.3869
	N2…..O3	3.0811				
	N3…..O4	3.0689	B3:0.0692			
	H5…..O2	1.9069				

IV. Conclusions

The results show that hydrogen peroxide has affected the pairs of adenine thymine and guanine cytosine and the size and power of hydrogen bonding in the base pair are affected. It found that the interactions mainly characterized by intermolecular hydrogen bonds. As a result, it changes the geometric structure of DNA. Therefore, this species may be cacerigenous with respect the human's cell.

References

[1]. I.R. Gould, P.A. Kollman, J. Am. Chem. Soc. 1994, 116, 2493

[2]. Y. Chun-Y.Y. Zhong-Zhi, School of Chemistry and Chemical Engineering, Liaoning Normal University, Dalian. 2011, 11, 6029

[3] P. Sun, A. Wu, N. Sun, X. Qiao, L. Shi and L. Zheng, Langmuir, 2018, 34, 2791-2799.

بیست و سومین کنفرانس شیمی فیزیک انجمن شیمی ایران
23rd ICS Physical Chemistry Conference
Chemistry Department,
Faculty of Science
Shahid Bahonar University of Kerman
Kerman, Iran
12-13 Jan 2022
ایران، کرمان
دانشگاه شهید باهنر کرمان
دانشکده علوم پایه، بخش شیمی
۲۳-۲۲ دی ماه ۱۴۰۰

Study of the Peptide Nucleic Acid (PNA)-RNA interactions using molecular dynamics simulation

Eghbal Omari[*], Seifollah Jalili[b], Atena Pakzadiyan[c]

[a]Department of Chemistry, K. N. Toosi University of Technology, Tehran, Iran, sjalili@kntu.ac.ir
[b]Department of Chemistry, K. N. Toosi University of Technology, Tehran, Iran, eghball.omar@gmail.com
[c]Department of Chemistry, K. N. Toosi University of Technology, Tehran, Iran, a.pakzadiyan@email.kntu.ac.ir

Abstract

Peptide Nucleic Acids (PNAs) are an important class of oligonucleotides. These molecules can attach to their complementary DNA or RNA strands and even form double strands (similar to DNA) together. Knowledge of the mechanism by which PNA interacts with RNA (or DNA) is important for the design and synthesis of PNAs. These studies can be performed using molecular dynamics simulations and make predictions about the strength of the interaction and the factors affecting it.

Keywords: Molecular dynamics simulation; Oligonucleotides; Peptide nucleic acids (PNAs); Synthesis.

I. Introduction

PNA was originally designed and developed as an imitation of an oligonucleotide for the detection of DNA, which binds to a large groove and forms a triplex. However, the PNA polyamide backbone is a very good structural imitation of the ribonucleic backbone of phosphate acids. Thus, PNA has attracted widespread attention in medicinal chemistry for the development of genetics, drugs, and genetic diagnosis [1][2,3] .

II. Methods

Gromacs software version 4.6.1 was used in all stages of molecular dynamics simulation. The force field selected in all stages is Charmm 27[2]. The solvent was then TIP3P water model. Equilibration in the NVT curve was performed using the LINCS algorithm for 1000 ps at a temperature of 310 K. The original simulation was performed for 20 ns. stages are Charmm 27. The solvent was TIP3P water model. Equilibration in the NVT curve was performed using the LINCS algorithm for 1000 ps at a temperature of 310 Kelvin [3,4].

III. Results and discussion

For the four structures, the analyzes of RMSF, Distance, and RMSD Distribution were calculated, respectively. According to the diagram, the flexibility of the two duplexes of RNA-PNA is almost equal. The maximum flexibility of the structure is related to the PNA-PNA duplex, the highest numerical value RMSF during the simulation time is related to the same duplex and is equal to 0.88, which indicates the highest fluctuation and the most instability among the four structures, in contrast to the highest stability and the least fluctuation with the numerical value RMSF is equal to 0.39 for RNA-RNA duplex (Figure 1).

At first, the distance between the atoms involved in the interaction in the PNA-PNA duplex is greater than the rest and fluctuates more over time, the most stable conditions

are related to the RNA(cug)-PNA duplex (Figure 2).

.

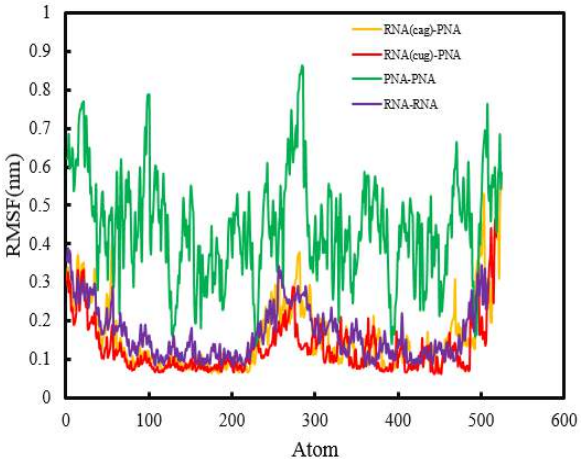

Fig. 1. Rmsf diagram of the four structures studied.

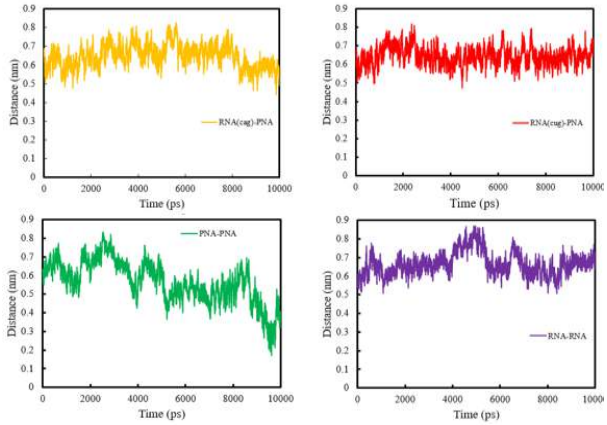

Fig. 2. Distance diagram of the four structures studied.

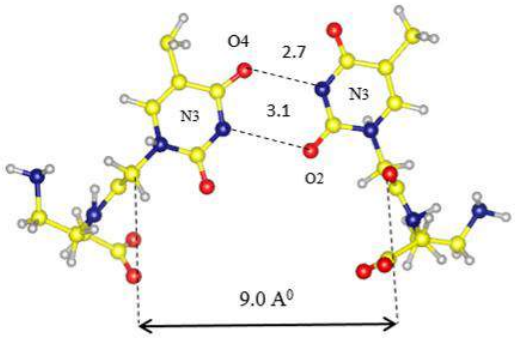

Fig.3. T–T base pairing interactions in the PNA–PNA duplex. Hydrogen are bonds and donor–acceptor distances indicated [6].

IV. Conclusions

PNA's role has been proposed as a primordial carrier of genetic information. Two conditions were set to support this speculation: that components of PNA be found in the primitive microorganisms and that sequence-specific PNA-PNA and PNA-RNA interactions be demonstrated[1]

.

References

[1] A. Kiliszek, K. Banaszak, Z. Dauter, W. Rypniewski, The first crystal structures of RNA–PNA duplexes and a PNA-PNA duplex containing mismatches—toward anti-sense therapy against TREDs, Nucleic Acids Res. 44 (2016) 1937–1943.

[2] K. Vanommeslaeghe, E. Hatcher, C. Acharya, S. Kundu, S. Zhong, J. Shim, E. Darian, O. Guvench, P. Lopes, I. Vorobyov, CHARMM general force field: A force field for drug-like molecules compatible with the CHARMM all-atom additive biological force fields, J. Comput. Chem. 31 (2010) 671–690.

[3] W.L. Jorgensen, J. Chandrasekhar, J.D. Madura, R.W. Impey, M.L. Klein, Comparison of simple potential functions for simulating liquid water, J. Chem. Phys. 79 (1983) 926–935.

[4] B. Hess, H. Bekker, H.J.C. Berendsen, J.G.E.M. Fraaije, LINCS: a linear constraint solver for molecular simulations, J. Comput. Chem. 18 (1997) 1463–1472.

بیست و سومین کنفرانس شیمی فیزیک انجمن شیمی ایران
23rd ICS Physical Chemistry Conference
Chemistry Department,
Faculty of Science
Shahid Bahonar University of Kerman
Kerman, Iran
12-13 Jan 2022
ایران، کرمان
دانشگاه شهید باهنر کرمان
دانشکده علوم پایه، بخش شیمی
۲۳-۲۲ دی ماه ۱۴۰۰

Study of electrochemical and structural properties of PTCDI molecule and some of its derivatives for the use in lithium-ion batteries

Faezeh Ebrahimi[a,*], Afshin Abbasi[a]

[a] *Department of Chemistry, University of Qom, Qom, Iran,*
**febrahimi313@gmail.com*

Abstract

3, 4, 9 and, 10-perylene tetracarboxylic diimide (PTCDI), is a promising electrode organic molecule for lithium-ion batteries (LIBs). However, it needs to be modified to receive better performance by molecular functionalization. In this study, we used different halogens as substitutions of this molecule and we considered their electrochemical and structural properties using Density Functional Calculations (DFT).

Keywords: Lithium-ion batteries; DFT calculations; electrochemical properties; organic electrodes; Halogenation.

I. Introduction

Lithium-ion batteries are the most susceptible type of rechargeable batteries which have received considered attention in recent decades have led to the development of prevailing electrical devices.

Despite the significant development of LIBS, the traditional production of these batteries is based on intermediate metal oxides, which are rare, expensive and, toxic elements.

Due to these disadvantages, the tendency to use organic materials instead of inorganics is increasing every day.

In recent years, small organic molecules, as well as large molecules and organic polymers have been studied in LIBs, and acceptable results have been recorded from the use of these molecules [1-3].

Most of these molecules have conjugate structures or benzene rings that allow electron transfer and conduction of electricity [4-6]. PTCDI is an organic substance that has presented potential application in LIBs [7].

I. Methods

To evaluate the structural and electrical properties of halogenated PTCDI, DFT calculations have been done using B3LYP functional and 6-31G(d) basis sets which is implemented in Gaussian 09 computational software. All the structures were fully optimized followed by vibrational frequency calculations to prove the real local minimum.

II. Results and discussion

PTCDI has eight hydrogens bonded to carbons. To substitute two hydrogens with halogen atoms sixteen structural isomers have appeared. All these structures were fully optimized using the same level of theory.

In the next step, two Li atoms were added in the positions of the anhydride oxygens and the final optimized structure is shown

Fig 1. The reaction of functionalized PTCDI (PTCDI-2X) with Li atoms can be discussed as follow:

$PTCDI\text{-}2X + 2Li \rightarrow PTCDI\text{-}2XLi_2$

The $PTCDI\text{-}2XLi_2$ compounds were then fully optimized. Vibrational frequency calculations let us calculate the Gibbs free energy difference (ΔG), The Enthalpy of the reaction (ΔH) as well as the electrical potential using the following equation.

$$\Delta E = -\frac{\Delta G}{nF}$$

Where F is the Faraday number. The results of the calculations of free energy differences, reaction enthalpies and voltages are summarized in table 1:

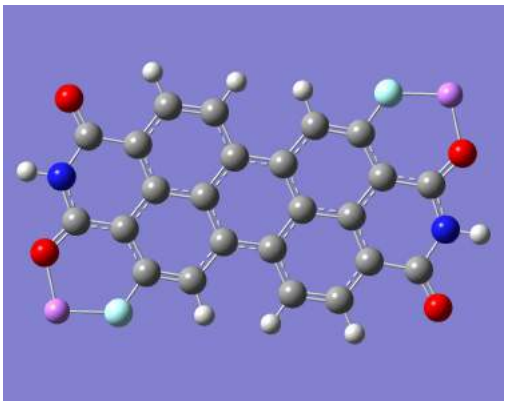

Fig. 1. Optimized structure of 2,8-DIFLUOROPTCDI- LI .

Table 1. Calculation of free energy and voltage and enthalpy:

Molecule name	ΔG (Kcal/mol)	E_f (V)	ΔH (Kcal/mol)
PTCDI-LI	-122.71	-2.66	-139.81
2,8-DIFLUOROPTCDI-LI	-115.08	-2.49	-132.12
2,8,DICHLOROPTCDI-LI	-104.43	-2.26	-120.48
2,8-DIBROMOPTCDI-LI	-116.96	-2.53	-131.79
2,8,DIIODOPTCDI-LI	-116.11	-2.51	-131.98

III. Conclusions

Our calculations show that halogen substitutions can influence the electrical properties as well as the molecular efficiency in LIBS.

The calculated electrical potentials of the halogens can be sorted as: F> Cl> Br = I, which shows the more electronegative element i.e., F represent better efficiency.

References

[1] P. Poizot, F. Dolhem, and J. Gaubicher, Curr. Opin. Electrochem., 2018, 9, 70–80.

[2] Gracia, R., & Mecerreyes, D., (2013). Polymers with redox properties: materials for batteries, biosensors and more. Polymer Chemistry, 4 (7), 2206–2214.

[3] Novák, P., Müller, K., Santhanam, K. S. V., & Haas, O., (1997). Electrochemically active polymers for rechargeable batteries. Chemical Reviews, 97 (1), 207–282.

[4] Deng, W., Shen, Y., Qian, J., Cao, Y., & Yang, H. (2015). A Perylene Diimide Crystal with High Capacity and Stable Cyclability for Na-Ion Batteries. ACS Appl. Mater & Interfaces, 7 , 21095-21099.

[5] Wu, D., Jing, F., Xi, X., Ma, L., Lu, D., Yang, P., & Liu, R., (2019). An Organic Solvent-free Approach towards PDI/Carbon Cloth Composites as Flexible Lithium Ion Battery Cathodes. Journal of Colloid and Interface Science, 538, 597-604.

[6] Bai, Y., Fu, W., Chen, W., Chen, Z., Pan, X., Lv, X., Wu, J., & Pan, X., (2019). Perylenetetracarboxylic diimide as a high-rate anode for potassium-ion batteries. Journal of Materials Chemistry A, 7, 24454–24461.

[7] Bai, Y., Fu, W., Chen, W., Chen, Z., Pan, X., Lv, X., Wu, J., & Pan, X., (2019). Perylenetetracarboxylic diimide as a high-rate anode for potassium-ion batteries. Journal of Materials Chemistry A, 7, 24454–24461.

بیست و سومین کنفرانس شیمی فیزیک انجمن شیمی ایران
23rd ICS Physical Chemistry Conference
Chemistry Department,
Faculty of Science
Shahid Bahonar University of Kerman
Kerman, Iran
12-13 Jan 2022
ایران، کرمان
دانشگاه شهید باهنر کرمان
دانشکده علوم پایه، بخش شیمی
۲۳-۲۲ دی ماه ۱۴۰۰

Investigation of the effect of electron donor and acceptor functional groups on the performance of PTCDI molecule for use in lithium-ion batteries

Faezeh Ebrahimi[a,*], Afshin Abbasi[a]

[a] *Department of Chemistry, University of Qom, Qom, Iran,*
**febrahimi313@gmail.com*

Abstract

One of the widely studied organic materials for use in lithium-ion batteries (LIBs) is 3, 4, 9, and 10-perylene tetracarboxylic diimide (PTCDI). The π-π aromatic arrangement and its stack structure and semiconducting property make this molecule suitable for use in the anode of LIBs. In this study, the effect of a variety of substitutions with different electronegativity on the performance of the PTCDI has been investigated using density functional theory calculations (DFT).

Keywords: Ion-lithium batteries; DFT calculations; electrochemical properties; organic electrodes; electron donor and acceptor functional groups.

I. Introduction

Today we see rapid and growing demand for various solutions to store electrochemical energy. This trend of demand is increasing rapidly with the increase of the planet's population and the change of people's lifestyles. In the meantime, the need for stronger electrochemical power supplies is felt in the three main applications of electric transport, portable and non-portable energy storage devices [1-4].

In recent years, small and large organic molecules and polymer have been studied in lithium batteries, and acceptable results have been recorded from the use of these molecules [5-7].

Previous studies have shown that the PTCDI base electrode produces a high capacity of 310 mAh/g with a high efficiency [8].

II. Methods

To evaluate the structural and electrical properties of PTCDI and its substitutions, DFT calculation have been done using B3LYP functional and the 6-31G(d) basis set which are implemented in Gaussian 09 computational software. All the structures were fully optimized followed by vibrational frequency calculations to proof the real local minimum.

III. Results and discussion

In this study four different functional groups i.e. -Methyl, -Vinyl, -OH and -NO2 were used as the substituted groups in the PTCDI molecule. It has eight hydrogens bonded to the perylene carbons. To substitute two hydrogens with two functional groups sixteen structural isomers have appeared. All these structures were fully optimized using the same level of theory.

In the next step, two Li atoms were added in the positions of the anhydride oxygens. The final optimized structure is shown Fig. 1.

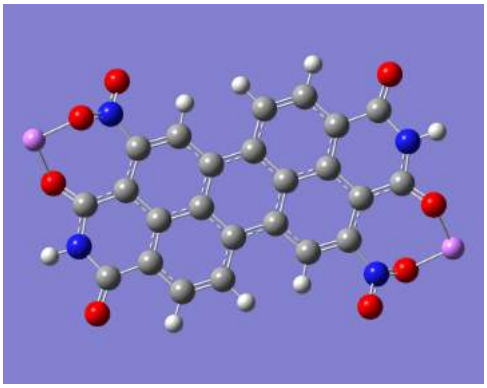

Fig. 1. Optimized structure of 2,8-NO2 PTCDI- LI

These compounds were then fully optimized. Vibrational frequencies calculations let us to calculate the Gibbs free energy differences (ΔG), The Enthalpy of the reactions (ΔH) as well as the electrical potentials that were obtained using the following equation:

$$\Delta E = -\frac{\Delta G}{nF}$$

Where F is the Faraday number. The results are summarized in Table 1:

Table 1. Calculation of free energy and voltage and enthalpy:

Molecule name	ΔG (Kcal/mol)	E_f (V)	ΔH (Kcal/mol)
PTCDI-LI	-122.71	-2.66	-139.81
2,8-DIHYDROXYPTCDI	-89.80	-1.94	-104.82
2,8-DIMETHYLPTCDI	-60.11	-1.30	-76.09
2,8-DIVINYLPTCDI	-103.24	-2.24	-122.07
2, 8-$(NO2)_2$ PTCDI	-135.52	-2.93	-156.76

IV. Conclusions

Since the higher electrical potential is a technical factor of the LIBs efficiency, from the results of Table 1 the following trend can be concluded:

-NO2 > PTCDI > -Vinyl > -OH > -Methyl

Hence, higher electronegative group of NO2 represents higher electrical potential and better efficiency.

References

[1] Whittingham, M. S., (1976). Electrical energy storage and intercalation chemistry. Science, 192 (4244), 1126–1127.

[2] Mizushima, K., Jones, P. C., Wiseman, P. J., & Goodenough, J. B. (1980). LixCoO2 (0<x<−1) a new cathode material for batteries of high energy density. Materials Research Bulletin, 15(6), 783–789.

[3] Moshtev, R., & Johnson, B., (2000). State of the art of commercial Li ion batteries. Journal of Power Sources, 91(2), 86–91.

[4] Goodenough, J. B., & Kim, Y. (2011). Challenges for rechargeable batteries. Journal of Power Sources, 196(16), 6688–6694.

[5] Poizot, P., Dolhem, F., & Gaubicher, J., (2018). Progress in all-organic rechargeable batteries using cationic and anionic configurations: toward low cost and greener storage solutions? Current Opinion in Electrochemistry, 9, 70–80.

[6] Gracia, R., & Mecerreyes, D., (2013). Polymers with redox properties: materials for batteries, biosensors and more. Polymer Chemistry, 4 (7), 2206–2214.

[7] Novák, P., Müller, K., Santhanam, K. S. V., & Haas, O., (1997). Electrochemically active polymers for rechargeable batteries. Chemical Reviews, 97 (1), 207–282.

[8] Bai, Y., Fu, W., Chen, W., Chen, Z., Pan, X., Lv, X., Wu, J., & Pan, X., (2019). Perylenetetracarboxylic diimide as a high-rate anode for potassium-ion batteries. Journal of Materials Chemistry A, 7, 24454–24461.

بیست و سومین کنفرانس شیمی فیزیک انجمن شیمی ایران
23rd ICS Physical Chemistry Conference
Chemistry Department,
Faculty of Science
Shahid Bahonar University of Kerman
Kerman, Iran
12-13 Jan 2022
ایران، کرمان
دانشگاه شهید باهنر کرمان
دانشکده علوم پایه، بخش شیمی
۲۳-۲۲ دی ماه ۱۴۰۰

Synthesis of nitrogen-doped carbon microspheres containing cobalt nanoparticles and its application in hydrogen release

Meisam khorashadizadeh, Vahid Saheb*
* *Department of Chemistry, Shahid Bahonar University of Kerman, Kerman, Iran, vahidsaheb@uk.ac.ir*

Abstract

Today, nanotechnology is a widespread and widely used science that is use in various industries by creating different properties in materials. Nanoparticles synthesized in different ways, one of these methods, hydrothermal synthesis method that is affordable and accessible.

In this study, hydrothermal synthesis method to produce carbon microspheres doped with nitrogen (NCCS) has been applied .In addition, a certain amount of cobalt nanoparticles placed on the surface of the substrate and catalyst to release hydrogen from metal hydride to ($NaBH_4$) provided.

Keywords: Nitrogen Doped Carbon Microsphere, Hydrothermal Synthesis, Cobalt Nanoparticles, Hydrogen Release, Sodium Borohydride.

I. Introduction

Public concerns about the depletion of fossil fuels and the problems associated with global warming and environmental pollution make the establishment of a clean and sustainable energy system a compelling need. As an alternative fuel, hydrogen is considered as a promising clean energy carrier in future energy system with high energy density and zero emission [1,2].

Recently, the potential use of NaBH4 has gained increasing attention as a promising source of hydrogen storage and generation by hydrolysis[3].

During the past decades, a variety of catalysts such as Lewis acids, metal complexes, precious metals, non-noble metals, and alloys have been developed for hydrogen generation using $NaBH_4$ hydrolysis [4].

To reduce aggregation of the catalyst particles and further improve the catalytic activity, various materials such as carbon, oxides, hydroxyapatite, clay, heteropolyanions, polymer/hydrogel, and Ni foamhave been chosen as the supports.[5]

II. Methods

First, using a hydrothermal method, a carbon substrate consisting of carbon microspheres doped with nitrogen was synthesized and then cobalt nanoparticles were placed on it to be used in the hydrogen release test at different temperatures.

Actually, by adding $NaBH_4$ solution, Co^{2+} ions are easily reduced in situ to cobalt metals, which precipitate uniformly on the surface of the NCCS support.

For comparison, nickel nanoparticles were used to evaluate the rate of hydrogen release for this catalyst. It should be noted that in these experiments, carbon microspheres and coffee grounds powder were used as the substrate and all these experiments were performed at a constant pH.

III. Results and discussion

The hydrogen release test from metal hydride has used to evaluate the

performance of the catalyst. The test conducted by an adiabatic system that finally calculate the activation energy of the reaction, the amount of primary energy necessary to release hydrogen from metal hydride calculated .Also, for further investigation and comparison between different nanomaterials, the catalyst was replaced with another metal and re-examined. From another perspective, catalyst to release hydrogen at different temperatures tested to evaluate its performance. According to the results, the performance of the catalyst has improved with temperature change and this result is completely different for catalysts and different substrates

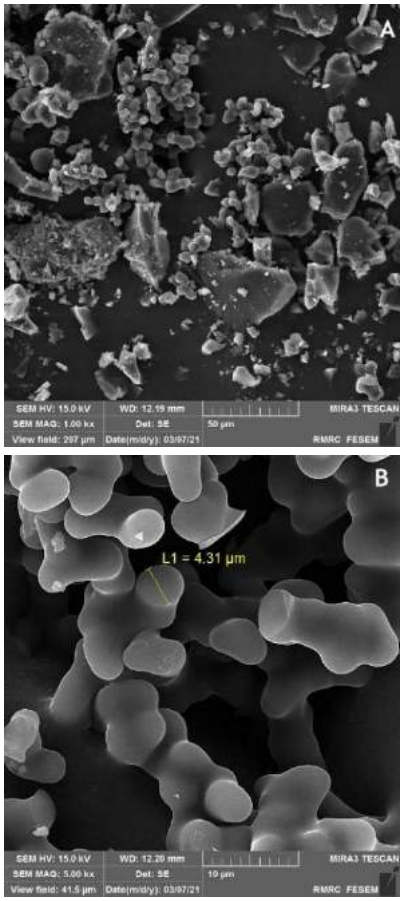

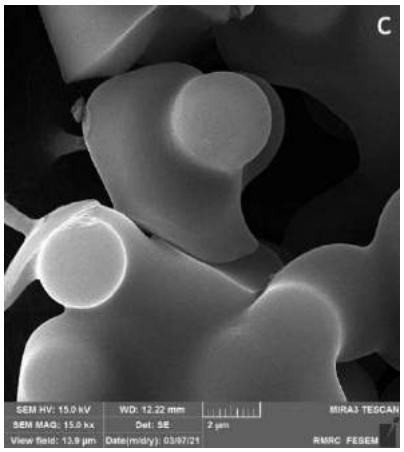

Fig. 1. FESEM images from nitrogen-doped carbon microspheres (NCCS)(A, B & C)

IV. Conclusions

In summary, nitrogen-doped colloidal carbon spheres (NCCS) were obtained by commercial glucose hydrothermal treatment and were first used as a substrate for the preparation of NCCS / Co catalysts with different CO loads by chemical reduction of Co^{2+} with $NaBH_4$. Co catalysts using NCCS substrate show excellent catalytic activity compared to $NaBH_4$ hydrolysis thanks to their unique hydrophilic surface which improves the contact between the catalysts and $NaBH_4$ in alkaline environment.

References

[1] Jie Zhu, Rong Li, Weiling Niu, Yanjun Wu, Xinglong Gou ,Journal of Power Sources 211 (2012) 33e39.

[2] H. Marty, Nature 472 (2011) 137.

[3] Niu W, Ren D, Han Y, Wu Y, Gou X, J Alloy Comp 2012;543:159e66.

[4] Zhu J, Li R, Niu W, Wu Y, Gou X, Int J Hydrogen Energy 2013;38(25):10864e70 .

[5]V.I. Simagina, O.V. Komova, A.M. Ozerova, O.V. Netskina, G.V. Odegova, D.G. Kellerman, O.A. Bulavchenko, A.V. Ishchenko, Appl. Catal A 394 (2011) 86e92.

بیست و سومین کنفرانس شیمی فیزیک انجمن شیمی ایران
23rd ICS Physical Chemistry Conference
Chemistry Department,
Faculty of Science
Shahid Bahonar University of Kerman
Kerman, Iran
12-13 Jan 2022
ایران، کرمان
دانشگاه شهید باهنر کرمان
دانشکده علوم پایه، بخش شیمی
۲۳-۲۲ دی ماه ۱۴۰۰

Electrochemical sensitive detection of a β-blocker drug using a nanostructured electrode based on a ferrite/graphene oxide nanocomposite

Asma Khoobi*

Department of Chemistry, Faculty of Sciences, University of Sistan and Baluchestan, Zahedan, 98135-674, Iran, a.khoobi@science.usb.ac.ir

Abstract

The present work reports designing of a new nanostructured sensor for analysis of atenolol as a β-blocker drug. At first, ferrite/graphene xide nanocomposite (FGON) is synthesized using ultrasonic process. Then, the structure and morphology of the samples are studied using different techniques such as Fourier transform infrared (FTIR), X-ray diffraction (XRD) and scanning electron microscopy (SEM). After confirmation of nanosized structure of the samples, they use an electrochemical sensor for determination of atenolol. The sensor is fabricated as FGON modified carbon paste electrode (FGON/CPE). The modification of the electrode shows a significant enhancement of the oxidation current of atenolol than the unmodified electrode. The electrochemical determinations at the surface of the nanostructured modified electrode present a wide dynamic linear range of 0.10-250.0 μM with a detection limit of 9.4 nM for atenolol. Finally, for investigation the applicability of the proposed electrochemical sensor, detection of the atenolol is performed in real complicated samples and acceptable recoveries are obtained.

Keywords: Nanostructured sensor; Ultrasonic irradiation; Structural analysis; Modification, Atenolol; Electrochemical studies.

I. Introduction

β-Blockers such as atenolol are one of the most commonly prescribed drugs all over the world. The drugs are applied for treatment of numerous diseases for example hypertension treatment, anginal attack prevention, heart failure, and myocardial infarction prevention [1,2]. But, some of the compounds have been misused by horses participating or athletes in highly competitive, and thus being prohibited as the doping agents [3]. Therefore, it is seemed to introduce a selective and sensitive procedure for detection of the compounds in real samples is necessary. Among the procedures that were described for β-blockers analysis, electrochemical techniques based on nanostructured electrodes are preferred due to their benefits for instance rapid detection, high selectivity and sensitivity, low cost and etc. In the present study, a new sensor based on (FGON/CPE) was used for sensitive and selective determination of atenolol.

II. Methods

All chemicals were applied in analytical grade. Deionized water was used for freshly preparation all of solutions. Atenolol, carbon graphite powder, paraffin oil, $Fe(NO_3)_3.9H_2O$, and other compounds were obtained from Merck. Synthesis of graphene oxide (GO) was performed using the modified Hummers' process [4]. Ultrasonic method was applied for preparation of ferrite nanostructure. Then, FGON was synthesized by a pre-graphenization method [5]. Finally, FGONs was used for fabrication of a modified sensor for detection of atenolol.

III. Results and discussion

The FTIR spectrum of the samples was studied in the range of 4000-400 cm^{-1} (Fig. 1).

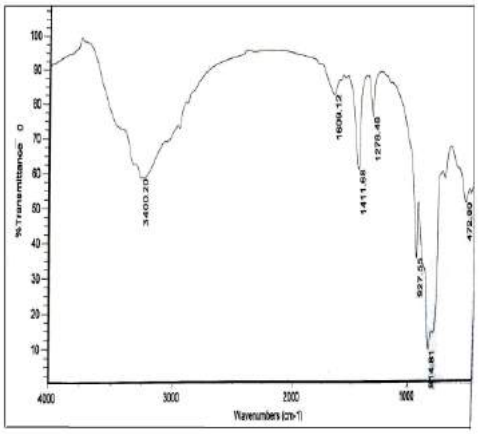

Fig. 1. FTIR spectrum of FGON.

Also, characterization and crystallite size of the samples were investigated using XRD. Sharp and strong peaks proposed the synthesized samples were well crystallized as FGON (Fig. 2). Furthermore, the crystallite size of the nanostructures was obtained 27.6 nm using Scherrer equation. Also, SEM was applied for surface studies. The micrograph indicated the formation of the nanostructures (Fig. 3). Therefore, the nanostructures can be potential sensing materials for electrochemical analysis.

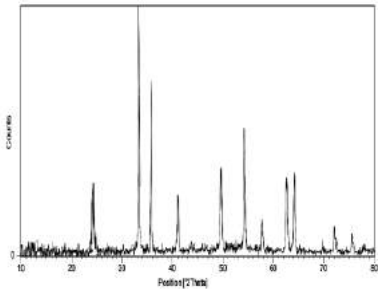

Fig. 2. XRD pattern of FGON

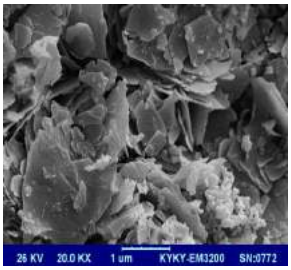

Fig. 3. SEM micrograph of FGON.

Differential pulse voltammetry was used for determination of atenolol at the surface of FGON/CPE in the optimized conditions. Therefore, a calibration curve based on voltammetric oxidation peak was plotted. Using the analysis of the data, limit of detection (3σ) of atenolol was estimated 9.4 nM with a dynamic linear range of 0.10-250.0 µM.

Investigation of the capability of the proposed method was checked by detection of atenolol in pharmaceutical and biological samples. The experiments showed the recovery ranges between 94.67-106.33% and 95.40%-103.80% for biological samples and pharmaceutical, respectively (Table 1). The data indicated that the proposed strategy can be effectively applied for the detection of atenolol in real complicated samples.

Table 1. Detection of atenolol in real samples at the surface of FGON/CPE.

Sample	No.	Spiked (µM)	Found (µM)	Recovery (%)
Human serum	**1**	0.0	Not detected	-
	2	3.00	3.19	106.33
	3	6.00	5.68	94.67
	4	9.00	8.84	98.22
Tablet	**1**	3.00	3.10	103.33
	2	5.00	4.77	95.40
	3	7.00	6.83	97.57
	4	10.00	10.38	103.80

IV. Conclusions

In this work voltammetric method was used for determination of trace amounts of atenolol using a FGON/CPE in the optimized chemical and instrumental conditions. After structural characterization, the nanostructures were applied for modification of the surface of a CPE for electrochemical studies of atenolol. Using the nanostructured modified electrode a low limit of detection and broad linear dynamic range was obtained. Also, detection of atenolol in real samples showed acceptable results that indicating the proposed sensor can be a potential material for drug analysis.

References

[1] V. Bhatia, A. Dhir and A. K. Ray, J. Photochem. Photobiol., A, 2021, 409, 113136.
[2] A. Ponkshe and P. Thakur, Mater. Today, 2019, 18, 1162-1175.
[3] M. Delamoye, C. Duverneuil, F. Paraire, P. Mazancourt and J.C. Alvarez, Forensic Sci. Int., 2004, 141, 23-31.
[4] M. Nawaz, M.U. Islam, M.A. Nazir, I. Bano, I.H. Gul and M. Ajmal, Ceram. Int., 2021, 47, 25505-25513.
[5] H.-J. Shin, K.K. Kim, A. Benayad, S.-M. Yoon, H.K. Park, I.-S. Jung, M.H. Jin, H.-K. Jeong, J.M. Kim, J.-Y. Choi and Y.H. Lee, Adv. Funct. Mater., 2009, 19, 1987-1992.

بیست و سومین کنفرانس شیمی فیزیک انجمن شیمی ایران
23rd ICS Physical Chemistry Conference
Chemistry Department,
Faculty of Science
Shahid Bahonar University of Kerman
Kerman, Iran
12-13 Jan 2022
ایران، کرمان
دانشگاه شهید باهنر کرمان
دانشکده علوم پایه، بخش شیمی
۲۲-۲۳ دی ماه ۱۴۰۰

Multivariate optimization method for designing an electrochemical selective nanostructured sensor in analysis of tyrosine

Asma Khoobi*

Department of Chemistry, Faculty of Sciences, University of Sistan and Baluchestan, Zahedan, 98135-674, Iran, a.khoobi@science.usb.ac.ir

Abstract

The present study reports simultaneous optimization of various parameters affecting in the oxidation peak current of tyrosine as a main amino acid in protein structures. All experimental variables containing chemical and instrumental parameters are simultaneously optimized. For achieving the purpose at first design of experiments (DoE) are considered before any experimental tests. Then, response surface methodology (RSM) is applied to find the optimized parameters. The electrochemical experiments for determination of tyrosine are accomplished at the surface of a nanostructured modified electrode. The electrode is fabricated using gold nanoparticles via a green approach. Voltammetric experiments are performed in the optimized conditions for determination of tyrosine using the nanostructured electrode. Analyzing of the data shows a linear dynamic range for tyrosine between 0.10-350.0 μM and the limit of detection is found to be 9.2 nM. Finally, the capability of the proposed modified sensor is confirmed using the detection of tyrosine in biological real samples.

Keywords: Eco-friendly green synthesis; Gold nanoparticles; Response surface methodology; Tyrosine; Voltammetric techniques; Sensing analysis.

I. Introduction

One of very important components of cells is proteins that have been composed from amino acids. The compounds create key roles in wide ranges of biological processes. Among of amino acids, tyrosine is a key amino acid that creates main roles in protein structures. Tyrosine is applied as protein-based supplements for treatment of numerous kinds of genetic disorder for example phenylketonuria. Also, the amino acid is being used for improving learning, memory [1,2]. The abnormal amount of tyrosine causes some human diseases. Parkinson's disease is result of increasing of level of tyrosine. Also, depression, alkaptonuria, hypochondrium, and albinism are due to lack of tyrosine [3]. Thus, it is seemed developing a rapid, simple, accurate and inexpensive method is necessary for analysis of low concentrations of the amino acid. In this study, onion peel was used for synthesis of gold nanoparticles as a stabilizing and reducing natural agent. Then, a carbon paste electrode based on the gold nanoparticles (CPE/GNPs) was fabricated and used for detection of tyrosine in biological complicated samples.

II. Methods

Tyrosine, $HAuCl_4$, carbon graphite powder, and other materials were obtained from Merck. H_3PO_4, H_3BO_3, CH_3COOH, and NaOH were used for adjusting of pH. Analytical grade of the chemicals was used in all experiments. For synthesis of GNPs, $HAuCl_4$ (1mM) and appropriate amount of onion peel was used and deionized water was added up to 10 mL. Then, color of the solution changed from yellow to ruby red. Next, the nanoparticles were used for fabrication of a nanostructured modified electrode for determination of tyrosine using electrochemical methods.

III. Results and discussion

UV-Vis spectroscopy was used for characterization of GNPs. For the colloidal gold a maximum UV-Vis absorption was obtained in 520 nm (Fig. 1) that indicating 24 nm diameter for colloidal GNPs [4].

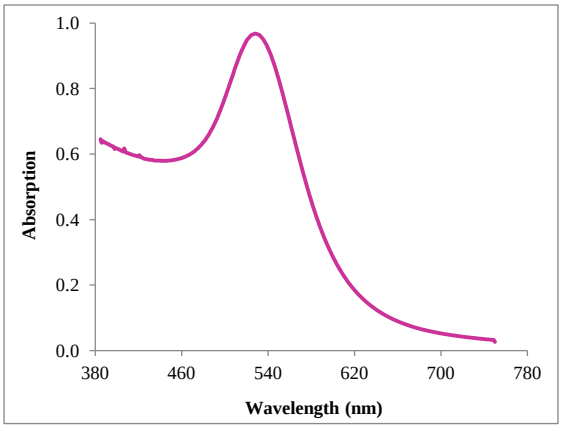

Fig. 1. The UV-Vis spectrum for GNPs.

Also, the morphology of the nanoparticles was examined using field emission scanning electron microscopy (FE-SEM). For investigation the interaction between all effective parameters in the determination of tyrosine DoE and RSM were used for voltammetric data. After multivariate optimization, differential pulse voltmmograms of tyrosine were obtained in different concentration and calibration curve was plotted. The results indicated the oxidation peak current of tyrosine shows two linear ranges of 0.10-8.0 μM and 8.0-350.0 μM with a limit of detection of 9.2 nM. Next, detection of tyrosine was accomplished in human blood serum samples. A standard addition method was applied and the recovery achieved between 94.6-103.1% suggesting the nanostructured sensor can be used successfully to detection of tyrosine in real samples.

IV. Conclusions

This work reports synthesis of GNPs by eco-friendly green approach. Then, the nanoparticles were applied as an electrochemical modified sensor for analysis of tyrosine. A multivariate optimization strategy was applied for simultaneous optimization of all factors on the determination of tyrosine. The strategy caused a sensitive determination of the analyte is obtained at the surface of CPE/GNPs. Also, the nanostructured electrochemical sensor has been successfully applied for detection of the amino acid in biological real samples.

References

[1] J. Zhang, J. Feng, Y. Tian, Y. Wu, X. Liu and Q. He, Microchem. J., 2021, 171, 106867.
[2] P. Deng, J. Xiao, J. Feng, Y. Tian, Y. Wu, J. Li and Q. He, Microchem. J., 2021, 165, 106106
[3] J. Tashkhourian, M. Daneshi and S. Nami-Ana, Anal. Chim. Acta, 2016, 902, 89-96.
[4] D. Tang, R. Yuan, Y. Chai, Y. Liu, J. Dai and X. Zhong, Anal. Bioanal. Chem., 2005, 381, 674-680.

بیست و سومین کنفرانس شیمی فیزیک انجمن شیمی ایران
23rd ICS Physical Chemistry Conference
Chemistry Department,
Faculty of Science
Shahid Bahonar University of Kerman
Kerman, Iran
12-13 Jan 2022
ایران، کرمان
دانشگاه شهید باهنر کرمان
دانشکده علوم پایه، بخش شیمی
۲۳-۲۲ دی ماه ۱۴۰۰

Anisotropic wetting characteristics of water droplet on phosphorene: A molecular dynamics simulation approach

Masumeh Foroutan[a] , Borhan Mostafavi Bavani [a,*]

[a] *Department of Physical Chemistry, School of Chemistry, College of Science, University of Tehran, Tehran, Iran.*

Abstract

In this study, using reactive molecular dynamics (MD) simulations, we investigated the structure and dynamic properties of water on the black phosphorene. Our simulations indicate that the diffusion of water molecules on the black phosphorene surface is anisotropic, which is in agreement with the recently reported experimental data. Moreover, the contact angle of water on phosphorene is proportional to the zigzag and armchair directions of surface. These findings thereby offer helpful insights into the mechanism of the wetting and transport of water at nanoscale, and provide a better foundation for future biomedical applications of phosphorene.

Keywords: Black phosphorene, Anisotropic, zigzag and armchair directions ,Reactive molecular dynamics simulations.

I. Introduction

Two-dimensional materials have attracted increasing attention due to their unique electrical[7], optical[2] , thermal[2] and mechanical properties4. Compared with many other 2D materials, black phosphorus possesses several unique characteristics,[5] such as a large direct band gap and high carrier mobility. In fact, few-layer phosphorene-based field-effect transistor has been recently demonstrated[3]. Besides, phosphorene is also promising for biological applications due to its little disruption to protein[14] and excellent performance in killing cancer cells[12]. Moreover, liquid exfoliation has been shown to be able to produce high-quality phosphorene,[11] which paves the way for applications of phosphorene in biological engineering.

Obviously, any biological applications of phosphorene require in-depth understanding of its interaction with biomolecules and fluids. In recent years, the wetting and diffusion behaviors of water in/on nanomaterials, such as graphene[8], carbon nanotube[10], boron-nitride[4], WS2 and MoS2 [1] have been extensively studied. We note, however, that the research on the interfacial behavior of water on phosphorene has just started[9]. Although the wetting and diffusion behaviors of water droplet on phosphorene surfaces have been studied,[9] the macroscopic contact angle of water droplet on phosphorene remains unexplored. To obtain this intrinsic property, water droplet with different sizes should be used[13] In addition, since phosphorene possesses a strong structural anisotropy[6] due to its puckered honeycomb lattice, thus for practical applications, it is important to

understand its directional dependence of macroscopic contact angle.

In this work, we first investigate the wetting behavior of a water droplet on phosphorene using reactive molecular dynamics simulations, with emphasis on the effect of water droplet size and the number of phosphorene layers. The findings revealed here may be useful for controlling the wettability of phosphorene, which may facilitate the applications of phosphorene in biological systems.

II. Methods

In this work, we used recently a set the developed ReaxFF parameters. In the simulations, water molecules in the initial state were arranged regularly in the three dimensional cube. The lateral dimensions of the singlelayer phosphorene were 198×198 $Å^2$. All the simulations were performed by using LAMMPS package. All the simulations were performed with periodic boundary conditions. The simulations were performed for 3 ns with an integration time step of 1 fs.

III. Results and discussion

Figs. 1 and 2 indicate (a) Initial structure and (b) equilibrium configuration of the simulation model. Red, white and green spheres represent the oxygen, hydrogen and phosphorus atoms, respectively. The contact angle of water droplet on a single-layer phosphorene surface along armchair and zigzag directions are shown in Fig. 3.

This anisotropic wettability could be explained by the anisotropic structure of phosphorene. It is known that phosphorene has a puckered structure, which exhibits a strong structural anisotropy. As a result, there is a larger pinning effect on water along armchair direction than zigzag direction. The larger pinning effect along armchair direction results in a larger restriction for wetting, causing it to be less hydrophilic. This structure-property based mechanism is evidenced by the fact that the droplet from the top view takes an ellipsoidal shape.

In addition to water contact angle, may also affect the structure of water near phosphorene. In order to understand the structure of the interfacial water molecules, we measured the density distribution function (DDF) of the oxygen atom along the direction normal to the surface(z axis) that indicates in the Fig. 4.

Fig. 6. Indicates the energy profil of water droplet on the phosphorene surface as a function of time of simulation. According to Fig. 5 the water droplet simulation system on the phosphorene surface is in equilibrium.

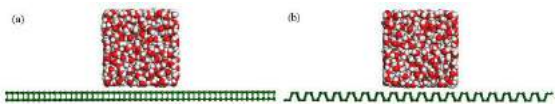

Fig. 1. Initial configuration simulation with 1000 water droplet on the phosphorene along (a) zigzag and (b) armchair directions

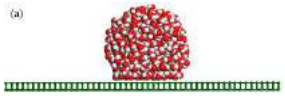

Fig. 2. Equilibrium configuration simulation with 1000 water droplet on the phosphorene along (a) zigzag directions

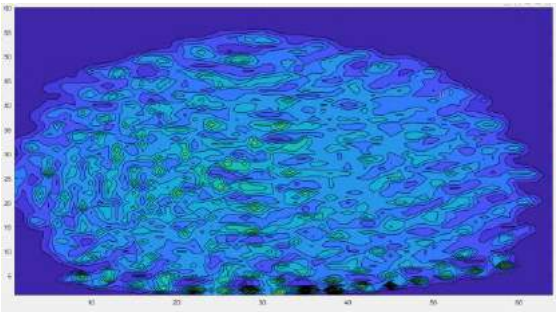

Fig. 3. Contour map of water droplet with 1000 water molecules on the phosphorene surface.

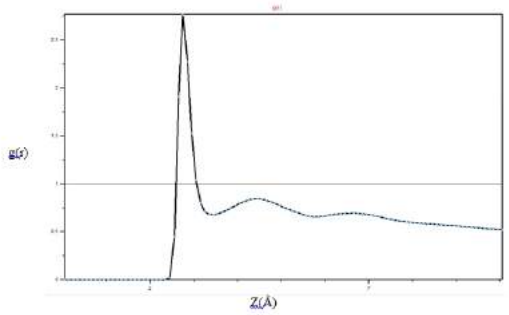

Fig. 4. The density distribution function of oxygen atoms g(z) as a function of the distance z .

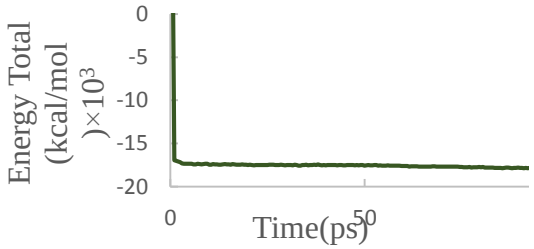

Fig. 5. The energy profile of water droplet on the phosphorene surface as a function of simulation time.

IV. Conclusions

The present study provided a molecular-level understanding of the wetting and diffusion behavior of a water droplet on the phosphorene sheet. Our study showed that phosphorene exhibited anisotropic wettability along armchair and zigzag directions, and the WCA increasing with increasing the droplet size in both directions. In addition, the macroscopic WCAs of water droplet on phosphorene along zigzag and armchair directions were predicted. Our study should help with understanding and manipulating the wetting and diffusive properties of liquid on phosphorene, with is critical for phosphoren's application in the fields of biomedicine and nanofluidics.

References

1. Philippe K Chow, Eklavya Singh, Bartolomeu Cruz Viana, Jian Gao, Jian Luo, Jing Li, Zhong Lin, Ana L Elias, Yunfeng Shi, and Zuankai Wang. 2015. Wetting of mono and few-layered WS2 and MoS2 films supported on Si/SiO2 substrates. *ACS nano* 9, 3: 3023–3031.
2. Xidong Duan, Chen Wang, Anlian Pan, Ruqin Yu, and Xiangfeng Duan. 2015. Two-dimensional transition metal dichalcogenides as atomically thin semiconductors: opportunities and challenges. *Chemical Society Reviews* 44, 24: 8859–8876.
3. M Umar Farooq, Arqum Hashmi, and Jisang Hong. 2015. Manipulation of magnetic state in armchair black phosphorene nanoribbon by charge doping. *ACS applied materials & interfaces* 7, 26: 14423–14430.
4. Weiwei Lei, David Portehault, Dan Liu, Si Qin, and Ying Chen. 2013. Porous boron nitride nanosheets for effective water cleaning. *Nature communications* 4, 1: 1–7.
5. Likai Li, Yijun Yu, Guo Jun Ye, Qingqin Ge, Xuedong Ou, Hua Wu, Donglai Feng, Xian Hui Chen, and Yuanbo Zhang. 2014. Black phosphorus field-effect transistors. *Nature nanotechnology* 9, 5: 372.
6. Weifeng Li, Yanmei Yang, Gang Zhang, and Yong-Wei Zhang. 2015. Ultrafast and directional diffusion of lithium in phosphorene for high-performance lithium-ion battery. *Nano letters* 15, 3: 1691–1697.
7. Yuan Liu, Nathan O Weiss, Xidong Duan, Hung-Chieh Cheng, Yu Huang, and Xiangfeng Duan. 2016. Van der Waals heterostructures and devices. *Nature Reviews Materials* 1, 9: 1–17.
8. Ming Ma, Gabriele Tocci, Angelos Michaelides, and Gabriel Aeppli. 2016. Fast diffusion of water nanodroplets on graphene. *Nature materials* 15, 1: 66–71.
9. G X Nie, J Y Huang, and J P Huang. 2016. Melting–Freezing Transition of Monolayer Water Confined by Phosphorene Plates. *The Journal of Physical Chemistry B* 120, 34: 9011–9018.
10. Himani Sharma, Dinesh C Agarwal, M Sharma, A K Shukla, D K Avasthi, and V D Vankar. 2014. Structure-modified stress dynamics and wetting characteristics of carbon nanotubes and multilayer graphene for electron field emission investigations.

بیست و سومین کنفرانس شیمی فیزیک انجمن شیمی ایران
23rd ICS Physical Chemistry Conference
Chemistry Department,
Faculty of Science
Shahid Bahonar University of Kerman
Kerman, Iran
12-13 Jan 2022
ایران، کرمان
دانشگاه شهید باهنر کرمان
دانشکده علوم پایه، بخش شیمی
۲۳-۲۲ دی ماه ۱۴۰۰

Development of molecularly imprinted polymer on ferric oxide nanoparticles modified electrode as electrochemical sensor for detection of the amount of human chorionic gonadotropin (hCG)

Solmaz Kia
Department of Engineering Sciences, Faculty of Advanced Technologies, University of Mohaghegh Ardabili, Namin, Iran.

Abstract

A novel molecularly imprinted electrochemical sensor based on Ferric oxide nanoparticles modified glassy carbon electrode was fabricated for detection of human chorionic gonadotropin (hCG). The stable proteins molecularly imprinted polymer films were made by electro-polymerization using aniline as functional monomer and hCG as the template. According to the results, the sensor showed a linear range from 1.0×10^{-10} to 1.0×10^{-7} g/cm^3 of hCG (R^2=0.9588) under optimal conditions with a detection limit of 0.6×10^{-10} g/cm^3. The calibration curve showed a 95.8% correlation of the data. In conclusion, the sensor has sensitivity, high stability and good repeatability.

Keywords: Molecularly imprinted electrochemical sensor; human chorionic gonadotropin; Fe3O4 nanoparticles; aniline; square wave voltammetry

I. Introduction

Human chorionic gonadotropin (hCG) is a chemical created by trophoblast tissue, tissue typically found in early embryos and which will eventually be part of the placenta. Measuring hCG levels can be helpful in identifying a normal pregnancy, pathologic pregnancy, and can also be useful following an aborted pregnancy. There is also a benefit in measuring hCG in a variety of cancers including choriocarcinoma and extra-uterine malignancies [1-3].

The term MIP based sensors refers to changing the surface of the transducer by arranging monomers around the target molecule to create specific effects in the polymers. The pattern is then removed from the formed polymer, leading to the high specificity of the analyte. The binding of the target protein is measured electrochemically by determining the oxidation behavior of the probe reaction at the modified electrode. In this research, we propose a new nanocomposite with molecular recognition capacity for hCG detection. The molecular imprinting technique was used for the formation of particular active sites relating to human growth hormone.

II. Methods

Magnetic Fe3O4 nanoparticles were prepared by co-precipitation of Fe2+ and Fe3+ ions in ammonia solution and treatment under hydrothermal conditions. The hCG imprinted polymer was then formed on Fe3O4 nanoparticles/glassy carbon electrode by cyclic voltammetry (CV) and hCG measured through square wave voltammetry (SWV). Elctropolymerization was done in a range of -0.3 to +0.9 V at a scan rate of 0.1 V.S-1 for 15 cycles. The accuracy of

MIP/Fe3O4/GCE formation was confirmed using the square wave voltammetry technique from -0.2 to +0.6 V, in 5mM solution of [Fe(CN)6] 3−/4− with 0.1 M KCl. To investigate selectivity of the sensor, direct competition between hCG, casein, Bovine serum albumin (BSA) and Urease to conjugate to MIP layer on the GC@Fe3O4 was employed. The human plasma samples analysis confirmed the applicability of the MIP/Fe3O4/GCE sensor to the assay of the human chorionic gonadotropin (hCG) molecules.

III. Results and discussion

The effects of main operational parameters such as pH, amount of Fe3O4 NPs, monomer and template, Incubation time of template rebinding, number of cycles and the number of CV scans were investigated and optimized. The optimization was carried out by one at a time optimization method. Fe3O4 NPs were used to increase the immobilized amount of imprinted cavities for adsorption of target molecules. The 4 mg/cm^3 of Fe3O4 NPs is the optimal value for use in the MIP structure, the time of 30 min was selected as optimal incubation time.

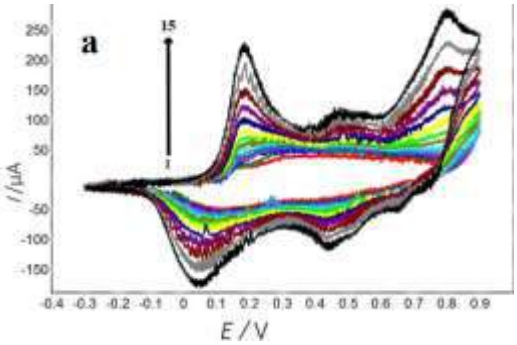

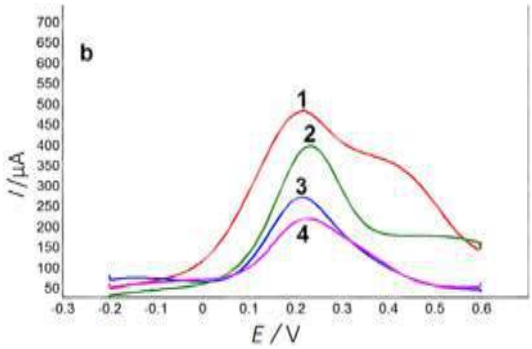

Fig. 1 Recorded voltammogram profiles (a) electro-polymerization of aniline in the presence of the hCG for the stepwise construction of the MIP and (b) SWV profile of the sensor; (1) MIP probe; (2) electro-polymerized probe after template molecule removal (3) electro-polymerized probe after rebinding with 25 ng/cm3 template and (4) electro-polymerized probe after rebinding with 12.5 ng/cm3 template. Experiments was done in K3[Fe(CN)6]/ K4[Fe(CN)6] solution (5mM) prepared in KCl (0.1M).

IV. Conclusions

This method has several advantages, including simple and rapid operation, high sensitivity, accurate selectivity, and can be widely used for screening of actual samples. In addition, this is first HGH analysis with high recovery in samples solution by MIP/Fe3O4 NPs/GCE.

References

[1] Montagnana M, Trenti T, Aloe R, Cervellin G, Lippi G. Human chorionic gonadotropin in pregnancy diagnostics. Clin Chim Acta. 2011 Aug 17;412(17-18):1515-20. [PubMed]

[2] Ong S, Beebeejaun H. The effect of physiological urine dilution on pregnancy test results in complicated early pregnancies. Br J Obstet Gynaecol. 1999 Jan;106(1):87-8. [PubMed]

[3] Cole LA. Immunoassay of human chorionic gonadotropin, its free subunits, and metabolites. Clin Chem. 1997 Dec;43(12):2233-43. [PubMed]

بیست و سومین کنفرانس شیمی فیزیک انجمن شیمی ایران
23rd ICS Physical Chemistry Conference
Chemistry Department,
Faculty of Science
Shahid Bahonar University of Kerman
Kerman, Iran
12-13 Jan 2022
ایران، کرمان
دانشگاه شهید باهنر کرمان
دانشکده علوم پایه، بخش شیمی
۲۳-۲۲ دی ماه ۱۴۰۰

Intermolecular potential energy surface for the X-H_3^+ system

Habib Jani pour, Mohammad R. Noorbala*, and Mansoor Namazian

Correspondence to: Mohammad R. Noorbala (E-mail: noorbala@yazd.ac.ir)
Department of Chemistry, Yazd University, Yazd, Iran, P.O. Box 89195-741

Abstract

The potential energy surface (PES) of X-H_3^+ (X is noble gas) system for different orientations of monomers towards each other is calculated by means of CCSD(T) method. The interaction energies obtained using the aug-cc-pVDZ and aug-cc-pVTZ basis sets are extrapolated to the complete basis set limit using extrapolated scheme. In order to improve the quality of the PES, fitting curve and counterpoise correction (CP) method were performed for the basis set superposition error (BSSE) for all calculations. Finally, a three-dimensional plot of intermolecular PES with its contour plot of the potential intermolecular interaction for the X-H_3^+ system is plotted.

Keyword: H_3^+; Intermolecular potential energy; ab initio computation; Fitting; contour plot.

I. Introduction

H_3^+ is the simplest tri-atom molecule [1] and one of the most abundant ions in the world. These ions are stable in the Interstellar medium (ISM) due to low temperature and pressure. The role of H_3^+ in the ISM is unique in order to make a comparison for the other molecular ions. Ab initio quantum calculations show that H_3^+ is capable of acting as a trap for noble gases by forming complexes in the gas phase [2]. Calculations were performed for different orientations of H_3^+ and X monomers with each other using different methods including CCSD(T) method and OAN(C) basis set [3]. In order to improve the quality of the PES, counterpoise correction (CP) method was carried out for the basis set superposition error (BSSE) for all calculations.

II. Methods

All calculations have been performed using the ORCA [4] program for the ab initio interaction energy calculations. We have performed the optimization method for all the points (12300). X-H_3^+ molecule potential energy calculation was performed using CCSD(T) method as a golden standard method [3] and with Dunning's correlation consistent basis sets (aug-cc-pVXZ, x=D,T) done [5,6]. The interaction energies are obtained using one of the newest basic sets OAN(C) and the high-level method of CCSD(T).

III. Results and discussion

Figure 1 and Table 1 shows the most stable orientation of the two monomers relative to the other orientations, due to the proximity of the electron cloud, two atoms of hydrogen and helium have the most interaction with each other. The corrected potential energy curves and its contour plot for the ϕ at the CCSD(T)/OAN(C) theoretical level are given in figure 2 (The angle of ϕ is the angle between the helium and H atoms that varies between zero and

360. θ is a dihedral angle between the He atom and the plane of H_3^+ species).

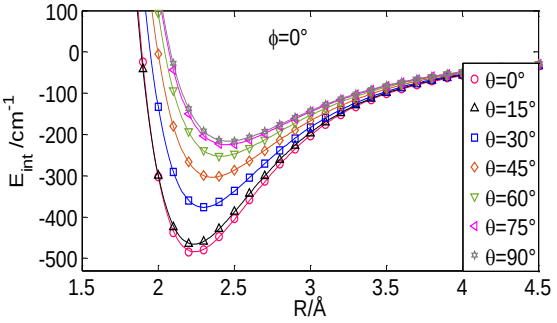

Fig. 1. BSSE corrected interaction energies of HeH_3^+ as a function of R for ϕ =0° and different θ angles.

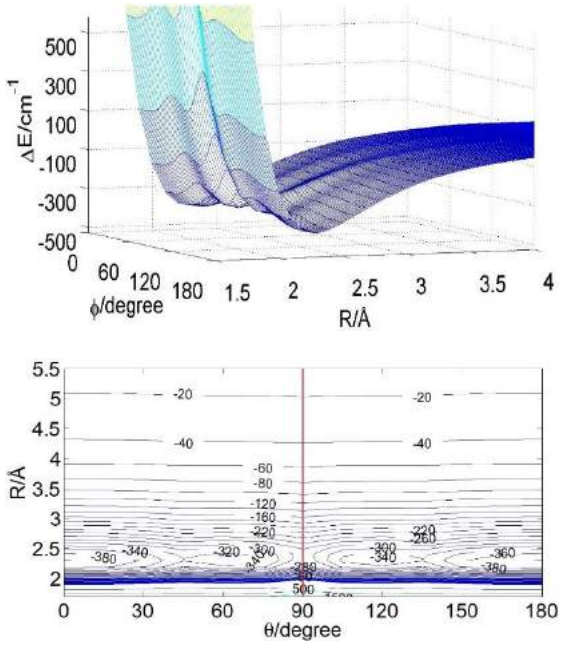

Fig. 2. The potential energy level curve of the intermolecular interaction and its contour plot have been shown. The contours are symmetric with respect to the dashed line. The energy labels are in cm^{-1}.

Table 1. The potential well depth (E_m), position of minimum potential well (R_m), width halfway of potential well (R_w) and sphere collision diameter (σ) obtained at CCSD(T)/ OAN(C) method.

	θ=0°			
ϕ	σ	E_m	R_m	R_w
0	1.893	-483.93	2.240	0.909
15	1.885	-470.75	2.230	0.911
30	1.924	-408.27	2.280	0.933
45	1.972	-342.59	2.330	0.974
60	2.000	-312.49	2.360	1.000

IV. Conclusions

In this research work, the IPES of X-H_3^+ has been calculated using ab initio calculations and density functional theory.

Results show that the configuration with ϕ and θ equal to zero degrees compared to the other orientations has the maximum depth of the potential well (E_m = -483.93 cm^{-1}) at σ=1.893 Å and the configuration that the helium atom is perpendicular to the H_3^+ molecule has the lowest stability (E_m= -216.23 cm^{-1}) at σ=2.082 Å.

References

[1] L. Lembo, H. Helm, D. Huestis, Chem. Phys., 1989, 90, 5299- 5308.
[2] F. Pauzat, Y. Ellinger, J. Pilmé, O. Mousis, J. Chem. Phys., 2009, 130, 174313-174328.
[3] P. Sun, A. Wu, N. Sun, X. Qiao, L. Shi and L. Zheng, Langmuir., 2018, 34, 2791-2799.
[3] M. Okoshi, T. Atsumi, H. Nakai, J. Comput. Chem., 2015, 36, 1075-1082.
[4] R. A. Kendall, T. H. Dunning Jr, R. J. Harrison, J. Chem. Phys., 1992, 96, 6796- 6806.
[5] T. H. Dunning Jr, J. Chem. Phys., 1989, 90, 1007-1023.
[6] M. Alipour, Int. J. Quantum Chem., 2014, 114, 255-260.

بیست و سومین کنفرانس شیمی فیزیک انجمن شیمی ایران
23rd ICS Physical Chemistry Conference
Chemistry Department,
Faculty of Science
Shahid Bahonar University of Kerman
Kerman, Iran
12-13 Jan 2022
ایران، کرمان
دانشگاه شهید باهنر کرمان
دانشکده علوم پایه، بخش شیمی
۲۳-۲۲ دی ماه ۱۴۰۰

The synthesis of smart nanoparticles to pH and their applications in industry and medicine

Beheshteh Sohrabi

Surface Chemistry Research Laboratory, Department of Chemistry, Iran University of Science and Technology, P.O. Box 16846-13114, Tehran, Iran.

Abstract

pH-responsive superhydrophobic surfaces (SHSs) have recently represented reliable ability in oil-water separation applications. In this work, for the first time we could develop a switchable SHS based on Titanium dioxide (TiO_2) and pH-responsive organic molecules using self-assembly method for oil-water separation and medical applications.

Keywords: Superhydrophobicity; Hollow sphere; pH sensitive; Smart nanoparticle; Nanobioreactor.

I. Introduction

The pH-responsive smart SHSs with water Contact angle (CA)>150° and surface free energy<10 mJ.m-2 which represent reversibly changeable interfacial properties in proper pH have recently attracted a lot of attentions because of their broad applications in optoelectronics, cell culture, microfluidic and (photo)catalyst [1, 2]. According to many reports, controlling surface wettability of SHSs as a main strategy to design an oil-water separation approach in industry or a nanobioreactor in medicine remains as a challenge for many years. In this work, for the first time, we could develop a switchable SHS based on (E)-4-(anthracen-9-yldiazenyl) benzoic acid (4-ABA) pH-responsive organic molecules and stearic acid (SA) using self-assembly method for oil-water separation applications. Also, a smart bioreactor was further developed by successfully bonding a surfactant to the hollow spherical titanium dioxide (TiO2) nanoparticles as a sensitive material to pH.

II. Methods

TiO_2-based transparent substrate prepared using glass substrate was cleaned by using concentrated HNO3/HCl/ethanol three time for ten minutes. Then dried in room temperature and, TiO_2 (99% Degussa anatase 25nm) paste was coated on clean glass using doctor blade deposition method. Also, TiO_2 – SiO_2 core-shell nanoparticles were synthesized by amorphous TiO_2 deposition on SiO_2 particles. First 0.15 g of SiO_2 powder with 100 ml ethanol with a magnetic stirrer were completely mixed. Then, an appropriate amount of ammonia and 1.5 ml of tetra butyl orthotitanate were added drop wise to the mixture. The resulting mixture was refluxed at 45 ° C for 3 hours.

III. Results and discussion

Surface chemical structure can be as a crucial factor for obtaining switchable surfaces. Changing in surface charge density has impact on the surface CA. Switchable surfaces that can change their CA, are obtained by intelligent applying Functional groups (FGs) of deposited

materials. Changing in wettability of SHSs are a strategy for designing of switchable surfaces for different applications. Therefore, the alternative charges of FGs of deposited molecules on SHS is a unique strategy for developing of switchable surfaces. Figure 1 showed the TiO_2@4-ABA/SA-based pH-responsive switchable hydrophilic/SHS with suitable structural design and stability on substrate for separation oil from water.

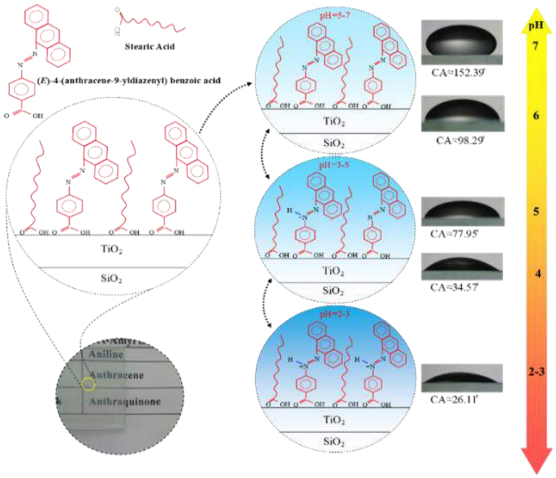

Fig. 1. The transparent sample of switchable superhydrophobic TiO2@4-ABA/SA-based plate.

To obtain hollow spheres of titanium dioxide, the core must be removed. This can be done with different materials that have the ability to remove the core. What is important at this stage, is the time and amount of the material used. Hydrofluoric acid and sodium hydroxide solution are usually used to remove SiO_2 core. In this work, 0.5 M NaOH solution was used. Figure 2. Shows SEM and TEM pictures of SiO_2-TiO_2 core-shell and TiO_2 hollow spheres. Fig. 3 shows the FTIR and NMR spectrum of surfactant synthesized from reaction of lysine amino acid and oleyl chloride was used for sensing of TiO_2 hollow nanoparticles to pH.

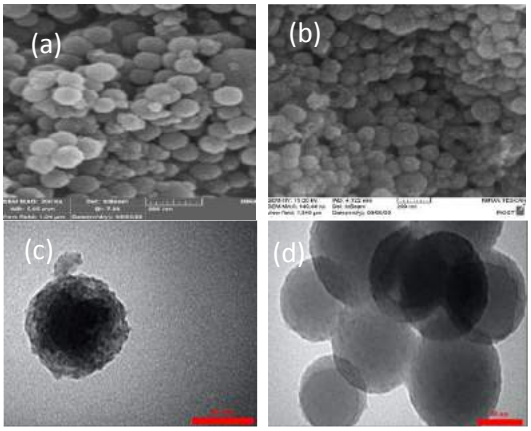

Fig. 2. (a) The SEM picture of SiO_2-TiO_2 core-shelle (b) The SEM picture of hollow TiO_2 nanoparticles (c) The TEM picture of SiO_2-TiO_2 core-shell (d) The TEM picture of hollow TiO_2 nanoparticles

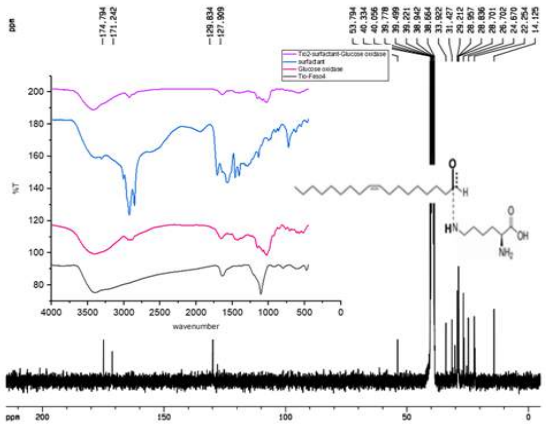

Fig. 3. Overview of surfactant molecules and its FTIR and NMR spectrum

IV. Conclusions

The results showed that the TiO_2 nanoparticls pH-responsivity are an appropriate option for oil water separation in broad range of pH. Significantly, the sensitivity of these nanoparticles to pH improves their specific application for the cancer therapy.

References

[1] Khanmohammadi Chenab, K., B. Sohrabi, and A. Rahmanzadeh, Superhydrophobicity: advancedbiological and biomedical applications. Biomaterials Science, 2019. 7(8): p. 3110-3137.

[2] Erbil, H. Yildirim. "Practical Applications of Superhydrophobic Materials and Coatings: Problems and Perspectives." Langmuir 36.10 (2020): 2493-2509.

بیست و سومین کنفرانس شیمی فیزیک انجمن شیمی ایران
23rd ICS Physical Chemistry Conference
Chemistry Department,
Faculty of Science
Shahid Bahonar University of Kerman
Kerman, Iran
12-13 Jan 2022
ایران، کرمان
دانشگاه شهید باهنر کرمان
دانشکده علوم پایه، بخش شیمی
۲۳-۲۲ دی ماه ۱۴۰۰

Investigation of intermolecular potential energy surface of CO-OCS system

Mohammad Hashim Abedi, Mohammad R. Noorbala*, and Mansoor Namazian

Correspondence to: Mohammad R. Noorbala (E-mail: noorbala@yazd.ac.ir)
Department of Chemistry, Yazd University, Yazd, Iran, P.O. Box 89195-741

Abstract

The potential energy surface (PES) for CO-OCS system is studied using CCSD(T) and QCSID(T) methods. Several basis sets of aug-cc-pVTZ, cc-pVTZ, aug-cc-pVDZ, cc-pVDZ and cc-pVQZ have been investigated; from which the aug-cc-pVTZ basis set is selected as the appropriate one. Then, the potential energy curves of three different shapes (T-shape, TO shape and X-shape) of the CO-OCS system such as the depth of the potential well, the position of the potential well in the half width and the diameter of the hard sphere have been studied. Finally, the CP correction was used to eliminate the BSSE error for all the calculations.

Keywords: Intermolecular potential energy surface; CO-OCS system; CCSD(T); BSSE.

I. Introduction

For developing quite a few of the domain of Physics, Biology and Chemistry, knowing the intermolecular potential energy surface is of great significance [1]. This potential is applicable in the calculation of many properties such as thermodynamic parameter, molecular relaxation rates, and transport coefficients [2]. Intermolecular potentials are obtainable by experimental methods including spectroscopic studies, molecular beam scattering experiments and speed of sound data [3-4].

Various theoretical researches on OCS-$(He)_N$ clusters have been done using Monte Carlo techniques. Interestingly, these techniques have been used for He clusters comprised of N_2O, CO_2, and HCCCN [5]. In this paper for the first time, the IPES has been calculated for the CO-OCS, using the CCSD(T)/aug-cc-pVTZ level of theory.

II. Method

For investigating the PES of the CO-OCS system, all CCSD(T) and QCISD(T) calculation methods were carried out using the Gaussian 09 software. For the consistent correlation of the system, the aug-cc-pVDZ, cc-pVTZ, aug-cc-pVTZ, cc-pVQZ, and cc-pVDZ basis sets have been used. First, CO and OCS monomers are optimized. Secondly, the calculations of the potential energy curves, for different orientations of two specific monomers were studied with respect to each other.

III. Results and discussion

In this paper, cc-pVDZ and cc-pVTZ and their corresponding enlarged basis sets, which have been obtained by adding the polarized functions, have been studied. Counterpoise correction (CP) has been applied in all the calculations for eliminating the BSSE error. The uncorrected and the corrected curves show the typical form of an interaction potential

Table 1 The values of the depth of the potential well, D_e, the position of the potential well, the half-width of $\Delta R_{1/2}$ and the collision diameter of the hard sphere σ have been calculated for the CO-OCS complex based on the uncorrected and corrected potentials using CCSD(T) method and different basis sets.

Methods/Basis Sets	$D_e(cm^{-1})$		R_e(Å)		$\Delta R_{1/2}$(Å)		σ(Å)	
	Uncorr.	Corr.	Uncorr.	Corr.	Uncorr.	Corr.	Uncorr.	Corr.
CCSD(T)/ cc-pVDZ	-132.25	25.89	3.70	4.30	0.96	1.27	3.26	3.83
CCSD(T)/aug-cc-pVDZ	-256.97	107.33	3.60	3.80	1.19	2.98	3.14	3.39
CCSD(T)/ cc-pVTZ	-142.77	70.83	3.70	3.90	2.86	2.85	3.29	3.48
CCSD(T)/aug-cc-pVTZ	-145.43	92.31	5.25	5.35	2.37	2.59	4.81	4.93
QCSID(T) cc-pVQZ	-142.41	--	3.70	--	2.67	--	3.27	--

consisting of attractive and repulsive parts that result in a potential well (Fig. 1).

The related parameters to the curves of the potential energy (Table 1) were described which are sensitive to the applied basis sets. By correction, the related values of the D_e and $\Delta R_{1/2}$ are remarkably changed. Therefore, it can be concluded that CP correction is necessary for the potential energy of the intermolecular interaction.

According to these calculations, adding the polarized functions to the consistent correlated basis sets results in the increment of the depth of the pontetial well in the uncorrected and corrected potentials and in the decrement of the half-width of the potential well in the corrected potential and its increase in the uncorrected potential in the CCSD(T) method. Furthermore, with the addition of the polarized functions cc-pVDZ basis set results in the decrement of the depth and the half-width of potential well. Also, the characteristics of the curve of the potential energy are sensitive to the changes in the basis sets.

IV. Conclusion

In this work, the effects of the five basis sets on the curves of the potential energies has been calculated using the CCSD(T) and QCISD(T) methods. The CP correction is used for eliminating the BSSE errors. The uncorrected and corrected curves calculated by CCSD(T) method present the repulsion and attraction forces based on the CP correction. In all the investigated basis sets, the related hard sphere to the corrected interacting potentials are remarkably more than the corresponding uncorrected potentials.

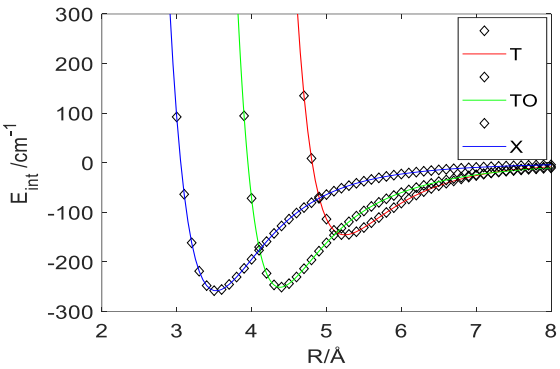

Fig. 1. The potential energy of the intermolecular interaction of the CO-OCS as a function of the R distance, obtained from CCSD(T) and the aug-cc-pVTZ basis set for T, TO, and X shapes.

References

[1] H. Sabzyan and M. R. Noorbala, J. Mol. Struct. THEOCHEM, 2003, 636(1-3), 185-193.
[2] M. R. Noorbala and H. Sabzyan, J. Mol. Struct. THEOCHEM, 2004, 678(1-3), 67-76.
[3] S. Tashakor, M. R. Noorbala and M. Namazian, Int. J. Quantum Chem., 2016, 116(20), 1477-1485.
[4] S. Tashakor, M. R. Noorbala and M. Namazian, Theor. Chem. Acc., 2017, 136, 1-10.
[5] H. Li, Y. Liu, W. Jäger, R. J. Le Roy and P. N. Roy, Can. J. Chem. 2010, 88(11), 1146-1154.

بیست و سومین کنفرانس شیمی فیزیک انجمن شیمی ایران
23rd ICS Physical Chemistry Conference
Chemistry Department,
Faculty of Science
Shahid Bahonar University of Kerman
Kerman, Iran
12-13 Jan 2022
ایران، کرمان
دانشگاه شهید باهنر کرمان
دانشکده علوم پایه، بخش شیمی
۲۳-۲۲ دی ماه ۱۴۰۰

Computational study of the synergistic effect of N, S atoms co-doping into monolayer graphdiyne nanosheet on hydrogen adsorption and storage

Monireh Dehkhodaei[a], Adel Reisi-Vanani[a,b,*]

[a] *Institute of Nano Science and Nano Technology, University of Kashan, Kashan, Iran*
[b] *Department of Physical Chemistry, Faculty of Chemistry, University of Kashan, Kashan, Iran, Fax: +98 3155912397; Tel: +98 3155912358, areisi@kashanu.ac.ir*

Abstract

In this work, the ability of adsorption and storage of the hydrogen by co-doped graphdiyne nanosheet with nitrogen and sulfur atoms under different positive and negative charges injection was investigated. For this aim, the first-principles calculations using the DFT-D3 method were used to evaluate the adsorption capacity by this structure.

Keywords: Graphdiyne; N-S co-doping; Charge injection; Hydrogen storage; DFT-D3 calculation.

I. Introduction

Today, the use of hydrogen clean fuel as an alternative to fossil fuels for energy production depends on its storage technology [1]. One of the most promising materials introduced for this purpose is 2D carbon structures, especially graphyne (GY) and graphdiyne (GDY), which have a variety of sp and sp^2 hybrids in their structure [2,3]. Studies have shown that for efficient storage of the hydrogen on these structures, structural modifications such as doping or decoration with different atoms, application of the electric field and charge injection, etc. can be very effective in improving the results [3,4].

II. Methods

All calculations were performed by the $DMol^3$ module of the Material Studio software by using density functional theory (DFT) with the correction of Grimme's scheme by GGA approximation method, with the help of PBE functional and DNP basis set. Studies were carried out on a 2×2 GDY supercell with a vacuum space of 20 Å. A global orbital cut-off radius of 5.2 Å and a grid of 7×7×1 Monkhorst-Pack k-points for the Brillouin zone were applied.

III. Results and discussion

The best site for N and S dopants in the structure of pristine GDY was determined. Applying of charge leads to an increase in the inhomogeneity of π bonds and a change in the band structure diagrams of the GDY. These changes are seen in Fig. 1. The adsorption energy of the first adsorbed H_2 molecule and the maximum number of H_2 molecules adsorbed on the nanosheets are given in Table 1 and Fig. 2, respectively. Results show that co-doping of N and S atoms improves adsorption energy of hydrogen molecule onto GDY nanosheet from -0.093 to -0.481 eV (about 5 times), while charge-injection promote it from -0.481 to -0.845 eV.

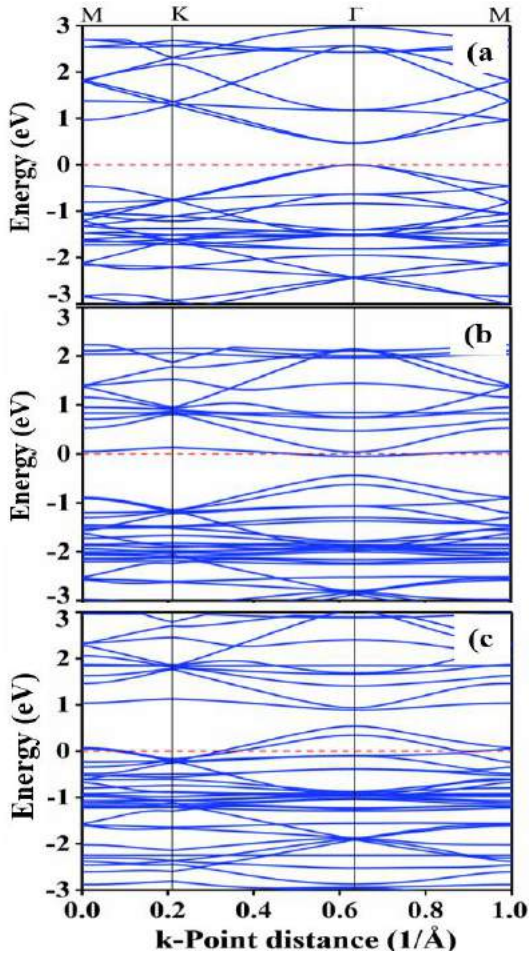

Fig. 1. Band structure of: a) pristine GDY, b) neutral, and c) +5 charged N,S co-doped GDY nanosheet.

IV. Conclusions

In this study, the effect of modifying the structure of GDY with N and S atoms and also injecting charge to improve H_2 adsorption was evaluated using DFT calculations. The results showed that the simultaneous doping of these atoms changed the nature of pristine GDY from an intrinsic semiconductor to a n-type semiconductor, and the structure maintained 6 H_2 molecules with an adsorption capacity of 4.84 wt%. By adding charge to the structure (specifically +5 charge), the adsorption energy is significantly increased and the structure is able to store 22 H_2 molecules with an adsorption capacity of 15.7 wt%. These observations show that the simultaneous use of two approaches of co-doping and charge injection can be effective in the design of H_2 adsorbents.

Table 1. The adsorption energy of the first adsorbed H_2 molecule (E_{ads}, eV).

Nanosheet	pristine GDY	neutral N,S-GDY	+5 charged N,S-GDY
E_{ads} (eV)	-0.093	-0.481	-0.845

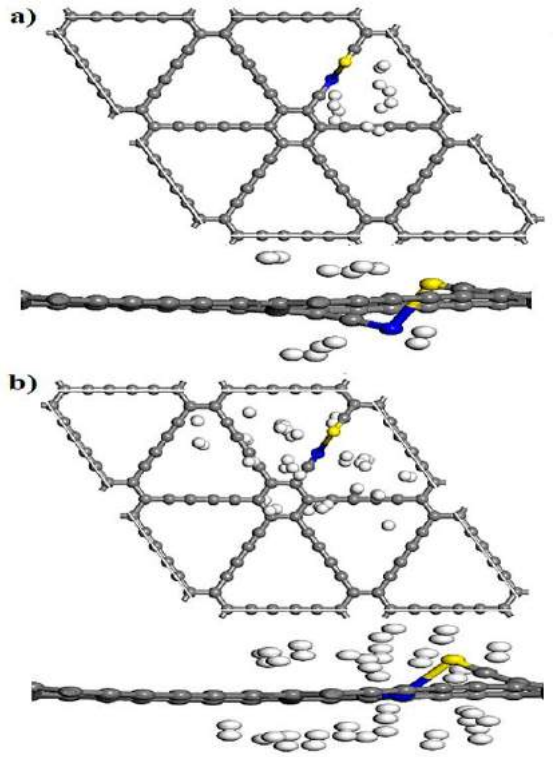

Fig. 2. Top and side views of relaxed structures of a) 6 H_2 molecules adsorbed on neutral N,S-GDY nanosheet, b) 22 H_2 molecules adsorbed on +5 charged N,S-GDY nanosheet.

References

[1] C. Tarhan and M. A. Çil, J. Energy Storage, 2021, 40, 102676.
[2] Y. Li, L. Xu, H. Liu and Y. Li, Chem Soc Rev, 2014, 43, 2572-2586.
[3] C. Huang, Y. Li, N. Wang, Y. Xue, Z. Zuo, H. Liu and Y. Li, Chem rev, 2018, 118, 7744-7803.
[4] A. Seif and K. Azizi, RSC adv, 2016, 6, 58458-58468.

بیست و سومین کنفرانس شیمی فیزیک انجمن شیمی ایران
23rd ICS Physical Chemistry Conference
Chemistry Department,
Faculty of Science
Shahid Bahonar University of Kerman
Kerman, Iran
12-13 Jan 2022
ایران، کرمان
دانشگاه شهید باهنر کرمان
دانشکده علوم پایه، بخش شیمی
۲۳-۲۲ دی ماه ۱۴۰۰

The effect of solvent evaporation time on the properties and performance of polymer membranes based on a mixture of polyvinyl chloride and polymethyl methacrylate

Alireza Khodabakhshi[a,]*, Alireza Pouyamehr [b]

[a] *Address: Department of Chemistry, Faculty of Science, Arak University, Arak, 38156-8-8349, Iran*
Email: A- Khodabakhshi@araku.ac.ir
[b] *Address: Department of Chemistry, Faculty of Science, Arak University, Arak, 38156-8-8349, Iran*
Email: pouyamehralireza23@yahoo.com

Abstract

In this study, the effect of evaporation time of tetrahydrofuran solvent on the properties and performance of polymeric membranes based on a mixture of two polymers, polyvinyl chloride and polymethyl methacrylate was investigated. For this purpose, after preparing a polymeric solution from the mentioned polymers, in the phase inversion process, the membranes were made using immersion method in non-solvent bath at evaporation times of 0, 15, 30 and 45 seconds. To investigate the effect of evaporation time on the properties of the prepared membranes, variables of water content, porosity, pore size, flux and membrane rejection were tested.

Keywords: Membrane; phase inversion; polymethyl methacrylate; evaporation time.

I. Introduction

Membrane processes are among the most widely used separation methods [1]. One of the manufacturing processes of polymeric membranes is the phase inversion process using the immersion bath method. The formation of membrane pores in this method is based on the exchange of solvent and non-solvent in the membrane film. By controlling the effective parameters in this process, different membrane structures can be obtained. One of these parameters is the evaporation time of the solvent, which is the distance between pulling the stretched film on a flat surface and placing it in a non-solvent bath [2].

II. Methods

To investigate the effect of evaporation time of tetrahydrofuran solvent on the properties and performance of polymeric membranes based on a mixture of polyvinyl chloride and polymethyl methacrylate, the membranes at evaporation times of 0, 15, 30 and 45 seconds was prepared. The polymeric ratio of polyvinyl chloride to polymethyl methacrylate was 70 to 30 and the preparation process was phase inversion process by immersion in non-solvent (water) method.

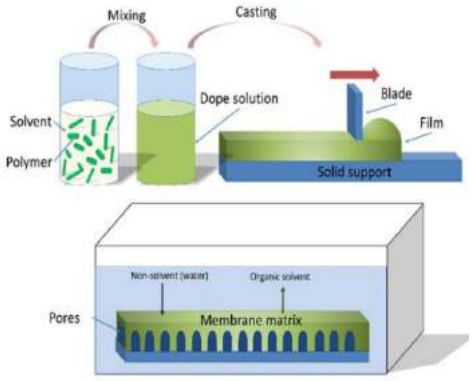

Fig. 1. Non-solvent phase inversion casting process [3]

Figure 1 shows a demo of this preparation process. To investigate the effect of

solvent evaporation time on the performance and properties of the prepared membranes, the variables of water content, porosity, pore size, flux and membrane rejection were used and calculated using the formulas of Figure 2.

$$\text{Water content} = \frac{W_w - W_d}{W_w} \times 100$$

$$\varepsilon = \frac{W_{wet} - W_{dry}}{A \times l \times d_w}$$

$$r_m = \sqrt{\frac{(2.9 - 1.75\varepsilon)8\eta lQ}{\varepsilon \times A \times \Delta P}}$$

$$Jv = Q/A.t$$

$$\text{Rejection } \% = 1 - \left(\frac{C_p}{C_f}\right) * 100$$

Fig.2. Water content equations, Porosity, The size of the cavities, flux and ion rejection [4].

III. Results and discussion

The values obtained from water content, porosity, pore size, flux and membrane rejection are shown in Table 1. The results show that increasing evaporation time has a significant effect on membrane performance. According to the obtained values, it was found that with increasing the evaporation time of the solvent, the values of water content, porosity, pore size and water flux for each membrane decreased and the rate of ion excretion had an increasing trend. According to the evaporation time of the membranes and the results obtained, it can be said that with increasing evaporation time during the evaporation stage, the surface of the stretched film loses more solvent and as a result the polymer concentration in the top layer of the film increases. Increasing the polymer concentration on the surface of the stretched film has led to the limitation of insoluble diffusion in the polymer film, which will delay the phenomenon of phase inversion, and as a result, cavitation at the membrane surface will be delayed and disturbed by the polymer chains. In other words, with increasing evaporation time, we will have membranes with smaller and smaller cavities and a higher percentage of ion repulsion.

Table 1 Values obtained from water content, porosity, pore size, water flux and copper ion rejection in four evaporation times 0, 15, 30 and 45 seconds

evaporation times (Second)	Water content (%)	Porosity (%)	pore size (m)	flux (L/ m^2.h)	rejection (%)
0	31.24	27	2.861×10^{-8}	43.21	29
15	24.53	20.56	1.852×10^{-8}	36.25	43.55
30	16.42	11.05	1.057×10^{-8}	10.41	50.61
45	9.23	7.13	9.034×10^{-9}	7.01	59.02

IV. Conclusions

The results showed that increasing the evaporation time of solvent had a significant effect on membrane performance. With increasing solvent evaporation time, water content, porosity, pore size and water flux decreased and rejection of the membrane increased.

References

[1] M. Takht Ravanchi, T. Kaghazchi and A. Kargari, Desalination, 2009,235,199-244.

[2] M. A . Alaei Shahmirzadi, S. Hosseini, G. Ruan and N. R. Tan, RSC Advances,2015,5,49080-49097.

[3] X . Dong, A. Al-Jumaily and I. C. Escobar, Membranes,2018,8(2),23.

[4] S.M. Hosseini, S.H. Amini, A.R. Khodabakhshi, E. Bagheripour and B. Van der Bruggen, Taiwan Institute of Chemical Engineers,2018,82,169-178.

بیست و سومین کنفرانس شیمی فیزیک انجمن شیمی ایران
23rd ICS Physical Chemistry Conference
Chemistry Department,
Faculty of Science
Shahid Bahonar University of Kerman
Kerman, Iran
12-13 Jan 2022
ایران، کرمان
دانشگاه شهید باهنر کرمان
دانشکده علوم پایه، بخش شیمی
۲۳-۲۲ دی ماه ۱۴۰۰

Theoretical study of the CO dissociation mechanism in [(η^5-C_5H_5) Fe $(CO)_2$(η^1-C_5H_5)]

Elham S. Tabatabaie[a*], Maryam Daghigh Asli[b]

[a]*Department of Chemistry, Alzahra University, P.O. Box 1993891176, Vanak, Tehran,Iran*
[b]*Department of Chemistry, Islamic Azad University, Central Tehran Branch,Shahrak Gharb, Tehran, Iran*

Abstract

in this study, using theoretical calculations of DFT density functions, CO substitution reactions in cyclopentadiene and indenyl ligands in complexes [(η^5-C_5H_5) Fe $(CO)_2$(η^1-C_5H_5)] (I) Which leads to the formation of sandwich complex Fe(η^5-C_5H_5)$_2$ were investigated. The free energy barrier of CO dissociation process for complex I was calculated. The first CO substitution giving an η^2-Cp complex has a higher barrier than the second CO substitution giving an η^5-Cp complex. This behavior was attributed to the increased degree of aromaticity of Cp in the transition state connecting the η^2-Cp complex to the η^5-Cp complex. Calculations show that first and second CO substitution reactions different take place through the formation of two monochromonyl Endo and Exo isomeric. Finally, it was found that the pathway is more accessible to the CO substitution reaction through the Exo-isomer intermediate.

Keywords: Density functional theory, activation energy barrier, first and second CO substitution reactions, cyclopentadienyl ligand, monocarbonyl intermediate, Exo isomer

I. I. Introduction

In 1970, Cotton and co-workers established that warming [Fe(η^5-Cp)(η^1-Cp)$(CO)_2$]leads to dissociation of carbonyl ligands and formation of the sandwich complex [Fe(η^5-Cp)$_2$].[1,2] Belmont et al. Generated η^3-cyclopentadienyl via UV radiation close to η^1-cyclopentadienyl complexes, It was observed experimentally that the loss of CO can occur upon warming of such η^1-Cp complexes, yielding the conversions of η^1-Cp to η^3-Cp and subsequently to η5-Cp [3].In this paper, a comprehensive study on the mechanism of CO exchange reactions in a series of metal-organic (I) complexe was investigated. In the following, the mechanism of dissociation of the first and second CO in the observed complexes, the formation of the sandwich complex was investigated using the theory of DFT density functions.

II. Computational details

Gaussian 03[4] was used to fully optimize all the structures reported in this paper at the B3LYP level [5,6] of density functional theory. The effective core potentials of Hay and Wadt with double-_ valence basis sets (LanL2DZ) [7-9] were chosen to describe Fe and P. The 6-31G(d) basis set was used for other atoms.31 Polarization functions were also added for Fe (f) 2.462 and P (d) 0.387).[10] This basis set combination will be referred to as BS1. Frequency calculations were carried out at the same level of theory for structural optimization. To further refine the energies obtained from the B3LYP/BS1 calculations, we carried out single-point. energy calculations for all the structures with a larger basis set (BS2). BS2 comprises the SDDALL [11,12] basis set with associated ECPs for the transition metals and 6-311++G (2d, p) basis set for the other atoms. To estimate the corresponding Gibbs free energies, the entropy corrections were calculated at the B3LYP/ BS1 level and added to the B3LYP/BS2 total energies. We have used the B3LYP /BS2// B3LYP / BS1energies throughout the paper unless otherwise stated. The natural bond orbital (NBO) program,[13] as implemented in Gaussian 03, was used to obtain natural populations of atoms.

III. Results and discussion

Figure 2 shows the energy profile for the CO dissociation process and the fluxional behaviors in [Fe(η^5-Cp) (η^1-Cp) $(CO)_2$]. Consistent with the previously undertaken studies by Romaoand Veiros on [Mo(η^5-Cp) (η^1-Cp) (N*t*Bu)$_2$] [14], [M(η^5-Cp) (η^1-Cp) $(CO)_2$] *n* can exist in the two isomers **1M** and **2M** due to therelative orientations of the η^1-Cp ligands. In isomer **1M**, the η1-Cp ligand points toward the η^5-Cp ligand, while in isomer **2M** the η^1-Cp ligand points toward one of the CO ligands. **1Fe** is calculated to be about 0.6 kcal/mol more stable than **2Fe**.[15] This result is in good agreement with the experimental observation in which **1Fe** is the only structure reported for [Fe(η^5-Cp) (η^1-Cp) $(CO)_2$]. **1M_TS** is the transition state structure connecting **1M** to **2M** (table1). According to Figure 2, a complex η3-Cp was proposed as an intermediate between complexes η1-Cp and η^3-Cp [16]. In contrast, our calculations show that the first CO substitution reaction by η^1-Cp yields an η^2-Cp intermediate instead of an η^3-Cp intermediate as the reaction product. The η^3-Cp complexes are calculated to be first-order saddle points on the PES, connecting two η^2-Cp complexes **3M** to each other. We also found that η^1-Cp-assisted CO substitution, giving **3M**, has a higher barrier than η^2-Cp-assisted CO substitution, giving **4M** (Figure 2 and Table 1). For instance, the barrier from **2Fe** to **3Fe** (27.7 kcal/mol) is calculated to be 9.4 kcal/mol higher than that from **3Fe** to **4Fe** (18.3 kcal/mol). This result, which agrees well with the experimental observations concerning the temperature dependence of CO loss, demonstrates that, in general, **2M** is much less labile than **3M**. Because the substitution reactions proceed via an Id (dissociative interchange) mechanism, it is expected that the CO ligand should bind more tightly to the metal center in 2M than in 3M. We also believe that, in **6M_TS** and **4M**, the aromaticity of the Cp ligand involved in the substitution reaction is noticeably recovered, making the CO substitution easier.

This claim finds support from NICS calculations. For example, the NICS (1) values of -5.7, -7.4, -1.3, -13.6, and -17.3 were computed for **2Fe**, **5Fe_TS**, **3Fe**, **6Fe_TS**, and **4Fe**, respectively, suggesting that the relevant Cp ligands benefit from the increased degree of aromaticity in **6Fe_TS** and **4Fe (Table1)**.

TABLE 1: NICS (1) Values Calculated for the Species 1M Using the B3LYP/BS2//B3LYP/BS1 Calculations

	complex	2Fe	5M_TS	3Fe	6M_Ts	4M
NICS (1)	(I)	-5.7	-7.4	-1.3	-13.6	-17.3

In addition, calculations show that the CO substitution reaction proceeds in two different directions Which results in the formation of two intermediates between the monocarbonyl Exo isomer (3M-Ib) and the endo isomer (3M-Ib) (Figure2). Comparison of activation energy barrier in Figure 1 for two pathways leading to the formation of two intermediates endo and Exo. The above argument confirms that the Exo isomer is more stable than the endo isomer. In the Exo isomer, the bond length between the metal and the intermediate carbon of the ligand is reduced compared to the endo isomer. which reduces the activation energy barrier of Exo isomer compared to endo isomer. Which is due to the strong interactions between the ligand (η^3-C_5H_5) and the metal. Therefore, the substitution reactions of Co proceed through the Exo isomer pathway.

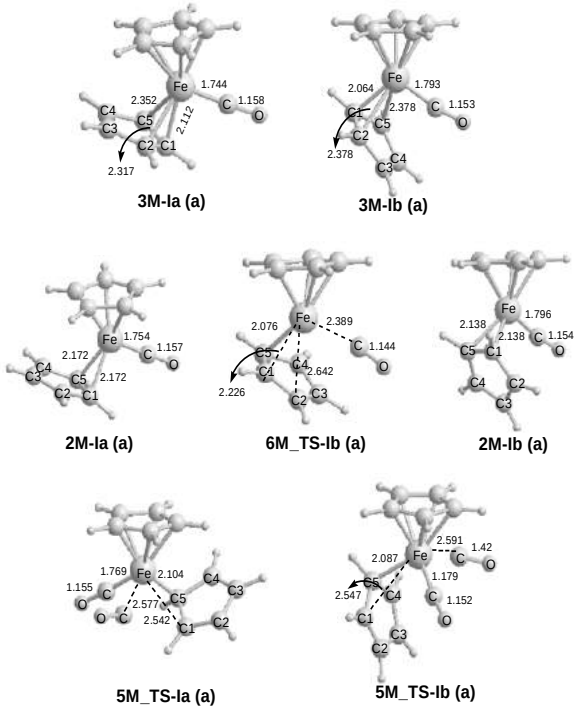

Figure 1. Optimized structures with selected structural parameters (bond length in Å) for some of the species involved in the energy profile shown in Figure 2.

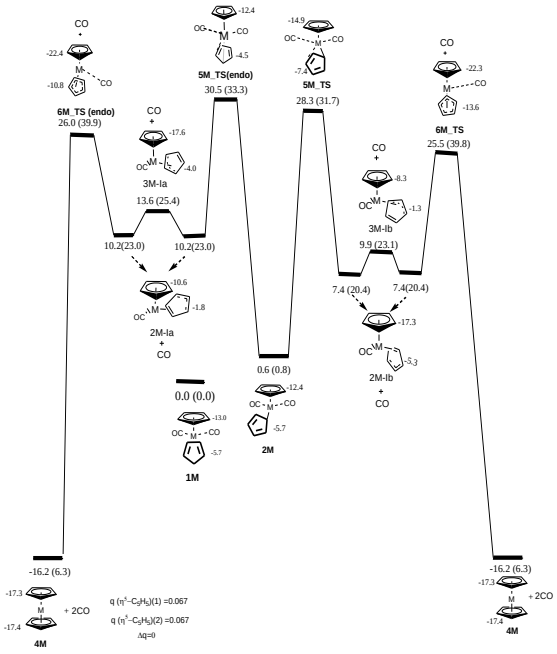

Figure 2. Energy profile calculated first and second CO substitution reactions in [Fe(η_5-Cp*) (η_1-Cp) $(CO)_2$]. The relative free energies and potential energies (in parentheses) obtained from the B3LYP/BS2//B3LYP/BS1 calculations are given in kcal/mol.

IV. Conclusions

In this investigation, density functional theory calculations were used to compare the CO substitutions reaction of the Cp (Cp=C_5H_5) ligand in the complexe (η^5-C_5H_5) Fe $(CO)_2$(η^1-C_5H_5) (I). the reaction dissociation of carbonyl ligands leads to the formation of sandwich complexe Fe(η^5-C_5H_5)$_2$. The activation energy barrier of CO substitutions reaction was calculated for I complexe. In addition, calculations show that the monocarbonyl complexes are stable in the Exo form and the CO substitution by endo η3-indenyl form never happens.

References

[1] Calderon, J. L.; Cotton, F. A.; Takats, J. *J. Am.Chem. Soc.* **1970**, *92*, 3801.
[2] Stradiotto, M.; Hughes, D. W.Brook, M. A.;*Organometallics* **1997**, *16*, 5563.
[3] Beimont, J. A.; Wrighton, M. S. *Organometallics* **1986**, *5*, 1421.
[4] Frisch, M. J.; et al. *Gaussian 03*, *re*Vision *B.05*; Gaussian, Inc.PA2003.
[5] Lee, C. T.; Yang, W. T.; Parr, R. G. *Phys. Re*V. *B* **1988**, *37*, 785.
[6] Becke, A. D. *J. Chem. Phys.* **1993**, *98*, 5648.Miehlich, B.; Stoll, H.; Preuss, H. *Chem. Phys. Lett.***1989**, *157*, 200.
[7] Hay, P. J.; Wadt, W. R. *J. Chem. Phys.* **1985**, *82*, 270.
[8] Wadt, W. R.; Hay, P. J. *J. Chem. Phys.* **1985**, *82*, 284.
[9] Hay, P. J.; Wadt, W. R. *J. Chem. Phys.* **1985**, *82*, 299.
[10] Hariharan, P. C.; Pople, J. A. *Theor. Chim. Acta* **1973**, *28*, 213.
[11] *Hollwarth, A.; Bohme, M.; Dapprich, S.; Ehlers, A. W.; Gobbi,A.; Jonas, V..; Frenking, G.Chem. Phys. Lett. 1993, 208, 237.*
[12] Bergner, A.; Dolg, M.; Kuechle, W.; Preuss, H. Mol.Phys. 1993, 80, 1431.
[13] Dolg, M.; Wedig, U.; Stoll, H.; J. Chem. Phys. 1987,86, 866.
[14] Roma˜o, C. C.; Veiros, L. F. Organometallics 2007, 26, 1777.
[15] The CCSD(T)/BS1//B3LYP/BS1 calculations also indicate that 1Fe is only 0.4 kcal/mol more stable than 2Fe. In conflict with the experiment that showed 1Fe is the only species isolated, our results predict that both 1Fe and 2Fe should be isolated. At present, we have no explanation for this discrepancy.
[16] Dolg, M.; Wedig, U.; Stoll, H.; Preuss, H. J. Chem. Phys. 1987, 86, 866.

بیست و سومین کنفرانس شیمی فیزیک انجمن شیمی ایران
23rd ICS Physical Chemistry Conference
Chemistry Department,
Faculty of Science
Shahid Bahonar University of Kerman
Kerman, Iran
12-13 Jan 2022
ایران، کرمان
دانشگاه شهید باهنر کرمان
دانشکده علوم پایه، بخش شیمی
۲۳-۲۲ دی ماه ۱۴۰۰

Computational study of external electric field effect on the electronic properties of a simple molecular wire

Reza Safari*, Hamid Hadi*

Department of chemistry, Faculty of science, University of Qom, Qom, Iran:
hadi.ha@fs.lu.ac.ac.ir and R.safari@qom.ac.ir

Abstract

In this study, external electric field effect (EF) on some of the electronic properties (such as atomic charge/energies, current/voltage curve and molecular cohesive energy) of a simple organic field-effect molecular wire, are studied, using quantum theory of atoms-in- molecules (QTAIM) and Landauer theory (LT). Analysis of the results obtained in this study showed that these proposed field-effect molecular wire has a suitable response to the applied external electric field (EF).

Keywords: Molecular wire; Nanoelectronics; QTAIM theory; Landauer theory; Field-effect device; Cohesive energy.

I. Introduction

Nanotechnology has expanded greatly due to its interdisciplinary nature. Reducing the dimensions of molecular electronic devices (such as molecular wires) increases their efficiency [1]. Therefore, in this study, external electric field effect on some electronic properties (such as atomic chare, bond paths, electron density and its Laplacian, atomic kinetic/virial energy, current/voltage curve and molecular cohesive energy) of an organic molecular wire are studied, using quantum theory of atoms-in-molecules (QTAIM, [2-3]) and Landauer theory (LT, [3]).

Also, the EF effect on molecular cohesive energy (as one of the factors affecting the stability of field-effect molecular devices) of this field-effect molecular wire is investigated, using following equation:

$$E_{Coh} = -(E_{tot} - \sum_i n_i E_i)/n \quad (1)$$

where E_{tot}, E_i, and n_i being the total energy of all designed molecules, the atomic energy and the number of atoms respectively and n is the total number of all atoms [4].

II. COMPUTATIONAL METHODS

The partitioning of the molecular space into atomic basins can be used to partition the overall electronic properties into atomic contributions, systematically. Also, based on as reported **[2],** the QTAIM remains equally valid in the presence of external field (EF). Thus, in this study, geometry optimization and calculation of the structural and electronic properties of the proposed field-effect molecular wire shown in Fig. 1, have been carried out at QTAIM/DFT-UB3LYP/6- 311G* level of theory, under different EF intensities (in the +x direction). For the gold atoms of the electrodes, LANL2DZ pseudopotential is used.

III. Results and discussion

Some of the electronic properties of these proposed molecular wire are studied, using

QTAIM and LT. Sample of these computational results are shown in Figs 1-3.

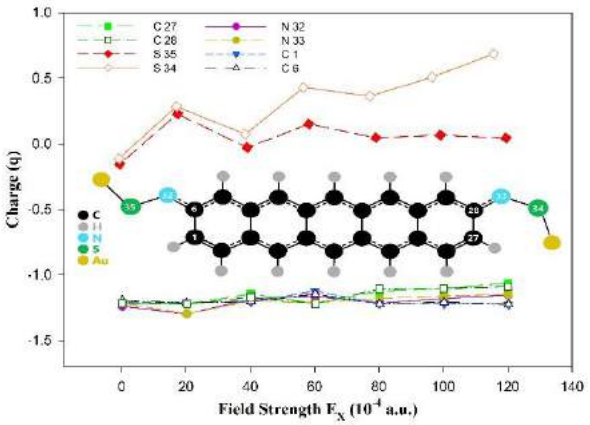

Fig 1. External electric field effect (EF) on the electronic atomic charges, of some atomic basins of the molecular wire is studied in this work.

EF=0 (a.u.)

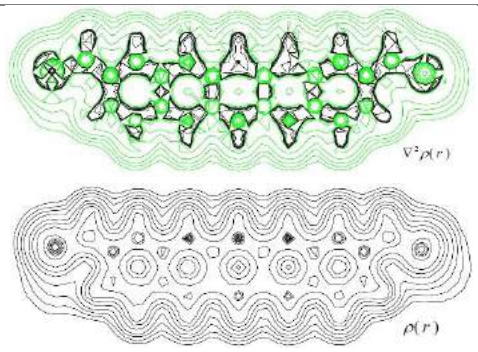

EF=0.006 (a.u.)

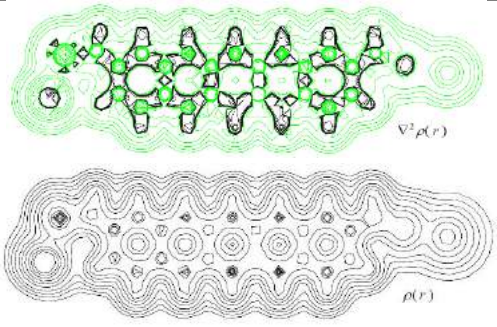

Fig 2. External EF on contour/local map of electron density ($\boldsymbol{\rho(r)}$), Laplacian electron density ($\boldsymbol{\nabla^2\rho(r)}$) of the molecula wire is studied in this work

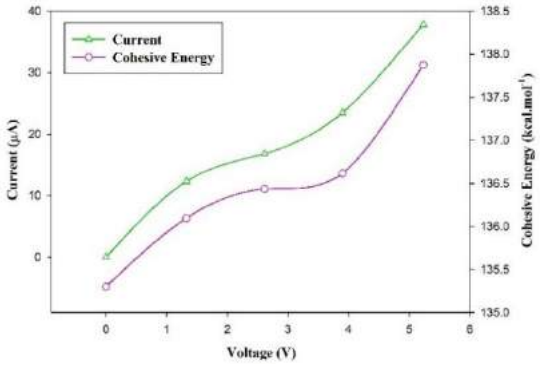

Fig 3. External EF effect on current/voltage curve (I/V) and molecular cohesive energy of the molecular wire is studied in this work.

Atomic scale analysis of the results obtained here shows that sulfur atoms play an important role in intra-molecular charge and energy transfer in this molecular wire. These results also show that the molecular cohesive energy varies non-linearly (with small amplitude oscillations) with EF.

IV. Conclusions

In this study, external EF effect on some of the electronic properties of the field-effect molecular wire shown in Fig.1, are studied, using QTAIM and Landauer theory (LT). Analysis of these results show that when an EF is applied to this molecular wire, the charge and energy are transfer between different atomic basins of this simple organic wire, and thus it is expected that this field-effect molecular wire has acceptable performance in real nanoelectronic circuits.

References

[1] M. Ratner, Nature Nanotechnology, 2013, 8, 378–38.

[2] C.F. Matta, R.J. Boyd, Quantum Biochemistry, *Wiley*, Weinheim, 2010.

[3] R. Landauer, Phys Lett A, 1981, 85, 91-93.

[4] H. hadi and H. shamluie, Computational and Theoretical Chemistry, 2021, 1206, 113494.

بیست و سومین کنفرانس شیمی فیزیک انجمن شیمی ایران
23rd ICS Physical Chemistry Conference
Chemistry Department,
Faculty of Science
Shahid Bahonar University of Kerman
Kerman, Iran
12-13 Jan 2022
ایران، کرمان
دانشگاه شهید باهنر کرمان
دانشکده علوم پایه، بخش شیمی
۲۳-۲۲ دی ماه ۱۴۰۰

Investigation of structure and chemical properties of hydroxycarbamide using quantum chemical calculations

Malihe Nazemian, Mansoor Namazian* and Mohammad R. Noorbala

Correspondence to: Mohammad R. Noorbala (E-mail: namazian@yazd.ac.ir)
Department of Chemistry, Yazd University, Yazd, Iran, P.O. Box 89195-741

Abstract

Hydroxycarbamide or hydroxyurea is a hydroxylated molecule of urea which has been widely used for decades to treat many neoplastic diseases. In this study, the zwitterion formation of hydroxycarbamide in the gas and solution phases is investigated. The conversion of hydroxycarbamide to its zwitterion form is as follows:

$$HO - NH - CO - NH_2 \rightarrow {}^{-}O - NH - CO - NH_3^{+}$$

The change of Gibbs free energy and equilibrium constant for this conversion has been investigated by means of high level ab initio methods. The results of this study help to understand the mechanism of this drug in biological systems.

Keyword: Hydroxycarbamide; zwitterion; Hydroxyurea; G4; ab initio.

I. Introduction

Hydroxycarbamide or hydroxyurea with the chemical formula $CH_4N_2O_2$ was first synthesized by Dassler and Stein in 1869. It is a hydroxylated molecule of urea and a water-soluble solid, colorless, crystalline and tasteless. Hydroxycarbamide has been widely used for decades to treat many neoplastic diseases, including leukemia and other blood disorders, including sickle cell anemia [1].

In chemistry, a zwitterion, also called an inner salt, is a molecule that contains an equal number of positively- and negatively-charged functional groups [2].

II. Methods

G3, G4MP2 and G4 theories are employed to investigate process of conversion of hydroxycarbamide to its zwitterion form in the gas phase and solution.

Zwitterion of hydroxycarbamide is studied in 21 solvents with different polarity using SMD continuous solvent model at the B3LYP/6-31G (2df, 2p) level of theory.

III. Results and discussion

The conversion of hydroxycarbamide to its zwitterion form is not spontaneous in the gas phase as the change of Gibbs energies are positive (Table 1). However, this process is spontaneous in aqueous solution. The non-aqueous solution, solvation energies have been calculated for a large number of solvents. Zwitterion form is more stable in polar solvents such as acetonitrile, methanol, ethanol and formic acid (Table 2). The higher the polarity, the higher the percentage of zwitterion form.

Table 1. The change of Gibbs energies (hartree) for the gas phase and solution.

	gas-phase	solution	
Method	ΔG	ΔG(total)	K
G3	0.081732	-0.0261392	15.9
G4MP2	0.085457	-0.0224142	10.7
G4	0.086318	-0.0215532	9.8

Table 2 . The change of Gibbs energies and equilibrium constant along with dielectric constants for the studied solvents.

Solvent	Dielec	ΔG(total) kJmol^{-1}	K
Water	78.4	-56.6	9.8
Acetonitrile	35.7	-23.9	2.6
Chloroform	4.7	2.2	0.9
Ethanol	24.9	-46.3	6.5
methanol	32.6	-54.4	9.0
Carbon Tetra Chloride	2.2	-24.9	2.7
Benzene	2.3	34.0	0.3
Toluene	2.4	32.1	0.3
Acetone	20.5	-17.6	2.0
Diethyl Ether	4.2	11.3	0.6
Pyridine	13.0	-10.9	1.5
Cyclo Pentanol	17.0	-37.2	4.5
Di Methyl Sulfoxide	46.8	-20.5	2.3
n-Octanol	9.9	-32.1	3.6
Anisole	4.2	11.3	0.6
TetraHydro Furan	7.4	-2.3	1.1
Aniline	6.9	-15.2	1.8
Dichloromethane	8.9	-10.9	1.6
DiChloro Ethane	10.1	-13.0	1.7
Formic Acid	51.1	-54.1	8.9
Nitro Benzene	34.8	-19.4	2.2

IV. Conclusions

The conversion of hydroxycarbamide to its zwitterion form has been studied:

$$HO-NH-CO-NH_2 \rightarrow {}^{-}O-NH-CO-NH_3^{+}$$

The change of Gibbs free energy and equilibrium constant for this conversion has been investigated by means of G3, G4MP2 and G4 high level methods.

Zwitterion of hydroxycarbamide is studied in 21 solvents with different polarity using SMD continuous solvent model at the B3LYP/6-31G (2df, 2p) level of theory. The zwitterion form is stable in water and polar solvents.

References

[1] A. S. Boyd, and K. H. Neldner, Hydroxyurea therapy, Journal of the American Academy of Dermatology, **1991**, 25, 518-524.

[2] Munz, D.; Meyer, K., Charge frustration in ligand design and functional group transfer. *Nat. Rev. Chem.* **2021**, *5*, 422-439.

بیست و سومین کنفرانس شیمی فیزیک انجمن شیمی ایران
23rd ICS Physical Chemistry Conference
Chemistry Department,
Faculty of Science
Shahid Bahonar University of Kerman
Kerman, Iran
12-13 Jan 2022
ایران، کرمان
دانشگاه شهید باهنر کرمان
دانشکده علوم پایه، بخش شیمی
۲۲-۲۳ دی ماه ۱۴۰۰

Effects of Water on the Formation and the Stability of Interfacial Nano-bubble: A Molecular Dynamic Simulation.

Maryam Hamzeh Joungheni*., Masumeh Foroutan

Department of Physical Chemistry, University of Tehran, Tehran, Iran, mrymhamzeh@ut.ac.ir

Abstract:

The stability and growth of a nano-bubble on a smooth surface are studied by molecular dynamics simulation in this work. We investigated the phase transition of an argon film on substrates. When the liquid atoms on obtain enough thermal energy, they convert into a nano-bubble. Our simulation reveal how pinning of the three-phase contact line on the surface can lead to the stability of the surface nano-bubble.

Keywords: Nano-bubble, Contact angle, Molecular dynamics simulation

I. Introduction

The existence of stable surface nano-bubbles was first proposed from measurements of long range forces between hydrophobic surfaces, which was later verified by atom force microscopy. The observed properties of surface nano-bubbles include very long lifetime and smaller contact angles than expected on the same substrate, which have attracted much theoretical attention(1).

The standard theory used to describe the bubble-nucleation phenomenon is the so-called classical nucleation theory (CNT). CNT is commonly used to predict the rate of nucleation(2).

The formation of nano-bubbles around nanoparticles is a phenomenon that has technological relevance in applications such as cancer treatment(3), catalytic reactions(4) and solar energy conversion(5).

The molecular dynamics simulation method (MD) is an available tool to describe the interaction between different particles and microscopic bubble nucleation process. It has become a popular tool to study the effects of solid-liquid interfacial wettability on phase transition with the development of computer technology (6).

II. Methods

In the present study, the simulation case are performed using package LAMMPS. The initial configuration of the simulation system is a cubic box including platinum, water, argon atoms. A periodic boundary is applied to the two direction. The L-J potential is presented to describe the interaction between atoms (7). During the simulation process, the cut-off radius is 3.5 σ and the position, velocity atoms are updated by a Velocity-Varlet algorithm.

Results and discussion

Based on analyses, for the smooth substrate, the nucleation position is related to the substrate temperature. The nan-bubble appears with the increase of substrate temperature, as the heating process continues, thermal energy exchanges between the fluid atoms.

III. Conclusions

In this work, the formation and growth processes of the nano-bubble on a smooth surfaces with heating time are showed. Then, quantitative analysis is performed using simulation results.

References:

[1] V. Craig, Soft Matter, 2011, 7(1), 40- 48.

[2] L. Farkas, Phys. Chem. 1927, 125, 236–242.

[3] E. Lukianova-Hleb, E. Hanna, J. Hafner, D. Lapotko, Nanotechnology 2010, 21, 085102.

[4] J. Adleman, D. Boyd, D. Goodwin, D. Psaltis, Nano Lett. 2009, 9, 4417–4423.

[5] O. Neumann, A. Urban, J. Day, S. Lal, P. Nordlander, N. Halas, ACS Nano 2012, 7, 42–49.

[6] M. ILIĆ M, M. PETROVIĆ M, V. STEVANOVIĆ, Therm. Sci. 2019, 23, 87-10

[7] G. Nagayama, P. Cheng, International Journal of Heat & Mass Transfer, 2004, 47, 501-513.

بیست و سومین کنفرانس شیمی فیزیک انجمن شیمی ایران
23rd ICS Physical Chemistry Conference
Chemistry Department,
Faculty of Science
Shahid Bahonar University of Kerman
Kerman, Iran
12-13 Jan 2022
ایران، کرمان
دانشگاه شهید باهنر کرمان
دانشکده علوم پایه، بخش شیمی
۲۳-۲۲ دی ماه ۱۴۰۰

Interaction of 5-Fluorouracil anti-cancer drug& $B_{12}P_{12}$ with adenine: DFT, AIM, ELF and NBO study

M. Rezaei Sameti [a]*, A. Rezaei

[a] *Department of Applied Chemistry, Faculty of Science, Malayer University, Malayer, 65174, Iran*

Abstract

The interaction of the 5-Fluorouracil anti-cancer drug & $B_{12}P_{12}$ complex with adenine in presence of static electric field was studied by density functional theory (DFT) computational method. The geometrical, structural properties, quantum and thermodynamic parameters, reduced density gradient (RDG), natural bond orbital (NBO) and atom in molecule topology (AIM) parameters are calculated and all results are analyzed. The gap energy between HOMO and LUMO orbitals and global hardness and electronegativity of system reduce significantly from pure state. The adsorption energy values for all studied models are negative and exothermic. The results of this studied confirm that the $B_{12}P_{12}$ nanocage can be useful carrier for delivery 5-FU anticancer drug to the target cells.

Keywords: $B_{12}P_{12}$ nanocage; adenine; 5-Fu drug; DFT; ELF

I. Introduction

One of the therapeutic challenge of medicine in the body is to deliver intelligently of the drug to the target cells with high accuracy. For this means various material are applied for making the sensitive drug delivery carriers. In the resent years, various nano materials such as nanotube, nano plat and nano cage are used for this purpose. The results of these studied indicated that the $B_{12}N_{12}$, $B_{12}P_{12}$ nanocages are a good candidate for delivery of various drugs. [1-4]. One of the effective drug for treatment of colorectal cancer, esophageal cancer, stomach cancer, pancreatic cancer, breast cancer, and cervical cancer [5-6].

II. Methods

All considered models are optimized at the WB97XD/LanL2DZ level of theory by Gaussian (09) package. The optimized structures are used to determine adsorption energy, NBO, and quantum parameters of 5-FU adsorption. Adsorption energy (Eads) of 5-FU on the surface of $B_{12}P_{12}$ and Adenin is calculated as follows [3-5]:

$$\Delta E = E_{B12P12/Flu-Adenin} - (E_{B12P12/Flu+}E_{Adenin}) \quad (1)$$

III. Results and discussion

The adsorption energies of all studied complex are negative and adsorption process is exothermic. In the presence of static electric field (SEF) the adsorption and interaction of drug & nanocage complex with adenine increase significantly from original state, this property may be more effective in the drug delivery carriers (DDCs) in the biological system. With adsorbing drug & nanocage and adenine the energy gap (E_{gap}), and global hardness (η) of decrease slightly

from original states, so the conductivity and reactivity of complex increase slightly from original states. The calculated values of electron localization function (ELF) and localized orbital locator (LOL) are in the range of 0 to 0.5 a.u, these results confirm that the nature of bonding between drug & nanocage with adenine is non-covalence (electrostatic) or weak covalence and this result is in agreement reduced gradient density (RDG) plots (Figs. 1, 2). The natural bond orbital (NBO) results demonstrate that with adsorbing 5-FU drug the donor electron effect of adenine increase, so the dipole moment of complex enhance.

Conclusions

The results of this study demonstrate that the bonding type between drug and adenine in the presence of nanocage and SEF filed is electrostatic. And with increasing the strong of SEF field the adsorption of drug on the adenine increase. The calculated results indicate that $B_{12}P_{12}$ nanocage in the presence of SEF field is a good candidate for drug delivery carriers of 5-FU anticancer drug in biological system.

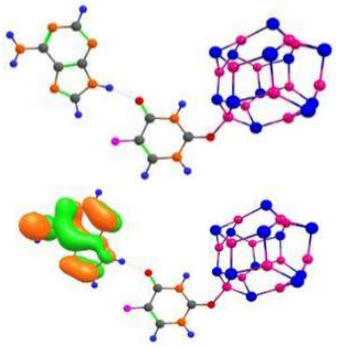

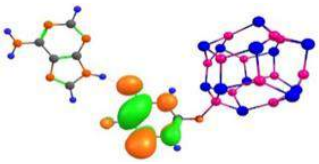

Fig. 1 The optimized and HOMO-LUMO structures of 5-FU& B12P12 complex with adenine.

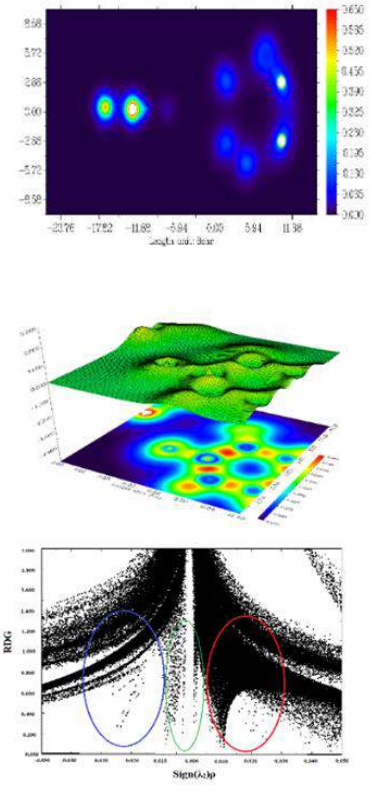

Fig. 2 the LOL, ELF and RDG plots of 5-FU& $B_{12}P_{12}$ complex with adenine.

References

[1] M. A. Graham, G. F. Lockwood, D. Greenslade, S. Brienza, M. Bayssas, E. Gamelin, Clin. Cancer Res. 2000, 6, 1205.

[2] M. F. Sorrentino, A.G. Truesdell, J. Cardiol. Cases, 2012, 6 (1), 20.

[3] M. Rezaei-Sameti, S. K. Abdoli, J. Mol. Str. 2020, 1205, 127593.

[4] M. Rezaei-Sameti, E. Shiravand, Adsorption, 2020, 26, 955.

[5] M Rezaei-Sameti and Kh Hadian, *Iranian. J. Phys.Res*, 2016, 16, 3.

[6] A. Y. Moore, *J. Dermatological Trea*t. 20 (6) (2009) 328–35.

بیست و سومین کنفرانس شیمی فیزیک انجمن شیمی ایران
23rd ICS Physical Chemistry Conference
Chemistry Department,
Faculty of Science
Shahid Bahonar University of Kerman
Kerman, Iran
12-13 Jan 2022
ایران، کرمان
دانشگاه شهید باهنر کرمان
دانشکده علوم پایه، بخش شیمی
۲۳-۲۲ دی ماه ۱۴۰۰

(Syntheses, characterization of SnO_2/ZnO nanocomposite as a Visible light-activated photocatalyst)

Farshad Soleimani[a], Iran Sheikhshoaie[a,*], Mahdiyeh Sheikhshoaei[b]
[a] *Department of Chemistry, Faculty of Science, Shahid Bahonar University of Kerman, 76175-133, Kerman, Iran*
[b] *Department of Minning, Faculty of Engineeing, Shahid Bahonar University of Kerman, 76175-133, Kerman, Iran*
E-mail: shoaie@uk.ac.ir

Abstract

In this work, the adsorption of methyl red dye on SnO_2/ZnO nanocomposite adsorbent was investigated. This nanocomposite was successfully synthesized by thermal method from a primary $SnCl_2$ loaded in MOF. The synthesized nano particles were characterized by X-ray diffraction (XRD), field emission scanning electron microscope (FE-SEM), X-ray analysis (**EDX**) and MAP analysis. This compound has high purity with crystalline structure. These results was also being compared with the standard XRD pattern of Zinc Tin Oxide (Reference code No. 01-074-2184) with Cubic crystal system and Fd-3m space group.

Keywords: Nanocomposite; Phtocatalyst; Tin oxide; FESEM; XRD; Methyl red; EDX, Zink oxide.

I. Introduction

A significant amount of colorful sewage is produced from a variety of industries, such as leather, textile, plastic and paper. Dyes containing toxic cationic and anionic compounds in industrial wastewater have adverse effects on the environment. Such a color drain can threaten the environment. Some colors have health hazards. The toxicity and carcinogenicity of these substances and their precursors are indicative of increased risk in aquatic life.

Photocatalysis has attracted a lot of attention as an effective process in the mitigation of environmental pollution.

SnO_2 is a semiconductor that is used in photocatalytic activities due to its cheapness, non-toxicity, high surface-to-volume ratio, thermal and chemical stability. In addition, ZnO with a band gap energy of 3.2 eV (similar to TiO_2) can serve as an photocatalyst in organic pollutants degradation due to its high quantum efficiency, high chemical stability, high photosensitivity, low cost, and ability to absorb a larger fraction of solar spectrum.

Hence, this study aimed to investigate the efficiency of SnO_2, ZnO photocatalysis to reduce an organic dye in sewage.

In order to find the optimal conditions, the parameters involved in the adsorption process were changed, such as pH of the solution, amount of adsorbent, the concentration of solution and temperature of the solution.

II. Methods

At first, $Zn(Mim)_2$ was synthesized by the solo-thermal method and then the element Sn was added to the initial composition using $SnCl_2$, the final structure of which was obtained as a nanocomposite [1-3]. In order to oxidize and form our desired structure,

$Sn/Zn(Mim)_2$ was heated at 800 ° C for 8 hours. FE-SEM, XRD and FT-IR analyzes were used for Characterization Figure 1 shows the XD pattern of the synthesized Zink Thin oxide. Finally, UV-vis spectroscopy was used to check the property the photocatalytic properties synthesized nanostructure. Typically the photocatalytic activities of desired amounts of as synthesized nano composite were assessed by the photodegradation of 50 ml Methyle red (MR) aqueous solution (with 5 ppm concentration in different pH). The suspension was set aside with magnetic stirring (500 RPM) at room temperature and dark conditions for 20 min to reach an adsorption–desorption equilibrium. After that the suspension was exposed to visible light for desired time (0 –55 min), at certain time intervals.

5 ml of the suspension was centrifuged to remove the photocatalyst. Then by measuring the absorption of MR in the filtrate at 518 nm using UV–Vis absorption spectrometer the photocatalytic activity and degradation process was monitored Figure 2.

III. Results and discussion

The final structure was examined by FT-IR, XRD and FESEM and was completely consistent with the literature.

Photocatalytic activity of Tin zink oxide was investigated by photocatalytic decolonization of methyl red (MR) under visible light irradiation. Moreover, the impact of initial molar concentrations of catalyst loading, initial pH of the solution and temperature on the rate of MR degradation process was studied. In addition, the photocatalytic degradation process can be explained in a terms of kinetic model.

IV. Conclusions

The results of this research can be examined from several perspectives. First, the nanoparticles have photocatalytic properties and are capable of producing free radicals by stimulation with ultraviolet light, and the other is the destruction of the desired color and contaminant in the presence of nanoparticles produced. Due to the importance of water and the prevention of any contamination from contaminated water, water purification by photocatalysts is a good approach. Nanoparticles of SnO_2@ZnO can be introduced as a suitable nanophotocatalyst for the destruction of pollutants.

References

[1]. Z. Zhang, Z. Yang, R. Wang, Z. Feng, X. Xie, Q. Liao, Electrochimica Acta, 2014, 134, 287-292.

[2]. [6] Y.F. Yuan, J.P. Tu, H.M. Wu, C.Q. Zhang, S.F. Wang, X.B. Zhao, Journal of Power Sources, 2007, 165, 905-910.

[3]. B. Liu, X. Zhang, H. Shioyama, T. Mukai, T. Sakai, Q. Xu, Journal of Power Sources, 2010, 195, 857-861..

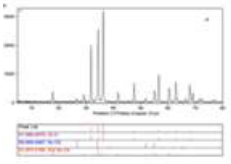

Fig. 1. XRD patten of SnO2/ZnO2 nano composite

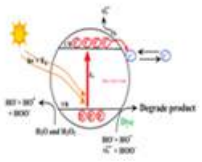

Fig. 2. Schematic mechanisem of degridation dye(SnO2/ZnO2)

بیست و سومین کنفرانس شیمی فیزیک انجمن شیمی ایران
23rd ICS Physical Chemistry Conference
Chemistry Department,
Faculty of Science
Shahid Bahonar University of Kerman
Kerman, Iran
12-13 Jan 2022
ایران، کرمان
دانشگاه شهید باهنر کرمان
دانشکده علوم پایه، بخش شیمی
۲۳-۲۲ دی ماه ۱۴۰۰

Adsorption of some monoatomic, diatomic and triatomic gases on graphene

Maryam A. Rafiei[a*], Mansoor Namazian[b]

[a] *Department of Chemistry, Faculty of Science, University of Tehran, Tehran, Tel: 02161111; maryam.rafiei@ut.ac.ir*
[b] *Department of Chemistry, Faculty of Science, Yazd University, Yazd, Tel: 03531232222; namazian@yazd.ac.ir*

Abstract

The present work aims to study the interaction between He, Ne, Ar, Kr, O_2, CO_2 and CS_2 molecules and monolayer graphene by means of density functional theory (DFT) calculations. In this study, we also include a detailed view on various configurations of approaching gases, different sites of graphene, equilibrium distances, levels of theory and models for the process of adsorption.

Keywords: Graphene; Adsorption; Noble gases; Oxygen; Density functional theory

I. Introduction

Graphene, a single-atom-thick two-dimensional honeycomb structure composed of carbon atoms [1]. It has attracted enormous attention due to its mechanical flexibility, electronic conductivity and optical transparency. Graphene has applications in a wide range of fields such as adsorption of gases, sensing, electronics, energy storage, biomedicine and catalysis. Various studies have been separately carried out on the adsorption of gases on graphene [2, 3], however, there is no systematic analysis of adsorption of monoatomic, diatomic and triatomic gases on graphene. Besides, their atomic/molecular configurations have not completely resolved.

II. Methods

All DFT calculations were carried out using the ORCA 4.2.1 program package [4]. Several different functionals and basis sets have been studied and the M06-2X [5] along with 6-311+G(d,p) basis set is used for the studied system.

III. Results and discussion

Different models including 2, 4, 7 and 19 hexagonal rings have been studied and 7 hexagonal rings which are composed of 36 atoms in the (x,y) plane are adequate for the present study (Fig. 1).

The adsorption energies for monoatomic noble gases are in the range of -3.7 to -10.3 kJ/mol. The smallest atom of He shows the lowest and Kr shows the highest energy in this range. For the diatomic molecule of O_2, the adsorption energy is -12.3 kJ/mol, whereas for the triatomic gases of CO_2 and CS_2 the energies are calculated as -19.4 and -25.5 kJ/mol, respectively. The equilibrium distances of the studied gases are 2.5, 2.9, 2.9, 3.3, 2.9, 3.0 and 3.4 Å for He, Ne, Ar, Kr, O_2, CO_2 and CS_2, respectively.

All different configurations and symmetric adsorption positions have been investigated. For the monoatomic gases and O_2, site H (at the center of a hexagonal ring) has been found as the best position,

whereas for the CO_2 and CS_2, site A (over a C atom) is more favorable. The best orientation for the studied polyatomic gases is found to be parallel. A summary of the results is shown in Table 1.

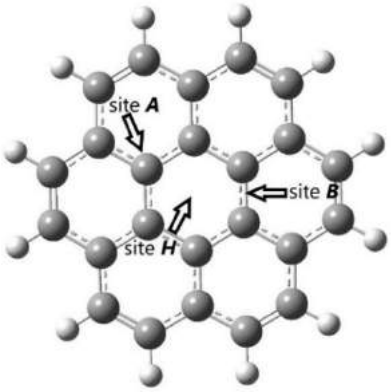

Fig. 1. Different sites of A, B and H for the 7-ring model of graphene

Table 1. The adsorption energies (E_{ads} in kJ/mol) and equilibrium distances (d_0 in Å) of He, Ne, Ar, Kr, O_2, CO_2 and CS_2 on different sites of graphene

Gas	Perpendicular						Parallel	
	Site **A**		Site **B**		Site **H**			
	E_{ads}	d_0	E_{ads}	d_0	E_{ads}	d_0	E_{ads}	d_0
He	-3.8	2.8	-3.0	3.0	-3.8	2.8	-	-
Ne	-5.7	2.9	-5.6	3.0	-5.7	2.9	-	-
Ar	-7.9	3.2	-8.0	3.3	-8.0	3.3	-	-
Kr	-9.6	3.3	-8.9	3.3	-9.6	3.3	-	-
O_2	-9.6	3.0	-9.5	3.9	-12.3	2.9	-13.5	3.0
CO_2	-8.4	2.9	-8.6	3.0	-10.8	2.9	-19.4	3.0
CS_2	-16.4	3.2	-16.7	3.2	-16.8	3.1	-25.5	3.4

IV. Conclusions

The adsorption behavior of He, Ne, Ar, Kr, O_2, CO_2 and CS_2 on graphene (with 7 hexagonal rings) was studied. The increase of adsorption energy and equilibrium distance from He to Kr is in agreement with the experiment that larger gases have stronger dipole-dipole interactions. Investigating of different configurations for O_2, CO_2 and CS_2 showed that a clear preference was parallel configuration with respect to the graphene. Among studied gases, CS_2 presented the highest adsorption energy.

References

[1] K. S. Novoselov, A. K. Geim, S. V. Morozov, D. e. Jiang, Y. Zhang, S. V. Dubonos, I. V. Grigorieva and A. A. Firsov, Science, 2004, 306, 666-669.

[2] X. Zhu, K. Liu, Z. Lu, Y. Xu, S. Qi and G. Zhang, Physica E, 2020, 117, 113827.

[3] L. H. Qu, X. L. Fu, C. G. Zhong, P. X. Zhou and J. M. Zhang, Materials, 2020, 13, 4945.

[4] F. Neese, WIREs Computational Molecular Science, 2012, 2, 73-78.

[5] Y. Zhao and D.G. Truhlar, Theoretical Chemistry Accounts, 2008, 120, 215-241.

بیست و سومین کنفرانس شیمی فیزیک انجمن شیمی ایران
23rd ICS Physical Chemistry Conference
Chemistry Department,
Faculty of Science
Shahid Bahonar University of Kerman
Kerman, Iran
12-13 Jan 2022
ایران، کرمان
دانشگاه شهید باهنر کرمان
دانشکده علوم پایه، بخش شیمی
۲۲-۲۳ دی ماه ۱۴۰۰

A theoretical study of solvent effects on vibrational frequencies of glycine

Javad Beheshtian[a], Zahra Hasanzadeh Tazeh Gheshlagh[b, *]

Department of Chemistry, Faculty of Science, Shahid Rajaee Teacher Training University
[a] Tehran, Tel: 09127179794; E-mail: J.Beheshtian@sru.ac.ir
[b] Tehran; Tel: 09355501061; E-mail: Hasanzadeh.206z@yahoo.com

Abstract

In the present work, we show that CPCM and IEFPCM methods are able to change the vibrational frequencies values of amino acid glycine in solution phase at theory of the levels MP2/6-311G ** and CISD/6-311G**. The findings of this report demonstrate that vibrational frequencies values with the methods for the glycine in solution phase may change in some cases. Comprehensively, almost equal and differ only slightly in some cases like the first observed frequency belongs to the OH tension. The CCO bend and CH_2 Asymmetric tension in MP2/6-311G ** and CCO bend, CCN bend and $CCNH_2$ twist vibrating movements are different.

Keywords: CPCM; DFT; IEFPCM; Glycine; Solution Phase; Vibrational Frequencies.

I. I. Introduction

Each of the different vibration modes of the molecule occurs at a specific frequency. As a general rule, bond tensions have higher vibrational energies. Bonding bends have lower energy and torsional movements have the lowest vibrational energy. Usually, the lowest vibrational frequencies are related to the twisting of the major parts of large molecules [1]. The significance of amino acids in chemistry is good fixed [2]. In this Letter, we demonstrate the change of vibrational frequencies values with the CPCM and IEFPCM methods [3] for glycine in solution phase.

II. Methods

The calculations of quantum mechanics in theory level by using MP2/6-311G ** and CISD/6-311G** theory method. In order to this, firstly the structure of glycine designed by using Chem Office software and initial optimization operated by using ChemBio 3D Ultra 12 software and AM1 method on asus- PC computer with a 2.20 GHz processor, used for finalization. Eventually, the final calculation operated in theory of the level MP2/6-311G ** and CISD/6-311G** in the solution phase [4, 5].

III. Results and discussion

For studying the **solvent effects on vibrational frequencies of glycine** whit CPCM and IEFPCM model at first optimization process performed. Then calculation of the **vibrational frequencies** containing CPCM and IEFPCM model glycine done. The structure of glycine is shown in Fig. 1 and the result of this research is presented in Table 1.

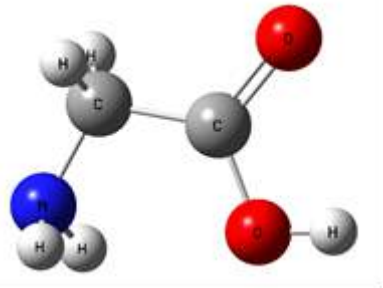

Fig. 1. Chemical structures of studied molecule (Glycine).

Table 1. Calculated vibrational frequencies (cm^{-1}) values with the CPCM and IEFPCM methods for glycine in solution phase.

	IEFPCM		CPCM	
Vibrating movements	MP2/ 6-311G **	CISD/ 6-311G**	MP2/ 6-311G **	CISD/ 6-311G**
OH tension	3849	4022	3849	4022
NH_2 Asymmetric tension	3625	3738	3625	3738
NH_2 Symmetric tension	3543	3665	3543	3665
CH_2 Asymmetric tension	3144	3210	3143	3210
CO tension	1841	1942	1841	1942
NH_2 and CH_2 Asymmetric motion	1418	1468	1418	1468
CCO bend	478	496	429	452
CCN bend	264	275	264	260
$CCNH_2$ twist	260	265	260	252

IV. Conclusions

In the present work, we chose to calculate vibrational frequencies values with the CPCM and IEFPCM methods for glycine in solution phase. According to our results, comparing the vibration motions in the solution phase with the CPCM and IEFPCM methods, it can be concluded that the observed frequencies for the motions under study are generally almost equal and differ only slightly in some cases. The first observed frequency belongs to the OH tension. In CCO bend and CH_2 Asymmetric tension vibrating movements in MP2/6-311G ** theory method and CCO bend, CCN bend and $CCNH_2$ twist Vibrating movements in CISD/6-311G** are different in both solution phase. Generally, we may say that the models are a convenient and versatile method to account for solvent effects.

References:

[1] Ren-Hui Zheng, Wen-Mei Wei and Yan-Ying Liu, Molecular Physics, 2021, 119, 4.

[2] Derbel ,Najoua, Koseoglu,Fitnat, Kilic,Esma, J.Phys.Chem, 2007, B111, 1470-1477.

[3] Shaymaa H. Abdulrahmana, Fanar M. Al-Healy, Egypt. J. Chem, 2021, 64, 4359 – 4367.

[4] Frisch M J,Trucks G W,Schlegel AB, Gaussian, Pittsburgh, PA, 1994.

[5] M. j. Frisch et al. GAUSSIAN 03, Revision C. 01, Gaussian Inc., Wallingford. CT, 2004.

بیست و سومین کنفرانس شیمی فیزیک انجمن شیمی ایران
23rd ICS Physical Chemistry Conference
Chemistry Department,
Faculty of Science
Shahid Bahonar University of Kerman
Kerman, Iran
12-13 Jan 2022
ایران، کرمان
دانشگاه شهید باهنر کرمان
دانشکده علوم پایه، بخش شیمی
۲۲-۲۳ دی ماه ۱۴۰۰

Theoretical Investigation of Structural and Electronic Properties of Azophenol Molecular Switches and its Derivatives

Morteza Zare*, Fatemeh Omidian

Department of Chemistry, Shahid Chamran University of Ahvaz, Ahvaz, Iran, m.zare@scu.ac.ir

Abstract

The quantum chemical calculations have been utilized for obtaining the equilibrium geometries and transition states of four azophenol molecular photoswitches. The transition structures were obtained for two mechanism (rotation and inversion). For all studied molecules, the trans isomers are more stable than the cis configurations both in the vacuum and ethanol solvent. The cis-to-trans thermal isomerization pathways were studied using relaxed potential energy surface scan. The transition structures were obtained and the barrier energies were predicted for rotation and inversion mechanisms. The rotation pathway was found to be preferred. The order of the calculated energy barriers are in very good agreement with the experimental relaxation times.

Keywords: Molecular photoswitches; Azophenol; Transition state; DFT.

I. Introduction

The design and development of new devices and machines at the molecular level, having the dimension of 10^{-9} m (nm), are guidelines for the modern and multidisciplinary field of nanotechnology. Molecular switches are a special type of molecular machines that can be switched between (at least) two distinguishable forms by the application of a chemical, electrochemical, photochemical, or thermal stimulus. Photoswitches are molecular switches where the different forms of a molecule can be inter-converted by means of a photochemical reversible process [1]. Magnetic, electrical or optical properties, through an external trigger signal is a very interesting design feature of new promising functional systems and smart materials [2]. Herein we focus on investigating the geometrical and electronic properies of four azophenol molecular photoswitches (Fig. 1).

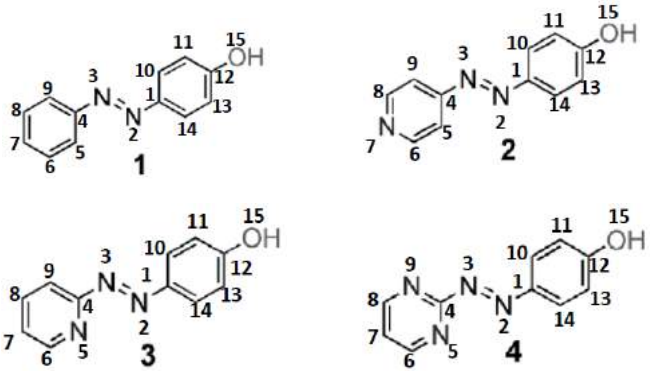

Fig1. Chemical structures of azo compounds.

II. Methods

Geometric structures were optimized using the DFT method at the B3LYP/6-311++G(d,p) level. We have also reported additional calculations by using Grimme's D3 dispersion corrected functional [3]. The transition state was investigated using the potential energy surface scan in both

inversion and rotational pathways around the angle and dihedral angle, respectively. All calculations were performed using Gaussian 09 [4] program.

III. Results and discussion

Energies and relative energies with respect to the more stable isomers are listed in Table 1. For all studied molecules, the trans isomers are more stable than the cis configurations both in the vacuum and ethanol solvent. Data in the presence of solvent are not shown here.

Table 1. Energies of cis and trans isomers (in au) and relative energies with respect to the trans isomers (in kcal.mol^{-1}).

	E /au	E_{rel}/ kcal.mol^{-1}
1trans	-649.206479	0
1cis	-648.185243	13.33
2trans	-664.243800	0
2cis	-664.223489	12.74
3trans	-664.242256	0
3cis	-664.225638	10.43
4trans	-680.281523	0
4cis	-680.266372	9.51

The transition structures for cis to trans thermal isomerization were obtained using the Berny algorithm. The angle C1-N2-N3 (**A**) and the dihedral angle C1-N2-N3-C4 (**D**) of the transition structures are listed in Table 2. The barrier energies were predicted for rotation and inversion mechanisms and presented in Table 2. The rotation pathway is found to be preferred. The order of the calculated energy barriers are in very good agreement with the experimental relaxation times (τ).

IV. Conclusions

In this article, geometric properties and vibrational frequencies are obtained using B3LYP(D3) method. The results show that the trans isomers of all four compounds have a stretched structure but cis isomers are twisted. The distinction between cis and trans isomers is of particular importance. The presence of ethanol has no significant effect on the molecular geometries. Based on the results, trans isomers are more stable than cis isomers both in the presence and in the absence of ethanol. The inversion and rotation pathways was studied for cis to trans thermal isomerization. The rotational mechanism is more favorable than the inversion pathway.

References

[1] A. Sinicropi, (2010). Biomimetic Photoswitches. *LA CHIMICA E L'INDUSTRIA*, *3*, 102

[2] J. Garcia- Amorós, M. Díaz- Lobo, S. Nonell and D. Velasco, Angew. Chem. Int. Ed., 2012, 51, 12820.

[3] S. Grimme, J. Antony, S. Ehrlich and H. Krieg, J. Chem. Phys., 2010, 132, 154104.

[4] M. J. Frisch, et al. Gaussian 09, Gaussian Inc, Wallingford CT, 2013.

Table 2. The angle C1-N2-N3 (**A**) and the dihedral angle C1-N2-N3-C4 (**D**) of the transition structures (in degree), energy barriers for cis to trans isomerization (in kcal.mol^{-1}) and relaxation time (τ).

	1		**2**		**3**		**4**	
	ROT	INV	ROT	INV	ROT	INV	ROT	INV
A C1-N2-N3	116.9	179.1	117.2	179.0	117.2	177.3	114.6	177.6
D C1-N2-N3-C4	-89.5	-125.6	-90.0	-115.2	-91.0	-179.2	-90.3	-178.3
ΔE	26.08	29.90	21.55	31.09	22.97	29.98	19.70	32.06
τ	0.0205		0.014		0.049		0.0064	

بیست و سومین کنفرانس شیمی فیزیک انجمن شیمی ایران
23rd ICS Physical Chemistry Conference
Chemistry Department,
Faculty of Science
Shahid Bahonar University of Kerman
Kerman, Iran
12-13 Jan 2022
ایران، کرمان
دانشگاه شهید باهنر کرمان
دانشکده علوم پایه، بخش شیمی
۲۲-۲۳ دی ماه ۱۴۰۰

Spectroscopic study of the applications of encapsulation of fenofibrate molecules with β-cyclodextrin in aqueous media

Elham Javanparast[a] and Nina Alizadeh[a*]

[a] Department of Chemistry, Faculty of Science, University of Guilan, P.O. Box: 19141, Rasht, Iran,

Abstract

The aim of this work was to study the physicochemical characterization of fenofibrate(FNB)-ßCD binary systems was carried out by Fourier transform infrared spectroscopy (FTIR) and ^{1}HNMR. Phase solubility analysis revealed enhancement in the solubility of fenofibrate. Phase solubility studies revealed 1:1 M complexation of fenofibrate with ßCD. The dissolution study revealed that the drug dissolution rate was improved by the presence of ßCD.

Keywords: Fenofibrate,β-Cyclodextrin, Complexation, Spectroscopy

I. Introduction

Fenofibrate (FNB) is an oral fibrate lipid lowering drug, which could markedly reduce elevated plasma concentrations of triglycerides, low density lipoprotein (LDL) and total cholesterol. As the compound is practically insoluble in water the oral bioavailability of the drug in humans is relatively low .The complex formation usually results in a modulation of the physicochemical and pharmaceutical properties of guest molecules, such as increased solubility and dissolution rate, improved chemical stability[1]. Cyclodextrins (CDs) form a group of structurally related oligosaccharides with cylindershaped cavities that have the capacity to form inclusion complexes with many drugs by taking a whole drug molecule, or a part of it, into the cavity[2].

The purpose of this study was to characterize the interaction between fenofibrate and ßCD, to study its effect on solubility and bioavailability of fenofibrate.

II. Methods

The possible interactions between fenofibrate and ßCD in both solid state and liquid states were investigated. The solid state interaction was investigated by fourier transform infrared (FTIR) spectroscopy. The interaction in solution was studied by phase solubility analysis and dissolution experiments. Fenofibrate and ßCD complexes were prepared in a molar ratio of 1:1 by physical mixture and freez drying method.

III. Results and discussion

The FTIR spectra of the systems of fenofibrate–ßCD and those of pure components are shown in Figure 1. IR spectra of complex showed changes from parent spectra i.e. pure drug and beta cyclodextrin. When the systems are compared, it can be observed that the ester

group stretching band at 1728 cm^{-1} broadens and shifts towards higher wavenumbers, indicating change in the intermolecular H-bonds of the drug upon complexation. Similar modifications were seen in the combination signal of the ester group, which indicates change in the interaction of this group when the complex is formed. In addition, the bands at 1050-1340 cm^{-1} corresponding to antisymmetric vibrations of the aryl ether group and C-O stretching of esters broaden in some cases and in others peaks vanish upon complexation.

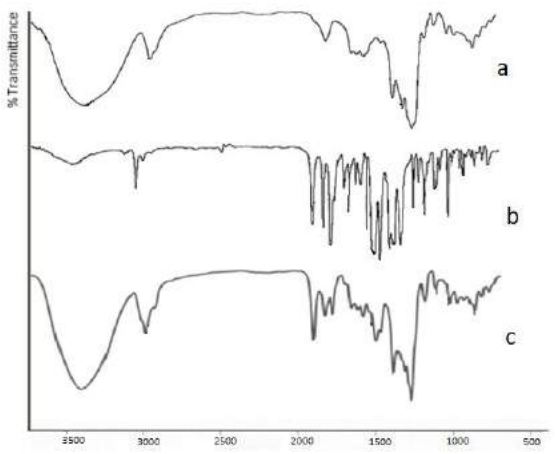

Fig. 1. FT-IR: β-cyclodextrin (a) Fenofibrate (b) complex β-cyclodextrin and fenofibrate (c)

In the IR spectra of inclusion complex, broadening of the peak was observed at 2913cm^{-1} due C-H stretching vibration while all other characteristic peaks of drug had disappeared indicating possible interaction between drug and cyclodextrin.

IV. Conclusions

It can be hypothesized that the solubility might be enhanced indicating that the ester moiety is partially enclosed in the apolar region of the cyclodextrin cavity. As such the linkage is stearically stabilized by the hydroxyl groups on the surface of the cyclodextrin molecule, which can otherwise mediate the nucleophilic attack on the carbonyl function of the fenofibrate molecule causing hydrolysis. So it can be concluded that the cyclodextrins might have formed the inclusion complex with fenofibrate in host-guest fashion, with central hydrophobic cavity of cyclodextrin acting as host for whole drug or part of it.

References

[1] Vogt, M., Kunath, K., Dressman, J.B.: Eur J Pharm. Biopharm., 68, 283–288 (2008).
[2] F. G. Gu1, Y. Wang, G. D. L. Meng, H. B. Han, C. Z. Wu1143–146 (2012).

بیست و سومین کنفرانس شیمی فیزیک انجمن شیمی ایران
23rd ICS Physical Chemistry Conference
Chemistry Department,
Faculty of Science
Shahid Bahonar University of Kerman
Kerman, Iran
12-13 Jan 2022
ایران، کرمان
دانشگاه شهید باهنر کرمان
دانشکده علوم پایه، بخش شیمی
۲۲-۲۳ دی ماه ۱۴۰۰

The Adsorption of Li and Li^+ on Silicene sheet: A DFT study

Javad Beheshtian[a], Zahra Hasanzadeh Tazeh Gheshlagh[b,*]

Department of Chemistry, Faculty of Science, Shahid Rajaee Teacher Training University
[a] Tehran, Tel: 09127179794; E-mail: J.Beheshtian@sru.ac.ir
[b] *Tehran; Tel: 09355501061; E-mail: Hasanzadeh.206z@yahoo.com*

Abstract

Using DFT calculations, we investigate the effect of adsorption defective silicene doped with Lithium (Li) and Lithium ion (Li^+). The calculated results show that the energy gap was the same in MV and DV vacancy modified defected silicene doped with Li but differences were seen in MV and DV vacancy modified defected silicene doped with Li+. Our results would present a new significant strategy to study new structures silicene-based devices and their interesting applications such as batteries.

Keywords: Density functional theory calculations, Doping, Silicene, Vacancy modification.

I. I. Introduction

Silicene has more properties than graphene, it has received more attention today [1]. Because it's enough space, high surface area and modify the properties of silicene through creating defect and adsorption or substitutional doping have attracted the researcher's attention [2, 3]. For this reason, we have investigated theoretically the creation of MV and DV vacancy modified defected silicene doped with Li and Li^+. It is proposed that defect and dope can affect energy gap of proposed structures .The goal of the present work was Comparison energy gap on MV and DV vacancy modified defected silicene doped with Li and Li^+.

II. Methods

Calculations were carried out within the framework of density functional theory (DFT) using a local density approximation scheme, as implemented in the Dmol3 package. The generalized-gradient approximation (GGA) for the exchange correlation functional with the parametrization of Perdew − Burke − Ernzerhof (PBE) was used [4-5]. The double numerical plus polarization (DNP) basis set, 4.4 basis file and Monkhorst-Pack k-point mesh of (6×6×1) and (4×4) supercell with a vacuum width of 60 ˚A.

III. Results and discussion

At first pristine silicene and then two types of vacancy on pristine silicene according to studies and type of issue optimized. Two types of studied vacancy include mono vacancy (MV), double vacancy (DV) and doping them whit Lithium (Li) and Lithium ion (Li+) done and their optimized structures are shown in Fig. 1.

As mentioned in the introduction, the following equation can be used to described the energy gap (*E*gap) of structures. where *E*gap is the energy gap for the optimized

equilibrium configuration of the mono-vacancy and double-vacancy with the A (A = Li and Li+) sited in the vacancy, EHOMO is the energy of HOMO of the silicene with the vacancy and E_{LOMO} is the energy of LOMO of the structures. The values of energy of HOMO (E_{HOMO}), LUMO (E_{LUMO}) and energy gap (Egap) for pristine and vacancy modified defected silicene presented in Table 1.

$$E\text{gap} = E_{HOMO} - E_{LUMO} \quad (1)$$

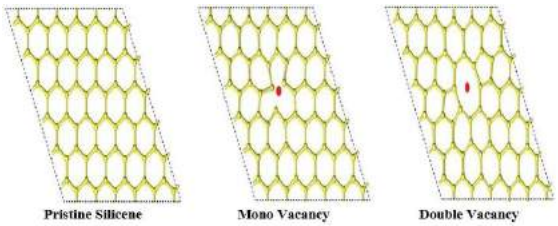

Fig. 1. Optimized models of suggested silicene: pristine silicene, MV and DV and defective structures.

Table 1. The energy of HOMO (E_{HOMO}), LUMO (E_{LUMO}) and energy gap(Egap) calculated for the single substitution doping on vacancy modified defected silicene structures whit Li and Li^+.

System	E_{HOMO} (ev)	E_{LUMO} (ev)	Egap (ev)
MV	-4.84	-5	0.16
MV-Li	-4.91	-5.13	0.22
MV- Li^+	-6.37	-6.38	0.01
DV	-4.74	-4.83	0.09
DV- Li	-4.99	-5.21	0.22
DV- Li^+	-6.33	-6.43	0.1

IV. Conclusions

In the present work, having investigated the electronic properties of silicene the change of energy gap in vacancy modified defected silicene structures doped with Li and Li+. According to the table1, the defect and doping whit Li and Li+ can affect the amount of energy gap and it can be changed apparently. The energy gap was the same in MV and DV vacancy modified defected silicene doped with Li but differences were seen in MV and DV vacancy modified defected silicene doped with Li^+. It was observed that the defect and doping can play an important role in energy gap.

References

[1] Md. Habibur Rahman, Emdadul Haque Chowdhury, Muhammad Rubayat Bin Shahadat, Md Mahbubul Islam, Computational Materials Science, 2021, 191.
[2] HuynhAnh Huy, Quoc Duy Ho, Truong QuocTuan, Ong Kim Le3, Nguyen Le Hoai Phuong, Dumbbell, Sci Rep, 2021, 11.
[3] Yang GM, Xu Q, Fan X, Zheng WT, The Journal of Physical Chemistry C, 2018, 122, 1903-1912.
[4] J. Perdew, Phys. Rev. Lett, 1996, 77, 18-28.
[5] Delley, B, J. Chem. Phys, 2000, 13, 7756-7764.

بیست و سومین کنفرانس شیمی فیزیک انجمن شیمی ایران
23rd ICS Physical Chemistry Conference
Chemistry Department,
Faculty of Science
Shahid Bahonar University of Kerman
Kerman, Iran
12-13 Jan 2022
ایران، کرمان
دانشگاه شهید باهنر کرمان
دانشکده علوم پایه، بخش شیمی
۲۲-۲۳ دی ماه ۱۴۰۰

The interaction of Phosgene gas with the pristine and B & Al doped $Si_{12}C_{12}$: A DFT and TD-DFT method

M. Rezaei Sameti[a]*, A. Rezaei, Masood Maleki

[a] *Department of Applied Chemistry, Faculty of Science, Malayer University, Malayer, 65174, Iran*

Abstract

In this project, the interaction and adsorption of the toxic phosgene ($COCl_2$) gas on the surface of pristine and B, Al-doped $Si_{12}C_{12}$ nanocage was investigated by density functional theory (DFT) and time dependent density functional theory (TD-DFT). Optimized structures were applied for calculating the geometrical and electrical parameters, adsorption energy, quantum parameters, and thermodynamic properties and reduced density gradient (RDG) scatter plots. The calculated results indicated that the adsorption energy and enthalpy values of all studied structures were negative and all processes were exothermic. With doping B and Al atoms the absolute values of adsorption energy increase significantly from pristine models, so doped models were a good candidate for adsorbing $COCl_2$ toxic gas. The gap energy and global hardness of nano cluster in the presence of doping atoms and $COCl_2$ gas decrease significantly, and also the conductivity, reactivity of nanocluster increase, this property demonstrated that the B, Al doped $Si_{12}C_{12}$ was a good sensor and absorber for detecting $COCl_2$ gas.

Keywords: SiC nanocage; B; Al doped; DFT; RDG

I. Introduction

Phosgene is the organic chemical compound with the formula $COCl_2$. It is a colorless gas; in low concentrations, its odor resembles that of freshly cut hay or grass. It is very poisonous and was used as a chemical weapon during World War I, where it was responsible for 85,000 deaths [1-2]. In addition to its industrial production, small amounts occur from the breakdown and the combustion of organochlorine compounds. In the last years various methods are used for detecting and adsorbing various toxic materials such as $COCl_2$. The results of previous researches confirmed that the doped nanocage has a most potential for adsorbing and detecting toxic materials in the environmental systems [3-4].

II. Methods

At first step, we considered 15 configurations for adsorption of $COCl_2$ on the surface of nanocage, all selected configuration are optimized at cam-B3LYP/6-31G (d, p) level of theory. By using Gaussian 09 package. From optimized models, the quantum parameters, thermodynamic properties in the gas phase and water solvent media, Uv-visible spectrum, density of states plots and reduced density gradient (RDG) are calculated.

III. Results and discussion

The geometrical results indicated that the bond length of nanocage around doping and

adsorbing position increase significantly from original values (see Fig. 1). These results confirm that the electrical properties of nanocage alter from pristine state. On the other hand the quantum parameters involving gap energy, global hardness, and electrophilicity of system decrease, so the conductivity and reactivity of nanocage increase (see Figs. 2 and 3). The adsorption energy and enthalpy values for interaction of $COCl_2$ gas with pristine and B, Al doped $Si_{12}C_{12}$ nanocage are negative and process are exothermic. With doping B and Al the absolute values of adsorption energy increased significantly from pristine model. The RDG results indicate that the nature bonding between $COCl_2$ and nano cage is physisorption and van der Walls type. The Uv-visible results show that with doping B, Al and adsorbing $COCl_2$ the optical properties of nanocage change slightly from pure state.

IV. Conclusions

The results of this study reveal that, B and Al doped $Si_{12}C_{12}$ nanocages are favorable candidate for making a selective filter or and sensitive sensor for adsorbing and detecting toxic $COCl_2$ gas from environmental systems.

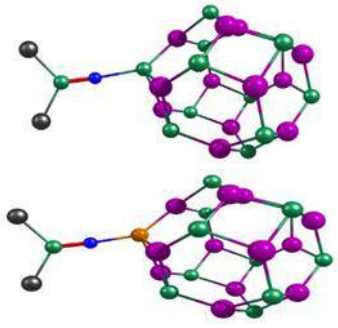

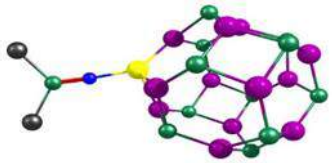

Fig. 1 The optimized structures of COCl2 adsorption on the pristine and B, Al doped Si12C12 nanocage

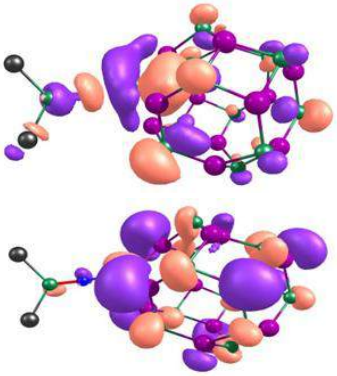

Fig. 2 The HOMO-LUMO plots for $COCl_2$ adsorption on the pristine and B, Al doped $Si_{12}C_{12}$ nanocage

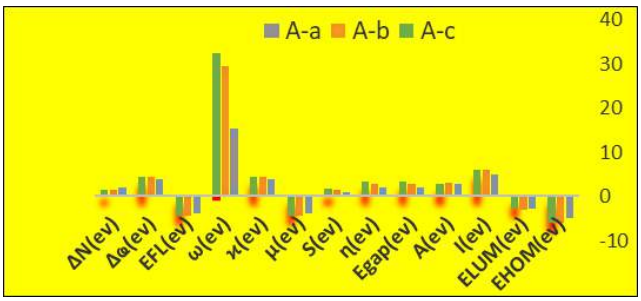

Fig. 3 The quantum parameters for $COCl_2$ adsorption on the pristine and B, Al doped $Si_{12}C_{12}$ nanocage

References

[1] M. Nakata, K. Kohata, T. Fukuyama, K. Kuchitsu, J. Mol. Spect. 83 (1980) 105–117.

[2]A. Zaboli, H. Raissi, F. Farzad, H. Hashemzadeh, J. Mole. Liq. 2020, 301,112435

[3] M. Rezaei-Sameti, E. Shiravand, Adsorption, 2020, 26, 955.

[4] M. Rakhshi, M. Mohsennia, H. Rasa, M. Rezaei Sameti, Vacuum, 2018, 155, 456.

بیست و سومین کنفرانس شیمی فیزیک انجمن شیمی ایران
23rd ICS Physical Chemistry Conference
Chemistry Department,
Faculty of Science
Shahid Bahonar University of Kerman
Kerman, Iran
12-13 Jan 2022
ایران، کرمان
دانشگاه شهید باهنر کرمان
دانشکده علوم پایه، بخش شیمی
۲۳-۲۲ دی ماه ۱۴۰۰

DFT study of promote hydrogen adsorption by borophene nanostructure decorated with Sc atom

Sima Roshan[a], Adel Reisi-Vanani [a,b,*], Simin Roshan [a]

[a] *Department of Physical Chemistry, Faculty of Chemistry, University of Kashan, Kashan, Iran*
[b] *Institute of Nano Science and Nano Technology, University of Kashan, Kashan, Iran*
E-mail: areisi@kashanu.ac.ir

Abstract

The use of hydrogen as a clean alternative to fossil fuels needs to overcome storage problems. In this study, we investigated the H_2 adsorption behavior on pristine and Sc decorated β_{12}-borophene, using DFT calculations. The results show that borophene decorated with Sc atom, can obliquely adsorb H_2 on B-B bonds with adsorption energy of -0.410 eV, while this value for H_2 on pristine borophene is -0.164 eV. Electrical conductivity and lack of magnetic properties are seen in DOS diagrams. Therefore, structural modification of borophene with Sc atom can greatly increase H_2 adsorption energy.

Keywords: Borophene; DFT; H_2 Storage.

I. Introduction

Experimental advances in the field of nanotechnology have identified H_2 as a suitable energy source with high-capacity of energy. The use of H_2 requires the discovery of an ideal storage space. Today, boron-based nanomaterials (Borophene), with their light weight have revolutionized in the conversion and storage of energy [1]. The most stable structure among borophene allotropes is β_{12}-borophene. The remarkable properties of the borophene cause that these materials have good potential for practical applications in various fields such as metal ion batteries, gas sensors and H_2 storage. In this study, application of the pristine and Sc decorated β_{12}-borophene for hydrogen storage applications was studied by DFT-D calculations.

I. Methods

All calculations of this study were performed using spin polarized DFT method in $DMol^3$ module of Materials Studio program. The GGA method with PBE correlation exchange functional were used. We also used Grimme's method and DFT-D3 corrections to consider the contribution of the weak Van der Waals interactions. In addition, we used a 7×7×1 gamma-centered Monkhorst-pack set of k-points. Adsorption energy (E_{ads}) of the H_2 molecule onto structures was calculated by the following equation:

$$E_{ads} = [E_{clx} - E_{M\text{-}borophene} - E_{H2}] \quad (1)$$

where E_{clx}, $E_{M\text{-}borophene}$ and E_{H2} are the energies of the complex, Sc-decorated borophene, and H_2 molecule, respectively.

II. Results and discussion

First, to investigate the adsorption properties of β_{12}-borophene, a 2×3 supercell was optimized. Next, we placed a Sc atom in eight different sites of the borophene, and for each structure, after optimization was calculated the adsorption

energy of the Sc atom on the sheet, based on "Eq. (1)". Results showed that after optimization, the center of hexagon site is the best for Sc decoration of borophene with the highest adsorption energy of -5.204 eV. Then, to investigate the H_2 adsorption on the structures, we placed a H_2 molecule in various sites of the Sc-β_{12} structure and in horizontal and vertical orientations. Fig. 1 shows the most stable configuration.

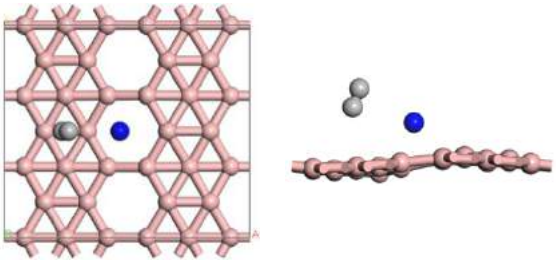

Fig. 1. Optimized configuration of the H_2-Sc-β_{12} from top and side views.

The adsorption energy of the H_2 molecule on the structures is obtained by "Eq. (1)". Our results show that adsorption energies on the pristine and Sc decorated borophene structures are about -0.164 and -0.410 eV, respectively (Table 1). Therefore, it can be said that the Sc decoration of the β_{12}-borophene is significantly effective to improve the H_2 adsorption energy.

Table 1. Adsorbtion energy (E_{ads}) of the H_2 on the borophene.

System	Final position	Final State	E_{ads} (eV)/H_2
H_2-β_{12}	H1	Vertical	-0.164
H_2-Sc-β_{12}	B2	Oblique	-0.410

Total density of state (DOS) diagrams for H_2-β_{12} and H_2-Sc-β_{12} systems are shown in Fig 2. The passage of conduction lines and the non-zero DOS at the Fermi level confirm the semi-metallic properties and conductivity of the structures. Also, the mirror image of the α and β lines shows that these structures have not magnetic properties.

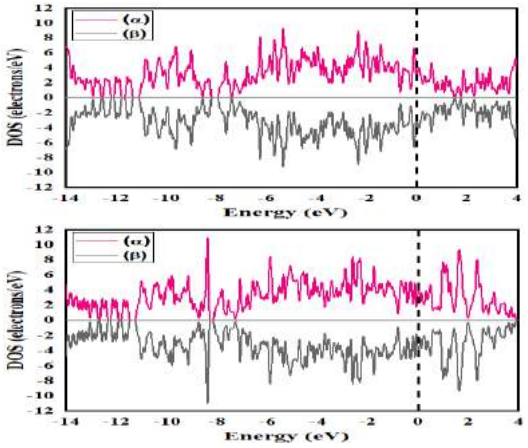

Fig. 2. DOS of systems H_2-β_{12} (top), H_2-Sc-β_{12} (down).

III. Conclusions

In summary, we investigated the storage of H_2 on the pristine and Sc decorated β_{12}-borophene using DFT calculations. Our study showed that the best sites with the highest adsorption energies for the H_2 adsorption in the β_{12} structure is B-B bonding. Also, the adsorption energy of the H_2 molecule after Sc decoration is about 2.5 times greater than it for pristine one. DOS diagrams confirm the electrical conductivity and lack of the magnetic properties of the structures. Therefore, it is concluded that the decoration of the Sc atom on β_{12}-borophene significantly increases the H_2 adsorption energy according to the DOE targets.

References

[1] B. Feng, J. Zhang, Q. Zhong, W. Li, S. Li, H. Li, P. Cheng, S. Meng, L. Chen and K. Wu, *Nature chemistry*, 2016, *8*(6), 563-568.

بیست و سومین کنفرانس شیمی فیزیک انجمن شیمی ایران
23rd ICS Physical Chemistry Conference
Chemistry Department,
Faculty of Science
Shahid Bahonar University of Kerman
Kerman, Iran
12-13 Jan 2022
ایران، کرمان
دانشگاه شهید باهنر کرمان
دانشکده علوم پایه، بخش شیمی
۲۲-۲۳ دی ماه ۱۴۰۰

Modification of the structural and electronic properties of Ni decorated borophene for hydrogen adsorption: A DFT study

Simin Roshan[a], Adel Reisi-Vanani [a,b,*], Sima Roshan [a]

[a] *Department of Physical Chemistry, Faculty of Chemistry, University of Kashan, Kashan, Iran*
[b] *Institute of Nano Science and Nano Technology, University of Kashan, Kashan, Iran*
E-mail: areisi@kashanu.ac.ir

Abstract

The use of the hydrogen as an ideal energy for replacement in fossil fuels requires a suitable storage technology. Following the synthesis of borophene, its use for H_2 storage was suggested. In this study, we investigate the adsorption of Ni atom on to β_{12}-borophene and its performance in H_2 storage using DFT calculations. The results of our calculations show that configuration with Ni atom and H_2 molecule in the center of hexagon site has the highest adsorption energy. The Ni atom binds to the surface of borophene with an adsorption energy of -4.402 eV. Also, adsorption energy of H_2 molecule on to pristine borophene is about -0.164 eV, and decoration of β_{12}-borophene with Ni atom can significantly improve it up to -0.619 eV, which is in line with the DOE targets. Also, β_{12}-borophene structure after Ni doping keeps conductivity and non-magnetic properties.

Keywords: Adsorption; H_2 Storage; DFT

I. I. Introduction

Using H_2 energy as a suitable choice for replacement of fossil fuels, requires light and inexpensive storage materials [1]. The advent of borophene, a two-dimensional nanostructure of boron atoms, has demonstrated its applications for H_2 storage. Experimental research on the borophene in 2015 by Manix and Feng, reports various phases for it, and shows that the most stable of them is β_{12} [2]. In the numerous studies for borophene, its applications in the field of the electrode, electrocatalysis, gas sensor and H_2 storage have been reported. The structural and electronic properties of the borophene cause that it is an excellent material for H_2 storage applications. Metal decoration can improve its H_2 adsorption behaviour, and in this study, we theoretically investigate this improvment by Ni decoration of β_{12} -borophene.

II. Methods

All calculations are performed using the spin-polarized DFT method by DMol^3 module implanted in Materials Studio package [3]. The GGA method and the PBE for the exchange correlation functional and the DNP basis set were applied. To measure dispersion Van der Waals interactions, Grimme's DFT-D3 method was used. For integration in Brillouin zone, the set of 7×7×1 k-points were used. The adsorption energy (E_{ads}) of H_2 molecule is calculated according to the following:

$$E_{ads} = E_{clx} - E_{metal\text{-}borophene} - E_{H2} \quad (1)$$

where E_{clx}, $E_{metal\text{-}borophene}$ and E_{H2}, are total

energy of the complex, metal decorated borophene and H_2 molecule, respectively.

III. Results and discussion

To investigate the adsorption of a single Ni atom on the β_{12}-borophene, we considered a 2×3 supercell with 30 boron atoms. We put Ni atom in eight various adsorption sites in β_{12}-borophene and optimized the structures. Adsorption energies were calculated according to "Eq 1". The results show that the center of hexagon is the best site to decorate the Ni atom on β_{12}-borophene with an adsorption energy of -4.402 eV. In the following, we put an H_2 molecule at different sites, vertically and horizontally, on the Ni decorated borophene. In the most stable configuration and after optimization, the H_2 lies horizontally and with a distance of 2.751 Å from borophene sheet (Fig. 1).

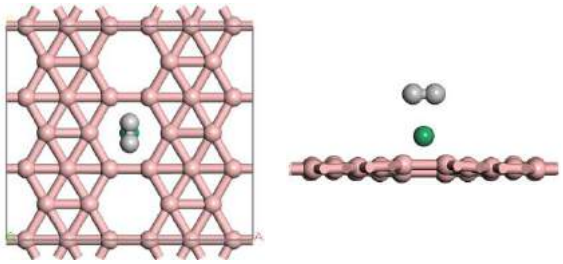

Fig. 1. Top and side views of the optimized configuration of the H_2-Ni-β_{12}.

In Table 1, the adsorption energy of the H_2 on the pristine and Ni-decorated borophene have been summarized.

Table 1. Adsorbtion energy (E_{ads}) of the H_2 on the borophene.

System	Final position	Final State	E_{ads} (eV)/H_2
H_2-β_{12}	H1	V	-0.164
H_2-Ni-β_{12}	H1	H	-0.619

The results in Table 1 show that the H_2 adsorption energy for Ni decorated borophene is about -0.619 eV. In comparison to this value for pristine β_{12}-borophene with an adsorption energy of -0.164 eV. It is seen that Ni decoration causes 3.77 times increasing in E_{ads}. Band structure diagrams for systems contain H_2 adsorbed on the pristine and decorated borophene in Fig 2 confirm that there is no band gap, and the semi-metallic and conductivity properties are preserved. The matching of the α and β lines indicates that there is no magnetic property.

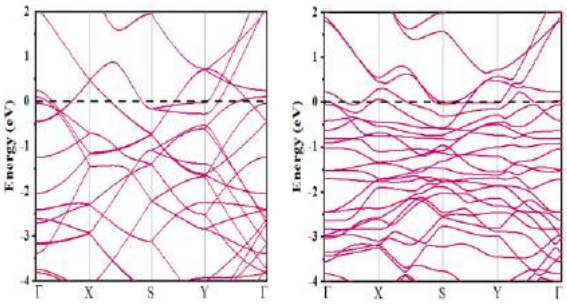

Fig. 2. Band structure of systems pristine (left), Ni-decorated (right), β_{12} of adsorbed by the H_2 molecule.

IV. Conclusions

In summary, we performed DFT calculations to evaluate the adsorption of H_2 in pristine and Ni decorated borophene. The center of hexagon site is the best for Ni atom and H_2 molecule. It was found that Ni decoration causes that an increasing about 3.7 times in E_{ads}. Also, Ni decoration causes no effect on the conductivity and magnetic properties of the borophene, and it can say that Ni-decorated borophene is suitable for H_2 storage applications in the future.

References

[1] R. Singh, A. Altaee and S. Gautam, *Heliyon*, 2020, e04487.

[2] B. Feng, J. Zhang, Q. Zhong, W. Li, S. Li, H. Li, P. Cheng, S. Meng, L. Chen and K. Wu, *Nature chemistry*, 2016, *8*(6), 563-568.

بیست و سومین کنفرانس شیمی فیزیک انجمن شیمی ایران
23rd ICS Physical Chemistry Conference
Chemistry Department,
Faculty of Science
Shahid Bahonar University of Kerman
Kerman, Iran
12-13 Jan 2022
ایران، کرمان
دانشگاه شهید باهنر کرمان
دانشکده علوم پایه، بخش شیمی
۲۲-۲۳ دی ماه ۱۴۰۰

Study of structure and study of chemical reactions of flucytosine and cytosine

Mahsa Azizi soreshjani, Mansoor Namazian*, and Mohammad R. Noorbala

Correspondence to: Mansoor Namazian (E-mail: namazian@yazd.ac.ir)
Department of Chemistry, Yazd University, Yazd, Iran, P.O. Box 89195-741

Abstract

Intramolecular hydrogen transfer for cytosine is investigated. By migration of hydrogen atom from nitrogen of cytosine to oxygen a different isomer is produced. Considering the new geometric position, fully optimization along frequency calculations and higher level of theory have been investigated using quantum chemical computation methods. The solubility of this compound in different solvents is also investigated. The results of this study are important in biochemistry of cytosine.

Keywords:

Cytosine; hydrogen transfer; G4MP2; DFT

I. Introduction

The intermolecular interaction of bases in DNA or RNA is of immense interest and significance to chemists and biologists alike. The interactions of these bases with metal cations, solvent molecules and other small molecules or ions would affect the structure and biological properties or process, which have been investigated widely [1–5]. One of the cytosine derivatives is flucytosine, which was first synthesized in 1957 as a potential antitumor agent [6-7]. Flucytosine is a small, water-soluble molecule that affects body tissues. Flucytosine was first used in 1968 to treat severe infections and meningitis and is still one of the oldest antifungal agents. Which is still in use [7].

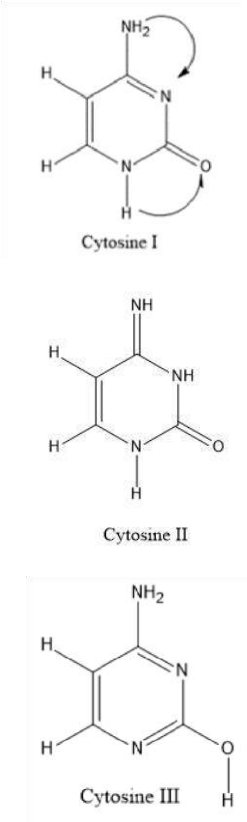

Fig. 1. The chemical structures of three different isomers of cytosine.

II. Methods

Geometry optimization and harmonic frequencies have been carried out using the density functional method B3LYP/6-31G(2df, p). Optimization with

M06-2X method with different basis sets 6-311+G (2df, 2pd), 6-311+G(df, pd), 6-311+G(d,p) were also investigated. Solvation energies are obtained by DMD model of solvation. G4MP2 and CBS-QB3 have been also employed.

III. Results and discussion

The chemical structures of three different isomers of cytosine are shown in Fig. 1. Total energies of different isomers of cytosine have been calculated and the relative energies are presented in Table 1. As seen in this table, isomer I is the most stable structure in aqueous solution. Therefore, the conversion of I to other iosmers is not favorable from thermodynamic point of view. The barriers for these conversions are also calculated and found to be very high.

Table 1. Relative energies of cytosine isomers by means of different methods (kJ/mol)

Method	I	II	III
G4MP2	-23.0	5.5	0.0
CBS-QB3	-23.2	7.4	0.0
M062X 6-311+G(2df,2pd)	-21.2	10.8	0.0
M062X 6-311+G(df,pd)	-20.7	11.3	0.0
M062X 6-311+G(d,p)	-20.5	11.5	0.0

IV. Conclusions

The chemical thermodynamics and kinetics for the conversion of cytosine to its different isomers have been studied and the results show that isomer I is the most stable isomer in aqueous solution. This is also true for other polar solvent such as ethanol.

References

[1] J. Sponer, P. Hobza, Chem. Rev., 1999, 99, 3247.

[2] J. Sponer, J. Leszczynski, P. Hobza, Biopolymers (Nucl. Acid Sci.) 2002, 61, 3.

[3] J. Munoz, J. Sponer, P. Hobza, M. Orozco, F. J. Luque, J. Phys. Chem. B., 2001, 105, 6051.

[4] K. S. Schmidt, J. Reedijk, K. Weisz, J. E.M. Basilio, J. E. Sponer, J. Sponer, B. Lippert, Inorg. Chem., 2002, 41, 2855.

[5] M. V. Vazquez, A. Moussatova, A. Martinez, O. Dolgounitcheva, V. G. Zakrzewski, J. V. Ortiz, J. Phys. Chem. A., 2004, 108, 5845.

[6] R. Duschinsky, E. Pleven, C. Heidelberger, J. Am. Chem. Soc., 1957, 79, 4559.

[7] C. Heidelberger, L. Griesbach, B. Montag, Cancer Res., 1958, 18, 305.

بیست و سومین کنفرانس شیمی فیزیک انجمن شیمی ایران
23rd ICS Physical Chemistry Conference
Chemistry Department,
Faculty of Science
Shahid Bahonar University of Kerman
Kerman, Iran
12-13 Jan 2022
ایران، کرمان
دانشگاه شهید باهنر کرمان
دانشکده علوم پایه، بخش شیمی
۲۲-۲۳ دی ماه ۱۴۰۰

Investigation of structural and electronic properties of GaN Nanosheet

Tara Ashouri[a*], Seifollah Jalili[b], Mohammad Ghassem Mahjani[c]
[a] *K. N. Toosi University of Technology, Tehran, Iran, tara_ashouri@email.kntu.ac.ir*
[b] *K. N. Toosi University of Technology, Tehran, Iran, sjalili@kntu.ac.ir*
[c] *K. N. Toosi University of Technology, Tehran, Iran, mahjani@kntu.ac.ir*

Abstract
We have performed the first-principles calculations on the structural and electronic properties of the 2D GaN nanosheet. In this work, the electronic properties of pristine GaN monolayer have been studied using a first-principles calculation based on DFT. The results unveil that these semiconductor monolayer sheets are promising materials for electrical sensors and due to their tunable bandgap semiconductor on the application of the electric field.

Keywords: Density functional theory; Two-dimensional Gallium nitride; Electronic properties, structural properties

I. Introduction

In recent years, two-dimensional materials are very interesting in materials science. They have high potential applications in nanostructures, such as nanodevices. Two-dimensional materials such as nanosheets have attracted much attention in the new project. Gallium nitride (GaN) has attracted increasing attention due to its extraordinary physical, optical, structural, mechanical, and electronic properties. The wide and direct bandgap of about 3.4 eV makes GaN an ideal material for the fabrication of blue and ultraviolet light-emitting diodes [4,5]. Recently, in first-principles calculations, it was found that GaN has stable monolayer honeycomb structure. [1, 2]

II. Methods

In this paper, the first principles based on DFT were calculated in the QUANTUM ESPRESSO package. The Perdew-Burke Ernzerhof (PBE) parametrization of the generalized gradient approximation (GGA). In order 5 × 5 × 1 GaN supercell was constructed. The cutoff energy for the plane-waves is chosen to be 40 Ry, and the supercell is large enough to ensure that the vacuum space is 15 A˚ to eliminate the interaction between periodic images.

III. Results and discussion

The nanostructures of GaN were optimized by the GGA method. The average Ga-N bond length is 1.87 A˚, which is very close to previous theoretical results and in good agreement with experimental ones [2, 3]. In contrast to a purely covalent bond in graphene, the bonds between Ga and N gain an ionic character. Therefore the charge will transfer from Ga to N [6]. Our calculated total density of states (DOS) and corresponding electronic band structure for GaN nanosheets are shown in Fig 3 and 2 respectively. The results are shown that group III-nitride nanosheets have semiconductor properties with a wide bandgap of 1.95 eV for GaN nanosheets. The calculated total density of states shows that the top of the valence band is mainly contributed by N atoms, while just beside the conduction band of the total DOS is mainly contributed by the Ga atom. All the above results are in good agreement with previous theoretical results [3, 4].

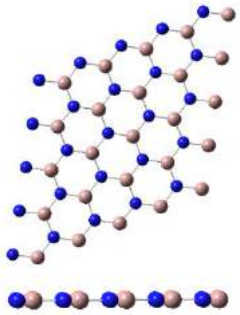

Fig. 1. Top view and side view of GaN Monolayer 5.5.1

Table 1. Cell parameter and atomic position in input file of VC-RELAX from Relax-Reference

Structure	Cell Size	Total Energy	Bond Length	Angle
Relax-Reference	a =14.77 b =14.77	-	1.67223	117.95540
Relax-14.77	a =14.77 b =14.77	-10885.65	1.70555	120.01143
Relax-14.87	a =14.87 b =14.87	-10885.94	1.71697	119.66178
Relax-14.97	a =14.97 b =14.97	-10886.20	1.72907	119.99320
Relax-15.07	a=15.07 b=15.07	-10886.43	1.74029	119.69781
Relax-15.17	a=15.17 b=15.17	-10886.62	1.75212	119.82958
Relax-15.37	a=15.37 b=15.37	-10886.94	1.77438	119.89538
Relax-15.57	a=15.57 b=15.57	-10887.17	1.79783	119.89519
Relax-15.77	a=15.77 b=15.77	-10887.31	1.82106	119.88488
Relax 15.97	a=15.97 b=15.97	-10887.38	1.84373	119.88306
Relax 16.07	a=16.07 b=16.07	-10887.38	1.85537	119.98837
Relax 16.17	a=16.17 b=16.17	-10887.37	1.86702	119.88422
Relax 16.27	a=16.27 b=16.27	-10887.35	1.87855	119.96179
Our Study	**a=16.04 b=16.04 c=25**	**-10887.41**	**1.85**	**119.91**

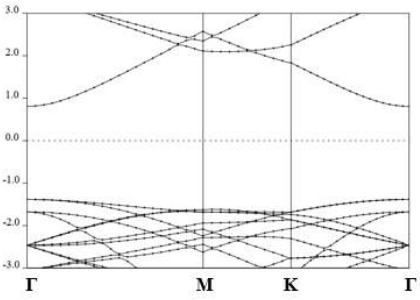

Figure 2. .Band Structure. E (eV) / K-Path [arb]-Energy is set to zero

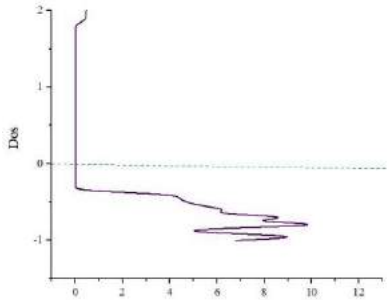

Figure 3. Density of States-Energy is set to zero

IV. Conclusions

We calculated the electronic and structural properties of the hexagonal GaN nanosheets by density functional theory in the generalized gradient approximation. The band structure, density of states of the GaN nanosheet were calculated systematically based on density functional theory. The results show that GaN nanosheet is an indirect bandgap semiconductor. The bandgap is 2.14 eV. This provides a theoretical basis for the design and application of GaN optoelectronic materials. These results propose a potential application for the development of h-GaN nanostructures in electronic and optoelectronic devices.

References

[1]. Xia, C., et al., The feasibility of tunable p-type Mg doping in a GaN monolayer nanosheet. Acta Materialia, 2013. 61(20): p. 7720-7725.

[2]. Ke, C., C. Tian, and Y. Gan, Tailoring the band gap in codoped GaN nanosheet from first principle calculations. Frontiers in Materials, 2020. 7: p. 124.

[3]. Qin, Z., et al., Orbitally driven low thermal conductivity of monolayer gallium nitride (GaN) with planar honeycomb structure: a comparative study. Nanoscale, 2017. 9(12): p. 4295-4309.

[4]. Roohi, H. and N.A. Ardehjani, Exploring the adsorption of CO toxic gas on pristine and M-doped (M= Ti, Cr, Fe, Ni and Zn) GaN nanosheets. New Journal of Chemistry, 2019. 43(38): p. 15280-15292.

بیست و سومین کنفرانس شیمی فیزیک انجمن شیمی ایران
23rd ICS Physical Chemistry Conference
Chemistry Department,
Faculty of Science
Shahid Bahonar University of Kerman
Kerman, Iran
12-13 Jan 2022
ایران، کرمان
دانشگاه شهید باهنر کرمان
دانشکده علوم پایه، بخش شیمی
۲۳-۲۲ دی ماه ۱۴۰۰

DFT study of structural, electronic and UV-Vis spectra properties of oligopyrrole chains as candidate conducting materials

Zeinab Ashrafi andHossein Nikoofard*

Faculty of Chemistry, ShahroodUniversity of Technology, Shahrood, Iran, nikomahdieh@yahoo.com

Abstract

Density functional theory (DFT) is used to study geometry structure, electronic and UV-Visible spectra properties for a series of oligopyrroles including di, tri, tetra, penta, hexa, hepta and octa-pyrrole. Analysis of the HOMO-LUMO band gap and the UV-visible spectral properties demonstrate the facility of hole transport for the oligopyrroles as a potential candidate for conducting polymers.

Keywords: Pyrrole; Density functional theory; Geometry structure; UV-Vis spectra.

I. Introduction

Pyrrole (Py) derivatives are an important feature in the organic conducting materials. A great number of conducting polymers based on Py have been extensively used in energy storage devices, electrochromic displays, electronic devices, and many other applications [1-3].

In the current work, we became interested to study the structural and electronic properties of the oligomers consisting of Py monomers via DFT calculations. Our aim was, to provide a distinct understanding and a new vision description of the geometric characteristics of the understudied oligo(Py)s such as their planarity and conjugated length; their opto-electronic properties, for example, the highest occupied molecular orbital (HOMO) and the lowest unoccupied molecular orbital (LUMO); the ionization potential (IP) and electron affinity (EA); and spectral properties.

II. Results and discussion

Addition of a monomeronto the Pyring could change the electron delocalization over the molecular structure of olig(Py)s. Delocalization of the π-electrons onto the molecular structure leads to a satisfactory resonance system, which corresponds to a narrow HOMO-LUMO gap (HLG). In Table 1, the alternating bond parameter(δ) for all oligomers are displayed. It was found that addition of a monomer onto oligomer chain led to a slight decrease in δ with respect to the parent monomer.This reduction for the radical cations becomes more considerable with respect to their neutral states.

Table 1. Calculated alternating parameter values (in A) for the studied pyrrole oligomers in neutral and radical states.

Species	Neutral state	Radical cation
Di-Py	0.0467	-0.0239
Tri-Py	0.0438	-0.0094
Tet-Py	0.0423	-0.0008
Pen-Py	0.0413	0.0047
Hex-Py	0.0406	0.0090
Hep-Py	0.0403	0.0123
Oct-Py	0.0399	0.0162

The HOMO and LUMO diagrams for the pentamer chain, as an example, are shown in Fig. 1. In the excitation process including the ground state (S_0) → first singlet excited state (S_1) may be primarily

assigned to the HOMO → LUMO transition corresponding to a $\pi^*-\pi$ excited singlet state. For all oligomers, the HOMO possess anti-bonding characters spared mostly over the π-bonds (C=C), although in the case of LUMO, it is composed of the ring atoms and joint monomer rings (C-C) with possessing bonding interactions.

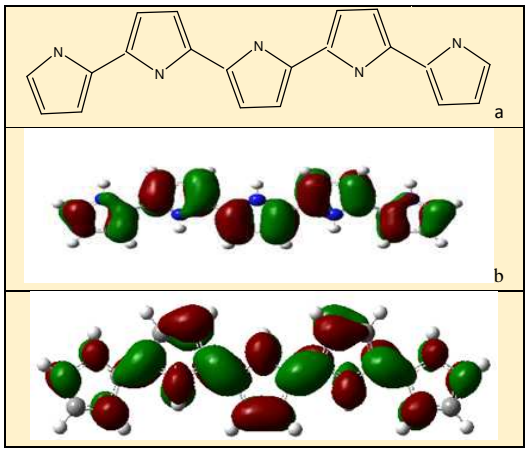

Fig. 1. The contour plots of HOMO (b) and LUMO (c) for the pen-Py (a).

The TD-DFT excitation energies (E_g) and longest wavelengths (λ_{max}) of the maximum absorption peak obtained for each oligomer derivative were calculated.

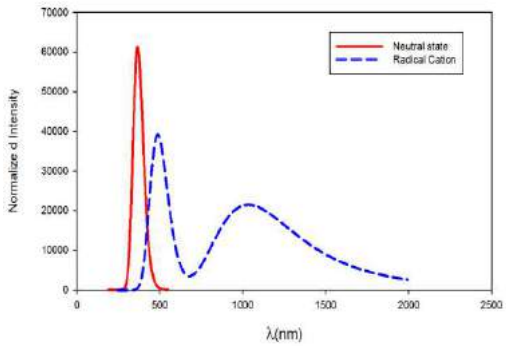

Fig. 2. Simulated absorption spectra for pen-Py in both the neutral and radical states.

As one can see in Fig. 2, an evident bathochromic shift corresponding to a decrease in the excitation energy was observed for pen-Py. In fact, the radical state of each oligo(Py) has larger λ_{max} values with respect to its ground state.

III. Conclusions

In this work, we showed the contributions of the DFT approaches to the detailed description of a series of oligomers derived from the Py monomers. Geometrical optimization carried out on the Py oligomers showed that the oligo(Py) chain has planar structure in the oxidation phase. It was found that the HOMO-LUMO gaps of the studied oligomers decreased with increase in the chain length. Moreover, the TD-DFT calculations carried out on the optimized oligomer structures showed that the growth of Py oligomers yielded an increase in the conjugation length, and thereby, a red shift to the absorption and emission spectra.

References

1.Skotheim, T.A.; Handbook of Conducting Polymers, 3rd Ed, CRC – Press, Boca Raton, 2002.
2. Bakhshi, A. K.;Bahalla, G.; Electrically conducting polymers:Materials of the twenty first century; Sci. Ind. Res., 2004, 63, 715.
3. Nikoofard, H.;Gholami, M., Theoretical investigation of structures and electronic states of a series of phenyl-capped oligothiophenes,ComptesRendusChimie, 2014, 17, 1034-1040.
4. Ocampo, C.; Casanovas, J.;Liesa, F.;Alemán, C.; Polymers and oligomers derived from pyrrole and N-hydroxymethylpyrrole: A theoretical analysis of the structural and electronic properties, Polymer, 2006, 47, 3257-3262.

بیست و سومین کنفرانس شیمی فیزیک انجمن شیمی ایران
23rd ICS Physical Chemistry Conference
Chemistry Department,
Faculty of Science
Shahid Bahonar University of Kerman
Kerman, Iran
12-13 Jan 2022
ایران، کرمان
دانشگاه شهید باهنر کرمان
دانشکده علوم پایه، بخش شیمی
۲۲-۲۳ دی ماه ۱۴۰۰

Effect of C^{α} -methylated residue on the folding behavior of p53 peptide: A Molecular Dynamics Study

Seifollah Jalili[a], Elham Zarurati [b]*

[a] *Department of Chemistry, K. N. Toosi University of Technology, Tehran, Iran, sjalili@kntu.ac.ir*
[b] *Department of Chemistry, K. N. Toosi University of Technology, Tehran, Iran, elhamzaroorati@yahoo.com*

Abstract

Disorders in protein-protein interactions are often the main cause of several diseases, making them attractive as drug targets. One of the cancer- associated protein -protein interactions is the Hdm2-p53 complex. Over expression of Hdm2 disrupts the normal activity of p53, which is commonly seen in cancer cells containing the p53 normal type. Disruption of the HDM2-p53 interaction to maintain p53 function is considered a therapeutic approach to cancer treatment. To inhibit unnatural PPIs, researchers are always look for strategies that interfere with these interactions. Helix mimetics containing Cα-methylated residues can be a good inhibitor for P53-Hdm2 interaction.

Keywords: P53; C^{α}-Me-α-residue; Molecular dynamics simulations.

I. Introduction

One of the cancer-associated protein -protein interactions is the Hdm2-p53 complex. Cancer is caused by mutations in the p53 peptide gene as well as over expression of Hdm2 protein. Inhibition of Hdm2-p53 interaction to reactivate p53 is a treatment for a variety of tumors [1]. In a MD study [2] on Np53 (ETFSDLWKLLPE) and Ep53 peptides with two different conformations (αR and PPII), they concluded that Ep53 could be a better inhibitor of Hdm2. Among unnatural-backbone units for increase the stability and helical content of peptides in the α- helix secondary structure, chiral C^{α}-Me-α-residues was compared to mimic the helical domain of the p53 protein [3,4]. Therefore, we designed VP53 peptide (ETFVDVWKVLVE) with αR conformation and to compare the folding behavior of designed peptide with NP53 peptide.

II. Methods

The initial backbone conformation of peptides, α-helix (ψ= -47º, φ=-57º) was prepared with hyperchem. MD simulations were performed by the Gromacs 5.0.7 simulation packages with Opls-AA force field. Two systems were solvated by cubic boxes of TIP3P water for 200 ns. The production run was performed under at 310 K and 1 atm pressure using Berendsen thermostat. The covalent bonds containing hydrogen atoms were constrained using LINCS algorithms. The Ewald summation was used to handle long-range electrostatic interactions.

III. Results and discussion

since short helical peptides are often not structurally stable, strategies to strengthen this secondary structure are important. For this purpose, Vp53 Peptide was designed.

The presence of four methylated Valine amino acids in Vp53 peptide caused less changes in the dihedral angles of these peptide. In this peptide, the dihedral angles of Trp7 residue appear slightly away from canonical secondary structural basin during the simulation, but the other intermediate residues of the peptide did not change probably due to the effect of neighboring methylated Valine amino acids.

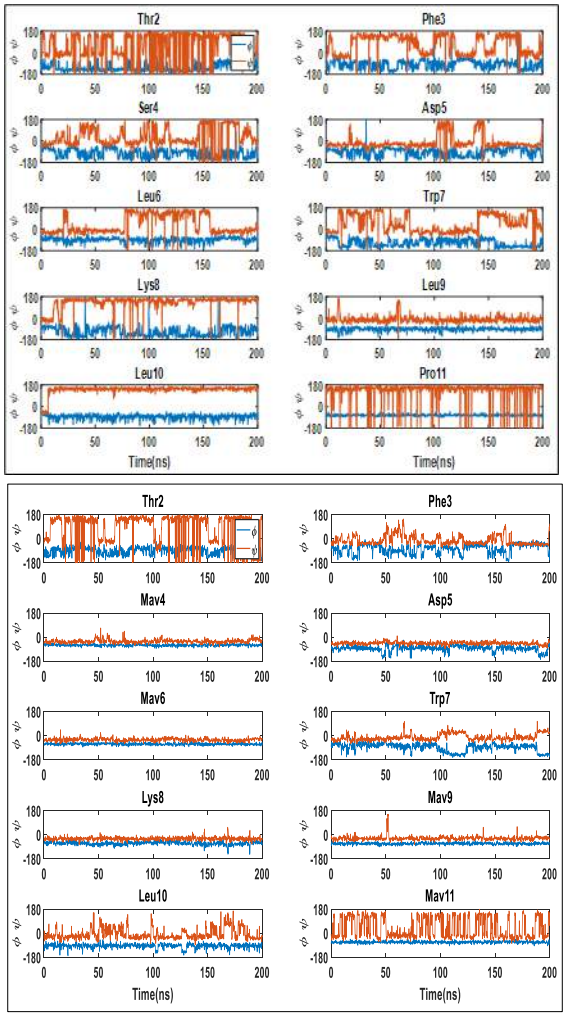

Fig1.Backbone dihedral angel distribution of Np53 and Vp53 obtained from 200 ns MD

Hydrogen bond plays an important role in the stability of secondary structures of protein. Figure 2 shows the average number of H-bonds formed Vp53 peptide is higher than Np53 peptide.

We obtained similar results for a p53 peptide that was methylated with the four C^{α}-Me-α-residues.

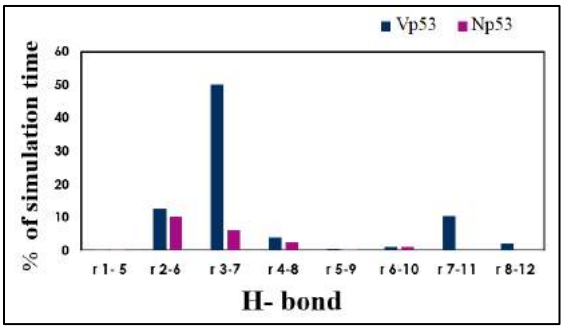

Fig. 2. Average backbone H-bonding pattern for two peptide. The X-axis shows the two residues between which a hydrogen bond is formed.

IV. Conclusions

In this study, the folding behavior of Vp53 synthetic peptide with Np53 peptide was investigated. The analysis shows that the Placement of methylene valine amino acids increased the content of the peptide helix, and the substitution of other methylated amino acids could be considered.

References

[1] Wang, S., Zhao, Y., Aguilar, A., Bernard, D. and Yang, C.Y., 2017. *Cold Spring Harbor perspectives in medicine*, *7*(5), p.a026245.

[2] Chattopadhyay S, Ajani H, Basu G. Peptide Science. 2016 Jan;106(1):51-61.

[3] George KL, Horne WS. Accounts of chemical research. 2018 Apr 19;51(5):1220-8.

[4] Pelay-Gimeno M, Glas A, Koch O, Grossmann TN. Angewandte Chemie International Edition. 2015 Jul 27;54(31):8896-927.

بیست و سومین کنفرانس شیمی فیزیک انجمن شیمی ایران
23rd ICS Physical Chemistry Conference
Chemistry Department,
Faculty of Science
Shahid Bahonar University of Kerman
Kerman, Iran
12-13 Jan 2022
ایران، کرمان
دانشگاه شهید باهنر کرمان
دانشکده علوم پایه، بخش شیمی
۲۲-۲۳ دی ماه ۱۴۰۰

Spectroscopy study on encapsulation of vitamin E (VE) as fat-soluble antioxidant via formation of beta cyclodextrin inclusion complexes

Parisa Azizi[a] and Nina Alizadeh[a*]
*[*a] Department of Chemistry, Faculty of Science, University of Guilan, P.O. Box: 19141, Rasht, Iran*

Abstract
In this paper, the study and synthesis of complexes derived from natural β-cyclodextrin as a host with vitamin E as a guest. Vitamin E is a group of eight fat soluble compounds that include four tocopherols and four tocotrienols. The characteristics and determination of their stability by spectroscopic method to improve the physical and chemical properties of vitamin E been paid.
Keywords: Natural cyclodextrin; Antioxidant effect; Vitamin E;

I. Introduction

One of the most remarkable features of CDs is their tendency to form solid inclusion complexes with a wide variety of solid, liquid and gaseous compounds by the process of molecular complexation. The complexes formed are called host–guest type of complexes[1,2]. Such type of complexes involves a guest molecule (drug) which is properly fitted into the lipophilic cavity of host[2-4].

II. Methods

In this study the formation of solid vitamin E and β-cyclodextrin inclusion complex at a 1:1 molar ratio was done according to a freeze-drying method. Vitamin E was dissolved in ethanol and β-cyclodextrin in water. Initially, β-cyclodextrin was dissolved in an aqueous solution, then vitamin E was added to this solution while the solution was stirred.

III. Results and discussion

Vitamin E has a wide range of use as food supplements and in pharmaceuticals; however, its poor solubility is a drawback for its use and processing. Inclusion complexation with CD molecules enables to overcome this challenge and enhance the water solubility of vitamin E compounds.

a)

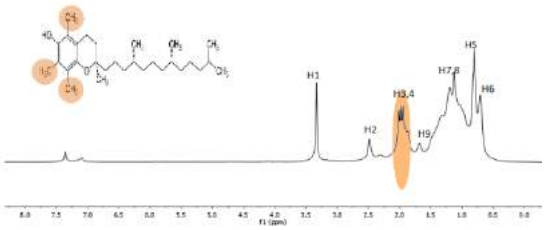

b)

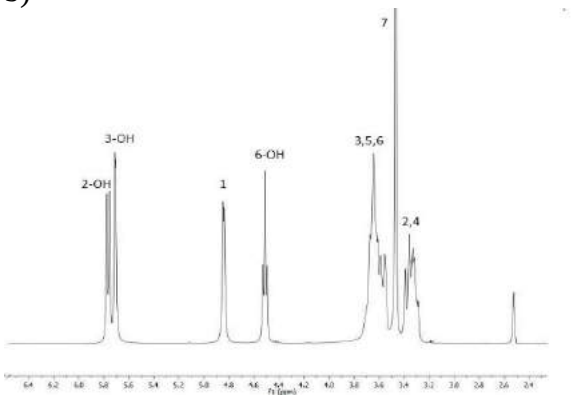

C)

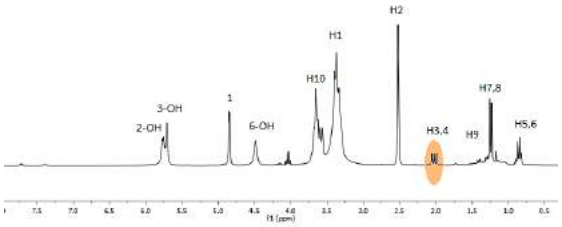

Fig. 1. H NMR spectrum of (**a**) a-tocopherol and (**b**) β- CD, (**c**) VE/ β-CD inclusion complex

IV. Conclusions

In this study, we have investigated the solubility and antioxidant property of inclusion complex of between Vitamin E and β-cyclodextrin. For this, antioxidant properties of vitamin E/ β-CD inclusion complex and pure vitamin E were tested by a model organic radical molecule (DPPH). More importantly, the water solubility of vitamin E was greatly enhanced for vitamin E/βCD inclusion complex sample due to the inclusion complexation. While pure vitamin E is insoluble in water, vitamin E/β-cyclodextrin inclusion complex web has displayed fast-dissolving behavior.

Additionally, vitamin E/β-cyclodextrin inclusion complex web has provided enhanced photostability for the sensitive vitamin E by the inclusion complexation in which vitamin E/β-cyclodextrin inclusion complex still kept its antioxidant activity even after exposure to UV-light.

In brief, using our results suggested that inclusion complex of vitamin E/β-cyclodextrin could have potential applications in food, pharmaceuticals, and healthcare owing to enhanced water-solubility, prolonged shelf life, and high photostability of vitamin E along with its efficient antioxidant activity.

References

[1] Neha Sharma, Ashish Baldi. Drug Delivery., 2016, 23:3, 729-747.

[2]U.Kemelbekov, Y.Luo, Z.Orynbekova, W.Saenger, 2010, J Incl Phenom Macrocycl Chem.

[3] Asli Celebioglu, Tamer Uyar, J. Agric. Food Chem. 2017, 65, 5404−5412.

[4] B. Tian, S. Hua, & J. Liu, Carbohydrate polymers, 2020, A review. 232, 115805.

بیست و سومین کنفرانس شیمی فیزیک انجمن شیمی ایران
23rd ICS Physical Chemistry Conference
Chemistry Department,
Faculty of Science
Shahid Bahonar University of Kerman
Kerman, Iran
12-13 Jan 2022
ایران، کرمان
دانشگاه شهید باهنر کرمان
دانشکده علوم پایه، بخش شیمی
۲۳-۲۲ دی ماه ۱۴۰۰

Prediction of oxidation potential for a series of oligopyrroles in THF solvent using DFT calculations

Zeinab Ashrafi andHossein Nikoofard*

Faculty of Chemistry, ShahroodUniversity of Technology, Shahrood, Iran, nikomahdieh@yahoo.com

Abstract

In this work, the standard oxidation potential (E_{ox}) of a series of oligopyrroles including di, tri, tetra, penta, hexa, hepta and octa-pyrrole was predicted using quantum mechanical calculations. The obtained results were compared with the available values of experimental data and an acceptable agreement was obtained. The results showed that with increasing the length of the oligomer chain and increasing the conjugation property of π-electron systems, the E_{ox} values also decrease. Finally, by extrapolating the data of studied oligomers, the oxidation potential for polypyrrole was predicted in THF solvent.

Keywords: Oxidation potential; Thermodynamic cycle; Oligopyrrole; Density functional theory.

I. Introduction

Conducting polymers have demonstrated to be one of the most versatile sets of materials since their serendipitous discovery by Shirakawa and co-workers in 1977 [1]. Arguably, in this materials,polypyrrolederivatives have attracted the attention of many groups due to their outstanding properties as energy storage devicesand highly conductive materials [2,3].

In competition with the new experimental results, a great number of theoretical research works have been carried out to study the structural, electronic, and optic properties of the conducting polymers, contributing to a better investigation and rationalization of the characteristics of these materials, and moreover, to predict those of yet unknown ones [2,3]. In the current work, we studied theoretically a series of oligopyrroles using a computation method based on the quantum chemical calculations.

II. Methods

The structure of studied species was optimized by means of the density functional theory at the level of B3LYP/6-31G (d,p) along with the polarizable continuous model in gas and tetrahydrofuran (THF) solvent.A thermodynamic cycle for calculating the Gibbs free energy values (ΔG^o) of the species in the gas and solvent phases was used(Scheme. 1).

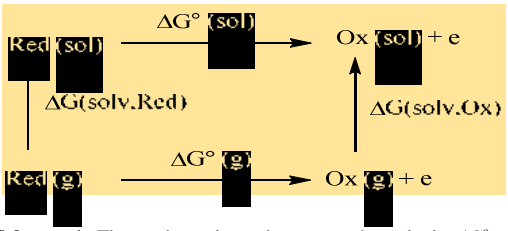

Scheme. 1. Thermodynamic cycle was used to obtain ΔG^o of oxidation reaction in the solution phase.

III. Results and discussion

The calculated values for the absolute thermochemical properties of molecules

can be used to determine the oxidationpotential. In this regard, it is necessary to use the following thermodynamic cycle (Scheme. 1), which is used for transferring all the species involved in the oxidation reaction from the gas phase to the solution phase. For comparison with the experimental data, the absolute values for the oxidation potential obtained were compared with the Hg_2Cl_2 reference electrode in non-aqueous phase [4], and they were collected in Table 1. According to this table, one can find a reasonable agreement between the calculated E_{ox} values and their experimental results for available data.

Table 1. Calculated oxidation potential values (in V) together with experimental values [4] for the studied pyrrole oligomers in THF solvent.

Species	E_{ox}/Hg_2Cl_2 (Cal.)	E_{ox}/Hg_2Cl_2 (Exp.)
Di-Py	0.60	0.62
Tri-Py	0.30	0.28
Tet-Py	0.12	0.16

The calculated E_{ox} values for PTs *vs.* the ionization potential (IP) values are plotted in Fig. 1. According to this figure, there is a good linear correlation between the $E_{ox}$and IP values. The results obtained show that extension of conjugated length lowers both the E_{ox} and IP valuesof oligopyrrolespecies.

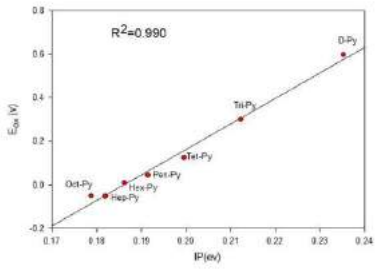

Fig. 1. Plot of the calculated E_{ox} (V) *vs.* IP (eV) values for oligopyrrole species.

In addition,the predicted oxidation potential valuesfor the studied oligomers was used to predict the E_{ox} value of polypyrrole.

IV. Conclusions

A density functional theory method based on the B3LYP / 6-31G (d, p) level of theory was used to calculate the oxidation potentialof a series of oligopyrroles in gas and THF media. The results obtained showed that an increase in the length of the oligomeric chain causes a reduction in E_{ox}values which is consistent with the results obtained from their electronic properties. The observed trend for oxidation potential of the studied samples showed a very good correlation with ionization energy and the highest occupied molecular orbital. The predicted oxidation potential values for the studied molecules are in good agreement with their experimental values.

References

1.Bakhshi, A. K.;Bahalla, G.; Electrically conducting polymers:Materials of the twenty first century; Scientific Industrial Research, 2004, 63, 715.

2. Liu, M. M.; Han, S. M.; Zheng, X. W.; Han, L. L.; Liu, T.; Yu, Z. Y.; Experimental and theoretical prediction of the redox potential of dopamine and its supramolecular complex with glycine, Int. J. Electrochem. Sci, 2015, 10, 235.

3. Nikoofard, H.; Kordnezhad, F.; Prediction of oxidation potential for a series of phenylthiophene derivatives, Comp. Theo. Chem.,2020, 256, 15-27.

4. Beitollahi, D.; Farrokhpour, H.; Khoshroo, A. R.; Computational and electrochemical studies on the redox reaction of 2-(2, 3-dihydroxy phenyl)-1, 3-dithiane in aqueous solution, Iran. J. Math. Chem., 2012, 3, 103-112.

بیست و سومین کنفرانس شیمی فیزیک انجمن شیمی ایران
23rd ICS Physical Chemistry Conference
Chemistry Department,
Faculty of Science
Shahid Bahonar University of Kerman
Kerman, Iran
12-13 Jan 2022
ایران، کرمان
دانشگاه شهید باهنر کرمان
دانشکده علوم پایه، بخش شیمی
۲۳-۲۲ دی ماه ۱۴۰۰

The effect of electrode materials on I–V characteristics behavior of 2,2,6,6-tetramethyl-3,5-heptanedione (a β-diketone) as molecular switch

Mohammad Eslah Aliabadi[a]*, Mohammad vakili[a], Ayoub Kanaani[b], Vahid Reza Darugar[a]

[a]*Department of Chemistry, Faculty of Science, Ferdowsi University of Mashhad, Mashhad, Iran*
E-mail: eslah.khosravi@gmail.com Tel: 09032431584
E-mail: vakili-m@um.ac.ir Tel: 05138805551
E-mail: vahidrezadarugar@mail.um.ac.ir Tel: 05138804065
[b]*School of Chemistry, Damghan University,Damghan,Iran*
E-mail: A.kanaani@yahoo.com Tel: 09155196389

Abstract

In this research, using nonequilibrium green's function (NEGF) integrated with density functional theory (DFT). We investigated the electronic transport properties of a β-diketone, 2,2,6,6-tetramethyl-3,5-heptanedione,as molecular wire.

Keywords: Switching behavior; β-diketone; Electronic transport; DFT-NEGF.

I. Introduction

In recent years, with the advancement of techniques for manipulating individual molecules, electronic devices based on single molecules have been considered one of the most promising candidates for today's silicon-based devices both for their novel physical properties and potential for device applications, such as negative differential resistance (NDR), switches, latches and rectifiers [1,2].

II. Methods

The transport calculations from 0.0 to 3.0 V at 300 K were done using the Landauer–Büttiker formula in the TranSIESTA package [3]. The Perdew–Burke–Ernzerhof (PBE) exchange-correlation functional is adopted for the generalized gradient approximation (GGA). A ξ plus single polarization (SZP) and double-ξ plus single polarization (DZP) basis sets were used for the electrons of electrode atoms and the organic atoms in the transport calculations, respectively. A k-grid sampling of 4×4×100 is used, together with a mesh cutoff energy of 150 Ry.

III. Results and discussion

The title molecule can be converted between two keto and enol forms [4]. The electronic transmission factors, on-off ratio, I–V characteristics, the alteration of the electrode materials, Y, (Y =Au, Ag, and Pt), and HOMO–LUMO gaps relevant to these forms are thoroughly discussed. It can be concluded that due to the deformation of the title molecule (enol→keto), there is a noticeable change in conductivity. It can be seen from these graphs, that the current in this electron device is significantly dependent on the electrode material.

Both enol and keto forms with different electrodes show that, the current in the enol form is always greater than that in the keto form. The I–V characteristics of the molecular switch with three different

electrode types (Au, Pt and Ag) were obtained and the results are shown in figure 1(a-c).

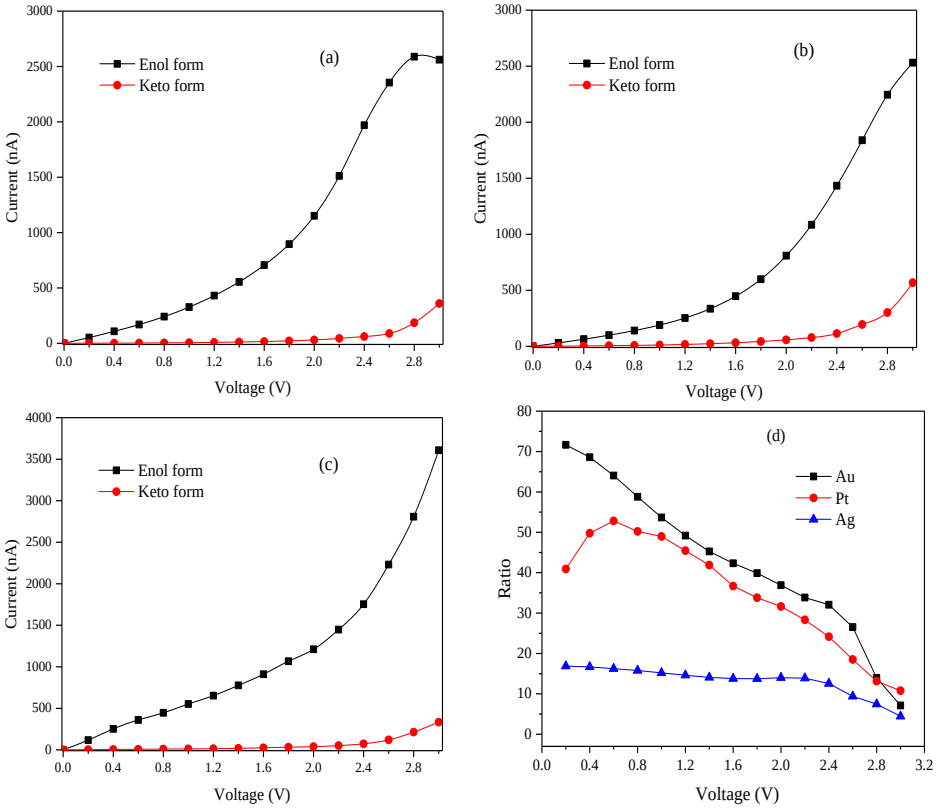

Fig1: The calculated I–V characteristics of the molecular switch with hollow site: (a) Au, (b) Ag, (c) Pt, (d) current switching ratio as a function of applied bias with different electrodes.

IV. Conclusions

The results showed that the title compound has the best switching performance in the Au electrode (see figure 1d).The highest and lowest changes in the current ratio are for the gold and silver electrodes, respectively. In the Pt electrode with increasing voltage, the current ratio increases and then decreases. But with increasing voltage, the current ratio in the Au and Ag electrodes decrease.

References

[1]H. Basch, R. Cohen, and M.A. Ratner, Nano Lett. 2005, 5, 1668.
[2]T. Frederiksen, M. Brandbyge, N.Lorente, and A.P.Jauho, Phys. Rev. Lett. 2004, 93, 256601.
[3] M. Brandbyge, J.-L. Mozos, P. Ordejón, J. Taylor and K. Stokbro, Phys Rev B. 2002, 65, 165401.
[4]M. Vakili, S.F. Tayyari, A.-R. Nekoei, H. Miremad, S. Salemi, and R. Sammelson, J. Mol. Struct. 970 (2010) 160-170.

بیست و سومین کنفرانس شیمی فیزیک انجمن شیمی ایران
23rd ICS Physical Chemistry Conference
Chemistry Department,
Faculty of Science
Shahid Bahonar University of Kerman
Kerman, Iran
12-13 Jan 2022
ایران، کرمان
دانشگاه شهید باهنر کرمان
دانشکده علوم پایه، بخش شیمی
۲۳-۲۲ دی ماه ۱۴۰۰

The I–V characteristics of methyl 3-oxobutanoate as molecular switch

Mohammad Eslah Aliabadi[a]*, Mohammad vakili[a], Ayoub Kanaani[b]

[a]Department of Chemistry, Faculty of Science, Ferdowsi University of Mashhad, Mashhad, Iran
E-mail: eslah.khosravi@gmail.com Tel: 09032431584
E-mail: vakili-m@um.ac.ir Tel: 05138805551
[b]School of Chemistry, Damghan University,Damghan,Iran
E-mail: A.kanaani@yahoo.com Tel: 09155196389

Abstract

In this research, using nonequilibrium green's function integrated with density functional theory, we investigate the electronic transport properties of a β-diketone (methyl 3-oxobutanoate) molecular wire induced by hydrogen transfer.

Keywords: Switching behavior; β-diketone; Electronic transport; DFT-NEGF.

I. Introduction

With the getting smaller of traditional electron devices and the advancement of nanotechnology and microfabrication, using molecules as components in atomic-scale circuits has become an attractive field and nanomaterials have become one of the most dazzling stars in the twenty-first century [1]. Heptane-3,5-dion molecular switch, which changes between enol and keto forms can be a good option for a molecular switch device, is one family member of β-diketone [2]. Formation of intramolecular hydrogen bonding (IHB) in cis-enol forms leads to increased resonance of π-conjugating electrons and also formation of six-membered chelated ring [3].

II. Methods

The transport calculations from 0.0 to 3.0 V at 300 K were done using the Landauer–Büttiker formula in the TranSIESTA package [4]. The Perdew–Burke–Ernzerhof (PBE) exchange-correlation functional is adopted for the generalized gradient approximation (GGA). A ξ plus single polarization (SZP) and double-ξ plus single polarization (DZP) basis sets were used for the electrons of electrode atoms and the organic atoms in the transport calculations, respectively. A k-grid sampling of 4×4×100 is used, together with a mesh cutoff energy of 150 Ry.

III. Results and discussion

The electronic transmission factors, on-off ratio, I–V characteristics, the alteration of the electrode materials, Y, and HOMO–LUMO gaps relevant to these forms are thoroughly discussed. It can be concluded that due to the deformation of the title molecule (enol→keto), there is a noticeable change in conductivity. The I–V characteristics of the molecular switch with three different electrode types (Au, Pt and Ag) were obtained (see figure 1a-c).

It can be seen from these graphs that the current in this electron device is significantly dependent on the electrode material. Both enol and keto forms with

different electrodes exhibit almost similar behaviors and regardless of the electrode type, the current in the enol form is always greater than that in the keto form.

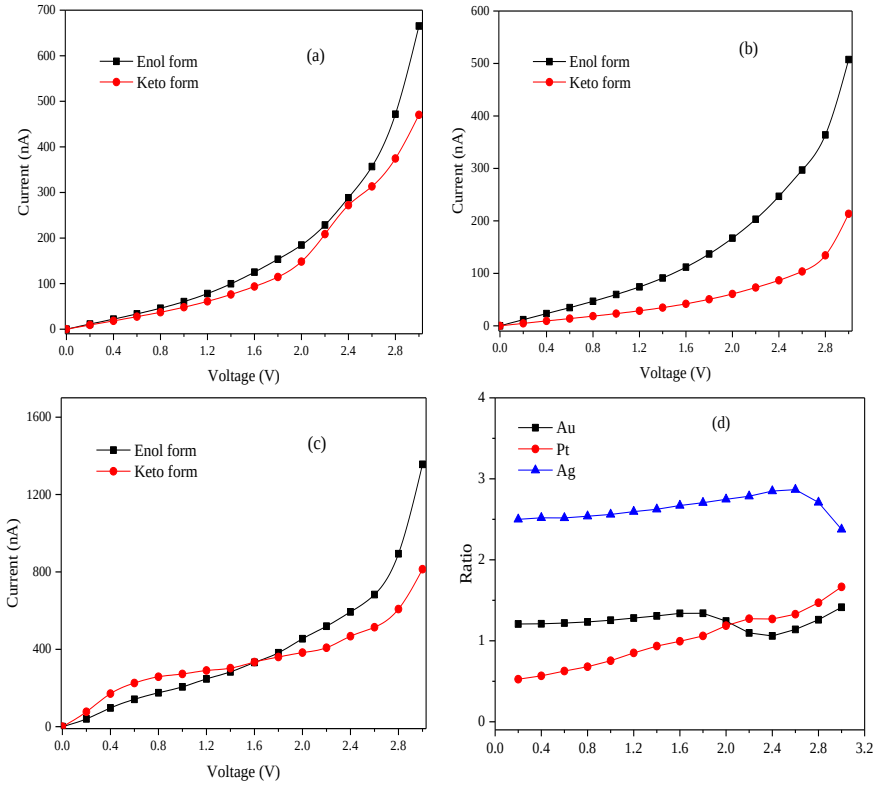

Fig 1: The calculated I–V characteristics of the molecular switch with hollow site: (a) Au, (b) Ag, (c) Pt, (d) current switching ratio as a function of applied bias with different electrodes.

IV. Conclusions

The highest and lowest changes in the current ratio are for the Ag and Pt electrodes, respectively. In the Pt electrode with increasing voltage, the current ratio increases. In Ag electrode, with increasing voltage up to 2.6 volts, the current ratio slightly increased and then decreased.

References

1]H. Basch, R. Cohen and M.A. Ratner, Nano Lett. 2005, 5, 1668
[2]S. Soltani-Ghoshkhaneh, M. Vakili, S.F. Tayyari and A.R. Berenji, J. Mol. Struct. 2016, 1103, 35
[3]S.F. Tayyari, M. Zahedi-Tabrizi, S. Laleh, Z. Moosavi-Tekyeh, H. Rahemi and Y.A. Wang, J. Mol. Struct. 2007, 827, 176.

بیست و سومین کنفرانس شیمی فیزیک انجمن شیمی ایران
23rd ICS Physical Chemistry Conference
Chemistry Department,
Faculty of Science
Shahid Bahonar University of Kerman
Kerman, Iran
12-13 Jan 2022
ایران، کرمان
دانشگاه شهید باهنر کرمان
دانشکده علوم پایه، بخش شیمی
۲۲-۲۳ دی ماه ۱۴۰۰

Investigation of Structural and Electronic Properties of SrS by FP-LAPW method

Leila Tohidi Asl [a], Hamdollah Salehi *[2,b]

[a] *Department of Science, Malek-e-Ashtar University of Technology, Esfahan, Iran*
[b] *Department of Physics, Faculty of Science, Shahid Chamran University of Ahvaz, Ahvaz, Iran*

Abstract

The equilibrium lattice constant and the optimal volume of strontium sulfide crystal were calculated by density functional theory with generalized slope approximation, which is very close to the experimental value, and this approximation was used to draw the density diagrams of the state and the band structure.

Keywords:
Density functional theory , SrS ,Wien2k

I. Introduction

The strontium sulfide crystal, has two crystalline phases, CsCl and NaCl. The crystalline phase of NaCl is used in many technologies, and accurate structural and electronic calculations can be helpful. Structural and electronic calculations of materials are usually done by both experimental and simulation methods. Due to the fact that crystal simulation is much easier and less expensive, in this paper we have tried to use this method and then for verification, the calculated values are compared with experimental values. The crystal structure of strontium sulfide in the NaCl phase is spatial group 225 (m3_mF). The experimental lattice constant obtained for this crystal is reported to be 6,024 angstroms. Also, the value of the band gap, which was calculated experimentally, is 3.60 electron volts [1].

II. Methods

Our calculations are performed with the calculation code Wien2K, which is based on density functional theory[2]. The generalized gradiant approximation is then used in this calculation code. We start by producing the structure with experimental values, then perform electronic calculations of the crystal and compare it with the experimental values.

III. Results and discussion

The crystal structure is simulated by considering the spatial group 225 (m3_mF) and the lattice constant values a, b, c = 6.24 and also α, β, γ = 90. The positions of the atoms are as follows: we place the first atom rS strontium with atomic radius 2.03 and atomic number 38 in position (0, 0 and 0) and the second S atom of sulfur with atomic radius 1.93 and atomic number 16 in position (We put 0.5, 0.5 and 0.5). After storage, the network constant value structure changed to 5.999 angstroms. The length of interatomic bonds was extracted in this case, which is 3 angstroms for the bond between Sr and S and 4.2426 angstroms for the bond between Sr and Sr. In the following calculations with the relaxed

structure, we set the percentage change of the radius of the sphere to zero. To separate the brain electrons and capacitance electrons, we set the separation energy to 6-Riedberg. The optimal values for the cut-off wave vector are 8 and for the K point the value is 2000 with 72 generators and meshes 12, 12, 12. In the continuation of strontium sulfide crystal calculations, we calculate the volume optimization to obtain the optimal equilibrium lattice constant for the crystal.

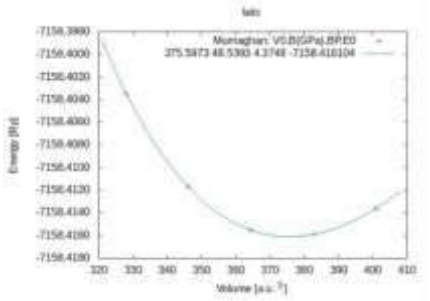

Fig. 1. The graph of total energy values with volume changes

The results of constant lattice optimization by GGA approximation for crystal potential function were calculated as 6.0611 angstroms from Mornagan method and 6.0609 angstroms from Beach Mornagan method. After optimizing all the important parameters of the structure, we performed self-consistent solution calculations with optimal values and generalized GGA slope approximation. The values of total energy and band gap for polarized spin mode were calculated as 7158.41586533 Riedberg and 2.531 electron volts, respectively. Also in the state without polarization spin, the total energy value is 7158.41586531 Riedberg and the band gap is 2.531 electron volts. Examining the density diagram of the total crystal states and comparing it with the total state density for each atom separately, we see that strontium atoms were predominant in the conduction band, and sulfur atoms prevailed in the core band.

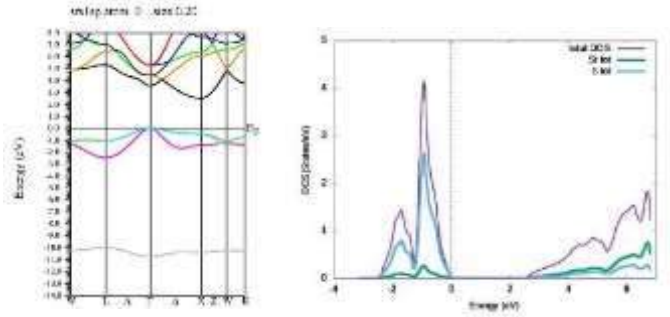

Fig. 2. Energy bands and Density of total states of SrS.

IV. Conclusions

According to the calculation, information can be obtained from the crystal. The crystal has a band gap between the electrons of the core and the electrons of the conduction layer. According to the generalized slope approximation, its value is more than 2 electron volts, but this value is not consistent with experimental calculations. The strontium sulfide crystal in this case has a semiconductor structure. By examining the orbitals of individual atoms and finding the dominant orbital, we can manipulate some properties of the crystal and achieve the desired results.

References

[1] S.Labidi , H.Meradji , M.Labidi , S.Ghemid , S.Drablia and F.El Haj Hassan , physics procedia2 ,2009 , 1205 - 1212

[2] P. Blaha, “Wien97, Vienna University of Technology, 1997. Improved and updated Unix version of the original copyrighted Wien code, which was published by P. Blaha, K. Schwarz, P. Sorantin, and SB Trickey”, Comput. Phys. Commun, vol **59**, ,1990.399.

بیست و سومین کنفرانس شیمی فیزیک انجمن شیمی ایران
23rd ICS Physical Chemistry Conference
Chemistry Department,
Faculty of Science
Shahid Bahonar University of Kerman
Kerman, Iran
12-13 Jan 2022
ایران، کرمان
دانشگاه شهید باهنر کرمان
دانشکده علوم پایه، بخش شیمی
۲۳-۲۲ دی ماه ۱۴۰۰

Comparison of 1,2-Ethanediol Synthesis Efficiency through Formose Reaction in the Presence of Aerosil and Montmorillonite Mineral Catalysts

Arash Vojood*, Mohammad Khodadadi-Moghaddam, Gholamreza Ebrahimzadeh-Rajaei

Department of Chemistry, Ardabil Branch, Islamic Azad University, Ardabil, Iran, voojod.a2012@gmail.com

Abstract

In the present paper, the efficiency of 1,2-ethanediol (ethylene glycol) synthesis was evaluated through Formose reaction (FR) and in the presence of Aerosil (fumed silica) catalyst at methanol solvent and compared with the synthesis of the same molecule through the same reaction but in the presence of Montmorillonite at water solvent. The results indicated that the amount of produced ethylene glycol through FR in the polar solvent of methanol will be lower in the presence of a fumed silica catalyst than the polar solvent of water in the presence of montmorillonite.

Keywords: Origin of life; Formose reaction; Ethylene glycol; Aerosil; Montmorillonite

I. I. Introduction

The origin of life on the planet Earth has been one of the humanity's most compelling enquiries since the cradle of civilization. The study of the origins of life is a challenging and fascinating subject, that involves the interplay of different disciplines such as biology, chemistry, physics, astronomy, geology, philosophy, and so forth. People are trying to understand the chemical origins of life [1, 2]. One of the interesting questions is where carbohydrates come from because they are the building blocks of DNA and RNA.

The prebiotic chemists suggested that sugar formation relied on the synthesis of Formose that was discovered in 1861 by a Russian chemist named Alexander Mikhaylovich Butlerow. The FR is very important to the question of the origin of life because it is considered as a potential synthesis route for the generation of complex monosaccharides and is a possible process whereby sugars form abiotically [3, 4]. In this study, the efficiency of 1,2-ethanediol synthesis was evaluated through FR and in the presence of Aerosil catalyst at methanol solvent and compared with the synthesis of the same molecule through the same reaction but in the presence of Montmorillonite at water solvent.

II. Methods

In this work, 23 ml of formalin with 200 ml of deionized water was transferred to a 250 ml three-necked flask and brought to a temperature of 60 °C. Then, sodium hydroxide solution (2M) was added to it to reach the desired pH, and finally 0.17 g of the Montmorillonite catalyst was added to the flask to start the reaction. Then, at the desired intervals, 5 ml of the mixture was

taken and these liquid samples were then dried in a rotary evaporator until turning into white solid samples, and after dissolving these solid samples in 5 ml of methanol, they were centrifuged for analysis in a GC-MS device [3].

III. Results and discussion

The main product of the FR under the conditions applied during this work is 1,2-ethanediol ($C_2H_6O_2$). Fig.1a shows the results (GC-MS) of the FR at pH =7.8 in the presence of a heterogeneous Aerosil catalyst at methanol solvent. The amount of ethylene glycol in the mixture increases from the beginning of the reaction and reaches a maximum amount of 0.89 mmol / dl during 630 minutes [5].

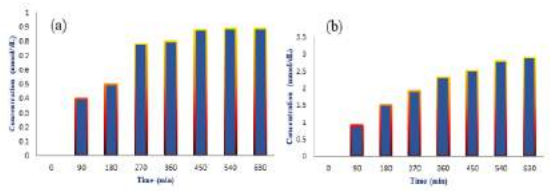

Fig. 1. Changes ethylene glycol concentration over time through the FR in the presence of (a) Aerosil and (b) montmorillonite mineral catalysts.

Fig.1b shows the results (GC-MS) of the FR at pH =7.5 in the presence of a mineral Montmorillonite catalyst at water solvent. The amount of ethylene glycol in the mixture increases from the beginning of the reaction and reaches a maximum amount of 2. 9 mmol / dl during 630 minutes [3]. A comparison between Figs. 1a and 1b (similar pHs) shows a reduction of more than twofold in the production of ethylene glycol in methanol solution.

IV. Conclusions

In the present work, the synthesis of ethylene glycol through FR (a non-biological reaction to produce sugars) at the presence of heterogenous Aerosil catalyst (Fig1. a) was compared with its synthesis through the same reaction but in the presence of Montmorillonite (Fig1. b) in terms of synthesis efficiency. The results indicated that the FR can be performed in aqueous or non-aqueous solvents such as ethanol and methanol (the simplest forms of alcohol). Moreover, the dielectric constant (symbol: ε) of methanol at 25 ºC (32.7) was lower than water (78.3). In fact, the dielectric constant of a solvent is a measure of its polarity. The higher the dielectric constant of a solvent, the more polar it is. So, the amount of produced ethylene glycol through FR in the polar solvent of methanol will be lower in the presence of an Aerosil catalyst than the polar solvent of water in the presence of Montmorillonite. This indicates the low efficiency and return rates of methanolic media (pH=7.8) compared to water with a pH of 7.5 in terms of ethylene glycol production. On the other hand, scientists now believe that the first germinations of life were established in the depth of the seas. In addition, Holy Quran mentioned water (the global solvent) as the origin of life both in terms of the emergence of the creatures and the continuation of life.

References

[1] A. P´erez-Villaa, F. Pietruccia and A. Saitta, Phys. Life. Rev., 2021, 34-35, 105135.

[2] S. Thripati and, R. O. Ramabhadran, J. Phys. Chem., 2017, 121, 8659-8674.

[3] A. Vojood and, et al, Chem. Methodol., 2021, 5, 422-432.

[4] A. Omran and et al, Life., 2020, 10, 125.

[5] A. Vojood and et al, J. of Applied Chemistry., 2021. doi:10.22075/CHEM.2021.22337.1942.

بیست و سومین کنفرانس شیمی فیزیک انجمن شیمی ایران
23rd ICS Physical Chemistry Conference
Chemistry Department,
Faculty of Science
Shahid Bahonar University of Kerman
Kerman, Iran
12-13 Jan 2022
ایران، کرمان
دانشگاه شهید باهنر کرمان
دانشکده علوم پایه، بخش شیمی
۲۲-۲۳ دی ماه ۱۴۰۰

Prebiotic Synthesis of Ethylene Glycol through Formose Reaction in Methanolic Medium

Arash Vojood

Department of Chemistry, Ardabil Branch, Islamic Azad University, Ardabil, Iran, voojod.a2012@gmail.com

Abstract

Formose reaction (FR) is very noteworthy in the context of prebiotic chemistry and origin of life. Because, this reaction is known as the basis of non-biological chemical reactions to produce sugars. Also, Alexander Mikhaylovich Butlerow discovered (Russian chemist) the FR in 1861. moreover, in this work, the FR is performed at pH =10.6 in the presence of an Aerosil (fumed silica) catalyst at methanol (the simplest forms of alcohol) solvent. The product observed in this reaction is 1,2-ethanediol (ethylene glycol). The present study shows that the efficiency of ethylene glycol (simplest diol) production by FR is low in methanolic medium.

Keywords: Origin of life; Prebiotic chemistry; Formose reaction; Methanol; Ethylene glycol

I. I. Introduction

The compound 1,2-ethanediol is a highly toxic organic liquid, colorless, and odor-less chemical with sweet taste. Its most common use is as an automotive antifreeze. Furthermore, 1,2-ethanediol was first developed in 1859 by a French chemist—Charles-Adolphe Wurtz—via saponification of ethylene glycol diacetate with potassium hydroxide [1, 2].

One of the most difficult problems of life to solve is understanding of how it started and one of the questions that has been raised about us is where we came from and how life started on our planet [3]. Life is a chemical life as we all already know, so chemistry plays an important role in the interdisciplinary endeavor to work on the issue of the origin of life. Therefore, the answers to the question of how organic complex molecules can be distinguished from simple ones and description of the possible mechanisms that move in prebiotic environments are on the shoulders of chemistry community [4, 2].

One of the plausible prebiotic synthesis routes is the Formose network. In fact, it is believed that FR is related to prebiotic sugar synthesis. Alexander Mikhaylovich Butlerow discovered the FR in 1861 [5]. On the other hand, a plausible setting for the FR may have existed in the Hadean epoch, 4.0–4.5 billion years ago (Ga). This was when planet Earth accreted and cooled into a volcanic world with a thick, CO2 rich atmosphere and water ocean due to volcanic outgassing. In this study, our focus is on the FR and synthesis of ethylene glycol through this reaction. The main product of the FR under the conditions applied during this work is

ethylene glycol with $C_2H_6O_2$ chemical formula, Scheme 1.

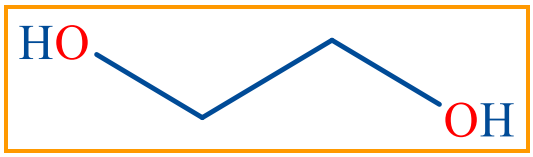

Scheme 1: Molecular structure of ethylene glycol

II. Methods

In this work, 100 ml of methanol with 11 ml of aqueous formaldehyde solution (formalin) was first transferred to a 250 ml three-necked flask and heated up to a temperature of 60 °C. Then, 2 M sodium hydroxide solution was added to bring it to the desired pH (10.6), and finally 0.08 g of the Aerosil catalyst was added to the flask to start the reaction. Then, at the desired intervals, 5 ml of the mixture was taken and these liquid samples were then dried in a rotary evaporator until turning into white solid samples, and after dissolving these solid samples in 5 ml of methanol, they were centrifuged for analysis in a GC-MS device [2].

III. Results and discussion

Fig.1 shows the results (GC-MS) of the FR at pH =10.6 in the presence of a heterogeneous Aerosil catalyst at methanol solvent. The amount of ethylene glycol in the mixture increases from the beginning of the reaction and reaches a maximum amount of 0.5 mmol / dl during 90 minutes.

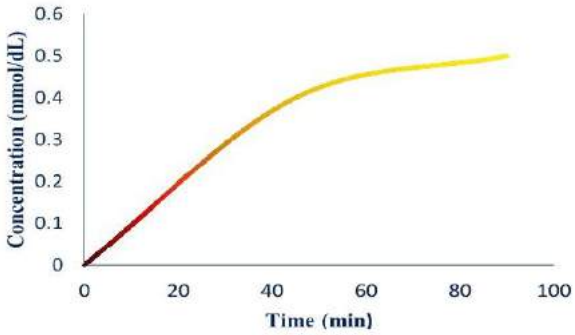

Fig. 1. Changes ethylene glycol concentration over time through the FR in Methanolic Medium.

IV. Conclusions

FR is very noteworthy in the context of prebiotic chemistry (chemistry, which occurred before life began or the chemistry which led to life on Earth, and possibly on other planets) and origin of life. Because, this reaction is known as the basis of non-biological chemical reactions to produce sugars [2, 5].

In the present work, the FR is performed at pH=10.6 in the presence of a fumed silica catalyst at methanol solvent. The product observed in this reaction is ethylene glycol. According to GC-MS results, the efficiency of ethylene glycol production by FR is low in methanolic medium. Also, if methanol solvent is used at pH of 10.6, 2,3-dihydroxypropanal (glyceraldehyde) with $C_3H_6O_3$ chemical formula, is not observed during the FR.

References

[1] H. Yue, Y. Zhao, X. Maa and J. Gong, Chem Soc Rev., 2012, 41, 4218-4244

[2] A. Vojood and et al, J. of Applied Chemistry., 2021. doi:10.22075/CHEM.2021.22337.1942.

[3] A. Biscans, life., 2018, 8, 57.

[4] A. Eschenmoser, Tetrahedron., 2007, 63, 12821-12844.

[5] A. Vojood and, et al, Chem. Methodol., 2021, 5, 422-432.

بیست و سومین کنفرانس شیمی فیزیک انجمن شیمی ایران
23rd ICS Physical Chemistry Conference
Chemistry Department,
Faculty of Science
Shahid Bahonar University of Kerman
Kerman, Iran
12-13 Jan 2022
ایران، کرمان
دانشگاه شهید باهنر کرمان
دانشکده علوم پایه، بخش شیمی
۲۳-۲۲ دی ماه ۱۴۰۰

Monitoring Dynamics of Membrane protein in lipid bilayer environment by solid-state NMR and Molecular Dynamics Simulations

Hafez Razmazm[a, b, c], Samuli Ollila[b], Ali Ebrahimi[c], Marta Bonaccorsi[d], Guido Pintacuda[d], Luca Monticelli[a]*

[a] *Molecular Microbiology and Structural Biochemistry, University of Lyon, CNRS, UMR5086, Lyon, France; E-mail: hafez.razmazma@ibcp.fr , luca.monticelli@ibcp.fr*
[b] *Institute of Biotechnology, University of Helsinki, Helsinki 00014, Finland; E-mail: samuli.ollila@helsinki.fi*
[c] *Department of Chemistry, University of Sistan and Baluchestan, Zahedan 98167-45845, Iran; E-mail: ebrahimi@chem.usb.ac.ir*
[d] *University of Lyon, Centre de RMN à Très hauts Champs, UMR 5280 CNRS, Villeurbanne, France; E-mail: guido.pintacuda@ens-lyon.fr*

Abstract

In this work, we developed novel methodology to measure order parameters (S^2) and spin relaxation rates (R1, R1ρ) of protein backbone and side chains in a lipid bilayer environment by solid state (SS) NMR spectroscopy; then we developed a protocol to calculate same NMR parameters from all-atom (AA) MD simulations. We applied the methodology to aquaporin 1 (AQP1), an important integral membrane protein. We find reasonable agreement between measured and calculated values.

Keywords: MD Simulation; AQP1; SS-NMR; NMR relaxation parameters (R1, R1ρ).

I. I. Introduction

Recent methodological and technical advancements in SS magic angle spinning NMR spectroscopy allow determining membrane protein structures at high-resolution in complex environments [1]. Information on dynamics can also be obtained from SS-NMR experiments [2], but this generally needs interpretation via molecular simulations, and the development of methods for linking molecular dynamics with NMR parameters is in its infancy. Here we simulated protein dynamics using the molecular dynamics technique, to develop a protocol for calculating NMR relaxation parameters from simulations. To establish a proof of concept, we tested our approach on a well-known protein, human aquaporin 1 (hAQP1) [3].

II. Methods

Simulation setup: The initial structure of AQP1 was obtained from the Protein Data Bank (PDB), entry 4CSK, then the extracellular loop C was refined using MODELLER program on the basis of the SS-NMR structure (PDB ID: 6POJ). Tetrameric model of AQP1 (including monomer A, B, C, and D; Fig1 A) were embedded into POPC/SOPS lipid bilayer along the Z-axis by applying the membrane builder module of CHARMM-GUI. The systems were solvated using the TIP3P water model and neutralized with 0.01 M NaCl ions (NMR conditions). The entire systems consisted of 24720 atoms.

Simulation Details: All MD simulations were performed using the GROMACS 2019.2 MD package [4] with the CHARMM36m AA force field. After

standard energy minimization (steepest descent algorithm), the resultant systems were equilibrated for 200 ns in isothermal-isobaric ensemble. Unrestrained production runs then proceeded for 6 μs in the NPT ensemble, with the temperature maintained at 298 K using the velocity-rescaling thermostat and the pressure maintained at 1 bar using the semi-isotropic Parrinello−Rahman barostat. Each system was replicated and assigned with different initial velocities to generate 3 independent simulations, 6 μs each.

III. Results and discussion

In this project, we first carried out AA MD simulations of AQP1 under conditions mimicking SS-NMR experiments (Fig. 1A). Our experimental collaborators previously obtained S^2 and R1, R1ρ for AQP1. Then we back-calculated the same parameters from MD simulations (Fig. 1B) using Python scripts.

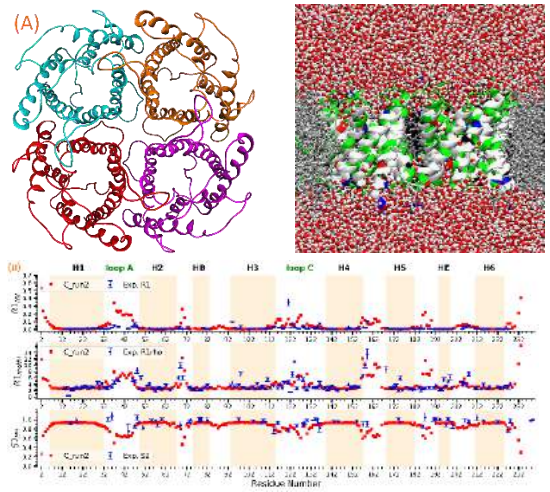

Fig. 1. (A) A top view (left) of the extracellular face of an AQP1 homotetramer and side view (right) of the simulation system. and (B) plots of experimental (blue) and simulated (red) S^2, R1 and R1ρ for monomer C of AQP1 protein.

By combining the R1ρ from experiments and simulations we extracted the protein rotational diffusion coefficient (5×10^2 s^{-1}); we found that rotational diffusion of AQP1 (under the experimental conditions tested here) is slower than expected. The protein backbone dynamics is very limited in the transmembrane region, while loops appear more mobile. Overall, the agreement between NMR and simulations is reasonable, but discrepancies in the loop region are significant, and can probably be ascribed to limitations in the AA force field.

IV. Conclusions

We developed algorithms (in the form of a python script) to back-calculate dynamic parameters from AA simulations in terms of S^2, R1 and R1ρ; then we used them to analyze a number of microsecond trajectories of AQP1. Our simulations demonstrate that the simulation trajectories give an atomic resolution interpretation for protein dynamics measured with SS NMR experiments.

References

[1] D. Lalli, M. N. Idso, L. B. Andreas, S. Hussain, N. Baxter, S. Han, B. F. Chmelka, and G Pintacuda, *J. Am. Chem. Soc*., 2017, 139, 13006-13012.

[2] M. Bonaccorsi, T. le Marchand, and G. Pintacuda, *Current Opinion in Structural Biology*, 2021, 70, 34-43.

[3] P. Agre, M. Bonhivers, and M. J. Borgnia, *J. Biol. Chem.*, 1998, 273, 14659–14662.

[4] M. J. Abraham, T. Murtola, R. Schulz, S. Pall, J. C. Smith, B. Hess, and E. Lindahl, *SoftwareX*, 2015, 1, 19−25.

Acknowledgement

The work has been performed under the Project HPC-EUROPA3 (INFRAIA-2016-1-730897), with the support of the EC Research Innovation Action under the H2020 Programme.

بیست و سومین کنفرانس شیمی فیزیک انجمن شیمی ایران
23rd ICS Physical Chemistry Conference
Chemistry Department,
Faculty of Science
Shahid Bahonar University of Kerman
Kerman, Iran
12-13 Jan 2022
ایران، کرمان
دانشگاه شهید باهنر کرمان
دانشکده علوم پایه، بخش شیمی
۲۳-۲۲ دی ماه ۱۴۰۰

Removal of Carbon Dioxide by Phosphonium-Based Amino Acid Ionic Liquids: Molecular Dynamics Simulation

Kobra Taji[a], **Fatemeh Moosavi**[b,*]

[a] *Department of Chemistry, Faculty of Science, Ferdowsi University of Mashhad, Mashhad, 9177948974, Iran, E-mail: ktaji4423@gmail.com*
[b] *Department of Chemistry, Faculty of Science, Ferdowsi University of Mashhad, Mashhad, 9177948974, Iran, E-mail: moosavibaigi@um.ac.ir*

Abstract

Molecular dynamics simulation was performed to capture CO_2 by using non-toxic solvents. Tetrabutylphosphonium cation coupled with glycinate amino acid anion was simulated in order to compare the functionalization effect on gas capturing. The results demonstrated that functionalized ionic liquid with carboxylic group is the most favoured ionic liquid and its interaction with CO_2 is due to the anion.

Keywords: Molecular Dynamics Simulation; Carbon Dioxide Capture; Phosphonium-based Ionic Liquids; Radial Distribution Function.

I. I. Introduction

The main reason for global warming is greenhouse gases; these gases include water vapor, carbon dioxide, methane, and nitrous oxide. Excessive emission of carbon dioxide has adverse effects on the global climate, leading to social and economic consequences. For this reason, the removal of carbon dioxide gas has been considered [1]. Phosphonium-based ionic liquids are of interest due to the chains around the phosphonium cation and the large space volume. They have a higher solubility compared to imidazolium ionic liquids [2]. In the present study, the removal of carbon dioxide gas with ionic liquids that have unique properties such as low vapor pressure, high thermal stability and physical and chemical adjustment has been done through proper coupling of cation and anion. These solvents are used as harmless environmental solvents and green ones [3].

II. Methods

Molecular dynamics simulation was performed with Materials Studio software [4] for 3 ns to investigate the removal of carbon dioxide. Here, glycinate amino acid anion coupled with tetrabutylphosphonium cation, $[P_{4444}][GLY]$, was simulated at ambient temperature and pressure. In addition, the studied ionic liquid cation was functionalized using different functional groups including –OH, –COOH, $–NH_2$, and $–OCH_3$. The geometry optimization in the gas phase for CO_2 and all target ionic liquids was carried out using DFT at B3LYP/6-311++G(d,p) level of theory. The wave number calculation was also performed at the same level of theory. The absence of negative values of Hessian matrix confirmed that the stationary point corresponds to a real minimum. In addition, the electrostatic surface potential (ESP) at the same level of theory was conducted to access more

accurate atomic charges. The temperature and pressure of NPT ensemble simulation box were controlled by with Andersen thermostat and Berendsen barostat.

III. Results and discussion

Ion pair binding energy is the highest in [P_{4444}][Gly] and is the lowest in [P_{4444}COOH][Gly]. According to the cation…anion pair correlation function, Figure 1, it can be understood that cation functionalization does not change the compactness of the system and the average distance between cation and anion is 4.80 Å. However, the intensity of the interaction shows reduction due to the functionalization. It can also shed light on the more space available for the gas to be absorbed in the [P_{4444}COOH][Gly]. Noticeably, comparing the radial distribution function, RDF, between the ionic liquid and the gas demonstrates that anion has the major role in gas solubility. The average distance between the glycinate anion and absorbed CO_2 gas is 3.40 Å and the [P_{4444}COOH][Gly] shows the most favorable interaction between the liquid and the CO_2 gas. Figure 2 illustrates that the target ionic liquids are able to absorb the CO_2 uniformly and make it dissolved.

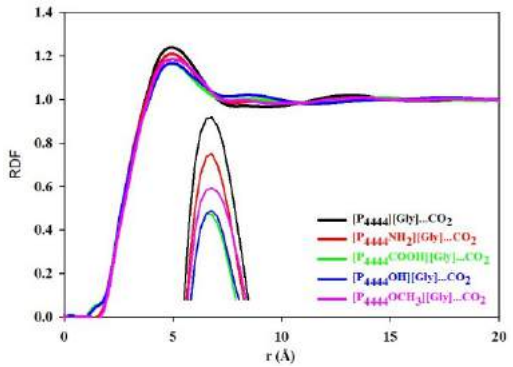

Fig. 1. Anion… cation RDF at the presence of CO_2. Magnification of the first peak is shown as a legend from COMPASS (version 2.8) force field.

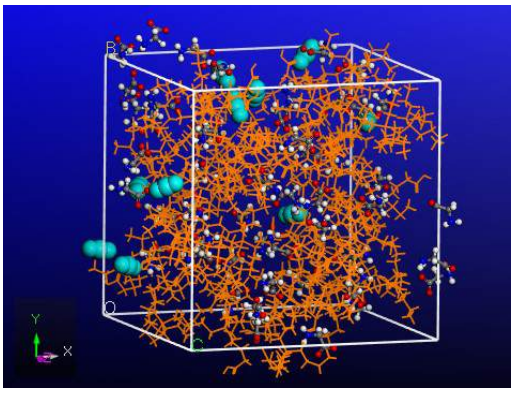

Fig. 2. Final snapshot of the simulation box; the orange is cation, the cyan is CO_2, and anion is shown in stick and ball model with O in red, C in dark gray, N in blue, and H atoms in white.

IV. Conclusions

It was observed that the functional group addition to the cation not only decreases the cation and anion interaction but also density of the liquid. As a result, the ionic liquid anion does tend to interact with the carbon dioxide. In general, the anion plays a critical role in the interaction because its radial distribution function occurred at a shorter distance. The compactness of ion pairs as well as the least mobility of captured gas demonstrated that functionalization with carboxylic acid is more favored for this purpose.

References

[1] M. Aghaie, N. Rezaei, and S. Zendehboudi, *Renewable and Sustainable Energy Reviews*, 2018, 96, 502.

[2] P. J. Carvalho, V. H. Álvarez, I. M. Marrucho, M. Aznar, and J. A. P. Coutinho, *The Journal of Supercritical Fluids,* 2010, 52, 258.

[3] Y. Xie, G. Liu, H. Nie, F. Yu, X. Xing, and H. Cui, *Energy Technology*, 2020, 8, 190.

[4] M. Meunier and S. Robertson, *Molecular Simulation*, 2021, 47, 537.

بیست و سومین کنفرانس شیمی فیزیک انجمن شیمی ایران
23rd ICS Physical Chemistry Conference
Chemistry Department,
Faculty of Science
Shahid Bahonar University of Kerman
Kerman, Iran
12-13 Jan 2022
ایران، کرمان
دانشگاه شهید باهنر کرمان
دانشکده علوم پایه، بخش شیمی
۲۳-۲۲ دی ماه ۱۴۰۰

Preparation of Ni/g-C_3N_4 nanocomposite as electrocatalyst for hydrogen evolution reaction

Maryam Heydarpour[a*], Shahram Ghasemi[b], Abdolah Omrani[b]

[a] *Physical Chemistry Division, University of Mazandaran, Postal Code 47416-95447, Babolsar, Iran*
[b] *Faculty of Chemistry, University of Mazandaran, Babolsar, Iran*
[*] *Corresponding to Maryam Heydarpour, E-mail: m.heidarpour@stu.umz.ac.ir*

Abstract

Developing stable and efficient electrocatalyst for hydrogen evolution reaction (HER) is greatly desirable for the production of hydrogen as a clean energy resource. Herein, we report a simple and effective approach to fabricate Ni/g-C_3N_4 elecrocatalysts, which can enhance the charge transfer rate and decrease the overpotential for HER.

Keywords: Electrocatalyst; Graphitic Carbon Nitride; Nickel nanoparticles; Hydrogen evolution reaction.

I. Introduction

Hydrogen (H_2) has been regarded as the most promising energy carrier alternative to fossil fuels due to the environmental intimacy nature and high gravimetric energy density [1]. g-C_3N_4 has received wide attention due to its high stability, non-toxicity, facile and low-cost synthesis [2]. Ni-based materials (Ni-based alloys and wide accessibility composites) are one of the most promising catalysts for HER [3].

II. Methods

Syntheses of g-C_3N_4: 4g urea was placed in alumina crucible with a cover and transferred to a muffle furnace under static air atmosphere and calcined at 550 ˚C for 3 h with a rate of 2 ˚C min^{-1} and then was cooled naturally and collected. **Syntheses of Ni/g-C_3N_4:** 50 mg g-C_3N_4 was dispersed in water and mixed with 25 mg $Ni(NO_3)_2.6H_2O$ for 18 h at room temperature followed by reduction with borohydride and stirring at 50 ˚C for 16 h. The catalyst was collected by centrifugation. **Electrode preparation:** The electrochemical studies were carried out in three-electrode cell by a series of testing methods. All the potentials were measured using Ag|AgCl (KCl saturated) reference electrode, but they were finally reported to RHE.

III. Results and discussion

Figure 1 shows the X-ray pattern of bulk g-C_3N_4 and Ni/g-C_3N_4. g-C_3N_4 shows two diffraction peak at 13.1˚ and 27.7˚, which corresponds to (100) and (002) planes respectively, (JCPDS 87-1526). Compared with the pure g-C_3N_4, the appeared peaks located at 44.5˚, 51.8˚ and 76.4˚ could be assigned to the (111), (200) and (220) crystal planes of Ni, indicating the presence of Ni (PDF # 65-2865) [4].

The electrocatalytic activities of bare GCE, g-C_3N_4/GCE and Ni/g-C_3N_4/GCE for HER were studied by linear sweep voltammetry (LSV) in N_2-saturated H_2SO_4 (0.5 M) solution at scan rate of 5 mV s^{-1}. Figure 2

shows the LSV curves of different electrodes. At the surface of GCE, the kinetic of the HER is slow and needs to high overpotential. At the surface of g-C_3N_4, the overpotential decreases and current density increases. Ni/g-C_3N_4/GCE shows better HER performance with the low overpotential of -0.25V at a current density of 100 mA cm^{-2}, compared to -0.5 V of g-C_3N_4/GCE. At the surface of Ni/g-C_3N_4/GCE, the onset potential of HER reduces substantially and current density increased which means the improvement in the kinetic of process due to the presence of transition metal nanoparticles. g-C_3N_4 has flake-like morphology with plenty of irregular interstitial pores, in which Ni nanoparticles are embedded. Tafel slopes as the intrinsic HER activity of the catalysts are obtained from the LSV curves. Generally, the lower Tafel slope of the catalyst means the faster kinetics and higher catalytic activity. The Tafel slopes are calculated to be 210 mV dec^{-1} (g-C_3N_4) and 145 mV dec^{-1} (Ni/g-C_3N_4).

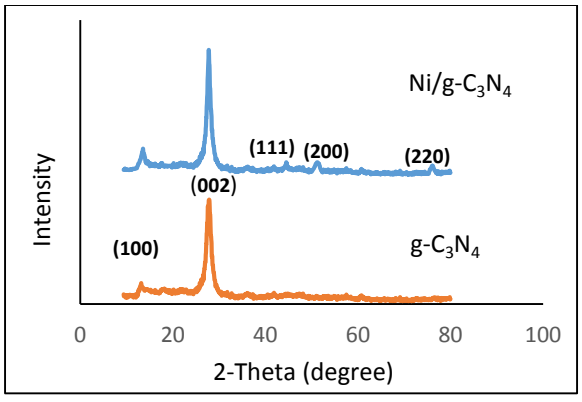

Fig. 1. XRD pattern of g-C_3N_4 and Ni/g-C_3N_4

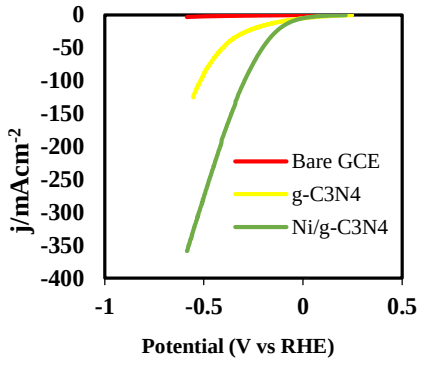

Fig. 2. LSV curves of bare GCE, g-C_3N_4, Ni/g-C_3N_4.

IV. Conclusions

In this work, the preparation of Ni/g-C_3N_4 nanocomposite is presented which used as catalyst for improvement of HER. Ni/g-C_3N_4/GCE showed good HER proficiency with low overpotential. Our results also state that the Ni/g-C_3N_4 would be high efficiency non-noble catalyst for HER.

References

[1] Zhou, Kai ling, zelin wang, Platinum single-atom catalyst coupled with transition metal/metal oxide heterostructure for accelerating alkaline hydrogen evolution reaction. Nature communications 2021, 12.1:1-10

[2] Hao, Qiang, Guohua jia, Graphitic carbon nitride with different dimensionalities for energy and environmental applications. Nano Research, 13(1), 18-37.

[3] Wang, Lixin, Yao li, (2017). Coral-like-structured Ni/C3N4 composite coating: an active electrocatalyst for hydrogen evolution reaction in alkaline solution. ACS Sustainable Chemistry & Engineering, 5(9), 7993-8003.

[4] Bi L, Xu D, Zhang L, Metal Ni-loaded gC3N4 for enhanced photocatalytic H2 evolution activity: the change in surface band bending. Physical Chemistry Chemical Physics. 2015;17(44):29899-905.

بیست و سومین کنفرانس شیمی فیزیک انجمن شیمی ایران
23rd ICS Physical Chemistry Conference
Chemistry Department,
Faculty of Science
Shahid Bahonar University of Kerman
Kerman, Iran
12-13 Jan 2022
ایران، کرمان
دانشگاه شهید باهنر کرمان
دانشکده علوم پایه، بخش شیمی
۲۳-۲۲ دی ماه ۱۴۰۰

Heavy metal removal by modified cellulose nano fibers(MCNF)

Atiyeh Amirafshar[a], Ali Ahmadpour[b,*]

[a] *Department of Chemical engineering, Ferdowsi University of Mashhad, Mashhad , Iran , at.amirafshar@um.ac.ir*
[b] *Department of Chemical engineering, Ferdowsi University of Mashhad, Mashhad , Iran , ahmadpour@ um.ac.ir*

Abstract

In this work, at the first step hardwood pulp was modified by the maleic anhydride; and then electrospinning of modified solution was carried out under different voltages. At last obtained fibres was washed with water and aqueous 70% (w/w) ethanol and prepared to use as a nano absorbent.

The synthesized absorbent was characterized by SEM and FTIR. The degree of substitution of modification reaction is 1-1.8 by titration method. The affection of other parameters like PH, Contact time and temperature on removal was studied. The results show that the modified CNF has a great capacity of absorption for Hg(II).

Keywords: Heavy metals removal; Electrospinnig; Cellulose nano fiber; Modification.

I. I. Introduction

Many studies has been carried out to remove heavy metals, but compare to other methods, adsorption could be more economic, flexible and efficient[1,2].

Cellulose as a cheap, abundant, renewable, and having hydroxyl functional groups could be a great material to start many reactions[3,4].

The aim of this work is to obtain nano fibers which previously modified by maleic anhydride to remove Hg(II) and investigate capacity of it.

II. Methods

Cellulose provided from waste paper. Industrial maleic anhydride was purchase from Tianjin No. 1 chemical reagent factory.. DMAc, LiCl salt and DMAP was from Shanghai Chemical Reagent Co., Ltd., China.

Hg(II) ions waste water was from an industrial field with the concentration of 0.002 $mol.L^{-1}$.

Waste papers was dried and shredded, then dissolved in LiCl/DMAc. DMAP as catalyst was added with maleic anhydride to modify cellulose.

Electrospinning of this solution was carried out under different voltages.

III. Results and discussion

The FTIR scpectra of MCNF and waste paper are presented in Fig.1. As demonstrated in this figure the relevant change observed in bands at about 1730, Which indicate that maleic anhydride was grafted onto cellulose surface. The band at 1730 is due to the stretching of carboxyl group(C=O).

Scanning electron micrographs presented in Fig.2. demonstrate the size of fibers before and after electrospinning. The desire diameter of cellulose fibers had obtained at 15Kv, collector distance of 12cm and flow rate of 5$ml.hr^{-1}$.

Obviously this nano fibers are more effective comparison to micro fibers[5].

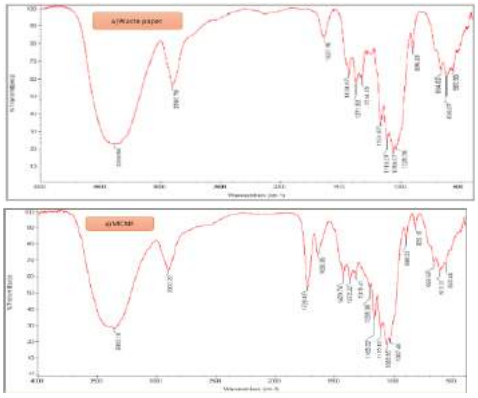

Fig.1.FTIR of waste paper and MCNF .a)waste paper. b) MNCNF

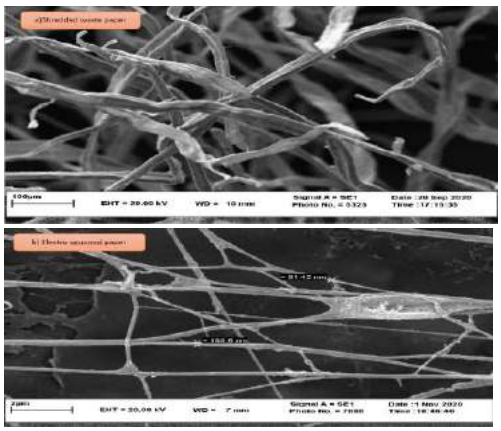

Fig.2. SEM images of a)waste paper b) MCNF

The removal of heavy metal ions from pollutant is dependent on PH of solution. PH range can effect on the surface charge and degree of ionization of the absorbate. A series of test was carried out at different PH values. Fig.3.a demonstrate that at the high PH adsorption was increased sharply, because of the reaction between hydroxyl groups and Hg(II) .So the optimum PH to remove Hg(II) is 5.5.

The effect of temperature on the adsorption of Hg(II) at the range of 10-60 ℃ was investigated. The adsorption capacity was changed from 10 to40℃ and negligible from 40 to 60 ℃.

The effect of stirring time on the adsorption was demonstrated in Fig.3.c. The adsorption rate increased till 32 min and the equilibrium time is around 400min.

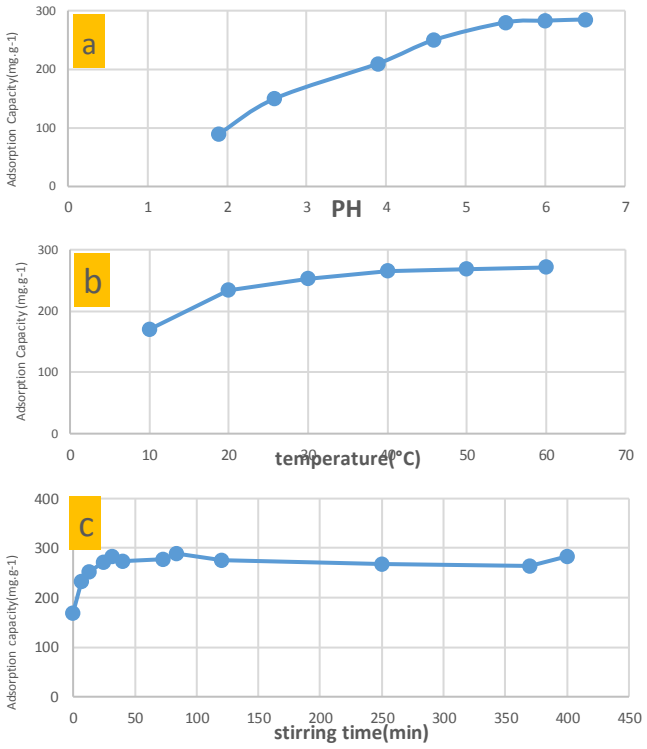

Fig.3. effect of a)PH b)temperature c)stirring time, on adsorption capacity.

IV. Conclusions

In this study, the possibility of using MCNF as adsorbent for Hg(II) ions has investigated. MCNF has a good adsorption capacity for Hg(II) and the maximum uptake of Hg(II) ions from its aqueous solution was found to be 275.2 $mg.g^{-1}$ at the optimum PH of 5.2 and 38 ℃ and stirring time of 32min.

References

[1]Trakulsujaritchok T, Noiphom N, Tangtreamjitmum N, Saeeng R (2011) J Mater Sci 46:5350.
[2] Reichert J, Binner JGP (1996) J Mater Sci 31:1231.
[3] Zhou YM, Jin Q, Zhu TW, Akama Y (2011) J Hazard Mater187:303.
[4]Gurgel LVA, Melo JCP, Lena JC, Gil LF (2009) BioresourTechnol 100:3214.
[5] Zhou, Y., Jin, Q., Hu, X., Zhang, Q., Ma, T., 2012b. Heavy metal ions and organic dyes removal from water by cellulose modified with maleic anhydride. J. Mater. Sci.47 (12), 5019e5029.

بیست و سومین کنفرانس شیمی فیزیک انجمن شیمی ایران
23rd ICS Physical Chemistry Conference
Chemistry Department,
Faculty of Science
Shahid Bahonar University of Kerman
Kerman, Iran
12-13 Jan 2022
ایران، کرمان
دانشگاه شهید باهنر کرمان
دانشکده علوم پایه، بخش شیمی
۲۲-۲۳ دی ماه ۱۴۰۰

Protein-Ligand Docking in Melatonin receptor

Mohammad Amiri* [a] , Mansour Namazian[a] , Maryam Dehestani[b]

[a] Department of Chemistry, University of Yazd, Yazd, Iran, mohammadamiri1985@yahoo.com [b] Department of Chemistry, Shahid Bahonar University of Kerman, Kerman,

Abstract

In this study, molecular docking of Melatonin receptor type a (MT1) and it's intrinsic Ligand, Melatonin (N-acetyl-5-methoxytryptamine) have been done. Inhibition constant (k_i) for the docking system was acceptable, also free energy shows good stability.

Keywords: Melatonin; Melatonin receptor; Docking; Inhibition constant; GPCR.

I. Introduction

Melatonin (Figure 1) is widely distributed in a variety of organisms, such as bacteria, algae, fungi, plants, vertebrates, and mammalians, including humans. In mammals, it is primarily produced by the pineal gland. Main role of this hormone is master sleep and circadian rhythm regulation [1]. Interactions between proteins and ligands is essential for drug design. In silico methods the first step to design the drug is molecular docking of the system receptor as target molecule (protein) and the drug as ligand.

Melatonin receptors, MT1 and MT2, belong to the most variety and most important group of protein, the G-protein-coupled receptor (GPCR) superfamily. GPCR also known as seven-(pass)-transmembrane domain receptors, 7TM receptors. They are called seven-transmembrane receptors because they pass through the cell membrane seven times [2]. The first crystallography structure of GPCR was introduced for rhodopsin [3]. Supply crystallography structure with good resolution is the first step to do molecular docking.

The crystallography structure for MT1 was introduced by Stauch and *et al.* in 2019[4].

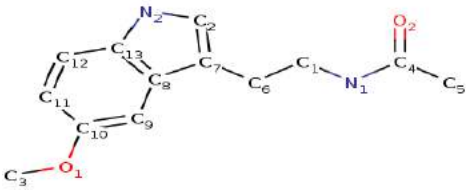

Fig. 1. Melatonin structure

II. Methods

Crystallography structure file (PDB file) for melatonin receptor type A (MT1) extract from RCSB site (6ME2 code) to provide PDB file for ligand (melatonin). We used ATB server before that the molecule have been optimized using B3LYP method of theory and 6–31 G basis set.

Auto Dock and Auto gride software have been used for docking, and using lamarckian genetic algorithm for search.

III. Results and discussion

Figure 2 shows the ligand docked into melatonin receptor. Calculations show the most important amino acids in interaction region are Glutamine 181 and Asparagine 162. k_i for the system calculated 250 nano molar.

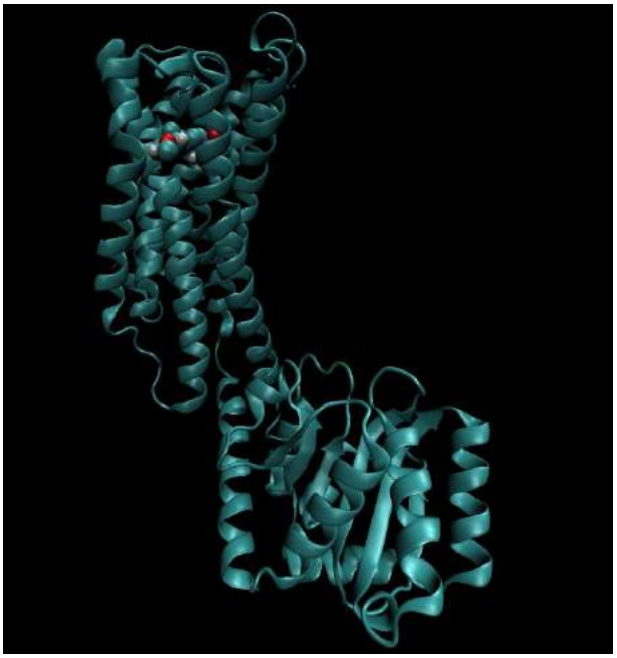

Fig. 2. Docked ligand into receptor body.

IV. Conclusions

Molecular docking can be the first step to introduce new drugs in silico, and as the second step MD simulation can be used to investigate interaction and stability of the system. In the present work, we can suggest new ligands for our receptor system and compare it with origin ligands.

References

[1] D.P. Zlotos, R. Jokers, E. Cenon. S. Rivara, J. Med. Chem., 2014, 8, 3161-3185.

[2] B. Trzaskowski, D. Latek, S. Yuan, U. Ghoshdastider, A. Debinski, S. Filipek, Curr. Med. Chem., 2012, 19, 1090–109.

[3] K. Palczewski, T. Kumasaka, T. Hori, C. A. Behnke, H. Motoshima, B. A. Fox , I. Le Trong, D. C. Teller, T. Okada, R. E. Stenkamp, M. Yamamoto, M. Miyano, Science, 2000, 289: 739–45.

[4] B. Stauch, L. C. Johansson, J. D. McCorvy, et al.. Nature, 2019, 569, 284–288

بیست و سومین کنفرانس شیمی فیزیک انجمن شیمی ایران
23rd ICS Physical Chemistry Conference
Chemistry Department,
Faculty of Science
Shahid Bahonar University of Kerman
Kerman, Iran
12-13 Jan 2022
ایران، کرمان
دانشگاه شهید باهنر کرمان
دانشکده علوم پایه، بخش شیمی
۲۳-۲۲ دی ماه ۱۴۰۰

A new Carbon allotrope: 2D Twin Graphene

Faezeh Taravat[a], Seifollah Jalili[b,] *

[a] *K. N. Toosi University of Technology, Tehran, Iran, faezeh.taravat@email.kntu.ac.ir*
[b] *K. N. Toosi University of Technology, Tehran, Iran, sjalili@kntu.ac.ir*

Abstract

In this research, the mechanical properties and electrical band structure of Twin graphene - a new two-dimensional carbon allotrope - were theoretically investigated. To this end, the first-principles calculations were applied. Here, the mechanical properties of the twin graphene sheets are investigated using DFT.

Keywords: Twin graphene; Mechanical properties; DFT; density of states.

I. Introduction

Twin graphene as a new two-dimensional carbon allotrope was discovered recently to use in various areas of nanotechnology [1, 2]. It is an allotrope that is like a graphene bilayer in which one layer is organically conjoined with another. Also, this structure is a direct semiconductor with an intrinsic bandgap of about 1 eV. Twin graphene deviates from the correlation because this structure essentially has two layers in the out-of-plane direction [3, 4].

II. Methods

In this research, the first-principles density functional theory was applied to all the calculations by using the Quantum Espresso package. The DFT + D2 method of Grimme was added in order to higher accurately describe van der Waals interactions. The cut-off energy of the plane-wave basis set is 500eV. simulation box with 12.24 × 12.24 × 20 Å3 included supercell of twin graphene.

III. Results and discussion

Twin Graphene is like a graphene bilayer in which one layer is organically conjoined with another. A primitive unit cell contains 18 atoms. There are two types of carbon atoms in twin graphene's structure, denoted C1 (on the surface planes) and C2 (on the mid-plane) respectively (Figure 1).

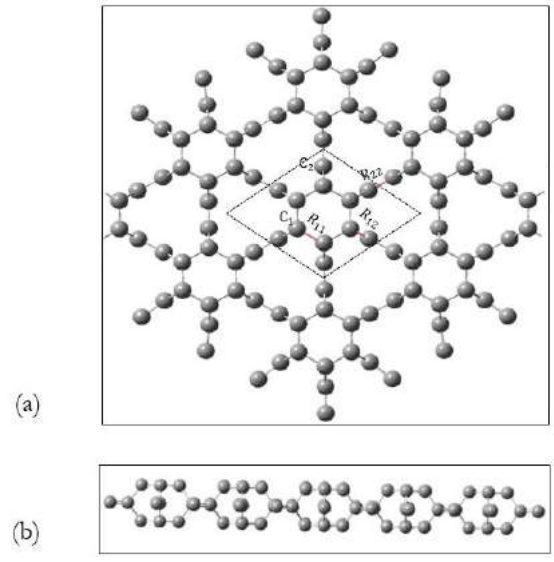

Fig. 1. Optimized structure of Twin Graphene. (a) Top and (b) side views of the lattice structure. The unit cell is marked inside top view.

The optimized structural parameters for twin graphene from the first-principles calculations are summarized in Table 1. The C1-C1 bond length, r11 = 1.42 Å, indicates C1 atoms have sp2 hybridization, whereas the C1–C2 (r12 = 1.54 Å) and C2– C2 (r22 = 1.35 Å) bond lengths exhibit featured characteristics of single

and double bonds. Other structural properties are exhibited in Table 1.

Table 1. Optimized lattice constant (a), bond lengths (r) and bond angles (θ) for twin graphene in different cell parameters.

Cell parameters	r_{11} (A°)	r_{22} (A°)	r_{12} (A°)	θ_{111} (deg)	θ_{112} (deg)	θ_{121} (deg)	θ_{122} (deg)
a = 12.1 b = 12.1 c = 20	1.41	1.33	1.52	120.08	108.40	102.12	129.03
a = 12.2 b = 12.2 c = 20	1.42	1.33	1.53	120.12	108.65	100.68	129.66
a = 12.3 b = 12.3 c = 20	1.42	1.34	1.53	120.14	109.01	99.50	130.27
a = 12.4 b = 12.4 c = 20	1.42	1.35	1.54	120.11	109.05	98.30	130.84
a = 12.6 b = 12.6 c = 20	1.43	1.36	1.56	119.87	109.58	95.78	132.10
a = 12.8 b = 12.8 c = 20	1.44	1.37	1.58	120.12	110.08	93.54	133.23
a = 13.1 b = 13.1 c = 20	1.45	1.40	1.61	120.21	110.63	99.44	134.71
a = 13.2 b = 13.2 c = 20	1.46	1.41	1.63	120.00	110.90	89.08	135.44
a = 13.3 b = 13.3 c = 20	1.46	1.41	1.64	120.09	110.97	88.57	135.60
a = 13.4 b = 13.4 c = 20	1.46	1.42	1.64	120.04	111.08	87.90	136.24
a = 13.5 b = 13.5 c = 20	1.47	1.42	1.65	120.06	111.38	86.86	136.51
Ref [1, 2]	1.43	1.33	1.55	120.00	112.40	80.60	139.70

The electronic band structure of twin graphene shows that this structure is a direct semiconductor (Figure 2).

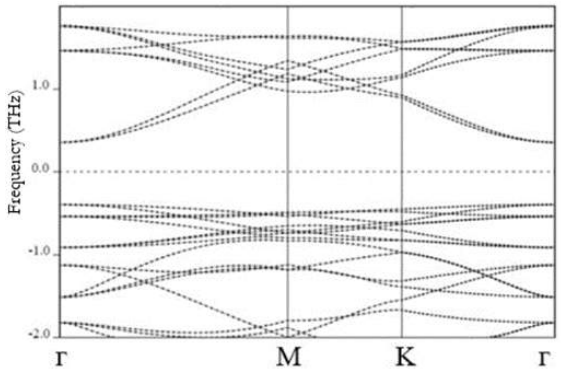

Fig. 2. Electronic band structure of twin graphene.

IV. Conclusions

In summary, by using DFT calculations, the electronic band structure and mechanical properties of Twin graphene are investigated. The excellent mechanical properties make twin graphene suitable to be used in nanoelectromechanical fields. Other properties for this structure can be useful for adsorption, batteries and etc.

References

1. Jiang, J.-W., et al., Twin graphene: A novel two-dimensional semiconducting carbon allotrope. Carbon, 2017. 118: p. 370-375.
2. Li, L., et al., First-principles studies on 3d transition metal atom adsorbed twin graphene. Applied Surface Science, 2018. 441: p. 647-653.
3. Zhang, R.-S. and J.-W. Jiang, The art of designing carbon allotropes. Frontiers of Physics, 2019. 14(1): p. 1-17.
4. Majidi, R. and T. Rabczuk, Structural and electronic properties of BN co-doped and BN analogue of twin graphene sheets: a density functional theory study. Journal of Physics and Chemistry of Solids, 2019. 135: p. 109115.

بیست و سومین کنفرانس شیمی فیزیک انجمن شیمی ایران
23rd ICS Physical Chemistry Conference
Chemistry Department,
Faculty of Science
Shahid Bahonar University of Kerman
Kerman, Iran
12-13 Jan 2022
ایران، کرمان
دانشگاه شهید باهنر کرمان
دانشکده علوم پایه، بخش شیمی
۲۳-۲۲ دی ماه ۱۴۰۰

Novel electrocatalysts for Hydrazine fuel cells: enhanced power generation by optimizing Bimetallic Ni-Co nanoparticles on Nickel Foam (NF)/ reduced graphene oxide as anode and mixed metal oxides as cathode

Tahereh Mohammadi[a], Karim Asadpour-Zeynali [a]* ,Mir Reza Majidi[b], Mir Ghasem Hosseini[c]

[a] *Department of Analytical Chemistry, Faculty of Chemistry, University of Tabriz, Tabriz 51666-16471, Iran*
[b] *Department of Analytical Chemistry, Faculty of Chemistry, Tabriz University, Tabriz, Iran*
[c] *Tabriz, Iran Electrochemistry Research Laboratory, Department of physical chemistry, Faculty of Chemistry University of Tabriz, Tabriz,Iran*

Abstract

One of the major challenges in liquid fuel cells is the provision of Membrane electrode assembly (MEA) electrocatalysts. In the present study, an attempt is made to make a fuel cell with liquid hydrazine fuel without Fixing catalytic inks on the Nafion. In this regard, the catalytic inks based on Ni-Co alloy on NF/ rGO is deposited as used anode and the mixture of iridium, tantalum and silisium oxide, mixed metal oxide electrodes (MMO) has been used cathode. The physical characterization of synthesized materials is investigated using Fourier transform infrared spectroscopy, scanning electron microscopy, energy-dispersive X-ray spectroscopy, and X-ray diffraction. Maximum power density values of 59 mW cm^{-2} at 60 °C are obtained for Ni_{50}-Co_{50} /rGO. The construction of this type of cells without the use of catalytic inks on Nafion has been done for the first time by the electrochemical research team of energy production and storage systems of the Faculty of Chemistry, University of Tabriz.

Keywords: Ni−Co nanoparticles ,direct hydrazine−hydrogen peroxide fuel cell ,Mixture of metal oxides, Nickel Foam.

I. Introduction

Fuel cells have been considered as the promising energy conversion devices with high energy density and broad operation temperature range. Among the liquid fuels, hydrazine is the most promising alternative for fuel cells. This is because that hydrazine is a carbon-free fuel with low cost and readily availability, and its synthesis is relative simple. The only problem needed to be concerned is its toxicity, whereas it can be stored as solid hydrazine by combining with amide or carbonyl groups and released upon contacting with warm water [1-3]. DHFC has attracted intensive attentions duo to its highly theoretical cell voltage (1.56 V) and high power density (5.4 KWh L^{-1}). DHFC can be operated at moderate temperature and the outcome is eco-friendly water [1-3].

II. Methods

Bimetallic Ni-Co nanoparticles on Nickel Foam (NF) reduced graphene oxide (rGO)

are fabricated by electrodeposition to be used as anode electrocatalysts for direct hydrazine-hydrogen peroxide fuel cells (DHHPFCs) (Fig.1). The physical characterization of synthesized materials is investigated using Fourier transform infrared spectroscopy, scanning electron microscopy, energy-dispersive X-ray spectroscopy, and X-ray diffraction. The electrochemical half-cell tests are used to study their electrocatalytic properties toward hydrazine oxidation in an alkaline solution. A direct hydrazine–hydrogen peroxide fuel cell is assembled using mixture of metal oxides (MMO) as a cathode and Ni-Co/ rGO as an anode.

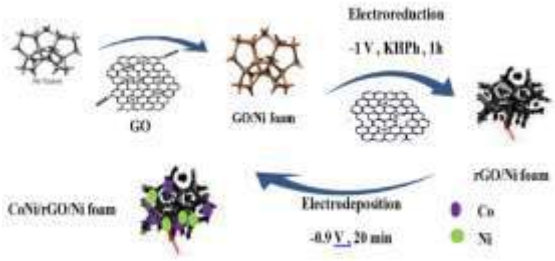

Fig1. The schematic image of CoNi/rGO/Ni foam synthesis process

III. Results and discussion

Fuel cell system includes stainless steel end plates, flow collectors Gold-plated stainless steel and graphite plates with a surface area of 5 cm^2 with grooves It is a spiral with a depth of 1 mm (Figure 2a). The cell performance was studied at different operation conditions. For example, the Figure 2b is illustrated the I–P and I–V curves for CoNi/rGO/Ni foam at different temperatures. Maximum power density values of 59 mW cm^{-2} at 60 °C are obtained for Ni_{50}-Co_{50} /rGO .

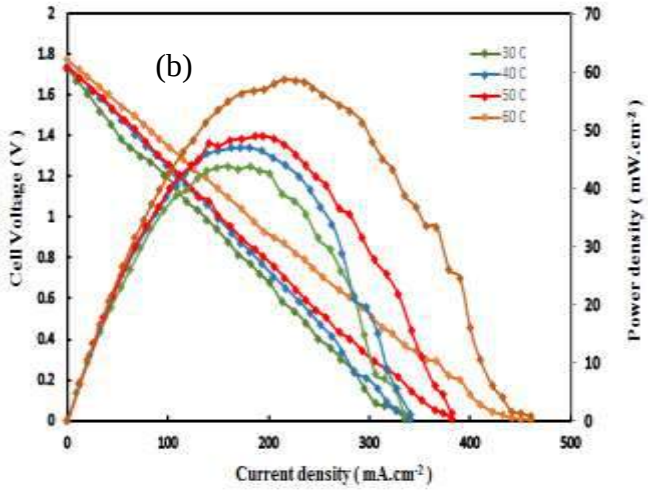

Fig. 2. .(a) Single fuel cell of PEM (b) The effect of temperature (30, 40,50, 60 °C) on V -I and I-P curves. Cathode: MMO and anode: Co-Ni/rGO/Ni foam.

IV. Conclusions

The power efficiency of DHHPFCs in this study with commercial liquid fuel cells is comparable to that of catalytic inks fixed on Nafion; instead, the cathode and anode preparation method is so convenient and accessible that a Nafion without any preparation can be used multiple times.

References

[1] Biaopeng Li, Congying Song, Jinling yin, Jun Yan, Ke Ye, Kui Cheng, Kai zhu, Dianxue Cao, Guiling Wang, International Journal of Hydrogen Energy, 2020, 45, 10569.

[2] Meisong Guoa, Yu Chenga, Yanan Yua, Jingbo Hua, Applied Surface Science, 416, 2017, 439.

[3] Mir Ghasem Hosseini , Raana Mahmoodi , Mehdi Abdolmaleki , New J.Chem., 2018, 42, 12222.

[4] Mir Ghasem Hosseini, M.M. Hosseini,Prot. Met. Phys.Chem. Surfaces, 2018, 54, 700.

بیست و سومین کنفرانس شیمی فیزیک انجمن شیمی ایران
23rd ICS Physical Chemistry Conference
Chemistry Department,
Faculty of Science
Shahid Bahonar University of Kerman
Kerman, Iran
12-13 Jan 2022
ایران، کرمان
دانشگاه شهید باهنر کرمان
دانشکده علوم پایه، بخش شیمی
۲۳-۲۲ دی ماه ۱۴۰۰

Validation of potential energy distribution by VEDA in vibrational assignment some of Copper (II) complexes with β-diketone ligands

Faezeh Ahmadi*[a], Mohammad Vakili[a], Vahidreza Darugar[a]

[a]*Department of Chemistry, Faculty of Science, Ferdowsi University of Mashhad, Mashhad, Iran*
E-mail: faezeh.ahmadi@mail.um.ac.ir Tel: 05138795457
E-mail: vakili-m@um.ac.ir Tel: 05138805551
E-mail: vahidrezadarugar@mail.um.ac.ir Tel: 05138804065

Abstract

In this research, validated the PED results were applied on the vibrational spectra of Copper (II) complexes of β-diketones family. The PED contributions compared with the GaussView animation of reported assignments, and their experimental IR and Raman shifts upon change of different substitution in β-position.

Keywords: VEDA; DFT; PED; GaussView; vibrational shifts.

I. Introduction

The Copper complexes of β-diketones and especially those of acetylacetone and its derivatives and their vibrational analyses have been studied [1–4]. Generally, the assignment of vibrational bands for the mentioned complexes described via two methods. The first GaussView animations of movements, and the second using potential energy distribution (PED) analysis by Vibrational Energy Distribution Analysis (VEDA) software [3]. In spite of numerous vibrational spectroscopy reported on the Copper complexes of β-diketones [1-4], but the quantitative analysis of vibrational spectra of these complexes has not been reported by VEDA software untill now. Lately, Darugar et al. validated the PED results on the β-diketones family [5].

II. Methods

The harmonic vibrational frequencies some of Copper (II) complexes of β-diketones family were calculated via density functional theory (DFT) at the B3LYP/6–311G(d) level of theory (see Fig. 1). The PED contributions were calculated via VEDA software [1].

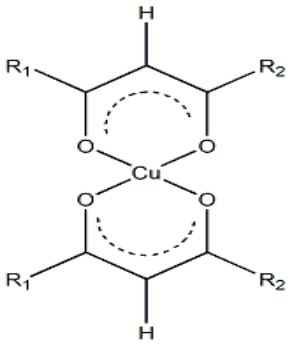

(a) R_1,R_2=CH_3 , (b) R_1,R_2=C_2H_5, (c) R_1R_2=Ph (d)R_1,R_2=Ph,CH_3

Fig. 1: The schematic of Copper (II) β-diketone complexes.

III. Results and discussion

Outcomes in Table 1 almost indicated the PED contributions, GaussView moving and observed vibrational shifts show the same results for the most of the vibrational bands which are not coupled, such as asymmetric and symmetric CH_3 stretching, CH_3 rocking modes and the phenyl ring vibrations. The most differences were detected in the below of 1000 cm^{-1} region, especially in the asymmetric and symmetric O-Cu-O stretching modes.

.**Table 1** The abridged most important fundamental bands of β-diketone complexes which shifted by change of substitution (shifting's are in cm^{-1} and PED's are in %).

Normal mode	$Cu(AA)_2$		$Cu(HPD)_2$		$Cu(BA)_2$		$Cu(DBM)_2$	
	PED	Shifting	PED	Shifting	PED	Shifting	PED	Shifting
νCHα	98	0	100	3	95	22	98	57
νaC=C–C=O	54	0	67	14	52	18	38	-26
νsC=C–C=O	79	0	65	9	….	-62	50	-33
νsCCC	36	0	….	55	39	-170	54	16
γCHα	96	0	80	-8	79	-10	71	-37
δCHα	54	0	50	-14	44	23	34	45
νaO-Cu-O	72	0	….	7	14	15	11	43
νsO-Cu-O	50	0	34	5	11	100	14	120

IV. Conclusions

The PED contributions compared with the GaussView animation of reported assignments, and their experimental IR and Raman shifts upon change of different substitution in β-position than that Cu(AA)2 as parent complex.

Hence, the calculated PED contributions by VEDA software do not well explain those vibrational bands shifts in these complexes, which are directly engaged with the Cu-O movements.

References

[1] M. H. Jamroz, SpectrochimicaActa Part A: Molecular and Biomolecular Spectroscopy 114 (2013) 220–230.

[2] S. Soltani-Ghockhaneh , Mohammad Vakili , Sayyed FaramarzTayyari , Ali Reza Berenji , Vahidreza Darugar , Journal of Molecular Structure 1197 (2019) 443_449

[3] M. Vakili, S.F. Tayyari, R. Afzali, SpectrochimicaActa Part A: Molecular and Biomolecular Spectroscopy 136 (2015)1827-1823

[4] A.-R. Nekoei, M. Vakili, M. Hakimi-Tabar, S. F. Tayyari, R. Afzali, H. G. Kjaergaard, SpectrochimicaActa Part A: Molecular and Biomolecular Spectroscopy 128 (2014) 272–279

[5] V.R. Darugar, M. Vakili; S. F. Tayyari, F. S. Kamounah, Journal of Molecular Graphics and Modelling 107 (2021) 107976.

بیست و سومین کنفرانس شیمی فیزیک انجمن شیمی ایران
23rd ICS Physical Chemistry Conference
Chemistry Department,
Faculty of Science
Shahid Bahonar University of Kerman
Kerman, Iran
12-13 Jan 2022
ایران، کرمان
دانشگاه شهید باهنر کرمان
دانشکده علوم پایه، بخش شیمی
۲۳-۲۲ دی ماه ۱۴۰۰

Metal-ligand bond strength in symmetric of Copper (II) β-diketone complexes by UV and TD-DFT approaches

Faezeh Ahmadi*[a], Mohammad Vakili[a], Vahidreza Darugar[a]

[a]*Department of Chemistry, Faculty of Science, Ferdowsi University of Mashhad, Mashhad, Iran*
E-mail: faezeh.ahmadi@mail.um.ac.ir Tel: 05138795457
E-mail: vakili-m@um.ac.ir Tel: 05138805551
E-mail: vahidrezadarugar@mail.um.ac.ir Tel: 05138804065

Abstract

In this research, the UV wavelengths in some of Copper (II) complexes of β-diketones with different substitutions in beta position, such as CH_3, C_2H_5, iso-pro, and t-But, were calculated and compared with their reported experimental UV bands.

Keywords: TD-DFT; UV-Vis; Copper (II) β-diketone complexes.

I. Introduction

The metal β-Diketones complexes are important molecules for researchers, because they are widely used in science and industry [1]. Recently, seyyed katouli et al. and soltani et al. analyzed the metal-ligand bond strength for some of β-diketones complexes by UV technique [2,3]. To our knowledge, the computational approach of UV spectra of these complexes has not been studied until now.

II. Methods

For this purpose, the UV wavelengths in some of Copper (II) complexes of β-diketones with different substitutions in beta position, such as CH_3, C_2H_5, iso-pro, and t-But, as symmetric complexes were calculated via time-depending density functional theory (TD-DFT) at the B3LYP/6–311G(d) level of theory (see Fig. 1)

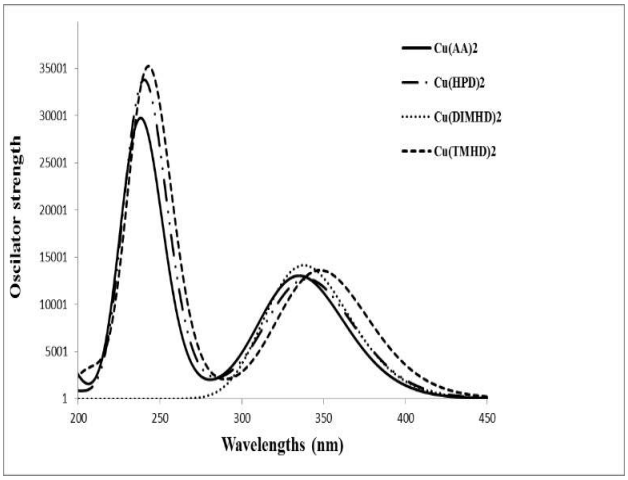

Fig. 1: The TD-DFT bands in Copper (II) β-diketone complexes.

III. Results and discussion

For copper (II) acetylacetonate, $Cu(AA)_2$, the calculated and experimental bands are at 235 (240) and 332 (307) nm [2]. In bis(3,5-heptanedionato)copper(II), $Cu(HPD)_2$, two bands are appeared at 239 (243) and 336 (310) nm. The numbers are in parenthesis due to reported experimental bands [3]. For copper (II) 2,2,6,6-tetramethylheptane-3,5-dionate, $Cu(TMHD)_2$, the bands is calculated at 242 and 348 nm. While in copper (II) 2,6-dimethylheptane-3,5-dione, $Cu(DIMHD)_2$, only an broad band is calculated at 336 nm.

IV. Conclusions

Hence, the first band at below of 250 nm, is assigned to ligand-to-metal charge transfer, while the other band at higher of 300 nm, are assigned to $\pi \rightarrow \pi^*$ transitions of chelated ring. This red shifts in wavelengths from $Cu(AA)_2$ to $Cu(TMHD)_2$ specifies that the resonance of chelated ring and Cu-O bond strength in these complexes according to following trend: $Cu(TMHD)_2 > Cu(DIMHD)_2 > Cu(HPD)_2 \geq Cu(AA)_2$.

References

[1] Włodzimierz Urbaniak, Katarzyna Jurek, Katarzyna Witt, AndrzejGora˛czko, Chemik 65 (4) (2011) 273-282.
[2] S. Seyedkatouli, M. Vakili, S.F. Tayyari, R. Afzali, J. Mol. Struct. 1160 (2018) 107-116.
[3] S. Soltani-Ghockhaneh, M.Vakili, S. F. Tayyari, A. R. Berenji, V. Darugar, J. Mol. Struct. 1197 (2019) 443-449.

بیست و سومین کنفرانس شیمی فیزیک انجمن شیمی ایران
23rd ICS Physical Chemistry Conference
Chemistry Department,
Faculty of Science
Shahid Bahonar University of Kerman
Kerman, Iran
12-13 Jan 2022
ایران، کرمان
دانشگاه شهید باهنر کرمان
دانشکده علوم پایه، بخش شیمی
۲۳-۲۲ دی ماه ۱۴۰۰

Molecular Structure at the Interfaces of Submonolayer Thin Films of Sexithiophene

Thorn A. Dramstad[a], Zahra Sohrabpour[b], Aaron M. Massari[c,*]

[a] *University of Minnesota, 207 Pleasant St. SE,Minneapolis, MN, USA 55454; Tel: 1 (612)626-8416; E-mail: drams002@umn.edu*
[b] *K. N. Toosi University of Technology, Kaviyan St E., Tehran, Iran; Tel: 21 8888 2991; E-mail: zsohrabpour@kntu.ac.ir*
[c] *University of Minnesota, 207 Pleasant St. SE,Minneapolis, MN, USA 55454; Tel: 1 (612)626-8416; E-mail: massari@umn.edu*

Abstract

Vibrational sum frequency generation (VSFG) spectroscopy with different polarization combinations was used to show that the average orientation of α-sexithiophene (6T) on a glass substrate for the 6T/glass interface changes with the thickness of the film. This is a result of 6T growth mechanism on glass, which was studied by AFM imaging. It was also shown that 6T on glass forms a wetting layer, and the buried interface experiences a change in environment after some critical deposition thickness, leading to a change in the orientation of the interfacial molecules.

Keywords: Sum Frequency Generation Spectroscopy (SFG); Sexithiophene (6T); Thin Film Interfaces.

I. Introduction

The growth of organic thin films is complex. In the early stages of film growth, many molecular materials deposit in a less ordered thin-film phase, distinct from their crystalline structure, which upon reaching a critical thickness converts into a crystalline bulk phase. [1,2]

In this study, the model organic semiconductor, α-sexithiophene (6T), has been studied at glass/6T (inner) and 6T/air (outer) interfaces.

To study interfacial structures, it is crucial to use experimental methods, such as VSFG spectroscopy, capable of characterizing at the interface. In this study, AFM was also incorporated to gain complementary information about the topography of the outer interface (6T/air).

II. Methods

6T samples were made by deposition on glass substrates using a home-built organic vapor deposition chamber. Topographic imaging was performed on a Bruker Dimension 5000 AFM. The VSFG spectroscopy was done using the Massari lab laser instrument. [3]

III. Results and discussion

AFM height imaging showed that the initial layers of 6T deposits as a wetting layer, as the film becomes thicker, large island-like features start forming. A structural change is experienced by 6T molecules at the outer interface but, the structure of the underlying 6T molecules, which is of importance for an electronic material, is unknown.

To determine structure and orientation at the inner interface VSFG spectroscopy with two polarization combinations was used. Samples with different thicknesses of 60, 20 and 11 nm were measured.

Polarized FTIR and Raman measurements have shown that 6T vibrational symmetric stretches are polarized along the in-plane short

molecular axis (M) and the asymmetric stretches along the molecular long axis (L) (Fig.1 inset). [4]

In VSFG, the sps polarization, samples the in-plane component of a transition dipole whereas the ssp measures the out-of-plane contribution. Higher frequency VSFG activity between 1457 cm^{-1} – 1460 cm^{-1} are characteristic of grain boundaries, which are aligned with the M axis of 6T (Fig. 1). The higher frequency mode shows up in both ssp and sps polarized VSFG spectra which would be expected of a disordered population. A lower frequency of 1420 cm^{-1}, present in the sps spectrum of the 60nm sample, is related to an inner ring M-axis mode.[5] So, for thicker samples, a higher population of the interfacial molecules are oriented with their short axis aligned between parallel and perpendicular to the surface.

Also, the inner interface frequencies are higher than the outer frequencies, suggesting the buried molecules are more constrained, resulting in a tighter bond.

When the film thickness is decreased from 20 to 11 nm nearly all VSFG signal amplitude disappears, except the peak near 1458 cm^{-1} (ssp spectrum). This indicates that the molecules are rotating so the M-axis on average, is nearly perpendicular to the substrate. However molecular orientation for a thicker film of a couple monolayers changes so the L-axis is perpendicular to the surface (end-on orientation). VSFG measurements were then carried out on a thickness gradient sample. At a thickness below ~7 nm the environment felt by the buried and exposed interfaces is identical. One possible explanation is that at these thicknesses the substrate forces are the dominant force in the sample.

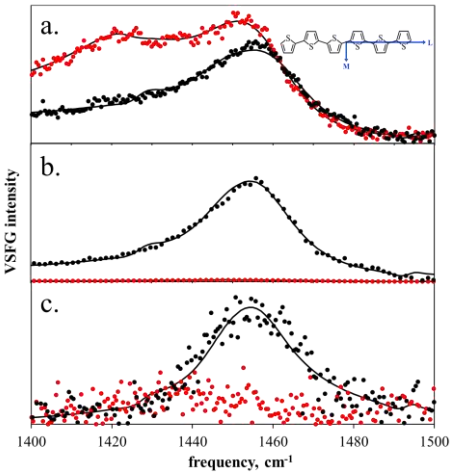

Fig. 1. VSFG spectra of 6T on glass with (a) 60 nm, (b) 20 nm, and (c) 11 nm thickness (ssp: black, sps: red, best fits: solid lines). Inset: molecular structure of 6T with transition dipole directions for the M and L modes.

IV. Conclusions

VSFG has shown that the average orientation of 6T on glass for the inner and outer interfaces depending on thickness, is different. This is a result of the 6T growth transition, which was confirmed by AFM. Also, by using different polarization combinations, it was shown that the environment of the 6T molecules at the inner and outer interfaces are identical only at ultrathin thicknesses.

References

[1] Jones, A.; Chattopadhyay, B.; Geerts, Y.; Resel, R., *Adv. Funct. Mater.*, 2016, *26* (14), **2233-2255**.
[2] Kowarik, S.; Gerlach, A.; Sellner, S.; Schreiber, F.; Cavalcanti, L.; Konovalov, O., *Phys. Rev. Lett.*, 2006, *96* (12), **125504**.
[3] Kearns, P.; Sohrabpour, Z.; Massari, A., *Opt. Express* 2016, *24* (17), **19863-19870.**
[4] Horowitz, G.; Bachet, B.; Yassar, A.; Lang, P.; Demanze, F.; Fave, J. L.; Garnier, F., *Chem. Mater.* 1995, *7*, **1337-1341**.
[5] Casado, J.; Katz, H.; Hernandez, V.; Navarrete, J., *Vib. Spectrosc*, 2002, *30* (2), **175-189**

بیست و سومین کنفرانس شیمی فیزیک انجمن شیمی ایران
23rd ICS Physical Chemistry Conference
Chemistry Department,
Faculty of Science
Shahid Bahonar University of Kerman
Kerman, Iran
12-13 Jan 2022
ایران، کرمان
دانشگاه شهید باهنر کرمان
دانشکده علوم پایه، بخش شیمی
۲۳-۲۲ دی ماه ۱۴۰۰

Electrochemical insight into the cytochrome c adsorption on graphene and graphene oxide/self assembled monolayer surfaces and study of its electron transfer kinetics

Vali Alizadeh[a,*], Ahmad Jamali Moghadam[a]

[a] *Department of Petroleum Engineering, University of Garmsar,Garmsar, Iran, va11180@yahoo.com*

Abstract

The electrochemical property of cyt c on graphene (G) and graphene oxide (GO)/self assembled monolayer (SAM) surfaces were investigated by electrochemical techniques. Electrochemical response of cyt c on G/SAM showed an increase in peak separation and reduction in peak current. Cyclic voltammetry (CV) and scanning electrochemical microscopy (SECM) results, suggest that the adsorption of cyt c on G/SAM is an unfavorable adsorption orientation for ET, so that the ET kinetics is higher on GO/SAM compared with G/SAM. The results show that cyt c is immobilized onto the GO/SAM surface by electrostatic interaction; whereas on G/SAM surface adsorbs by hydrophobic interaction.

Keywords: Graphene; Self Assembled Monolayer; Cytochrome c; Electron Transfer Kinetics.

I. Introduction

A hybrid of metalloproteins and carbon nanoparticles on electrode surfaces are of great relevance to a broad spectrum of potential applications such as biosensors, bioelectronics and, biochips [1,2]. Cyt c plays an essential role in electron transfer (ET) chain in mitochondria. The adsorption of cyt c on solid electrodes impedes the ET between cty c and the electrode surfaces [2,3]. However, the nanoscale materials, e.g. carbon nanomaterials that facilitate the protein ET at electrode surfaces have attracted much attention [4]. In this work, first the Au electrode modified by hexanethiol SAM, then modified by G and GO nanoparticles. Afterward, cyt c adsorbed on G/SAM and GO/SAM surfaces to study of ET kinetics.

II. Methods

Electrochemical measurements were carried out using a CHI-900 scanning electrochemical microscopy that uses a combination of stepper motors and an XYZ piezo block in order to position the ultramicroelectrode (UME). A gold disc electrode (Au), Au/SAM/G/cyt c and Au/SAM/GO/cyt c hybrid systems served as working electrode for CV and SECM experiments. An Ag/AgCl (3M KCl) electrode was used as the reference electrode. EIS measurements were carried out using an Autolab PG30 electrochemical analyzer, fitted with FRA2 module boards in presence of 0.5 mM $Fe(CN)_6^{-3/-4}$ at a potential of 0.25 V. Frequencies were swept between 10 kHz and 100 mHz with an amplitude of 5 mV rms sinusoidal potential modulation.

III. Results and discussion

The results indicate that the adsorbed cyt c on both surfaces maintains its structure (Fig. 1). But the difference in ET kinetics on Au/SAM/G and Au/SAM/GO should be attributed to the cyt c orientation relative to the surface. On the Au/G/SAM, cyt c is less prone to direct ET since the electrons reach the electrode surface over a long distance. But the ET facilitates from Au/GO/SAM surface to the cyt c due to the heme ring is much closer to the GO surface.

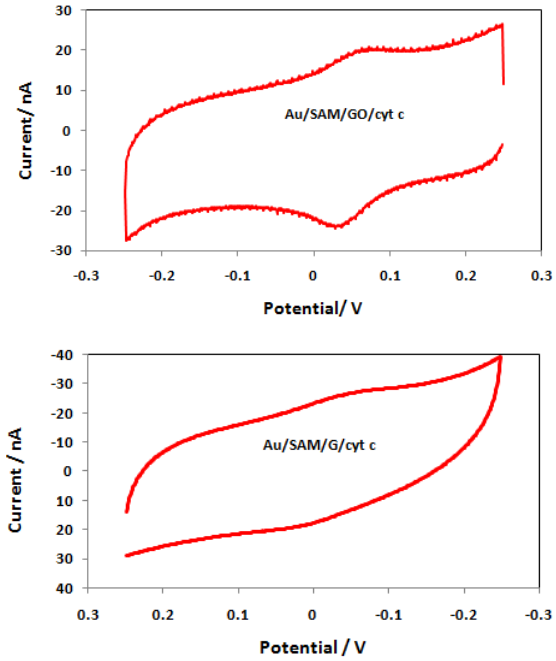

Fig. 1. Cyclic voltammetry of cyt c on GO (above) and G (below) prepared hybrid system in 44 mM phosphate buffer solution at scan rate 20 mV/s.

IV. Conclusions

Cyt c adsorbed on G and GO modified surfaces in two different interaction strategies, hydrophilic and hydrophobic interaction, respectively. The heme plane in cyt c far away from the G surface, which is not conductive to ET but is close to the GO surface, which makes ET prone. These findings have a guiding role in the development of biosensors.

References

[1] T.S. Wong and U. Schwaneberg, Curr. Opin. Biotechnol., 2003, 14, 590-596.
[2] T. Noll and G. Noll, Chem. Soc. Rev., 2011, 40, 3564-3576.
[3] J. Xu and E.F. Bowden, J. Am. Chem. Soc., 2006, 128, 6813-6822.
[4] S.F. Kiew, L.V. Kiew, H.B. Lee, T. Imae and L.Y. Chung, J. Controlled Release, 2016, 226, 217-228.

بیست و سومین کنفرانس شیمی فیزیک انجمن شیمی ایران
23rd ICS Physical Chemistry Conference
Chemistry Department,
Faculty of Science
Shahid Bahonar University of Kerman
Kerman, Iran
12-13 Jan 2022
ایران، کرمان
دانشگاه شهید باهنر کرمان
دانشکده علوم پایه، بخش شیمی
۲۳-۲۲ دی ماه ۱۴۰۰

Study of tunneling electron transfer on Graphene nanoplatelet /Self assembled monolayer modified gold electrode by electrochemical techniques

Vali Alizadeh[a,*], **Ahmad Jamali Moghadam**[a]

[a] *Department of Petroleum Engineering, University of Garmsar,Garmsar, Iran, va11180@yahoo.com*

Abstract

The electrochemical property of graphene nanoplatelet on self assembled monolayer (SAM) was investigated. A gold electrode was modified by octanethiol to produce SAM, next graphene nanoplatelet adsorbed on SAM to obtain a graphene/SAM electrode. The prepared electrode was characterized by ferrocenemethanol as a redox probe, and cyclic voltamettry (CV) and scanning electrochemical microscopy (SECM) techniques. The experimental results showed that the tunneling electron transfer can be restored by graphene nanopalatelet. The electron transfer rate of ferrocenemethanol on graphene/SAM modified electrode was evaluated quantitatively by SECM, and equal to 4.5×10^{-2} cm s^{-1}.

Keywords: Graphene Nanoplatelet; Electron Transfer; Cyclic Voltammetry; Frerrocenemethanol; Self Assembled Monolayer.

I. Introduction

Graphene has several advantages in electrochemical applications, such as huge surface area, high conductivity, and bears high π-conjugation; in addition graphene nanoplatelets formed by stacked graphene sheets with a typical thickness of 2-10 graphene layers are equally important. The spontaneous formation of a self-assembled monolayer (SAM) of alkanthiols onto a gold electrode can establish useful structures on the electrode surface. The SAM of long carbon chains acts as an insulation barrier which can block ET between the bare electrode and redox species in solution. However, ET can be restored, and the redox processes through the SAM can be investigated with attachment of nanomaterials to the SAM. The present work studies the fabrication and characterization of graphene/SAM modified gold electrode and the kinetics of graphene sheet mediated ET on such chemically modified electrodes [1-3].

II. Methods

Electrochemical measurements were carried out using a CHI-900 scanning electrochemical microscopy that uses a combination of stepper motors and an XYZ piezo block in order to position the ultramicroelectrode (UME). A gold disc electrode (Au) and Au/SAM/Graphene served as working electrode for CV and SECM experiments. An Ag/AgCl (3M KCl) electrode was used as the reference electrode.

III. Results and discussion

The graphene nanoplatelet are first dispersed in ethanol and then adsorbed onto the surface of prepared Au/SAM. The electrochemical properties of the Au/SAM and Au/SAM/graphene electrodes were characterized by CV. Compared with the CV curve of the ferrocenemethanol on the bare Au electrode, no redox peaks were obtained on the Au/SAM electrode, indicating that the SAM greatly hinders the heterogeneous ET between the electrode and the redox species in solution. After the adsorption of graphene nanoplatelet on the surface of the SAM, the cyclic voltammogram shows a nearly reversible ET behavior just as that observed for a bare gold electrode under the same conditions and suggesting that the heterogeneous ET blocked by the SAM is largely restored by graphene nanoplatelet. The ET kinetics of ferrocenemethanol was explored on the Au/SAM/graphene electrode using both CV and SECM in a more quantitatively way. Since ET kinetics obtained for a conventional electrode by CV is always affected by the iR drop, it was evaluated by employing SECM. The apparent heterogeneous rate constant was evaluated to be equal to 4.5×10^{-2} cm s^{-1} by fitting the theoretical and experimental approach curves.

IV. Conclusions

An Au/SAM/graphene electrode was prepared and evaluated by CV. The kinetics of the ET of ferrocenemethanol was effectively blocked by SAM. However, the adsorption of graphene nanoplatelets can restore ET between substrate Au electrode and ferrocenemethanol. Graphene nanoplateles mediates ET between the Au electrode and ferrocenemethanol as an electron relay stations. SECM as a powerful technique was applied to determine ET kinetics.

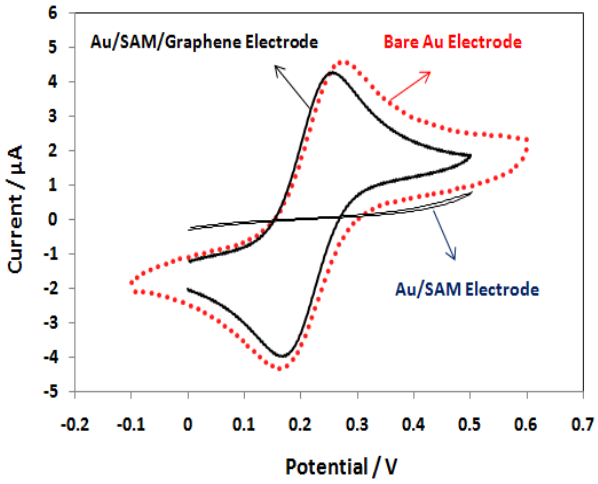

Fig. 1. Cyclic voltammograms of 0.1 mM ferrocenemethanol on Bare Au, Au/SAM and Au/SAM/Graphene electrodes in 100mM phosphate buffer solution at scan rate 50 mV/s.

References

[1] X. Wang, L. Zhi and K. Mullen, Nano Lett., 2008, 8, 323-227
[2] M. Pumera, Langmuir, 2007, 23, 6453-6458.
[3] H. O. Finklea, S. Avery and M. Lynch, Langmuir, 1987, 3, 409-413.

بیست و سومین کنفرانس شیمی فیزیک انجمن شیمی ایران
23rd ICS Physical Chemistry Conference
Chemistry Department,
Faculty of Science
Shahid Bahonar University of Kerman
Kerman, Iran
12-13 Jan 2022
ایران، کرمان
دانشگاه شهید باهنر کرمان
دانشکده علوم پایه، بخش شیمی
۲۳-۲۲ دی ماه ۱۴۰۰

Enol-keto swching Schif base ligand Salicylidenemethyl Furylamine

Ahmad Jamali Moghadame[a]*, Valli alizade[b],

[a]*University of Garmsar P.O.Box 3581755796, Garmsar, Iran; E-mail: a.jamalimoghaddam@fmgarmsar.ac.ir*
[b]*University of Garmsar P.O.Box 3581755796, Garmsar, Iran; E-mail: v.alizadeh@fmgarmsar.ac.ir*

Abstract

Potential energy surfaces (PES) for the ground and excited state intramolecular proton transfer (ESIPT) processes in N-salicilydenemethylfurylamine (SMFA) have been studied using CC2 level of theory. Our calculations suggest the non-viability of ground state intramolecular proton transfer. Excited states PES calculations support the existence of ESIPT process in SMFA. The calculated results show that the intramolecular hydrogen bond were formed in the S_0 state, and upon excitation, the intramolecular hydrogen bonds between -OH group and nitrogen atom would be strengthened in the S_1 state, which can facilitate the proton transfer process effectively. The minimum energetic level of the S_1 state along the PT coordinate lies in the short distance to the long distance of OH, which corresponds to the new bond formation of H−N. A barrierless reaction path directs the system back to the enol-type minimum of the S_0 potential energy surface. According to calculation results, a trans-keto type structure obtained from photoexcitation of the enol, can be responsible for the photochromoic effect, thus closing the photocycle of title compound.

Keywords: Schiff Base, Intramolecular Proton Transfer, Photochromism).

I. I. Introduction

From the beginning of the 21th century, the research for molecular switches based on light-induced conformational changes has been a hot topic. Schiff Base molecules represent a class of advanced materials widely employed in photonic and optoelectronic applications. Usually, ortho-hydroxy Schiff bases display two possible tautomeric forms, the enol-imine and the keto-amine forms. Depending on the tautomers, two types of intramolecular hydrogen bonds can exist in Schiff bases: O—H···N in enol-imine and N—H···O in ketoamine tautomers that resulted photochromic effect of salicylaldehyde Schiff bases [1-3].

II. Methods

The ab initio calculations have been performed with the TURBOMOLE program package. With the correlation-consistent polarized valence double-ζ (cc-pVDZ) basis set the ground and lowest excited singlet states equilibrium geometry have been obtained in the (RI-MP_2) and (RI-CC_2) level of theory respectively[4-5].

III. Results and discussion

The first step of this work is looking for the most stable structure of title compound. The most stable structure in ground state (S_0) at the MP2/cc-pVDZ

level of theory is enol form (E). While the excited state proton transfer (ESPT) is mainly achieved after the S1 geometry optimization of the E form at the CC2 level as keto form (K), (see Fig. 1). The minimum potential energy (MPE) profiles of E in the S0 state and in the lowest excited state, determined along the PT (OH distance) and along the torsion of the of the methylamine group (dihedral angle of θ (C1–C2–C7–N1)) are shown in Fig. 2. The results showed that after optical excitation of E to the first excited singlet state, a spontaneous (barrier-free) PT reaction occurs.

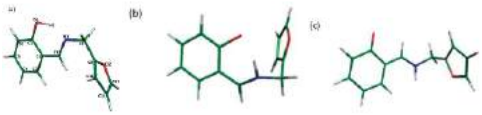

Fig. 1. Optimized geometries and numbering pattern: (a) the most stable configuration of the enol form of SMFA (calculated at the MP2/cc-pVDZ level of theory); (b) the S1 optimized structure of cis-keto form of SMFA (determined at theCC2/cc-pVDZ geometry optimization of the E form); (c) the optimized geometry structure of trans-keto form of SMFA obtained at the MP2/cc-pVDZ level of theory

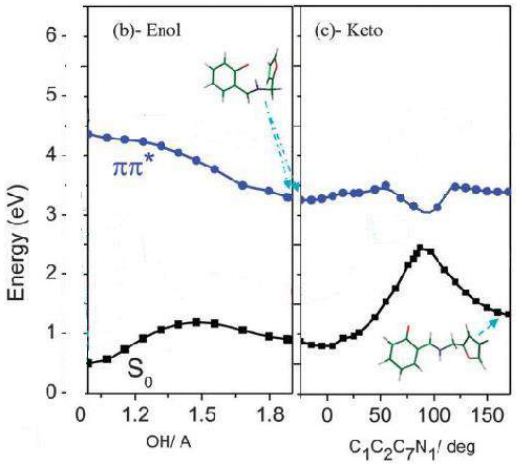

Table 2.) Potential energy curves of the S0 state (squares) and the S1 state (circles), as the functions the torsional reaction path and the hydrogen transfer reaction path. The energy origin is the energy of minimum enol in the ground state

IV. Conclusions

The proton transfer is the main character of SMFA at the excited state. In contrast to the ground state, the PT process is significantly exoergic in the excited state. From the barrierless potential energy curve of the enol form at the excited state, one can conclude the fast dynamics for such ESIPT. The calculations indicate that the trans-keto form produced by UV excitation of Enol form is a strong UV/vis absorber and should be highly photostable.

References

[1] H.Durr,H. Bouas-Laurent, "Photochromism: Molecules and Systems", 2003, 2nd Ed.; Elsevier: Amsterdam.

[2] M. Irie, Chem. Rev, 100 (2000) 1685-1716

[3] M. Z. Zgierski, J. Chem. Phys, 115 (2001) 8351–8358.

[4] Ahlrichs, R.; Bär, M.; Häser, M.; Horn, H.; Kölmel, C, Chem. Phys. Lett, 162 (1989) 165−169

[5] Christiansen,O.; Koch, H.; Jørgensen, Chem. Phys. Lett, 243 (1995) 409−418.

بیست و سومین کنفرانس شیمی فیزیک انجمن شیمی ایران
23rd ICS Physical Chemistry Conference
Chemistry Department,
Faculty of Science
Shahid Bahonar University of Kerman
Kerman, Iran
12-13 Jan 2022
ایران، کرمان
دانشگاه شهید باهنر کرمان
دانشکده علوم پایه، بخش شیمی
۲۳-۲۲ دی ماه ۱۴۰۰

Enol-keto switching in N-Salicylidene-2-Bromoethylamine Schiff base ligand

Ahmad Jamali Moghadame[a]*, Valli alizade[b],

[a]University of Garmsar P.O.Box 3581755796, Garmsar, Iran; E-mail: a.jamalimoghaddam@fmgarmsar.ac.ir
[b]University of Garmsar P.O.Box 3581755796, Garmsar, Iran; E-mail:v.alizade@fmgarmsar.ac.ir

Abstract

The Excited state reaction coordinates and the consequent energy profiles of a Schiff Base N-Salicylidene-2-Bromoethylamine (NSBA) have been investigated at the CC2 level of theory. The electron-driven proton transfer and torsional deformation have been identified as the most important photochemical reaction coordinates. The potential energy profiles of the ground and the lowest excited singlet state are calculated. In contrast to the ground state, the excited state potential energy profile shows a barrier-less dissociation pattern along the O–H stretching coordinate which verifies the proton transfer reaction at the S_1 state and the intramolecular hydrogen bonds between -OH group and nitrogen atom would be strengthened in the S_1 state. According to calculation results, a trans-keto type structure obtained from photoexcitation of the enol, can be responsible for the photochromoic effect of title compound. Furthermore, our results confirm the properties of hydrogen bonds can induce changes in geometric or electronic structure parameters and suggestion that aromatic Schiff Bases are potential candidates for optically driven molecular switches.

Keywords: Schiff Base, Intramolecular Proton Transfer, Photochromism).

I. I. Introduction

Excited-state reactions play important roles in the electronic properties of materials and biological systems, including their photoinduced functions. Aromatic Schiff bases and their metal complexes have recently attracted considerable attention because of their interesting and important properties such as biological activities, chemodosimeter, molecular tweezers, photochemical behavior, ionophores, catalytic activities, and pH-responsive [1]. Aromatic Schiff bases belong to a broad family of molecular systems whose photophysics is determined by the excited state intramolecular proton-transfer (ESIPT) reaction. Photochromic Schiff bases represent a special group of ESIPT systems, whose depopulation routes of the excited molecule are particularly complex. Besides the PT reaction cycle, returning the system to its original state through the back-PT, a large portion of molecules may be trapped in the ground state as metastable photochromic species. The photochromism and tautomerism features make extensive applications for Schiff bases in the laser dyes, molecular switches, nonlinear optical properties and molecular electronic devices [2-3].

Methods

The ab initio calculations have been performed with the TURBOMOLE program package [3]. With the correlation-

consistent polarized valence double-ζ (cc-pVDZ) basis set the ground and lowest excited singlet states equilibrium geometry have been obtained in the (RI-MP2) and (RI-CC2) level of theory respectively[4].

II. Results and discussion

The first step of this work is looking for the most stable structure of title compound. The most stable structure in ground state (S_0) at the MP2/cc-pVDZ level of theory is enol form (E). While the excited state proton transfer (ESPT) is mainly achieved after the S_1 geometry optimization of the E form at the CC2 level as keto form (K), (see Fig. 1). The minimum potential energy (MPE) profiles of E in the S_0 state and in the lowest excited state, determined along the PT (OH distance) and along the torsion of the methylamine group (dihedral angle of θ (C1–C2–C7–N1)) are shown in Fig. 2. The Fig. 2, illustrates that the enol form is a typical excited-state intramolecular proton transfer (ESIPT) system. The minimum energy profiles were obtained by optimization of molecular geometry for fixed values of the reaction coordinate for ground and excited states, performed respectively at the MP2/cc-pVDZ or CC2/cc-pVDZ level of theory.

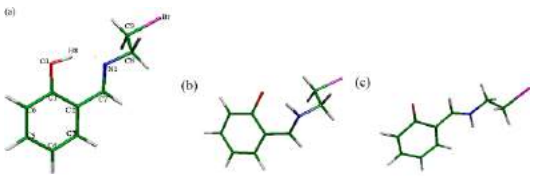

Figure. 1: Optimized geometries and numbering pattern: (a) the most stable configuration of the enol form of NSBA (calculated at the MP2/cc-pVDZ level of theory); (b) the S_1 optimized structure of cis-keto form of NSBA (determined at the CC2/cc-pVDZ geometry optimization of the E form); (c) the optimized geometry structure of trans-keto form of NSBA obtained at the MP2/cc-pVDZ level of theory.

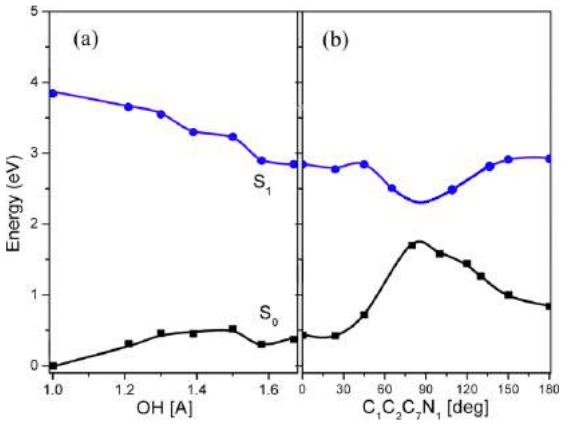

Fig. 2. Potential energy curves of the S0 state (squares) and the S_1 state (circles), as the functions of hydrogen transfer reaction path in the enol form of NSBA (a) and torsional reaction path in the keto form of NSBA (b). The energy origin is the energy of minimum enol in the ground state

III. Conclusions

The computational results of the present work suggest the following features of the photophysics of NSBA. The molecule is proton transfer from the hydroxyl group to the imine group. This reaction is predicted to be essentially barrier-less and thus extremely fast. The system switches from the S_1 surface to the S_0 surface and thus possible that the global minimum structure of NSBA is restored with a probability very close to unity, which is a requirement for the function of SBEA as an effective photostabilizer.

References

[1] H. Durr, H. Bouas-Laurent, "Photochromism: Molecules and Systems", 2003, 2nd Ed.; Elsevier: Amsterdam.

[2] M. Irie, Chem. Rev, 100 (2000) 1685-1716

A. L. Sobolewski and W. Domck, J. Phys. Chem. A, 111 (2007) 11725–11735.

[3] Ahlrichs, R.; Bär, M.; Häser, M.; Horn, H.; Kölmel, C, Chem. Phys. Lett, 162 (1989) 165−169

[4] Christiansen, O.; Koch, H.; Jørgensen, Chem. Phys. Lett, 243 (1995) 409−418.

بیست و سومین کنفرانس شیمی فیزیک انجمن شیمی ایران
23rd ICS Physical Chemistry Conference
Chemistry Department,
Faculty of Science
Shahid Bahonar University of Kerman
Kerman, Iran
12-13 Jan 2022
ایران، کرمان
دانشگاه شهید باهنر کرمان
دانشکده علوم پایه، بخش شیمی
۲۲-۲۳ دی ماه ۱۴۰۰

Quantum Chemical study of the Jahn – Teller Effect on the Distortions of XO_2 (X = O, S, Se, Te) Systems

Ali Esmaeili [a]

[a] *Department of Chemistry, Education,Markazi,mahallat.*
esmaeili.ali42031@gmail.com

Abstract

Preliminary researches provided essential information about the optimized configuration of triatomic XO_2 (X = O, S, Se, Te) systems, which were bent in the ground state and linear in their first excited state. The Jahn-Teller effects including the Jahn-Teller (JTE), the Renner-Teller effect (RTE), and the pseudo Jahn–Teller effect (PJTE) are parts of the most important reasons for structural distortion in the high–symmetry configurations for each molecular system. This study purpose was to investigate the dependence between PJT parameters including the vibronic coupling constant values (F), energy gap between reference states (Δ), and initial force constant (K_0). In all above mentioned molecules stability were increased with the reduction in the symmetry level. This increment was attributed to the PJTE. The vibronic coupling interaction between the ground (Σg), and the first excited states (Πu) through the PJTE problem (PJT (Σg+ Πu) × Πu) was because of the asymmetry and molecules bending phenomenon. The hardness difference parameter Δ[η (C_{2V}) -η ($D_{\infty h}$)] decreases from O to Te (30.42, 22.66, 22.65, 22.58 Kcal/mol). These changes could explain the trend, which were observed for the $D_{\infty h} \longrightarrow C_{2V}$ conversion process.

Keywords: the Jahn-Teller effect, vibronic interactions, Ab initio, Quantum, symmetry breaking

I. Introduction

Among the nanomaterials, supramolecular compounds are a group of nanoscale carriers with outstanding applications. Supramolecular nanocarriers are a diverse class of nanomateri- als whose interaction with the guest molecule is based on non-covalent interactions. Due to their reversible non-covalent in- teractions with guest molecules, this class of nanomaterials can alter their morphology, structure, or performance in response to some stimuli such as temperature, pH, light, enzyme, and inhibitory factors .

II. Methods

This study investigated the dependence between the PJT parameters (the vibronic coupling constant values (F), energy gap between reference states (Δ), and initial force constant (K_0). The configuration properties, global hardness, global electronegativity, and natural loads of XO_2 compounds (X = O, S, Se, Te) were attained by the means of time-dependent density functional theory (TD-DFT) (LC-$_W$PBE / Def2-TZVPP, B3LYP / Def2-TZVPP),

III. Results and discussion

Tables 1 and 2 displayed differences in electron energy ($E_0 = E_{ele} + ZPE$) between $D_{\infty h}$ and C_2v configurations from the compounds **1** to **4**, optimized with the B3LYP / Def2-TZVPP and LC-wPBE / Def2-TZVPP theory levels. Also, the zero point energy (ZPE) and energy parameters Δ [ZPE ($D_{\infty h}$) - ZPE (C_{2V})] of $D_{\infty h}$ and C_2v configurations for compounds **1** to **4** are summarized in the Tables 1 and 2 as followings:

The vibronic analysis is displayed in the $D_{\infty h}$ symmetry with 4 negative frequencies. These frequencies and their force constant values were summarized in Table 3. The vibronic modes symmetry of the negative frequencies are presented in the Fig. 1. The vibronic modes would change the molecular symmetry from the linear ($D_{\infty h}$) to the curved state (C_2v). The configurations distortion with the highest symmetry ($D_{\infty h}$) of compounds from **1** to **4** are because of the PJTE. These distortions main shares from configurations with the highest symmetry ($D_{\infty h}$) to (C_2v) the corresponding compounds symmetry are mainly because of the PJTE by mixing the ground (Σg) with the excited states (Πu). The mixing of Ψ_{HOMO} (Σg) and Ψ_{LUMO} (Πu) orbitals in these compounds is because of the PJTE two-level problem (Σg + Πu) × Πu.

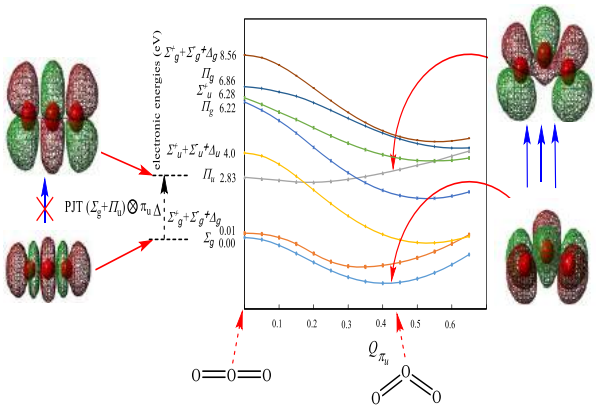

IV. Conclusions

This study purpose was to investigate the stability of the curved form (C_{2V}) of XO_2 molecules (X = O, S, Se, Te) with theory levels of (LC-$_W$PBE / Def2-TZVPP, B3LYP / Def2-TZVPP) and indicated that:

In all the molecules studied, stability level increases with reduction in the symmetry level. The elevated stability is attributed to the PJTE. The vibronic coupling interaction between the ground (Σg), and the first excited states (Πu) throughout the PJTE problem (PJT (Σg+ Πu) × Πu) is because of the asymmetry and molecules bending phenomenon. An increase in the stability of curved configurations (C_{2V}) in comparison with the linear configurations ($D_{\infty h}$) is compatible with the minimum energy principles (MEP), and maximum hardness principles (MHP).

References

[1] I B Bersuker, The Jahn–Teller Effect, Cambridge University Press, Cambridge, UK (2006)

[2]G.Kouchzkzadeh;D.Nori-Shargh,*Chem. Chem. Phys* **17** 29251-29261 (2015)

[3] W Zou, M Filatov and D Cremer, *Int. J. Quant. Chem* **112** 3277 (2012)

[4] H Kayi, I B Bersuker and J E Boggs, *J. Mol. Struct* **108** 1023 (2012)

بیست و سومین کنفرانس شیمی فیزیک انجمن شیمی ایران
23rd ICS Physical Chemistry Conference
Chemistry Department,
Faculty of Science
Shahid Bahonar University of Kerman
Kerman, Iran
12-13 Jan 2022
ایران، کرمان
دانشگاه شهید باهنر کرمان
دانشکده علوم پایه، بخش شیمی
۲۳-۲۲ دی ماه ۱۴۰۰

Symmetry breaking in the linear configurations of SX2 (X=F, Cl, Br, I): Pseudo-Jahn-Teller effect parameters, hardness and electronegativity

Ali Esmaeili [a]

[a] *Department of Chemistry, Education,Markazi,mahallat.esmaeili.ali42031@gmail.com*

Abstract

The instability of the curved structure in SX2(X=F ,Cl ,Br ,I) molecules due to the pseudo Jahn-Teller effect(PJTE) was investigated as an original PJTE study, which were bent in the ground state and linear in their first excited state.The effective parameters in vibronic coupling between reference states [HOMO(Πu)→ LUMO(Σg)] have been investigated in linear structures(D∞h).Calculations at the B3LYP/Def2-TZVPP level of theory produced the structural parameters, corrected electronic energies, electro negativity and hardness.The natural bond orbital (NBO)interpretation is associated with [Lp(3)X →σ*(1)S-X] to obtain stabilization energy (E(2)),vibronic coupling constant(Fij) and energy gaps between reference states(Δ).The interactions and effectiveness of these parameters with the structural parameters of the desired compounds were the focus of the study. In all above mentioned molecules stability were increased with the reduction in the symmetry level. The hardness difference parameter Δ[η (C2V) - η (D∞h)] decreases from F to I (44.05, 37.13, 30.19, 25.14 Kcal/mol).These changes could explain the trend, which were observed for the D∞h→ C2V conversion process.

Keywords: Pseudo-Jahn-Teller effect,vibronic coupling constant, The natural bond orbital, Stabilization energy

Introduction

These investigations indicate that the cause of the deviation from the linear structure in these combinations is the PJT-effect (PJTE). This effect converts high symmetry configurations in to low symmetry ones. In such system, electron transfer from the highest occupied molecular orbitals (HOMO) to the lowest unoccupied molecular orbitals (LUMO)changes the entire electron configuration.

The Jahn-Teller (JT) effect is one of the most fascinating researches of structure distortions that has been widely considered in experimental and theoretical studies for several years. Three types of JT distortions are the JT distortions of molecules in a degenerate electronic ground state, Pseudo JT (PJT) distortions in nondegenerate electronic states, and Renner-Teller (RT) distortions in a linear system.Any structural distortion of a polyatomic system is a consequence of the JT, PJT, or RTeffects.

Methods

All calculations were performed with the Gaussian09 program suite.The standard Def2-TZVPP basis set was used in the calculations. Using the hybrid functional of the B3LYP method, geometry optimization was conducted at each

stationary point found, confirming its identity as an energy minimum. The correlations between structural parameters and PJT parameters were investigated using natural bond orbital (NBO) interpretations

Results and discussion

Tables 1 and 2 displayed differences in electron energy ($E_0 = E_{ele} + ZPE$) between $D_{\infty h}$ and C_2v configurations from the compoundsSF_2,SCl_2,SBr_2andSI_2 optimized with the B3LYP / Def2-TZVPP and LC-wPBE / Def2-TZVPP theory levels.

The vibronic analysis is displayed in the $D_{\infty h}$ symmetry with 4 negative frequencies. These frequencies and their force constant values were summarized in Table 3. The vibronic modes symmetry of the negative frequencies are presented in the Fig. 1. The vibronic modes would change the molecular symmetry from the linear ($D_{\infty h}$) to the curved state (C_2v). The configurations distortion with the highest symmetry ($D_{\infty h}$) of compounds from **1** to **4** are because of the PJTE. These distortions main shares from configurations with the highest symmetry ($D_{\infty h}$) to (C_2v) the corresponding compounds symmetry are mainly because of the PJTE by mixing the ground (Σg) with the excited states (Πu). The mixing of Ψ_{HOMO} (Σg) and Ψ_{LUMO} (Πu) orbitals in these compounds is because of the PJTE two-level problem (Σg + Πu) × Πu.

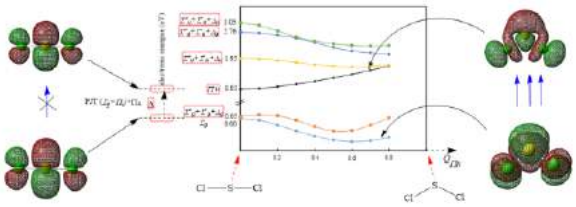

Figure 2: Energies of the ground and excited states and their change along the distortion coordinate $Q_{(\Pi u)}$of SX_2 molecules in the ($D_{\infty h}$).

Conclusions

In this investigation, we studied the instability of linear structure in SX2(X=F, Cl, Br, I) molecules at the B3LYP/Def2-TZVPP level of theory and observed the following: 1-In the studied molecules, descending of symmetry increased the stability of the molecule. This increase of stability is associated with the PJTE. 2-The vibronic coupling interaction between the (Σg) ground and the first (Πu) excited states through the PJT (Σg+Πu)×Πu PJTE problem was the causes of the symmetry breaking phenomenon and the curved in the studied molecules.

3-The increased stability of C2V structures in compared to D∞hstructures were compatible with the principles of minimum energy (MEP), and maximum hardness (MHP). 4-The differences between the E(2) values of strongest interaction for these structures decrease with decreasing of electronegativity of halogen and showed agood linear correlation with EJT.

References

[1] I.B Bersuker, The Jahn–Teller Effect, Cambridge University Press, Cambridge, UK (2006)

[2]G.Kouchzkzadeh;D.Nori-Shargh,*Chem.Chem. Phys.*,2015 ,**17** ,29251-29261.

[3] W Zou, M Filatov and D Cremer, *Int. J. Quant. Chem.*, 2012,**112,** 3277.

[4] H Kayi, I B Bersuker and J E Boggs, *J. Mol. Struct.*, 2012, **108,** 1023.

Compound	E_0	ΔE	r_{S-X}	$\Delta[r_{S-X}(D_{\infty h})-r_{S-X}(C_{2v})]$	θ_{S-X-S}	$\Delta[\theta_{X-S-X}(D_{\infty h})-\theta_{X-S-X}(C_{2v})]$
SF_2						
C_{2v}	-597.942923	0.0	1.6051	0.077	98.728	81.27
$D_{\infty h}$	-597.856811	54.036	1.6824		180.0	
SCl_2						
C_{2v}	-1318.662194	0.0	2.0390	0.130	104.130	75.87
$D_{\infty h}$	-1318.579631	51.244	2.1696		180.0	
SBr_2						
C_{2v}	-5546.584767	0.0	2.2067	0.132	105.359	74.64
$D_{\infty h}$	-5546.510188	46.80	2.3386		180.0	
SI_2						
C_{2v}	-993.838783	0.0	2.4088	0.137	106.870	73.13
$D_{\infty h}$	-993.769122	43.713	2.5463		180.0	

Table 1: Absolute energy (a.u),relative energy (kcal mol^{-1}),Structural parameters of linear ($D_{\infty h}$) and distorted (C_{2v}) configurations at B3LYP/Def2-TZVPP level of theory for 1 to 4.

Compound	SF_2	SCl_2	SBr_2	SI_2
ν_1	-386.6320	-323.6811	-282.2956	-289.3103
Force constant	2.1462	2.0281	1.6683	1.7207
Δ	2.84	0.93	0.57	0.08

Table 2: Calculating vibrational frequencies(cm^{-1}) of compounds 1-4.

Compound	r_{min}	E(min)	E_{JT}
SF_2	0.5	-597.9474138	54.48
SCl_2	0.6	-1318.6640357	51.71
SBr_2	0.7	-5546.5868663	47.21
SI_2	0.8	-993.8405051	44.05

Table 3: Minimum Absolute Energy Along the coordinate of the (Πu) Vibration ,Minimum Energy Point(Å) and JT Stabilization Energy(E_{JT},Kcal/mol)of SX_2 molecules(X=F,Cl,Br,I) at the B3LYP/Def2-TZVPP level of theory.

بیست و سومین کنفرانس شیمی فیزیک انجمن شیمی ایران
23rd ICS Physical Chemistry Conference
Chemistry Department,
Faculty of Science
Shahid Bahonar University of Kerman
Kerman, Iran
12-13 Jan 2022
ایران، کرمان
دانشگاه شهید باهنر کرمان
دانشکده علوم پایه، بخش شیمی
۲۳-۲۲ دی ماه ۱۴۰۰

Oxygen permeation through graphdiyne membrane

Maryam A. Rafiei[a*], **Ali Maghari**[b]

[a] *School of Chemistry, College of Science, University of Tehran, Tehran, Tel: 02161111; maryam.rafiei@ut.ac.ir*
[b] *School of Chemistry, College of Science, University of Tehran, Tehran, Tel: 02161111; maghari@ut.ac.ir*

Abstract

The present work aims to study the permeance of oxygen molecule through monolayer graphdiyne (GDY) by means of density functional theory (DFT) calculations. Various configurations of oxygen molecule, different sites of GDY, levels of theory and models for the adsorption process have been carried out by the ORCA program package.

Keywords: Graphdiyne; Membrane; Oxygen; Density Functional Theory

I. Introduction

Graphdiyne (GDY), a two-dimensional allotrope of graphene, is first synthesized in 2010 by Li's group [1]. It is constructed by substituting some carbon-carbon bonds in graphene with uniformly distributed diacetylenic linkages. GDY has attracted enormous attention due to its electronic, optical and mechanical properties. It has one-atom thickness and natural intrinsic uniform pores to guarantee the desired gas permeation. Recently, several studies have been separately carried out to explore the gas permeation property through [2, 3].

II. Methods

All DFT calculations were performed by using the ORCA 4.2.1 program package [4]. Several different functionals and basis sets have been studied and the PBE [5] along with def2/SVP basis set was used for the studied system.

III. Results and discussion

Different models including 1, 4, 8 and 18 pores have been studied and GDY with one pore and three hexagonal rings which is composed of 42 atoms in the (x,y) plane is adequate for the present study. All different distances and angles for oxygen molecule along with the GDY have been investigated. The obtained adsorption energy and equilibrium distance are -10.5 kJ/mol and 2.37 Å, respectively (Fig. 1). The transition structure of gas diffusion in the GDY membrane was studied by NEB-CI method. The electrostatic and van der Waals interactions between the oxygen molecule and membrane increase gradually with the decreasing of its distance, and reach the maximum value when the oxygen molecule is in center of the pore, perpendicularly. Total lowdin charges of the oxygen molecule at different positions with respect to GDY have been studied and its values have confirmed the previous results. The diffusion of oxygen molecule shows energy barrier of 12.5 kJ/mol. Cohesive energy as a property of membrane stability has been calculated and the result was 497.682 kJ/mol, which indicates that GDY has strong bonding in this study. The normal bond length of the oxygen molecule

has been changed as $\pm$10% for investigating consequence of applying field on system and results have shown that mentioned changes had no significant effect on adsorption energy, equilibrium distance and saddle point. Studies on passing multiple oxygen molecules through GDY have shown that two or more oxygen molecules cannot pass through one pore of GDY at the same time.

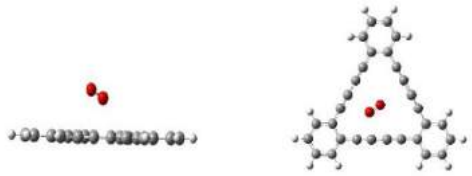

(a) (b)

Fig. 1. (a) side and (b) top views of adsorption configuration O_2 on GDY

IV. Conclusions

The adsorption and permeance behavior of oxygen molecule through GDY (with one pore and three hexagonal rings) was studied. The obtained values of equilibrium distance, adsorption energy and energy barrier was 2.37 Å, -10.5 and 12.5 kJ/mol, respectively. This study showed that GDY-O_2 had a good stability and only one oxygen molecule could pass through a pore of GDY.

References

[1] G. Li, Y. Li, H. Liu, Y. Guo, Y. Li and D. Zhu, Chemical Communications, 2010, 46, 3256-3258.
[2] M. Bartolomei, E. Carmona-Novillo, M. I. Hernández, J. Campos-Martínez, F. Pirani and G. Giorgi, The Journal of Physical Chemistry C, 2014, 118, 29966-29972.
[3] Y. Jiao, A. Du, S. C. Smith, Z. Zhu and S. Z. Qiao, Journal of Materials Chemistry A, 2015, 3, 6767-6771.
[4] F. Neese, WIREs Computational Molecular Science, 2012, 2, 73-78.
[5] J. P. Perdew and Y. Wang, Physical review B, 1992, 45, 13244

بیست و سومین کنفرانس شیمی فیزیک انجمن شیمی ایران
23rd ICS Physical Chemistry Conference
Chemistry Department,
Faculty of Science
Shahid Bahonar University of Kerman
Kerman, Iran
12-13 Jan 2022
ایران، کرمان
دانشگاه شهید باهنر کرمان
دانشکده علوم پایه، بخش شیمی
۲۳-۲۲ دی ماه ۱۴۰۰

The effect of wall structure on sound

Fahimeh Mokhtari[a], Mohammad Kmalvand[b,*]

[a] *Department of Physical Chemistry, Yazd University, Yazd, Iran, fahimehmokhtari@stu.yazd.ac.ir*
[b] *Department of Physical Chemistry, Yazd University, Yazd, Iran, Kamalvand@yazd.ac.ir*

Abstract

Sound wave propagation in argon gas is simulated using molecular dynamics (MD) to determine the attenuation of acoustic energy at high frequencies. This study shows the effect of sound source and reflector wall structure on sound parameters in a system containing argon gas. This approach shows that using structurless wall instead of a real wall does not significantly change the results for sound components and the resulting sound velocity value is closer to the experimental data.

Keywords: Sound speed; Structurless wall; Sound attenuation; Molecular dynamics simulations; LAMMPS.

I. Introduction

Noise is a common problem in almost every engineering application incorporating a mechanical device or fluid motion that can act as a noise generating source, such as home appliances, buildings, vehicles, and aircraft [1]. An effective technique for limiting noise to an acceptable level is to block the sound transmission path and absorb the sound energy using acoustic porous absorbers [2]. Molecular dynamics (MD) is a suitable method to simulate the of nanoscale sound absorption. In addition, the simulations would need to be extended into the millisecond time scale to permit the study of acoustic wave propagation in the audible frequency range (0.02-20 kHz), which would require considerable computational resources. Thus, performing MD simulations to explore acoustic absorption mechanisms at the nanoscale in the audible frequency range would not be feasible with the available computational resources. Therefore, the study of MD simulations for sound wave propagation is limited to acoustic frequencies in the gigahertz (GHz) range [3]. Nicholas and Alejandro studied the propagation of high-frequency sound waves in a dilute gas using the Monte Carlo Direct Simulation (DSMC) technique [4].Yano studied acoustic waves using molecular dynamics, although their focus was on qualitative discussion of wave propagation [5]. Ayub et al. studied the waveform created in the vicinity of the source, by a sine wave oscillation wall consisting of high-frequency solid argon particles [6]. The difference between this article and others is that instead of a wall composed of solid argon particles, a structureless wall has been used which in addition to reducing the difference between the speed of sound from the simulation and experimental data also saves computation time.

Methods

Molecular dynamics (MD) simulations were performed to propagate sound waves at a frequency of 1.5 GHz. The amplitude of the simulation has transverse dimensions

$L_x = L_y = 15.5$ nm and length $L_z = 150$ nm, which is approximately equal to half the sound wavelength ($L \approx 4\lambda/7$). Figure 1 shows a diagram of the simulation domain. The simulation domain ended in the z direction with a reflective structureless wall and a structurless wall was used as the audio source. Wall oscillation occurs by imposing a sine velocity in the z direction. Periodic boundary conditions were used in the directions perpendicular to the wave propagation. The simulation after 2ns equilibrated at temperature T= 273 K and pressure P= 1 atm with gas ρ= 1.8 Kgm^3. Then the oscillation of the piston with a velocity amplitude V= 0.15c= 49.69 m/s started sinusoidally to move the system with a sound wave with a frequency of 1.5 GHz. A Nose-Hover thermostat was used to control the gas temperature because the work done on the gas by the sound source causes the gas to heat up. A time step of 0.5 fs was used during gas equilibrium and a time step of 1 fs was used during wave propagation. This simulation run at approximately 67 ns, which is equivalent to 100 cycles of the emission wave cycle.

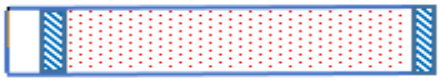

Fig 1. Schematic of MD simulation domain for acoustic wave propagation in argon gas.

II. Results and discussion

The non-linear fitting of the standing wave equations can be used to predict the acoustic parameters such as the sound speed (c) and attenuation coefficient (m) from the wave pattern of the particle velocity. Figure 2 shows the waveform of the cosine and sine components of the velocity amplitude for the simulation data obtained from the structurless wall and real wall.

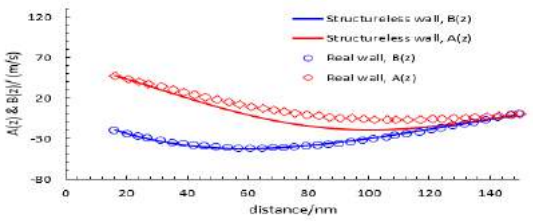

Fig 2. Non-linear curve fit to cosine and sine components, A(z) and B(z), of the velocity amplitude as a function of distance for acoustic wave frequency f =1.5GHz. The predicted values for sound speed and attenuation for structurless wall and solid argon wall respectively are: c = 397 m/s, m = 0.895m-1 and c = 435 m/s, m = 0.914m-1 [6].

III. Conclusions

As can be seen in Figure 2, there is no noticeable difference in the velocity curve of the two systems with the structurless and real walls. On the other hand, the value of sound speed obtained in this article is closer to the experimental sound speed (c = 307 m/s). Also, due to the reduction in the number of particles in the system with unstructured walls, computation time is dramatically reduced.

References

[1] M.J. Crocker, and J.P. Arenas, Use of sound-absorbing materials. Handbook of noise and vibration control, 2007, 696-713.
[2] J.P. Arenas, and M.J. Crocker, Recent trends in porous sound-absorbing materials. Sound & vibration, 2010, 44(7), 12-18.
[3] M. Allen, and D. Tildesley, Comput Simul Liq, Oxford University Press, Oxford, 1989.
[4] N.G. Hadjiconstantinou, and A.L. Garcia, Molecular simulations of sound wave propagation in simple gases. Physics of Fluids, 2001, 13(4), 1040-1046.
[5] T. Yano, Molecular dynamics study of sound propagation in a gas. in AIP conference proceedings, American Institute of Physics, 2012.
[6] M. Ayub, et al., Molecular dynamics simulations of classical sound absorption in a monatomic gas. Journal of Sound and Vibration , 2018, 421, 319-333.

بیست و سومین کنفرانس شیمی فیزیک انجمن شیمی ایران
23rd ICS Physical Chemistry Conference
Chemistry Department,
Faculty of Science
Shahid Bahonar University of Kerman
Kerman, Iran
12-13 Jan 2022
ایران، کرمان
دانشگاه شهید باهنر کرمان
دانشکده علوم پایه، بخش شیمی
۲۳-۲۲ دی ماه ۱۴۰۰

Comparison of thermal theory and density theory of flame propagation for evaluating the flammability limits of fuel-air-diluent mixtures

Ali M. Nassimi[a]*, Ghazal Shafiee[b]

[a] *Department of Chemistry, Sharif University of Technology, Tehran, Iran ; Tel: +98 21 6616 5377; E-mail: a.nassimi@sharif.edu*

[b] *Department of Chemistry, Sharif University of Technology, Tehran, Iran ; Tel: +98 21 6616 5318; E-mail: Gh4.shafiee@gmail.com*

Abstract

Present work, with general reference to the density theory of flame propagation, describes a model that considers the effect of inert gas dilution on the flammability limits of the fuel-diluent mixtures and compares these results with experimental data and the results obtained from thermal theory.

Keywords: Flammability limits; Explosive limits; Adiabatic flame temperature; Density factor.

I. Introduction

Lower flammability limit (LFL) and upper flammability limit (UFL) define the gas concentrations between which a flame propagates after ignition. These two limits are very important safety considerations. It is common to add an Inert gas to the flammable gas mixtures and vapors to reduce the probability of combustion and explosion. Since it is not practical to measure flammability limits for mixtures with every composition, a method that predicts flammability limits seems essential [1].

According to the thermal theory of flame propagation, a flame can only propagate above a specific temperature threshold; similarly, according to the density theory of flame propagation, flame only propagates above a specific density factor threshold. Nassimi et al. defined density factor as the ratio of the flammable mixture density before ignition to after ignition density [2], [3].

II. Methods

First, the adiabatic flame temperature and density of the resulting mixture corresponding to each equivalence ratio, φ, are calculated by "Chemical Equilibrium and Applications" (CEA) software. Where equivalence ratio, φ, is the ratio of available fuel to the total fuel needed to stoichiometrically consume all available oxidant. Chemical equilibrium is calculated for a range of diluent ratios in fuel, as a function of the equivalence ratio. Next, the graph of AFT (DF)-φ is drawn. AFT (DF) values are then calculated using this graph for φ_{LEL} and φ_{UEL}. These parameters show the equivalence ratio for the mixture at the LFL and the UFL, respectively. This is depicted in figure (1) for NH_3.

Past work in our group used a general version of the thermal theory of flame propagation and introduced a general version of density theory of flame propagation to predict flammability limit for flammables for which experimental FL data are not available [2], [3]. Present work uses specific versions of thermal theory and density theory for predicting FLs of fuel-inert mixtures. This work assumes the same adiabatic flame temperature at the FLs as

pure combustible chemicals to predict the UFL and the LFL of the mixtures of fuel and diluent in different ratios. In the same way, this work uses the same density factor at the FL as pure combustible chemicals to predict the LFL and UFL of the flammable gas-inert mixtures.

Estimates are based on thermal theory and density theory for mixtures of methane, propane, propylene, and isobutane fuels with diluents of nitrogen, carbon dioxide, and chloroform in the presence of air as oxidizer.

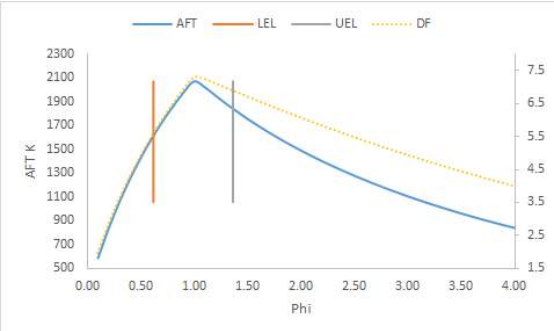

Fig. 1. AFT (right vertical axis) and DF (left vertical axes) based on the values of equivalence ratio (φ) for NH_3.

III. Results and discussion

This work reports that density theory predicts LFL of the fuel-diluent mixtures as well as thermal theory. For UFL, nevertheless, density theory was much more accurate than thermal theory for the most part. Note the caveat that the fuel type and the diluent can lead to varying accuracy in the calculated results.

IV. Conclusions

The present study proposes using the adiabatic flame temperature of pure combustible chemicals at lower flammability limits to determine lower flammability limits of fuel-diluent mixes in different ratios. It is also suggested that the density factor at upper flammability limits of pure combustible chemicals be used to estimate the upper flammability limits of mixtures of fuel and diluent in various proportions.

References

[۱] Liaw H. J, Chen C. C, Chang C. H, Lin N. K, and Shu C. M, *Industrial & Engineering Chemistry Research* Model To Estimate the Flammability Limits of Fuel−Air−Diluent Mixtures Tested in a Constant Pressure Vessel, 2012, 51

[۲] Nassimi A. M, Jafari M, Farrokhpour H, and Keshavarz M. H, *Chemical Engineering Science* Constants of explosive limits, 2017, 173, 384

[۳] Nassimi A. M, *Fire and Materials* Predicting flammability limits through thermal theory and density theory of flame propagation, 2021, 1-8

بیست و سومین کنفرانس شیمی فیزیک انجمن شیمی ایران
23rd ICS Physical Chemistry Conference
Chemistry Department,
Faculty of Science
Shahid Bahonar University of Kerman
Kerman, Iran
12-13 Jan 2022
ایران، کرمان
دانشگاه شهید باهنر کرمان
دانشکده علوم پایه، بخش شیمی
۲۳-۲۲ دی ماه ۱۴۰۰

Investigation of Spin Coating Technique on Efficiency of Zn(II) doped- $LaCrO_3$ Perovskite Solar Cells

Zohreh Rashidi Ranjbar*, Solmaz Morshedi Nodez

Address: Department of Chemistry, Faculty of Sciences, Shahid Bahonar University of Kerman, Kerman, Iran;
**Email:zoh.rashidi@gmail.com*

Abstract:

High-efficiency solar cells are rarely used in normal applications today due to their very complex structure and very expensive raw materials. The use of perovskite solar technology is very cheap and it has a simple process for processing into photovoltaic cells. In this project, $LaCrO_3$/Zn(II) doped perovskite structure was by co-precipitation method in the perovskite structure. We used spin coating technique for producing photo anode. The structure, shape and morphology of all compounds were identified. Using UV-Vis spectroscopy, the energy gap was calculated. At the end, estimated performances from two techniques, doctor blade and spin coating, were compared.

Keywords:
Solar cell; Energy gap; Spin coating; Perovskite.

I. Introduction

Perovskite solar cells are low cost, easy preparation and flexibility and have become the research focus in the field of photovoltaic technology [1]. Thin film solar cells are a promising approach for photovoltaics and offer a wide variety of choices in device design and fabrication [2]. There are various techniques in thin film coating such as Chemical Vapor Deposition (CVD) and Physical Vapor Deposition (PVD) and spin coating method [3].

Herein, we synthesize $LaCrO_3$/Zn(II) doped perovskite by co-precipitation method. Then, we use spin coating for the fabrication of thin film of solar cell layers. The comparison in performances was done between two techniques, doctor blade and spin coating.

II. Methods

To prepare $LaCrO_3$/Zn(II) doped, stoichiometric amounts of lanthanum nitrate and chromium nitrate (1:1 ratio) and 0.5 mmol of zinc(III) chloride were dissolved in 10 mL methanol. This mixture is stirred with the help of a magnetic stirrer at 90 ℃ for 10 min. After adding 0.1 M NaOH up to the solution doped sample were precipitated. 5drops of sample is taken and dispensed at the center of the glass substrate and rotated at 200 rpm.

III. Results and discussion

The synthesis of $LaCrO_3$/Zn(II) doped perovskite thin film for solar cell application by using spin coating technique has successfully done and were characterized using different analytical techniques (IR spectroscopy, X-ray powder Diffraction (XRD), Energy Dispersive X-ray Spectroscopy (EDAX)).

The absorbance spectrum of $LaCrO_3$/Zn(II) doped was obtained by UV–Vis spectroscopy. The optical band gap of $LaCrO_3$/Zn(II) doped is calculated by using Tauc's Plot (Figure 1). The value is about 3.12 eV. It shows the semiconductor behavior of $LaCrO_3$/Zn(II) doped.

To investigate photovoltaic properties, FTO/ TiO_2/ $LaCrO_3$/Zn(II) doped /electrolyte/C/FTO were fabricated.

The results showed the power conversion efficiency of $LaCrO_3$/Zn(II) doped perovskite solar cells is 0.019% with the open circuit voltage (Voc) of 0.107 V, the short circuit current density (Jsc) of 76 mA/cm^2 and the filling factor (FF) of 0.54% (Table 1).

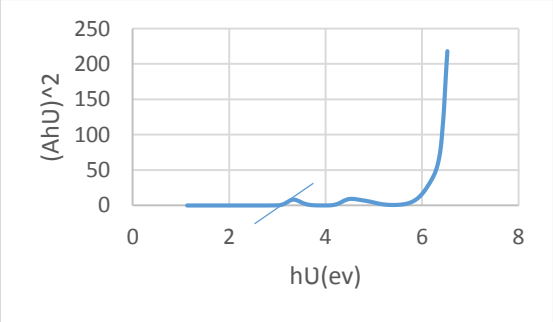

Fig. 1. Tauc plot of $LaCrO_3$/Zn(II) doped perovskite.

Table 1. **Photovoltaic parameters of $LaCrO_3$/Zn(II) doped perovskite soalr cells**

Parameter	V_{oc} (mV)	J_{sc}(mA/cm^2)	FF(%)	PCE(%)
	106.9	76	0.54	0.0192

IV. Conclusions

In this study, the effect of spin-coating method on photovoltaic property of $LaCrO_3$/Zn(II) doped perovskite was analyzed. The performances from two techniques, doctor blade and spin coating, were compared and there was not dramatically difference between these two methods.

References

[1] J.-H. Lee, K. Jung and M.-J. Lee, *Journal of Alloys and Compounds*, 2021, 879, 160373-160381.

[2] N. M. Laya, R. R. Zohreh, *Journal of Alloys and Compounds*, 2019, 785, 117-124.

[3] A.V. Shah, H. Schade, M. Vanecek, J. Meier, E. Vallat-Sauvain, N. Wyrsch, Kroll, C. Droz, J. Bailat, *Prog. Photovolt: Res. Appl.* 2004, 12, 113–142.

بیست و سومین کنفرانس شیمی فیزیک انجمن شیمی ایران
23rd ICS Physical Chemistry Conference
Chemistry Department,
Faculty of Science
Shahid Bahonar University of Kerman
Kerman, Iran
12-13 Jan 2022
ایران، کرمان
دانشگاه شهید باهنر کرمان
دانشکده علوم پایه، بخش شیمی
۲۳-۲۲ دی ماه ۱۴۰۰

Calculation of non-adiabatic coupling terms between the ground X^2A_1 and first excited A^2B_2 electronic states of NO_2 molecule

Afsaneh Nazari[a,*], Maryam Dehestani[a] Leila Zeidabadinejad[a]

[a] *Department of Chemistry, Shahid Bahonar University of Kerman, Kerman, Iran, nazari.afsane@yahoo.com*

Abstract

In the present work, the non-adiabatic coupling terms are investigated between the ground X^2A_1 and the first excited A^2B_2 electronic states of NO_2 molecule. At the first, the high-level quantum chemical method like CASSCF is applied to determine the conical intersection geometry between the ground and the first electronic states. The changes of non-adiabatic coupling terms with bond angular and bond length are computed by Molpro program. The calculations have been carried out in three contours around one atom. Finally The conversion of adiabatic to diabatic angle have been calculated for this molecule.

Keywords: Non-adiabatic coupling, quantum chemical method, Conical intersection, Molpro program

Introduction

Conical intersections (CIs) play a major role in the excited-states dynamics of simple polyatomic systems [1]. In the pervious studies, conical intersection is important in the molecular spectroscopy [2]. The investigation of the conical intersection is based on the following potential matrix [3,4]:

$$W = k\begin{pmatrix} y & x \\ x & -y \end{pmatrix} \qquad (1)$$

In attention to Eq(1), k is a constant and x and y are Cartesian coordination [3]. The none- adiabatic coupling term can be defined as :

$$\tau_{12} = \langle \psi_1 | \nabla \psi_2 \rangle \qquad (2)$$

Where, ψ_1 and ψ_2 are the diabatic eigenfunctions [3].

NO_2 is difficult system to evaluate in the cross-section of two lowest electronic states.

I. Methods

The location of the conical intersection geometry between the ground and first electronic states is explored and Molpro program is employed to obtain the changes of non-adiabatic coupling terms with bond angular and bond length. All calculations are carried out by CASSCF/cc-pVTZ level of theory [5].

II. Results and discussion

In this research, the conical intersection of NO_2 is occurred between the ground X^2A_1 and the first excited A^2B_2 electronic states at bond length 1.47Å and bond angular 108°. Also, non-adiabatic coupling terms are investigated in three contours around one atom including q= 0.2,0.3and 0.4Å. Fig.1 demonstrates the desired contour along the bond and angle at which the non-adiabatic coupling is computed. The values of r_{2x} and θ_x are respectively 1.07Å and 126°. The conversion of adiabatic to diabatic angle can be expressed :

$$\alpha(\Gamma) = \oint_\Gamma dQ.\lambda(Q|\Gamma) = n\pi \qquad (3)$$

Table 1 displays the values of α_{12} for NO_2 molecule. In q=0.4Å, the value of α_{12} is not multiple of π due to the perturbation is created. The plots of changes τ_{r2} and τ_{φ} in terms of φ for q=0.4Å are represented in Figs. 2and 3. In order to Fig2, τ_{r2} changes the sign at $\varphi = 190°$ and the significant deviation is observed at $\varphi = 196°$. Fig3, demonstrates which the values of τ_{φ} is minus from $\varphi = 0°$ to $\varphi = 200°$. It is concluded that the conical intersection for NO_2 molecule comes out at q=0.4Å.

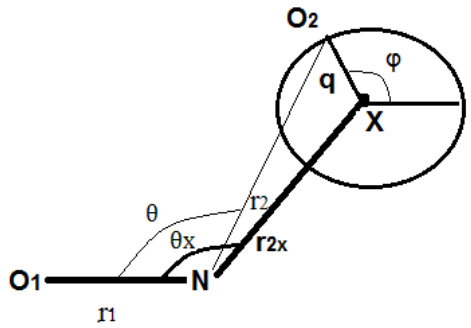

Fig. 1. The integral contour along a circular path with radius q, equilibrium bond length r_1=1.204 Å and equilibrium bond angular $\theta = 134°$.

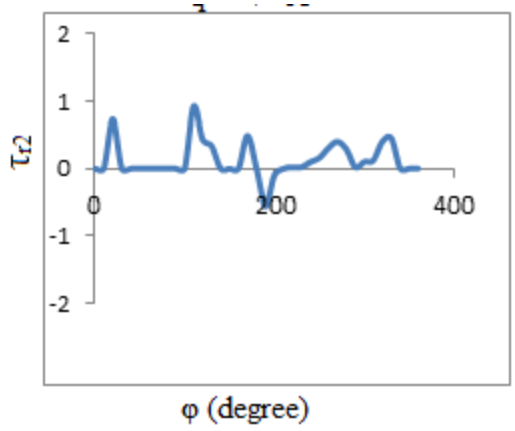

Fig. 2. The diagram of changes of τ_{r2} in terms of φ

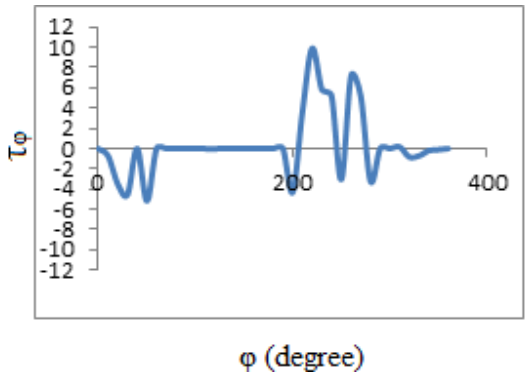

Fig. 3. The diagram of changes of τ_{φ} in terms of φ

Table 1 The values of α_{12} for NO_2 molecule

q(Å)	α_{12}	cos α_{12}
0.2	6.7858	0.8763
0.3	3.2673	-0.9921
0.4	2.9531	-0.9821

III. Conclusions

In the present research, non-adiabatic coupling terms between the ground X^2A_1 and the first excited A^2B_2 electronic states of NO_2 molecule are assessed theoretically. The conical intersection for NO_2 is located at bond length 1.47Å and bond angular 108°. CASSCF/cc-pVTZ level of theory is used to determine conical intersection. The changes of non-adiabatic coupling terms with bond angular and bond length are computed by Molpro program. At q=0.4Å, there is perturbation in NO_2 molecule. It is found that conical intersection occurs in this q.

References

[1] Y. Arasaki, K. Takatsuka, and W. Kwanghsi, J. Chem. Phys., 2010,129, 124307.
[2] M. Bear, Chem. Phys., 2000, 259,123-147.
[3] M. Bear, A. M. Mebel, and R. Englam, Chem. Phys. Lett., 2002,354, 243-250.
[4] M. Baer, Chem. and A. Alijah, Phys. Lett., 2000, 24, 489-493.
[5] R. Krishnan, M. Frisch, and J. A. Pople, J. Chem. Phys., 1980, 72, 650-654.

بیست و سومین کنفرانس شیمی فیزیک انجمن شیمی ایران
23rd ICS Physical Chemistry Conference
Chemistry Department,
Faculty of Science
Shahid Bahonar University of Kerman
Kerman, Iran
12-13 Jan 2022
ایران، کرمان
دانشگاه شهید باهنر کرمان
دانشکده علوم پایه، بخش شیمی
۲۳-۲۲ دی ماه ۱۴۰۰

Photocatalytic activity of co-doped TiO_2 nanoparticles under UV and visible light

Rezvaneh Amrollahi

[a] *Department of Physics, Iran University of Science and Technology, Tehran, Iran*

*AmrollahiR@iust.ac.ir

Abstract

M/TiO_2 (M=Ag,Cr,Cu,V,Pt) was synthesized by standard sol-gel methods. The resulting materials were extensivelly characterized by means of X-ray diffraction (XRD), BET surface-area measurements, Raman spectroscopy, and UV-Vis spectroscopy and Transmission electron microscopy (TEM). UV-Vis spectroscopy demonstrated a clear shift in the absorbance of the catalysts towards the visible light region. The photocatalytic activity of M/TiO_2 was evaluated in the oxidation of methylcyclohexane (MCH) under the illumination of UV and visible light. The conducted reactions were monitored by in situ ATR-FTIR technique. The photocatalytic acivity of Cr/TiO_2 showed much better conversion of MCH under visible light illumination compared with the parent of other M/TiO_2.

Keywords: TiO_2, photocatalysis, selective oxidation, nanoparticles and methylcyclohexane.

I. I. Introduction

Photocatalysis has been reported to be a feasible method to synthesize various products of hydrocarbon oxidation. Among many photocatalysts, TiO_2 is the most promising for practical use because it has the most efficient activity, the highest stability and the lowest cost. Unfortunately, TiO_2 is only effective under ultraviolet irradiation (<387 nm) which accounts for only 4% of the solar energy due to its large band gap (3.2 eV for anatase), and hence, improving the photocatalytic activity of TiO_2 in the visible region is a major focus of the TiO_2 photocatalysis research community [1,2].

Various approaches have been studied including doping with metal ions (e.g. V, Cr, Fe, Co, Mn, Mo, Ni, Cu, Y, Ce, and Zr) or nonmetallic elements (e.g., S, C, N) to enhance In this study, we address the M/TiO_2 (M=Cr, V, Cu, Ag, Pt) prepared by sol-gel method. The photocatalytic activity of photocatalysts tested in liquid phase conversion of methylcyclohexane to methylcyclohexanone. Photocatalytic activity was assessed by *in situ* ATR-FTIR spectroscopy.

II. Methods

TiO_2 nanoparticles (NPs) were prepared by standard sol-gel methods. After one day, the suspension was dried in the oven (80 ^{o} C) for 8 hours. The obtained powders were calcined at 400 o C for 1 hour under air. Doped TiO_2 samples (M/TiO_2) were prepared by adding a metal precursor to the mQ water prior to the TTIP to provide a doping level of 1wt%. Platinum (Pt), chromium (Cr), vanadium (V), silver (Ag) and coper (Cu) were chosen as metal-ion dopants in this study.

III. Results and discussion

UV-Vis spectroscopy was employed to investigate absorption characteristics of the

metal doped TiO_2 photocatalysts. The UV-vis absorption spectra are presented in Figure 1. The UV–vis spectrum of sol-gel TiO_2 is also shown for comparison. As expected, the absorption edge of TiO_2 is located at approximately 395 nm. The IR spectra of the products formed by MCH oxidation after photoexcitation at 425 nm or 375 nm of M/TiO_2 (M=Cr, V, Cu, Pt and Ag) for a period of 100 minutes, are compared in Figures 2a and 2b, respectively. Clearly, the Cr/TiO_2 sample is photocatalytically more active than others at both conditions (illumination at 375 or 425 nm). On the other hand, the Cr/TiO_2 and V/TiO_2 samples show much more significant conversion at 375 nm as compared to at 425 nm.

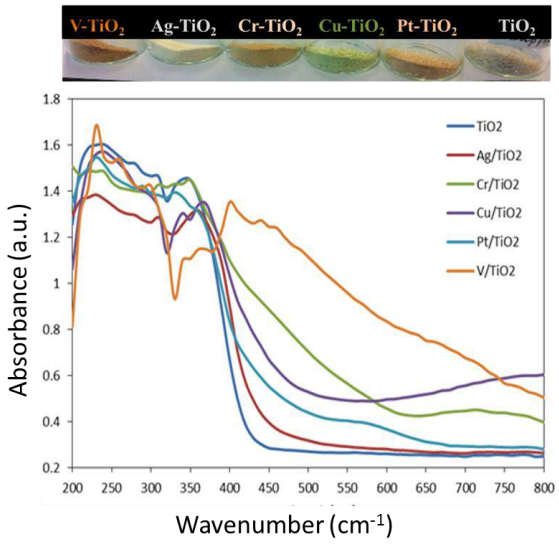

Figure 1: The UV-Vis spectrum of by M/TiO_2 (M=Cr, V, Cu, Pt, Ag) as compared to TiO2 sample.

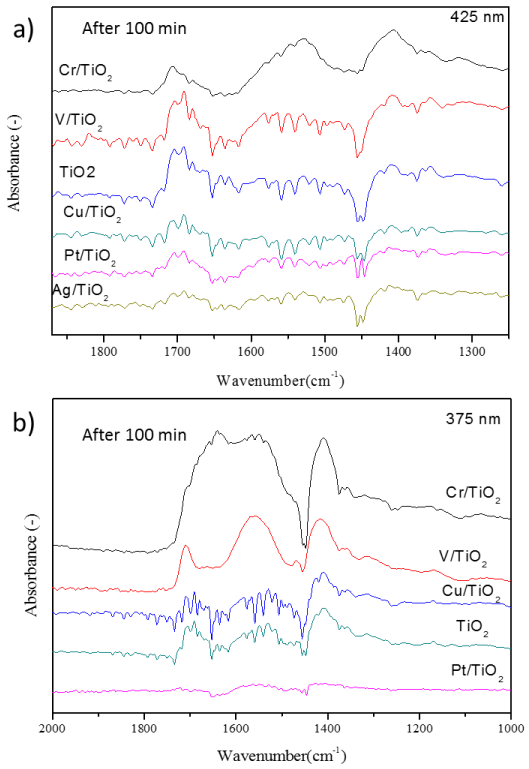

Figure2: The collected spectra of photo oxidation of MCH catalyzed by M/TiO_2 (M=Cr, V, Cu, Pt or Ag) and TiO_2. Illumination at 425 nm (a) or 375 nm (b) was applied. Spectra were measured in ATR mode after 100 min of reaction time.

IV. Conclusions

In conclusion, of the dopants investigated (Ag,Cu, Pt, V, Cr and Cu), Cr is the most effective in promoting visible light activity of TiO_2 in the oxidation of MCH. The Apparent Quantum Efficiency (AQE) of the most effective catalyst amounts to 4.5%.

References

[1] R. Amrollahi, M.S. Hamdy, G. Mul, Understanding promotion of photocatalytic activity of TiO_2 by Au nanoparticles, Journal of Catalysis, 319 (2014) 194-199.

[2] Y. Ding, Y. Wang, L. Zhang, H. Zhang, C.M. Li, Y. Lei, Preparation of TiO_2-Pt hybrid nanofibers and their application for sensitive hydrazine detection, Nanoscale, 3 (2011) 1149-1157.

بیست و سومین کنفرانس شیمی فیزیک انجمن شیمی ایران
23rd ICS Physical Chemistry Conference
Chemistry Department,
Faculty of Science
Shahid Bahonar University of Kerman
Kerman, Iran
12-13 Jan 2022
ایران، کرمان
دانشگاه شهید باهنر کرمان
دانشکده علوم پایه، بخش شیمی
۲۳-۲۲ دی ماه ۱۴۰۰

Room temperature selective (photo) catalytic oxidation of ethanol to acetaldehyde over Pt/WO_3

Rezvaneh Amrollahi

[a] *Department of Physics, Iran University of Science and Technology, Tehran, Iran*

*AmrollahiR@iust.ac.ir

Abstract

Oxidation of ethanol to acetaldehyde is of relevance to synthetic chemistry and development of sensors for detection of gas phase ethanol. It is demonstrated by gas phase analysis and diffuse reflectance infrared Fourier transform spectroscopy (DRIFTS) that a Pt/WO_3 composite shows significant activity in oxidative dehydrogenation of ethanol to acetaldehyde at room temperature. DRIFTS also demonstrates consecutive surface chemistry occurs, yielding predominantly ethyl acetate. The oxidation state of the most active Pt particles is determined to be Pt0, rather than PtO. Illumination has very little effect on surface reactivity and selectivity, but promotes formation of gas phase acetaldehyde.

Keywords: Photocatalyst, Selective oxidation, Nano materials, Pt/WO_3

I. Introduction

WO_3 has outstanding stability in acidic conditions, and favorable electron conductive properties. Besides in photocatalysis, WO_3 is used in electrochromic displays, gas sensors, solar energy devices, and field-emission devices. Several methods, including thermal evaporation, sol-gel processes, and hydrothermal reactions, have been reported for synthesis of WO_3 (nano) particles. To enhance performance of WO_3, in particular in sensing and photocatalytic applications, functionalizing of the material with noble metals such as Pt, Au, or Pd has been demonstrated effective. However, in both sensing of alcohol concentrations in aerobic conditions, as well as in gas phase catalytic oxidation of alcohols, little is known with respect to the oxidation state of the most active Pt particles, and the chemical transformations of ethanol occurring upon interaction with the catalyst (or sensor) surface. Here we report such insight on the basis of analysis of DRIFTS. The relevance of the data for sensor applications will be discussed in detail.

II. Results and discussion

Figure 1 illustrates TEM images of Pt/WO_3 (imp). Pt nanoparticles are present with an average size of 2.66 nm, with the smallest particles being 1.14 nm, and the largest approximately 4.69 nm.

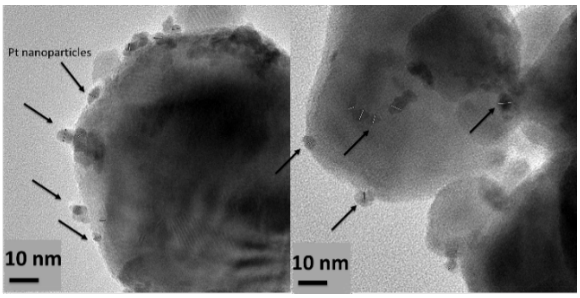

Figure 1. TEM images of Pt/WO_3 (imp)

It also appears that isolated Pt particles are present in other domains of the WO_3 particles.

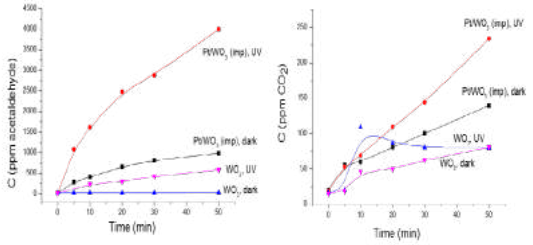

Figure 2. Concentration of products vs reaction time for ethanol oxidation over Pt/WO_3 (imp) and WO_3 in the absence or presence of illumination by a 365 nm LED source. (Left) acetaldehyde and (Right) CO_2. The product composition was measured by GC analysis.

The obtained product distributions of the oxidation of ethanol as a function of time (reaction in dark or

illumination) are shown in **Figure 2.** Oxidation of ethanol catalyzed by Pt/WO_3 yields a significant gas phase concentration of acetaldehyde. A very small amount of CO_2 was formed as detected by the GC analysis.

Remarkably, the quantities of acetaldehyde and CO_2 produced by WO_3 were significantly smaller than in the case of Pt/WO_3. The addition of Pt thus results in both a higher acetaldehyde production rate, and a significantly higher rate in formation of CO_2. Surprisingly, for Pt/WO_3, acetaldehyde formation was observed as well without any illumination. This phenomenon was not observed for WO_3.

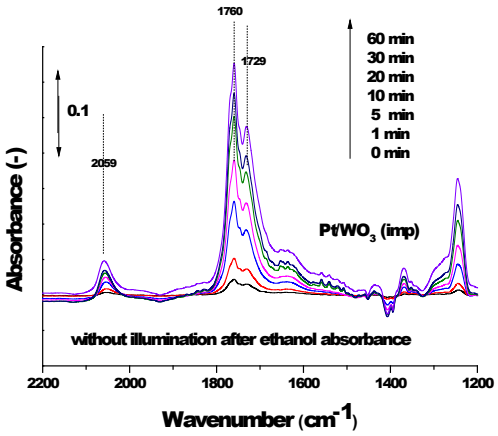

Figure 3. Time resolved DRIFT spectra in the 2200–1200 cm^{-1} region obtained during oxidation of ethanol over Pt/WO_3 (imp) in the dark.

The acetaldehyde amounts observed, allow for calculation of a rate of around 0.01 mmol/g/hr over Pt/WO_3 (imp) at 365 nm. Also, given the used light intensity, an apparent quantum efficiency of 1.25% to acetaldehyde can be calculated, defined as the amount of moles produced (per hour), divided by the amount of photons which entered the reactor (8×10^{-5} einsteins/h at 365 nm). Photocatalytic conversion using catalyst coatings based on TiO_2. These values are in the same order of magnitude as normally observed in Surface chemistry.

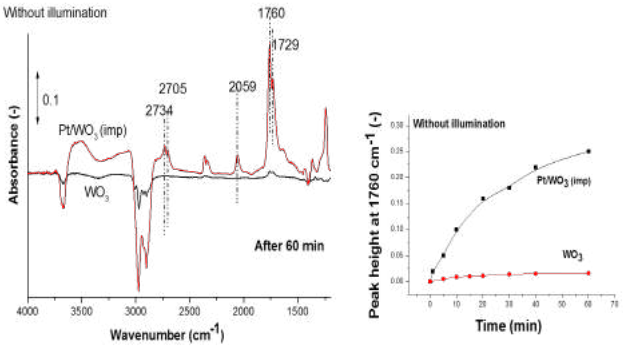

Figure 4. (Left) DRIFT spectra obtained after 60 minutes of oxidation of ethanol without illumination over Pt/WO_3 (imp) and WO_3. (Right) Development of peak height at 1760 cm^{-1} as a function of time for the same experiments.

The analysis of the surface chemistry occurring during the oxidation of ethanol over Pt/WO_3 is shown in **Figure 3** as a function of reaction time (from 0 to 60 min). The *in situ* DRIFTS spectra were obtained in the absence of illumination. Two strong bands grow in at 1760 and 1729 cm^{-1}. The 1729 cm^{-1} band is assigned to the ν (C=O) vibration of acetaldehyde (**Figure 4**).

III. Conclusions

The activity and selectivity of Pt/WO_3 materials depend strongly on the nature of the Pt species. By impregnation, a significant fraction of Pt was formed (approximately 50% of Pt was in the metallic state) and this resulted in an effective catalyst. The activity could be further improved by hydrogenation of the impregnated sample, which contained exclusively. The rate of formation of surface adsorbed acetaldehyde was not much affected by the absence or presence of light, while the gas phase production rate was significantly higher in the presence of light. We propose this is due to light stimulated desorption of the product acetaldehyde.

IV. References

[1] Amrollahi, R., Wenderich, K., Mul, G. Room Temperature Oxidation of Ethanol to Acetaldehyde over Pt/WO_3. *Adv. Mater. Interfaces*, 3: 1600266. doi: 10.1002/admi.201600266

بیست و سومین کنفرانس شیمی فیزیک انجمن شیمی ایران
23rd ICS Physical Chemistry Conference
Chemistry Department,
Faculty of Science
Shahid Bahonar University of Kerman
Kerman, Iran
12-13 Jan 2022
ایران، کرمان
دانشگاه شهید باهنر کرمان
دانشکده علوم پایه، بخش شیمی
۲۳-۲۲ دی ماه ۱۴۰۰

Synthesis of silver nanoparticles in aqueous and organic media and their application in increasing the efficiency of dye sensitized solar cells

Sheybani Nazila [a,*]; Roohllamini Nejad Dr Hossein[b]; Saheb Dr Vahid[c]

[a] *Address: Department of physics, Shahid Bahonar University of Kerman, Kerman; Tel: 09162481753; E-mail: Na.sheybani96@gmail.com*
[b] *Address: Department Of Physics, Shahid Bahonar University Of Kerman, Kerman; Tel: 09132430180; E-mail: rooholamini@uk.ac.ir*
[c] *Address: Department Of chemistry, Shahid Bahonar University Of Kerman, Kerman; Tel: 09173165106; E-mail: vskermanu@gmail.com*

Abstract

In this paper,synthesized silver was examined with two different solvents. first synthesized from silver nanoparticles in aqueous medium (sludge green) and then in an organic medium (gray).the silver nanoparticles synthesized in the cell were then used, the plasmonic effect of such substances increasing the efficiency of the plasmonic dye sensitized solar cell. in the first cell, we used N719 as a dye and silver nanoparticles (prepared in aqueous medium) and the calculated efficiency was 3%.in the second cell, we used N719 as dye and silver nanoparticles (prepared in organic medium) and the calculated efficiency was 2.89%.in the third cell, we used N719 as a dye and the calculated efficiency was 1.7%.

Keywords: Dye-sensitized solar cell, Synthesis of silver nanoparticles, Surface plasmon resonance

I. I. Introduction

The idea of supplying the earth with solar energy is a promising way to bridge the gap between our energy supply and our increasing energy demand. Silver nanoparticles increase light flux due to their wavelength of intensification in the visible range and their ability to absorb and scatter

II. Methods

The first method of silver synthesis in aqueous medium: weigh 1g of glucose, 0.170g of silver nitrate ($AgNo_3$) and 0.094g ($NaBH_4$) with a balance and prepare a solution of 0.1M silver nitrate ($AgNo_3$) and a solution of 0.2 M ($NaBH_4$) then in the solution Pour 1g of glucose nitrate, dissolve it, place a magnet in the solution, and place it on the heater at 70° C under complete rotation until H_2 is released. Then add the solution ($NaBH_4$) to the solution at 70° C using a burette and the color of the solution will slowly change to jade green [1].the second method of silver synthesis in organic medium: add oleic acid drop by drop to 50ml of 0.1M $AgNo_3$ solution to saturate the solution and place in a water bath at 50 ° C at 400 rpm, then add n-butylamine to ph= 11 turn green and add formic acid at the end and allow the reaction to produce for two hours. before cooling to room temperature, ethanol is added to the solution and placed in a vacuum oven to dry and the powder is gray [2].three N719 color-sensitive plasmonic solar cells were fabricated for comparison.silver synthesized.in the first cell, n aqueous medium on The surface of TiO_2 was used. first, the titanium dioxide paste is spread by dr blaide method and the optimal thickness of 16 micrometr is placed at a temperature of 450 °C. After cooking ,the synthesized silver nanoparticles are layered and placed at 70 ° C for 10 minutes

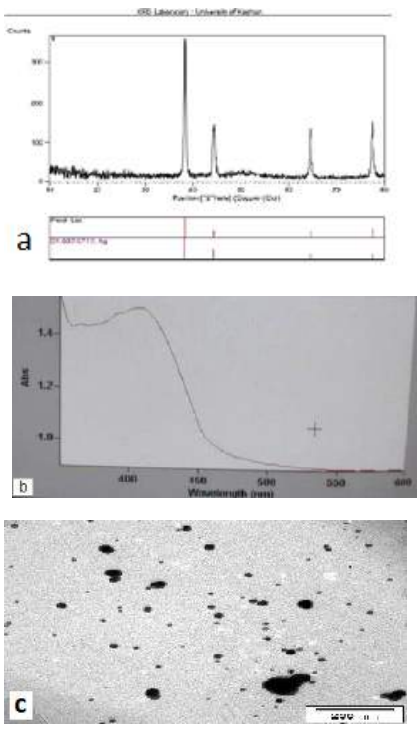

Figure 1: a) X-ray diffraction diagram for silver nanoparticles synthesized in aqueous medium,b) UV-visible absorption spectrum for silver nanoparticles synthesized in aqueous medium. c) TEM

and soaked in N719 (0.4 M) dye solution for 24 hours to uniformly layer the dye molecules due to the plasmonic effect of silver nanoparticles as well as the rapid electron transfer in silver amplified photoanode in TiO_2 nanoparticles, the efficiency is improved and the light current is generally increased. in the case of silver cells synthesized in organic medium, dye-sensitive solar cells were added. TiO_2 and dye N719 were layered in the third cell.

III. Results and discussion

Synthesis of silver nanoparticles was performed with two different solvents. synthesized silver was used in dye solar cells. in cell 1, by placing the synthesized silver in aqueous medium, it stimulates the dye N719 and leads to better absorption of photons.in cell 2, by absorbing the synthesized silver in an organic medium adjacent to the dye N719, less adsorption was performed than in cell 1. in the reference cell 3, due to the absence of plasmonic nanoparticles, we have less absorption than other cells. Current density-voltage diagrams of cells 1, 2 and 3 are shown in figure 2 and table 1.

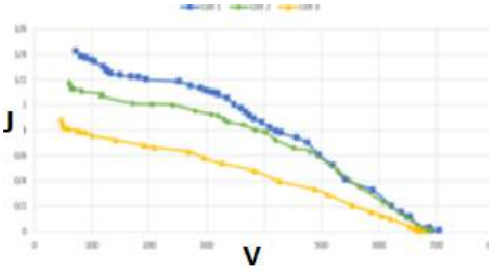

Figure 2: Current density curve (mA /cm^2) -volt (mV

Table 1. Solar cell efficiency 1,2, 3

Parameters	V_{oc}	J_{sc}	ϩ
1.N719+ Ag_1	706.2	1.378	3%
2. N719+Ag_2	690	1.176	2.9%
3. N719	679	0.88	1.727%

IV. Conclusions

Here, the synthesized silver nanoparticles were then applied to the dye-sensitive solar cell. The size of nanoparticles synthesized in aqueous medium is 13 nanometers and they are spherical. The absorption spectrum of nanoparticles is 420 nm and the x-ray diffraction for silver nanoparticles shows that several peaks at angles of 38.27°,42.71°, 64.32 °and shows 77.65°, which is related to plates with crystal structure of 111,200,220, 311, respectively. The surface plasmon effect of silver nanoparticles as well as faster electron transfer in photo anodes and increases efficiency.

References

[1] Shi, Yu-yuan, et al. "Size-controlled and large-scale synthesis of organic-soluble Ag nanocrystals in water and their formation mechanism." *Progress in Natural Science: Materials International* 2011

[2] Chen, Ming, et al."Conversion of the surface property of oleic acid stabilized silver nanoparticles from hydrophobic to hydrophilic based on host guest

بیست و سومین کنفرانس شیمی فیزیک انجمن شیمی ایران
23rd ICS Physical Chemistry Conference
Chemistry Department,
Faculty of Science
Shahid Bahonar University of Kerman
Kerman, Iran
12-13 Jan 2022
ایران، کرمان
دانشگاه شهید باهنر کرمان
دانشکده علوم پایه، بخش شیمی
۲۳-۲۲ دی ماه ۱۴۰۰

A theoretical study on the enantiomeric selectivity of β-cyclodextrin enantiomeric towards 1-(4 bromophenyl) ethanol enantiomers

Fatemeh Mirzaei[a], Effat Jamalizadeh[a,*], Ali Mohebbi[b]

[a] *Department of Chemistry, Shahid Bahonar University of Kerman, Kerman, Iran, jamalizadeh@uk.ac.ir*
[b] *Department of Chemical Engineering, Shahid Bahonar University of Kerman, Kerman, Iran*

Abstract

This study aims to theoretically investigate the enantiomeric selectivity of β-cyclodextrin (β-CD) towards 1-(4-bromophenyl) ethanol enantiomers. In this regards, the host-guest interaction of β-CD with 1-(4-bermophenyl) ethanol enantiomers has been studied by the semi-empirical (Pm6) method. Studies have The resulted theoretical data are in good agreement with the experimental results.

Keywords: Enantiomeric selectivity; Cyclodextrin; 1-(4-bromophenyl) ethanol enantiomers

I. Introduction

Chirality has special applications in various industries, particularly the pharmaceutical industry. There are many reasons in contemporary science that make the separation of enantiomers in chirality environment important [1]. 1-(4-bromophenyl) ethanol is an acetophenone derivative. Several papers on acetophenone and its derivatives report the reduction of microbial properties of various microorganisms. [2].

II. Methods

This theoretical study focuses on the interaction between 1-(4-bromophenyl) ethanol enantiomers with β-CD. All the structures were first drawn separately in a complex mode by GaussView software. After that, the structures drawn with Gaussian 09 software [3] were optimized by Semi-empirical (Pm6) method such a way that the best conformations and energies are obtained. The interaction energies of β-CD and the enantiomers at five conformations are calculated. The five conformations are as follows: In the first conformation, the enantiomer is situated inside the β-CD ring (1) and in the second conformation, the enantiomer is located on top of the β-CD ring (2) (the side with higher substitution for β ring) and in the third conformation, the enantiomer is positioned in the beneath of β-CD ring (3) (the side with lower substitution for β-ring) and in the fourth conformation, the enantiomer is placed such a way that its ring is close to β-CD ring (4) and in the fifth conformation, the enantiomer is located next to the β-CD ring by its substituent (5).

III. Results and discussion

Figure (1) shows the optimized structures of the host-guest complex (S)-1-(4-bromophenyl) ethanol and β-CD (S-β-CD)

as well as (R)-1-(4-bromophenyl) ethanol and β-CD (R-β-CD) in the best conformation and energy. The interaction energies of the host-guest complexes were calculated by the subtraction of the electronic energy of the host-guest enantiomer β-CD (EAB) complex from the summation of the enantiomer (EA) and β-CD (EB) electronic energies in the individually optimized states with the identical basic set (Table 1). Furthermore, the interaction energy of the intended host-guest complexes compared to that for the complex with enantiomer (EA) and β-CD (EB) in complex structure (Table 1). The interaction energy values indicate that the complexes constituted of enantiomers with β-CD are more stable in one conformation compared to other conformations and among R,S enantiomers, the complex of S-enantiomer with β-CD has more negative interaction energy and therefore is more stable. The obtained results are consistent with the experimental results related to the selectivity of β-CD for 1-(4-bromophenyl) ethanol enantiomers [4].

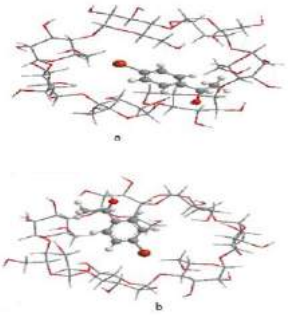

Fig. 1. The optimized complexes **a)** S-β-CD, **b)** R-β-CD by PM6 level of theory

Table 1 Interaction energy values for complexes of β-CD with R,S enantiomers in electron volts (eV).

system	$E_{int}(S-\beta-CD)$	$E'_{int}(S-\beta-CD)$	$E_{int}(R-\beta-CD)$	$E'_{int}(R-\beta-CD)$
1	-0.558	1.998	-0.370	-0.681
2	-0.266	-0.293	-0.221	-0.241
3	-0.211	-0.217	-0.254	-0.262
4	-0.298	-0.325	-0.185	-0.188
5	-0.18	-0. 977	-0. 977	-0.304

IV. Conclusions

The results shown that the interaction energy of (S)-1-(4-bromophenyl) ethanol in the conformation where the enantiomer is inside the β-CD ring has a more negative value with respect to (R)-1-(4-bromophenyl) ethanol enantiomer compared to that of the other conformations.

References

[1] S. Izumoto, and H. Nishi, Int. J. Res., 1999,20, 197-189.
[2] Z. Kani, and E. B. Kurbanoglu, J. Bio. Tech., 2008, 99, 1549-1552.
[3]M.J. Frisch, and et al. Gaussian 09, G09W. Gaussian Inc, Wallingford, USA. 2009.
[4] J. Tang, S. Zhang, Y. Lin, J. Zhou, L. Pang, X, Nie, B. Zhao, and W. Tang, Nature, 2015,5,11523.

بیست و سومین کنفرانس شیمی فیزیک انجمن شیمی ایران
23rd ICS Physical Chemistry Conference
Chemistry Department,
Faculty of Science
Shahid Bahonar University of Kerman
Kerman, Iran
12-13 Jan 2022
ایران، کرمان
دانشگاه شهید باهنر کرمان
دانشکده علوم پایه، بخش شیمی
۲۳-۲۲ دی ماه ۱۴۰۰

DFT study on free radical scavenging activity of new kind of polysaccharide molecule in solution phase

Maryam Fazeli, Mina Ghiasi*

Department of Chemistry, Faculty of Physics and Chemistry, Alzahra University, Tehran, Iran
E-mail: ghiasi@alzahra.ac.ir
ma.fa2285@gmail.com

Abstract

The Amanita caesarea polysaccharide is composed of α-D-glucose and α-D-lyxose at a ratio of 2:1. We used a quantum mechanical approach to shed light on the antioxidant ability of this compound in solution phase. Calculation of reaction enthalpies for the free radical scavenging by this polysaccharide, and research the lowest energy geometry for all studied molecules were calculated by density functional theory (DFT), B3LYP and UB3LYP for close and open shell systems respectively with split-valance 6-31G** basis set using Gaussian 2009 software. The analysis of the bond dissociation enthalpy (BDE) values and of the radicals to determine the delocalization possibilities clearly shows the importance of the 9-OH group in antioxidant reactivity.

Keywords: Amanita caesarea; antioxidant; DFT; HAT; BDE

I. Introduction

Oxidative stress is caused by an imbalance in the redox state of the body, during which an increase in the body's free radicals leads to tissue damage. Oxidative stress damage is involved in many types of diseases, including neurological diseases and cancers. Increasing free radicals cause change in the structure and function of the body's major biological molecules and lead to tissue damage. Reactive Oxygen Species (ROS) is one of the most important oxidants and the main factor of oxidative damage to the body's biological molecules. The most reactive oxygen species is the hydroxyl radical ($OH^{\bullet}$). Antioxidants, as the first defensive line against free radicals, reduce or prevent oxidative stress by reacting with free radicals and reactive species. Today, the use of natural antioxidants is very useful to fight free radicals. Different types of mushrooms are scattered all over the world. Edible mushrooms have medicinal and nutritional properties and are used to protect the heart, prevent cancer and so on [1,2]. Amanita caeserea is one of the mushrooms that has shown good antioxidant properties. The structure of Amanita caeserea polysaccharide is composed of α-D-glucose and α-D-lyxose in a ratio of 2:1, Figure 1 [3]. In this study, Free radical scavenging is monitored by Amanita caeserea polysaccharide using density functional theory.

II. Methods

Geometric optimization and vibration frequencies were performed at the level of B3LYP/6-31G**, Figure 2. All reported chemical properties including implicit

solvent (water) effects were calculated. Atoms with the O-H group were named according to Figure 1. Its chemical structure was plotted using Chemdraw software. In order to achieve the best location for scavenging and evaluation of the preferred free radical scavenging mechanism, we use the following mechanism:

Bond Dissociation Enthalpy (BDE): The stability of the hydroxyl group depends on the amount of BDE. The lower BDE values, the lower stability of the O-H bond, so the bond is broken easily. This action increases the antioxidant capacity of the desired compound. This parameter is calculated according to Equation 1 in standard conditions of 1atm and 298.15K [4].

$$BDE=H(RO^{\bullet}) + H(H^{\bullet}) - H(ROH) \qquad (1)$$

III. Results and discussion

The Bond dissociation enthalpy (BDE) in water phase was calculated at the level of theory B3LYP/6-31G**. The values of bond dissociation enthalpy are presented in Table 1. BDE values range from a minimum of 405.18 Kcal/mol to a maximum of 416.32 Kcal/mol. The antioxidant capacity is determined by the HAT mechanism of the Amanita caeserea molecule by the donor site 9-OH, with a minimum BDE of 405.18 Kcal/mol. The simplest donor of the $H^{\bullet}$ atom is found in the 9-OH position.

Table 1. O–H bond dissociation enthalpy (BDE) in kcal/mol obtained by the B3LYP/6-31G ** method.

OH-P	2-OH,3-OH,4-OH,6-OH,8-OH-9-OH,14-OH,15-OH,16-OH
BDE	**413,412.86,410.48,406.86,416.32,405.18,414.60,410.32,408.96**

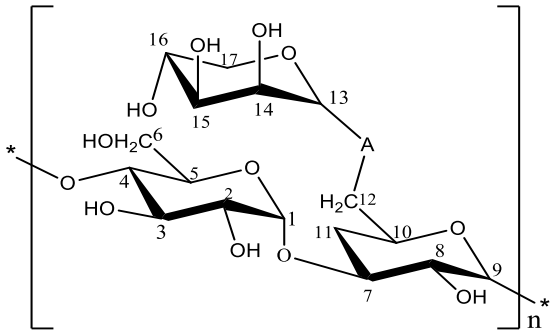

Fig. 1. Structure of the Amanita caeserea polysaccharide

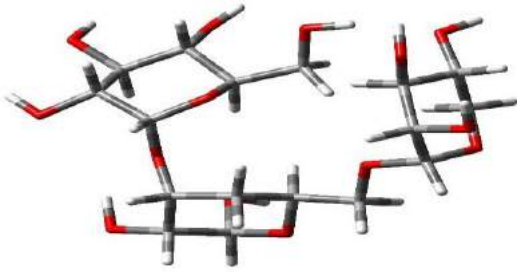

Fig. 2. The optimized structure of Amanita caeserea compound.

IV. Conclusions

In this study, the antioxidant capacity of Amanita caeserea molecule in water phase was reviewed by HAT mechanism. B3LYP/6-31G** density functional theory was used to calculate BDE. The results show that Amanita caeserea can be used as an acceptable natural antioxidant. The minimum bond dissociation enthalpy value is 405.18 Kcal/mol, which indicates the 9-OH position as a suitable position for $H^{\bullet}$ separation and reaction with free radicals.

References

[1] R. Siegel, D. Naishadham, A. Jemal, A Cancer Journal for Clinicians, 2013, 63,11

[2] J. E. Klaunig, L. M. Kamendulis and B. A. Hocevar, journal of toxicol pathol, 2010, 38, 96

[3] Y. Zhu, X. Ding, M. Wang, Y. Hou , W. Hou and C. Yue, journal of molecular medicine reports, 2016, 14, 3947

[4] Y. Zheng, G. Deng, R. Guo, D. Chen and Z. Fu, Journal of Molecular Sciences, 2019, 20, 1450

بیست و سومین کنفرانس شیمی فیزیک انجمن شیمی ایران
23rd ICS Physical Chemistry Conference
Chemistry Department,
Faculty of Science
Shahid Bahonar University of Kerman
Kerman, Iran
12-13 Jan 2022
ایران، کرمان
دانشگاه شهید باهنر کرمان
دانشکده علوم پایه، بخش شیمی
۲۳-۲۲ دی ماه ۱۴۰۰

Density Functional Theory Studies on the Antioxidant Mechanism of Fucoidan Polysaccharide Extracted from Seaweed

Maryam Fazeli, Mina Ghiasi*

Department of Chemistry, Faculty of Physics and Chemistry, Alzahra University, Tehran, Iran
E-mail: ghiasi@alzahra.ac.ir
ma.fa2285@gmail.com

Abstract

Fucoidans, sulfated polysaccharides that are isolated from brown seaweed, have strong antioxidant activity. The antioxidant activity of Fucoidan was reviewed through the main antioxidant mechanism of Hydrogen Atom Transfer (HAT) by density functional theory (DFT) at the level of DFT/B3LYP/6-31G** theory. The discriminant thermochemical properties, such as the bond dissociation enthalpy in the solution phase, were calculated. Analysis of values of bond dissociation enthalpy (BDE) and determination of localization probabilities clearly shows the importance of the 4-OH group in antioxidant reactivity.

Keywords: Fucoidan; Antioxidant; DFT

I. I. Introduction

Reactive Oxygen and nitrogen (RONS) species are unstable and highly reactive molecules that are physiologically produced during metabolic phases, especially in the electron transfer phase. Excessive increase in active species or defects in the antioxidant system typically lead to oxidative stress, and these molecules eventually cause biological macromolecules damage. Due to the destruction of important cells and molecules, the body has an extended antioxidant defense system [1]. Antioxidants are generally regenerative substances which are found both inside and outside cells and have the capacity to react with free radicals and reactive species. Research shows that Fucoidan polysaccharide reflect good antioxidant activity that can be used as a natural antioxidant. Fucoidan is a sulfated polysaccharide extracted from brown seaweed. Fucoidan mainly contains of L-Fucose and Sulphate ester groups, Figure1. This molecule is an excellent antioxidant and has great potential to protect the body against free radical damage [2,3]. Therefore, the main purpose of this study is to investigate the antioxidant capacity of Fucoidan molecule at the level of B3LYP/6-31G** theory in the water phase.

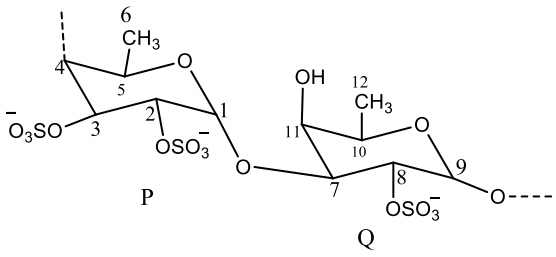

Fig. 1. Chemical structure of Fucoidan polysaccharide.

II. Methods

All DFT calculations have been done by Gaussian 2009 software. The geometry of all molecules, including radicals, has been completely optimized with a basis set of

6-31G**, by using the B3LYP function. Aqueous phase data were obtained for geometry of the study optimized species. Thermodynamic properties were calculated at T=298.15K. BDE was investigated as the most important factor to determine the antioxidant properties. The bond dissociation enthalpy is a suitable parameter to describe the decomposition of H$^{\bullet}$ from OH bond, Which according to Equation 1, is the difference in the heat of formation of the main molecule, ROH, and the corresponding radical, RO$^{\bullet}$.

$$BDE = H(RO^{\bullet}) + H(H^{\bullet}) - H(ROH) \quad (1)$$

H(ROH) and H(RO$^{\bullet}$) indicate the main molecule and the radical shape of the molecule, respectively.

The corresponding radical is also dissociate from the main molecule according to the following equation.

$$R\text{-}OH \rightarrow R\text{-}O^{\bullet} + H \quad (2)$$

The enthalpy of calculated H(H$^{\bullet}$) is as 0.956Kcal/mol [4].

III. Results and discussion

The most stable conformer of the optimized Fucoidan molecule at the B3LYP/6-31G** level in aqueous solvent is shown in Figure 2. Table 1 indicates the BDE values of the calculated OH groups. The OH corresponding to each of the BDEs is identified according to the carbon number in Figure 1. The data indicated in Table 1 show that the OH group at position 4-OH, located in the P-ring, with the value of Bond Dissociations Enthalpy equivalent to 412.17Kcal/mol is the most prone place of hydrogen transfer. At 298.15K, through the HAT mechanism, different values of hydrogen atom transfer from position are specified. Finally, the order of the bond dissociation enthalpy values for the Fucoidan molecule is as follows:

4-OH<9-OH<2-OH<8-OH<11-OH<3-OH

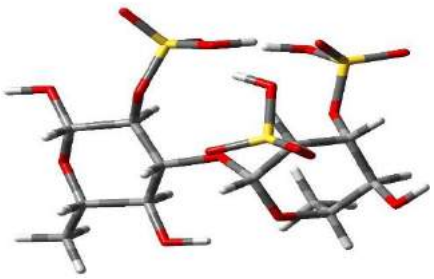

Fig. 2. The optimized structure of Fucoidan compound.

Table 1. DFT calculated parameter of free radical scavenging activity (BDE) for Fucoidan (in kcal/mol).

OH-P	2-OH	3-OH	4-OH	8-OH	9-OH	11-OH
BDE	413.57	422.01	412.17	414.07	412.20	414.84

IV. Conclusions

In this work, the BDE values for the Fucoidan molecule in aqueous solvent were investigated. The results were obtained by using the level of B3LYP/6-31G** and indicated that position 4-OH has the lowest value of BDE equal to 412.17Kcal/mol and this position shows a greater tendency for losing H$^{\bullet}$. Calculations indicate that this molecule has antioxidant property.

References

[1] Manisha, W. Hasan, R. Rajak and D. Jat, Journal of Advanced Research and Review, 2017, 2, 110

[2] A. Yadav, R. Kumari, J. P. Mishra, S. Srivatva and S. Prabha, 2016, 9, 1328

[3] H. Wang, Y. M. Liu, Z.M. Qi, S.Y. Wang, S. X. Liu, X. Li, H.J. Wang and X. C. Xia, Journal of Medicinal Chemistry, 2013, 20, 2899

[4] Z. Markovic, D. MilenKovic, J. Dorovic, J. M. D. Markovic, V. Stepanic, B. Lucic, D.Amic, Journal of Food Chemistry, 2012, 134, 1754

بیست و سومین کنفرانس شیمی فیزیک انجمن شیمی ایران
23rd ICS Physical Chemistry Conference
Chemistry Department,
Faculty of Science
Shahid Bahonar University of Kerman
Kerman, Iran
12-13 Jan 2022
ایران، کرمان
دانشگاه شهید باهنر کرمان
دانشکده علوم پایه، بخش شیمی
۲۳-۲۲ دی ماه ۱۴۰۰

Calculation of Structural and Electronic Properties of CaB_2 in The Orthorhombic Phase

Hamdollah Salehi*[1], Akram Eskandari

Department of Physics, Faculty of Science, Shahid Chamran University of Ahvaz, Ahvaz, Iran

Abstract

In this paper, the structural and electronic properties of calcium diboride in the orthorhombic phase are calculated and investigated. The calculations are performed using density functional theory and with quasi-potential method and generalized slope approximation by Espresso quantum computational code.

Keywords: structural properties; quantum Espresso; calcium diboride

I. Introduction

One of the most interesting candidates for the higher Tc transition temperature is the hypothetical simple hexagonal CaB_2 (calcium diboride) with the same crystal symmetry as MgB_2, where all Ca atoms have been replaced by Mg atoms [1].

Since CaB_2 will have superconducting properties, it will be significantly useful and applicable in science and industry in the near future

II. Method Description

In these calculations, quasi-potentials made by ultra-soft method and constant load have been used .

Table 1 . Calculated structural parameters of CaB2 composition in OsB2 phase and comparison with other results

Calculated quantities	Present work		others work
	GGA	LDA	theoretical [2]
a(a.u)	14.099	17.698	14.097
b(a.u)	7.965	6.636	5.936
c(a.u)	7.055	7.050	7.054
b/a	0.565	0.375	-
c/a	0.5004	0.3984	-
B(Gpa)	36.3	45.2	96
B'	4.24	5.75	3.576
$V_0(a.u)^3$	700.708	1358.83	-
$E_0(Ry)$	-173.36826	-26.07826	– 15.757

III. results and discussions

A: Structural properties

One of the important parameters in these calculations is the lattice constants. Using the Murnaghan equation, we plot the total energy diagram in terms of the initial cell volume for the corresponding

1 Corresponding author: Salehi_h@scu.ac.ir

values of a, where the volume corresponding to the minimum total energy (E_0) is the same as the optimal volume (V_0) and a lattice constant corresponding to this volume will be the optimal lattice constant.

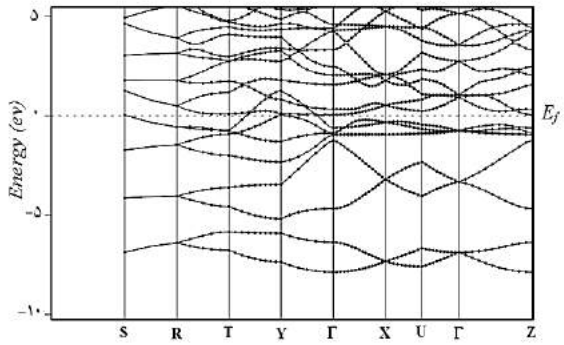

Figure 1. Energy bands of CaB2 compound in O3B2 phase.

Band structure

The band structure of CsB_2 in the direction of different symmetrical lines without considering the spin interaction is plotted in Figure (1).

The density diagram of the total states in the range -45ev to 5ev is plotted in Figure (2). The peaks observed in the -40eV to -20eV range are related to the involvement of core and quasi-core orbitals.

The figure of super electron density in the orthorhombic phase on coordinate plane (101) has been investigated. The high density of the lines around the bond B-B is a sign of high load density due to the presence of a covalent bond. There is also a metal bond between Ca-Ca atoms due to the homogeneous density of the lines.

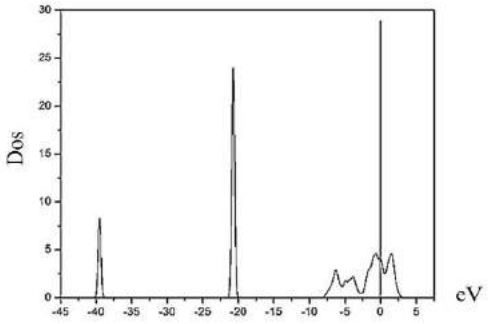

Figure 2: Density of total states of CaB_2 in the OsB_2 phase.

IV. Conclusions

The structure of the energy band in these phases has a dual degenerate near the Fermi level, which plays an important role in superconductivity. This study also confirms the metallic properties of calcium diboride.
The results obtained from density of states investigation show that calcium diboride does not have a band gap, which itself indicates the metallic properties of this compound. This

study also shows that the composition has a large lattice constant and a high density of states at the Fermi level, both of which are desirable properties for having a high temperature.

I. References

[1] S.V. Okatove, A. L. Ivanovskii, Yu. E. Medvedeva, (2001), The Electronic band structure of superconducting MgB_2 and related borides CaB_2, MgB_6 and CaB_6. Phys. State. Sol (b), 225, No1, R3 – R5.

[2] M. B. Ozisik, K. Colakoglu, E. Deligoz, (2012), Crystal structure, elastic, and lattice dynamical properties of BeB_2, NaB_2 and CaB_2 from the first principle, Journal of physics and Chemistry of Solids 73, 593 – 598.

بیست و سومین کنفرانس شیمی فیزیک انجمن شیمی ایران
23rd ICS Physical Chemistry Conference
Chemistry Department,
Faculty of Science
Shahid Bahonar University of Kerman
Kerman, Iran
12-13 Jan 2022
ایران، کرمان
دانشگاه شهید باهنر کرمان
دانشکده علوم پایه، بخش شیمی
۲۳-۲۲ دی ماه ۱۴۰۰

The effect of alkyl vs halogen side groups on the stability of Boron-Heterocyclic Carbenes: A computational DFT study

Babak Golzadeh[a], Shima Kazeri-shandiz[a]*, Alireza Akbari[a]

[a] *Address: Department of Chemistry, Payame Noor University, P.O. Box 19395-3697, Tehran, Iran*
Fax: +982122441511; Tel: +982123320000; E-mail: s.kazeri@yahoo.com

Abstract

The Boron-Heterocyclic Carbenes (BHCs) are divalent five-membered species in which two electron-deficient boron atoms flank the divalent carbon atom. The side groups attached to boron atoms have important role on their stability via singlet-triplet energy gap ($\Delta E_{t\text{-}s}$). In this study the stability of X_2BHCs bearing three alkyl groups (X= Me, iPr, tBu) is compared to those with halogen (X= F, Cl, Br) side groups. Results show greater $\Delta E_{t\text{-}s}$ for X_2BHCs with X= Me, iPr, tBu. All structures are bent (puckered). M06/def2-tzvp level of theory is applied for this purpose. All calculations are carried out using Guassian 09 program package.

Keywords: Boron heterocyclic carbenes; BHC; singlet-triplet energy gap; side groups.

I. Introduction

Replacing the two nitrogen atoms of Arduengo's N-heterocyclic carbenes (NHCs) with electron deficient boron atoms forms B-heterocyclic carbenes (BHCs) which may appear destabilizing at first glance. Yet, among the 40 optimized singlet (s) and triplet (t) BHCs and their Si, Ge, Sn and Pb homologues (BHEs), eight species are found that show higher stability than their corresponding NHEs for exhibiting wider singlet–triplet energy gaps ($\Delta E_{t\text{-}s}$), at B3LYP/TZ2P, as well as CBS-QB3 and G4MP2 ab initio levels [1]. Here, we are planning to study about the stability of some B-Heterocyclic carbenes and silylenes with some alkyl side groups and compare them to their halogen analogues.

II. Methods

The geometries of X_2BHE divalent species (scheme 1) ($C_2H_2B_2X_2E$; E=C, Si X= F, Cl, Br, Me, iPr, tBu) are optimized using B3LYP [2] and M06 [3] density functionals in conjunction with def2-TZVP basis sets. The calculations are carried out using the GAUSSIAN 09 program package. The vibrational frequencies show that all structures obtained are minima on the potential energy surface.

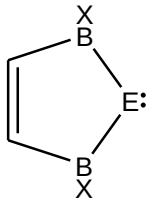

E = C, Si
X=F, Cl, Br, Me, iPr, tBu

Singlet & triplet
electronic configuration

Scheme 1

III. Results and discussion

All divalent species in this study are optimized with their two electronic configurations; singlet and triplet. In all calculated species with both introduced

methods the absolute values of the energy of each singlet species is greater than its corresponding triplets. All singlet species are bent or puckered with an average puckering angle of about 65°. On the other hand, all triplet species are planar. The energy gap between singlet and triplet configurations in each compound is our major feature for the comparison of their stability. Fig. 1 demonstrates the values of singlet-triplet energy gap ($\Delta E_{t\text{-}s}$) according to the sizes of halogen and alkane side substituents.

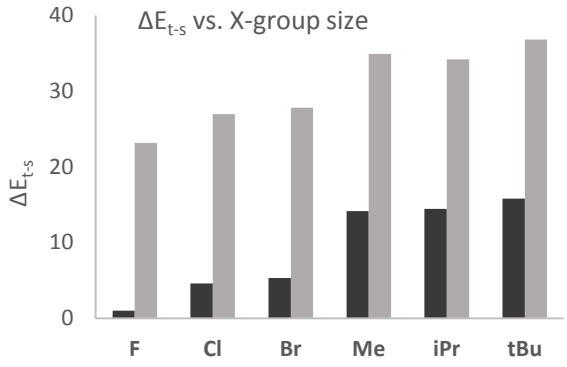

Fig. 1. ΔEt-s vs. X-group sizes for X2BHEs; E=C, Si X= F, Cl, Br, Me, iPr, tBu calculated at M06/def2-TZVP level of theory.

It is obviously shown that the average values of $\Delta E_{t\text{-}s}$ are larger for alkane side groups whether in carbenes or in silylenes. On the other hand, all silylenes under study show $\Delta E_{t\text{-}s}$ in comparison with their corresponding carbenes.

IV. Conclusions

Results exhibits that among 24 singlet and triplet carbenes and silylenes with the formulae $C_2H_2B_2X_2E$ and X= F, Cl, Br, Me, iPr, tBu substituents on boron atoms of the heterocycle, the silylene (X_2BHSi) species with alkane substituents have the largest amounts of $\Delta E_{t\text{-}s}$ and hence are the more stable than other species in present study. $(tBu)_2BHSi$ is the most stable. On the other hand, the carbenes with halogen substituents on boron atoms own the minimum values of $\Delta E_{t\text{-}s}$ and are the least stable. Totally, it is concluded that the size of bulkier alkyl substituents dominate the mesomeric effects of halogen substituents.

References

[1] A. Akbari, B. Golzadeh, S. Arshadi, M.Z. Kassaee, *RSC Advances*, 2015, 54, 43319.
[2] C. Lee, W. Yang, R.G. Parr, *Physical Review B, 1988, 37, 785.*
[3] Y. Zhao, D.G. Truhlar, *Theoretical Chemistry Accounts*, 2008, 120, 215.

بیست و سومین کنفرانس شیمی فیزیک انجمن شیمی ایران
23rd ICS Physical Chemistry Conference
Chemistry Department,
Faculty of Science
Shahid Bahonar University of Kerman
Kerman, Iran
12-13 Jan 2022
ایران، کرمان
دانشگاه شهید باهنر کرمان
دانشکده علوم پایه، بخش شیمی
۲۳-۲۲ دی ماه ۱۴۰۰

The nature of M-L bond in some B-heterocyclic carbenes in their complexes with G11 transition metals: A theoretical survey

Babak Golzadeh[a], Shima Kazeri-shandiz[a]*, Alireza Akbari[a]

[a] *Address: Department of Chemistry, Payame Noor University, P.O. Box 19395-3697, Tehran, Iran*
Fax:+982122441511; Tel: +982123320000; E-mail: s.kazeri@yahoo.com

Abstract

Boron-Heterocyclic Carbenes (BHCs) are organometallic ligands, and their coordination chemistry with transition metals, is interesting. Here, quantum chemical calculations at M06/def2-tzvp and BP86/TZ2P levels are applied for the calculation of X_2BHC-MCl; M=Cu(I), Ag(I), Au(I) with F, Cl and Br side groups. Results display that the interaction energies (ΔE_{int}) for C−M bond follow the trend for the G11 transition metals as Au(I) > Cu(I) > Ag(I). The nature of C−M bond in the complexes is evaluated using energy decomposition analysis (EDA) and excited transition state-natural orbitals for chemical valance (ETS-NOCV). The E_{int} in X_2BHC−MCl complexes studied here is largely electrostatic.

Keywords: Boron heterocyclic carbenes; transition metals; Complex; EDA-VOCV

I. Introduction

Significant advances have occurred in the preparation and isolation of heterocyclic divalents and their corresponding adducts, whether from main group elements or transition metal complexes [1]. Among them, the compounds derived from 5-membered boron heterocyclic carbenes (BHC) [2] inspired from those of corresponding N-heterocyclic carbenes (NHCs) could be interesting for various fields of science and technology.

In this study, some X_2BHC species with electron-withdrawing (X=F, Cl, Br) side groups on boron atoms are mentioned.

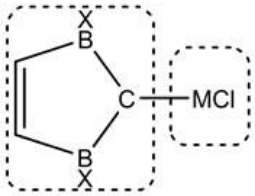

Scheme 1

Then, the complex compound is formed between the X_2BHE with group 11 metal chlorides (MCl; M=Cu(I), Ag(I), Au(I)) (Scheme 1). Interaction energies (ΔE_{int}) and the study of the nature of bonds in view of dative and electron-sharing are best described through energy decomposition analysis (EDA). As a final point, the extracted images from excited transition state-natural orbitals for chemical valence (ETS-NOCV) calculations helps to visualize more details of interaction between E and M atoms.

II. Methods

The geometries of X_2BHC−MCl (scheme 1) complex species are optimized using M06 density functional in conjunction with def2-TZVP basis sets using the G09 program package. In the EDA, the energy of bond formation of the fragments during interaction is the sum of four major

components as following:

$\Delta E_{int} = \Delta E_{elstat} + \Delta E_{Pauli} + \Delta E_{orb} + \Delta E_{disp}$

where ΔE_{elstat} is electrostatic interaction, ΔE_{Pauli} is Pauli repulsion, ΔE_{orb} is orbital interaction, and ΔE_{disp} is dispersion energy between two fragments. Here the EDA of complexes is carried out at BP86-D3/TZ2P(ZORA) with C1 symmetry using the program package ADF2009.01 [3].

III. Results and discussion

The results of EDA for $X_2BHC-MCl$ complexes with M=Cu, Ag, Au, and X= F, Cl, Br show that the average ΔE_{int} is -72, -51 and -83 for Cu, Ag and Au complexes, respectively (the E−M bond interaction energies (E_{int}) between the X_2BHE and MCl fragments follow the order of Au>Cu>Ag). The main component of E_{int} in all $X_2BHC-MCl$ complexes in this project is the electrostatic interaction (ΔE_{elstat}) which is about 63% of E_{int}. The average percentage of ΔE_{orb} which is used for finding a good explanation of chemical bonds is 36.

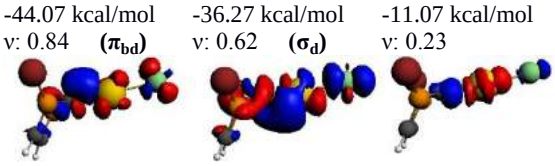

Fig. 1. Deformation densities associated with the most important orbital interactions for selected $Br_2BHC-MCl$ (M=Cu, Ag, Au) complexes at BP86-D3/TZ2P(ZORA)//M06/def2-TZVP

From the point of view of divalent atoms (E), the carbene complexes ($\mathbf{1}_X-MCl$; $\bar{E}_{int}$= -68.3 kcal.mol^{-1}) possess definite larger values of interaction energy in comparison with the silylenes ($\mathbf{2}_X-MCl$; $\bar{E}_{int}$= -54.2 kcal.mol^{-1}). With the help of deformation density ($\Delta\rho$) calculations, one can observe the covalent bond between the two interacted fragments *i.e.*, X_2BHE and MCl. in all carbene complexes ($X_2BHC-MCl$) in this project, there is one interaction from the donor orbital of the divalent atom (E) of the BHE to the acceptor orbital of metal atoms (M) which is displayed as $\sigma_{E\rightarrow M}$ (σ_d: σ-donation). In addition, there are two interactions from the M donor orbital to the acceptor orbital of E; one of which is $\pi_{E\leftarrow M}$ (π_{bd}: π-back donation), and the other is $\sigma_{E\leftarrow M}$ (σ_{bd}: σ-back donation).

IV. Conclusions

In all $X_2BHE-MCl$ complexes the electrostatic interaction ($\overline{\Delta E}_{elstat}$= 65%) is almost as twice as the orbital interaction

In all $X_2BHE-MCl$ complexes, there is one E→M (σ_d) deformation density.

For M→E back-donation, in $\mathbf{1}_X-MCl$ complexes there is one π_{bd} and one σ_{bd}, but in $\mathbf{2}_X-MCl$ complexes, there two π_{bd} (one $\pi_\perp$ and one $\pi_\parallel$).

V. References

[1] G. Frenking, N. Fröhlich, *Chemical Reviews*, 2000, 100, 717.

[2] A. Akbari, B. Golzadeh, S. Arshadi, M.Z. Kassaee, *RSC Advances*, 2015, 54, 43319.

[3] ADF2008.01, SCM, Theor Chem, Vrije Univ, Amsterdam, the Netherlands.
http://www.scm.com. https://doi.org/

بیست و سومین کنفرانس شیمی فیزیک انجمن شیمی ایران
23rd ICS Physical Chemistry Conference
Chemistry Department,
Faculty of Science
Shahid Bahonar University of Kerman
Kerman, Iran
12-13 Jan 2022
ایران، کرمان
دانشگاه شهید باهنر کرمان
دانشکده علوم پایه، بخش شیمی
۲۳-۲۲ دی ماه ۱۴۰۰

Simultaneous voltammetric determination of acetaminophen and isoniazid by using magnetic nanocomposite modified screen printed graphite electrode

Fariba Garkani Nejad[a,*], Zahra Dourandish[a], Iran Sheikhshoaie[a], Hadi Beitollahi[b]

[a]*Department of Chemistry, Shahid Bahonar University, Kerman, Iran, garkani.f1991@gmail.com*

[b]*Environment Department, Institute of Science and High Technology and Environmental Sciences, Graduate University of Advanced Technology, Kerman, Iran*

Abstract

In this work, an electrochemical sensor based on a screen-printed graphite electrode (SPGE) modified with Fe_2MoO_4 magnetic nanocomposite was prepared for determination of acetaminophen (AC). The limit of detection (LOD) of the method for AC was 0.05 μM and the sensor demonstrated a dynamic linear range from 0.15–500.0 μM for analysis of AC. Moreover, the Fe_2MoO_4/SPGE was used for the simultaneous determination of AC and isoniazid (INZ). In co-existence system containing AC and INZ, the developed sensor exhibited well-defined and separate DPV peaks (i.e., 630 mV) for these analytes**.**

Keywords: Screen-printed graphite electrode; Acetaminophen; Isoniazid.

I. Introduction

Drug analysis is a very important aspect of scientific research. Drugs are very diverse compounds in terms of structure and chemical properties. The action of these compounds is highly dose-dependent. Each drug has a therapeutic range, and the existence of drug at concentrations lower than the minimum level causes weak beneficial effects for patients, while concentrations above than maximum limit cause side effects, which may be dangerous for patients. Today, the establishment of methodologies for drug monitoring in pharmaceutical and biological sampls is essential for patients' safety [1]. Further attention has been recently attracted towards electrochemical methods because of their portability, short analysis times, inexpensive equipment, good sensitivity and potential for miniaturization, thereby making them promising analytical applications. Developments in nanostructured materials offer attractive opportunities in the fabrication of electrochemical sensors [2].

II. Methods

For preparation of Fe_2MoO_4/SPGE, 1 mg of prepared Fe_2MoO_4 nanocomposite was added into aqueous solution (1 ml), followed by sonication for 30 min to give a homogeneous suspension. Then, 5 μL of suspension was dispersed on the surface of SPGE as dropwise. Following the evaporation of solvent, the surface of electrode was washed for several times with deionized water to clean free modifier molecules and subsequently air-dried.

III. Results and discussion

Figure 1 displays cyclic voltammetric responses from the electrochemical oxidation of 200.0 μM AC at the surface of unmodified SPGE (curve a) and Fe_2MoO_4/SPGE (curve b). The results showed that the oxidation of AC is weak at the surface of the unmodified SPGE, but the presence Fe_2MoO_4 nanocomposite at

the surface of SPGE could enhance the peak current and decrease the oxidation potential. These results indicates the good ability of Fe_2MoO_4/SPGE to AC oxidation.

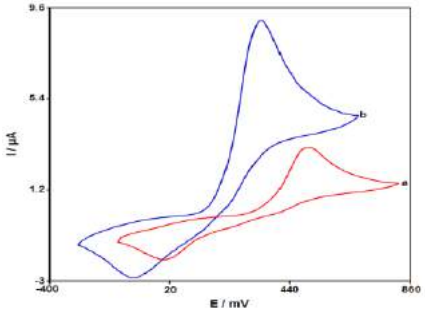

Figure 1. Cyclic voltammograms of (a) unmodified SPGE, (b) Fe_2MoO_4/SPGE in 0.1 M PBS (pH 7.0) in the presence of 200.0 µM AC at the scan rate 50 mVs^{-1}.

Differential pulse voltammograms (DPVs) for determination of AC is shown in Figure 2. Figure 2 shows that with increasing concentration of AC from 0.15–500.0 µM the Ipa increasing with a small shifting in the oxidation potentials. The plot of Ipa versus the concentration of AC was plotted as shown in Figure 2 (inset) and it shows almost straight line with good linearity with the linear regression equation Ipa(µA) = $0.0421C_{AC}$ (µM) + 0.7945 (R^2 = 0.9995). The LOD was calculated 0.05 µM.

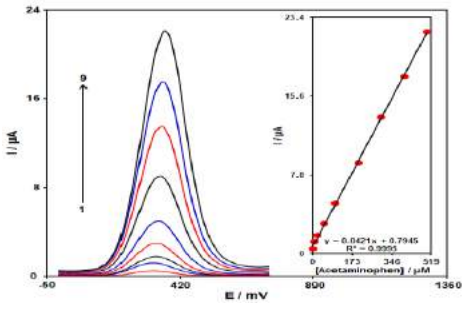

Figure 2. DPVs of Fe_2MoO_4/SPGE in 0.1 M PBS (pH 7.0) containing different concentrations of AC. Numbers 1–9 correspond to 0.15, 5.0, 20.0, 50.0, 100.0, 200.0, 300.0, 400.0 and 500.0 µM of AC. Inset: plot of the peak current as a function of AC concentration in the range of 0.15-500.0 µM.

Ac and INZ have been simultaneously determined by changing their concentration. Results obtained by voltammetry indicated complete anodic peaks at potentials of 330 mV and 960 mV that respectively correspond to AC and INZ oxidation. The peak oxidation current at different AC and INZ concentrations respectively showed a linear relationship of 5.0 to 400.0 µM and 5.0 to 500.0 µM (Figure 3A and 3B). These results indicate the feasibility of quantifying both analytes, at the same time, using the Fe_2MoO_4/SPGE.

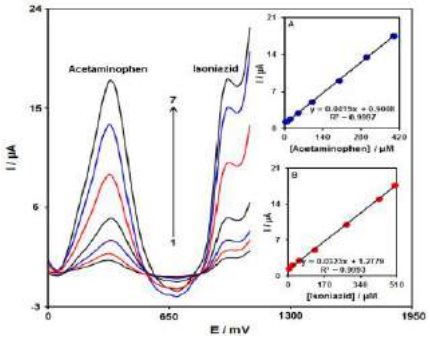

Figure 3. DPVs of Fe_2MoO_4/SPGE in 0.1 M PBS (pH=7.0) with various concentrations of AC+INZ. Numbers 1–7 respectively are corresponding to 5.0+5.0, 20.0+20.0, 50.0+50.0, 100.0+125.0, 200.0+275.0, 300.0+425.0 and 400.0+500.0 µM of AC and INZ. Insets: (A) plot of Ipa versus AC concentrations, (B) plot of Ipa versus INZ concentrations.

IV. Conclusions

The results of this study showed that Fe_2MoO_4/SPGE had excellent electrocatalytic activity towards AC. The oxidation peak currents of AC were proportional with its concentration in the ranges 0.15-500.0 µM, with LOD of 0.05 µM. In addition, the modified electrode was applied for simultaneous determination of AC and INZ.

References

[1] R. Thakur and A. Devi, Int. J. Appl. Pharm. Sci. Res., 2021, 6, 57-62.

[2] C. Zhu, G. Yang, H. Li, D. Du and Y. Lin, Anal. Chem., 2015, 87, 230.

بیست و سومین کنفرانس شیمی فیزیک انجمن شیمی ایران
23rd ICS Physical Chemistry Conference
Chemistry Department,
Faculty of Science
Shahid Bahonar University of Kerman
Kerman, Iran
12-13 Jan 2022
ایران، کرمان
دانشگاه شهید باهنر کرمان
دانشکده علوم پایه، بخش شیمی
۲۳-۲۲ دی ماه ۱۴۰۰

Screen-printed electrode modified with graphene quantum dots for detection of acetylcholine

Zahra Dourandish[a], Fariba Garkani Nejad[a,*], Iran Sheikhshoaie[a], Hadi Beitollahi[b]

[a]*Department of Chemistry, Shahid Bahonar University, Kerman, Iran, garkani.f1991@gmail.com*

[b]*Environment Department, Institute of Science and High Technology and Environmental Sciences, Graduate University of Advanced Technology, Kerman, Iran*

Abstract

In this paper a sensor to detect acetylcholine on the basis of graphene quantum dots (GQD) modified screen printed electrode (GQD/SPE) is reported. Under optimized conditions, GQDs/SPE exhibits excellent acetylcholine sensing attributes in the range of 1.0–800.0 μM with 0.3 μM of detection limit.

Keywords: Acetylcholine; Graphene quantum dots; Screen printed electrode; Voltammetry.

I. Introduction

As a prominent neurotransmitter, acetylcholine (ACh) widely exists in the peripheral and central nervous systems. Especially in human central nervous system, ACh plays an important role in memory, learning, attention, sleeping and consciousness [1, 2]. Acetylcholine level apparently is related to various neural disorders such as Alzheimer's disease, progressive dementia and schizophrenia [3]. Detecting ACh in biological samples is therefore important in neuronal cholinergic system research. electrochemical sensors have been demonstrated with several advantages such as fast analysis, high sensitivity and selectivity, no interference effect, real-time analysis and relatively low cost. The working electrodes may be modified to improve the analytical signal, the detection range, the sensitivity, stability, and the selectivity of this technique [4, 5]. Graphene quantum dots are single layer to tens of layer of graphene with size less than 30 nm. GQDs present exceptional properties including large specific surface area, low toxicity, good water solubility, excellent photoluminescence, good thermal conductivity, and excellent electrical conductivity [6]. Due to these unique properties, GQDs have been widely utilized in electrochemical sensing platforms. At the present study, we reported fabrication of a graphene quantum dots modified screen printed electrode and its application to determination of acetylcholine by voltammetry techniques.

II. Methods

A stock solution of GQDs in 1 mL of the aqueous solution was prepared by dispersing 1 mg of GQDs with ultrasonication for 1h, while 2 μL of aliquots of the GQD/H_2O suspension solution was cast on the carbon working electrodes, followed by waiting until the solvent was evaporated at room temperature.

III. Results and discussion

Fig. 1 depicts the cyclic voltammetry (CV) responses for electro-oxidation of 100.0

μM acetylcholine at the unmodified SPE (curve b) and GQD/SPE (curve a). The peak potential occurs at 725 mV due to the oxidation of acetylcholine, which is about 215 mV more negative than the unmodified SPE. Also, GQD/SPE shows much higher anodic peak currents for the oxidation of acetylcholine compared to the unmodified SPE, indicating that the modification of the unmodified SPE with GQDs has significantly improved the performance of the electrode towards acetylcholine oxidation.

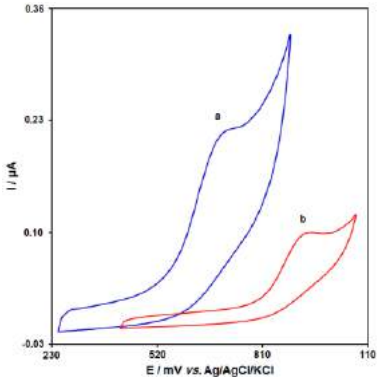

Fig. 1. CVs of a) GQD/SPE and b) SPE in the presence of 100.0 μM of acetylcholine in 0.1 M PBS (pH 7.0). In all cases, the scan rate was 50 mV s^{-1}.

The electro-oxidation peak currents of acetylcholine on the surface of GQD/SPE can be used to determine acetylcholine in the solution. Differential pulse voltammetry (DPV) experiments were performed by using GQD/SPE in 0.1 M phosphate buffer solutions (PBS) containing various individual concentrations of acetylcholine (Fig. 2). The results show that the electrocatalytic peak currents of acetylcholine oxidation at the surface of GQD/SPE were linearly dependent on acetylcholine concentrations over the linear dynamic range of 1.0-800.0 μM while the limit of detection (LOD) (3σ) was obtained as 0.3 μM.

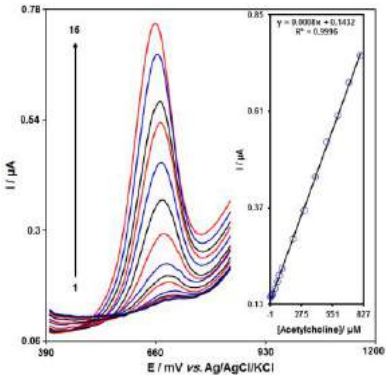

Fig. 2. DPVs of GQD/SPE in 0.1 M PBS (pH 7.0) containing different concentrations of acetylcholine. Numbers 1–15 correspond to 1.0, 5.0, 10.0, 20.0, 40.0, 60.0, 80.0, 100.0, 200.0, 300.0, 400.0, 500.0, 600.0, 700.0 and 800.0 μM of acetylcholine. The inset shows the plot of the peak current as a function of the acetylcholine concentration in the range of 1.0-800.0 μM.

IV. Conclusions

In this paper, GQD/SPE sensor was developed for studying voltammetric response of acetylcholine. This sensor significantly enhanced the oxidation peak current and decreased the oxidation peak potential of acetylcholine. The peak current was linear with acetylcholine concentration from 1.0 to 800.0 μM, and the detection limit was about 0.3 μM.

References

[1] G. Vinodhkumar, R. Ramya, M. Vimalan, I. Potheher and A. Cyrac Peter, Prog. Chem. Biochem. Res., 2018, 1, 40-49.
[2] S. Çevik, S. Timur and Ü. Anik, Microchim. Acta, 2012, 179, 299-305.
[3] S. Hou, Z. Ou, Q. Chen and B. Wu, Biosens. Bioelectron., 2012, 33, 44-49.
[4] A. Shamsi and F. Ahour, Adv. J. Chem. Section A, 2020, 4, 22-31.
[5] E.R. Santana, C.A. de Lima, J.V. Piovesan and A. Spinelli, Sens. Actuators B: Chem., 2017, 240, 487-496.
[6] J. Zhao, G. Chen, L. Zhu and G. Li, Electrochem. Commun., 2011, 13, 31-33.

بیست و سومین کنفرانس شیمی فیزیک انجمن شیمی ایران
23rd ICS Physical Chemistry Conference
Chemistry Department,
Faculty of Science
Shahid Bahonar University of Kerman
Kerman, Iran
12-13 Jan 2022
ایران، کرمان
دانشگاه شهید باهنر کرمان
دانشکده علوم پایه، بخش شیمی
۲۳-۲۲ دی ماه ۱۴۰۰

Synthesis of nitrogen-doped carbon microspheres containing palladium nanoparticles and its application in hydrogen release using formic acid

Sare Mezginezhad[*], **Vahid Saheb**[*]
[*] *Department of Chemistry, Shahid Bahonar University of Kerman, Kerman, Iran, vahidsaheb@uk.ac.ir*

Abstract

Today, nanotechnology is widely used to synthesize materials with new properties. Synthesized metal nanoparticles have the ability to effectively catalyze organic reactions due to their high surface to volume ratio and are therefore significant as efficient catalysts. In this project, the preparation of stabilized palladium nanoparticles on a substrate of nitrogen-doped carbon microspheres was first investigated. At the beginning of the operation, hydrogen release reactions were performed with formic acid by formulated catalyst and compared with other cobalt and nickel nanocatalysts. According to the obtained data and calculation of reaction activation energy, significant results for hydrogen release from Formic acid was obtained.

Keywords: Nitrogen Doped Carbon Microsphere, Hydrothermal Synthesis, Palladium Nanoparticles, Hydrogen Release, Formic Acid.

I. Introduction

Finding a suitable alternative of fossil fuel resources as an energy source is a main concern in the 21st century as the termination of fossil fuels resources, increasing environmental pollution and energy shortages [1,2].

In this context, hydrogen is considered to be one of the proper alternative candidates for future energy because of its high energy density and copious sources [3,4].

Among LOHC materials, formic acid (FA, HCOOH) is one of the major products from biomass processing To reduce aggregation of the catalyst particles and further improve the catalytic activity, various materials such as carbon, oxides, hydroxyapatite, clay, heteropolyanions, polymer/hydrogel, and Ni foamhave been chosen as the supports.[5]

FA exhibits characteristics of a high hydrogen content (4.4 wt %), nontoxicity, and easy storage and transportation, and it is regarded as a potential carrier for the production and storage of hydrogen.[6]

Hydrogen can be generated from FA via a dehydrogenation pathway (HCOOH → CO2 + H2). The dehydration pathway (HCOOH → CO + H2O) producing CO as the impurity, which is toxic for fuel cell catalysts, is an undesired side reaction and must be strictly controlled.[7]

II. Methods

First, using a hydrothermal method, a carbon substrate consisting of carbon microspheres doped with nitrogen was synthesized and then palladium nanoparticles were placed on it to be used in the hydrogen release test at different temperatures.

During the preparation of the desired carbon substrate, we observed that before the synthesis of the dye the solution was transparent to the color of water and after the synthesis of the dye the solution turned

black with an almost dark brown precipitate which was observed under a optial microscope, they were clearly visible.
We used formic acid as a reducing agent in catalyst synthesis as well as in hydrogen release tests as a hydrogen carrier.

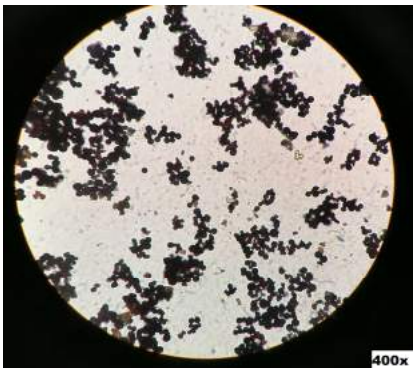

Fig. 1. Optical microscope image of NCCS (400X)

III. Results and discussion

The hydrogen release test from formic acid [FA] has used to evaluate the performance of the catalyst. The test conducted by an adiabatic system that finally calculate the activation energy of the reaction, the amount of primary energy necessary to release hydrogen from formic acid calculated .Also, for further investigation and comparison between different nanomaterials, the catalyst was replaced with another metal and re-examined. From another perspective, catalyst to release hydrogen at different temperatures tested to evaluate its performance. According to the results, the performance of the catalyst has improved with temperature change and this result is completely different for catalysts and different substrates

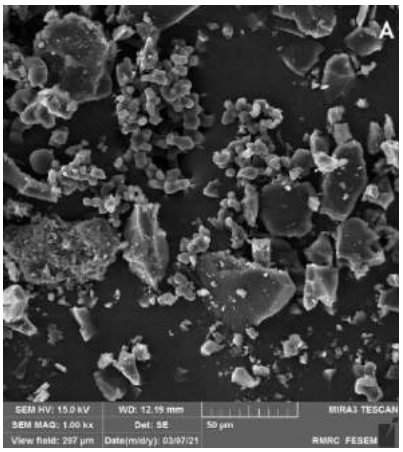

Fig. 2. FESEM image from nitrogen-doped carbon microspheres (NCCS)

IV. Conclusions

By synthesizing nitrogen-doped carbon microspheres by hydrothermal method, using glucose monohydrate, which is a cost-effective, inexpensive and available material, an ideal carbon substrate for catalytic nanoparticles can be obtained.

By using various support materials and synthetic strategies, a wide range of highly active metal NP catalysts were developed, which demonstrate considerable potential for the clean, efficient generation of H2 from FA under convenient conditions.

References

[1] Ghiyasiyan-Arani , Salavati-Niasari, The Journal of Physical Chemistry C. 2018;122(29):16498.
[2] Salehabadi A, Salavati-Niasari M, Ghiyasiyan-Arani MJournal of Alloys and Compounds,2018.
[3] Razavi FS, Morassaei MS, Salehabadi A, Ghiyasiyan-Arani, Journal of Alloys and Compounds. 2019.
[4] Mellmann, D.; Sponholz, P.; Junge, H.; Beller, M, Chem. Soc. Rev. 2016.
[5] Zhu, Q.-L.; Xu, Q Energy Environ. Sci.2015.
[6] Grasemann, M.; Laurenczy, G, Energy Environ. Sci. 2012.
[7] Jiang, H.-L.; Singh, S. K.; Yan, J.-M.; Zhang, X.-B.; Xu, Q, ChemSusChem 2010.

بیست و سومین کنفرانس شیمی فیزیک انجمن شیمی ایران
23rd ICS Physical Chemistry Conference
Chemistry Department,
Faculty of Science
Shahid Bahonar University of Kerman
Kerman, Iran
12-13 Jan 2022
ایران، کرمان
دانشگاه شهید باهنر کرمان
دانشکده علوم پایه، بخش شیمی
۲۳-۲۲ دی ماه ۱۴۰۰

Proposing a trajectory-based algorithm to solve the quantum-classical Liouville equation in the mapping basis

Sahand Nikzat[a], **Ali Nassimi**[b]*

[a] *Address: Sharif University of Technology, Tehran,; Tel:+98 91 4901 1368; E-mail: sahandnikzat@gmail.com*
[b] *Address: Sharif University of Technology, Tel: +98 21 6616 5377; E-mail: a.nassimi@sharif.edu*

Abstract

In the current study, by term-by-term comparison of the mapping quantum-classical Liouville equation (MQCLE) with the continuity equation, a trajectory-based algorithm is derived to solve MQCLE.

Keywords: Quantum-classical Liouville dynamics, Open quantum systems, Molecular dynamics algorithms

I. Introduction

Pursuing dynamics of quantum processes in complex and many-body systems has been an enduring task. A myriad of such systems are of great interest in physics and chemistry. Even though these systems consist of many parts, one may slit the whole system into two parts: a small part of the system whose properties must be studied as our primary target called a subsystem. Subsystem degrees of freedom are treated quantum mechanically. The rest of the system, regarded as less significant for our purposes, is called bath.

Bath degrees of freedom are treated classically. In this approach, the quantum subsystem may be considered an open quantum system with various interactions with the classical bath. Devising an algorithm to describe dynamics of such systems is difficult since the computational cost rises exponentially with the number of degrees of freedom [1,2]. This rapid rise motivates the construction of a range of approximate methods, among which the quantum-classical Liouville equation (QCLE) is our main focus. Where "t" denote time, $X = (R, P)$ is the concise notation of bath's canonical pair, $[\hat{A}, \hat{B}] = \hat{A}\hat{B} - \hat{B}\hat{A}$ denotes a quantum commutator where $\hat{A}$ and $\hat{B}$ are the operators, and $\{\hat{A}, \hat{B}\} = \frac{\partial \hat{A}}{\partial q}\frac{\partial \hat{B}}{\partial p} - \frac{\partial \hat{A}}{\partial p}\frac{\partial \hat{B}}{\partial q}$ is the Poisson bracket[1]. As you may notice, both operators depend on the canonical pair of the system.

II. Methods

In QCLE, the Hamiltonian and density matrix are operators in the Hilbert space of the subsystem while they are functions in the phase space of the bath. The mapping representation of this equation provides a phase-space-like description of discrete

$$\frac{\partial}{\partial t}\hat{\rho}_W(t) = -\frac{i}{\hbar}\left[\hat{H}_W(X), \hat{\rho}_W(X,t)\right] + \frac{1}{2}\left(\left\{\hat{H}_W(X), \hat{\rho}_W(X,t)\right\} - \left\{\hat{\rho}_W(X,t), \hat{H}_W(X)\right\}\right) \quad (1)$$

$$\frac{\partial}{\partial t}\rho_m(x,X,t) = \{H_m,\rho_m(t)\}_{x,X} + \frac{\hbar}{8}\sum_{\lambda\lambda'}\frac{\partial h^{\lambda\lambda'}}{\partial R}\left(\frac{\partial}{\partial r_{\lambda'}}\frac{\partial}{\partial r_\lambda} + \frac{\partial}{\partial p_{\lambda'}}\frac{\partial}{\partial p_\lambda}\right)\cdot\frac{\partial}{\partial P}\,\rho_m(t) \quad (2)$$

quantum states through mapping each state onto single-excitation states of fictitious harmonic oscillators [1-3].

Where $x=(r,p)$ is the canonical pair of mapping states of the subsystem, subscript "m" denotes the mapping form of each operator, while λ and λ' indicate mapping states corresponding to the subsystem's states. The second term on the right side of Eq (2) is responsible for a portion of the back reaction of the quantum subsystem on the classical environment [1,3]. In order to take the effect of this second term into account, we use an analogy with the continuity equation[4]. By comparing the continuity equation with the MQCLE, a set of equations of motion is obtained for the coordinates and momenta of the bath and subsystem mapping variables. To gain further insight into the nature of these equations, one may associate them with the equations that were obtained via omitting the second term in the equation. We realize that the only difference between these two sets of dynamical equations is an extra and complex part of the equation describing dynamics of the bath's momenum[3-5]. This part of the equation includes second derivatives of mapping variables, and since the numeric calculation of the second derivatives is challenging, it complicates the solution of the dynamics.

III. Results and Discussion

If we start with the Hermitian density matrix of the subsystem, map the subsystem states over fictitious harmonic oscillator states, and then take Wigner transform to describe it in the mapping basis. We will obtain the mapping density that can be inserted into the mentioned equations of motion. The resulting equation lends itself to Monte Carlo integration. Performing Verlet's time integration in the given time steps over the Monte Carlo's trajectories, we will be able to simulate the dynamics of the whole system.

IV. Conclusion

It can be inferred that the time evolution of each system and every ensemble of trajectories is obtainable. Despite the mapping Poisson bracket case where trajectories could evolve independently, trajectories are not behaving in the same way for the complete mapping quantum-classical Liouville equation. These coupled trajectories are the source of dissipation and decoherence of the system-bath description[1,4,5].

References

[1] R. Kapral, J. Phys.: Condens. Matter, 2015, 27, 3201

[2] H.Kim, A.Nassimi, and R. Kapral, J. Chem. Phys., 2008, 129, 8, 4102

[3] A.Nassimi, S.Bonella, and R. Kapral, J. Chem. Phys., 2010, 133, 13, 4115

[4] A.Kelly, R. Van Zon, J. Schofield, and R. Kapral, J. Chem. Phys., 2012, 136, 8, 4101

[5] CC. Wan, J. Schofield, J. Chem. Phys., 2002, 116, 2, 4494

بیست و سومین کنفرانس شیمی فیزیک انجمن شیمی ایران
23rd ICS Physical Chemistry Conference
Chemistry Department,
Faculty of Science
Shahid Bahonar University of Kerman
Kerman, Iran
12-13 Jan 2022
ایران، کرمان
دانشگاه شهید باهنر کرمان
دانشکده علوم پایه، بخش شیمی
۲۳-۲۲ دی ماه ۱۴۰۰

Theoretical investigations of the pyrimidine derivatives

Khadijeh shekoohi[a,*]

[a] *Department of Chemistry, Darab Branch, Islamic Azad University, Darab 7481783143-196, Iran*
E-mail: *sh.shekoohi@gmail.com*

Abstract

This study used, the density functional theory (DFT) methods to evaluate the geometrical properties, the lowest unoccupied molecular orbital (LUMO) and the highest occupied molecular orbital (HOMO) analysis and the molecular electrostatic potential (MEP) of pyrimidine derivatives containing oxindole.

.

Keywords:density functional theory, molecular electrostatic potential.

I. Introduction

Recently, pyrimidine derivatives have become one focus in the development of agrochemicals because of their high biological activity as herbicides, insecticides and fungicides[1].We study of pyrimidine derivatives with Density Functional Theory Calculation. This compounds synthetized with three-component reaction[2]that fig 1 shown this reaction. To investigate the correlation between molecular structure and properties quantum chemical study has been performed.

II. Computational details

The molecular properties of the compounds under investigation were determined by density functional theory (DFT). The DFT method using hybrid gradient-corrected (three-parameter nonlocal) exchange functional by Becke with the gradient corrected (nonlocal) correlation functional of Lee, Yang and Parr has been employed for all computations[3]. The first all compounds were optimized geometrical structures using B3LYP and 6-311G* basis set without any geometrical constraints. All the stationary structures in the gas phase have been fully optimized. All the calculations were performed by using GAUSSIAN03 program package .

III. Results and discussion

The corresponding molecular orbital pictures for the complexes obtained from their optimized geometries are visualized in Fig. 2.We have calculated the HOMO–LUMO orbital energy and HOMO–LUMO gap for all these compounds**.(**see Table 1).

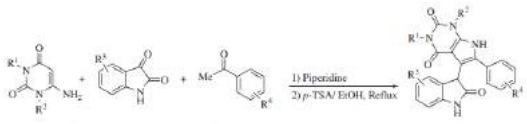

product	R^1	R^2	R^3	R^4
4i	H	H	H	H
4m	H	Me	H	H
4a	Me	Me	H	H

Fig2. Synthesis of 2-oxoindolin-3-yl-pyrrolo[2,3-d]pyrimidine-2,4(3H,7H)-diones under the optimized conditions[2].

According to Fig. 2, it has been observed that the LUMO surfaces is located on whole molecule but the HOMO surfaces lies on part of molecule. It is found that 4a have larger gap between HOMO LUMO gap therefore this molecule is inert respect

to 4i,4m. In the molecule 4m has the highest dipole moment among the complexes as shown in Table 1.

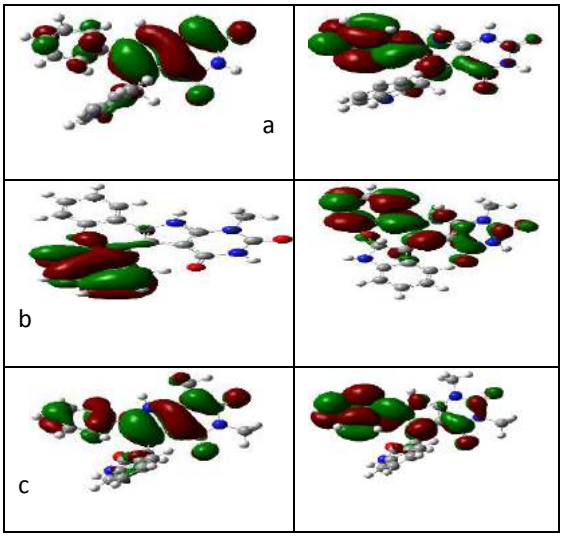

Fig.2. The isodensity plots of (a) 4i, (b) 4m and (c) 4a frontier orbitals

Table1.The computed properties of complexes

	E/a.u	Dipole/ deby	E_{HOMO} /ev	E_{LUMO} /ev	gap
4i	-1215.576	6.348	-5.649	-1.409	4.2
4m	-1254.897	6.522	-4.342	-1.281	3.1
4a	-1294.255	5.457	-5.643	-1.077	4.5

The molecular electrostatic potential (MEP) is related to the electronic density information on the molecular regions that are more susceptible to electrophilic or nucleophilic interactionAny molecule creates an electrostatic potential around itself[4].

Different values of electrostatic potential at MEP maps are shown by different colors which are mainly red, yellow, green, light blue and blue. The colors between red and green in MEP maps are related to electrophilic reactivity while the colors between green and blue in MEP maps is related to nucleophilic reactivity.

To predict reactive sites of electrophilic and nucleophilic attacks for the investigated compounds, MEP at the B3LYP/6-311g* optimized geometry was calculated. The MEP surfaces for 4m have been shown in Fig. 3.

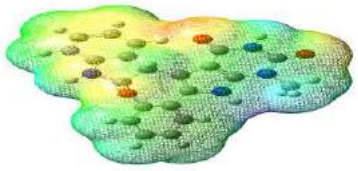

Fig3. Molecular electrostatic potential surface of 4m.

The negative sites of compounds **4a**, **4m**, **4i** are mostly focused on the Oxygen therefore, these sites have a high electron density and are appopriate for electrophilic attack (see Figure 3).

IV Conclusions

The design of pyridine derivatives containing a oxindol moiety were investigated using at the DFT /6-311G* theoretical level. The calculated results showed that highest gap energe between HOMO and LUMO is observed for molecule **4a** (R_1=R_2=CH_3, R_3=R_4=H)

References

[1] Huang, S.Q.; Zhang, Z.X.; Xu, H.H.; Zeng, D.Q., 2018, 44,81.

[2] K. Rad-Moghadam *, S.C Azimi Tetrahedron,2012,68, 9706.

[3] A.D. Becke, Density-functional thermochemistry. III. The role of exact exchange, J. Chem. Phys. 1993, 98,5648. C. Lee, W. Yang, R.G. Parr, Phys. Rev. 1988, B 37 785.

[4] S. R. Kumar, N. Vijay, K. Amarendra, P. Onkar, and S. Leena, Res J. Recent. Sci.2012, 1, 11

بیست و سومین کنفرانس شیمی فیزیک انجمن شیمی ایران
23rd ICS Physical Chemistry Conference
Chemistry Department,
Faculty of Science
Shahid Bahonar University of Kerman
Kerman, Iran
12-13 Jan 2022
ایران، کرمان
دانشگاه شهید باهنر کرمان
دانشکده علوم پایه، بخش شیمی
۲۳-۲۲ دی ماه ۱۴۰۰

Structural and Dynamic Properties of Cesium Metal by Molecular Dynamics Simulation

Khadijeh Shekoohi[a], **Mohammad Hadi Ghatee** [b,*]

[a] *Department of Chemistry, Darab Branch, Islamic Azad University, Darab 7481783143-196, Iran*
E-mail: *sh.shekoohi@gmail.com*
[b,*] *Department of Chemistry, Shiraz University, Shiraz 71454, Iran* ;E-mail:*ghatee@susc.ac.ir*

Abstract

In this study, by using the Gupta model potential, a series of Molecular dynamic simulations(MD) carried out to calculate the properties such as, density, pair distribution function $g(r)$, and surface tension of liquid cesium. These properties are investigated in wide range of temperatures of 400 to 1500K. Good agreements with experiment are observed for the simulated properties.

Keywords: molecular dynamic simulation, Gupta potential ,Pair correlation, surface tension

I. Introduction

In general experimental measurement at high temperatures and pressures for liquid metals is difficult and leads to a poor accuracy. In the last decade, the dynamic properties of liquid metals have been studied from a theoretical point [1,2] in our research group. A few MD simulation of liquid Cs have been performed. However, in the case of liquid cesium, not much work has been done to obtain vapor–liquid coexistence.

II. Computational details

We used the *n*-body Gupta potential [3], the Gupta potential parameters for cesium metal are reported in[3].All the simulation has been performed by using classical molecular dynamic method**,** using DL-POLY version 2.17. A cubic periodic boundary condition was employed throughout the simulations. The simulations were performed at constant number of molecule-volume-temperature (*NVT*), and Berendsen thermostat is considered for fixing the temperature in both the cases. We have considered box with 6500 atoms. We have performed simulation from low temperature to boiling point and high temperature (400-1500K).

III. Results and discussion

The pair correlation function of cesium at 323K is shown in Fig. 1 and compared with experimental pair correlation function. We observe that for structural properties of liquid Cs is in rather good agreement with the result of MD simulation and experimental data.

Surface tension, among other physical properties of metals, is a basis for studying the surface properties of the liquid state as well as the solvation property from practical and theoretical point of view.

Periodic boundary condition is applied in the three directions. We started with the construction of the simulation box (see Figure. 2) with the liquid slab in the center of a rectangular box. A time step of 1 fs was applied. After equilibration, simulation was performed for 4 ns at each

temperature for analysis. Bulk density was simulated by averaging the density of the bulk portion of the slab. The surface tension can be calculated by integrating the difference of the normal and tangential components of the pressure tensor across the interface. In the case of system with two interfaces the surface tension is calculated as: $\gamma = \frac{1}{2}\int_0^{Lz} dZ(p_n(z) - p_t(z))$

The value of γ was calculated from the components of pressure tensor of the simulation box: $\gamma = -b_z(P_{xx} + P_{yy} - 2P_{zz})/4$

whereb_z is the length of the simulation box along *z*-axis, e.g., along principle slab axis perpendicular to the liquid/vapor interface, and P_{xx}, P_{yy}, and P_{zz} are the principal components of the pressure tensor. The results of surface tension calculation in the range T = 298-723K are shown in Fig3. and compared with the experiments[4].

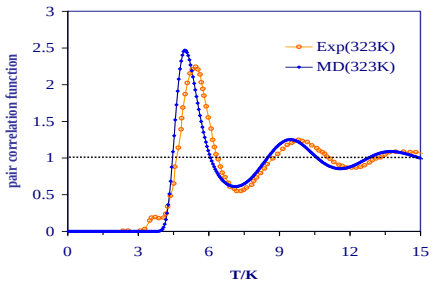

Figure 1. Pair correlation function *g*(*r*) for Cs. Results of this work is compared with the experimental results of Waseda[5] at 323K and atmospheric pressure.

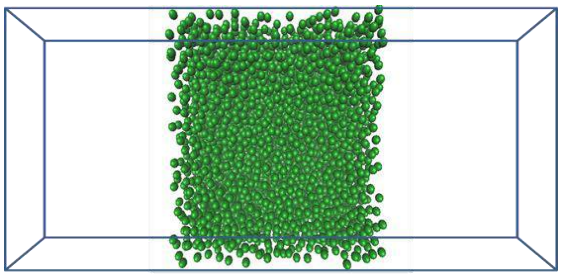

Fig2. A Snapshot of the simulated slab

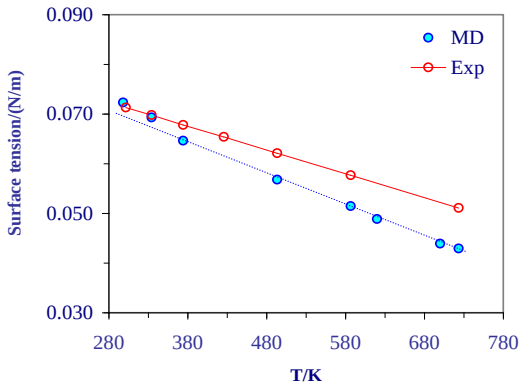

Figure 3. Surface tension (mNm^{-1}) from simulation, experimental

II. Conclusions

The molecular dynamics simulation with Gupta model predict liquid density of Cs having similar trend with the experimental density over the temperature range T= 400 to 1500K.The simulated surface tension leads to results with low deviations (with respect to the experimental) at low T's, though surface tension with higher deviations is produced at high temperatures.

References

[1] M.H. Ghatee, M. Bhadori, *Fluid Phase Equilib*,**2003**, 205, 339.

[2]M.H. Ghatee, M. Sanchooli, *Fluid Phase Equilib.*,**2003**,214, 197.

[3] F.Ducastelle, *J.phys.*(paris).,**1970**, 31, 1055.

[4] Handbook of Thermodynamic and Transport Propertiesof Alkali Metals, ed, R.W. Ohse Academic Press, Oxford, UK, 1985.

[5]R. Winter, F. Hensel, T. Bodensteiner, W. Glaser, Ber. Bunsenges.*Phys. Chem*. **1987**,91, 1327.

بیست و سومین کنفرانس شیمی فیزیک انجمن شیمی ایران
23rd ICS Physical Chemistry Conference
Chemistry Department,
Faculty of Science
Shahid Bahonar University of Kerman
Kerman, Iran
12-13 Jan 2022
ایران، کرمان
دانشگاه شهید باهنر کرمان
دانشکده علوم پایه، بخش شیمی
۲۳-۲۲ دی ماه ۱۴۰۰

Conical Intersection and Non-adiabatic Dynamics on Potential Energy Surfaces of H_2S^+ ion

Elahe Khosravi- Mashizi[a], Maryam Dehestani[a*], Elahe Mirzaie- Khaliabadi[a]

[a] *Department of Chemistry, Shahid Bahonar University of Kerman, Kerman, Iran,*
dehestani@uk.ac.ir

Abstract

In this work, we tried to find a suitable computational method for determining equilibrium structures and harmonic vibrational frequencies of the two lowest electronic states of H_2S^+. To understand non-adiabatic dynamics at conical intersections, we calculated the potential energy surfaces of excited electronic states, $^2A_1$ and $^2B_2$ by using MRCIQ method with CASSCF wave functions as reference functions with full valence complete active space comprising 17 electrons that are free to active orbitals with Aug-cc-pVQZ basis set. In this paper, we consider linear vibronic coupling model and evaluate vibronic coupling constant, diabatic frequencies for three modes of H_2S^+.

Keywords: Potential Energy Surface, Electronic State, Conical Intersection, Hydrogen sulfide ion

I. Introduction

H_2S^+ cation radical is a subject of experimental studies. Numerous studies have been conducted on the role of H_2S^+ in interstellar chemistry [1-3].

Potential energy surfaces and vibrational frequencies of states $^2A_1$, $^2B_1$ and $^2B_2$ of H_2S^+ ion are calculated by using MRCI method and cc-pvQz basis set. The conical intersection is determined between two states $^2A_1$, and $^2B_2$.

II. Methods

The electronic structure calculations of H_2S^+, for the two first excited electronic states were performed using ab initio calculations including CASSCF method with full-valence complete active space, comprising 17 electron that are active orbitals with Aug-cc-pVQZ basis set.

To check the effect of the dynamical electronic correlation on the geometries, and harmonic frequencies, we have examined the MRCI, CASSCF, CASPT2 and also MRCIQ methods with Aug-cc-pVQZ and Aug-cc-pV5Z basis sets. Comparing the results obtained at these computational levels with the experimental values shows that the MRCI computational level with CASSCF wave functions as reference functions with full valence complete active space give accurate equilibrium geometry and vibrational frequencies in first three electronic states of H_2S^+. All calculations are carried out with MOLPRO package. Since asymmetric stretching mode decreases the symmetry of molecule from C_{2v} to C_s, electronic energies and normal coordinates were calculated in both point groups (C_{2v} and

C_s). In the present study, we consider the linear vibronic coupling model and evaluate vibronic coupling constant, diabatic frequencies for three vibrational modes bending (ω_1), symmetric stretching (ω_2) and antisymmetric stretching (ω_3) using Mathematica program.

III. Results and discussion

In the first step in this paper, we tried to find a suitable computational method for investigating equilibrium structures and harmonic vibrational frequencies of the first electronic states of H_2S^+. Then we reexamined the existence of a conical intersection between $^2A_1$ (first excited electronic state) and $^2B_2$ (second excited electronic state) electronic states with MRCI Aug-cc-pVQZ level of theory and obtained the equilibrium geometry of this conical intersection. We obtained that at bond length 1.35 Å the conical intersection occurs between $^2B_2$ and $^2A_1$ states at the bond angle of 71.2º (Figs. 1 and 2).

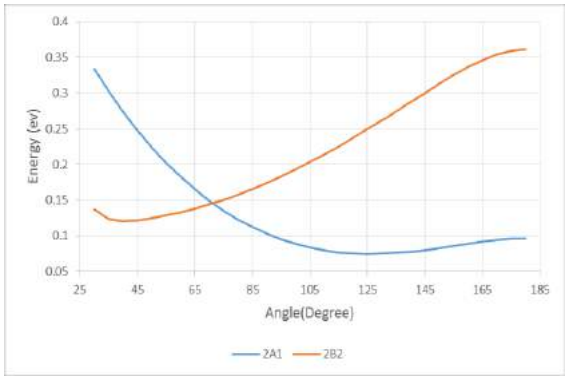

Fig. 1 Adiabatic potential energy curves changes in terms of bond angle at equilibrium bond length 1.357A°

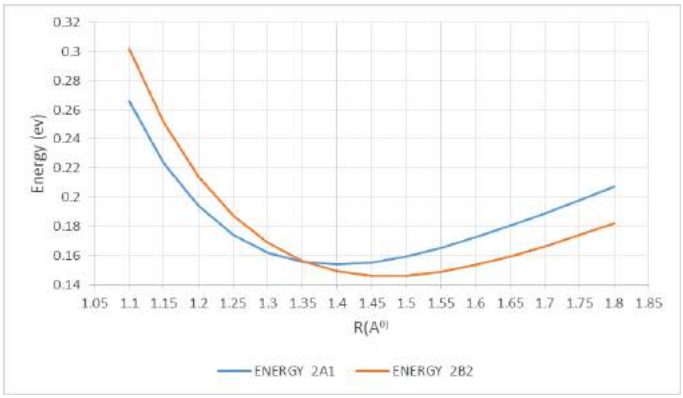

Fig. 2 Adiabatic potential energy curves changes in terms of bond length at the bond angle 71.2º

Since the non-adiabatic dynamics play an important role in characterizing molecular properties, we considered a linear vibronic coupling Hamiltonian model and evaluated vibronic coupling constant, non adiabatic frequencies for three modes of H_2S^+ (including bending, symmetric stretching and anti-symmetric stretching modes), bilinear and quadratic coupling constants for diabatic potentials.

IV. Conclusion

The first $^2A_1$ and second $^2B_2$ excited electronic of H_2S^+ cation can be coupled with each other by anti-symmetric stretching mode.

References

[1] D. Smith, N. G. Adams, W. Lindinger, 1981, J. Chem. Phys. 75(7), 3365-3370.

[2] G. F. Stowe, R. H Schultz, C. A. Wight, P. B. Armentrout, 1990, Int. J. Mass Spect. Ion Proc. 100, 177-195.

[3] G. Duxbury, C. Jungen, A. Alijah, J. P., Maier, D. Klapstein, 2014, Mol. Phys. 112(23), 3072-3084.

بیست و سومین کنفرانس شیمی فیزیک انجمن شیمی ایران
23rd ICS Physical Chemistry Conference
Chemistry Department,
Faculty of Science
Shahid Bahonar University of Kerman
Kerman, Iran
12-13 Jan 2022
ایران، کرمان
دانشگاه شهید باهنر کرمان
دانشکده علوم پایه، بخش شیمی
۲۲-۲۳ دی ماه ۱۴۰۰

Semi-industrial synthesis of magnetic Fe_3O_4@SiO_2@Me nanopowder to visualization of latent fingerprints

Akbar Mobaraki*

[a] *Department of Chemistry, Kharazmi University, 49 Mofateh St., Tehran 15719- 14911 (Iran);*

akbar.mobaraki@khu.ac.ir

Abstract

In this study a magnetic nanopowder for the development of latent fingerprints in semi-industrial scale was prepared. Instrumental techniques such as VSM and TEM were used to characterize the nanopowders. To show that the achieved structure and properties are well-suited for forensic science, fingerprints developed using the Fe_3O_4@SiO_2@Me nanopowders were applied on the sheet of paper. The nanopowder, Fe_3O_4@SiO_2@Me, offers simple synthesis process, convenient use for routine casework and low price**.**

Keywords: Surface chemistry, Magnetic nanopowder; Fingerprint; Fe_3O_4.

I. Introduction

Detection, imaging, and identification of latent fingerprints with powder is one of the most common forensic techniques for crime investigation [1, 2]. The dusting method greatly helps policemen in screening the potential criminal scenes and capturing fingerprint clues that are left behind when surfaces are handled with bare hands. In the dusting method, the dry powder particles adhere to the latent fingerprints residue on the surface. Therefore, the choice of the type and characters of used powder can depend on the properties of the particles, surfaces, and the type of the remained fingerprint. In this case, sufficient color contrasts with the surface, particle size, the shape of the fingerprint powders as well as by what method lifting of the particles from the surface are the critical factors [3]. Among various dusting agents, much attention has been focused on magnetic nanoparticles (MNPs) because easier fingerprint lifting by means of a permanent and ordinary magnet and higher visibility of the latent fingerprints.

As part of our efforts in surveying magnetic materials [4], we have semi-industrial scale prepared and characterized Fe_3O_4@SiO_2@Me magnetic fingerprint nanopowders (MFNPs) (Fig. 1a). Moreover, application and evaluation of the MFNPs to achieve clear and visible fingerprints on the paper surface to develop latent fingerprints were performed.

II. Methods

Fe_3O_4 MNPs was achieved using the procedure rendered by Zhang and co-workers [5]. The Fe_3O_4@SiO_2@Me MFNPs were prepared with grafting of the tetraethoxysilane (TEOS) and trimethoxymethylsilane (TMMS) precursors on the Fe_3O_4 MNPs, respectively.

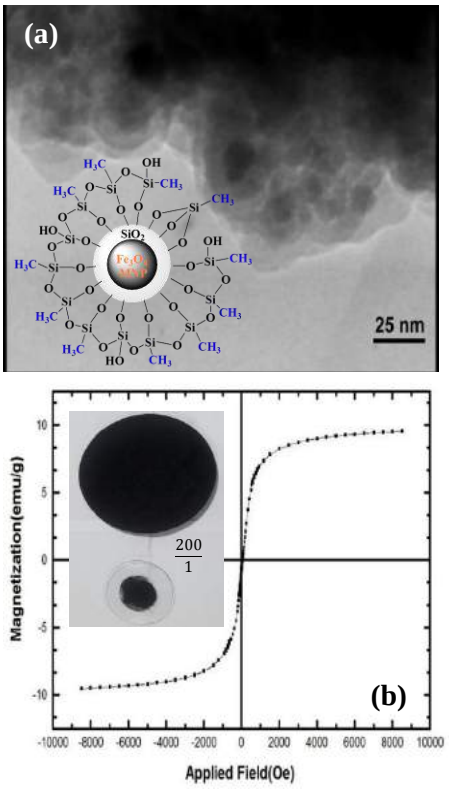

Fig. 1. (a) Schematic representation and TEM image of the Fe_3O_4@SiO_2@Me MFNPs. (b) VSM magnetization curves and scale-up synthesis of the Fe_3O_4@SiO_2@Me MFNPs.

We improved the synthetic procedure to pre-industrial scale in 200 times larger than laboratory scale in practice (Fig. 1b).

III. Results and discussion

To evaluate the magnetic properties of the obtained MFNPs, vibrating sample magnetometer (VSM) measurements at room temperature were performed (Fig. 1b). The Fe_3O_4@SiO_2@Me MFNPs exhibit the saturation magnetization (Ms) of 9.6 emu/g. To investigate the morphology and texture of the Fe_3O_4@SiO_2@Me MFNPs, the resultant nanopowders were characterized with using TEM image (Fig. 1a). It can be observed that the average particle diameters of synthesized MFNPs were approximately 25 nm. In our investigation, the 'in situ photographing' method was used. Using MFNPs, latent fingerprints photos taken from various individuals on the sheet of paper in the Fig. 2 were produced and rendered.

Fig. 2. Photos taken from individuals latent fingerprint developed with Fe_3O_4@SiO_2@Me MFNPs on the sheet of paper.

IV. Conclusions

In conclusion, we have semi-industrial scale prepared and characterized, a simple and efficient magnetic nanopowder, Fe_3O_4@SiO_2@Me, which has been used as a dusting agent for the development of latent fingerprints. Instrumental techniques such as VSM and TEM have shown suitable magnetic and texture properties of the prepared MFNPs. Finally, latent fingerprints photos taken from various individuals on the sheet of paper show the MFNPs is an efficient dusting agent.

References

[1] J.S. Gurbuz, *J. Forensic. Sci.*, 2015, 60, 727.
[2] P. Hazarika, *Angew. Chem. Int. Ed.*, 2012, 51, 3524.
[3] G.S. Sodhi, *Forensic. Sci. Int.*, 2001, 120, 172.
[4] A. Mobaraki, *ACS Comb. Sci.*, 2014, 16, 352.
[5] Q. Zhang, *Green Chem.*, 2012, 14, 201.

بیست و سومین کنفرانس شیمی فیزیک انجمن شیمی ایران
23rd ICS Physical Chemistry Conference
Chemistry Department,
Faculty of Science
Shahid Bahonar University of Kerman
Kerman, Iran
12-13 Jan 2022
ایران، کرمان
دانشگاه شهید باهنر کرمان
دانشکده علوم پایه، بخش شیمی
۲۳-۲۲ دی ماه ۱۴۰۰

A study on the releasing process of benzotriazole from magnetized halloysite nanocapsules

Sima Shahdadi, Maryam Akhondi, Effat Jamalizadeh
Department of Chemistry, Shahid Bahonar University of Kerman, Kerman, Iran
jamalizadeh@uk.ac.ir

Abstract
Today, several methods are developed for the improvement of corrosion resistance and the increase of alloy performances. Among these methods is the application of corrosion inhibitors. One new method that is currently studied is the synthesis of capsules with an inhibitor stored inside so that the inhibitor is released in a corrosive media. In this study, the releasing process of benzotriazole inhibitor from magnetized halloysite nanocapsules has been investigated by UV-vis spectroscopy. The obtained results indicate that in a corrosive medium, the inhibitors are gradually released into the solution.

Keywords: Nanocapsule, Magnetic Halloysite, Inhibitor, Corrosion.

I. Introduction

Halloysites have been studied as capsules synthesized with different methods from different shells [1]. Also, nanohalloysites are utilized as capsules for corrosion inhibitors [2]. Furthermore, various composites are synthesized by halloysite and Fe3O4 [3]. In this investigation, the releasing process of inhibitor from magnetized halloysite nanocapsules has been studied. One most important reason for magnetizing halloysites is their response to the magnetic field so that they can be easily collected from the media.

II. Methods

In this research, halloysite nanotubes powder of New Zealand China Clay Ltd. (Auckland, New Zealand) have been used. Benzotriazole, polyallylamine (100%) and polystyrene sulfonate (30%) have been purchased from Sigma Aldrich, USA. Iron chloride (100%), iron chloride hexahydrate (99%), ammonia (96%), hydrochloric acid (37%) were obtained from Merck.

The halloysite powder was mixed with iron chloride hexahydrate, iron chloride and water, and then the solution was refluxed. After 24 h, ammonia was added dropwise. Finally, the deposit was collected by a magnet and dried.

Then, benzotriazole was dissolved in water and after that, the magnetized halloysite was added to the solution. After 1 h, the solution was dried during stirring and collected using a centrifuge. Finally, benzotriazole was loaded into the magnetic halloysite.

To Generation polymer shell over the magnetic halloysite, polyallylamine hydrochloride was mixed with a solution comprising the magnetic halloysite and then collected with a centrifuge. In the next step, polystyrene sulfonate was added to the solution and the generate

nanocapsules were collected by a centrifuge.

The release of inhibitor in aqueous hydrochloric acid solution at pH 5 in the range of 15 min to 48 h was performed with a UV-Vis system.

III. Results and Discussion:

Figure 1 shows the TEM image of the halloysite nanotubes utilized in this investigation. Figure 2 indicates the results obtained from UV-VIs analysis. The results of UV-Vis showed that the inhibitor is gradually released from the halloysite nanocapsules. As shown in the figure, the release of the benzotriazole inhibitor is carried out at pH 5 up to 48 h. As well, according to the obtained results, the releasing rate of inhibitor is higher during the early times. The results also indicate that the releasing rate of the inhibitor is reduced during the period of 26 to 48 h and ends after 48 h.

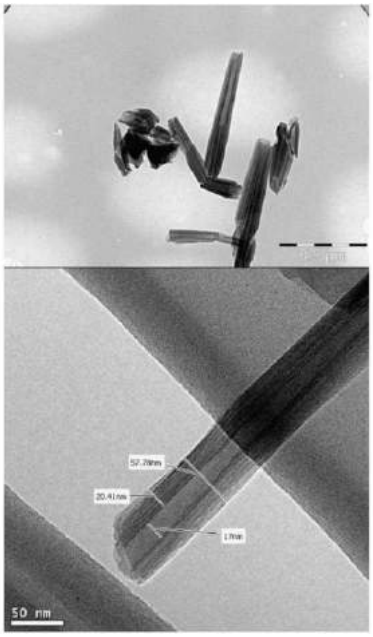

Figure 1. TEM image of halloysite nanotubes

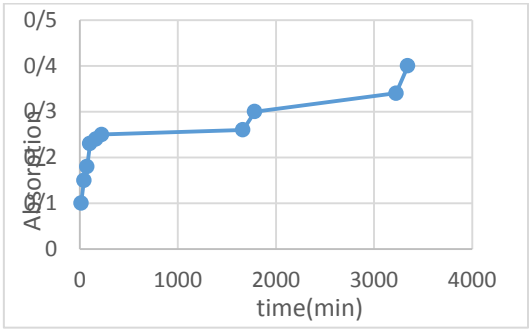

Figure 2: The releasing process of inhibitor from halloysite nanocapsules over time.

IV. Conclusions

The obtained results indicate the releasing of inhibitor at pH 5 over time.

The releasing rate of inhibitor in the first hours is higher than that in the last hours.

The releasing process ends after 48 h.

These nanocapsules can interact with the media and gradually release the inhibitor.

References

[1]. Duan J, Liu R, Chen T, Zhang B, Liu J. Halloysite nanotube-Fe3O4 composite for removal of methyl violet from aqueous solutions. Desalination. 2012;293:46-52.

[2]. Mu B, Wang W, Zhang J, Wang A. Superparamagnetic sandwich structured silver/halloysite nanotube/Fe 3 O 4 nanocomposites for 4-nitrophenol reduction. RSC Advances. 2014;4(74):39439-45.

[3]. Song X, Zhou L, Zhang Y, Chen P, Yang Z. A novel cactus-like Fe3O4/Halloysite nanocomposite for arsenite and arsenate removal from water. Journal of Cleaner Production. 2019;224:573-82.

[4] Maziarz P, Matusik J. Halloysite composites with Fe3O4 particles: the effect of impregnation on the removal of aqueous Cd (II) and Pb (II). Mineralogia. 2017;48.

[5] Hajizadeh Z, Maleki A, Rahimi J, Eivazzadeh-Keihan R. Halloysite Nanotubes Modified by Fe 3 O 4 Nanoparticles and Applied as a Natural and Efficient Nanocatalyst for the SymmetricalHantzsch Reaction. Silicon. 2020;12(5):1247-56.

بیست و سومین کنفرانس شیمی فیزیک انجمن شیمی ایران
23rd ICS Physical Chemistry Conference
Chemistry Department,
Faculty of Science
Shahid Bahonar University of Kerman
Kerman, Iran
12-13 Jan 2022
ایران، کرمان
دانشگاه شهید باهنر کرمان
دانشکده علوم پایه، بخش شیمی
۲۳-۲۲ دی ماه ۱۴۰۰

Investigation of the Equilibrium Parameters of Vinyl Cyanide as an Astrochemical Molecule Using Quantum Calculations

Arya Saboori Amleshi [a], Danial Mohammadi [*], Maryam Dehestani[b]

[a] *Department of Chemistry, Shahid Bahonar University of Kerman, Kerman, Iran, arya.saboori.a@gmail.com*

[b] *Department of Chemistry, Shahid Bahonar University of Kerman, Kerman, Iran, dehestani@uk.ac.ir*

[*] *Department of Chemistry, Shahid Bahonar University of Kerman, Kerman, Iran, danialmoh14@gmail.com*

Abstract

Vinyl cyanide, a molecule with planar geometry, has been presented as a strong candidate, forming Azotosomes on Titan's hydrocarbon-abundant lakes and seas. To further investigate the parameters of vinyl cyanide, three computational approaches DFT, MP2, and CCSD(T) were implemented. The results with the highest accuracy concerning the experimental data presented in the literature and data obtained from Atacama Large Millimeter/submillimeter Array (ALMA) have been selected and presented.

Keywords: Astrochemistry; Computational Chemistry; Vinyl cyanide; Quantum Calculations; Molecular Spectroscopy

I. Introduction

Astrochemistry studies the formation, destruction, and excitation of molecules in interstellar environments and their impact on the structure, dynamics, and evolution of astronomical objects [1]. It is required to obtain highly accurate calculations of astrochemical molecules equilibrium parameters, such as rotational and vibrational constants [2]. Vinyl cyanide (IUPAC Name: prop-2-enenitrile) with the molecular formula of CH_2CHCN has a high astrochemical and astrobiological value, using the archival data from the Atacama Large Millimeter/submillimeter Array (ALMA), which was gathered over a sequence of studies from February to May 2014, vinyl cyanide seems to be the best current candidate for the development of cell vesicles and membranes known as "azotosomes" on Titan's hydrocarbon-abundant lakes and seas [3,4]. Additionally, vinyl cyanide's ground and vibrationally excited states have been detected in interstellar space in the 80 - 280 GHz frequency range in Orion-KL with IRAM-30 m [5].

II. Methods

Using coupled cluster (CCSD(T)), Density-functional theory, and Møller–Plesset (MP2) methods in conjunction with three Dunning's correlation consistent basis sets; cc-pVTZ, cc-pVQZ, and cc-pV5Z [6], the rotational constants have been directly determined. The accuracy of each approach has been evaluated with respect to experimental data obtained from ALMA's archival data [3].

III. Results and discussion

In this study, equilibrium rotational constants of vinyl cyanide have been calculated with three different methods, including CCSD(T), B3LYP, and MP2 methods with cc-pVTZ, cc-pVQZ, and cc-pV5Z basis sets, to compare the accuracy

and efficiency of each method. In Table 1, the calculated parameters and CPU time of each approach have been presented. Since the MP2/cc-pV5Z, CCSD(T)/cc-pVQZ, and CCSD(T)/cc-pV5Z theory levels were overwhelmingly complicated, the calculations were not time efficient. According to the rotational constants of theoretical and experimental data [7], the MP2/cc-pVQZ and CCSD(T)/cc-pVTZ theory levels have shown to be more accurate. However, based on the CPU time of the corresponding calculations, the accuracy and calculation efficiency of the MP2/cc-pVQZ theory level stands out among the other mentioned approaches.

Table 1. Rotational constants and CPU time of different approaches: The calculations were conducted using Gaussian 09, and the experimental data was obtained from the ALMA archives; Computation system specifications: CPU model: Intel(R) Xenon(R) CPU E5-2650 V4 @ 2.20HHz; Number of processors shared: 40; Memory (RAM): 10GB

Vinyl Cyanide		Theoretical						Experimental
		DFT (B3LYP functional)			MP2		CCSD(T)	
		cc-pVTZ	cc-pVQZ	cc-pV5Z	cc-pVTZ	cc-pVQZ	cc-pVTZ	
Rotational Constants (GHz)	A	51.51501	51.46941	51.46941	49.93099	49.94778	50.15697	49.85069
	B	4.97515	4.98071	4.98071	4.94948	4.97202	4.96223	4.97121
	C	4.53698	4.54125	4.54125	4.50311	4.52189	4.51550	4.51382
CPU time (H:M)		00:15	02:30	39:29	01:44	29:16	666:53	

The total electric dipole moment of vinyl cyanide observed by MP2/cc-pVQZ theory level is 3.865 Debye. Also, the most intense vibrational frequency peaks and the related symmetry of the molecule have been listed in Table 2. Additionally, the calculated IR spectra of vinyl cyanide using MP2/cc-pVQZ theory level have been presented in Figure 1.

Table 2. Vibrational frequencies (GHz) with the highest peak and the related symmetry of the molecule.

Frequency (GHz)	Symmetry
6843.696 (1)	A'
21041.269 (4)	A"
29352.099 (6)	A"
30459.715 (7)	A"

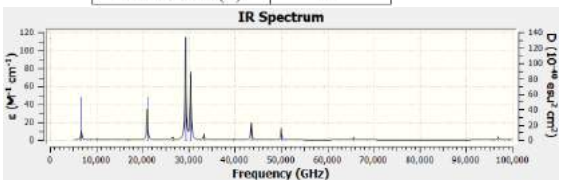

Fig. 1. The calculated IR spectrum of vinyl cyanide using MP2/cc-pVQZ

IV. Conclusions

Although many scholars have compared the accuracy of different quantum mechanical methods for many compounds [1], vinyl cyanide has not been studied enough. In the current study, quantum mechanical calculations have been explored for vinyl cyanide. Based on the observations in this study, the MP2/cc-pVQZ theory level was demonstrated to be dependable and time-efficient. The IR spectrum, the dipole moment of vinyl cyanide was presented in the paper. In future studies, the rotational spectra will be derived from the mentioned calculations.

References

[1] E.Herbst, and J.T. Yates Jr, Chemical reviews, 2013. 113(12): p. 8707-8709.
[2] M.Biczysko, J. Bloino, and C. Puzzarini, Wiley Interdisciplinary Reviews: Computational Molecular Science, 2018. 8(3): p. e1349.
[3] M.Y.Palmer, et al., Science advances, 2017. 3(7): p. e1700022.
[4] J. Stevenson, J. Lunine, P. Clancy, Sci. Adv. 1, e1400067 (2015).
[5] A.López, et al., Astronomy & Astrophysics, 2014. 572: p. A44.
[6] A.K.Wilson, T. Van Mourik, and T.H. Dunning Jr, Journal of Molecular Structure: THEOCHEM, 1996. **388**: p. 339-349.
[7] M.K.Sharma, Heliyon, 2019. 5(8): p. e02384.

بیست و سومین کنفرانس شیمی فیزیک انجمن شیمی ایران
23rd ICS Physical Chemistry Conference
Chemistry Department,
Faculty of Science
Shahid Bahonar University of Kerman
Kerman, Iran
12-13 Jan 2022
ایران، کرمان
دانشگاه شهید باهنر کرمان
دانشکده علوم پایه، بخش شیمی
۲۳-۲۲ دی ماه ۱۴۰۰

Semiempirical Quantum Calculations of Chiral Pillararene decorated with Alpha-hydroxyglycine for Enantioseparation of D-glucose and L-glucose

Arya Saboori [a], Amir Fallah lalehzari [b], Effat Jamalizadeh [*]

[a] *Department of Chemistry, Shahid Bahonar University of Kerman, Kerman, Iran, arya.saboori.a@gmail.com*
[b] *Department of Chemistry, Shahid Bahonar University of Kerman, Kerman, Iran, amirfallah623@gmail.com*
[c] *Department of Chemistry, Shahid Bahonar University of Kerman, Kerman, Iran, jamalizadeh@uk.ac.ir*

Abstract

Glucose, consumed widely every day, has two L and D enantiomers. The semiempirical PM7 method was utilized to investigate enantiomer separation of glucose with different enantioselective pillararenes. Also, alpha-hydroxyglycine-pillar[6]arene (AHGP6) has been introduced as a new glucose enantioselective molecule, and the separation of glucose enantiomers by differently decorated pillararene has been calculated. Also, the effect of pillararenes' ring size on the enantioseparation has been investigated.

Keywords: Enantiomer separation; Glucose; Pillararene; Semiempirical quantum calculations; PM7

I. Introduction

Chirality changes the way compounds interact in a biological environment; therefore, enantiomer separation is a helpful way to take advantage of the desired results with a specific enantiomer [1]. Although the separation of L and D enantiomers of glucose can affect the food industry[2], theoretical studies on glucose are limited.

The key point in enantiomer separation is the non-covalent interaction between host and guest molecules [3, 4]. Therefore, to separate enantiomers efficiently, it is essential to use a host molecule with many chiral centers, forming strong non-covalent bonds with the guest molecule. Pillararene is a significant enantiomer-selective molecule, appeared in scientific papers as an enantioselective molecule [4]. Although the enantiomer separation of glucose has not been studied much, in a recent paper, the selectivity of l-alanine decorated pillar[6]arene (LAP6) had been studied experimentally and theoretically at the B3LYP/6-31G* level. In the current study, the energy of pillararene and glucose enantiomers as a host-guest system was investigated through semiempirical quantum calculations PM7, which is known as an efficient approach, besides describing non-covalent interactions aligned to the experimental data. According to the literature, PM7 has improved in describing non-covalent bonds compared to PM6 [3].

II. Methods

The initial structures of L/D-glucose and pillararenes were prepared in GaussView 6.0.16. As shown in Fig. 1, all structures were optimized through the semiempirical PM7 method using Gaussian 09 software.

Moreover, the energy of the optimized host-guest system was compared to the enantioselectivity of different pillararenes.

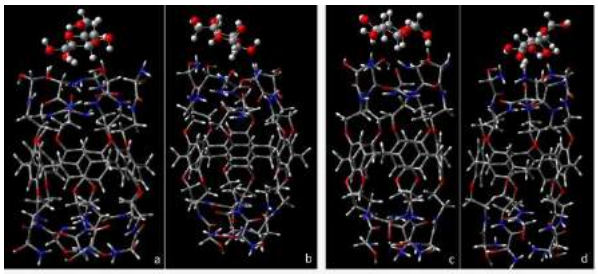

Fig. 1. Optimized Complex of Pillararenes and Enantiomers of Glucose; a,b: D-glucose and L-glucose with AHGP6 respectively; c,d: D-glucose and L-glucose with AHGP6, respectively.

Results and discussion

The total energy between D-glucose and LAP6 system is less than L-glucose and LAP6, which demonstrates stronger non-covalent bonds between D-glucose and LAP6, leading to the separation of L and D glucose. This is consistent with the experimental data in the literature.

In this work, AHGP6 was introduced as a new molecule to separate glucose enantiomers. The non-covalent bonds have been reinforced compared to LAP6 since substituted hydroxyl groups form strong hydrogen bonds with glucose. The optimization and the lower energy calculation of L/D-glucose and AHGP6 shows that AHGP6 can be a good candidate for the experimental separation of glucose enantiomers.

As shown in table 1., to explore possible impacts of pillararene's ring size on the enantiomer separation, the interaction energy of alpha-hydroxyglycine-pillar[5]arene (AHGP5) and alpha-hydroxyglycine-pillar[7]arene (AHGP7) with glucose enantiomers have been calculated. Considering the magnitude of difference between the energy of L/D-glucose and pillararenes mentioned in table 1., the AHGP5 shows an excellent selectivity towards glucose enantiomers.

Table 1. Energies of the system with glucose enantiomers and different pillararenes

Energy (Hartree)	LAP6	AHGP5	AHGP6	AHGP7
D-Glucose	-2.3748	-2.7218	-3.2309	-3.6372
L-Glucose	-2.3743	-2.7472	-3.2157	-3.6301
Magnitude of difference	0.0005	0.0254	0.0152	0.0071

III. Conclusions

The selectivity of alpha-hydroxy glycine decorated pillararenes towards glucose enantiomers has been shown to have stronger non-covalent bonds compared to l-alanine groups. Moreover, the calculation of total energy of L/D-glucose and different ring size of pillararenes demonstrated alpha-hydroxyglycine-pillar[5]arene with the highest selectivity compared to other molecules mentioned in this paper, leading to better enantiomer separation of glucose.

References

.1 Maier, N.M., P. Franco, and W. Lindner, *Separation of enantiomers: needs, challenges, perspectives.* Journal of Chromatography A, 2001. **906**(1-2): p. 3-33.

.2 Dubovski, N., et al., *Sweet chirality: the taste of L and D glucose stereoisomers.* bioRxiv, 202.0

.3 Hostaš, J., J. Řezáč, and P. Hobza, *On the performance of the semiempirical quantum mechanical PM6 and PM7 methods for non-covalent interactions.* Chemical Physics Letters, 2013. **568**: p. 161-166.

.4 Sun, Y., et al., *A biomimetic chiral-driven ionic gate constructed by pillar [6] arene-based host–guest systems.* Nature communications, 2018. **9**(1): p. 1-7.

بیست و سومین کنفرانس شیمی فیزیک انجمن شیمی ایران
23rd ICS Physical Chemistry Conference
Chemistry Department,
Faculty of Science
Shahid Bahonar University of Kerman
Kerman, Iran
12-13 Jan 2022
ایران، کرمان
دانشگاه شهید باهنر کرمان
دانشکده علوم پایه، بخش شیمی
۲۳-۲۲ دی ماه ۱۴۰۰

Effect of hydrophobic surface of ethyl-bridged periodic mesoporous organosilica functionalized sulfonic acid in the catalytic performance and product selectivity

Akbar Mobaraki[a,*], Babak Karimi[b], Hamid M. Mirzaei[b]

[a] *Department of Chemistry, Kharazmi University, 49 Mofateh St., Tehran 15719-14911, Iran; akbar.mobaraki@khu.ac.ir*
[b] *Department of Chemistry, Institute for Advanced Studies in Basic Sciences (IASBS), Zanjan 45137-6731, Iran; E-mail: karimi@iasbs.ac.ir*

Abstract

In this study we attest whether the hydrophobic/hydrophilic balance in the surface of solid catalysts might influence their catalytic performance. Therefore, two nanocatalyst were prepared and water adsorption-desorption isotherms of that, Et-PMO-Me-PrSO_3H (**1b**) in comparison to SBA-15-PrSO_3H (**1a**) have been measured. Effect of the hydrophobic surface of the **1b** was investigated in the synthesis of benzimidazole.

Keywords: Surface hydrophobicity, Benzimidazole, Periodic mesoporous organosilica, Catalyst.

I. Introduction

Periodic mesoporous organosilica (PMO) compound was first introduced in 1999, built from bridge organosilica precursor [$(RO)_3$Si-R-Si$(OR)_3$], through the surfactant self-assembly approach analogous to that used in preparation of ordered mesoporous silicates [1]. These materials have gained increasing interest because of their high surface area, adjustable pore size, and uniform organic moieties distribution inside the pore wall, and also highly tunable physicochemical properties such as hydrothermal and mechanical stabilities by varying the nature and extent of organic groups inside the pore wall and surface functionalization. Considering the hydrophilic nature of the most heterogeneous catalysts, the major problem is mass transfer phenomena in chemical reactions. Therefore, the hydrophobic/hydrophilic balance of surface of the solid catalysts could significantly influence their catalytic performance and product selectivity. Along the line in this hypothesis and our continuous interest in tuning and optimizing of hydrophobic/hydrophilic characteristic of the surface of the catalysts to gain more selective catalyst in recent years [2, 3], herein, our purpose is utilization of ethane-bridges PMO based sulfonic acid (**1b**) as a catalyst with hydrophobic surface and nanopores in the synthesis of benzimidazole.

II. Methods

Organosulfonic acid-functionalized PMO, Et-PMO-Me-PrSO_3H (**1b**), and SBA-15-PrSO_3H (**1a**) were synthesized according to the methods of Hamoudi et. al. [4] and Karimi et. al. [5], respectively.

III. Results and discussion

The textural and structural properties of **1b** synthesized for the current work was determined by elemental analysis (sulfur content 0.8 mmol.g^{-1} measured), and

transmission electron microscopy (TEM) image (Fig. 1).

To attest whether the hydrophobicity-acidity of catalyst and its selectivity toward reaction could influence both conversion and selectivity pattern of product in this study, we measured water adsorption-desorption isotherm of **1b** in comparison to **1a** in the gas phase at 25 °C. As can be shown, **1a** has a large water adsorption, indicating the hydrophilic nature of solid. In contrary, the **1b** showed much lower water uptake under the same condition, demonstrating the hydrophobic nanospaces of its (Fig. 2).

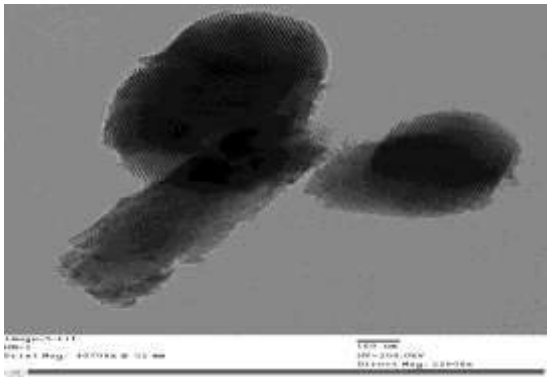

Fig. 1. TEM image of Et-PMO-Me-PrSO$_3$H.

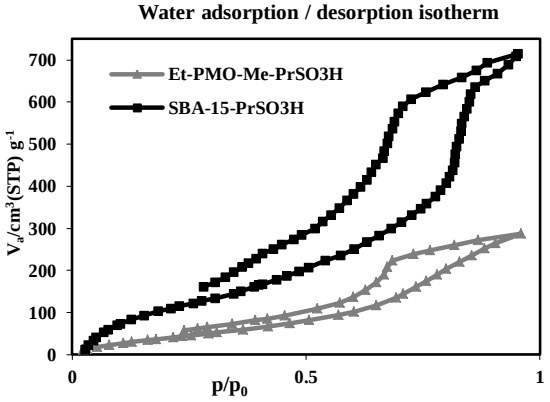

Fig. 2. Water adsorption-desorption of **1a** and **1b** solid acids.

To examine the possibility of our objective route to synthesis of benzimidazole, we have developed an efficient procedure for the synthesis of it from tandem reaction of isothiocyanate with 2-aminoaniline under solvent-free condition. A significant selectivity toward 1,3-dihydrobenzimidazole-2-thione (**A**) was observed by using **1b** as a hydrophobic solid acid.

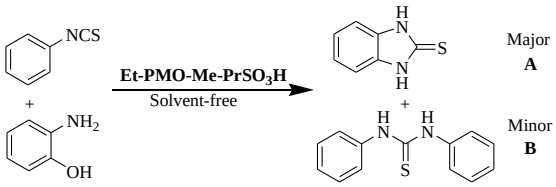

Fig. 3. Selectivity toward 1,3-dihydrobenzimidazole-2-thione **A** in the presence of Et-PMO-Me-PrSO$_3$H (**1b**) solid acid.

IV. Conclusions

In summary, we have prepared a solid acid, Et-PMO-Me-PrSO$_3$H (**1b**), with hydrophobic nature of surfaces and nanospaces to develop an efficient and practical procedure for the synthesis of benzimidazole under solvent-free conditions. A significant selectivity toward 1,3-dihydrobenzimidazole-2-thione (**A**) was observed which can be attributed to the surface hydrophobicity of **1b** which caused an easy diffusion of reactant into the nanopores of its where the catalytic sites are located, followed exclusion of the reaction polar products or by-products from the hydrophobic pores.

References

[1] S. Inagaki and O. Terasaki, J. Am. Chem. Soc., 1999, 121, 9611-9614.
[2] A. Mobaraki, B. Movassagh and B. Karimi, Appl. Catal. A: Gen., 2014, 472, 123-133.
[3] A. Mobaraki, B. Movassagh and B. Karimi, ACS Comb. Sci., 2014, 16, 352-358.
[4] S. Hamoudi and S. Kaliaguine, Micropor. Mesopor. Mater., 2004, 71, 17-25.
[5] B. Karimi and D. Zareyee, Org. Lett., 2008, 10, 3989-3992.

بیست و سومین کنفرانس شیمی فیزیک انجمن شیمی ایران
23rd ICS Physical Chemistry Conference
Chemistry Department,
Faculty of Science
Shahid Bahonar University of Kerman
Kerman, Iran
12-13 Jan 2022
ایران، کرمان
دانشگاه شهید باهنر کرمان
دانشکده علوم پایه، بخش شیمی
۲۳-۲۲ دی ماه ۱۴۰۰

Puckering angle in charged B-heterocyclic divalents: A computational DFT study

Babak Golzadeh[a,*]

[a] *Address: Department of Chemistry, Payame Noor University, P.O. Box 19395-3697, Tehran, Iran*
Fax: +982122441511; Tel: +989357820005; E-mail: b.golzadeh@pnu.ac.ir

Abstract

The introduction of electron-withdrawing groups such as boryl substituents flanking the divalent center (Ë) produces Boron-Heterocyclic divalents (BHEs); a good model of pull–pull carbene story profiting from the ability of boron to stabilize a lone pair in an adjacent position. Every bent singlet structure for all studied species is more stable. The stability of the singlets with a puckered geometry (D1≅66°) is achieved via cross-ring hyperconjugative interactions. Here, we decide to add positive and negative charges to each singlet BHE species and see what happens for their puckering.

Keywords: Boron heterocyclic divalents; BHE; puckering; singlet.

I. Introduction

Boron-Heterocyclic divalents (BHEs) which are the homologues of N-heterocyclic carbenes (NHCs) with the two nitrogen atoms replaced with boron atoms are introduced by Akbari et al [1]. In their initial study, they found that some of the heavier congeners of BHEs from group 14 (e.g. E=Ge, Sn and Pb) have larger singlet-triplet energy gap ($\Delta E_{t\text{-}s}$) in comparison with analogues NHEs. Each singlet species has a bent structure in its five-membered ring which we say it is "puckered". The puckering angle has an average amount of 66°. The heavier congeners have greater puckering angle in comparison with carbenes and silylenes. Here, we plan to optimize the BHE structures with one and two negative charges (-1 and -2) and also one positive charge (+1). The puckering angles will be compared with each other.

II. Methods

The geometries of X_2BHE divalent species (scheme 1) ($C_2H_2B_2X_2E$; E=C, Si X= F, Cl, Br, Me, iPr, tBu) and their charged species are optimized using BLYP [2] density functionals in conjunction with TZP basis sets (ZORA for heavy elements; Sn, Pb and I are applied). Whenever necessary, the spin polarization with restricted/unrestricted considerations has been truly applied. The calculations are carried out using the ADF 2013.01 program package. The vibrational frequencies show that all structures obtained are minima on the potential energy surface.

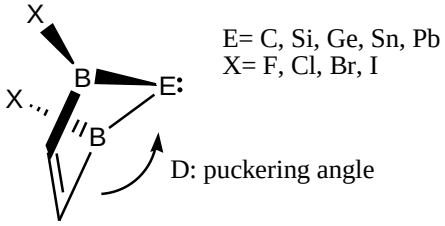

Scheme 1

III. Results and discussion

All divalent species in this study (X_2BHEs: E=C, Si, Ge, Sn, Pb; X= F, Cl, Br, I) with singlet electronic configuration are optimized with BLYP/TZVP level of theory. In the next step, the calculations are performed on X_2BHE^{-1}, X_2BHE^{-2} and X_2BHE^{+1} species. All singlet species are bent or puckered with an average puckering angle of about 65°. The average value for the puckering angle of X_2BHE^{+1} species is 67.6°. this is expectable because the lack of electron in lone-pair orbital of Ë atom pushes the ring to optimize itself in a condition that make stronger overlap with the C=C π bonding orbital. This results in a more bent situation of the ring and hence more puckering angle. On the other hand, the average amount of puckering angle for all X_2BHE^{-1} and X_2BHE^{-2} species is 30.5° and 0.0, respectively. It seems the 5-membered ring is getting wide open and getting to a planar structure. The reason lies behind the fact that the filling of electron density in empty orbital of Ë atom saturates it and decreases the tendency for the interaction of divalent atom with the C=C π bonding orbital. Fig 1 illustrates the four sample optimized structures of the aforementioned species and the increase and decrease in the puckering angle is obvious visibly.

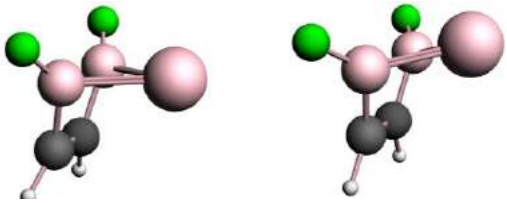

F_2BHGe^{+1} D= 68.8°

F_2BHGe D= 59.6°

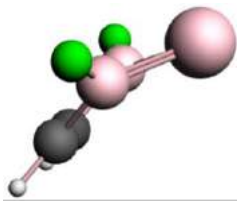

F_2BHGe^{-1} D= 29.9°

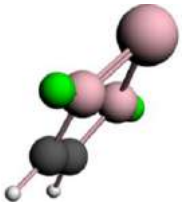

F_2BHGe^{-2} D= 0.0°

Fig. 1. Optimized structures of singlet F_2BHGe and its +1, -1 and -2 charged species at BLYP/TZP level of theory.

IV. Conclusions

Results exhibits that the singlet $C_2H_2B_2X_2Ë$ with E= C, Si, Ge, Sn, Pb and X= F, Cl, Br, I are more puckered when they are positively charged and less puckered when they have negative charges. The more the negative charge, the less the puckering of the heterocycles. Also, the results demonstrate that the puckering of the rings are because of the overlap between the empty orbital of Ë and the C=C π bonding orbital rather than the B—B overlap. It is also interesting that in all -2 charged species, the puckering angle is ≅0.0°.

References

[1] A. Akbari, B. Golzadeh, S. Arshadi, M.Z. Kassaee, *RSC Advances*, 2015, 54, 43319.
[2] C. Lee, W. Yang, R.G. Parr, *Physical Review B, 1988, 37, 785.*
[3] Y. Zhao, D.G. Truhlar, *Theoretical Chemistry Accounts*, 2008, 120, 215.

بیست و سومین کنفرانس شیمی فیزیک انجمن شیمی ایران
23rd ICS Physical Chemistry Conference
Chemistry Department,
Faculty of Science
Shahid Bahonar University of Kerman
Kerman, Iran
12-13 Jan 2022
ایران، کرمان
دانشگاه شهید باهنر کرمان
دانشکده علوم پایه، بخش شیمی
۲۳-۲۲ دی ماه ۱۴۰۰

Study of Electronegative effect of halogen substations on thermodynamic values of PTCDA molecule for use in lithium batteries

Fatemeh Alimohammadi[a]*, Dr. Afshin Abbasi[a],

[a] *Department of Chemistry, University of Qom, Qom, Iran,*
**fateme7557@gmail.com*

Abstract

3,4,9,10-perylenetetracarboxylic dianhydride (PTCDA) is a known organic substance that has an aromatic core and two groups of anhydrids. This molecule has been used as a cathode in lithium batteries. Studies show that by polymerizing PTCDA or using its derivatives, a longer periodic life can be achieved. One way of the efficiency improvement is to functionalize molecule with electronagive elements or particles. In this work, we have studied the effect of halogen substitutions on PTCDA in the presence of lithium element using the density functional calculations (DFT) method.

Keywords: lithium-ion batteries, DFT calculations, electrochemical properties, organic electrodes, Halogenation

I. Introduction,

Over the past two decades, lithium battery technology has made significant progress in the field of mobile electrical appliances and electric vehicles. Electrochemical technology for energy storage at the grid level also has the potential to move away from fossil fuels to renewable energy sources. Researchers have been looking at options to increase the energy density of lithium-ion batteries to meet the growing demand for lightweight and compact batteries with high energy storage capacity.

II. Methods

To evaluate the thermodynamic properties of PTCDA, the lithiation energy was computed through DFT. Structures were fully optimized at the B3LYP level of theory with the basis set 6-31G(d) and confirmed as true local minima by vibrational frequency analyses. Gaussian 09 package was adopted to perform the computations.

III. Results and discussion

In this study, we placed four halogens i.e., F, Cl, Br, I as substitute in PTCDA molecule and investigated their effect on the PTCDA molecule. First, one or two halogen atoms were replaced by hydrogens at PTCDA in all the possible positions. With two halogens on PTCDA for instance, sixteen structural isomers were appeared. All these structures were first fully optimized and followed by vibrational frequency calculations. Then two lithium were located close to the carboxylic oxygens in both part of the molecule which is shown in Fig. 1.

All structures were fully optimized. The optimized structures were used to calculate vibration frequencies, Enthalpy, and the Gibbs free energy the electrical potentials were calculated using the following equation:

$$\Delta E = -\frac{\Delta G}{nF}$$

Where F is the Faraday number. The results of the calculations of free energy differences, and the voltages are summarized in table 1

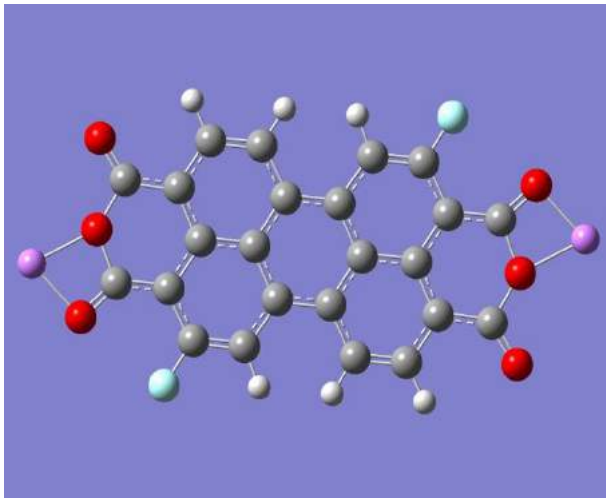

Fig.1. optimized structure of 5,11, difluoro PTCDA-Ll

Table 1. The Gibbs free energies and the electrical potentials of di-halogenated PTCDA

Structures	Δ G (kcal/mol)	Ef volt
PTCDA-Li	-103.25	-2.23
Di Fluoro PTCDA-Li	-107/260	-2.32
DiCholoro PTCDA-Li	-98/8747	-2.14
Di Bromo PTCDA-Li	-109/090	-2.36
Di Iodo PTCDA-Li	-123/560	-2.67

Conclusions

The results on table 1 shows that the computed electrical potentials do not follow a simple trend. However, most of the halogens improve the electrical potentials with respect to the unfunctionalized molecule. Therefore, halogenation could be one way of molecular improvement for the uses in LIBs.

References

1. Whittingham, M. S., (1976). Electrical energy storage and intercalation chemistry. Science, 192 (4244), 1126–1127.

2. Mizushima, K., Jones, P. C., Wiseman, P. J., & Goodenough, J. B. (1980). LixCoO2 (0<x<−1) a new cathode material for batteries of high energy density. Materials Research Bulletin, 15(6), 783–789.

3. Moshtev, R., & Johnson, B., (2000). State of the art of commercial Li ion batteries. Journal of Power Sources, 91(2), 86–91.

4. Goodenough, J. B., & Kim, Y. (2011). Challenges for rechargeable batteries. Journal of Power Sources, 196(16), 6688–6694.

5. Cho, J., Jeong, S., & Kim, Y., (2015). Commercial and research battery technologies for electrical energy storage applications. Progress in Energy and Combustion Science, 48, 84–101.

بیست و سومین کنفرانس شیمی فیزیک انجمن شیمی ایران
23rd ICS Physical Chemistry Conference
Chemistry Department,
Faculty of Science
Shahid Bahonar University of Kerman
Kerman, Iran
12-13 Jan 2022
ایران، کرمان
دانشگاه شهید باهنر کرمان
دانشکده علوم پایه، بخش شیمی
۲۳-۲۲ دی ماه ۱۴۰۰

B-heterocyclic plumbylenes: A computational study

Babak Golzadeh[a]

[a] *Address: Department of Chemistry, Payame Noor University, P.O. Box 19395-3697, Tehran, Iran*
Fax:+982122441511; Tel: +982123320000; E-mail: s.kazeri@yahoo.com

Abstract

B-heterocyclic plumbylenes (BHPbs) are compounds in which the nitrogen atoms of an Arduengo cyclic carbene are replaced with electron deficient boron atoms and the divalent carbon atom is replaced with Pb. Here we study the geometrical parameters and stability of these species via their singlet-triplet energy gaps in relation with their HOMO-LUMO energy gap.

Keywords: Boron heterocyclic plumbylenes; singlet; triplet; energy gap

I. Introduction

Significant advances have occurred in the preparation and isolation of heterocyclic divalents. Now as ever before, researchers are fascinated with group 14 divalents including carbenes, silylenes, germylenes, stannylenes, and plumbylenes.

dialkyl and diarylplumbylenes have been isolated and characterized by Lappert et al. Despite the toxicity of lead which has somewhat hampered its scrutiny, several examples of N-heterocyclic plumbylenes (NHPbs) have surfaced [1]. In this study, we are trying to survey the B-Heterocyclic Plumbylenes with new theoretical levels other than worked before [2].

II. Methods

The geometries of singlet and triplet X_2BHPb (X=F, Cl, Br, I) (scheme 1) species are optimized using OPBE density functional in conjunction with TZP basis sets with ZORA for Pb and I atoms using the ADF program package [3]. All singlet species are bent (dihedral angle ≅ 64.2°) and all triplet species are planar. To confirm the nature of the stationary species, frequency calculations are carried out.

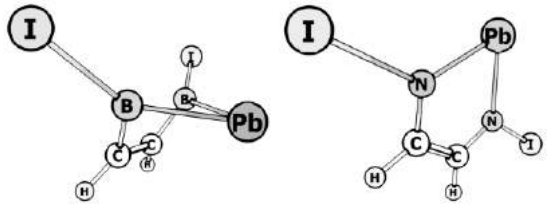

scheme 1 singlet (right) and triplet (left) I_2BHPb

III. Results and discussion

We begin discussing our calculated data on BHPbs, by estimating their stability through singlet-triplet energy gaps (ΔE_{st}) and energetic advantages of puckering for singlet states. Calculated energy differences between HOMO and LUMO of singlet states, $\Delta E_{(LUMO-HOMO)}$, for the halogenated BHPbs appear to have linear relationships with the corresponding ΔE_{st} values. They show correlation coefficients (R^2) of 0.95 (Fig. 1). The amounts of ΔE_{st} for X= F, Cl, Br and I are 20.67, 24.27, 25.26 and 22.53 kcal/mol, respectively (F<Cl
I). On the other hand, the corresponding values of $\Delta E_{(LUMO-HOMO)}$ with respect to halogens from F to I are 1.128, 0.411 0.366 and 0.669 eV (F>Cl<Br<I). The smallest value of ΔE_{st} for

F_2BHPb owns the largest value of $\Delta E_{(LUMO–HOMO)}$. This implies that in spite of the easier promotion of one electron from the lone-pair in sp^2 hybrid orbital to the empty p orbital of the divalent Pb atom, the HOMO and LUMO are largely separated from each other. This may be related to the geometrical change from bent (puckered geometry) to planar.

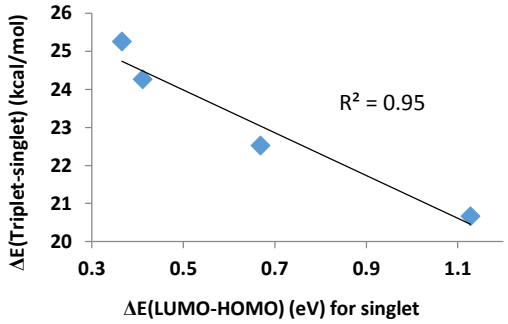

Fig. 1. Linear relationships between singlet LUMO–HOMO energy gaps $\Delta E_{(LUMO-HOMO)}$, and their corresponding singlet–triplet energy separations (ΔE_{st}), for X_2BHPb (X=F, Cl, Br, I)

IV. Conclusions

The challenging introduction of electron-withdrawing groups such as boryl substituents flanking the Plumbylenic center (Pb) produces a good model of pull-pull carbene story profiting from the ability of boron to stabilize a LP in an adjacent position. Every bent singlet structure (puckering angle ≅ 64.2° average) for all studied species is more stable than its corresponding planar triplet. There are linear relations between ΔE_{st} and $\Delta E_{(LUMO-HOMO)}$ and also between ΔE_{st} and the atomic size of the divalent atom for each species.

V. References

[1] J. Barrau and G. Rima, Coordination Chemistry Reviews, 1998, 178-180, Part 1, 593.

[2] A. Akbari, B. Golzadeh, S. Arshadi, M.Z. Kassaee, *RSC Advances*, 2015, 54, 43319.

[3] ADF2008.01, SCM, Theor Chem, Vrije Univ, Amsterdam, the Netherlands.
http://www.scm.com. https://doi.org/

بیست و سومین کنفرانس شیمی فیزیک انجمن شیمی ایران
23rd ICS Physical Chemistry Conference
Chemistry Department,
Faculty of Science
Shahid Bahonar University of Kerman
Kerman, Iran
12-13 Jan 2022
ایران، کرمان
دانشگاه شهید باهنر کرمان
دانشکده علوم پایه، بخش شیمی
۲۳-۲۲ دی ماه ۱۴۰۰

Theoretical Aspects of Bonds in the Complexes Benzoxapine Derivatives with Phosphoinositide -3- kinase delta

Samira Baravardi[a], Maryam Dehestani[*b] , Leila Zeidabadinejad[c]

[a]*Shahid Bahonar University of Kerman, Kerman, Iran; E-mail: samira.baravardii@gmail.com*
[b] *Shahid Bahonar University of Kerman, Kerman, Iran; E-mail: dehestani@uk.ac.ir*
[c]*Shahid Bahonar University of Kerman, Kerman, Iran, E-mail: lzeidabadi@yahoo.com*

Abstract

The aim of this work is to theoretically study the interaction of benzoxazepine derivatives with amino acids arginine and tryptophan of Phosphoinositide -3- kinase delta (PI3Kδ) using 6-31G (d) / B3LYP theory level. In this study, two directions have been considered to investigate the formation of a complex between benzoxazepine derivatives and PI3Kδ, through different aryl groups connected to carbon atoms 8 and 9, the benzene rings form the benzoxazepine complex. QTAIM results showed that there were some hydrogen bond interactions between benzoxazepine derivatives and the active space PIK3δ.

Keywords: Benzoxazepine derivatives; Density functional theory; Phosphoinositide-3-kinase delta (PI3Kδ); Quantum theory of atoms in molecules (QTAIM)

I. Introduction

The phosphoinositide-3-kinase delta (PI3Kδ) is a potent selective inhibitor extracted from the morpholine pyrimidine nucleus [1]. Benzoxazepine is a two-ring heterocyclic organic compounds of a benzene ring attached to the oxazepine ring Benzoxazepines inhibit the growth of breast cancer cells and are non-toxic. Breast cancer is the leading cause of cancer mortality among women [2]. In this work, we study the interaction of benzoxazepine derivatives on active space amino acids arginine and tryptophan of PI3Kδ using density functional theory.

II. Methods

In this research, first all the structures were drawn separately and in a complex state using Gauss view software [3]. Drawing of each complex was done in two ways. In the first case, benzoxazepine derivatives were obtained from the binding of different aryl groups to C8 of the benzene ring, and in the second case, from the bonding of different aryl groups to C9 of the benzene ring, and then its complexes are drawn with active space amino acids (tryptophan and arginine) PI3Kδ and optimized at 6-31G (d) / B3LYP theory level to obtain the best structures and energies. Quantum theory of atoms in molecules (QTAIM) is one of the most important theoretical techniques in the study of bonds. 2000-AIM software was used to perform these calculations.

III. Results and discussion

Figures (1-a)-(1-d) show the structure of benzoxazepine derivatives, the aryl groups (A-F) attached to carbon atoms C8 and C9 of the benzene ring benzoxazepin, the optimized structures of the benzoxazepine derivatives complex resulting from the bonding of aryl C group to C8 atom with (arginine and tryptophan amino acids) PI3Kδ in the best position and energy, and

the bond critical points (BCP) complex of benzoxazepine derivatives due to the bonding of aryl C groups to C8 with amino acids arginine and tryptophan PI3Kδ obtained from AIM calculations, respectively. The topological parameters at bond critical point for the interacting positions of the benzoxazepine derivatives and PI3Kδ complex from group C to C8 are determined and reported in Table (1). According to the data in Table (1) and Figure (1-d) related to the complex of benzoxazepine derivatives due to the bonding of aryl group C to C8 with (arginine and tryptophan amino acids) - Gb/Vb value for H51 --- O91 bond, 0.973798 a.u and the amount of total energy density (H_b) for this interaction is negative, which indicates that this interaction is somewhat covalent (moderate hydrogen bond). The value of -Gb/Vb and also the amount total energy density for other bonds are greater than one and positive, respectively, which indicates these interactions are non-covalent and have a weak hydrogen bond. They are electrostatic in nature. Charge electron density (ρ_b) less than 0.1 a.u. also indicates the non-covalent interactions in this complex.

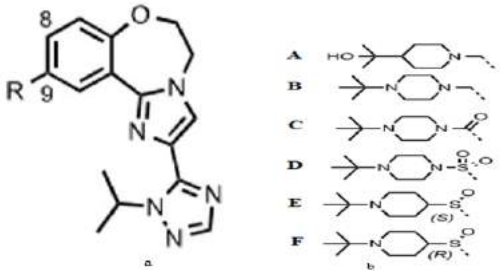

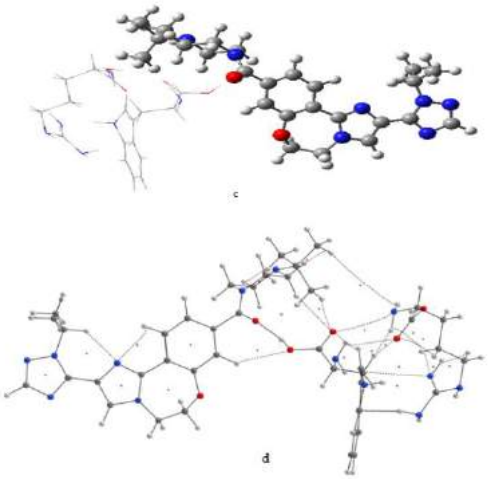

Fig 1 a) Structure of benzoxazepine derivatives **b)** Aryl groups (A-F) attached to carbon atoms C8 and C9 of the benzene ring Benzoxazepin **c)** Optimized structures of the benzoxazepine derivatives complex resulting from the bonding of aryl C group to C8 atom with PI3Kδ **d)** bond critical points (BCP) complex of benzoxazepine derivatives due to the boding of aryl C groups to C8 with PI3Kδ.

Bond	Bond Length(Å)	$\rho_{(r)b}$	H_b	- G_b/V_b
O_{15}---H_{99}	2.64	0.0072	0.0008	1.1822
O_{50}---H_{89}	2.73	0.0048	0.0009	1.3106
H_{51}---O_{91}	1.80	0.0345	-0.0007	0.9737
O_{15}---H_{108}	2.96	0.0031	0.0008	1.5227

Table 1: Topological parameters at BCP (ρ(r), Hb and - Gb/Vb (in a.u.)) of benzoxazepine derivative and PI3Kδ complex of the from different aryl groups C connected to C8 atom.

IV. Conclusions

The results show that the H51 --- O91 bond in this complex is somewhat covalent (moderate hydrogen bond).

References

[1] B.S. Safina, R.L. Elliott, A.K. Forrest, R.A. Heald, J.M. Murray, J. Nonomiya, J. Pang, L. Salphati, E.M. Seward, S.T. Staben, M. Ultsch, J. Med. Chem. Lett., 2017, 8 (9), 936-940.

[2] A. Jemal, F. Bray, M.M. Center, J. Ferly, E. Ward, D. Forman, Cancer. J. Clin. 2011, 61 (2), 69-90.

[3] Frisch, J. et al. Gaussian 09, G09W.Gaussian Inc, Wallingford, USA. 2009.

بیست و سومین کنفرانس شیمی فیزیک انجمن شیمی ایران
23rd ICS Physical Chemistry Conference
Chemistry Department,
Faculty of Science
Shahid Bahonar University of Kerman
Kerman, Iran
12-13 Jan 2022
ایران، کرمان
دانشگاه شهید باهنر کرمان
دانشکده علوم پایه، بخش شیمی
۲۳-۲۲ دی ماه ۱۴۰۰

Kinetic of Synthesis Pincer Ligand based on Thiol Precursor

Sayed Jalal Razavizade[a], Farahnaz Eshraghi[a,*], Saeed Vatani[b]

[a] *Central laboratory, University of Technology of Isfahan, Isfahan, Iran, jamalizadeh@uk.ac.ir*
[b] *Department of Chemistry, Shahreza Islamic Azad University, Isfahan, Iran*

Abstract

The kinetics of aliphatic pincer ligand based on SNS (bis(2-(μ^1-sulfanyl)ethyl)amine) has been studied by utilizing DFT calculation in the gas phase. The reaction between bis(2-chloroethyl)amine and different thiols has followed with S*N*2 mechanism.

Keywords: pincer ligand; thiol; kinetic

I. I. Introduction

Today, tridentate pincer ligands and their complexes in comparison to metal - complexes based on mono/bidentate ligands have been attracted the attention of researchers [1, 2]. Moulton and et.al in 1976 have synthesized the pincer ligand for the first time [3] and were named by Van Koten in 1987. These type ligands are coordinated into the metals which were leading to increasing their ability to adjust the reactivity, selectivity, and thermal stability to form a suitable and desired complex. Consequently, the existence unique features of the pincer complexes based on pincer ligand lead to significant application such as catalysis, electrocatalyst, supramolecules, sensor, medicine, solar fuels, and etc [4, 5]

II. Methods

DFT calculations were directed by the Gaussian 09 program. All structures of reactants, transition states, and products have optimized using the B3PW91 method. The standard 6-31G (d) basis set was adopted for H, N, C, Cl, and S atoms. The calculations were done in the gas phase. Also Eyring equation has used to calculate the rate constants of the reactions:

$$k(T) = \frac{k_B T}{h} e^{-\Delta G^{\neq}/RT}$$

III. Results and discussion

The reaction between bis(2-chloroethyl)amine and thiols has followed with SN2 mechanism.

We have used different thiol for synthesis of aliphatic pincer ligand in two steps, According to data, (4-aminophenyl)methanethiol, cyclopentanethiol, and propane-1-thiol in first step have the lowest activation free energy ($\Delta G_1^{\neq}$) and the highest rate constant (k1). Among three thiols, the $\Delta G_2^{\neq}$ and k_2 of the reaction for propane-1-thiol were 43 kcal/mol and 1.8×10^{-19} s^{-1}, respectively at second step. propane-1-thiol has the highest rate constant compared to the (4-aminophenyl)methanethiol and cyclopentanethiol, Fig. 1 has been shown The optimized structures of important

structural different thiol in first and second steps.

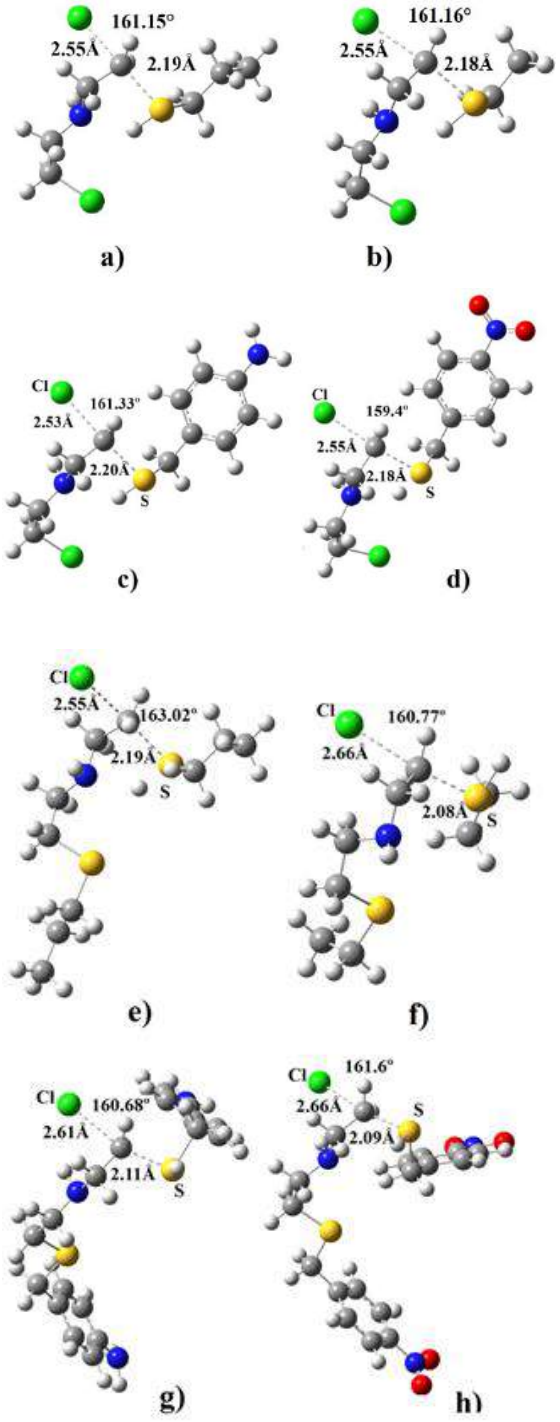

Fig. 1. TS structures in first step (a-d) and second step

Table 1. Table 1: The $\Delta G^{\neq}$ and k for different thiol

RSH	$\Delta G_1^{\neq}$ (kcal/ mol)	k_1 (s^{-1})	$\Delta G_2^{\neq}$ (kcal/ mol)	k_2 (s^{-1})
propane-2-thiol	47	2.09×10^{-22}	52.90	9.85×10^{-27}
2,5-dimethylfuran-3-thiol	48.08	3.38×10^{-23}	40.63	9.84×10^{-18}
cyclopentanethiol	45.74	1.76×10^{-21}	52.60	1.63×10^{-26}
ethanethiol	45.95	1.23×10^{-21}	51.41	1.22×10^{-25}
2-methylpropane-2-thiol	52.08	3.93×10^{-26}	48.39	$2.\times10^{-23}$
propane-1-thiol	**45.90**	**1.34×10^{-21}**	**43**	**1.8×10^{-19}**
(4-aminophenyl)methanethiol	45.41	3.07×10^{-21}	49.86	1.67×10^{-24}
(4-nitrophenyl)methanethiol	48.30	2.33×10^{-23}	53.04	7.77×10^{-27}

IV. Conclusions

The study kinetic of SNS pincer ligand with SN2 reactions in gas phase has been carried out by DFT calculations. The result has been shown that propane-1-thiol has highest constant rate.

References

[1] S.Werkmeister, J.Neumann, K.Junge, and M.Beller, *Chem. Eur*, 2015, 21, 12226-12250.
[2] S. H.Hosseini, N.Zohreh, S.Alipour, C.Busuioc, and R. Negrea, *Catal. Commun*, 2018, 108, 93-97.
[3] C. J. Moulton, and B. L. Shaw, *Dalton Transactions*, 1976, 11, 1020-1024.
[4] G. Van Koten, *PURE. APPL CHEM*, 61, 1681-1694 (1989).
[5] L.Soobramoney, M. D.Bala, and H. B. Friedrich *Dalton Trans*, 2014, 43, 15968-15978

بیست و سومین کنفرانس شیمی فیزیک انجمن شیمی ایران
23rd ICS Physical Chemistry Conference
Chemistry Department,
Faculty of Science
Shahid Bahonar University of Kerman
Kerman, Iran
12-13 Jan 2022
ایران، کرمان
دانشگاه شهید باهنر کرمان
دانشکده علوم پایه، بخش شیمی
۲۳-۲۲ دی ماه ۱۴۰۰

Theoretical studies of interaction of small Cobalt clusters with Oxygen, Hydrogen and Ethylene

Elham DehghanPisheh [a]*, Ali Haidar Pakiari[b]

[a] *Department of Chemistry, Shiraz University, Shiraz, Iran, e.dehghanpishe@gmail.com*
[b] *Department of Chemistry, Shiraz University, Shiraz, Iran*

Abstract

In this study, after calibration of DFT and selecting the best xc-functional, to evaluate the active sites of small Cobalt clusters (Co_n, n =2 - 4) which had been reported before, the interactions of small Cobalt clusters with Oxygen (O_2), Hydrogen (H_2) and Ethylene (C_2H_4) have been investigated. The results show the complete consistency of experiments, pure active sites, and our results.

Keywords: Calibration of DFT; Interaction of Small Cobalt clusters; Oxygen; Hydrogen; Ethylene.

I. I. Introduction

Cobalt clusters are the important compounds in an industry in catalytic processes such as Cobalt Fischer–Tropsch catalysts [1]. On the other hand, in the theoretical aspects, Cobalt clusters are very awkward systems in optimizing and any hints about their structures can be extremely helpful in developing their theoretical framework. Cobalt systems, such as other transition metals (TM), have near-degeneracy correlation between diffuse ns orbitals and contracted, partially filled (n-1) d orbitals and such conditions result in failure of the highly accurate wavefunction methods such as multi-reference (MR) and multireference configuration interaction (MR-CI) approaches. In this situation, density functional theory (DFT) has become a powerful tool for theoretical chemists to calculate many molecular properties of TM compounds such as their structural parameters, and energetic properties with impressive accuracy. To analyze the nature of bonds, natural bond orbital analysis (NBO) paves the way.

II. Methods

We have used DFT & NBO to calculate electrical and geometrical structures of interactions of Cobalt clusters with O_2 and C_2H_4. DFT has been used with selected xc-functional by calibration B3P86 and 6-311++G* basis set.

III. Results and discussion

Finding a suitable xc-functional and basis set of specific chemical species, is called calibration of DFT in such a way that the results can match with experimental values. The process had been done for small Cobalt clusters before and their active sites were also reported [2]. This calibrated DFT is applicable for the interaction analysis parts, too. The reported active sites are also the ones which O_2, H_2 and C_2H_4 selected to attack when interacting with small Cobalt

clusters. So, the results are in good agreement with pure Cobalt clusters [2]. The optimum structure was reported in accordance with the best energy and multiplicity. The experimental results reported that H_2 didn't interact with Co_n [3]. Our calculations also show that H_2 molecules do not make any bonds with all Co_n clusters and the reaction is repulsive. The nature of the Co-Co bonds adjacent to O_2, C_2H_4 are analysed in detail. Our studies consider NBO analysis results which let us know the nature of each bond, percentage of its orbital hybridizations, occupancy and energy of each individual bond. We also report total Lewis and non-Lewis parts of α and β-spin parts, and their NBO shapes. Thermodynamic properties (binding energy, interaction energy and Gibbs free energy) have been used as a guide as to how acceptable these interactions should be. The sample of NBO analysis for Co_3/O_2 are listed in Table 1.

When we have formation of bonds between two species, we report it as "new" bonds. Cobalt clusters (dimer and trimer) react with O_2 and make new bonds. Trimer makes additional products from decomposition of cluster and oxygen molecules and then products react again and make new compounds. Cobalt tetramer and oxygen molecules both decompose and make three new compounds. Interactions between Co_n and C_2H_4 do not make new bonds, instead making van der Waals complexes. The experimental bond energies of Co_n are in good agreement of our calculated binding energies [4].

Table 1. NBO Descriptors of Co_3/O_2 disigma (for α and β-spin parts), Showing Bonding Orbital (σ, π), Hybridization, Occupancy and Energy of Each Bond

NBO bond	h_A-h_B% [a]	Occ [b]	Energy [c]	NBO shape
β -spin				
1.$\sigma_{Co_{(3)}\text{-}O_{(4)}}$	$d_z^{44.2}$-$p_y^{81.0}$	0.97	-396.29	
2.$\sigma_{Co_{(2)}\text{-}O_{(5)}}$	$d_{x^2-y^2}^{67.1}$-$p_y^{99.3}$	0.92	-281.04	
3.$\pi_{Co_{(3)}\text{-}O_{(5)}}$	$d_{x^2-y^2}^{76.8}$-$p_x^{99.2}$	0.93	-218.42	
4.$\pi_{Co_{(3)}\text{-}O_{(4)}}$	$p_z^{51.5}$-$p_z^{99.9}$	0.94	-202.52	
5.$\pi_{Co_{(3)}\text{-}O_{(5)}}$	$d_{yz}^{52.2}$-p_z^{100}	0.93	-199.77	
6.$\sigma_{Co_{(1)}\text{-}Co_{(2)}}$	$s^{71.5}$- $s^{53.6}$	0.97	-172.01	
7.$\sigma_{Co_{(1)}\text{-}Co_{(2)}}$	$d_{xy}^{80.9}$-$p_y^{97.2}$	0.95	-158.98	
α-Spin				
1.$\sigma_{Co_{(3)}\text{-}O_{(4)}}$	$s^{65.7}$-$p_y^{72.5}$	0.95	-418.24	
2.$\pi_{Co_{(3)}\text{-}O_{(4)}}$	$d_{xy}^{87.7}$-$p_x^{97.2}$	0.95	-234.63	
3.$\sigma_{Co_{(1)}\text{-}Co_{(2)}}$	$s^{96.7}$- $s^{77.5}$	0.99	-203.63	

a - hA-hB%= type of maximum hA-hB%, b - occ=occupancy, c –Energy is in kcal/mol

IV. Conclusions

The electronic structure of adsorption of O_2 on Co_n could be beneficial in modeling a new effective promising catalyst. C_2H_4 can serve as a well-defined type of alkyl group in their interaction with Co_n. The detailed structures of their multiplicities, bond lengths, energies, nature of their bonds are in absolute agreement with pure Co_n and experiments data.

References

[1] K. Jeske, A.C.Kizilkaya, I.Lopez-Luque, N.Pfander, M. Bartsch, P.Concepcion and G.Prieto ACS Catal., 2021, 11, 4784-4798.

[2] A.H.Pakiari, and E. DehghanPisheh. Struct Chem., 2016, 27 (2), 583-593.

[3] M. E. Geusic, M. D. Morse, and R. E. Smalley, J. Chem. Phys., 1986, 23, 203.

[4] David A. Hales, C.X. Su, Li Lian, and P. B. Armentrout, J. Chem. Phys., 1994, 100, 1049.

بیست و سومین کنفرانس شیمی فیزیک انجمن شیمی ایران
23rd ICS Physical Chemistry Conference
Chemistry Department,
Faculty of Science
Shahid Bahonar University of Kerman
Kerman, Iran
12-13 Jan 2022
ایران، کرمان
دانشگاه شهید باهنر کرمان
دانشکده علوم پایه، بخش شیمی
۲۳-۲۲ دی ماه ۱۴۰۰

Redefining density theory fuel universe for improving flammability limit prediction

Aylan Rafiee Oskouee[a], Ali M. Nassimi[b*]

a Chemistry Department, Sharif University of Technology, Tehran, Iran, Tel: +98(21)66165318; Email: Aylin.Rafiee@ch.sharif.edu
b Chemistry Department, Sharif University of Technology, Tehran, Iran, Tel: +98(21)66165377; Email: a.nassimi@sharif.edu

Abstract

In previous studies molecular structure was used to define density theory fuel universe as the set of compounds whose flammability limits can be calculated by means of thermal or density theory of flame propagation. This study, shows that redefining density theory fuel universe based on thermodynamic criteria result in greater accuracy for predicted flammability limits.

Keywords: Flammability limit; Density factor; Adiabatic flame temperature; Thermal theory of flame propagation; Density theory of flame propagation

I. Introduction

Many flammable, toxic and hazardous materials are used in the chemical industry, which pose great safety challenges in the process of preparation, production, storage and transportation. In this regard, studies on the flammability limits (FLs) of flammable materials are important and necessary. Upper flammability limit (UFL) also called upper explosive limit (UEL) is the greatest fuel concentration in a fuel-air gaseous mixture which enables self-propagation of a flame. Lower flammability limit (LFL) also called lower explosive limit (LEL) is the least fuel concentration in a fuel-air gaseous mixture which enables self-propagation of a flame. We model combustion as

$$\varphi C_c H_h O_o N_n Cl_l Br_b S_s + 4.773 l_s \rightarrow combustion\ products \quad (1)$$

Where the equivalence ratio φ is the ratio of fuel to oxygen over the stoichiometric ratio of fuel to oxygen and l_s is the stoichiometric oxygen requirement for each fuel molecule, $l_s = \frac{(2C+\frac{(h-l-b)}{2}-o+2s)}{2}$.

Density factor (DF) is defined as the ratio of the mixed density of reactants $\rho_{fuel\text{-}ox}$ to the mixture density of products $\rho_{prod.}$ It has been shown that for a large set of fuels (TTFU[1]) DF is concentrated around its mean value [1].

$$DF = \frac{\rho_{fuel-ox}}{\rho_{prod}} = \frac{4.773 l_s \rho_{air} + \varphi \rho_{fuel}}{(4.773 l_s + \varphi)\rho_{prod}} = \frac{T_f}{T_i}\left[\frac{4.773 l_s M_{air} + \varphi M_{fuel}}{(4.773 l_s + \varphi) M_{prod}}\right] \quad (2)$$

Where T_f and T_i are, respectively, final and initial temperature, M_{air}, M_{fuel} and M_{prod} are, respectively, the average molecular mass of air, molecular mass of fuel and the average molecular mass of combustion products [2].

II. Methods

Thermal theory proposes the existence of a theoretical threshold temperature (TTT) that at a flame temperature greater than the TTT, flame propagation is possible and at a temperature smaller than the TTT, the flame cannot propagate. By considering the same TTT for different fuels and limiting the fuels to

[1] Thermal Theory Fuel Universe

set of thermal theory fuel universe, the LFL is obtained with a good approximation, but for the UFL, the prediction accuracy is quite limited. To predict the UFL, since the DF at the UFL has a greater concentrated around the mean compared with the adiabatic flame temperature, for the UFL, density theory can be used. Density theory of flame propagation uses the assumption that the density factor at each FL is constant for different fuels. We have redefined thermal theory fuel universe and called it density theory fuel universe to increase prediction accuracy for FLs [2]. In redefining DTFU thermodynamic properties such as enthalpy of formation (ΔH_f) and combustion enthalpy (ΔH_c) of compounds are considered. A set of 133 compounds are considered, of which 26 compounds are excluded because of their ΔH_f and 18 compounds are excluded because of their ΔH_c, finally 89 compounds remain with negative value of ΔH_f and value of ΔH_c less than -1500 kJ/mole. To test the validity of this assumptions chemical equilibrium with applications (CEA) is used to calculate combustible mixture equilibrium composition, adiabatic flame temperature (T_{ad}) and after equilibration density of combustible mixture. Using these data T_{ad} vs ϕ and DF vs ϕ are plotted for every compound under study. These plots are used to interpolate the values of T_{ad} and DF corresponding to UFL and LFL [3].

III. Results and discussion

In this study, thermal theory of flame propagation and density theory of flame propagation are tested on 133 fuel compounds. Mean absolute percentage error (MAPE) in predicted values of FLs and thermodynamic properties of these compounds are compared. It is shown that for compounds that have positive enthalpy of formation or enthalpy of combustion greater than -1500 kJ/mole exhibit large values of Mean absolute percentage error.

Table 1: Mean absolute percentage error (MAPE) for thermal theory predicted (TTP) and density theory predicted (DTP) values of lower flammability limit (LFL) and upper flammability limit (UFL) for members of density theory fuel universe.

TTP LFL MAPE	DTP LFL MAPE	TTP UFL MAPE	DTP UFL MAPE
10.00	9.48	17.99	16.88

IV. Conclusions

This work suggests using thermal theory of flame propagation for predicting LFL and density theory of flame propagation for predicting UFL for members of DTFU. DTFU is defined as the set of flammables with negative enthalpy of formation and combustion enthalpy less that -1500 kJ/mol. MAPE for predicting FLs of members of DTFU using both density theory and thermal theory are reported in Table 1. Precision of this method is comparable with far more involved, state of the art detailed kinetic modeling of combustion.

References

[1] A. M. Nassimi, M. Jafari, H. Farrokhpour and M. H. Keshavarz, "Constants of explosive limits," *Chem. Eng. Sci.*, vol. 173, pp. 384-389, 2017.

[2] A. M. Nassimi, *Predicting flammability limits through thermal theory and density theory of flame propagation*, Fire Mater., 2021.

[3] A. Nassimi and A. Rafiee, *"Comparing density theory of flame propagation and thermal theory of flame propagation for evaluating flammability limits",* under review, (2021).

[1] Density Theory Prediction

بیست و سومین کنفرانس شیمی فیزیک انجمن شیمی ایران
23rd ICS Physical Chemistry Conference
Chemistry Department,
Faculty of Science
Shahid Bahonar University of Kerman
Kerman, Iran
12-13 Jan 2022
ایران، کرمان
دانشگاه شهید باهنر کرمان
دانشکده علوم پایه، بخش شیمی
۲۳-۲۲ دی ماه ۱۴۰۰

Predicting Lower and Upper Flammability Limits

Ali Mohammad Nassimi[a*], Mahour Aghakhani[b*]

[a] *Chemistry Department, Sharif University of Technology, Azadi Street, Tehran*
[b] *Chemistry Department, Sharif University of Technology, Azadi Street, Tehran, and Science Department, Tehran University*

Abstract

In this work, direct and indirect use of the quantitative structure-property relationship (QSPR) is used to predict the explosive limits. The indirect use of QSPR was through first predicting either density factor (DF)---defined as the ratio of the density of the reactant mixture (ρ_r) to the density of the product mixture (ρ_P)---or adiabatic flame temperature (AFT)---defined as the temperature attained when all of the chemical reaction heat released heats combustion products---at the flammability limit.

Keywords: Quantitative structure property relationship; Flammability limits; Density factor; Adiabatic flame temperature

I. Introduction

A fuel and oxidant mixture can give rise to a self-propagating flame if the oxidant/fuel ratio is within a specific range. The boundaries of this range are called explosive limits. In calculation of flammability limits from adiabatic flame temperature, the existence of the flammability limits is considered to be a consequence of existence of a minimum sustaining temperature for the flame—thermal theory. Lower flammability limit (LFL)—defined as the least fuel concentration capable of self-propagating a flame—and upper flammability limit (UFL)—defined as the greatest fuel concentration capable of self-propagating a flame—are properties of a fuel-oxidizer mixture [1]. Flammability limit (FL) values are frequently reported as volume percentage in air, they can also be studied in other oxidants [2]. Knowing these limits is crucial for the safety of design in the chemical industry. The values of these limits are essential to prevent accidental explosions during chemical processes. [3]

II. Methods

Past work discussed graphing AFT or DF vs. equivalence ratio, φ, thus establishing the equivalence between flammability limit values and values of AFT or DF at the flammability limits. To calculate the flammability limits, AFT at the flammability limits and DF at the flammability limits, each is assumed to be a linear combination in the form of the group frequency/property value multiplied by its coefficient; this results in our desirable property. Coefficient values are derived from linear regression. Group frequency/molecular property are deduced from molecular formula. For example, CH_4 has 1 type 0 carbon and 4 hydrogens with a molecular weight of 16.04 gram/mol.

III. Results and discussion

In this work, according to the average relative errors, it is proved that by using the QSPR, the greatest accuracy in predicted FL values can be achieved by calculating FLs through values of density factors. Thus, this work suggests calculating flammability limits through the values of density factor predicted by a QSPR. Table 1 shows the average relative errors of the calculated values of DF and AFT at FLs according to our calculations. It is easy to see that QSPR produces DF and AFT at FLs with greater accuracy compared with values of FLs themselves. Thus we suggest calculating

flammability limits via first calculating DF at the FL and then using the equivalence of the values of DF at FLs and FL values as explained in references [1] and [2].

Table 1: The average relative errors of our method.

	LFL	UFL
PDF	0.071	0.111
PAFT	0.1	0.134
PFL	0.51	0.258

IV conclusion

Average relative errors of a group of compounds whose flammability limits are calculated through DF at FL are respectively 0.088 for LEL and 0.17 for UEL. The results show a better accuracy in indirect way. Thus, this work suggests using a specific version of density theory of flame propagation for calculating FLs.

References

[1] Nassimi, A. M., Jafari, M., Farrokhpour, H., & Keshavarz, M. H. (2017). Constants of explosive limits. *Chemical Engineering Science*, *173*, 384-389.

[2] Nassimi, A. M. (2021). Predicting flammability limits through thermal theory and density theory of flame propagation. *Fire and Materials*.

[3] Albahri, T. A. (2013). Prediction of the lower flammability limit percent in air of pure compounds from their molecular structures. *Fire safety journal*, *59*, 188-201.